The Choline Metabolite-Interacting Proteome of Mammalian Cells: Discovery and Significance

A thesis

submitted in partial fulfilment of the requirements

for the degree of

Doctor of Philosophy

by

Aditi Dixit

20132008

INDIAN INSTITUTE OF SCIENCE EDUCATION AND RESEARCH (IISER)

PUNE, INDIA

2022

Dedicated to the loving memory of my Nana and Nani

Certificate

Certified that the work incorporated in the thesis entitled "**The Choline Metabolite-Interacting Proteome of Mammalian Cells: Discovery and Significance**" submitted by Ms. Aditi Dixit was carried out by the candidate under my supervision. The work presented here or any part of it has not been included in any other thesis submitted previously for the award of any degree or diploma from any other university or institution.

Date: April 7th, 2022

Dr. Jeet Kalia

Thesis advisor

Declaration

I declare that this written submission represents my ideas in my own words and where others' ideas have been included, I have adequately cited and referenced the original sources. I also declare that I have adhered to all principles of academic honesty and integrity and have not misrepresented or fabricated or falsified any idea/data/fact/source in my submission. I understand that violation of the above will be cause for disciplinary action by the institute and can also evoke penal action from the sources which have thus not been properly cited or from whom proper permission has not been taken when needed.

Date: April 7th, 2022 Aditi Dixit

Registration No. 20132008

Acknowledgements

I express my sincere gratitude to my advisor, Dr. Jeet Kalia for guiding me throughout my doctoral studies and for nurturing an encouraging lab atmosphere. Jeet is one of the most passionate scientists I have come across and I have been immensely fortunate to have learnt the importance of hard work and perseverance from him. I am grateful to him for believing in me at times when I had very little confidence in myself. I thank him for not only providing me with the independence in executing my experiments, but also for the support and guidance when I needed it the most. Jeet's constant pursuit of leaning new concepts, and the breadth of his scientific knowledge and interests never ceases to amaze me and I aspire to imbibe these qualities from him.

I offer my heartfelt and sincere appreciation to Jeet for being persistent in my graduate school training. Under his tutelage, I have not only learnt the significance of seeking rigor in pursuing science, but also the discipline of keeping myself updated with the relevant literature for my project. I feel privileged to have Jeet teach me how to perform experiments and more importantly, how to critique them. I particularly want to thank him for the opportunity and space that he has given me in exploring and venturing beyond the comfort zones of my expertise.

In addition to being an incredible advisor, Jeet has also been a remarkable mentor. In times of my personal crises, Jeet has very been a patient listener and has also been very kind in sharing his perspectives with me that have often been very helpful. Jeet finds genuine joy in supporting the lab members in achieving their goals not only within the lab but also after their graduate school. From troubleshooting a TLC condition with me to analyzing huge proteomics datasets, I have seen Jeet work very hard on each of our projects at every stage. I had known that he is far more ambitious for his students than we have been for ourselves, and I had the privilege of experiencing it personally during my postdoc search. Jeet has helped me work on my applications like they were his own. He has edited multiple drafts of my cover letters and my CV. I fall short on words every time I think of Jeet's contribution in my development as a researcher. I take immense pride in my training and I truly am grateful for his mentorship.

I thank the former members of the Kalia lab–Debayan Sarkar, Rahul Nisal, Chitra Shanbhag and Nitin Tagad, with whom I had shared the pleasure of working and having fun at work. I thank them for their support especially in the initial days of my graduate school journey. I want to especially thank my postdoctoral colleague–Dr. Gregor P. Jose for training me on biology-based experiments. I joined the laboratory with almost no experience in performing biological experiments and Gregor had very kindly and patiently taken me under his wing. I thank Gregor for patiently training me on the biochemistry experiments and bringing me out of my comfort zone. I am grateful to him for being the source of positivity in the lab and also for introducing me to the game of badminton at Pune, that I often continue to enjoy. I also want to extend my gratitude to the current members of my lab–Yashaswi Singh, Satyajit Mishra, Manas, Saswati Biswal and Dr. Tanveer Alam Khan for maintaining an enjoyable and supportive atmosphere in the lab. I thank Sumita Majhi and Subhadeep Duari for helping me on my molecular biology and recombinant protein production experiments. I also would like to acknowledge the support that I received from the previous members of the lab–Avni Jain, Avinil Das Sharma, Namita Bhoi, Sahil Bhardwaj, Anusree V.S., and Dheerendra Singh.

I thank my research advisory committee–Dr. Thomas Pucadyil, Dr. H. N. Gopi and Dr. S. G. Srivatsan for their valuable feedback and evaluations during my research progress.

I would take this opportunity to acknowledge the administration at IISER Pune for providing and maintaining the state-of-the-art facilities for aspiring researchers like myself. I would also like to thank the hospitable administration at IISER Bhopal. Moving to a new institute was challenging for my lab members and myself, and I am deeply thankful to IISER Bhopal's administration for being a gracious host to all of us and also in providing unrestricted access to all research facilities. I thank the laboratories of Drs. Sanjeev Shukla and Nagaraj Balasubramanian for providing access to the EVOS cell imaging system, Dr. Ankur Gupta for providing access to a UV-Visible spectrophotometer, and Dr. Himanshu Kumar for providing access to a Zeiss Axio Vert.A1 microscope and a Biorad microtiter plate reader. I also would like to thank Dr. Sourav Datta's lab for providing unrestricted access to use the ChemiDoc imager in their lab.

I am deeply grateful to our group's collaborator, Prof. Matthew Shoulders and my advisor, Dr. Jeet Kalia for providing me with a unique opportunity to visit the Shoulders laboratory at the

Department of Chemistry, MIT, Boston, towards the end of my graduate school. I consider myself most fortunate as this visit offered me a chance to learn about the chemogenetic control of the unfolded protein response (UPR), from one of the leading research groups working on it, the Shoulders laboratory. In addition to learning new biological concepts, I also sincerely thank Prof. Shoulders for hosting me in Boston and providing me with a unique opportunity to visit the research groups that I was interested in joining for my postdoctoral studies. It brings me great joy to write that my visit to Boston has been one of the most positive experiences so far in my young career as a researcher and I whole heartedly thank my advisor, Dr. Jeet Kalia and Prof. Shoulders for arranging it for me. This endeavor would not have been possible without the generous support received from the MISTI grant from MIT, that was jointly awarded to Prof. Shoulders and my advisor, Dr. Jeet Kalia. Additionally, I would like to thank Betty Lou, the administrative staff with the Shoulders group, and Kathryn Yammine, a graduate student in the Shoulders laboratory, for making sure all arrangements were in place upon and after my arrival and for the rest of my visit. I also learnt a lot from my discussions with Seo-yeon on her co-IP experiments and I thank Jess for devoting time to demonstrate the revival and subculture of the UPR-activable HEK293 cell lines.

I am indebted to my friends from the Integrated PhD batch of 2013 who have made this journey memorable. We have shared some amazing trips and memories together that I will continue to cherish forever. I found great friends in Mehak and Deepak who supported me whenever I needed them. Mehak had not only helped me sail through the coursework that I found challenging during our MS program, but also been my confidante in every step of the way since then. I am deeply grateful to Deepak for his kindness and patience. I am indebted to them for not only sharing my joy but also my hardships. I thank Anshul, Adarsh, and Bharat for offering support and advice on many occasions when I needed it, and even at times when I did not need one! I would also like to thank Dhriti, Shivani, Sandip, Neeladri, Anish, Divya, Ron, Jay, Akhila, Kashyap and Amar for wonderful memories on many trips that we had taken together. Thank you all for making my Ph.D. journey truly special.

I could not have undertaken this journey without the unconditional love and support of my parents. They have acted as my pillars of strength through thick and thin and I am eternally

grateful for them. I thank my siblings–Mini and Vibhu for taking care of Maa and Papa during the times when I believe I should have been there to support them. They have always had my back and their presence in my life has provided me with a sense of immense security and comfort. I also would like to thank Rajat, my brother-in-law for supporting and providing comfort to me and my family in times of need. Lastly, I would like to take this opportunity to thank my dear late grandparents, my Nana and Nani, for their teachings and sacrifices, and for believing in me.

Synopsis

The Choline Metabolite-Interacting Proteome of Mammalian Cells: Discovery and Significance

Submitted by: Aditi Dixit

Thesis Advisor: Dr. Jeet Kalia

Indian Institute of Science Education and Research (IISER), Pune

Dr. Homi Bhabha Road, Pashan, Pune-411008,

Maharashtra, India

Metabolites interact with proteins and regulate several physiological processes such as energy production, signal transduction, cellular communication, biosynthesis of proteins and nucleic acids, and interconversion to other metabolites. The identification and functional elucidation of protein-metabolite interactions is therefore, imperative for understanding cellular physiology. The goal of my thesis is the discovery of the mammalian cellular proteome that interacts with the metabolites of the dominant eukaryotic choline lipid biosynthetic pathway, the Kennedy pathway and the characterization of the functional significance of those interactions.

Although the pathways for the biosynthesis and catabolism of choline lipids are well characterized, the role of these lipids and those of their biosynthetic precursor metabolites including choline, phosphocholine, CDP-choline and glycerophosphocholine as modulators of cellular proteins is poorly understood. This is important because abnormal choline metabolism is surfacing as a characteristic feature of malignant transformation. Notably, cellular levels of total choline content, phosphocholine, glycerophosphocholine, and levels of PC and SM lipids are grossly altered in many types of cancers including breast, prostate, and ovarian. Our understanding of the physiological roles of elevated choline metabolite levels in cancer progression is however, limited. Therefore, to determine the role of choline metabolites in

mammalian cells, profiling the proteins that interact with choline metabolites and lipids, is of vital importance and, in this thesis, I have developed technology to achieve the same.

In **Chapter 1** of this thesis, I discuss the role of cellular metabolites as co-factors, substrates or inhibitors for target protein. Furthermore, I focus my discussion on another important aspect of metabolites where they serve as allosteric modulators of protein function, *i.e.*, when metabolites modulate a protein's function by interacting at a site that is different from the active site. I highlight the significance of such interactions by describing a few pioneering examples of allosteric protein-metabolite relationships that regulate the activity of enzymes such as pyruvate kinase, phosphofructokinase, and ATP synthase. Additionally, I also provide a brief overview on how traditional structural biology-based and biochemical methods have facilitated the detection and characterization of metabolite-protein interactions. Discussions on more recent studies on mass spectrometry-based workflows shed light on how they have accelerated the identification of novel metabolite-protein interactions within cells. Photoaffinity labeling has contributed tremendously towards the discovery of global landscape of metabolite-protein interactions.

In the later part of this chapter, I provide a detailed account of the advantages and limitations of various types of photoaffinity labels that have been used to manipulate cellular systems. This survey further elaborates on how diazirines have emerged as one of the most popular photoaffinity tags for the metabolic labeling of a variety of cellular metabolites. Lastly, after concluding from the literature review on the techniques that have been used for the identification of metabolite-protein interactions, I propose a chemoproteomics-based strategy to discover the choline metabolite-interacting proteome of mammalian cells. This method involves rationally designing a bifunctional choline analog appended with a diazirine group (to covalently capture metabolite-interacting proteins upon UV irradiation) and an alkynyl or an azido group (to isolate the resultant protein-metabolite conjugates) that is capable of metabolically labeling choline metabolites in mammalian cells and deploying it to identify interacting partners of choline metabolites in cells.

To design a bifunctional choline analog that readily labeled all choline metabolites and lipids in cells, I decided to evaluate the promiscuity of the Kennedy pathway with respect to accepting structurally diverse surrogates of choline as substrates. In **Chapter 2**, I describe the structure-

activity relationship-based studies wherein I tested the metabolic labeling efficiency of nine structurally distinct alkynyl or azido analogs of choline via lipidomics and cellular imaging, and found that all of them showed robust metabolic incorporation in HEK293 cells. These studies revealed the remarkable promiscuity of the Kennedy pathway.

Encouraged from these findings, in **Chapter 3**, I tested several β-diazirine containing bifunctional alkynyl/azido choline analogs for metabolic incorporation into the Kennedy pathway by performing the lipidomics and cellular imaging experiments. These studies revealed that although most of the β-diazirine choline analogs successfully labeled choline metabolites and lipids, the resultant bifunctional choline metabolites in cells were inefficient in generating substantial yields of UV-crosslinked protein conjugates. Upon further investigation, I found that β-diazirine containing bifunctional alkynyl/azido choline metabolites were unstable in mammalian cells as they were further metabolized into making large amounts of diazirine devoid alkynyl/azido choline metabolites in cells. Lastly, I showed the physiological relevance of this transformation by performing lipidomics experiments on HEK293 cells labeled with isotopic trimethyl D9 choline. These studies unveiled a novel choline lipid headgroup remodeling mechanism involving sequential dealkylation and methylation that has important implications for fundamental lipid biology.

The pursuit of an ideal bifunctional alkynyl/azido diazirine choline analog was concluded by the development of the γ-diazirine choline analogs. The lipidomics and imaging experiments performed on these analogs in **Chapter 4** demonstrated their robust metabolic incorporation in mammalian cells and the stability of their resultant metabolites in mammalian cells. Moreover, the in-gel fluorescence experiments revealed that the bifunctional γ-diazirine labeled choline metabolites showed successful UV-mediated crosslinking with the interacting proteins. Encouraged from these results, I employed my proposed chemoproteomics workflow to identify 674 “high-confidence” choline metabolite-interacting protein hits in HEK293 cells. Survey of our protein hits revealed that the mammalian choline metabolite-interacting proteome is enriched in functionally diverse proteins, a large subset of which are known drug targets, thereby demonstrating the tremendous potential of choline metabolite-interacting proteins for drug development.

To determine the physiological significance of the choline metabolite-protein interactions, I performed functional studies on six selected protein hits in **Chapter 5**, one of which is the attractive multifunctional anticancer target protein p32. Orthogonal binding experiments such as the DARTS assay revealed that p32 specifically binds with phosphocholine. ELISA studies on p32 revealed that phosphocholine is a potent and general modulator of the binding of this protein with a variety of its interacting partners. These results have important ramifications in cancer biology and implicate phosphocholine in mechanisms underlying HIV-1 infectivity and the inflammation response. Furthermore, out of the five other enzymes tested, choline metabolites were shown to modulate three of them—lactate dehydrogenase, citrate synthase and malic enzyme.

Taken together, the work described herein provides insights into choline lipid biology and sheds light on the physiological relevance of choline metabolites outside of their well-established roles as intermediates in the cellular choline lipid biosynthetic pathway. I anticipate that the results of the experiments on the p32 protein will set the stage for studies focused on interrogating the functional relevance of the interactions of choline metabolites and lipids on other protein hits that our chemoproteomic approach has identified.

Table of Contents

Dedication……ii

Certificate……..iii

Declaration……..iv

Acknowledgements……..v

Synopsis……..ix

Table of Contents……..xiii

List of Figures……...……xvi

List of Tables……...….xxi

List of Schemes……..xxiii

List of Abbreviations……...xxv

Chapter 1: Introduction ……...1

1.1 Protein-Metabolite Interactions…….2

1.2 Methods to Detect Protein-Metabolite Interactions ……..4

1.3 Discovering the Choline Metabolite-Interacting Proteome: Motivation and Strategy……..15

1.4 References……18

Chapter 2: The Structure-Activity Relationship Studies Aimed at Interrogating the Promiscuity of the Kennedy Pathway……27

2.1 Introduction……..28

2.2 Results and Discussion……29

2.3 Conclusions……..37

2.4 Experimental Methods…….39

2.5 ^{1}H and ^{13}C-NMR Spectra for the Synthetic Procedures of Analogs **1**-**9**……..59

2.6 References……75

Chapter 3: β-Diazirine Cholines as Metabolic Labeling Probes for Choline Metabolites…….77

3.1 Introduction……..78

3.2 Results and Discussion……78

3.3 Conclusions……..91

3.4 Experimental Methods…….93

3.5 ^{1}H and ^{13}C-NMR Spectra for the Synthetic Procedures of Analogs **10**-**15**……...119

3.6 References……..143

Chapter 4: γ-Diazirine Cholines as Metabolic Labeling Probes for Choline Metabolites……...144

4.1 Introduction……145

4.2 Results and Discussion……..145

4.3 Conclusions……157

4.4 Experimental Methods……...…159

4.5 ^{1}H and ^{13}C-NMR Spectra for the Synthetic Procedures of Analogs **20** and **21**…..…175

4.6 References……..…180

Chapter 5: Functional Studies Aimed at Determining the Role of Choline Metabolites in Protein Function……...……183

5.1 Introduction……184

5.2 Results and Discussion……..186

5.3 Conclusions……203

5.4 Experimental Methods……...204

5.5 References……..214

Conclusions and Future Directions……..219

Appendix……..222

A.1 TIC, XIC and LipidView Plots for the Lipidomics Experiments Performed in Figure 3.6……...223

A.2 TIC, XIC and LipidView Plots for the Lipidomics Experiments Performed in Figure 4.5……230

A.3 Data for Figures 4.8-4.11……..235

Rights and Permissions……..324

List of Figures

Figure No.	Figure title	Page No.
1.1	The X-ray crystal structure of the allosteric sites of ATCase in complex with ATP, CTP, UTP and Mg^{2+}ion	5
1.2	Schematic representation of the workflow for large scale identification of metabolites bound to the enzymes involved in ergosterol biosynthetic pathway in yeast cells by affinity chromatography	7
1.3	Schematic representation of the workflow for the global analysis of protein-metabolite interactions in *Arabidopsis thaliana* cell lysates using PROMIS	8
1.4	Schematic representation of the workflow for the identification of protein-metabolite interactions in cell lysates by using LiP-SMap, SPROX and TPP	10
1.5	Chemical structures of the three major photocrosslinking groups and their corresponding reactive intermediates generated after photoactivation	12
1.6	The experimental workflow of photoaffinity-based identification of protein-metabolite interactions in cells	13
1.7	Kennedy pathway and our strategy to identify the binding partners of its intermediates	16
2.1	Azido choline (**2**) and alkynyl choline analogs (**1**, **3**-**9**) tested for metabolic labeling of cellular choline metabolites	29
2.2	Imaging workflow for characterizing the metabolic labeling of choline analogs in HEK293 cells	30
2.3	A diagrammatic representation for the use of the PIS mode to detect non-natural choline lipids	31
2.4	Metabolic labeling studies on analog **1** via lipidomics and cellular imaging	32

2.5	Metabolic labeling studies on analog **2** via lipidomics and cellular imaging	33
2.6	Metabolic labeling studies on analog **3** via lipidomics and cellular imaging	34
2.7	Metabolic labeling studies on analog **4** via lipidomics and cellular imaging	35
2.8	Metabolic labeling studies on analog **5** via lipidomics and cellular imaging	36
2.9	Metabolic labeling studies on analog **6** via lipidomics and cellular imaging	37
2.10	Metabolic labeling studies on analog **7** via lipidomics and cellular imaging	38
2.11	Metabolic labeling studies on analog **8** via lipidomics and cellular imaging	39
2.12	Metabolic labeling studies on analog **9** via lipidomics and cellular imaging	40
3.1	Metabolic labeling studies on β-diazirine choline analog **10**	79
3.2	Metabolic labeling studies on β-diazirine choline analog **11**	80
3.3	Uncaging and stability studies of **11**	81
3.4	Testing the cellular conversion of **11**-labeled metabolites/lipids to **1**-labeled lipids	82
3.5	Testing the cellular conversion of **11**-labeled metabolites/lipids to **10**-labeled lipids	83
3.6	Estimate of **1**-, **10**-and **11**-labeled lipids formed from the cellular administration of **11**	85

3.7	Metabolic labeling studies on β-diazirine choline analog **12**	86
3.8	Metabolic labeling studies on β-diazirine choline analog **13**	87
3.9	The C_{α}–C_{β}bond cleavage hypothesis to explain the formation of **1**-and **10**-labeled lipids in **11**-administered cells	88
3.10	Metabolic labeling studies on β-diazirine choline analog **15**	89
3.11	A general scheme depicting our dealkylation-methylation hypothesis for the cellular turnover of β-diazirine choline compounds	91
3.12	Testing the N–C bond cleavage hypothesis on cells administered with D9 choline	92
4.1	Metabolic labeling studies on γ-diazirine choline analog **20**	146
4.2	Metabolic labeling studies on bifunctional γ-diazirine choline analog **21**	147
4.3	Testing the cellular conversion of **21**-labeled metabolites/lipids to **1**-labeled lipids	148
4.4	Testing the cellular conversion of **21**-labeledmetabolites/lipids to **20**-labeled lipids	149
4.5	Estimate of **1**-, **20**-, and **21**-labeled lipids formed from the cellular administration of **21**	150
4.6	Testing the crosslinking efficiency of **21**-labeled choline metabolites in cells.	151
4.7	Comparing the crosslinking efficiency of **21**with other alkynyl/azido choline derivatives and in presence of choline in cells	152
4.8	Identification of the choline metabolite and lipid-interacting proteome of HEK293 cells by using the γ-diazirine choline analog **21**	153

4.9	Subcellular distribution of our choline metabolite-interacting proteins	154
4.10	The functional classification of the high-confidence protein hits	156
4.11	The classification of the high-confidence protein hits as per their roles in diseases	157
5.1	Recombinant production and biotinylation of His-p32	187
5.2	DARTS analysis of the binding of choline metabolites to p32	188
5.3	Studies on the modulation of p32 binding to HA by choline metabolites	190
5.4	Characterization of the effect of choline metabolites on the binding of p32 to Lyp-1via ELISA	191
5.5	Characterization of the effect of choline metabolites on the binding of p32 to acetylated-Tat peptide via ELISA	192
5.6	Characterization of the effect of choline metabolites on the binding of p32 to MCP1 via ELISA	193
5.7	Characterizing the effect of choline metabolites on the activity of lactate dehydrogenase	194
5.8	Characterizing the activity of citrate synthase in presence of choline metabolites and lipids	196
5.9	Characterizing the activity of malic enzyme in presence of choline metabolites and lipids	198
5.10	Characterizing the activity of GAPDH in presence of choline metabolites and lipids	200
5.11	Characterizing the activity of glutamate dehydrogenase in presence of choline metabolites and lipids	202

A1	Kinetics for the formation of the metabolically labeled choline lipids produced in HEK293 cells cultured in presence of **11**	224
A2	Characterization of the metabolically labeled choline lipids produced in HeLa cells cultured in presence of **11**	226
A3	Characterization of the metabolically labeled choline lipids produced in MDA-MB-231 cells cultured in presence of **11**	228
A4	Kinetics for the formation of the metabolically labeled choline lipids in HEK293 cells cultured in presence of **21**	231
A5	Characterization of the metabolically labeled choline lipids produced in HeLa cells cultured in presence of **21**	232
A6	Characterization of the metabolically labeled choline lipids produced in MDA-MB-231 cells cultured in presence of **21**	234

List of Tables

Table No.	Table title	Page No.
2.1	Compound parameters used for the PIS of lipids labeled with the choline analogs **1**-**9**	56
3.1	Compound parameters used for the PIS of lipids labeled with the choline analogs **10**-**15**	115
4.1	Compound parameters used for the PIS of lipids labeled with the γ-choline analogs **20** and **21**	164
4.2	Details of antibodies used for Western blot experiments	171
A1	The list of 902 proteins identified from the sixplex TMT experiment with the 674 "high-confidence" protein hits (enrichment ratio ≥ 2 and p value ≤ 0.05) written in red	235
A2	The table contains the list of 674 high-confidence protein hits categorized according to their subcellular localization and their localization in membrane and soluble compartments as per the UniProt database	267
A3	A list of our high-confidence protein hits (HEK293 cell proteins) that were also identified in HeLa cells as PC lipid-binding proteins by Yao and co-workers (reference number 6 cited in Chapter 4).	280
A4	A list of our high-confidence protein hits (HEK293 cell proteins) that are homologs of the yeast PC lipid-binding mitochondrial proteins identified by de Kroon and co-workers (reference number 7 cited in Chapter 4)	282
A5	The list of 674 high-confidence protein hits categorized according to their protein class as per the PANTHER classification system	283
A6	A protein-wide list of the enzymes among the high-confidence protein hits categorized according to their catalytic mechanisms as per the UniProt database	294

A7	List of the gene IDs of our high-confidence protein hits that are genetically linked to various disease classes as per the DAVID bioinformatics resource	299
A8	The gene IDs for the high-confidence protein hits categorized with respect to the number of the types of cancer they are overexpressed in as per the Oncomine database	303
A9	The list of 250 proteins among our 674 high-confidence protein hits that were identified as DrugBank targets on the UniProt database	316

List of schemes

Scheme No.	Scheme Title	Page No.
2.1	Synthesis of propargyl choline **1**	41
2.2	Synthesis of butynyl choline **3**	42
2.3	Synthesis of hexynyl choline **4**	43
2.4	Synthesis of dipropargyl choline **5**	43
2.5	Synthesis of propargyl butynyl choline **6**	45
2.6	Synthesis of benzyl propargyl choline **7**	47
2.7	Synthesis of diethyl propargyl choline **8**	48
2.8	Synthesis of tripropargyl choline **9**	49
2.9	Synthesis of rhodamine alkyne **S9**	52
3.1	Synthesis of diazirine choline **10**	94
3.2	Synthesis of propargyl diazirine choline **11**	98
3.3	Synthesis of azido diazirine choline **12**	102

3.4	Synthesis of propargyl ethyl diazirine choline **13**	107
3.5	Synthesis of propargyl methyl diazirine choline **15**	110
4.1	Synthesis of **γ**-diazirine choline **20**	160
4.2	Synthesis of propargyl γ-diazirine choline **21**	162

List of Abbreviations

ABTS	2,2'-azino-bis(3-ethylbenzothiazoline-6-sulfonic acid
CoASH	coenzyme A
acetyl-CoA	acetyl coenzyme A
ADP	adenosine diphosphate
AGC	automatic gain control
α-KG	alpha ketoglutarate
ATCase	aspartate transcarbamoylase
ATP	adenosine triphosphate
BSA	bovine serum albumin
CAD	collision activated dissociation
cAMP	cyclic adenosine monophosphate
CDP	cytidine diphosphate
cGMP	cyclic guanosine monophosphate
CID	collision induced dissociation
COX	cytochrome c oxidase
CS	citrate synthase
CTP	cytidine triphosphate
CuAAC	copper-(I)-assisted alkyne-azide cycloaddition
dAMP	deoxyadenosine monophosphate
DARTS	drug affinity responsive target stability

DAVID	database for annotation, visualization and integrated discovery
DCM	dichloromethane
dCMP	deoxycytidine monophosphate
dGMP	deoxyguanosine monophosphate
DIPEA	*N*,*N*-diisopropylethylamine
DMEM	Dulbecco's modified eagle medium
DMF	dimethylformamide
DMSO	dimethylsulfoxide
DNA	deoxyribonucleic acid
dTMP	deoxythymidine monophosphate
DTNB	5,5-dithiobis-(2-nitrobenzoic acid)
DTT	dithiothreitol
dUMP	deoxyuridine monophosphate
ECL	electrogenerated chemiluminescence
ECM	extracellular matrix
EDTA	ethylenediaminetetraacetic acid
ELISA	enzyme-linked immunoassay
ESI	electrospray ionization
F-6-P	fructose-6-phosphate
FBP	fructose-1,6-bisphosphate
FBS	fetal bovine serum

G-3-P	DL-glyceraldehyde-3-phosphate
GAPDH	glyceraldehyde 3-phosphate dehydrogenase
GART	Glycinamide ribonucleotide transformylase
GFP	green fluorescent protein
GLUD1	glutamate dehydrogenase 1
GPC	glycerophosphocholine
GS1	ion source gas 1
GS2	ion source gas 2
h	hours
HA	hyaluronic acid
HCD	higher energy collisional dissociation
HEK	human embyonic kidney
HEPES	4-(2-hydroxyethyl)-1-piperazineethanesulfonic acid
HILIC	hydrophilic interaction liquid chromatography
HIV	human immodeficiency virus
HPLC	high-performance liquid chromatography
HRMS	high-resolution mass spectrometry
HRP	horseradish peroxidase
HSP	heat shock protein
IgG	immunoglobulin G
IPTG	isopropyl β-D-1-thiogalactopyranoside

ITC	isothermal titration calorimetry
kD/kDa	kilodaltons
K_m	Michaelis Constant
LB	Luria–Bertani
LC-MS/MS	Liquid chromatography- tandem mass spectrometry
LDH	lactate dehydrogenase
LiP-SMap	limited proteolysis -small molecule mapping
LMSD	Lipid Maps structure database
m	minutes
m/z	mass-to-charge ratio
ME	malic enzyme
mRNA	messenger ribonucleic acid
MS/MS	tandem mass spectrometry
NAD+	nicotinamide adenine dinucleotide
NADH	reduced nicotinamide adenine dinucleotide
NADP+	nicotinamide adenine dinucleotide phosphate
NADPH	reduced nicotinamide adenine dinucleotide phosphate
Ni-NTA	nickel-nitrilotriacetic acid
nLC	nano liquid chromatography
NMR	nuclear magnetic resonance
NP-40	non-indent 40

OXPHOS	oxidative phosphorylation
PAL	photoaffinity label
PANTHER	protein analysis through evolutionary relationships
PARP1	poly ADP-ribose polymerase 1
PBS	phosphate buffered saline
PBST	phosphate buffered saline/tween-20
PC	phosphatidylcholine
PCNA	proliferating cell nuclear antigen
PFA	paraformaldehyde
PGRMC1	progesterone receptor membrane component 1
PCTP	phosphatidylcholine transfer protein
PIS	precursor ion scan
PK	pyruvate kinase
PKM2	pyruvate kinase isoform M2
PMA	phosphomolybdic acid
*p*TsCl	para-toluenesulfonyl chloride
PVDF	polyvinylidene fluoride
RFP	red fluorescent protein
RT	retention time
s	seconds
SAH	*S*-adenosyl homocysteine

SAICAR	succinylaminoimidazolecarboxamide ribose-5′-phosphate
SDS	sodium dodecyl sulfate
SDS-PAGE	sodium dodecyl sulfate-polyacrylamide gel electrophoresis
SM	sphingomyelin
SPR	surface plasmon resonance
SPROX	stability of proteins from rates of oxidation
TBAF	tetrabutyl ammonium fluoride
TBDMSCl	tertiary-butyldimethylsilyl chloride
TBS	tris buffered saline
TBTA	tris((1-benzyl-4-triazolyl)methyl)amine
TCEP	tris(2-carboxyethyl)phosphine
TEA	*N*,*N*,*N*-triethylamine
TFA	trifluoroacetic acid
THF	tetrahydrofuran
TIC	total ion chromatogram
TLC	thin layer chromatography
TMS	tetramethylsilane
TMT	tandem mass tag
TOF	time-of-flight
TPP	thermal protein profiling
UHPLC	ultra-high-performance liquid chromatography

UTP	uridine triphosphate
UV	ultra violet
VDAC1	voltage-dependent anion-selective channel 1
V_{max}	maximal reaction rate
XIC	extracted ion chromatogram

Chapter 1

Introduction

1.1 Protein-Metabolite Interactions

Metabolites are small molecules that serve as either intermediates or end-products of metabolic pathways. They mediate a multitude of physiological events such as energy production, signal transduction, cellular communication, genetic/epigenetic regulation, biosynthesis of proteins and nucleic acids, and interconversion to other metabolites.[1-5] Metabolites orchestrate the vast array of these functions either directly or indirectly by binding or interacting with proteins and thereby modulating their functions. Classically, metabolites have been characterized to engage with the target protein at the active site in the form of a substrate, cofactor, inhibitor or the product of an enzymatic reaction.

Metabolites also act as allosteric modulators of proteins.[6-9] Allosteric regulation refers to influencing the function of a protein by binding of a metabolite at a site that is distant from the active site of the protein. The first example of an allosteric relationship was documented by Christian Bohr and co-workers in 1904, wherein they described that the binding of carbon dioxide modulated the binding affinity of a protein called hemoglobin towards its substrate, *i.e.*, oxygen.[10] This relationship was termed as "Bohr effect" and has been investigated extensively to delineate the mechanism of hemoglobin's activity.[11] The term "allosteric inhibition", however, was first coined by Jacques Monod and Francois Jacob in 1961 where they discussed the role of metabolites as enzyme inhibitors that were not "steric analogs of the substrate".[12] Following these observations, decades of research on allosteric mechanisms inspired Monod to propose allostery as the "second secret of life."[13] In this section of my thesis, I will discuss a few noteworthy examples of allosteric/regulatory protein-metabolite interactions that are significant for protein function.

One of the prominent examples of an allosteric protein-metabolite interaction is between the glycolytic enzyme, pyruvate kinase (PK) and its interacting partners. PK is a tightly regulated enzyme in the glycolysis pathway that converts its substrate, phosphoenolpyruvate to pyruvate. It is also known to bind to several endogenous metabolites other than its substrate, such as fructose-1,6-bisphosphate (FBP), serine, adenosine triphosphate (ATP), alanine and phosphotyrosine.[14, 15] While metabolites such as FBP and serine allosterically activate PK, ATP, alanine and

phosphotyrosine are known to allosterically inhibit it.[16-18] These protein-metabolite interactions have been shown to be critical for the regulation of PKM2 in disease states such as cancer.[9]

Another key regulatory enzyme from the glycolysis cycle, phosphofructokinase (PFK) that converts fructose-6-phosphate (F-6-P) and ATP to FBP and adenosine diphosphate (ADP), has been shown to be tightly regulated by interactions with endogenous metabolites such as citrate, ADP, and phosphoenolpyruvate.[19, 20] These metabolites regulate PFK by binding to it at different sites and modulate the protein in varying capacities. For example, citrate and phosphoenolpyruvate have been shown to inhibit human and bacterial PFK respectively,[19, 20] and ADP activates the latter.[19]

In a recent example, alpha-ketoglutarate (α-KG), a TCA cycle intermediate, was demonstrated to bind to the subunit β of ATP synthase, also known as the complex V of the electron transport chain and inhibits it.[21] The authors also characterized the functional relevance of this protein-metabolite interaction and found it to be critical in regulating the life-span of *C. elegans*.

The aforementioned examples establish that in addition to their well-appreciated roles as substrates or co-factors in life-sustaining pathways, metabolites also have additional protein targets in cells and many of these protein-metabolite interactions have physiological ramifications. Consequently, the identification of the proteins that metabolites interact with in the cell and the elucidation of how those interactions influence protein function are vital for understanding the extended physiological roles of these metabolites.

In a very interesting study published by Joshua D. Rabinowitz and co-workers in 2009, the total concentration of 103 intracellular metabolites was determined to be around 300 mM in *E. coli*. whereas the total concentration of proteins is nearly 7 mM.[22] The number of cellular metabolites largely exceeded the number of proteins and this is indicative of the presence of an intricate network of protein-metabolite interactions, many of which are unknown. Significant progress has been made to identify and characterize protein-protein[23, 24] and protein-DNA interactions,[25] however, the development of methodologies to investigate a much more intricate network of protein-metabolite interactions has been lagging behind.[26-28] In this chapter of my thesis, I will discuss about the technologies available for detection and characterization of protein-metabolite

interactions, their profound contributions towards understanding the extended roles of metabolites, and their limitations.

1.2 Methods to Detect Protein-Metabolite Interactions

1.2.1 Biochemical and structural biology-based methods

Traditionally, biochemical and structural biology methods have been successfully employed to identify numerous protein-metabolite interactions. Biochemical methods that have largely been used to detect protein-metabolite interactions involve performing functional studies on purified proteins of interest in the presence of the metabolites under *in vitro* conditions. One of the prime examples involves the discovery of ATP as a negative modulator and fructose-2,6-bisphosphate as an activator of the glycolytic enzyme, PFK. In a study published in 1981, micromolar concentrations of fructose-2,6-bisphosphate was shown to restore the activity of PFK and relieved the enzyme of its inhibition that was caused by elevated concentrations of ATP.[29] The identification of such a functionally significant protein-metabolite interaction was done by partially purifying PFK from a rat liver homogenate containing many interfering enzymes and performing enzymatic assays on it.

Structural biology-based methods such as X-ray crystallography have been used since decades to visualize the structure of a protein bound to its substrate or other metabolites or drugs that acts as modulators of proteins.[30] These methods have been very insightful in providing the atomic level description of a metabolite-bound protein structure. One of the key examples is the regulation of aspartate transcarbamoylase or ATCase, the first enzyme of the pyrimidine biosynthetic pathway by nucleotides, ATP, CTP and UTP.[31] ATCase is a tightly regulated enzyme that condenses carbamoyl phosphate and L-aspartate to generate *N*-carbamyl-L-aspartate and is a representative allosteric enzyme that possesses distinct binding sites for binding substrates and metabolic allosteric modulators. ATP is known to activate the enzyme whereas CTP and UTP are known to inhibit the same.[32] In 2013, Gregory M. Cockrell and co-workers used X-ray crystallography to reveal the binding sites of ATCase with ATP, CTP and UTP, complexed with magnesium ions (Figure 1.1).[33] The structural analysis complemented with enzymatic assays on purified ATCase

helped the authors propose a novel mechanism in which CTP and UTP inhibited the protein and dispelled other alternate hypotheses that had been prevalent since past few decades. Such an example demonstrates that both structural biology and biochemical methods provide valuable insights into the protein-metabolite interactions and their role in functional modulation of the protein. These methods, however, possess several limitations because, a) they are performed in isolated systems that lack the physiological complexity, b) they are dependent on laborious purification steps of proteins that is required for both structural and functional studies, c) both crystallography and *in vitro* enzymatic assays are not high-throughput in nature as many proteins are difficult to purify and/or crystallize especially membrane proteins, d) these techniques cannot capture any low affinity and transient interactions that are typically present in protein-metabolite

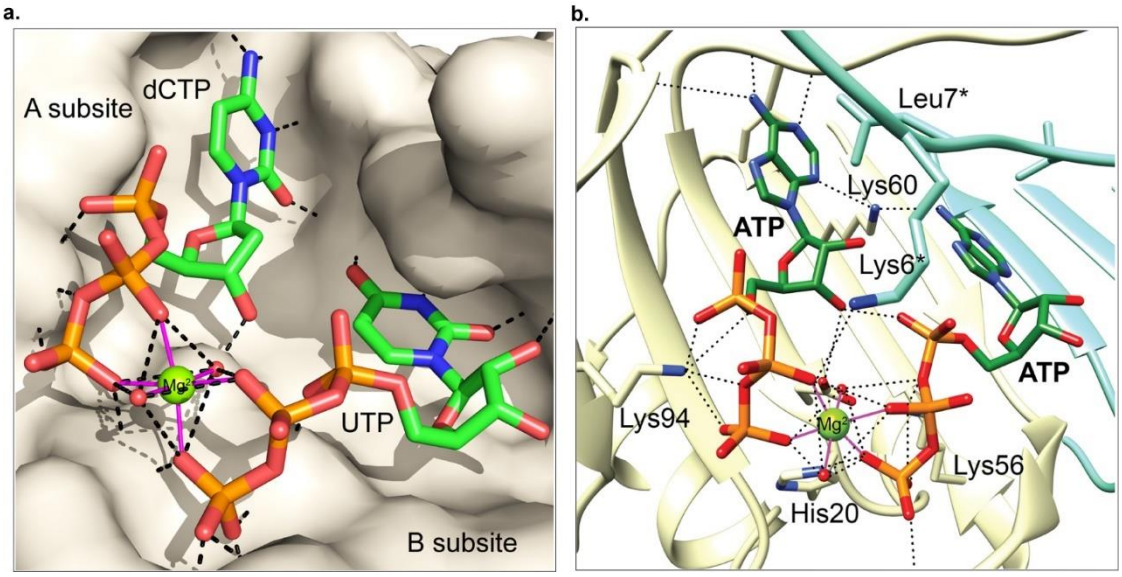

Figure 1.1. The X-ray crystal structure of the allosteric sites of ATCase in complex with ATP, CTP, UTP and Mg^{2+} ion. a) The regulatory sites A and B of ATCase are shown by the surface representation and the protein-bound CTP and UTP are shown in stick representation. The green Mg^{2+} ion is shown in co-ordination with the nucleotides and water molecules that act as ligands are shown by red spheres. The hydrogen bonds are represented by the dashed bonds. b) The X-ray crystal structure of ATCase bound to two molecules of ATP and Mg^{2+} at a regulatory site r6 of the enzyme. The amino-acids marked with asterisk belong to the r1 chain. The green Mg^{2+} ion is shown in co-ordination with the nucleotides and water molecules that are shown by red spheres. The hydrogen bonds are represented by dashed bonds. This figure is adapted from the paper authored by Krantrowitz and co-workers (PDB ID 4FYX).[33]

complexes, and e) these methods are biased and are dependent on the choice of proteins and are incapable of mapping the global landscape of protein-metabolite interactions.

1.2.2 Mass spectrometry-based methods

Mass spectrometry-based approaches have contributed tremendously towards the discovery of metabolite-interacting proteins and have overcome the many limitations of structural biology-based methods that I have discussed above. Recent advances in mass spectrometry have enabled researchers to couple it with several biochemical techniques such as size exclusion chromatography and affinity chromatography to mine protein-metabolite interactions under physiological or near-physiological conditions.[34, 35] Proteins bound with metabolites exhibit several differences in their properties compared to the unbound proteins in cells, such as differences in thermal meting temperature, susceptibility towards proteolysis, and differences in elution profiles of an unbound protein *vs* metabolite-bound protein over a chromatographic separation column.[36-38] These differences have been used by researchers to distinguish a protein-metabolite complex in cell lysates or live cells from the unbound protein. These mixtures are eventually subjected to quantitative proteomics and/or metabolomics to identify protein-metabolite interactions. In this section of my thesis, I will discuss about the prominent methodologies that employed mass spectrometry to identify novel protein-metabolite interactions, their contributions in expanding the database for protein-metabolite interactions, and their limitations.

An elegant protein-centric approach was used by Michael Snyder and co-workers in 2010, wherein they used affinity chromatography and untargeted metabolomics to discover known and several novel metabolite binding partners of 21 enzymes involved in ergosterol biosynthesis in yeast cells.[39] Ergosterol that is structurally analogous to cholesterol, is a major structural and signaling component in *Saccharomyces cerevisiae*. As schematically depicted in Figure 1.2, the authors targeted each of the 21 ergosterol biosynthetic enzymes and individually overexpressed them in yeast cells as fusion proteins with IgG binding domains. The yeast cells were lysed and the metabolite-bound protein that was expressed as a fusion protein with an IgG binding domain was enriched from the resultant lysate by performing affinity purification on IgG resin. The protein-metabolite complexes were eluted from the resin and the bound metabolites were separated from

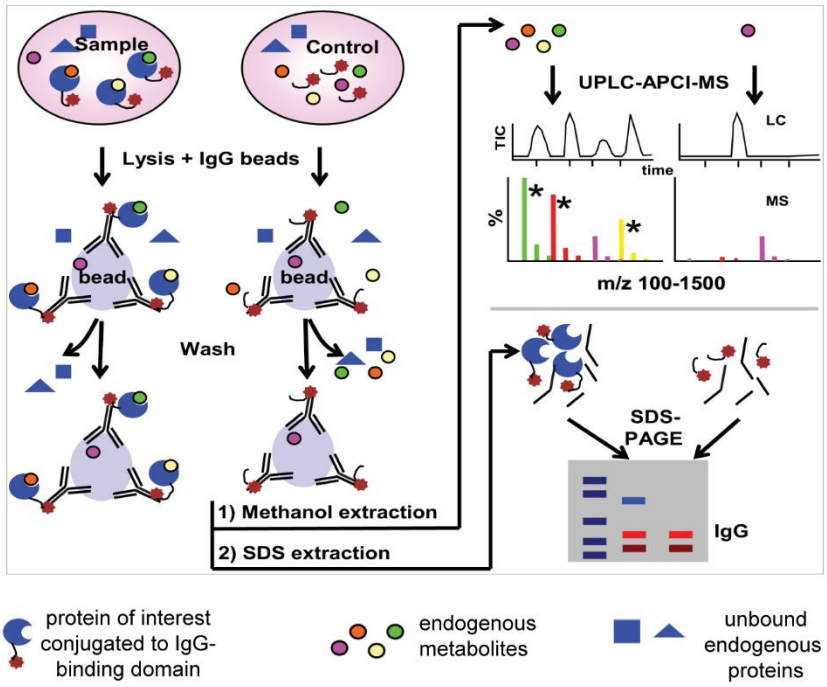

Figure 1.2. Schematic representation of the workflow for large-scale identification of metabolites bound to the enzymes involved in ergosterol biosynthetic pathway in yeast cells by affinity chromatography. The protein of interest is overexpressed in yeast cells as a fusion protein with an IgG binding domain. Control cells express the IgG binding domain tag without the protein of interest. The cells are then lysed and the lysate is subjected to a resin conjugated to IgG. The metabolite-bound protein complex is captured on these beads the resultant assembly is subjected to methanol extraction to separate the protein-bound metabolites that are further subjected to LC-MS/MS for identification. The IgG conjugated protein that is precipitated as a result of the methanol extraction is resolved on SDS-PAGE for characterization. This figure is adapted from the paper authored by Snyder and co-workers.[39]

their complexes by performing methanolic extractions on them. The metabolite extracts were then analyzed by LC-MS/MS for identification. Using this strategy, the authors found that 16 out of 21 enzymes involved the ergosterol biosynthesis were associated with metabolites other than their products or substrates. This large scale-analysis also revealed novel regulatory roles of ergosterol by virtue of its interaction with protein kinase Ypk1. Integrating affinity chromatography with mass spectrometry helped the authors generate a map of metabolites that interact with a certain protein of interest. This study also set the stage for identification of other protein-metabolite interactions, for example, a follow-up study used the same technology to discover many novel

binding partners of the mammalian phosphatidylcholine transfer protein (PCTP) that included lipids like sphinganine, sphingosine, behenic acid and linoleamide.[40] In another example, succinylaminoimidazolecarboxamideribose-5′-phosphate (SAICAR), an intermediate of the purine nucleotide synthesis pathway was found to specifically bind to PKM2 in glucose-depleted cancer cells. Further biochemical assays demonstrated that this interaction is responsible for cancer cell survival under low glucose conditions.[41] Although this approach helped the authors uncover several novel metabolite-protein interactions, however, it is limited to a protein of interest and cannot be utilized for the discovery of global metabolite-interacting proteome.

In the next example, I will discuss about an unbiased approach that was employed by Daniel Veyel and co-workers in 2018 to reveal a global network of known and putative protein-metabolite interactions.[38] This technology, named protein–metabolite interactions using size separation or PROMIS combined size-exclusion chromatography with quantitative metabolomics and proteomics to reveal a map of nearly 140 metabolites and 5000 proteins from *Arabidopsis thaliana* lysates, a few of which were mined for binding interactions. In this method, cell lysates derived from *Arabidopsis thaliana* were subjected to size-exclusion chromatography. The free metabolites expectedly eluted in the later fractions owing to their low molecular weight, whereas the protein-bound metabolites co-eluted with the corresponding unbound proteins in the higher molecular

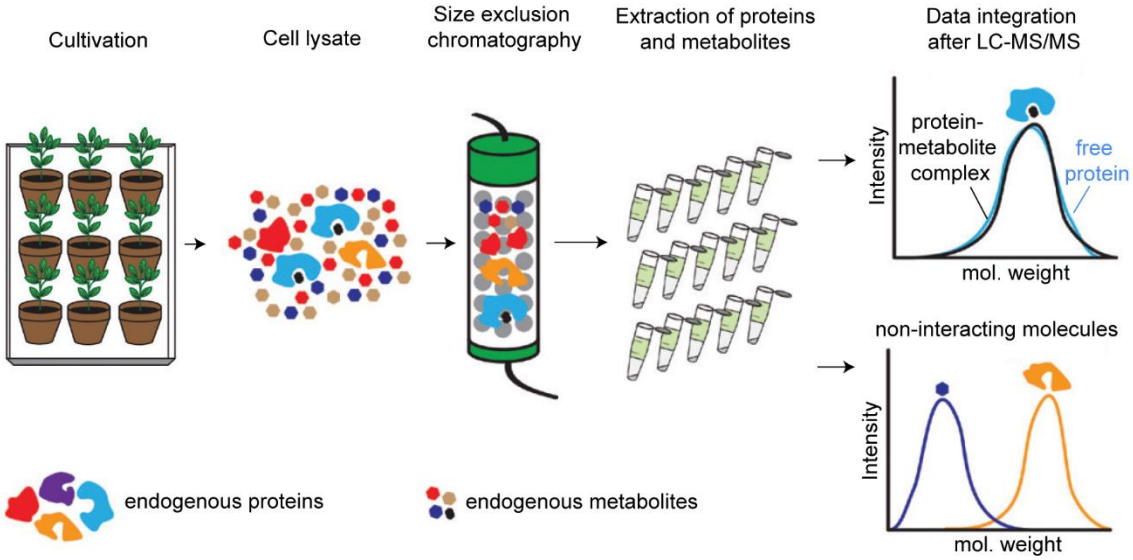

Figure 1.3. Schematic representation of the workflow for the global analysis of protein-metabolite interactions in *Arabidopsis thaliana* cell lysates using PROMIS. This figure is adapted from the review authored by Skirycz and co-workers.[26]

weight-containing initial fractions. All the elution fractions were further subjected to separate metabolite and protein extractions and their identity were determined by performing metabolomics and proteomics on the extracted samples (workflow depicted in Figure 1.3 above). This method not only validated numerous known protein-metabolite interactions, but also confirmed several predicted interactions. PROMIS was also successful in predicting many novel protein-metabolite interactions including the binding of glyceraldehyde-3-phosphate dehydrogenase (GAPDH) with the dipeptide Tyr-Asp. A similar workflow was employed another group wherein, they identified putative small molecule-protein interactions in yeast cell lysates by co-eluting the bound protein complexes with their unbound counterparts on a non-denaturing anion exchange column.[42]

Although the targeted metabolite-centric approaches such as the one developed by the Snyder group or untargeted global interactome-wide approaches such as PROMIS are significant breakthroughs into the growing repertoire of the technologies available for the identification of protein-metabolite interactions, they suffer from certain limitations. For example, the methodology developed by the Snyder group requires overexpression of a protein of interest that may cause undesired physiological changes in cells. Consequently, this may give rise to results that may be irrelevant in native physiological context. Moreover, overexpression of some proteins may cause cytotoxicity. Success of techniques such as PROMIS is dependent on the co-elution of the unbound and metabolite-bound protein on a size-separation column, however, co-elution is not confirmatory evidence of a binding interaction. Therefore, PROMIS suffers from the occurrence of high rates of false positive results.

A metabolite/ligand-bound protein exhibits additional stability towards proteolysis, and towards chemical or heat-induced denaturation compared to its unbound state. These changes in properties are exploited in many metabolite-centric mass spectrometry-based approaches to discover several novel protein-metabolite interactions.[36, 37, 43] Limited proteolysis was integrated with quantitative proteomics to discover cellular binding partners of endogenous metabolites by Paola Picotti and co-workers in a robust workflow called limited proteolysis-small molecule mapping or LiP-SMap (schematically depicted in Figure 1.4, top panel).[37] Herein, the yeast cell lysate treated with the metabolite of interest was subjected to non-specific proteolysis and the samples were subjected to mass spectrometric detection of the digested peptides. The proteins that were bound to the treated metabolite would show increased stability towards protease-mediated digestion and therefore,

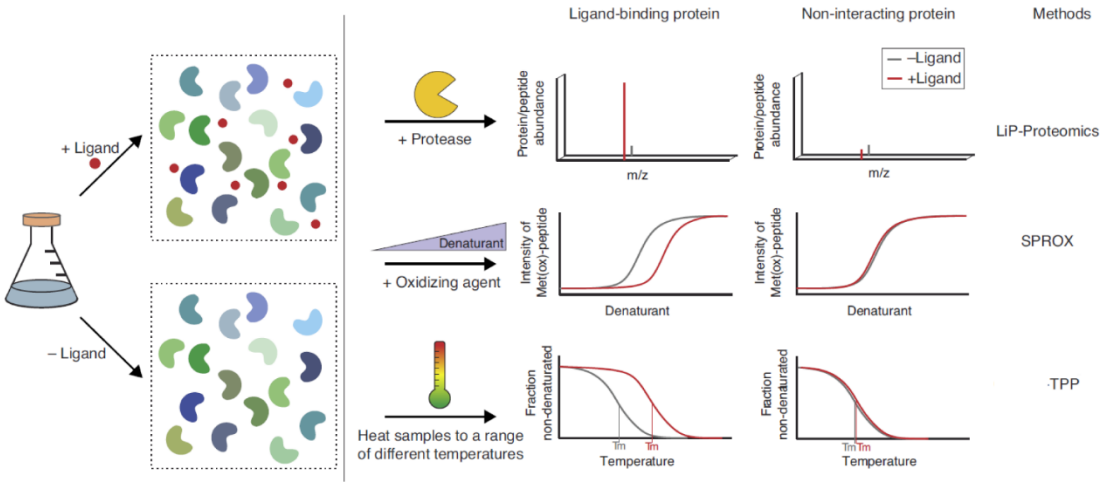

Figure 1.4. Schematic representation of the workflow for the identification of protein-metabolite interactions in cell lysates by using LiP-SMap (top), SPROX (middle) and TPP (bottom). This figure is adapted from the review authored by Sauer and co-workers.[28]

were identified by the mass of the corresponding undigested peptide, whereas the same protein was identified by its digested fragments in the lysate samples devoid of any treatment. This work led the investigators to find a proteome-wide list consisting of more than 1500 protein-metabolite interactions and 7000 putative binding sites. Several of these novel interactions were characterized as allosteric in nature or as protein-substrate relationships.

In an orthogonal method, the metabolite/ligand binding of a protein was determined by the extent of protection of a bound protein from oxidation in presence of a denaturant.[43, 44] In this technology called stability of proteins from rates of oxidation or SPROX, the cell lysates were treated with the metabolite of interest (or not) and the lysates were aliquoted into multiple fractions and the fractions were treated with an increasing concentration of a denaturant such as guanidine and a constant concentration of an oxidizing agent such as hydrogen peroxide (schematically depicted in Figure 1.4, middle panel). Each of these samples was labeled with an isobaric tag and the abundance of the oxidized protein is quantified in each sample using tandem mass spectrometry. The proteins that showed a shift in the plot for the EC_{50} value of the denaturant *vs* the rate of oxidation were deemed as metabolite-bound. This analysis was successful in providing an unbiased protein-wide list of cellular targets of endogenous metabolites such as NAD^+ and ATP in yeast cell lysates.[45, 46]

Ligand induced stability also confers stability to proteins from heat induced-denaturation. Thermal shift assays have been used for decades to screen libraries of small molecules for binding with a pure protein.[47, 48] In a method called thermal protein profiling (TPP), researchers combined thermal melting of proteins with TMT-based quantitative proteomics to discover protein targets of known drugs in mammalian cell lysates.[36] In this method, cancer cell lysates were treated with staurosporine (a broad-spectrum inhibitor of protein kinases) and aliquoted into several fractions. The control samples were treated with the vehicle. Each fraction was heated with increasing temperature to induce denaturation of the proteins. The denatured proteins were separated from the protein mixture by centrifugation and the intact proteins were retained in the supernatant. The latter was further subjected to quantitative proteomics to calculate the abundance of intact proteins. The staurosporine-bound proteins would be protected from denaturation and hence, a change in the thermal melting temperature for such proteins was observed (depicted in Figure 1.4, bottom panel). This resulted in identification of more than 50 protein targets for staurosporine in mammalian cells. TPP is a powerful approach as it reveals a global interaction landscape for known as well as novel small molecules of pharmacological importance. This technology, additionally, has also been used to detect the protein binding partners for endogenous metabolites in cells and in cell lysates. Using TPP-MS/MS, several known and novel binding partners of metabolites such as ATP, cyclic nucleotides (cAMP and cGMP), and deoxynucleotides (dAMP, dGMP, dUMP, dTMP, dCMP) were detected in cell lysates.[49, 50]

Taken together, these multifaceted methods involving ligand induced-protein stability such as SPROX, TPP-MS and LiP-SMap have made significant advancements in mapping the interaction landscape of several metabolites at a cellular level. However, in some cases, metabolite binding may not significantly influence protein stability, therefore, these methods suffer from reporting false negative protein hits. Moreover, many regulatory protein-metabolite interactions are low-affinity or transient in nature that may evade detection. In the next section, I will describe how photoaffinity labeling overcomes the aforementioned limitations.

1.2.3 Photoaffinity labeling coupled with mass spectrometry

Photoaffinity labeling when integrated with quantitative proteomics has been demonstrated as a powerful alternate approach to covalently capture protein-metabolite interactions in cells. In this

approach, the metabolite of interest is derivatized with a photoactivable group that upon irradiation with UV light, generates a highly reactive intermediate that forms a covalent bond with the neighboring binding partners. The first example of photoaffinity-based labeling of a protein was reported for chymotrypsin in 1962 by F. H. Westheimer and co-workers,[51] wherein the enzyme was chemically derivatized at the active site with a photoactive diazo group and the resultant modified enzyme (diazoacetyl chymotrypsin, as the authors termed it) was photolyzed by exposing it to UV light to generate a highly reactive carbene species that eventually crosslinked with the neighboring water molecules. The advent of photoaffinity labeling has revolutionized research in chemical biology and medicinal chemistry primarily because of its ability to identify protein-ligand complexes and to map ligand-binding sites in isolated as well as cellular systems.[52]

An ideal photoactivable analog of a small molecule or a metabolite has three major requirements: minimal structural perturbation compared to the parent molecule so as to retain the latter's biological activity within cells, its stability in the absence of UV light and at physiological pH values, and photoactivation at long UV wavelengths so as to minimize the biological damage in cells. Three major types of photoactivable groups that qualify most of these aforementioned requirements are benzophenones, aryl azides, and diazirines (structures depicted in Figure 1.5).

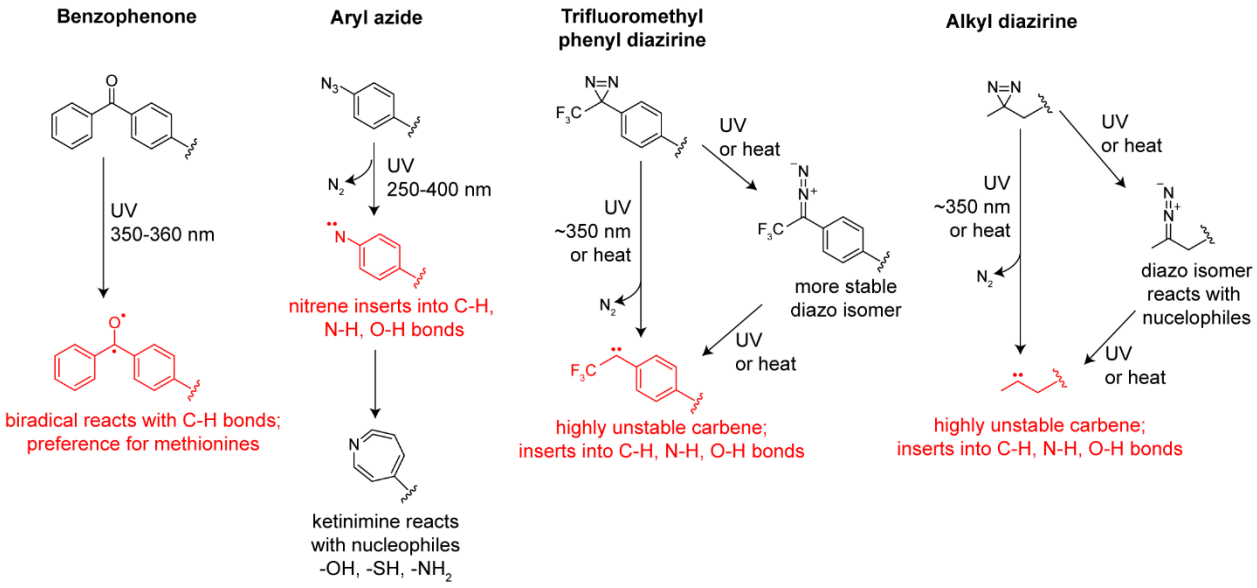

Figure 1.5. Chemical structures of the three major photocrosslinking groups and their corresponding reactive intermediates generated after photoactivation. This figure is adapted from the review authored by Kohler and co-workers.[52]

While all three functional groups photolyze under near longer UV wavelengths (~350-400 nm), their activation generates different reactive intermediates. Benzophenone generates a biradical after photoactivation, whereas aryl azides generate nitrene and both aryl and aliphatic diazirine groups generate a highly reactive carbene species. All three intermediates are capable of inserting into C-H, N-H and O-H bonds (Figure 1.5).

A typical workflow for photoaffinity-based identification of protein targets that bind to a metabolite of interest in cells involves the cellular administration of a bifunctional metabolite derivative labeled with a photocrosslinkable group (such as diazirine, or aryl azide, or benzophenone), and a bioorthogonal affinity group (usually alkyne or azide), followed by UV-mediated crosslinking of the protein-metabolite complex, biotinylation of the protein-metabolite conjugate, its affinity chromatography-based enrichment and mass spectrometry to obtain a protein-wide list of metabolite binding proteins (depicted in Figure 1.6 below).

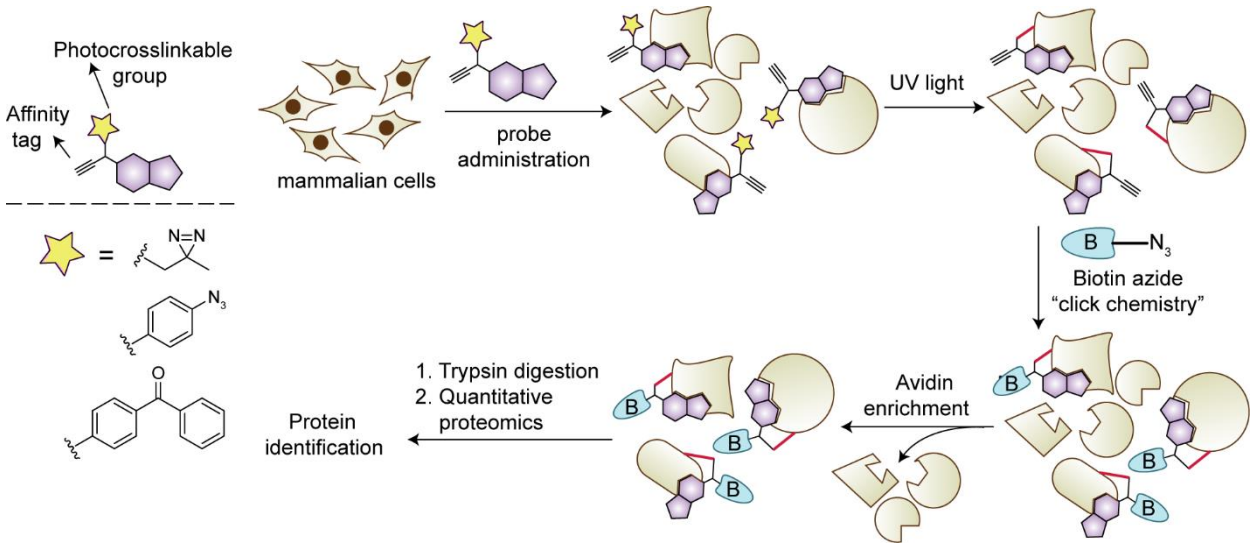

Figure 1.6. The experimental workflow of photoaffinity-based identification of protein-metabolite interactions in cells.

Benzophenone derivatives of metabolites have been employed to map binding sites on purified proteins and also to identify protein binding partners in cells. In 1974, benzophenone derivative of a peptide hormone called pentagastrin was first used to determine its binding sites on pure bovine serum albumin (BSA) via UV-mediated crosslinking.[53] Since then, benzophenone has been

appended with several biomolecules such as inositol triphosphate, phosphatidylcholine lipids, phosphatidyl glycerol lipids, nucleotides such as ATP and ADP to report their protein-binding partners.[54] Benzophenone as a photoactivable group offers high chemical stability and increased crosslinking yields to the probe, however, its use to label smaller cellular metabolites remains limited due to its bulky structure that may perturb the biological activity of the probe and its preference for crosslinking towards methionine.[55]

Aryl azides release nitrogen upon UV irradiation and form a highly unstable nitrene intermediate that can insert into the neighboring C-H, C-N, N-H, O-H bonds thereby enabling crosslinking with the neighboring molecules. Jeremy R. Knowles and co-workers developed the first aryl azide probe in 1969, 4-fluoro-3-nitrophenyl azide to crosslink to antibodies such as bovine γ-globulin.[56] Laboratories of Edmond Bauerlein and Anton de Kroon also synthesized phenyl azide derivatives of phosphatidylethanolamine[57] and phosphatidylcholine lipids[58] respectively and incorporated them into cellular lipid bilayers to determine the binding partners of the corresponding bifunctional lipids. Although nitrenes are very powerful crosslinking agents, their precursor aryl azides suffer from a few limitations in their usage in a biological environment that include: a) the phenyl azide group uncages at ~260 nm and irradiation at such shorter wavelengths can cause significant damage to the endogenous nucleic acids and proteins, and b) the subsequent nitrene intermediate can also rearrange to form a relatively stable ketinimine intermediate (see Figure 1.5) that shows preference towards crosslinking with nucleophilic groups such as thiols, hydroxyl or amino groups that eventually compromises the photocrosslinking yields of the aryl azide probe.[59]

The development of diazirine groups as photocrosslinking agents have overcome the aforementioned drawbacks of benzophenones and aryl azides. Diazirines are highly strained three-membered cyclic compounds that contain one carbon atom and two nitrogen atoms (see Figure 1.5 for structure). Upon exposure to UV light (~350 nm), diazirines undergo photolysis to release the highly reactive carbene species that inserts into the neighboring C-H, N-H and O-H bonds. The first use of diazirines on biomolecules was pioneered by Har Gobind Khorana's group and Frederic M. Richards' group is 1980 where both laboratories derivatized phosphatidylcholine lipids with diazirines.[60, 61] While Khorana's work studied the photophysical properties of diazirine-labeled PC lipids, Richards' study determined the binding sites of the photoactive choline lipids with Gramicidin A in liposomal preparations. The use of diazirine has since then revolutionized the

interactome mapping because of the following advantages that it endows on the bifunctional metabolite derivatized with it: a) its relatively smaller size compared to other photocrosslinkable groups offers minimal structural perturbation at the protein binding site, b) its thermal and chemical stability has enabled researchers to use it in diverse biological samples, and c) the subsequent carbene species has a small lifespan of nanoseconds[62, 63] that affords higher crosslinking rates and precludes non-specific crosslinking that may occur due to diffusion of the probe in the biological sample. Owing to these strengths, researchers have used diazirine labeled biomolecules since decades to map protein-protein interactions, protein-nucleotide interactions, and protein-drug interactions.[64, 65]

More recent examples involve the use of bifunctional probes for labeling a metabolite, *i.e.*, probes that are labeled with a diazirine group (to covalently capture the otherwise reversible protein-metabolite interaction) and an affinity tag such as an alkyne or an azide group (to isolate the protein-metabolite conjugate) in photoaffinity-based mapping of protein-metabolite interactions. Research from Benjamin Cravatt's laboratory has contributed significantly towards the design of bifunctional derivatives of endogenous metabolites such as *S*-adenosyl homocysteine (SAH), sterols, arachidonic acid, and their application in finding the protein binding partners of these metabolites in mammalian cells.[66-68] The interactome of other endogenous lipids such as fatty acids,[69] sphingosine,[70, 71] and phosphatidic acid[72] has also been determined in cells by using the bifunctional diazirine modified analogs of these lipids or their precursors.

1.3 Discovering the Choline Metabolite-Interacting Proteome: Motivation and Strategy

Detection and characterization of biomolecular interactions has long been a subject of investigation. In the previous sections of this chapter, I have described the importance of the protein-metabolites interactions on protein function and the methods that are used to identify them. The goal of my thesis was the discovery of the mammalian cellular proteome that interacts with the metabolites of the dominant eukaryotic choline lipid biosynthetic pathway, the Kennedy pathway (Figure 1.7a). This extensively studied pathway[73, 74] starts with the cellular uptake of the nutrient, choline, followed by its sequential conversion into phosphocholine, cytidine 5'-diphospho

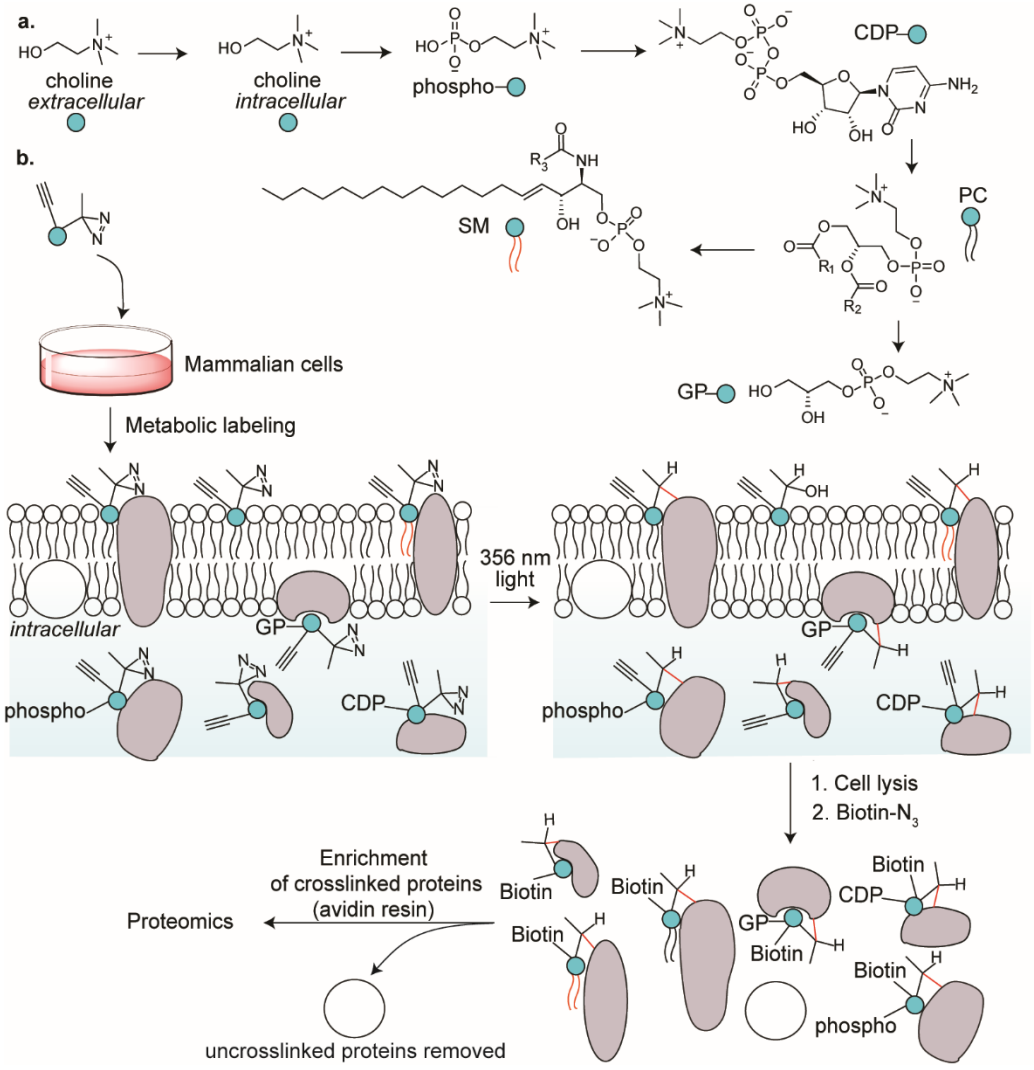

Figure 1.7. Kennedy pathway and our strategy to identify the binding partners of its intermediates. (a) The metabolism of choline in mammalian cells, and (b) our strategy of leveraging it to identify the choline metabolite and lipid-interacting proteome of mammalian cells. R_1, R_2 and R_3 represent alkyl groups and the abbreviations CDP, PC, SM and GP denote cytidine 5'-diphosphocholine, phosphatidylcholine, sphingomyelin and glycerophospho respectively.

(CDP) choline and finally to the lipids, phosphatidylcholine (PC) and sphingomyelin (SM), that are catabolized to glycerophosphocholine (GPC).

Choline lipids are the most abundant lipid species in mammalian cells. In addition to acting as structural components in mammalian cells, they have profound roles in cellular signaling[75, 76] and

modulation of the functions of membrane proteins as well.[77, 78] Although the studies focused on the cellular roles of choline lipids are in abundance, similar studies on the physiological functions of the other Kennedy pathway metabolites independent of their roles as intermediates in the choline lipid biosynthesis and catabolic pathways are limited. The identification of cellular proteins that they bind to within cells is imperative for filling this knowledge gap. While choline lipid-interacting proteins have been profiled previously for mitochondrial membrane preparations from yeast and in mammalian cells,[58, 79] the identity of the proteins that interact with polar choline metabolites has not yet been reported.

Notably, the cellular levels of total water-soluble choline-containing metabolites (referred to as tCho and comprising choline, phosphocholine, CDP choline and GPC taken together, not including choline lipids) have been demonstrated to be elevated in a variety of cancers including brain, prostate, breast and ovarian cancer.[80, 81] In epithelial ovarian cancer cells, for example, the tCho levels were measured to be as high as 7 mM and phosphocholine levels were enhanced 3-8 fold as compared to those in the immortalized non-tumoral cell variants.[82] Among the choline metabolites, phosphocholine levels in particular are observed to be elevated in cancer cells with concentrations as high as 9 mM reported in the triple negative breast cancer cell line, MDA-MB-231.[83] Indeed, elevated tCho and phosphocholine levels have emerged as hallmarks of cancer and the development of non-invasive approaches for the measurements of their cellular levels is being actively pursued for diagnosis and monitoring disease progression.[80-82] Nevertheless, the roles of the elevated levels of choline metabolites in disease physiology have not yet been unraveled. The discovery of the proteins that these metabolites bind to in cells followed by the characterization of the ramifications of these interactions on protein function can provide valuable insights into the mechanisms underlying cancer progression.

Owing to the advantages that were discussed in section 1.2.3 above, I decided to pursue the discovery of the choline metabolite-interacting proteome of mammalian cells by employing photoaffinity labeling. This would entail the cellular administration of a bifunctional choline analog appended with a photocrosslinkable tag such as the diazirine group and an affinity tag such as the alkyne group. After its successful cellular internalization, the bifunctional choline metabolite would eventually be employed as a substrate for the Kennedy pathway thereby labeling all the subsequent choline metabolites (*i.e.*, phosphocholine, CDP choline, PC, SM, and GPC) with the

non-natural diazirine and alkyne groups. UV-irradiation of the metabolically labeled cells would lead to chemical crosslinking of all bifunctional choline metabolites with their respective interacting partners via diazirine chemistry and the resultant crosslinked proteins would be biotinylated via copper (I) assisted alkyne-azide cycloaddition (CuAAC). Subsequently, these proteins would be isolated via avidin/streptavidin affinity chromatography and subjected to protease treatment followed by mass spectrometry leading to their identification. This approach would enable the discovery of choline metabolite and lipid-interacting proteins in the native cellular milieu (schematically depicted in Figure 1.7b).

In the later upcoming chapters of my thesis, I will discuss about how I developed a bifunctional choline analog appended with the alkyne and diazirine groups and used it to metabolically label choline metabolites and the PC and SM lipids in HEK293 cells. My work began with structure-activity relationship studies aimed at interrogating the promiscuity of the Kennedy pathway with respect to accepting choline analogs as precursors. This study involved the evaluation of a small library of choline analogs as probes for metabolically labeling choline lipids by employing the imaging and lipidomics approaches (Chapter 2). The results of these studies guided the design of bifunctional alkynyl/azido diazirine choline probes (Chapter 3), one of which proved to be ideal for the proposed chemoproteomics-based application and enabled me to discover the choline metabolite and lipid-interacting proteome of mammalian cells (Chapter 4). In the pursuit of the development of a stable bifunctional choline analog, I also discovered a novel choline lipid headgroup remodeling mechanism in cells (Chapter 3). Finally, in Chapter 5, I describe my functional experiments on few of the choline metabolite-interacting protein hits that revealed that choline metabolites modulate their function thereby demonstrating the importance of these interactions in cellular physiology.

1.4 References

1. Wang, Y. P.; Lei, Q. Y., Metabolite sensing and signaling in cell metabolism. *Signal Transduct Target Ther* **2018,** *3*, 30.

2. Metallo, C. M.; Vander Heiden, M. G., Understanding metabolic regulation and its influence on cell physiology. *Mol Cell* **2013,** *49* (3), 388-98.

3. Li, F.; Xu, W.; Zhao, S., Regulatory roles of metabolites in cell signaling networks. *J Genet Genomics* **2013,** *40* (7), 367-74.

4. Etchegaray, J. P.; Mostoslavsky, R., Interplay between Metabolism and Epigenetics: A Nuclear Adaptation to Environmental Changes. *Mol Cell* **2016,** *62* (5), 695-711.

5. Lu, C.; Thompson, C. B., Metabolic regulation of epigenetics. *Cell Metab* **2012,** *16* (1), 9-17.

6. Gerosa, L.; Sauer, U., Regulation and control of metabolic fluxes in microbes. *Curr Opin Biotechnol* **2011,** *22* (4), 566-75.

7. Swint-Kruse, L.; Matthews, K. S., Allostery in the LacI/GalR family: variations on a theme. *Curr Opin Microbiol* **2009,** *12* (2), 129-37.

8. Sola-Penna, M.; Da Silva, D.; Coelho, W. S.; Marinho-Carvalho, M. M.; Zancan, P., Regulation of mammalian muscle type 6-phosphofructo-1-kinase and its implication for the control of the metabolism. *IUBMB Life* **2010,** *62* (11), 791-96.

9. Macpherson, J. A.; Anastasiou, D., Allosteric regulation of metabolism in cancer: endogenous mechanisms and considerations for drug design. *Curr Opin Biotechnol* **2017,** *48*, 102-110.

10. Bohr, C.; Hasselbalch, K.; Krogh, A., Ueber einen in biologischer Beziehung wichtigen Einfluss, den die Kohlensäurespannung des Blutes auf dessen Sauerstoffbindung übt1. *Skandinavisches Archiv Für Physiologie* **1904,** *16* (2), 402-12.

11. Riggs, A. F., The Bohr effect. *Annu Rev Physiol* **1988,** *50*, 181-204.

12. Monod, J.; Jacob, F., Teleonomic mechanisms in cellular metabolism, growth, and differentiation. *Cold Spring Harb Symp Quant Biol* **1961,** *26*, 389-401.

13. Monod, J., *Chance and Necessity: Essay on the Natural Philosophy of Modern Biology*. Penguin Books Ltd.: 1977.

14. Jurica, M. S.; Mesecar, A.; Heath, P. J.; Shi, W.; Nowak, T.; Stoddard, B. L., The allosteric regulation of pyruvate kinase by fructose-1,6-bisphosphate. *Structure* **1998,** *6* (2), 195-210.

15. Chaneton, B.; Hillmann, P.; Zheng, L.; Martin, A. C. L.; Maddocks, O. D. K.; Chokkathukalam, A.; Coyle, J. E.; Jankevics, A.; Holding, F. P.; Vousden, K. H.; Frezza, C.; O'Reilly, M.; Gottlieb, E., Serine is a natural ligand and allosteric activator of pyruvate kinase M2. *Nature* **2012,** *491* (7424), 458-62.

16. Carbonell, J.; Feliu, J. E.; Marco, R.; Sols, A., Pyruvate kinase. Classes of regulatory isoenzymes in mammalian tissues. *Eur J Biochem* **1973,** *37* (1), 148-56.

17. Ashizawa, K.; Kato, H.; McPhie, P.; Cheng, S.-y., Regulation of thyroid hormone binding to its cytosolic binding protein by L-α-alanine. *Biochem Biophys Res Commun* **1990,** *167* (2), 587-92.

18. Christofk, H. R.; Vander Heiden, M. G.; Wu, N.; Asara, J. M.; Cantley, L. C., Pyruvate kinase M2 is a phosphotyrosine-binding protein. *Nature* **2008,** *452* (7184), 181-86.

19. Evans, P. R.; Farrants, G. W.; Hudson, P. J., Phosphofructokinase: structure and control. *Philos Trans R Soc Lond B Biol Sci* **1981,** *293* (1063), 53-62.

20. Webb, B. A.; Forouhar, F.; Szu, F. E.; Seetharaman, J.; Tong, L.; Barber, D. L., Structures of human phosphofructokinase-1 and atomic basis of cancer-associated mutations. *Nature* **2015,** *523* (7558), 111-14.

21. Chin, R. M.; Fu, X.; Pai, M. Y.; Vergnes, L.; Hwang, H.; Deng, G.; Diep, S.; Lomenick, B.; Meli, V. S.; Monsalve, G. C.; Hu, E.; Whelan, S. A.; Wang, J. X.; Jung, G.; Solis, G. M.; Fazlollahi, F.; Kaweeteerawat, C.; Quach, A.; Nili, M.; Krall, A. S.; Godwin, H. A.; Chang, H. R.; Faull, K. F.; Guo, F.; Jiang, M.; Trauger, S. A.; Saghatelian, A.; Braas, D.; Christofk, H. R.; Clarke, C. F.; Teitell, M. A.; Petrascheck, M.; Reue, K.; Jung, M. E.; Frand, A. R.; Huang, J., The metabolite alpha-ketoglutarate extends lifespan by inhibiting ATP synthase and TOR. *Nature* **2014,** *510* (7505), 397-401.

22. Bennett, B. D.; Kimball, E. H.; Gao, M.; Osterhout, R.; Van Dien, S. J.; Rabinowitz, J. D., Absolute metabolite concentrations and implied enzyme active site occupancy in Escherichia coli. *Nat Chem Biol* **2009,** *5* (8), 593-99.

23. Smits, A. H.; Vermeulen, M., Characterizing Protein-Protein Interactions Using Mass Spectrometry: Challenges and Opportunities. *Trends Biotechnol* **2016,** *34* (10), 825-34.

24. Phizicky, E. M.; Fields, S., Protein-protein interactions: methods for detection and analysis. *Microbiol Rev* **1995,** *59* (1), 94-123.

25. Dey, B.; Thukral, S.; Krishnan, S.; Chakrobarty, M.; Gupta, S.; Manghani, C.; Rani, V., DNA-protein interactions: methods for detection and analysis. *Mol Cell Biochem* **2012,** *365* (1-2), 279-99.

26. Luzarowski, M.; Skirycz, A., Emerging strategies for the identification of protein-metabolite interactions. *J Exp Bot* **2019,** *70* (18), 4605-18.

27. Diether, M.; Nikolaev, Y.; Allain, F. H.; Sauer, U., Systematic mapping of protein-metabolite interactions in central metabolism of Escherichia coli. *Mol Syst Biol* **2019,** *15* (8), e9008.

28. Diether, M.; Sauer, U., Towards detecting regulatory protein-metabolite interactions. *Curr Opin Microbiol* **2017,** *39*, 16-23.

29. Van Schaftingen, E.; Jett, M. F.; Hue, L.; Hers, H. G., Control of liver 6-phosphofructokinase by fructose 2,6-bisphosphate and other effectors. *Proc Natl Acad Sci U S A* **1981,** *78* (6), 3483-86.

30. Changeux, J. P., 50 years of allosteric interactions: the twists and turns of the models. *Nat Rev Mol Cell Biol* **2013,** *14* (12), 819-29.

31. Lipscomb, W. N., Aspartate transcarbamylase from Escherichia coli: activity and regulation. *Adv Enzymol Relat Areas Mol Biol* **1994,** *68*, 67-151.

32. Kantrowitz, E. R.; Lipscomb, W. N., Escherichia coli aspartate transcarbamoylase: the molecular basis for a concerted allosteric transition. *Trends Biochem Sci* **1990,** *15* (2), 53-59.

33. Cockrell, G. M.; Zheng, Y.; Guo, W.; Peterson, A. W.; Truong, J. K.; Kantrowitz, E. R., New paradigm for allosteric regulation of Escherichia coli aspartate transcarbamoylase. *Biochemistry* **2013,** *52* (45), 8036-47.

34. Guo, H.; Peng, H.; Emili, A., Mass spectrometry methods to study protein-metabolite interactions. *Expert Opin Drug Discov* **2017,** *12* (12), 1271-80.

35. Li, S.; Shui, W., Systematic mapping of protein-metabolite interactions with mass spectrometry-based techniques. *Curr Opin Biotechnol* **2019,** *64*, 24-31.

36. Savitski, M. M.; Reinhard, F. B.; Franken, H.; Werner, T.; Savitski, M. F.; Eberhard, D.; Martinez Molina, D.; Jafari, R.; Dovega, R. B.; Klaeger, S.; Kuster, B.; Nordlund, P.; Bantscheff, M.; Drewes, G., Tracking cancer drugs in living cells by thermal profiling of the proteome. *Science* **2014,** *346* (6205), 1255784.

37. Piazza, I.; Kochanowski, K.; Cappelletti, V.; Fuhrer, T.; Noor, E.; Sauer, U.; Picotti, P., A Map of Protein-Metabolite Interactions Reveals Principles of Chemical Communication. *Cell* **2018,** *172* (1-2), 358-372 e23.

38. Veyel, D.; Sokolowska, E. M.; Moreno, J. C.; Kierszniowska, S.; Cichon, J.; Wojciechowska, I.; Luzarowski, M.; Kosmacz, M.; Szlachetko, J.; Gorka, M.; Meret, M.; Graf, A.; Meyer, E. H.; Willmitzer, L.; Skirycz, A., PROMIS, global analysis of PROtein-metabolite interactions using size separation in Arabidopsis thaliana. *J Biol Chem* **2018,** *293* (32), 12440-53.

39. Li, X.; Gianoulis, T. A.; Yip, K. Y.; Gerstein, M.; Snyder, M., Extensive in vivo metabolite-protein interactions revealed by large-scale systematic analyses. *Cell* **2010,** *143* (4), 639-50.

40. Schrick, K.; Bruno, M.; Khosla, A.; Cox, P. N.; Marlatt, S. A.; Roque, R. A.; Nguyen, H. C.; He, C.; Snyder, M. P.; Singh, D.; Yadav, G., Shared functions of plant and mammalian StAR-related lipid transfer (START) domains in modulating transcription factor activity. *BMC Biol* **2014,** *12*, 70.

41. Keller, K. E.; Tan, I. S.; Lee, Y. S., SAICAR stimulates pyruvate kinase isoform M2 and promotes cancer cell survival in glucose-limited conditions. *Science* **2012,** *338* (6110), 1069-72.

42. Chan, J. N.; Vuckovic, D.; Sleno, L.; Olsen, J. B.; Pogoutse, O.; Havugimana, P.; Hewel, J. A.; Bajaj, N.; Wang, Y.; Musteata, M. F.; Nislow, C.; Emili, A., Target identification by chromatographic co-elution: monitoring of drug-protein interactions without immobilization or chemical derivatization. *Mol Cell Proteomics* **2012,** *11* (7), M111 016642.

43. Strickland, E. C.; Geer, M. A.; Tran, D. T.; Adhikari, J.; West, G. M.; DeArmond, P. D.; Xu, Y.; Fitzgerald, M. C., Thermodynamic analysis of protein-ligand binding interactions in

complex biological mixtures using the stability of proteins from rates of oxidation. *Nat Protoc* **2013,** *8* (1), 148-61.

44. West, G. M.; Tang, L.; Fitzgerald, M. C., Thermodynamic analysis of protein stability and ligand binding using a chemical modification- and mass spectrometry-based strategy. *Anal Chem* **2008,** *80* (11), 4175-85.

45. Dearmond, P. D.; Xu, Y.; Strickland, E. C.; Daniels, K. G.; Fitzgerald, M. C., Thermodynamic analysis of protein-ligand interactions in complex biological mixtures using a shotgun proteomics approach. *J Proteome Res* **2011,** *10* (11), 4948-58.

46. Geer, M. A.; Fitzgerald, M. C., Characterization of the Saccharomyces cerevisiae ATP-Interactome using the iTRAQ-SPROX Technique. *J Am Soc Mass Spectrom* **2016,** *27* (2), 233-43.

47. Pantoliano, M. W.; Petrella, E. C.; Kwasnoski, J. D.; Lobanov, V. S.; Myslik, J.; Graf, E.; Carver, T.; Asel, E.; Springer, B. A.; Lane, P.; Salemme, F. R., High-density miniaturized thermal shift assays as a general strategy for drug discovery. *J Biomol Screen* **2001,** *6* (6), 429-40.

48. Niesen, F. H.; Berglund, H.; Vedadi, M., The use of differential scanning fluorimetry to detect ligand interactions that promote protein stability. *Nat Protoc* **2007,** *2* (9), 2212-21.

49. Sridharan, S.; Kurzawa, N.; Werner, T.; Gunthner, I.; Helm, D.; Huber, W.; Bantscheff, M.; Savitski, M. M., Proteome-wide solubility and thermal stability profiling reveals distinct regulatory roles for ATP. *Nat Commun* **2019,** *10* (1), 1155.

50. Lim, Y. T.; Prabhu, N.; Dai, L.; Go, K. D.; Chen, D.; Sreekumar, L.; Egeblad, L.; Eriksson, S.; Chen, L.; Veerappan, S.; Teo, H. L.; Tan, C. S. H.; Lengqvist, J.; Larsson, A.; Sobota, R. M.; Nordlund, P., An efficient proteome-wide strategy for discovery and characterization of cellular nucleotide-protein interactions. *PLoS One* **2018,** *13* (12), e0208273.

51. Singh, A.; Thornton, E. R.; Westheimer, F. H., The Photolysis of Diazoacetylchymotrypsin. *J Biol Chem* **1962,** *237* (9), PC3006-PC3008.

52. Tanaka, Y.; Bond, M. R.; Kohler, J. J., Photocrosslinkers illuminate interactions in living cells. *Mol Biosyst* **2008,** *4* (6), 473-80.

53. Galardy, R. E.; Craig, L. C.; Jamieson, J. D.; Printz, M. P., Photoaffinity Labeling of Peptide Hormone Binding Sites. *J Biol Chem* **1974,** *249* (11), 3510-18.

54. Dorman, G.; Prestwich, G. D., Benzophenone photophores in biochemistry. *Biochemistry* **1994,** *33* (19), 5661-73.

55. Wittelsberger, A.; Thomas, B. E.; Mierke, D. F.; Rosenblatt, M., Methionine acts as a "magnet" in photoaffinity crosslinking experiments. *FEBS Lett* **2006,** *580* (7), 1872-76.

56. Fleet, G. W. J.; Porter, R. R.; Knowles, J. R., Affinity labelling of antibodies with aryl nitrene as reactive group. *Nature* **1969,** *224* (5218), 511-12.

57. Gao, Z.; Bauerlein, E., Identifying subunits of ATP synthase TF_0.F1 in contact with phospholipid head groups. Alpha-subunits are labeled selectively by a new photoreactive phospholipid designed for hydrophilic photolabeling. *FEBS Lett* **1987,** *223* (2), 366-70.

58. Gubbens, J.; Ruijter, E.; de Fays, L. E.; Damen, J. M.; de Kruijff, B.; Slijper, M.; Rijkers, D. T.; Liskamp, R. M.; de Kroon, A. I., Photocrosslinking and click chemistry enable the specific detection of proteins interacting with phospholipids at the membrane interface. *Chem Biol* **2009,** *16* (1), 3-14.

59. Schrock, A. K.; Schuster, G. B., Photochemistry of phenyl azide: chemical properties of the transient intermediates. *J Am Chem Soc* **1984,** *106* (18), 5228-34.

60. Erni, B.; Khorana, H. G., Fatty acids containing photoactivable carbene precursors. Synthesis and photochemical properties of 3,3-bis(1,1-difluorohexyl)diazirine and 3-(1,1-difluorooctyl)-3H-diazirine. *J Am Chem Soc* **1980,** *102* (11), 3888-96.

61. Brunner, J.; Richards, F. M., Analysis of membranes photolabeled with lipid analogues. Reaction of phospholipids containing a disulfide group and a nitrene or carbene precursor with lipids and with gramicidin A. *J Biol Chem* **1980,** *255* (8), 3319-29.

62. Toscano, J. P.; Platz, M. S.; Nikolaev, V., Lifetimes of Simple Ketocarbenes. *J Am Chem Soc* **1995,** *117* (16), 4712-13.

63. Ford, F.; Yuzawa, T.; Platz, M. S.; Matzinger, S.; Fülscher, M., Rearrangement of Dimethylcarbene to Propene: Study by Laser Flash Photolysis and ab Initio Molecular Orbital Theory. *J Am Chem Soc* **1998,** *120* (18), 4430-38.

64. Das, J., Aliphatic diazirines as photoaffinity probes for proteins: recent developments. *Chem Rev* **2011,** *111* (8), 4405-17.

65. Dubinsky, L.; Krom, B. P.; Meijler, M. M., Diazirine based photoaffinity labeling. *Bioorg Med Chem* **2012,** *20* (2), 554-70.

66. Horning, B. D.; Suciu, R. M.; Ghadiri, D. A.; Ulanovskaya, O. A.; Matthews, M. L.; Lum, K. M.; Backus, K. M.; Brown, S. J.; Rosen, H.; Cravatt, B. F., Chemical Proteomic Profiling of Human Methyltransferases. *J Am Chem Soc* **2016,** *138* (40), 13335-43.

67. Hulce, J. J.; Cognetta, A. B.; Niphakis, M. J.; Tully, S. E.; Cravatt, B. F., Proteome-wide mapping of cholesterol-interacting proteins in mammalian cells. *Nat Methods* **2013,** *10* (3), 259-64.

68. Niphakis, M. J.; Lum, K. M.; Cognetta, A. B., 3rd; Correia, B. E.; Ichu, T. A.; Olucha, J.; Brown, S. J.; Kundu, S.; Piscitelli, F.; Rosen, H.; Cravatt, B. F., A Global Map of Lipid-Binding Proteins and Their Ligandability in Cells. *Cell* **2015,** *161* (7), 1668-80.

69. Haberkant, P.; Raijmakers, R.; Wildwater, M.; Sachsenheimer, T.; Brugger, B.; Maeda, K.; Houweling, M.; Gavin, A. C.; Schultz, C.; van Meer, G.; Heck, A. J.; Holthuis, J. C., In vivo profiling and visualization of cellular protein-lipid interactions using bifunctional fatty acids. *Angew Chem Int Ed Engl* **2013,** *52* (14), 4033-38.

70. Haberkant, P.; Stein, F.; Hoglinger, D.; Gerl, M. J.; Brugger, B.; Van Veldhoven, P. P.; Krijgsveld, J.; Gavin, A. C.; Schultz, C., Bifunctional Sphingosine for Cell-Based Analysis of Protein-Sphingolipid Interactions. *ACS Chem Biol* **2016,** *11* (1), 222-30.

71. Hoglinger, D.; Nadler, A.; Haberkant, P.; Kirkpatrick, J.; Schifferer, M.; Stein, F.; Hauke, S.; Porter, F. D.; Schultz, C., Trifunctional lipid probes for comprehensive studies of single lipid species in living cells. *Proc Natl Acad Sci U S A* **2017,** *114* (7), 1566-71.

72. Yu, W.; Lin, Z.; Woo, C. M.; Baskin, J. M., A Chemoproteomics Approach to Profile Phospholipase D-Derived Phosphatidyl Alcohol Interactions. *ACS Chem Biol* **2021**.

73. Kennedy, E. P.; Weiss, S. B., The Function of Cytidine Coenzymes in the Biosynthesis of Phospholipides. *J Biol Chem* **1956,** *222* (1), 193-214.

74. Gibellini, F.; Smith, T. K., The Kennedy pathway--De novo synthesis of phosphatidylethanolamine and phosphatidylcholine. *IUBMB Life* **2010,** *62* (6), 414-28.

75. Chakraborty, M.; Jiang, X. C., Sphingomyelin and its role in cellular signaling. *Adv Exp Med Biol* **2013,** *991*, 1-14.

76. Vance, J. E.; Vance, D. E., Phospholipid biosynthesis in mammalian cells. *Biochem Cell Biol* **2004,** *82* (1), 113-28.

77. Ramu, Y.; Xu, Y.; Lu, Z., Inhibition of CFTR Cl- channel function caused by enzymatic hydrolysis of sphingomyelin. *Proc Natl Acad Sci U S A* **2007,** *104* (15), 6448-53.

78. Xu, Y.; Ramu, Y.; Lu, Z., Removal of phospho-head groups of membrane lipids immobilizes voltage sensors of K+ channels. *Nature* **2008,** *451* (7180), 826-29.

79. Wang, D.; Du, S.; Cazenave-Gassiot, A.; Ge, J.; Lee, J. S.; Wenk, M. R.; Yao, S. Q., Global Mapping of Protein-Lipid Interactions by Using Modified Choline-Containing Phospholipids Metabolically Synthesized in Live Cells. *Angew Chem Int Ed Engl* **2017,** *56* (21), 5829-33.

80. Glunde, K.; Bhujwalla, Z. M.; Ronen, S. M., Choline metabolism in malignant transformation. *Nat Rev Cancer* **2011,** *11* (12), 835-48.

81. Glunde, K.; Penet, M. F.; Jiang, L.; Jacobs, M. A.; Bhujwalla, Z. M., Choline metabolism-based molecular diagnosis of cancer: an update. *Expert Rev Mol Diagn* **2015,** *15* (6), 735-47.

82. Podo, F.; Sardanelli, F.; Iorio, E.; Canese, R.; Carpinelli, G.; Fausto, A.; Canevari, S., Abnormal choline phospholipid metabolism in breast and ovary cancer: Molecular bases for noninvasive imaging approaches. *Curr Med Imaging* **2007,** *3* (2), 123-37.

83. Mori, N.; Wildes, F.; Takagi, T.; Glunde, K.; Bhujwalla, Z. M., The Tumor Microenvironment Modulates Choline and Lipid Metabolism. *Front Oncol* **2016,** *6*, 262.

Chapter 2

The Structure-Activity Relationship Studies Aimed at Interrogating the Promiscuity of the Kennedy Pathway

This chapter is adapted with permission from the publication: Dixit, A.; Jose, G. P.; Shanbhag, C.; Tagad, N.; Kalia, J. Metabolic labeling-based chemoproteomics establishes choline metabolites as protein function modulators. *ACS Chem. Biol.* **2022**, *17*, 2272–2283. Copyright 2022 American Chemical Society.

2.1 Introduction

To globally map the cellular targets of choline metabolites in mammalian cells, we envisioned developing a robust technology that relies on metabolic labeling of cellular choline metabolites and lipids, and entails the cellular administration of bifunctional derivative of choline that is appended with a photocrosslinkable group and an affinity tag. Based on the previous literature,[1-4] we reasoned that an ideal bifunctional choline surrogate should contain a minimalist UV-crosslinkable diazirine group and an alkyne or an azide group for the affinity purification of the protein-metabolite conjugate. The metabolic labeling of cellular choline metabolites with these non-natural groups would result in the trafficking of all the labeled choline metabolites and choline lipids within cells in a manner identical to that of the natural metabolites. This approach would enable us to subsequently capture the choline metabolite–protein interactions upon UV-mediated crosslinking followed by biotinylation, affinity chromatography-based enrichment and mass spectrometry to identify choline metabolite and lipid-interacting proteins (Figure 1.7b).

A critical prerequisite for the success of our approach for the discovery of the choline metabolite-interacting proteome of mammalian cells is the amenability of these metabolites to undergo metabolic labeling with choline analogs. In this regard, we were encouraged by the pioneering work of Adrian Salic and co-workers demonstrating successful metabolic labeling of mammalian choline lipids with the alkynyl choline derivative, propargyl choline[5] (compound **1**, Figure 2.1) and also by azido choline[6] (compound **2**, Figure 2.1). Although these studies provided a valuable starting point, our approach relies on the choline lipid biosynthetic machinery to be amenable to accommodating more substantial structural alterations to the choline scaffold as compared to those present in these previous tested compounds, as in addition to the alkyne tag, our application required the choline analog to be appended with the diazirine group as well. Consequently, a more detailed exploration of the promiscuity of the choline lipid biosynthetic machinery with respect to choline analogs was warranted.

Our work began with structure-activity relationship studies aimed at interrogating the promiscuity of the Kennedy pathway with respect to accepting choline analogs as precursor substrates. To evaluate the degree of structural alterations on choline that are accommodated by the Kennedy pathway enzymes, we designed a small library of choline analogs (compounds **1**-**9**, Figure 2.1; the

synthetic procedures and compound characterization details for all compounds are described in section 2.4) and evaluated their ability to metabolically label mammalian choline metabolite and lipids. This library contained analogs where the *N*-methyl group on choline was substituted with alkynyl groups possessing different chain lengths, or two of the three, or all three *N*-methyl groups were substituted with either an alkynyl group or a combination of alkynyl and alkyl groups (analogs **1**, **3**-**9**, Figure 2.1). We also synthesized azido choline (compound **2**, Figure 2.1) to test whether biorthogonal groups other than the alkyne group are accepted by the cellular biosynthetic machinery.

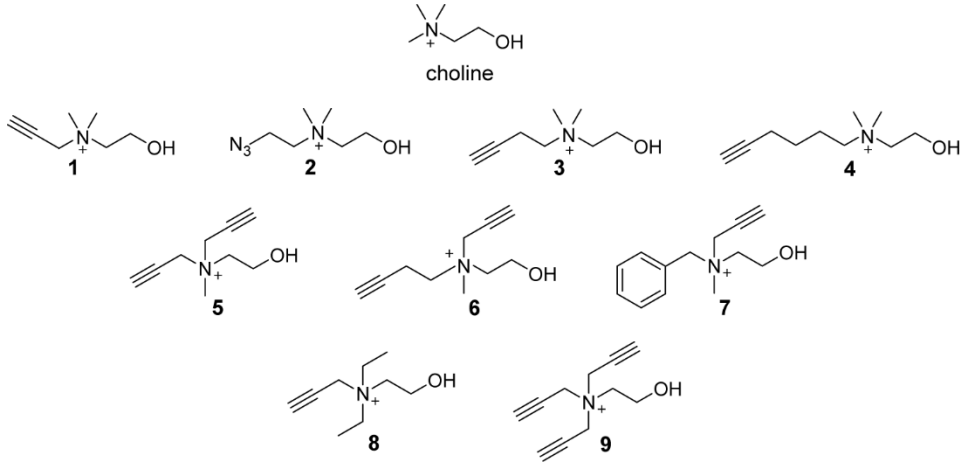

Figure 2.1. Azido choline (**2**) and alkynyl choline analogs (**1**, **3**-**9**) tested for metabolic labeling of cellular choline metabolites

2.2 Results and Discussion

We used two methods to characterize metabolic labeling of choline metabolites and lipids with the aforementioned choline analogs, cellular imaging and lipidomics. We performed cellular imaging as a preliminary test for metabolic labeling of choline metabolites. Our imaging experiments involved incubating HEK293 cells in culture with choline analogs (**1**-**9**, Figure 2.1) followed by treating the cells with either rhodamine alkyne (for the azido analog **2**) or azido fluorescein (for **1** and the other alkynyl cholines, **3**-**9**) under CuAAC conditions. The imaging protocol that we followed was identical to that reported by Salic and co-workers for imaging choline lipids of NIH-3T3 cells metabolically labeled with propargyl choline lipids (Figure 2.2).[5]

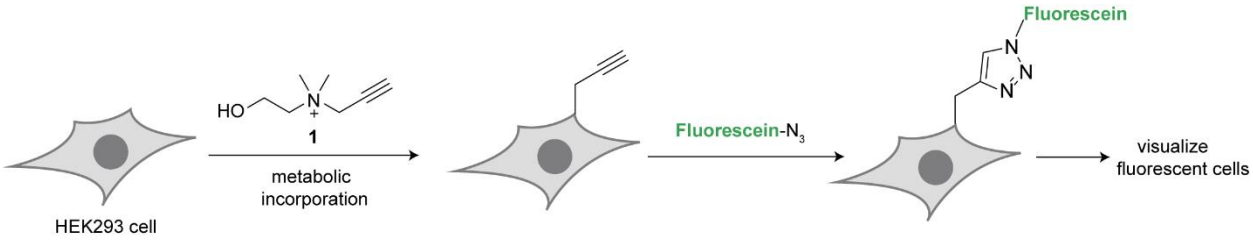

Figure 2.2. Imaging workflow for characterizing the metabolic labeling of choline analogs in HEK293 cells. The HEK293 cells in culture were administered with the alkynyl/azido choline analog (compound **1** has been shown here for representation) and its metabolic incorporation was tested by treating the cells with azido/alkynyl fluorescent dyes under click chemistry conditions followed by visualizing the fluorescent cells under the microscope.

In addition to cellular imaging, we also performed lipidomics to test the metabolic labeling of each of the choline analogs (**1**-**9**). Our lipidomics experiments entailed subjecting lipids extracted from HEK293 cells treated with the choline analogs to LC-MS/MS analysis on a HILIC column in the precursor ion scan (PIS) mode[7, 8] wherein all the parent ions that upon fragmentation yielded daughter ions corresponding to the phospho derivatives of the administered choline analogs were identified (described schematically in Figure 2.3). Since PC and SM lipids are the end products of the Kennedy pathway (Figure 1.7a), the characterization of the metabolic labeling of these lipids with our choline analogs was also, by extension, a readout of the metabolic labeling status of the choline metabolites that serve as precursor metabolites in the pathway (Figure 1.7a).

Consistent with the previous reports,[5, 6] propargyl choline (**1**) and azido choline (**2)** labeled the choline lipids efficiently as demonstrated by the appearance of intense fluorescence upon imaging (first image in the left panel of Figures 2.4a and 2.5a). The cellular administration of equimolar amounts of choline along with either **1** or **2** resulted in an attenuation of fluorescence intensity (second image in the left panel of Figures 2.4 and 2.5) demonstrating that these compounds served as choline surrogates as the presence of the preferred natural substrate resulted in a reduction of metabolic labeling by the non-natural analogs (second image in the left panel of Figures 2.4a and 2.5a).

Lipidomics analysis on lipids isolated from cells administered with **1** and **2** gave intense peaks for the labeled lipids on the total ion chromatograms (TICs; right panel of Figures 2.4a and 2.5a) The

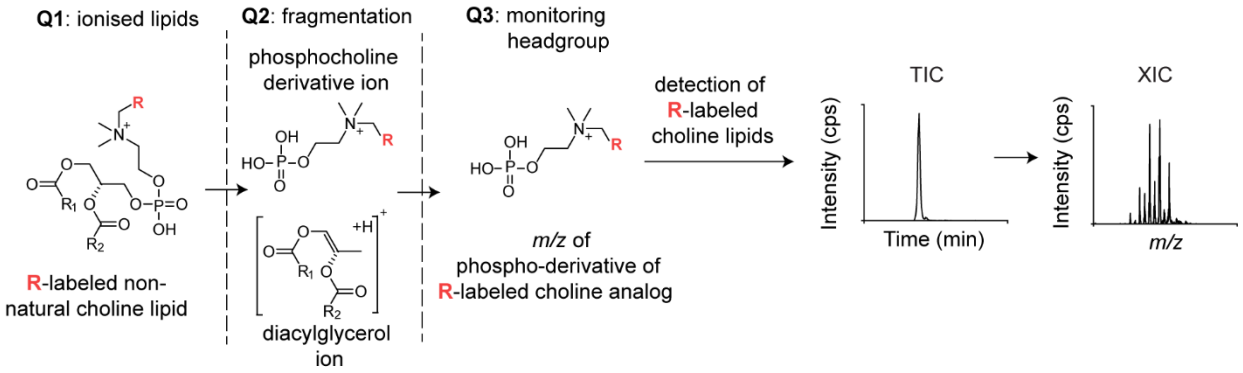

Figure 2.3. A diagrammatic representation for the use of the PIS mode to detect non-natural choline lipids. A representative ionized non-natural choline lipid with **R**-labeled phosphocholine as its headgroup and R_1 and R_2 as its hydrophobic tails, travels from the first quadrupole (Q1) of the QTRAP4500 instrument to the second quadrupole (Q2) where it is fragmented by collision activated dissociation (CAD) into the diacylglycerol ion and the ion of the phospho-derivative of the **R**-labeled choline analog. The third quadrupole (Q3) scans for the *m/z* of the fragment ion corresponding to the phospho-derivative of **R**-labeled choline analog. All parent ions that yield this fragment ion in the Q3 are detected, yielding a peak on the total ion chromatogram (TIC) which is further processed by the Analyst software to generate the extracted ion chromatogram (XIC) that shows the *m/z* values for all the **R**-labeled choline lipids.

mass spectra representing the labeled lipid species detected within the TIC peaks are depicted in the extracted ion chromatograms (XICs; right panel of Figures 2.4a and 2.5a) and the analysis of these XICs by the LipidView software revealed the identity of all the choline lipids metabolically labeled with these analogs (Figures 2.4b and 2.5b). Consistent with the previous reports for other mammalian cells such as NIH3T3,[5, 6] we found that the three most intense **1**- and **2**-labeled PC lipid species in HEK293 cells were 34:1, 32:1 and 36:2. The imaging and the lipidomics results from the treatment of **1** and **2** in HEK293 cells established a robust experimental workflow that was needed to test other more elaborate analogs of choline.

We next synthesized butynyl choline (compound **3** in Figure 2.1) and hexynyl choline (compound **4** in Figure 2.1) and tested them for metabolic labeling via the imaging and lipidomics workflow as described above. We found that both **3** and **4** showed successful metabolic incorporation as represented by the cellular imaging and lipidomics analysis (Figures 2.6 and 2.7). Imaging

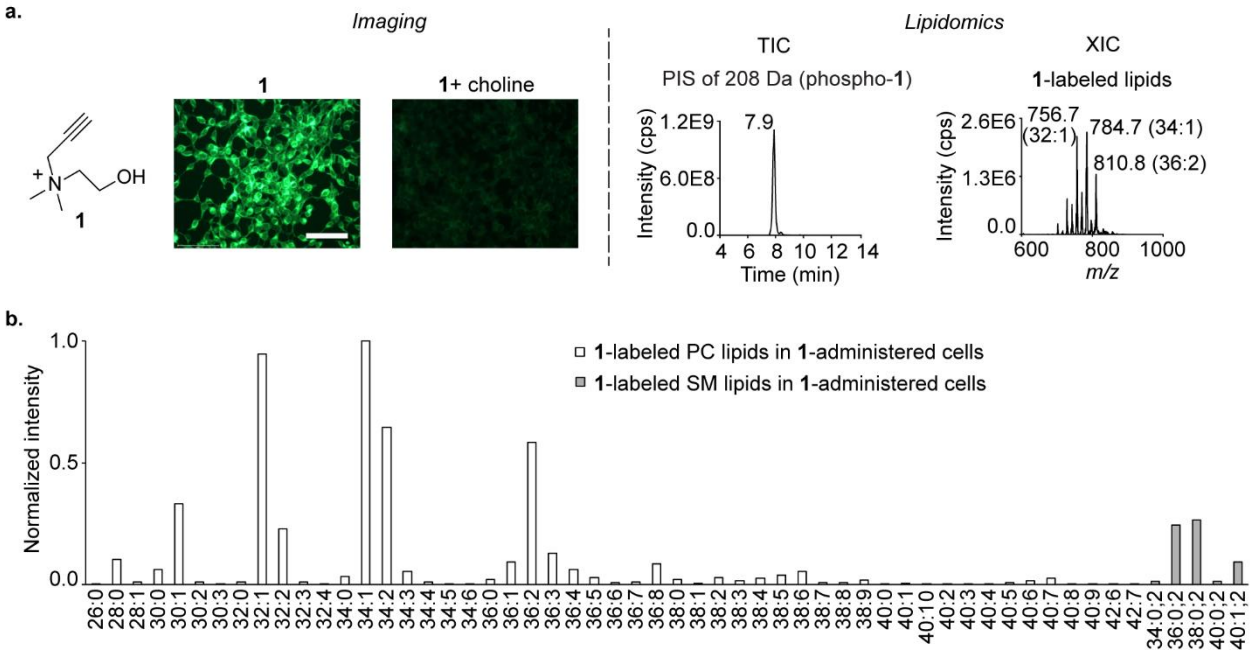

Figure 2.4. Metabolic labeling studies on analog **1** via lipidomics and cellular imaging. a) *Left*: HEK293 cells were cultured for 24 h in the presence of either analog **1** (2 mM; left) or choline chloride along with the analog **1** (2 mM of each; right), subsequent to which the cells were fixed and treated with 5-azido fluorescein under click chemistry conditions and imaged. The scale bar represents 100 μm. *Right*: The TIC and XIC plots obtained by employing a PIS of 208 Da (the *m/z* for phospho-**1**) on lipids extracted from HEK293 cells cultured for 24 h in the presence of compound **1** (2 mM). b) A bar graph obtained from the LipidView software denoting all **1**-labeled PC and SM lipids identified from the XIC depicted above. The *y*-axis has been normalized to the most intense peak *i.e.*, lipid 34:1 of the XIC.

experiments on cells administered with butynyl choline (**3**) yielded intense fluorescence whereas the hexynyl derivative (**4**) yielded a substantially lower fluorescence signal suggesting that the former was a much more proficient choline metabolic labeling probe than the latter. This conclusion was supported by the lipidomics experiments that revealed that the intensity of the TIC peak obtained for the labeled lipids extracted from HEK293 cells treated with **3** (~2.0E8; right panel of Figure 2.6a) was more than 10-fold higher than that obtained for **4** (~1.6E7; right panel of Figure 2.7a). The metabolic labeling levels were observed to reduce with increasing structural dissimilarity of the analogs with respect to choline, as demonstrated by a sequential decrease in the TIC peak intensities going from compound **1** to **4** (TICs in the right panel of Figures 2.4a-

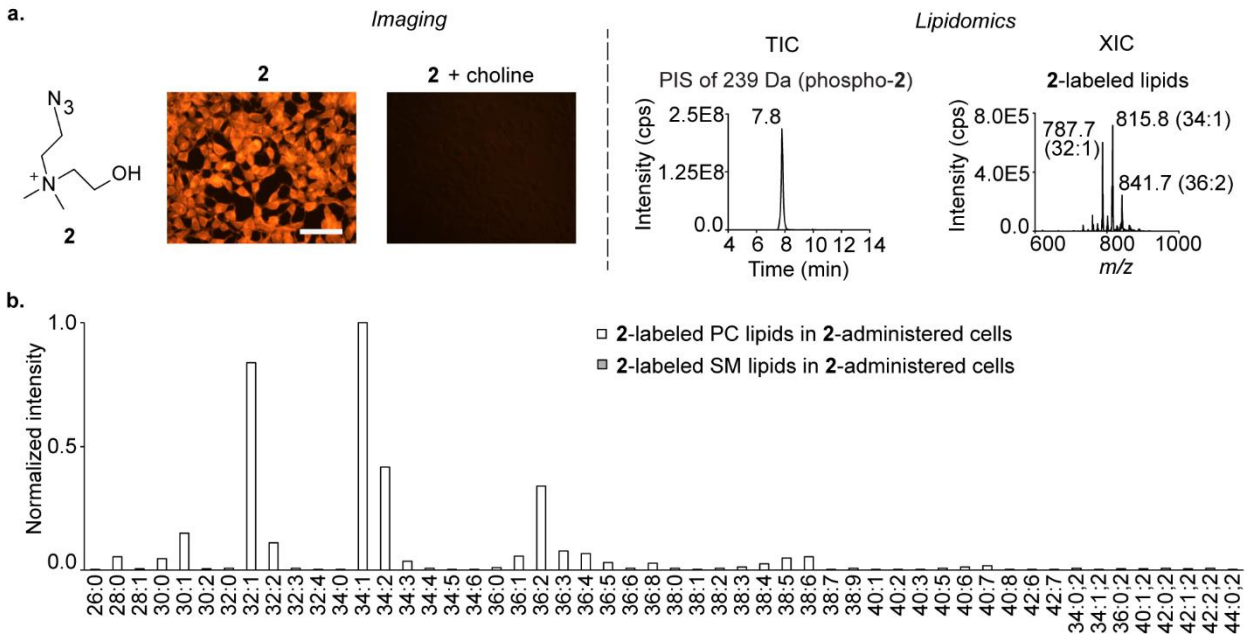

Figure 2.5. Metabolic labeling studies on analog **2** via lipidomics and cellular imaging. a) *Left*: HEK293 cells were cultured for 24 h in the presence of either analog **2** (2 mM; left) or choline chloride along with the analog **2** (2 mM of each; right), subsequent to which the cells were fixed and treated with 5-azido fluorescein under click chemistry conditions and imaged. The scale bar represents 100 μm. *Right*: The TIC and XIC plots obtained by employing a PIS of 239 Da (the *m/z* for phospho-**2**) on lipids extracted from HEK293 cells cultured for 24 h in the presence of compound **2** (2 mM). b) A bar graph obtained from the LipidView software denoting all **2**-labeled PC and SM lipids identified from the XIC depicted above. The *y*-axis has been normalized to the most intense peak *i.e.*, lipid 34:1 of the XIC.

2.7a).

We tested compounds **5**, **6** and **7** for metabolic incorporation into the Kennedy pathway. Whereas compounds **3** and **4** retained two of the three *N*-methyl groups of choline, compounds **5**, **6** and **7** retained only one of them (Figure 2.1). Interestingly, the dialkynyl choline analogs **5** and **6** also metabolically labeled choline lipids as demonstrated by the appearance of clear peaks on the TICs and XICs for the expected labeled choline lipid species with **5** being much more efficient, yielding more than 10-fold higher TIC peak (right panels of Figure 2.8a and 2.9a) and substantially higher fluorescence intensity in the imaging experiment as compared to **6** (left panels of Figures 2.8a and 2.9a).

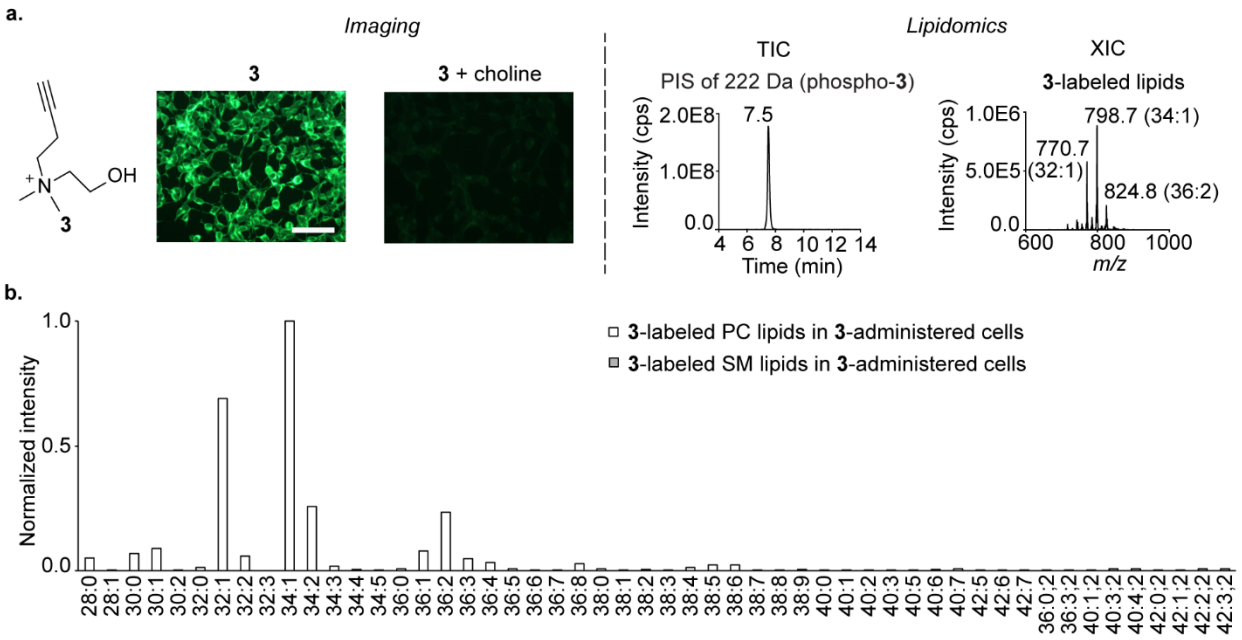

Figure 2.6. Metabolic labeling studies on analog **3** via lipidomics and cellular imaging. a) *Left*: HEK293 cells were cultured for 24 h in the presence of either analog **3** (2 mM; left) or choline chloride along with the analog **3** (2 mM of each; right), subsequent to which the cells were fixed and treated with 5-azido fluorescein under click chemistry conditions and imaged. The scale bar represents 100 μm. *Right*: The TIC and XIC plots obtained by employing a PIS of 222 Da (the *m/z* for phospho-**3**) on lipids extracted from HEK293 cells cultured for 24 h in the presence of compound **3** (2 mM). b) A bar graph obtained from the LipidView software denoting all **3**-labeled PC and SM lipids identified from the XIC depicted above. The *y*-axis has been normalized to the most intense peak *i.e.*, lipid 34:1 of the XIC.

Remarkably, the replacement of one of the methyl groups of choline with the significantly bulkier benzyl group (compound **7**; Figure 2.1) was also well-tolerated by the choline biosynthetic machinery, yielding a TIC intensity of ~5.0E6 (Figure 2.10), demonstrating the tremendous promiscuity of the choline biosynthesis machinery of mammalian cells with respect to accepting choline derivatives. It is important to note that, although, the TIC showed a prominent signal intensity of ~5.0E6 units for **7**-labeled choline lipids (Figure 2.10b), the imaging panel shows negligible fluorescence above background for **7**-labeled choline lipids (Figure 2.10a) suggesting that lipidomics is a more sensitive method for characterization of metabolic labeling than imaging. Notably, as expected in normal phase chromatography, the retention time values corresponding to the peaks for the labeled lipids were observed to reduce with increasing hydrophobicity of the

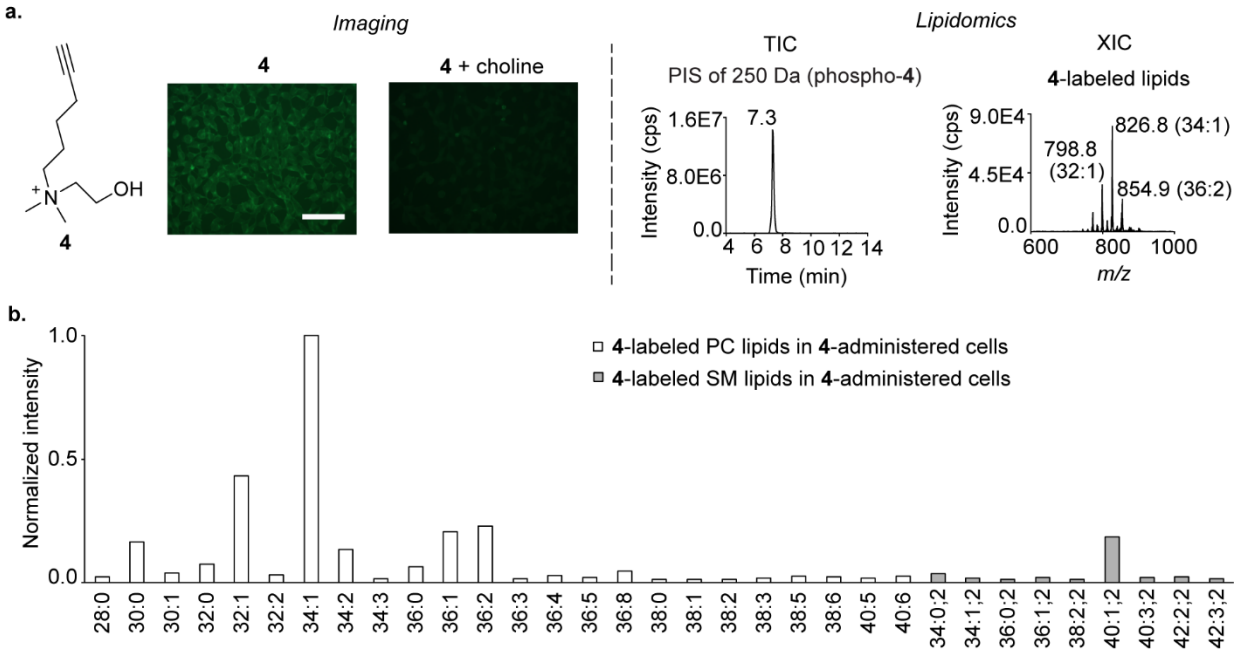

Figure 2.7. Metabolic labeling studies on analog **4** via lipidomics and cellular imaging. a) *Left*: HEK293 cells were cultured for 24 h in the presence of either analog **4** (2 mM; left) or choline chloride along with the analog **4** (2 mM of each; right), subsequent to which the cells were fixed and treated with 5-azido fluorescein under click chemistry conditions and imaged. The scale bar represents 100 μm. *Right*: The TIC and XIC plots obtained by employing a PIS of 250 Da (the *m/z* for phospho-**4**) on lipids extracted from HEK293 cells cultured for 24 h in the presence of compound **4** (2 mM). b) A bar graph obtained from the LipidView software denoting all **4**-labeled PC and SM lipids identified from the XIC depicted above. The *y*-axis has been normalized to the most intense peak *i.e.*, lipid 34:1 of the XIC.

choline analogs, going from 7.9 min for compound **1** to 6.5 min for **7** (TICs in Figures 2.4-2.10).

We also tested compounds **8** and **9** where all three of the *N*-methyl groups of choline were substituted to longer alkyl chains. (Figure 2.1). Consistent with the results obtained for compound **7**, lipidomics analysis revealed that both **8** and **9** showed successful metabolic labeling of choline lipids (right panels of Figures 2.11a and 2.12a) and that the extent of labeling was not high enough to yield intense fluorescence signals from the cellular imaging experiments (left panels of Figures 2.11a and 2.12a).

These results further consolidated the previous findings that lipidomics is a more sensitive

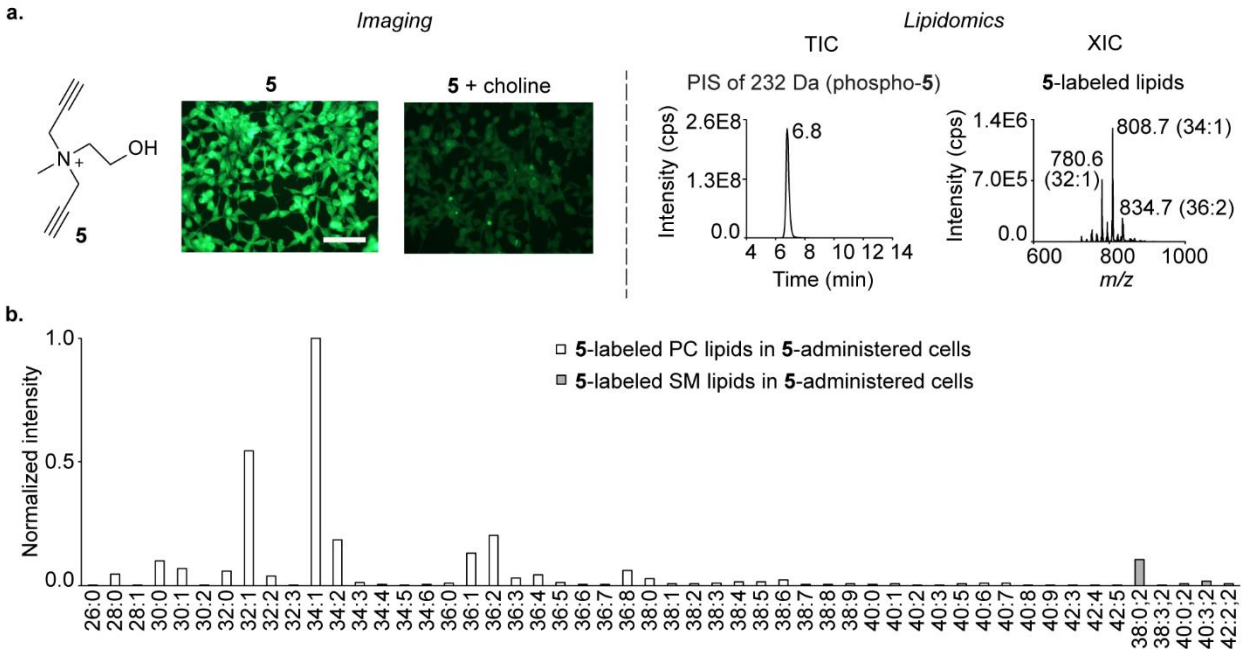

Figure 2.8. Metabolic labeling studies on analog **5** via lipidomics and cellular imaging. a) *Left*: HEK293 cells were cultured for 24 h in the presence of either analog **5** (2 mM; left) or choline chloride along with the analog **5** (2 mM of each; right), subsequent to which the cells were fixed and treated with 5-azido fluorescein under click chemistry conditions and imaged. The scale bar represents 100 μm. *Right*: The TIC and XIC plots obtained by employing a PIS of 232 Da (the *m/z* for phospho-**5**) on lipids extracted from HEK293 cells cultured for 24 h in the presence of compound **5** (2 mM). b) A bar graph obtained from the LipidView software denoting all **5**-labeled PC and SM lipids identified from the XIC depicted above. The *y*-axis has been normalized to the most intense peak *i.e.*, lipid 34:1 of the XIC.

method for the characterization of metabolic labeling of choline lipids than imaging. Specifically, when the TIC peaks' intensities reduced to ~E6 units (for compounds **7**-**9**, Figures 2.10-2.12), the imaging experiments did not yield detectable fluorescence signals. Interestingly, we also observed that as the signal intensities of the TIC peaks decreased from compound **1** to **9**, *i.e.*, from ~E9 to ~E6 units respectively (compare TICs on Figures 2.4a-2.11a), the number of labeled choline lipid species also decreased (compare LipidView plots on Figures 2.4b-2.11b). The most abundant non-natural PC lipid species across all the analogs, however, remained the same, *i.e.*, 34:1, 32:1 and 36:2.

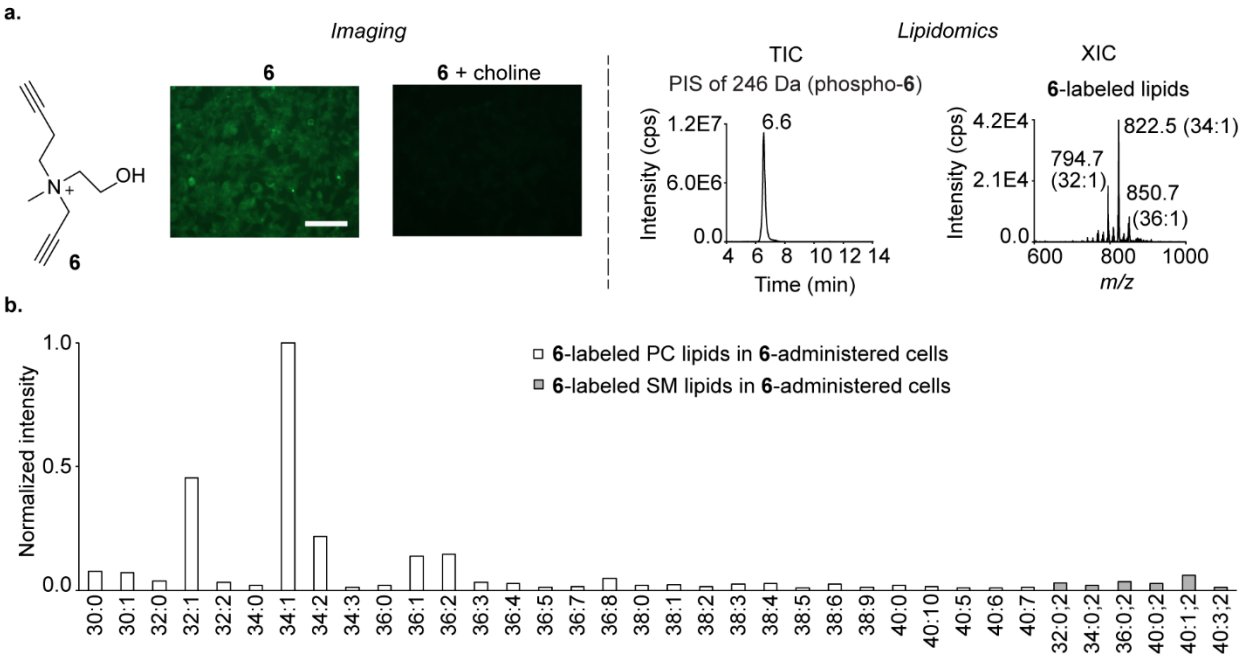

Figure 2.9. Metabolic labeling studies on analog **6** via lipidomics and cellular imaging. a) *Left*: HEK293 cells were cultured for 24 h in the presence of either analog **6** (2 mM; left) or choline chloride along with the analog **6** (2 mM of each; right), subsequent to which the cells were fixed and treated with 5-azido fluorescein under click chemistry conditions and imaged. The scale bar represents 100 μm. *Right*: The TIC and XIC plots obtained by employing a PIS of 246 Da (the *m/z* for phospho-**6**) on lipids extracted from HEK293 cells cultured for 24 h in the presence of compound **6** (2 mM). b) A bar graph obtained from the LipidView software denoting all **6**-labeled PC and SM lipids identified from the XIC depicted above. The *y*-axis has been normalized to the most intense peak *i.e.*, lipid 34:1 of the XIC.

2.3 Conclusions

In this chapter, I have described the development of a robust experimental workflow to characterize the metabolic labeling efficiency for nine choline analogs via cellular imaging and lipidomics. The results from the structure-activity relationship studies revealed that the choline lipid biosynthetic machinery is remarkably flexible with respect to accepting structurally elaborate choline analogs as demonstrated by the TICs in Figures 2.4-2.12. Notably, cells metabolically labeled with the most elaborate analogs (**4** and **6-9**) did not yield intense fluorescence signals (Figures 2.7 and 2.9-2.12, left panel) despite confirmation of metabolic labeling via lipidomics (the corresponding right panels). These results demonstrated the higher sensitivity of our PIS

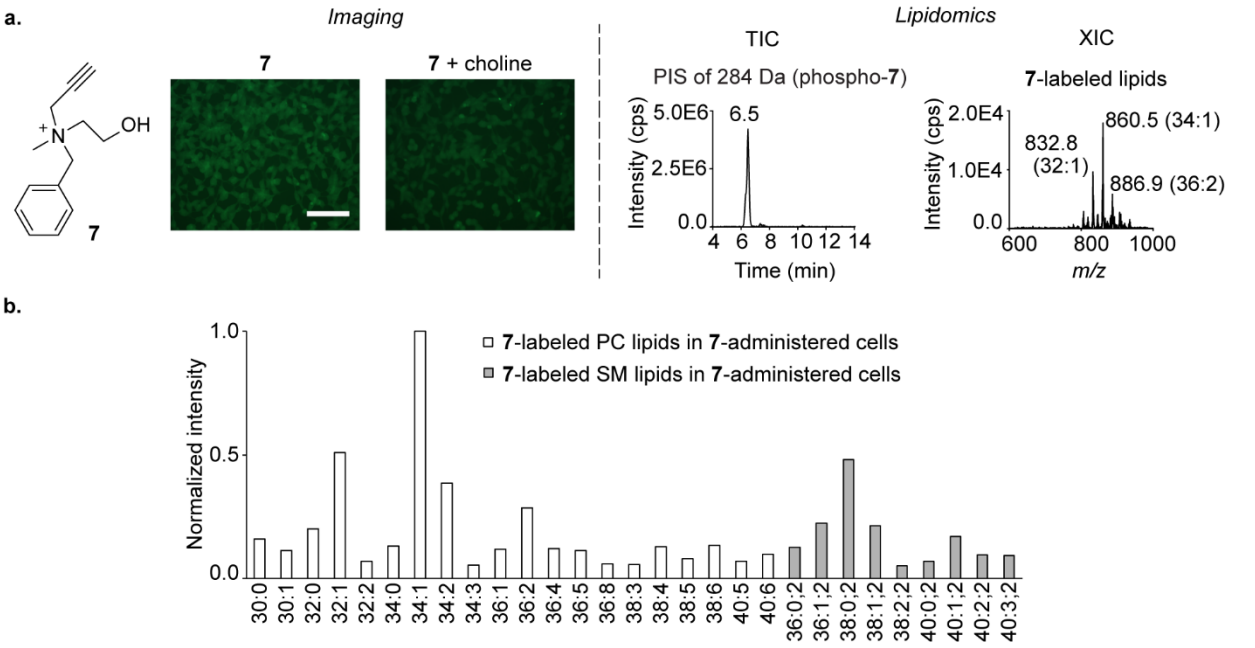

Figure 2.10. Metabolic labeling studies on analog **7** via lipidomics and cellular imaging. a) *Left*: HEK293 cells were cultured for 24 h in the presence of either analog **7** (2 mM; left) or choline chloride along with the analog **7** (2 mM of each; right), subsequent to which the cells were fixed and treated with 5-azido fluorescein under click chemistry conditions and imaged. The scale bar represents 100 μm. *Right*: The TIC and XIC plots obtained by employing a PIS of 284 Da (the *m/z* for phospho-**7**) on lipids extracted from HEK293 cells cultured for 24 h in the presence of compound **7** (2 mM). b) A bar graph obtained from the LipidView software denoting all **7**-labeled PC and SM lipids identified from the XIC depicted above. The *y*-axis has been normalized to the most intense peak *i.e.*, lipid 34:1 of the XIC.

lipidomics workflow as compared to our version of click chemistry-based imaging for characterizing metabolic labeling. In fact, fluorescence imaging as a means to characterize metabolic labeling was compatible with only those analogs (**1**, **2, 3** and **5**) that yielded TIC peak intensities of the order of E8 or above for the labeled lipids.

One important insight from these studies was that extending the chain length of alkyl substituents on the choline nitrogen atom results in reduced metabolic labeling efficiency as is evident when comparing the fluorescence imaging intensities and lipidomics TIC data for compounds **1**, **3** and **4** in Figures 2.4, 2.6 and 2.7. Interestingly however, the replacement of two *N*-methyl groups of

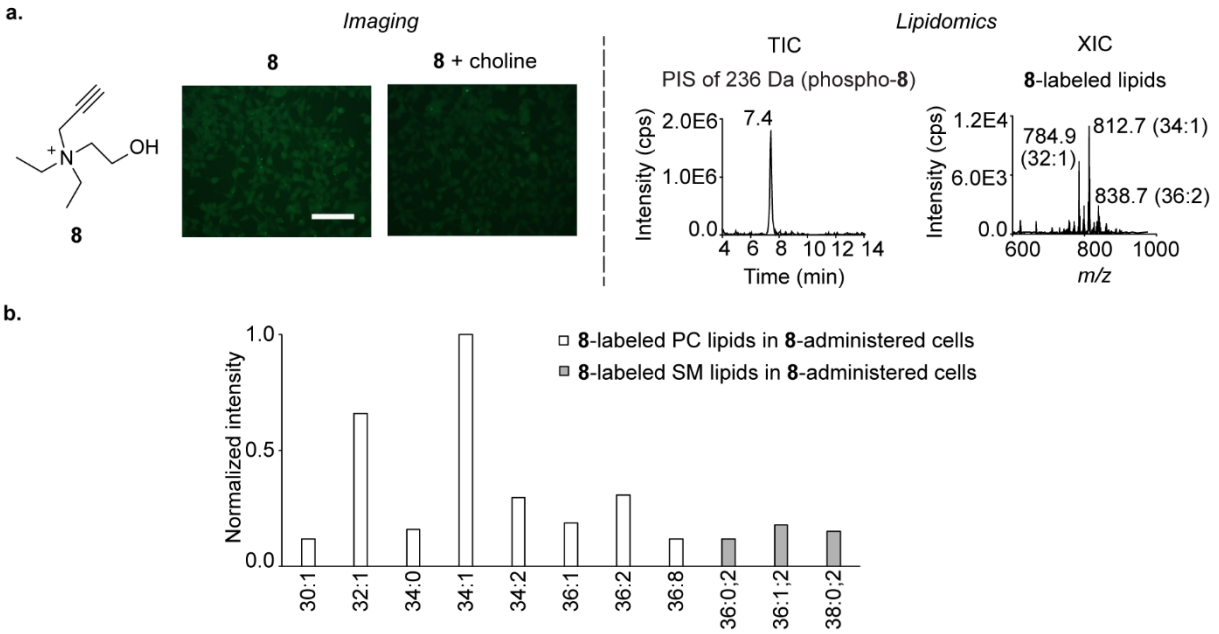

Figure 2.11. Metabolic labeling studies on analog **8** via lipidomics and cellular imaging. a) *Left*: HEK293 cells were cultured for 24 h in the presence of either analog **8** (2 mM; left) or choline chloride along with the analog **8** (2 mM of each; right), subsequent to which the cells were fixed and treated with 5-azido fluorescein under click chemistry conditions and imaged. The scale bar represents 100 μm. *Right*: The TIC and XIC plots obtained by employing a PIS of 236 Da (the *m/z* for phospho-**8**) on lipids extracted from HEK293 cells cultured for 24 h in the presence of compound **8** (2 mM). b) A bar graph obtained from the LipidView software denoting all **8**-labeled PC and SM lipids identified from the XIC depicted above. The *y*-axis has been normalized to the most intense peak *i.e.*, lipid 34:1 of the XIC.

choline with longer alkyl substituents (as in compounds **5, 6** and **7**) showed robust incorporation in the choline lipid biosynthetic machinery. The results of this survey of choline analogs as probes for metabolic labeling, therefore, provided valuable insights into the structural framework within which to design bifunctional choline analogs containing both the diazirine and the alkyne groups.

2.4 Experimental Methods

2.4.1 Materials

All organic synthesis reactions were performed in oven-dried glassware. Chemical reagents

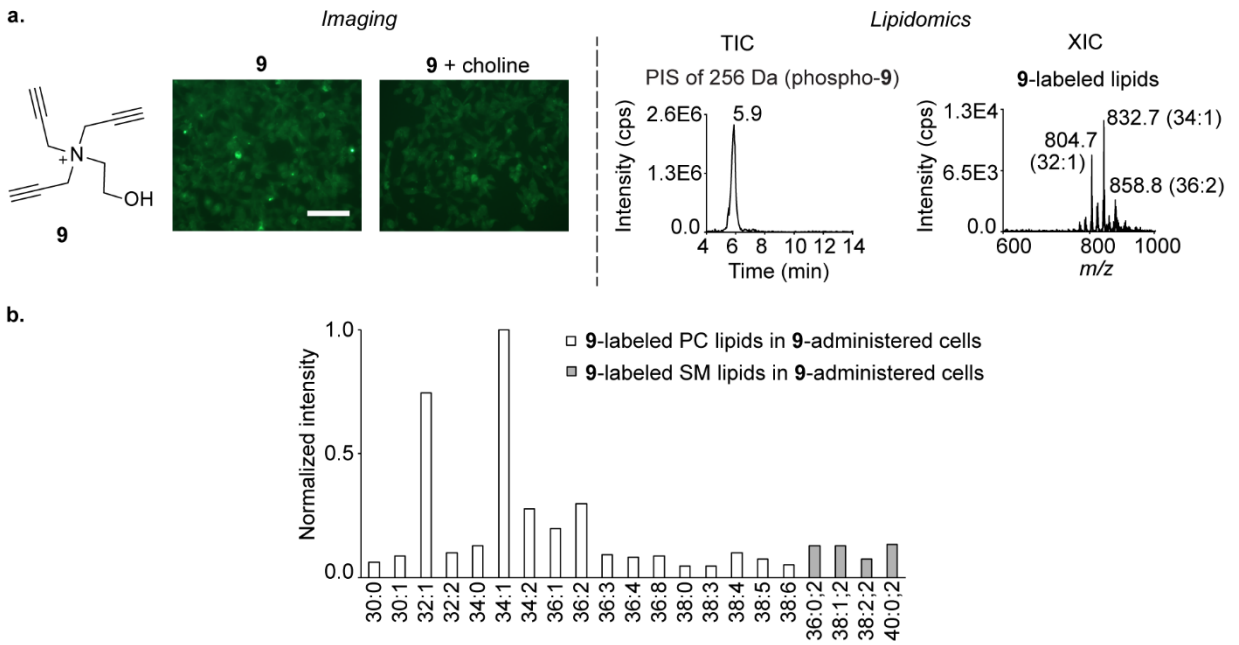

Figure 2.12. Metabolic labeling studies on analog **9** via lipidomics and cellular imaging. a) *Left*: HEK293 cells were cultured for 24 h in the presence of either analog **9** (2 mM; left) or choline chloride along with the analog **9** (2 mM of each; right), subsequent to which the cells were fixed and treated with 5-azido fluorescein under click chemistry conditions and imaged. The scale bar represents 100 μm. *Right*: The TIC and XIC plots obtained by employing a PIS of 256 Da (the *m/z* for phospho-**9**) on lipids extracted from HEK293 cells cultured for 24 h in the presence of compound **9** (2 mM). b) A bar graph obtained from the LipidView software denoting all **9**-labeled PC and SM lipids identified from the XIC depicted above. The *y*-axis has been normalized to the most intense peak *i.e.*, lipid 34:1 of the XIC.

for organic synthesis were purchased either from Sigma-Aldrich or Alfa Aesar and were used without purification. Distilled water was used for reaction work-ups, and ultrapure Type 1 water was used for buffer preparations and LC-MS experiments. The progress of chemical reactions was monitored by thin layer chromatography (TLC) using 0.25 mm Merck precoated (60 F254) silica gel plates. For visualization of TLC spots, UV light of wavelength 254 nm (for UV active compounds) and 365 nm (for fluorescent compounds) was used. In some cases, TLC spots were visualized using ninhydrin and phosphomolybdic acid (PMA) staining solutions. Purifications were performed using column chromatography on silica gel (100-200 mesh). Reagents for cell culture-based experiments such as Dulbecco's modified eagle medium (DMEM), fetal bovine

serum (FBS), penicillin-streptomycin solution, 0.05% Trypsin-EDTA solution were purchased from Gibco (ThermoFisher Scientific).

2.4.2 Instrumentation and software

^{1}H and ^{13}C-NMR spectra were acquired either on a Bruker Avance III HD Ascend 400 MHz or a Bruker Avance III HD Ascend 500 MHz spectrometer and the raw files were processed on the Mestrenova software (Mestrelab Research). Chemical shifts are reported as parts per million (δ) relative to tetramethylsilane (TMS) as internal standard and coupling constants (*J* values) in Hertz (Hz). Multiplicities are indicated as follows: s (singlet), d (doublet), t (triplet), q (quartet), dd (doublet of doublet), bs (broad singlet), td (triplet of a doublet) and m (multiplet). High-resolution mass spectra (HRMS) were recorded on HRMS-ESI-Q-Time-of-Flight LC/MS (Synapt G2, Waters). Cellular imaging was performed on an EVOS-M7000 cell imaging system (Invitrogen). Lipidomics was performed on a triple quadrupole mass spectrometer (QTRAP 4500 system from Sciex) equipped with an Exion UHPLC from Sciex. All mass spectra (TIC and XIC) were analyzed on the Analyst software (Sciex) and lipid species were identified by using the LipidView software (Sciex). All mammalian cells in culture were incubated in a Galaxy 170S CO_2 incubator (Eppendorf).

2.4.3 Synthetic schemes and procedures

Scheme 2.1 Synthesis of propargyl choline **1**

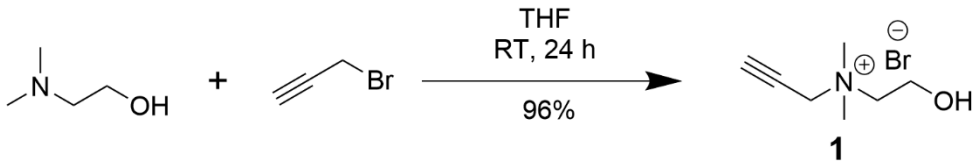

1

Propargyl choline (1)

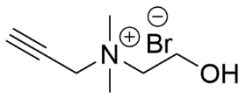

1

To an ice-cold solution of 2-dimethylaminoethanol (2 g, 22.4 mmol, 1 eq.) in THF (6 mL), 80% (*w*/*w*) propargyl bromide solution in toluene (2.89 mL, 26.9 mmol, 1.2 eq.) was added dropwise and the resultant mixture was stirred at 0 °C for 15 min. Subsequently, the mixture was warmed

to room temperature and stirred for 24 h. The light-brown precipitate thus formed was collected by filtration and washed with cold THF (100 mL) to give **1** as a white solid (4.52 g, 96%).

^{1}H NMR (400 MHz, DMSO-d6) δ 5.34 (t, *J* = 5.0 Hz, 1H), 4.48 (d, *J* = 2.4 Hz, 2H), 4.07 (t, *J* = 2.5 Hz, 1H), 3.85 (q, *J* = 4.8 Hz, 2H), 3.49 – 3.47 (m, 2H), 3.16 (s, 6H).

^{13}C NMR (100 MHz, DMSO-d6) δ 82.9, 72.6, 64.7, 54.9, 54.5, 50.6.

HRMS (ESI): $C_7H_{14}NO^+$; Calculated mass, $[M]^+$ 128.1070; Observed mass, $[M]^+$ 128.1.

Azido choline (2)

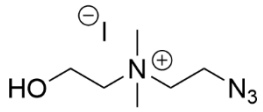

2

Azido choline **2** was synthesized according to a previously reported procedure.[6]

Scheme 2.2 Synthesis of butynyl choline **3**

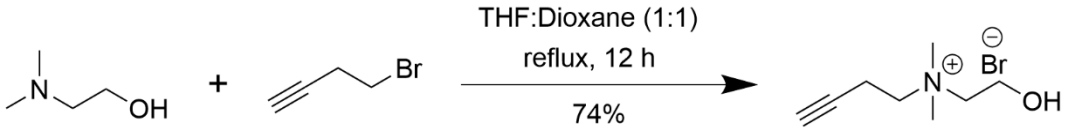

3

Butynyl choline (3)

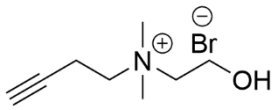

3

To a solution of 2-dimethylaminoethanol (0.5 mL, 4.97 mmol, 1 eq.) in a mixture of THF and dioxane (4 mL of a 1:1 solution), 4-bromobutyne (0.7 mL, 7.45 mmol, 1.5 eq.) was added and the reaction mixture was refluxed for 12 h. Subsequently, the solvent was evaporated under reduced pressure and the resultant brown residue was dissolved in ethanol (5 mL) and stored at -20 °C overnight. The precipitate thus obtained was collected, washed with cold ethanol (50 mL), and vacuum-dried to give dirty-white crystals of **3** (0.82 g, 74 %).

^{1}H NMR (400 MHz, DMSO-d6) δ 5.30 (t, *J* = 4.8 Hz, 1H), 3.82 (bs, 2H), 3.56 (t, *J* = 7.6 Hz, 2H), 3.43 (t, *J* = 4.8 Hz, 2H), 3.10 (s, 6H), 2.77 (t, *J* = 6.4 Hz, 2H).

^{13}C NMR (100 MHz, DMSO-d6) δ 79.9, 74.2, 65.5, 62.5, 55.4, 51.5, 13.5.

HMRS (ESI): $C_8H_{16}NO^+$; Calculated mass, $[M]^+$ 142.1226; Observed mass, $[M]^+$ 142.1232.

Scheme 2.3 Synthesis of hexynyl choline **4**

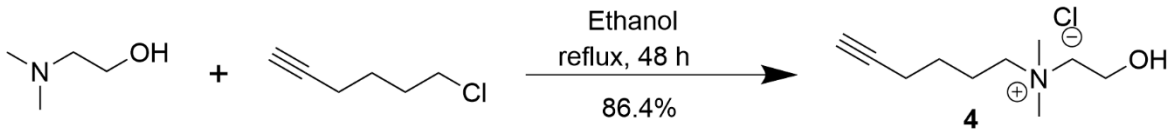

Hexynyl choline (4)

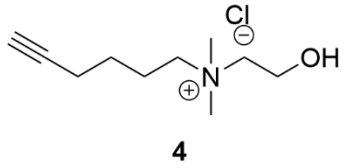

To a solution of 2-dimethylaminoethanol (0.5 mL, 4.12 mmol, 1 eq.) in ethanol (11 mL), 6-chlorohexyne (2 mL, 16.5 mmol, 4 eq.) was added and the resulting mixture was refluxed for 48 h. Subsequently, the solvent was removed under reduced pressure to give a heterogeneous mixture of a white solid and a yellow viscous oil. This mixture was dissolved in acetone (2 mL) and incubated in a dry ice-acetone cooling mixture at -78 °C for 1 h. A white precipitate was observed to form. The yellow solution was decanted and the precipitate was triturated with ice-cold acetone (3 × 2 mL) to give **4** as a white solid (0.88 g, 86.4%).

^{1}H NMR (400 MHz, DMSO-d6) δ 5.51 (t, *J* = 5.2 Hz, 1H), 3.81 (bs, 2H), 3.40 – 3.34 (m, 2H), 3.07 (s, 6H), 2.86 (t, *J* = 2.4 Hz, 1H), 2.23 (td, *J* = 6.8 Hz, 2.4 Hz, 2H), 1.80 – 1.72 (m, 2H), 1.49 – 1.42 (m, 2H).

^{13}C NMR (100 MHz, DMSO-d6) δ 83.8, 71.8, 64.6, 63.5, 54.8, 50.9, 24.9, 22.5, 21.1, 17.3.

HRMS (ESI): $C_{10}H_{20}NO^+$; Calculated mass, $[M]^+$ 170.1539; Observed mass, $[M]^+$ 170.1544.

Scheme 2.4 Synthesis of dipropargyl choline **5**

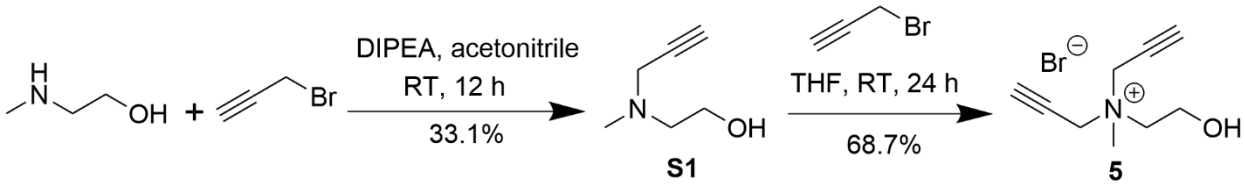

2-(methyl(prop-2-yn-1-yl)amino)ethan-1-ol (S1)

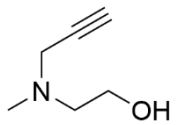

S1

To an ice-cold solution of acetonitrile (5 mL) containing *N*-methylaminoethanol (0.5 g, 6.65 mmol, 1.0 eq.) and *N*,*N*-diisopropylethylamine (1.0 mL, 6.0 mmol, 0.9 eq.), 80% (*w*/*w*) propargyl bromide solution in toluene (0.65 mL, 6.0 mmol, 0.9 eq.) was added dropwise. The resultant reaction mixture was stirred at 0 °C for 30 min and then allowed to warm to room temperature and stirred for 12 h. Subsequently, the solvent was removed under reduced pressure and the residue was dissolved in dichloromethane (25 mL) and washed with saturated sodium bicarbonate solution (25 mL). The aqueous layer was further washed with dichloromethane (3 × 25 mL). The organic layers were pooled, dried by adding anhydrous sodium sulfate, filtered and concentrated under reduced pressure and subjected to silica gel column chromatography (10% methanol in ethyl acetate) to afford **S1** as a yellow-colored oil (0.25 g, 33.1%).

^{1}H NMR (400 MHz, $CDCl_3$) δ 3.61 (t, *J* = 5.2 Hz, 2H), 3.39 (d, *J* = 2.4 Hz, 2H), 2.63 (t, *J* = 5.2 Hz, 2H), 2.35 (s, 3H), 2.23 (t, *J* = 2.4 Hz, 1H).

^{13}C NMR (100 MHz, $CDCl_3$) δ 78.4, 73.4, 58.7, 57.0, 45.8, 41.3.

HRMS (ESI): $C_6H_{12}NO$; Calculated mass, $[M+H]^+$ 114.0913; Observed mass, $[M+H]^+$ 114.0924.

Dipropargyl choline (5)

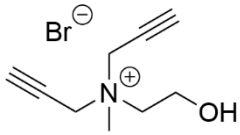

5

An ice-cold solution of **S1** (50.5 mg, 0.45 mmol, 1 eq.) in THF (1 mL) was treated with 80% (*w*/*w*) propargyl bromide in toluene (59 µL, 0.54 mmol, 1.2 eq.). The resultant solution was stirred under ice-cold conditions for 30 min and then at room temperature for 24 h. A yellow oil was observed to settle down at the bottom of the round-bottomed flask which upon trituration with ice-cold chloroform (8 × 2 mL), followed by drying under reduced pressure gave **5** as a pale-yellow solid (71.2 mg, 68.7%).

^{1}H NMR (400 MHz, DMSO-d6) δ 5.44 (m, 1H), 4.49 (t, *J* = 2.4 Hz, 4H), 4.12 (t, *J* = 2.4 Hz, 2H), 3.87 (bs, 2H), 3.54 (t, *J* = 5.2 Hz, 2H), 3.18 (s, 3H).

^{13}C NMR (100 MHz, DMSO-d6) δ 83.6, 71.9, 62.8, 54.7, 52.4, 48.3.

HRMS (ESI): $C_9H_{14}NO^+$; Calculated mass, $[M]^+$ 152.1070; Observed $[M]^+$ 152.1077.

Scheme 2.5 Synthesis of propargyl butynyl choline **6**

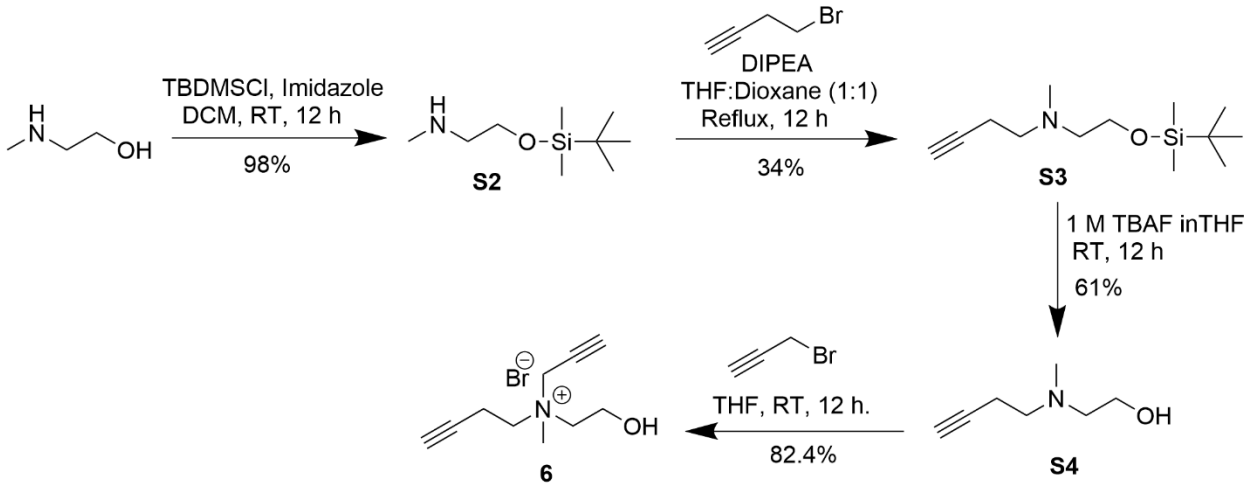

2-((*t*-butyldimethylsilyl)oxy)-*N*-methylethan-1-amine (S2)

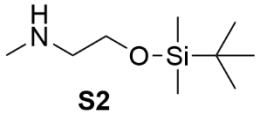

To an ice-cold solution of *N*-methylaminoethanol (3 g, 39.9 mmol, 1 eq.) and imidazole (2.85 g, 41.9 mmol, 1.05 eq.) in dichloromethane (30 mL), was added an ice-cold solution of solution of *t*-butyldimethylsilylchoride (6.33 g, 42 mmol, 1.05 eq.) in dichloromethane (20 mL) under nitrogen atmosphere. Before mixing these two solutions, nitrogen gas was bubbled through each of them for 30 min. The resultant solution was allowed to warm to room temperature and stirred for 12 h. The reaction mixture was subsequently washed with 50 mL of water and the organic layer was concentrated under vacuum to give **S2** as a white solid (7.43 g, 98%).

^{1}H NMR (400 MHz, $CDCl_3$) δ 3.76 (t, *J* = 5.2 Hz, 2H), 2.74 (t, *J* = 5.2 Hz, 2H), 2.49 (s, 3H), 0.89 (s, 9H), 0.06 (s, 6H).

^{13}C NMR (125 MHz, $CDCl_3$) δ 59.7, 51.4, 34.1, 26.0, 18.4, -5.3.

HRMS (ESI): $C_9H_{23}NOSi$; Calculated mass, $[M+H]^+$ 190.1622; Observed $[M+H]^+$ 190.1634.

***N*-(2-((*t*-butyldimethylsilyl)oxy)ethyl)-*N*-methylbut-3-yn-1-amine (S3)**

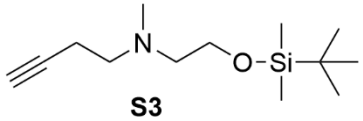

S3

To a solution of **S2** (1 g, 5.3 mmol, 1 eq.) and *N*,*N*-diisopropylethylamine (0.9 mL, 5.3 mmol, 1.0 eq.) in a mixture of THF and dioxane (15 mL of a 1:1 solution), 4-bromobutyne (0.5 mL, 5.3 mmol, 1 eq.) was added dropwise. After refluxing the resultant mixture for 12 h, the solvent was removed under reduced pressure and the residue was dissolved in dichloromethane (15 mL) and washed with saturated solution of sodium bicarbonate (2 × 20 mL). The organic extracts were combined, dried by adding anhydrous sodium sulfate and concentrated under reduced pressure. The resultant residue was subjected to silica-gel column chromatography (15% ethyl acetate in hexane) to yield **S3** as a yellow oil (436.5 mg, 34%).

^{1}H NMR (400 MHz, $CDCl_3$) δ 3.71 (t, *J* = 6.4 Hz, 2H), 2.67 (t, *J* = 7.5 Hz, 2H), 2.57 (t, *J* = 6.4 Hz, 2H), 2.37 – 2.33 (m, 2H), 2.32 (s, 3H), 1.96 (s, 1H), 0.89 (s, 9H), 0.06 (s, 6H).

^{13}C NMR (125 MHz, $CDCl_3$) δ 83.1, 69.0, 61.8, 59.3, 56.8, 42.9, 26.1, 18.5, 17.2, -5.2.

HRMS (ESI): $C_{13}H_{27}NOSi$; Calculated mass, $[M+H]^+$ 242.1935; Observed $[M+H]^+$ 242.1956.

2-(but-3-yn-1-yl(methyl)amino)ethan-1-ol (S4)

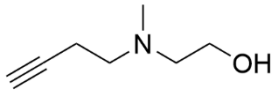

S4

To a round-bottomed flask containing **S3** (800 mg, 3.31 mmol, 1 eq.) in THF (30 mL), tetrabutylammonium fluoride (4.96 mL of a 1 M solution in THF, 4.96 mmol, 1.5 eq.) was added. After stirring the mixture at room temperature for 12 h, the solvent was removed under reduced pressure and the residue was subjected to using silica gel column chromatography (5% methanol in ethyl acetate) to yield **S4** as a yellow liquid (255.0 mg, 61%).

^{1}H NMR (400 MHz, $CDCl_3$) δ 3.58 (t, *J* = 5.2 Hz, 2H), 2.64 (t, *J* = 7.2 Hz, 2H), 2.57 (t, *J* = 5.2 Hz, 2H), 2.38 – 2.34 (m, 2H), 2.30 (s, 3H), 1.98 (t, *J* = 2.4 Hz, 1H).

^{13}C NMR (125 MHz, $CDCl_3$) δ 82.7, 69.4, 58.54, 58.50, 55.9, 41.5, 17.4.

HRMS (ESI): $C_7H_{13}NO$; Calculated mass, $[M+Na]^+$ 150.0889; Observed $[M+Na]^+$ 150.0912.

Propargyl butynyl choline (6)

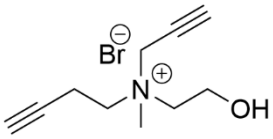

6

To an ice-cold solution of **S4** (255 mg, 2 mmol, 1 eq.) in THF (3 mL), 80% (*w*/*w*) propargyl bromide in toluene (260 µL, 2.4 mmol, 1.2 eq.) was added and the resultant mixture was stirred under ice-cold conditions for 15 min and then at room temperature for 12 h. A brown precipitate was observed to settle down at the bottom of the round-bottomed flask which upon trituration with ice-cold chloroform (15 × 2 mL) followed by drying under vacuum gave **6** as a viscous yellow liquid (406.4 mg, 82.4%).

^{1}H NMR (400 MHz, DMSO-d6) δ 5.39 (t, *J* = 4.8 Hz, 1H), 4.50 (s, 2H), 4.10 (s, 1H), 3.88 – 3.81 (m, 2H), 3.67 – 3.57 (m, 2H), 3.52 – 3.49 (m, 2H), 3.14 (s, 3H), 2.80 (t, *J* = 6.7 Hz, 2H).

^{13}C NMR (100 MHz, DMSO-d6) δ 83.4, 79.3, 74.2, 72.2, 62.9, 59.7, 54.9, 52.7, 48.6, 13.1.

HRMS (ESI): $C_{10}H_{16}NO^{+}$; Calculated mass, $[M]^{+}$ 166.1226; Observed mass $[M]^{+}$ 166.1234.

Scheme 2.6 Synthesis of benzyl propargyl choline **7**

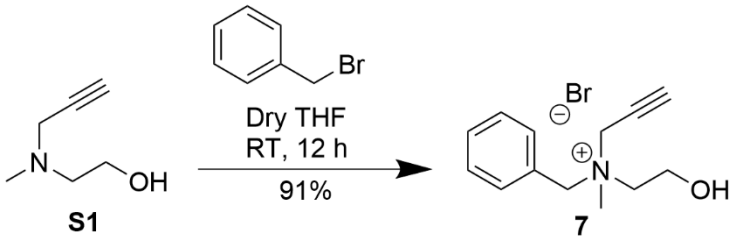

S1 **7**

Benzyl propargyl choline (7)

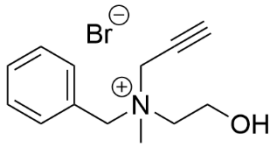

7

A round-bottomed flask charged with **S1** (0.3 g, 2.6 mmol, 1 eq.) was purged with nitrogen gas and anhydrous THF (4 mL) was added. This solution was stirred at 0 °C and 80% (*w*/*w*) propargyl bromide in toluene (1.57 mL, 6.6 mmol, 5.0 eq.) was added dropwise under nitrogen atmosphere. After 15 min, this reaction mixture was warmed to room temperature and stirred for another 24 h.

The resulting white precipitate was filtered, washed with diethyl ether (10 × 5 mL), and dried under reduced pressure to afford **7** as a white solid (91%).

^{1}H NMR (400 MHz, DMSO-d6) δ 7.64 – 7.50 (m, 5H), 5.44 (t, *J* = 4.8 Hz, 1H), 4.70 (q, *J* = 12.8 Hz, 2H), 4.32 (t, *J* = 2.4 Hz, 2H), 4.17 (t, *J* = 2.4 Hz, 1H), 3.96 – 3.92 (m, 2H), 3.50 – 3.43 (m, 2H), 3.06 (s, 3H).

^{13}C NMR (100 MHz, DMSO-d6) δ 133.1, 130.5, 129.1, 127.4, 83.7, 72.6, 65.2, 62.6, 54.7, 51.4, 47.5.

HRMS (ESI): $C_{13}H_{18}NO^{+}$; Calculated mass, $[M]^{+}$ 204.1383; Observed $[M]^{+}$ 204.1390.

Scheme 2.7 Synthesis of diethyl propargyl choline **8**

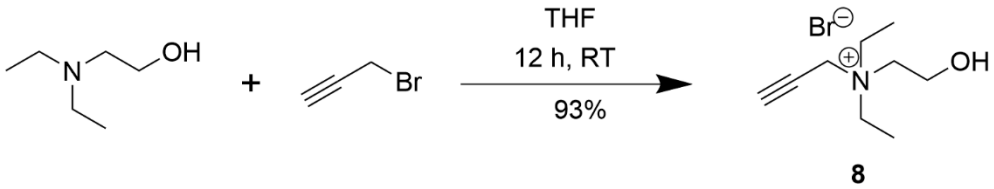

8

Diethyl propargyl choline (8)

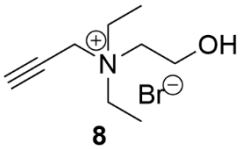

8

To an ice-cold solution of 2-diethylaminoethanol (1.13 mL, 8.55 mmol, 1 eq.) in THF (10 mL), 80% (*w*/*w*) propargyl bromide solution in toluene (0.73 mL, 8.53 mmol, 1 eq.) was added dropwise. The reaction mixture was stirred at 0 °C for 30 min and then at room temperature for 12 h to yield a precipitate. This precipitate was collected, washed with ice-cold THF (10 × 10 mL) and then vacuum dried to yield **8** as a dirty-white solid (1.24 g, 93%).

^{1}H NMR (400 MHz, DMSO-d6) δ 5.34 (t, *J* = 5.2 Hz, 1H), 4.41 (d, *J* = 2.4 Hz, 2H), 4.03 (t, *J* = 2.8 Hz, 1H), 3.84 – 3.80 (m, 2H), 3.46 – 3.38 (m, 6H), 1.24 (t, *J* = 7.2 Hz, 6H).

^{13}C NMR (100 MHz, DMSO-d6) δ 82.5, 72.2, 59.0, 54.5, 48.6, 7.6.

HRMS (ESI): $C_{9}H_{18}NO^{+}$, Calculated mass, $[M]^{+}$ 156.1383; Observed mass, $[M]^{+}$ 156.1398.

Scheme 2.8 Synthesis of tripropargyl choline **9**

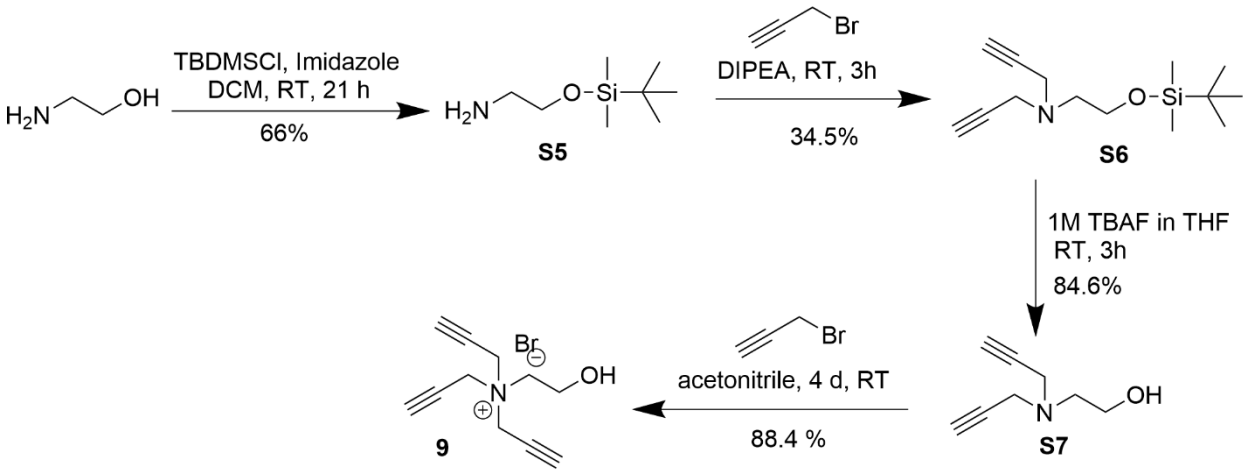

2-((*t*-butyldimethylsilyl)oxy)ethan-1-amine (S5)

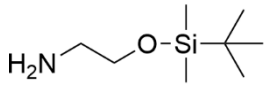

S5

To a solution of aminoethanol (4.8 mL, 240 mmol, 1 eq.) in dichloromethane (120 mL), imidazole (17.99 g, 264 mmol, 1.1 eq.) was added. Nitrogen gas was bubbled into this mixture for 30 min and subsequently, the solution was stirred under ice-cold conditions for 15 min. A solution of *t*-butyldimethylsilylchoride (39.78 g, 264 mmol, 1.1 eq.) in dichloromethane (120 mL) was prepared and was also subjected to nitrogen gas treatment as described above. This solution was transferred into the flask containing aminoethanol and imidazole in dichloromethane by using a gas-tight syringe. The resultant turbid mixture was stirred at room temperature for 21 h following which it was washed with water (250 mL). Subsequently, the organic layer was dried by adding anhydrous sodium sulfate, and vacuum dried to afford **S5** as a yellow liquid (15.72 g, 65.6%).

^{1}H NMR (500 MHz, $CDCl_3$) δ 3.65 (t, *J* = 5.25 Hz, 2H), 2.94 (s, 2H), 2.81 (t, *J* = 5.25 Hz, 2H), 0.89 (s, 9H), 0.06 (s, 6H).

^{13}C NMR (125 MHz, $CDCl_3$) δ 64.5, 44.1, 26.1, 18.5, -5.2.

HRMS (ESI): $C_8H_{21}NOSi$, Calculated mass, $[M+H]^+$ 176.1465; Observed mass, $[M+H]^+$ 176.1470.

***N*-(2-((*t*-butyldimethylsilyl)oxy)ethyl)-*N*-(prop-2-yn-1-yl)prop-2-yn-1-amine (S6)**

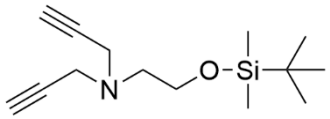

S6

To a round-bottomed flask containing **S5** (7.6 g, 40.8 mmol, 1 eq.) dissolved in dichloromethane (50 mL), *N*,*N*-diisopropylethylamine (4.3 mL, 24.5 mmol, 0.6 eq.) was added and the flask was cooled to 0 °C. To this mixture, a solution of 80% *w*/*w* propargyl bromide in toluene (2.64 mL, 24.5 mmol, 0.6 eq.) in dichloromethane (30 mL) was added dropwise and the resultant mixture was stirred at 0 °C for 30 min and then allowed to warm up to room temperature and stirred for 4 h. The orange solution thus obtained was washed with saturated sodium bicarbonate solution (2 × 80 mL), dried by adding anhydrous sodium sulfate, concentrated under reduced pressure and the residue was subjected to silica gel column chromatography (10% ethyl acetate in hexane) to yield **S6** as a yellow liquid (6.16 g, 34.5%).

^{1}H NMR (500 MHz, $CDCl_3$) δ 3.75 (t, *J* = 6.05 Hz, 2H), 3.50 (d, *J* = 2.3 Hz, 4H), 2.70 (t, *J* = 6.05 Hz, 2H), 2.21 (t, *J* = 2.3 Hz, 2H), 0.89 (s, 9H), 0.06 (s, 6H).

^{13}C NMR (125 MHz, $CDCl_3$) δ 79.2, 73.0, 62.4, 55.2, 43.2, 26.1, 18.4, -5.2.

HRMS (ESI): $C_{14}H_{25}NOSi$, Calculated mass, $[M+H]^+$ 252.1778; Observed mass, $[M+H]^+$ 252.1795.

2-(di(prop-2-yn-1-yl)amino)ethan-1-ol (S7)

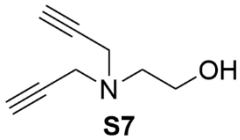

S7

To a solution of **S6** (541.1 mg, 2.15 mmol, 1 eq.) in THF (45 mL), tetrabutylammonium fluoride (3.4 mL of a 1 M solution in THF, 3.4 mmol, 1.5 eq.) was added and the resultant orange-colored reaction mixture was stirred at room temperature for 3 h. After removing the solvent under reduced pressure, the residue was subjected to using silica gel column chromatography (5% methanol in ethyl acetate) to yield **S7** as a yellow liquid (250 mg, 84.6%).

^{1}H NMR (500 MHz, $CDCl_3$) δ 3.64 (t, *J* = 5.25 Hz, 2H), 3.47 (d, *J* = 2.3 Hz, 4H), 2.74 (t, *J* = 5.2 Hz, 2H), 2.24 (t, *J* = 2.25 Hz, 2H).

^{13}C NMR (125 MHz, $CDCl_3$) δ 78.7, 73.4, 58.8, 54.6, 42.3.

HRMS (ESI): $C_8H_{11}NO$; Calculated mass, $[M+Na]^+$ 160.0733 ; Observed $[M+Na]^+$ 160.0753.

Tripropargyl choline (9)

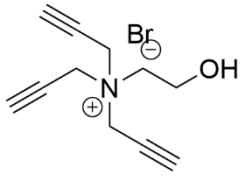

9

To an ice-cold solution of **S7** (180.2 mg, 1.31 mmol, 1 eq.) in acetonitrile (3 mL), 80% *w/w* solution of propargyl bromide in toluene (0.42 mL, 3.93 mmol, 3 eq.) was added dropwise. Stirring this mixture for 4 d at room temperature yielded a white precipitate that was collected and triturated with ice-cold chloroform (10 × 5 mL) which upon drying under reduced pressure gave compound **9** as a white solid (507 mg, 88.4%).

^{1}H NMR (500 MHz, DMSO-d6) δ 5.48 (t, *J* = 4.95 Hz, 1H), 4.54 (d, *J* = 2.35 Hz, 6H), 4.16 (t, *J* = 2.3 Hz, 3H), 3.93 – 3.90 (m, 2H), 3.61 (t, *J* = 4.95 Hz, 2H).

^{13}C NMR (125 MHz, DMSO-d6) δ 84.1, 71.3, 61.2, 54.6, 50.6.

HRMS (ESI): $C_{11}H_{14}NO^+$; Calculated mass, $[M]^+$ 176.1070; Observed $[M]^+$ 176.1084.

Scheme 2.9 Synthesis of rhodamine alkyne **S9**

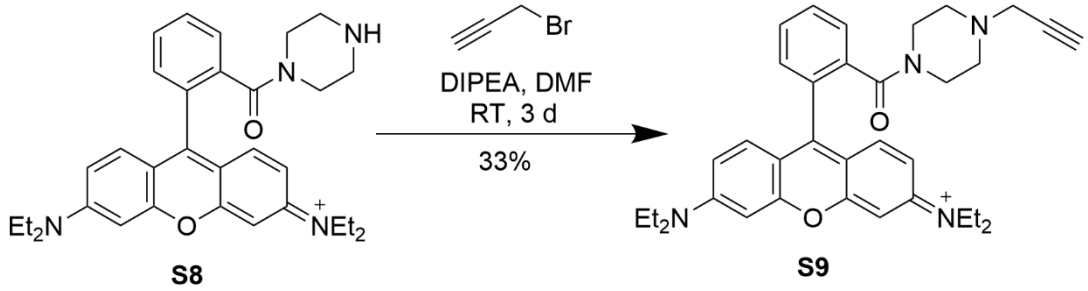

Rhodamine alkyne (S9)

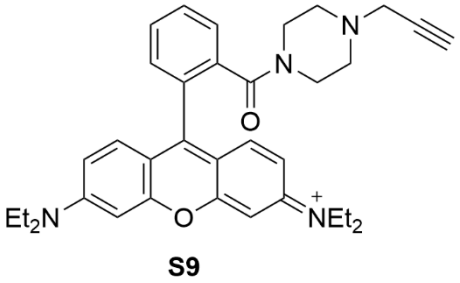

Rhodamine B piperazine amide (**S8)** was synthesized according to a previously reported method.[9] To an Al-foil wrapped round-bottomed flask charged with **S8** (100 mg, 0.18 mmol, 1 eq.) in DMF (1 mL), a solution of 80% *w/w* propargyl bromide in toluene (75 µL, 0.69 mmol, 3.75 eq.) and *N*,*N*-diisopropylethylamine (47 µL, 0.27 mmol, 1.5 eq.) in DMF (1 mL) was added dropwise and the mixture was stirred at room temperature for 3 d. Subsequently, the solvent was removed under reduced pressure and the concentrated residue was dissolved in ethyl acetate (50 mL) and washed with saturated sodium bicarbonate solution (1 × 50 mL). The aqueous layer was washed with ethyl acetate (3 × 50 mL) and 1:3 *v/v* solution of isopropanol and dichloromethane (15 × 50 mL). The organic layers were combined, dried by adding anhydrous sodium sulfate and concentrated under reduced pressure. The residue was subjected to silica gel column chromatography (10% methanol in dichloromethane) to afford 35.1 mg of **S9** as a deep purple solid (33%).

^{1}H NMR (400 MHz, $CDCl_3$) δ 7.69 – 7.67 (m, 2H), 7.56 – 7.54 (m, 1H), 7.38 – 7.35 (m, 1H), 7.28 (s, 1H), 7.27 (s, 1H), 7.01 – 6.98 (m, 2H), 6.84 (d, *J* = 2.4 Hz, 2H), 3.70 – 3.6 (m, 8H), 3.45 – 3.35 (m, 4H), 3.25 (d, *J* = 2.4 Hz, 2H), 2.38 – 2.35 (m, 4H), 2.26 (t, *J* = 2.4 Hz, 1H), 1.34 (t, *J* = 7.2 Hz, 12H).

^{13}C NMR (100 MHz, $CDCl_3$) δ 167.6, 157.9, 155.8, 135.6, 132.3, 130.4, 130.3, 130.1, 127.8,

114.3, 113.9, 96.6, 74.0, 51.7, 51.1, 47.5, 46.7, 46.3, 41.7, 12.81.

HRMS (ESI): $C_{35}H_{41}N_4O_2^+$; Calculated mass, $[M]^+$ 549.3224; Observed mass, $[M+H]^+$ 549.3249.

5-Azidofluorescein (S10)

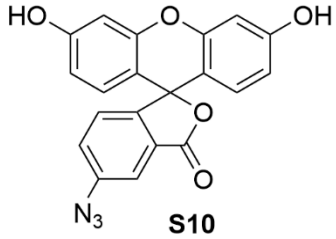

S10

5-Azidofluorescein (**S10**) was synthesized according to a previously reported method.[10]

2.4.4 General procedure for cell culture

HEK293 cells were cultured in DMEM medium supplemented with 10% FBS, 100 units/mL penicillin, and 100 µg/mL streptomycin (complete media) in a humidified CO_2 incubator maintaining 5% CO_2 levels and a temperature of 37 °C. All the treatments and incubations of HEK293 cells performed in a CO_2 incubator were done in an incubator maintaining 5% CO_2 levels, and a temperature of 37 °C.

2.4.5 Procedure for the characterization of metabolic labeling by cellular imaging

(i) *Imaging metabolically labeled choline lipids*: 0.2 million HEK293 cells were seeded in 1 mL of complete media in a 24-well plate. After a 12 h incubation in a CO_2 incubator, 10 µL of 200 mM stock solutions of choline analogs in PBS were administered into each well (final concentration: 2 mM). The same volume of PBS devoid of choline analogs was added in the control wells. After a further 24 h incubation in a CO_2 incubator, cells were washed with PBS (2 × 500 µL) at room temperature and fixed by incubating them in formaldehyde (250 µL of a 3.7% *w/v* solution in PBS) for 2 h at 4 °C. The fixed cells were washed with TBS (2 × 500 µL) and then incubated in a click reaction cocktail (250 µL) for 30 min at room temperature under dark. The click reaction cocktail was made in 0.1 M Tris-HCl buffer at pH 8.5 and contained 1 mM $CuSO_4.5H_2O$ (added from a stock of 500 mM in water), 100 mM L-ascorbic acid (added from a stock of 500 mM in water) and 20 µM 5-azidofluorescein (added from a stock of 10 mM in DMSO) for imaging alkynyl choline analogs or 20 µM rhodamine alkyne (added from a stock of 1.25 mM

in DMSO) for imaging cells treated with azido choline analogs. After completion of this 30 min-long incubation, the cells were washed with TBS (1 × 500 µL), 0.5 M NaCl (1 × 500 µL) and then again with TBS (1 × 500 µL). Finally, 250 µL TBS was added to each well and the cells were imaged using the EVOS-M7000 cell imaging system. All images were acquired by using a 40× objective either under the GFP channel (for analogs **1**, **3**-**9**) or the RFP channel (for analog **2**) and the representative images are provided in Figures 2.4-2.12 (for analogs **1**-**9**). Each experiment was performed three times by administering the cells with the aforementioned choline analogs into three separate wells and performing the imaging experiment as described above.

(ii) *Choline competition*: 0.2 million HEK293 cells were seeded in 1 mL of complete media in a 24-well plate. After 12 h of incubation in a CO_2 incubator, choline chloride (10 µL of a 200 mM solution in PBS) and the choline analog (10 µL of a 200 mM solution in PBS) were added. After a further 24 h incubation in a CO_2 incubator, cells were treated in the same way as mentioned in section 2.4.5 (i) for cellular imaging. All images were acquired by illuminating the cells with the same exposure that was used to acquire images for the corresponding choline analog treatments without any co-administration with choline. Each experiment was performed in triplicate.

2.4.6 Procedure for the characterization of metabolic labeling by lipidomics

(i) *Extraction of lipids from HEK293 cells*: For all lipidomics experiments, 3 million cells in 10 mL of complete medium were seeded into two 10 cm sterile culture dishes (for each treatment) and incubated for 24 h in a CO_2 incubator. Subsequently, 317 µL of 65 mM solutions of choline analogs in PBS (final concentration of each analog in each flask was 2 mM) were administered and after a 24 h-long incubation in a CO_2 incubator, the adhered cells were washed with ice-cold PBS (2 × 5 mL), resuspended in ice-cold PBS (5 mL), pooled in a centrifuge tube and centrifuged at 1,000 *g* for 5 min at room temperature. The supernatant was then aspirated off and the lipids were extracted from the resultant pellet by using modified Bligh Dyer method.[5] Briefly, the cell pellet was treated with a mixture of chloroform and methanol (1 mL of a 1:2 *v*/*v* solution), vortexed for 1 min, followed by addition of chloroform (0.5 mL) and 1 M NaCl (0.5 mL), and again vortexed for 1 min. Phase separation was achieved by centrifuging the mixture at 3,220 *g* at room temperature for 30 min. The lower lipid-enriched organic layer was separated and dried using a benchtop vacuum concentrator at room temperature. For compound parameter optimization via

direct infusion method, the dried lipid samples were redissolved in chloroform (1 mL) and 40 µL of this lipid stock solution was added to a mixture of chloroform/methanol/300 mM ammonium acetate in water such that the final composition was 300/665/35 (*v*/*v*/*v*) and the final volume of the lipid mixture was 1.2 mL. For all LC-MS/MS analysis, the dried lipids were dissolved in a mixture of chloroform and methanol (200 µL of a 1:1 *v*/*v* solution). For all control experiments, the procedure described above was followed without administration of any choline derivatives.

(ii) HPLC method details: Lipids extracted from cells were fractionated on a 2.6 µm Kinetex HILIC column (I.D. 100 × 2.1 mm, 100 Å, Phenomenex). TICs were generated using the PIS modes for various non-natural choline head groups (see Figure 2.3 for an explanation of the PIS mode) on the HILIC column using a binary gradient. The elution protocol used is summarized below:

Mobile Phase A: 95:5 Acetonitrile: Water (both acetonitrile and water contained 10 mM ammonium acetate)

Mobile Phase B: 1:1 Acetonitrile: Water (both acetonitrile and water contained 10 mM ammonium acetate)

Gradient:

0 to 1 min: 100% A

1 to 5 min: 100% A to 90% A

5 to 13 min: 90% A to 70% A

13 to 25 min: 70% A to 100% A

25 min to 39 min: 100% A (for column re-equilibration)

Flow rate: 0.5 mL/min

Column oven temperature: 40 °C

Sample volume: 10 µL of lipid solution extracted from cells.

(iii) *Mass-spectrometry details*: Lipids eluted from the HILIC column were analyzed and detected on an AB Sciex 4500 QTRAP mass spectrometer equipped with an ESI source heated to 400 °C. The scan speed was maintained at 200 Da/sec. The electrospray capillary was held at +5500 volts, curtain gas was set at 35 (arbitrary units), CAD gas was maintained at the medium level and the two ion source gases GS1 and GS2 were set at 50 and 60 (arbitrary units) respectively. The PIS mode (schematically described in Figure 2.3) was used for detecting all the non-natural or native choline lipids to generate the TICs and all TICs depicted in the Figures 2.4-2.12 are representative of at least three biological replicates. The TIC peaks were processed on the Analyst software to generate the XICs. The compound parameters (declustering potential, entrance potential, collision energy, and collision cell exit potential) were optimized by ramping each of them against the intensity by the direct infusion method. Native choline lipids were detected by employing a PIS of 184.1 Da (*m/z* for phosphocholine) and the compound parameters were optimized separately. For characterizing metabolic labeling with alkynyl/azido-substituted choline analogs **1**-**9**, the PIS masses of their corresponding phosphoryl derivatives, and the optimized compound parameters for the PIS of 184.1 Da (*m/z* for phosphocholine) were used. Each TIC was background-subtracted with the corresponding blank chromatogram. The details of compound parameters for the detection of metabolic incorporation of each analog using PIS mode are listed in Table 2.1 below.

Table 2.1. Compound parameters used for the PIS of lipids labeled with the choline analogs **1**-**9**

S. No.	Head group	PIS mode mass (Da)	Declustering Potential (volts)	Entrance Potential (volts)	Collision Energy (volts)	Collision cell Exit Potential (volts)
For native and alkynl/azido-substituted choline lipids						
1.	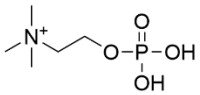 phosphocholine (native lipids)	184.1	110.0	7.8	30.9	5.2
2.	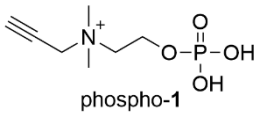 phospho-**1**	208.1				

3.	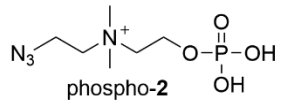 phospho-**2**	239.1	110.0	7.8	30.9	5.2
4.	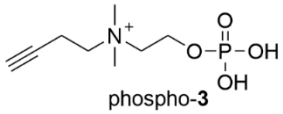 phospho-**3**	222.1				
5.	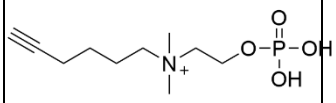 phospho-**4**	250.1				
6.	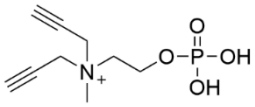 phospho-**5**	232.1				
7.	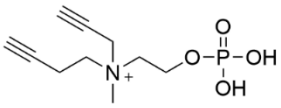 phospho-**6**	246.1				
8.	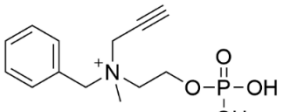 phospho- **7**	284.1				
9.	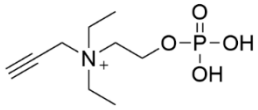 phospho-**8**	236.1				
10.	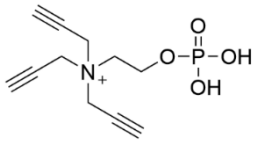 phospho-**9**	256.1				

(iv) *Identification of non-natural lipids using the LipidView software*: To identify the choline lipids labeled with non-natural headgroups **1-9**, the corresponding XIC was processed using the LipidView (AB Sciex, version 1.2) software[11] by manually modifying its database. Peaks were corrected for isotopic overlap and were processed by setting a mass tolerance of 0.5 Da, with a

minimum intensity of 0.1% and a minimum signal-to-noise ratio of 10.[12, 13] The subsequent phospholipid species were then verified by Lipid Maps structure database (LMSD)[14] and the ones absent from this platform were excluded from the analysis. Each PC lipid is annotated by using two numbers; for example, 34:2 where 34 is the sum of carbon atoms in the two fatty acyl chains and 2 is the total number of double bonds present in the two fatty acyl chains of the corresponding PC lipid. Each SM lipid species is annotated by using three numbers; for example, 40:1;2 where 40 is the sum of the carbon atoms in sphingosine back bone and the fatty acyl chain, 1 is the total number of double bond(s) present in the sphingosine backbone and the fatty acyl chain, and 2 is the sum of the hydroxyl groups present on the sphingosine backbone including the phosphorylated hydroxyl group at C-1 position of the sphingosine backbone.

2.5 ^{1}H and ^{13}C-NMR Spectra for the Synthetic Procedures of Analogs 1-9

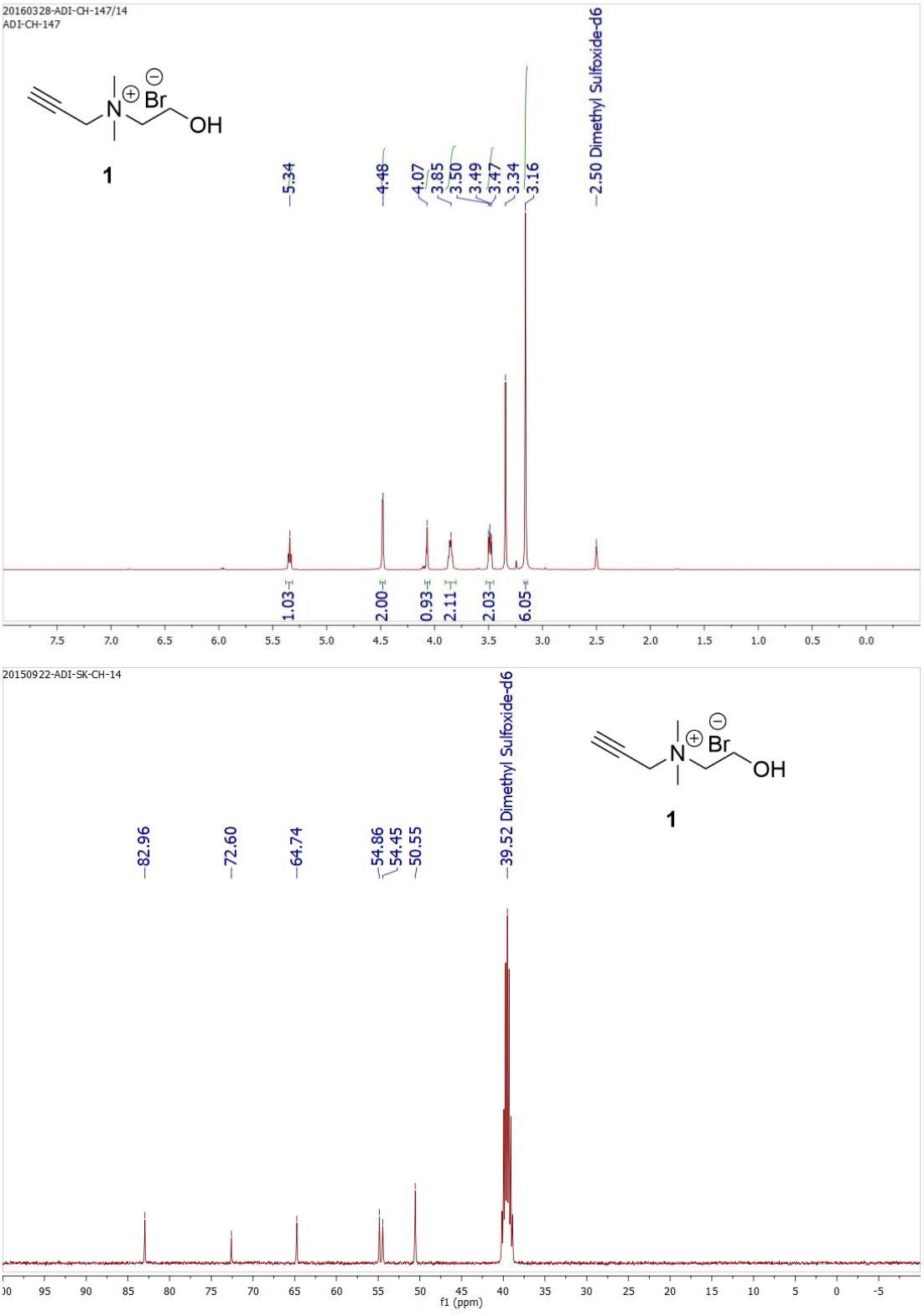

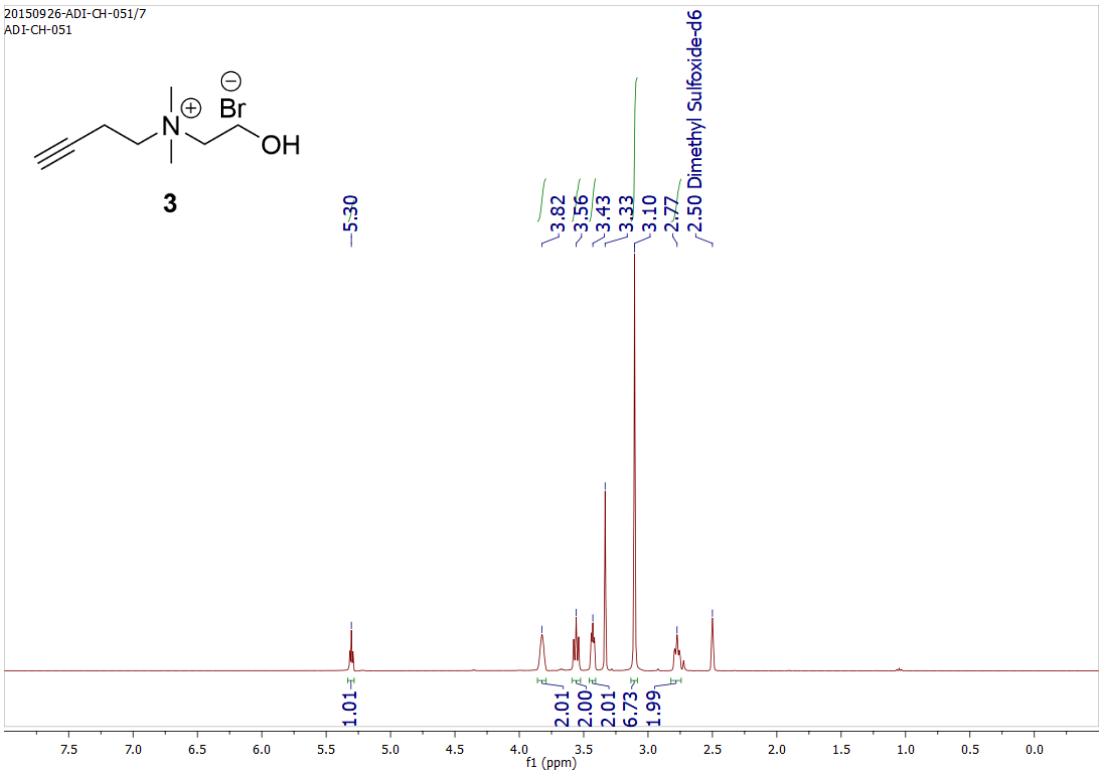
20150926-ADI-CH-051/7
ADI-CH-051
Br
OH
3
5.30
3.82
3.56
3.43
3.33
3.10
2.77
2.50 Dimethyl Sulfoxide-d6
1.01
2.01
2.00
2.01
6.73
1.99
f1 (ppm)

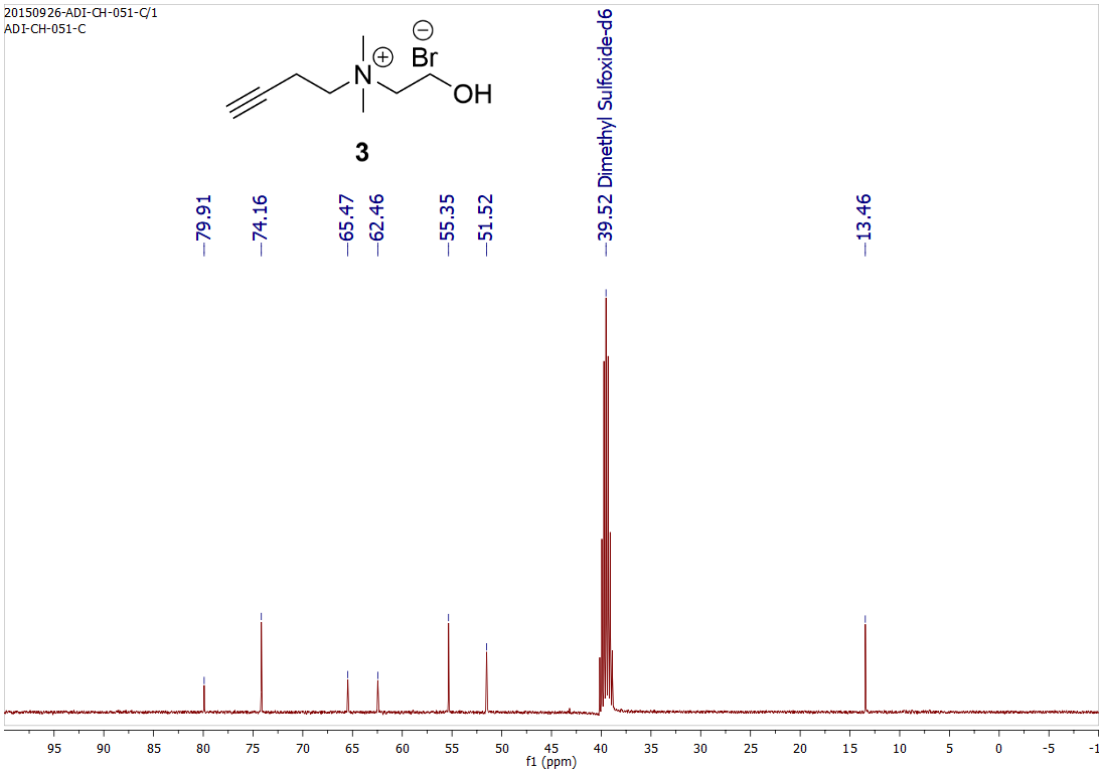
20150926-ADI-CH-051-C/1
ADI-CH-051-C
Br
OH
3
79.91
74.16
65.47
62.46
55.35
51.52
39.52 Dimethyl Sulfoxide-d6
13.46
f1 (ppm)

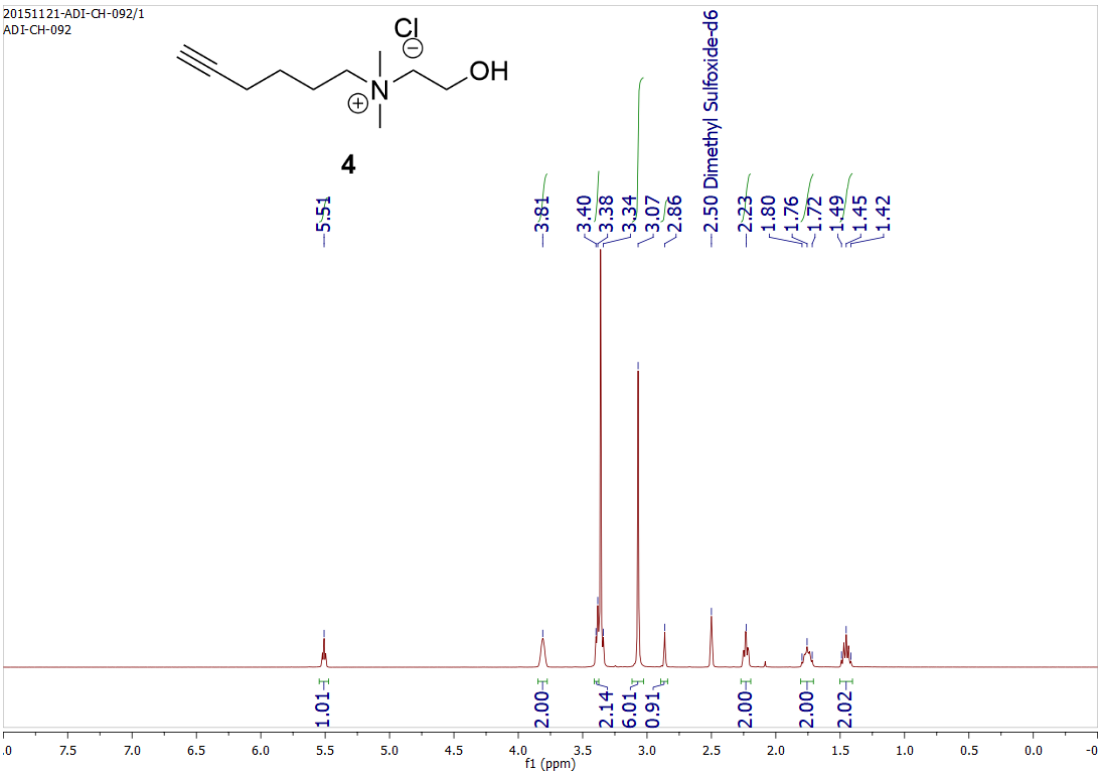
20151121-ADI-CH-092/1
ADI-CH-092
Cl
OH
N
4
5.51
3.81
3.40
3.38
3.34
3.07
2.86
2.50 Dimethyl Sulfoxide-d6
2.23
1.80
1.76
1.72
1.49
1.45
1.42
1.01
2.00
2.14
6.01
0.91
2.00
2.00
2.02
f1 (ppm)

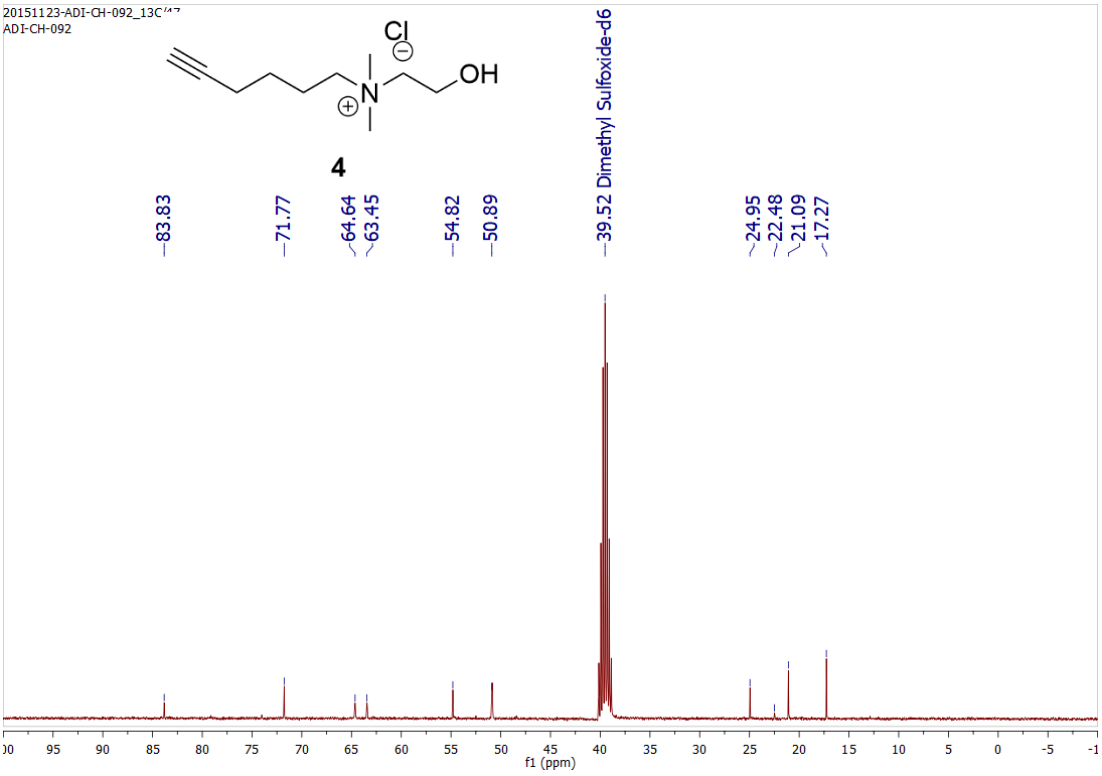
20151123-ADI-CH-092_13C
ADI-CH-092
Cl
OH
N
4
83.83
71.77
64.64
63.45
54.82
50.89
39.52 Dimethyl Sulfoxide-d6
24.95
22.48
21.09
17.27
f1 (ppm)

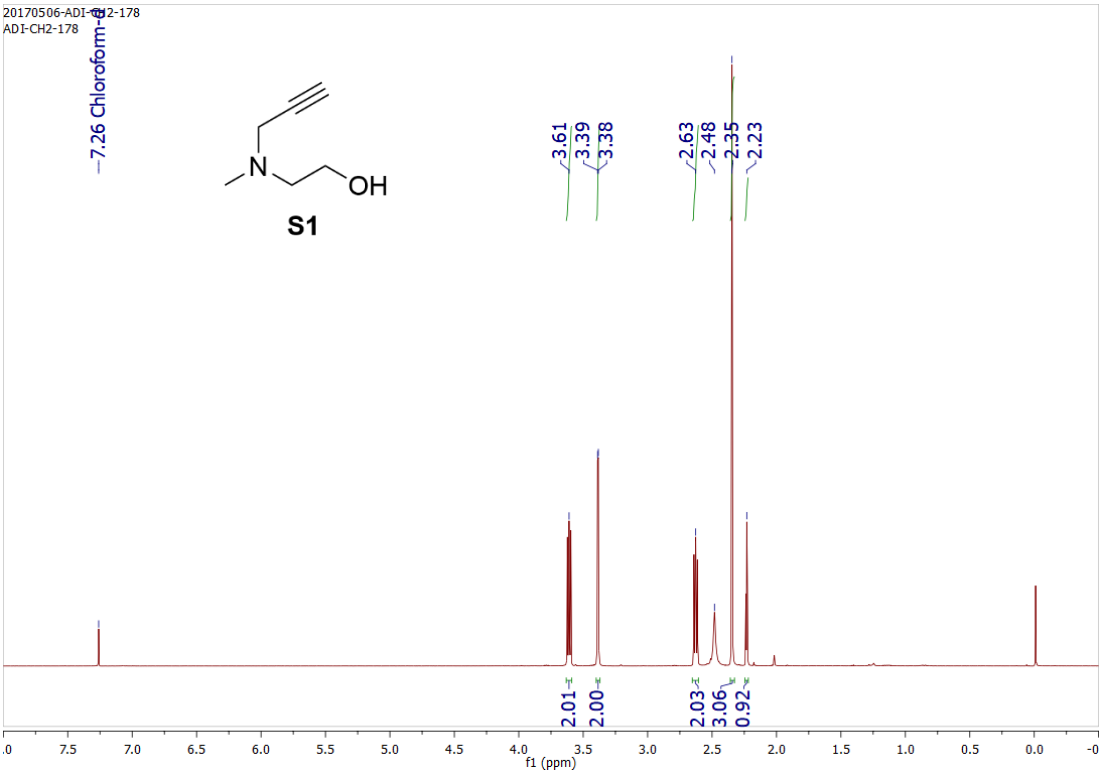
20170506-ADI-CH2-178
ADI-CH2-178
7.26 Chloroform-d
N
OH
S1
3.61
3.39
3.38
2.63
2.48
2.35
2.23
2.01
2.00
2.03
3.06
0.92
f1 (ppm)

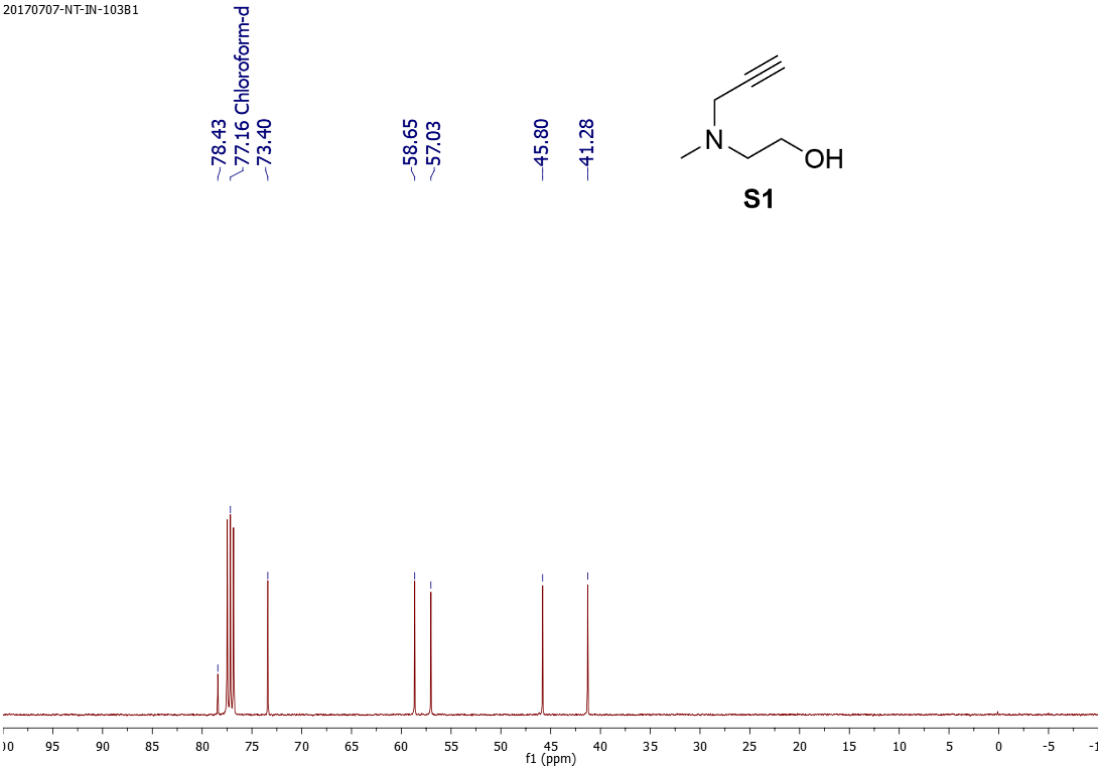
20170707-NT-IN-103B1
78.43
77.16 Chloroform-d
73.40
58.65
57.03
45.80
41.28
N
OH
S1
f1 (ppm)

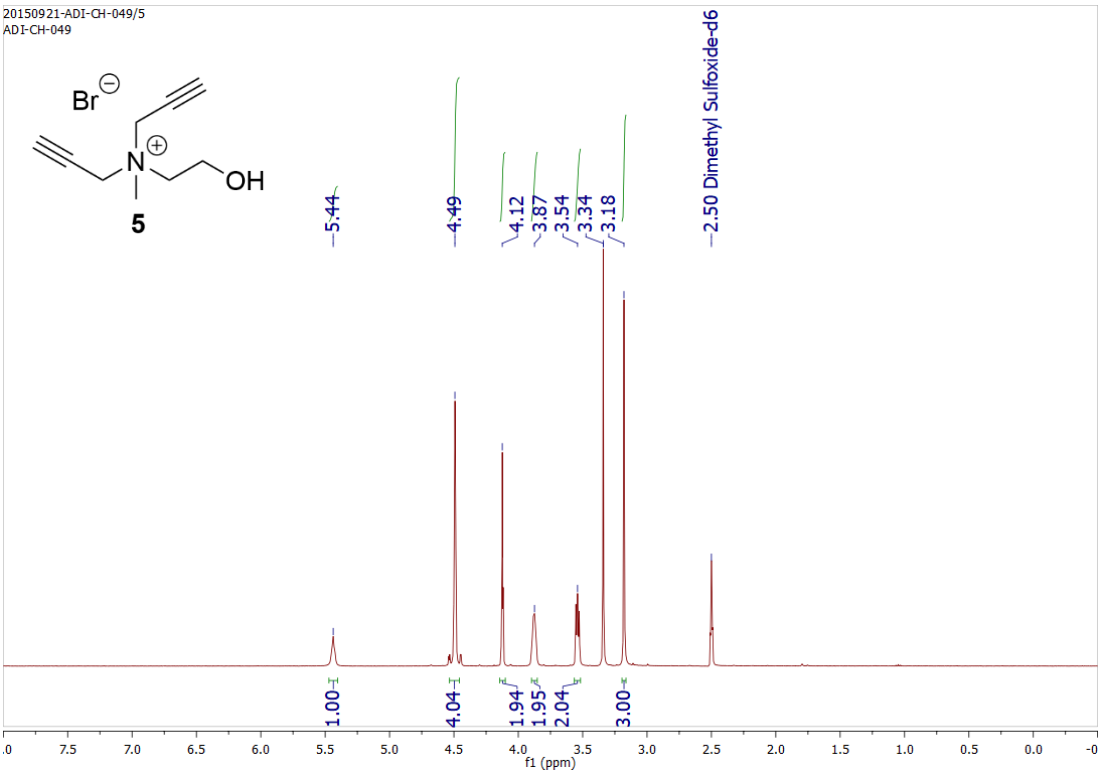
20150921-ADI-CH-049/5
ADI-CH-049
Br
N
OH
5
5.44
4.49
4.12
3.87
3.54
3.34
3.18
2.50 Dimethyl Sulfoxide-d6
1.00
4.04
1.94
1.95
2.04
3.00
f1 (ppm)

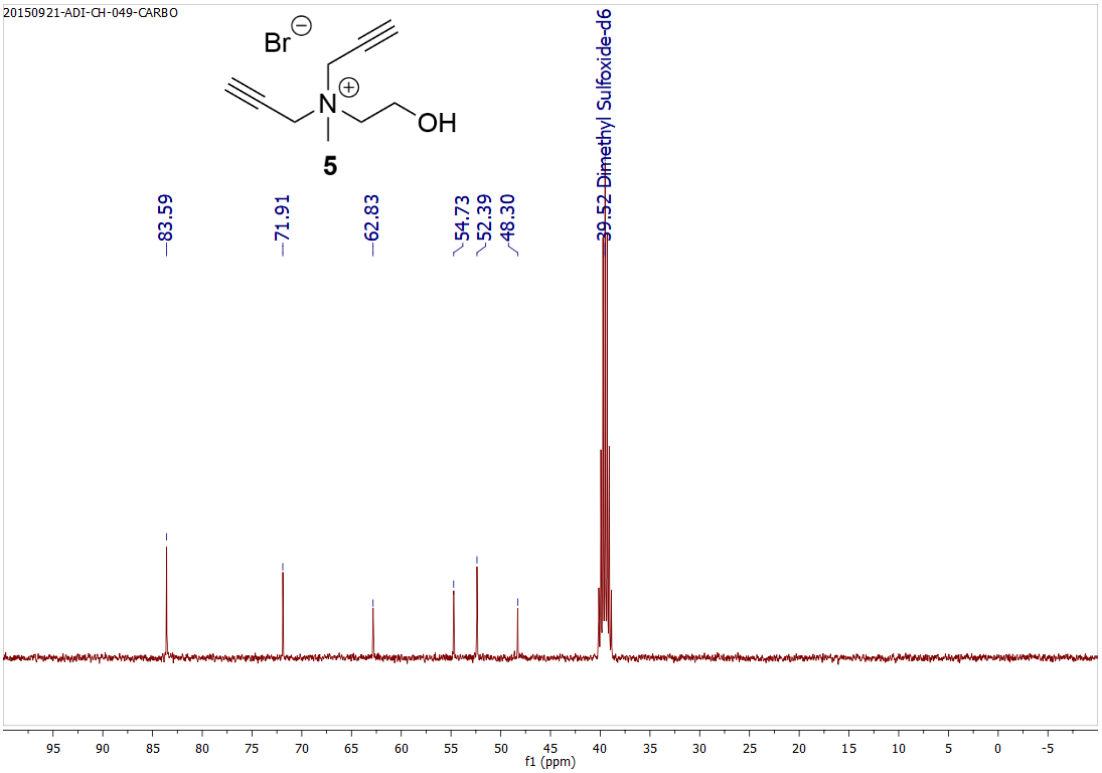
20150921-ADI-CH-049-CARBO
Br
N
OH
5
83.59
71.91
62.83
54.73
52.39
48.30
39.52 Dimethyl Sulfoxide-d6
f1 (ppm)

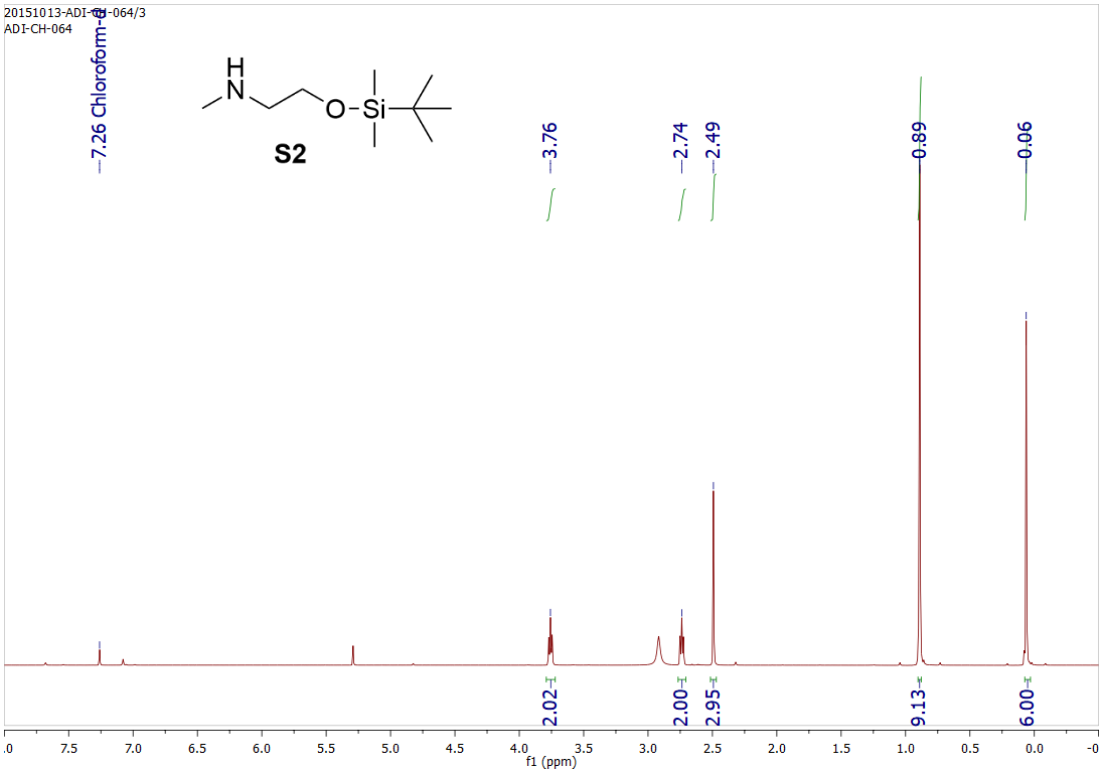
20151013-ADI-CH-064/3
ADI-CH-064
7.26 Chloroform-d
3.76
2.74
2.49
0.89
0.06
S2
2.02
2.00
2.95
9.13
6.00
f1 (ppm)

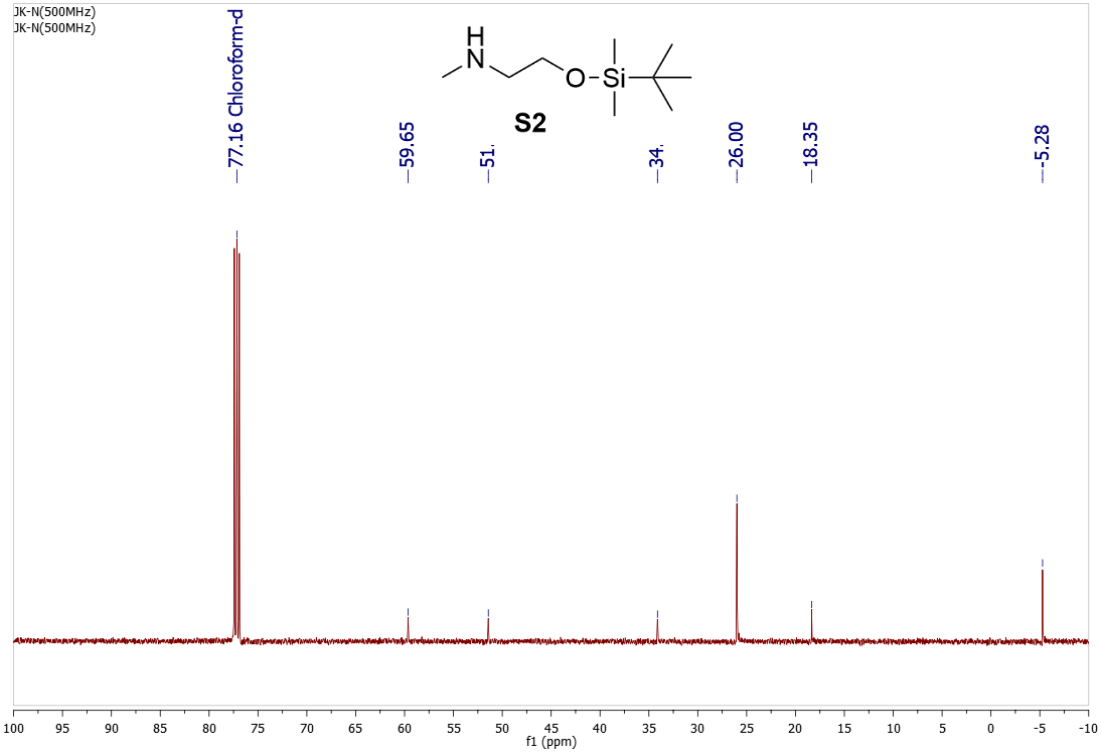
JK-N(500MHz)
JK-N(500MHz)
77.16 Chloroform-d
59.65
51.
34.
26.00
18.35
-5.28
S2
f1 (ppm)

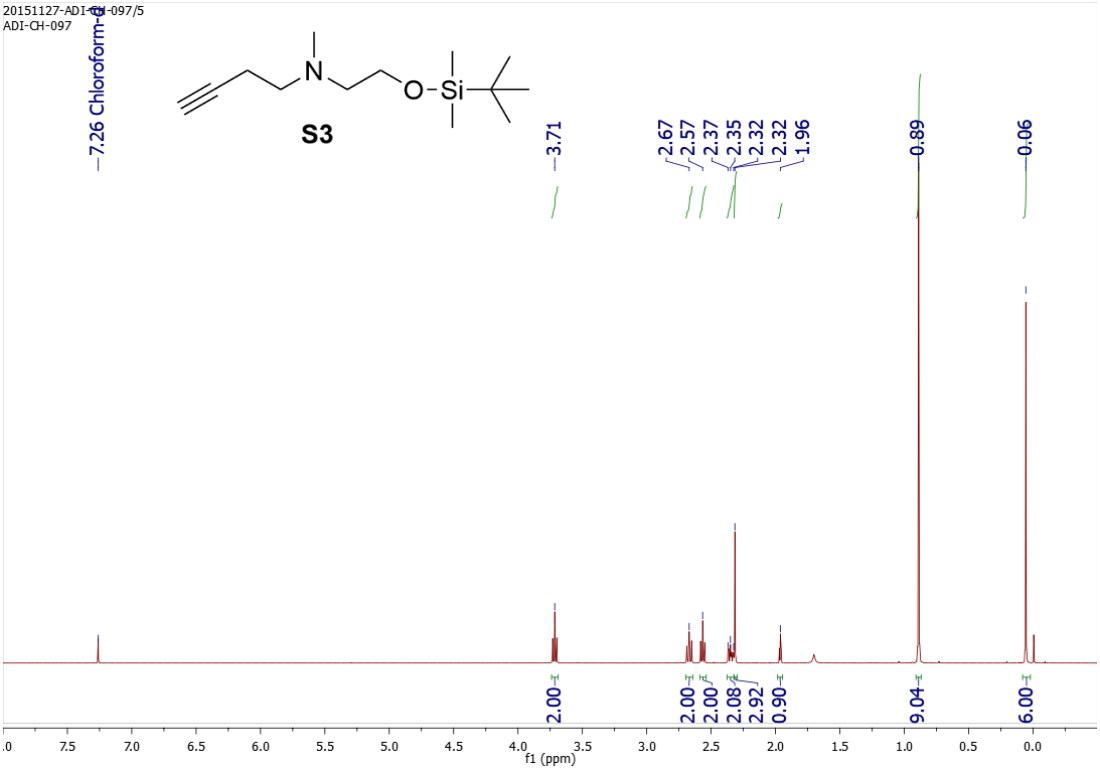
20151127-ADI-CH-097/5
ADI-CH-097
7.26 Chloroform-d
3.71
2.67
2.57
2.37
2.35
2.32
2.32
1.96
0.89
0.06
S3
2.00
2.00
2.00
2.08
2.92
0.90
9.04
6.00
f1 (ppm)

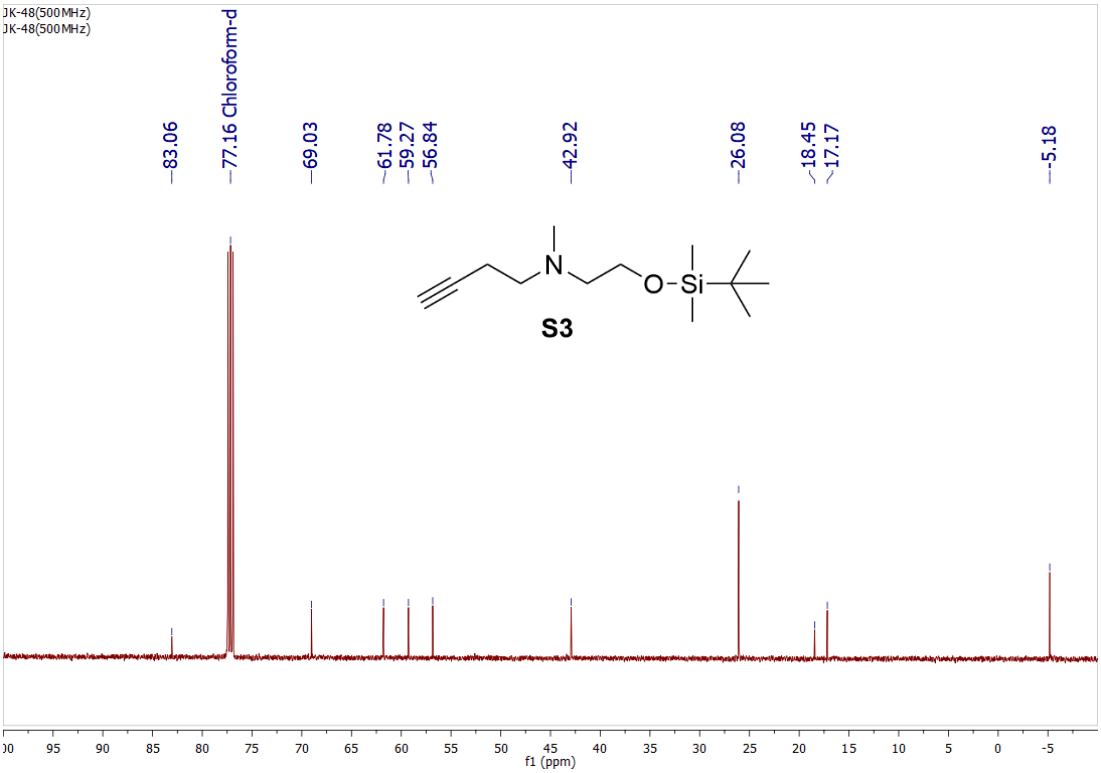
JK-48(500MHz)
JK-48(500MHz)
83.06
77.16 Chloroform-d
69.03
61.78
59.27
56.84
42.92
26.08
18.45
17.17
-5.18
S3
f1 (ppm)

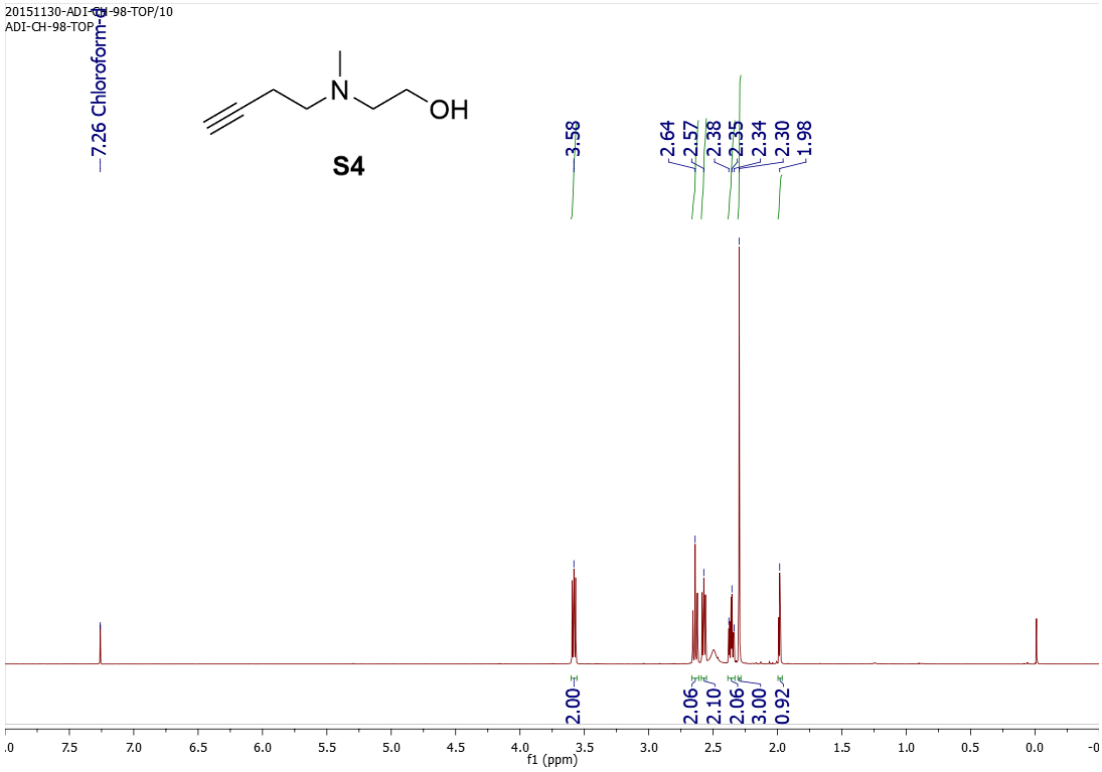
20151130-ADI-CH-98-TOP/10
ADI-CH-98-TOP
7.26 Chloroform-d
3.58
2.64
2.57
2.38
2.35
2.34
2.30
1.98
2.00
2.06
2.10
2.06
3.00
0.92
f1 (ppm)
S4

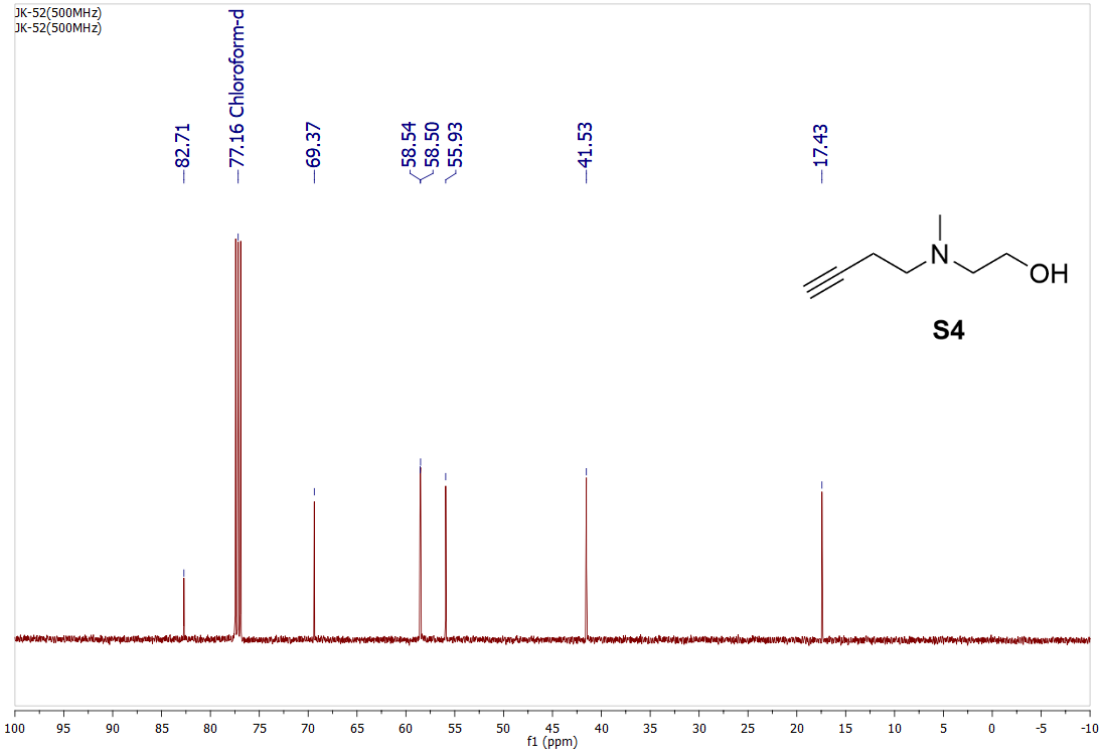
JK-52(500MHz)
JK-52(500MHz)
82.71
77.16 Chloroform-d
69.37
58.54
58.50
55.93
41.53
17.43
f1 (ppm)
S4

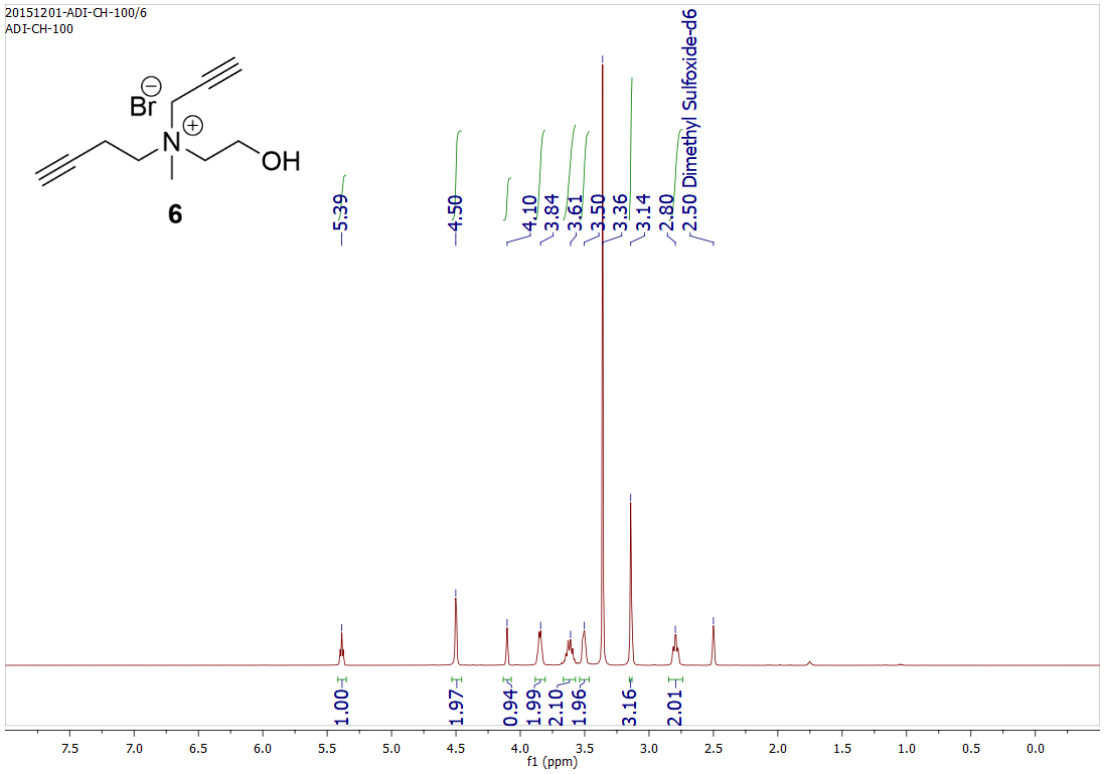
20151201-ADI-CH-100/6
ADI-CH-100
Br
N
OH
6
5.39
4.50
4.10
3.84
3.61
3.50
3.36
3.14
2.80
2.50 Dimethyl Sulfoxide-d6
1.00
1.97
0.94
1.99
2.10
1.96
3.16
2.01
f1 (ppm)

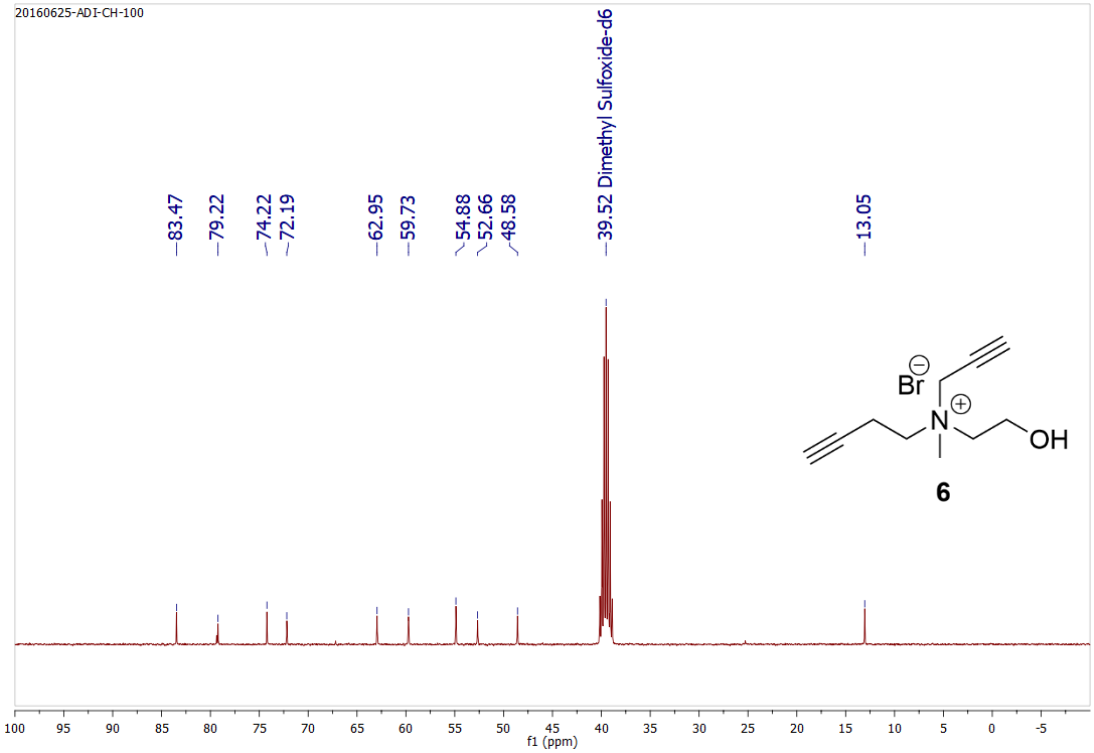
20160625-ADI-CH-100
83.47
79.22
74.22
72.19
62.95
59.73
54.88
52.66
48.58
39.52 Dimethyl Sulfoxide-d6
13.05
Br
N
OH
6
f1 (ppm)

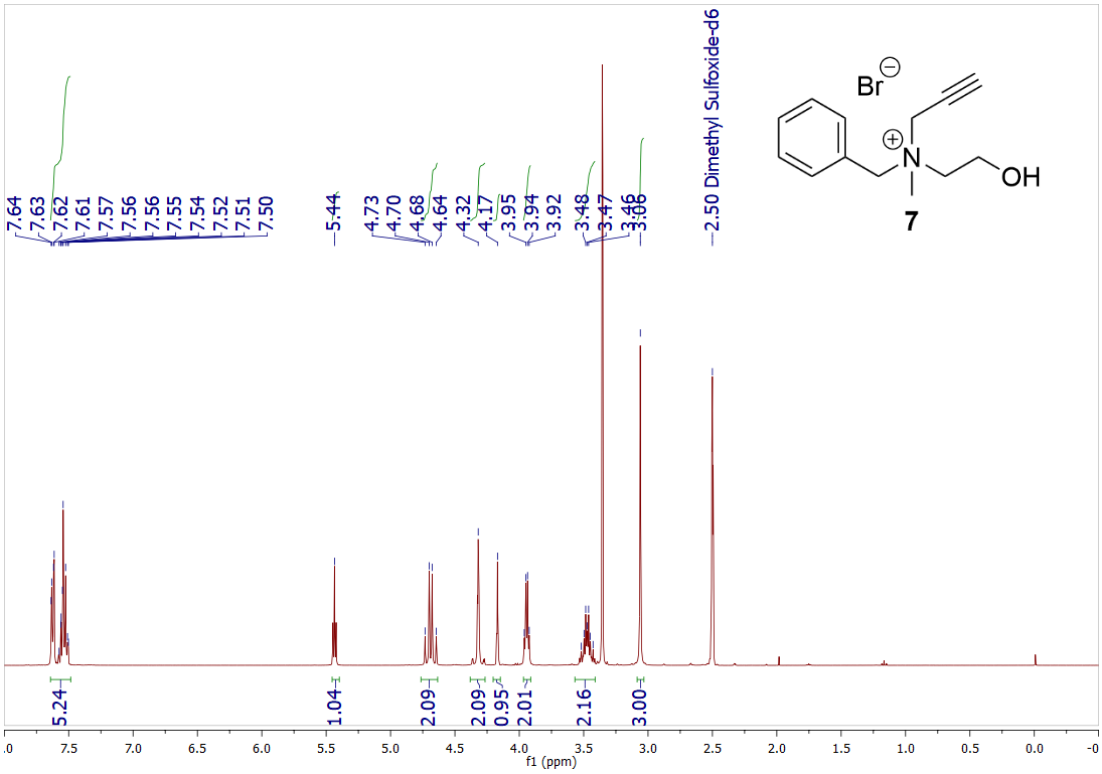
7.64
7.63
7.62
7.61
7.57
7.56
7.56
7.55
7.54
7.52
7.51
7.50
5.44
4.73
4.70
4.68
4.64
4.32
4.17
3.95
3.94
3.92
3.48
3.47
3.46
3.08
2.50 Dimethyl Sulfoxide-d6
Br
N
OH
7
5.24
1.04
2.09
2.09
0.95
2.01
2.16
3.00
f1 (ppm)

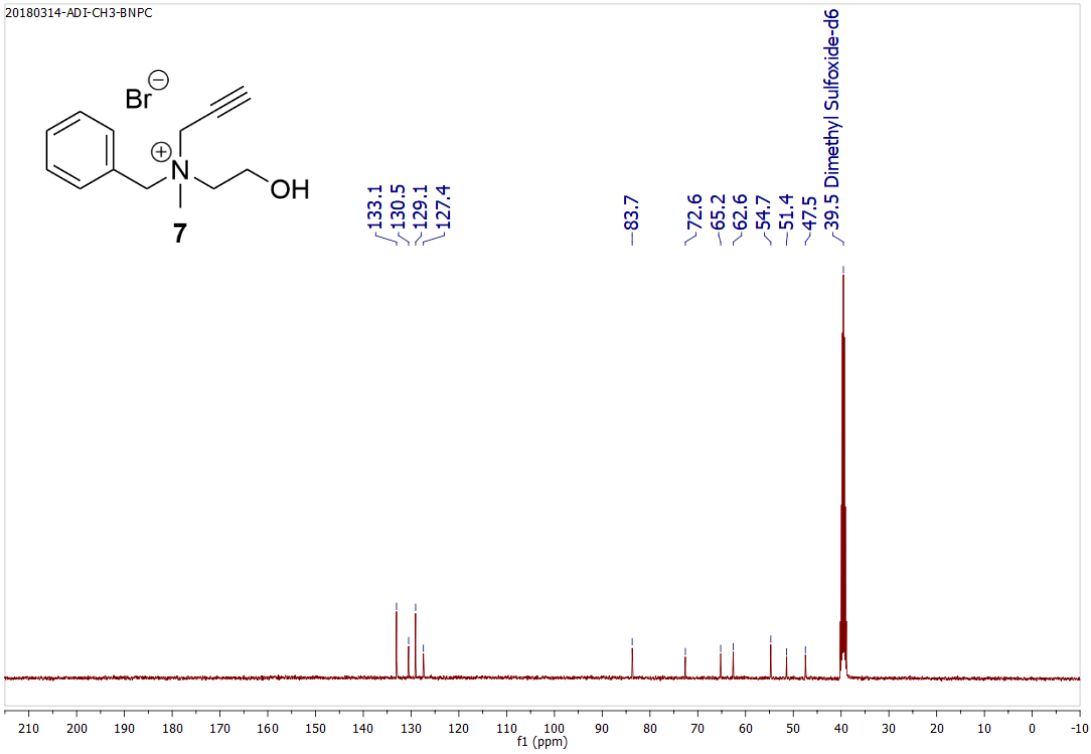
20180314-ADI-CH3-BNPC
Br
N
OH
7
133.1
130.5
129.1
127.4
83.7
72.6
65.2
62.6
54.7
51.4
47.5
39.5 Dimethyl Sulfoxide-d6
f1 (ppm)

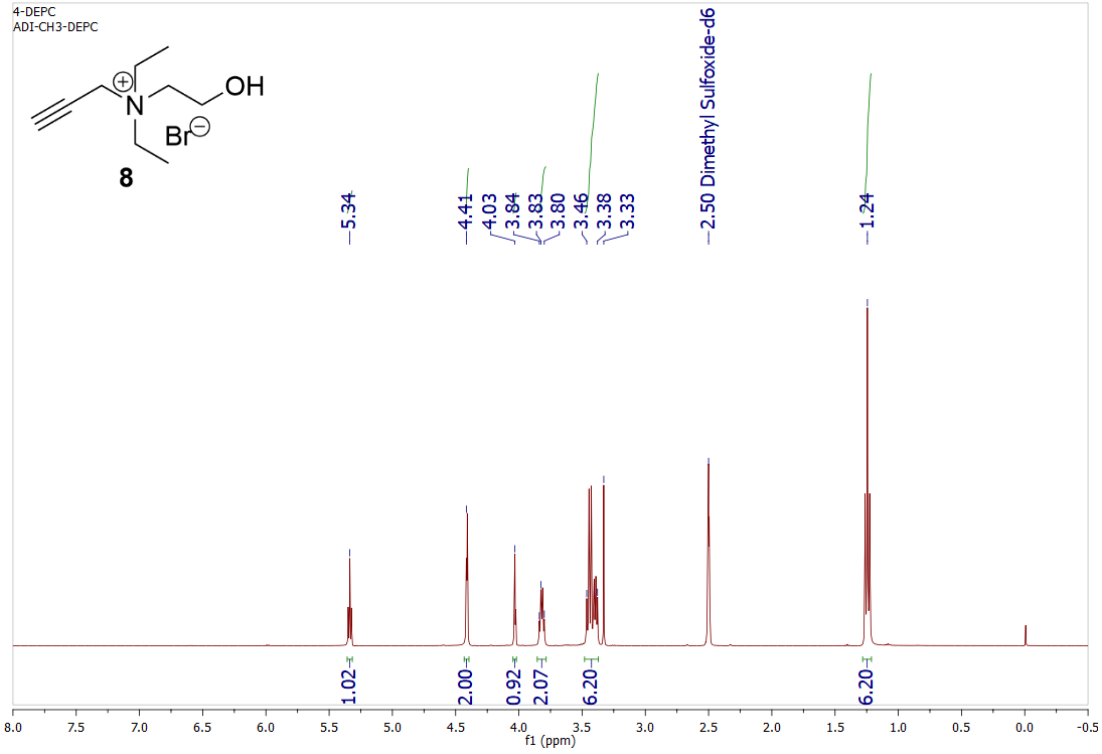
4-DEPC
ADI-CH3-DEPC
OH
N
Br
8
5.34
4.41
4.03
3.84
3.83
3.80
3.46
3.38
3.33
2.50 Dimethyl Sulfoxide-d6
1.24
1.02
2.00
0.92
2.07
6.20
6.20
f1 (ppm)

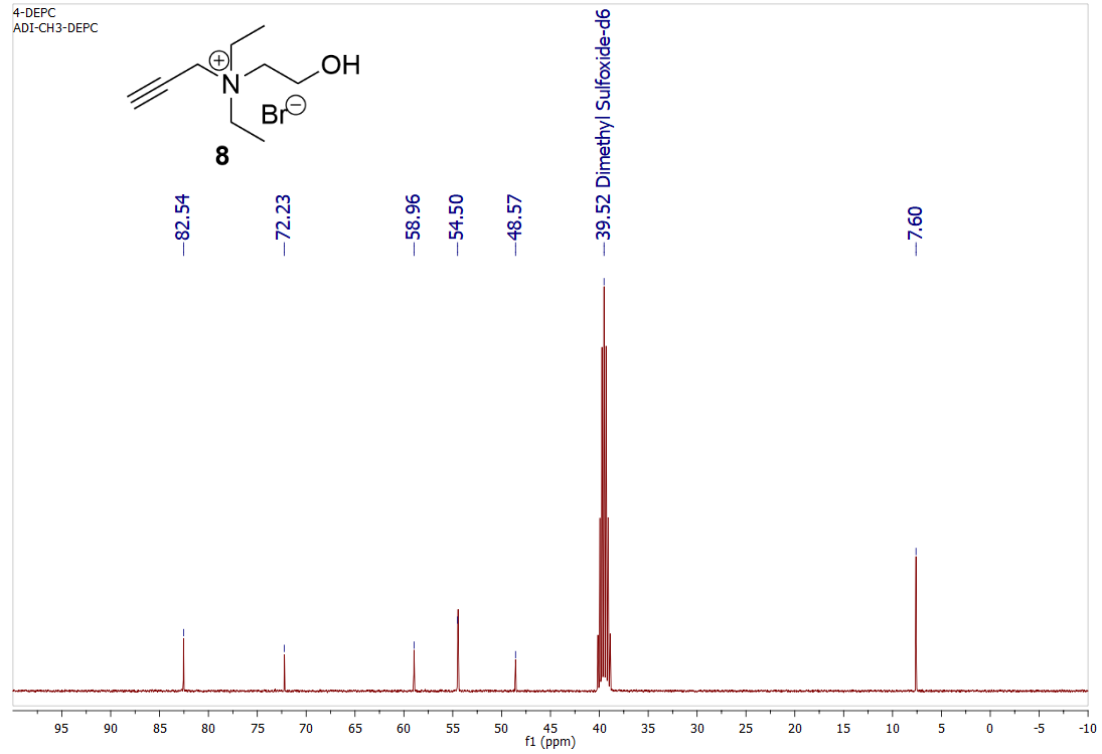
4-DEPC
ADI-CH3-DEPC
OH
N
Br
8
82.54
72.23
58.96
54.50
48.57
39.52 Dimethyl Sulfoxide-d6
7.60
f1 (ppm)

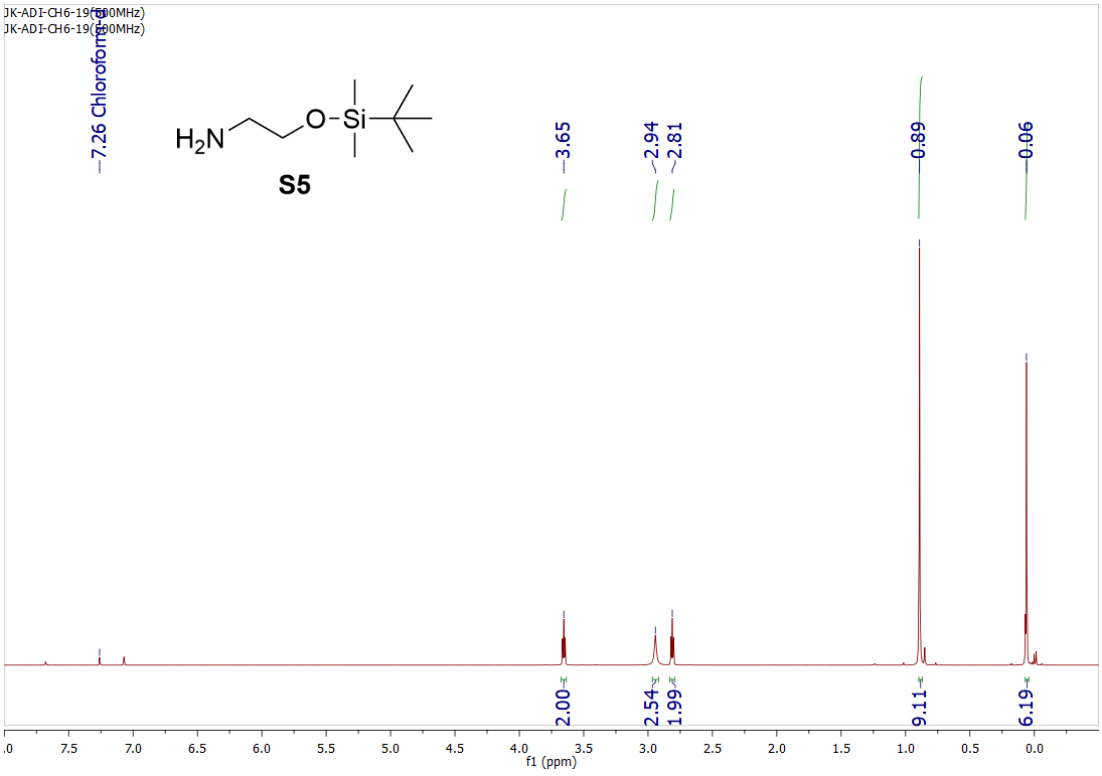
JK-ADI-CH6-19(500MHz)
JK-ADI-CH6-19(500MHz)
7.26 Chloroform-d
3.65
2.94
2.81
0.89
0.06
S5
2.00
2.54
1.99
9.11
6.19
f1 (ppm)

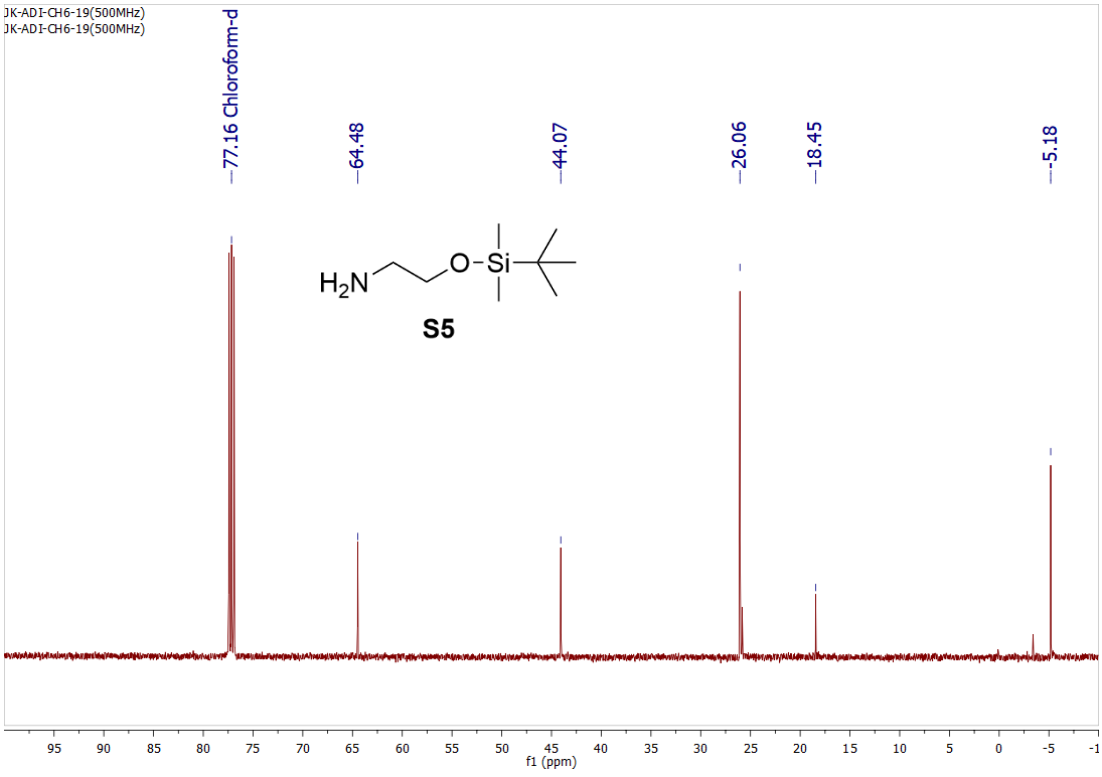
JK-ADI-CH6-19(500MHz)
JK-ADI-CH6-19(500MHz)
77.16 Chloroform-d
64.48
44.07
26.06
18.45
-5.18
S5
f1 (ppm)

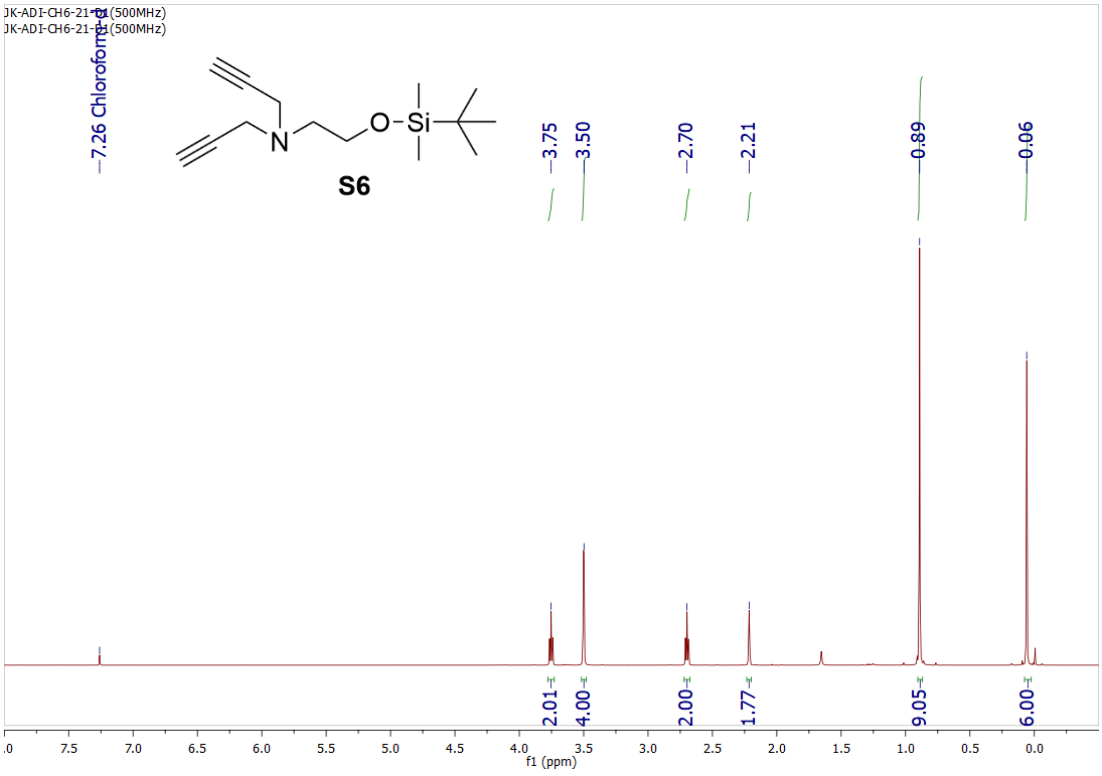
JK-ADI-CH6-21-D1(500MHz)
JK-ADI-CH6-21-D1(500MHz)
7.26 Chloroform-d
3.75
3.50
2.70
2.21
0.89
0.06
S6
2.01
4.00
2.00
1.77
9.05
6.00
f1 (ppm)

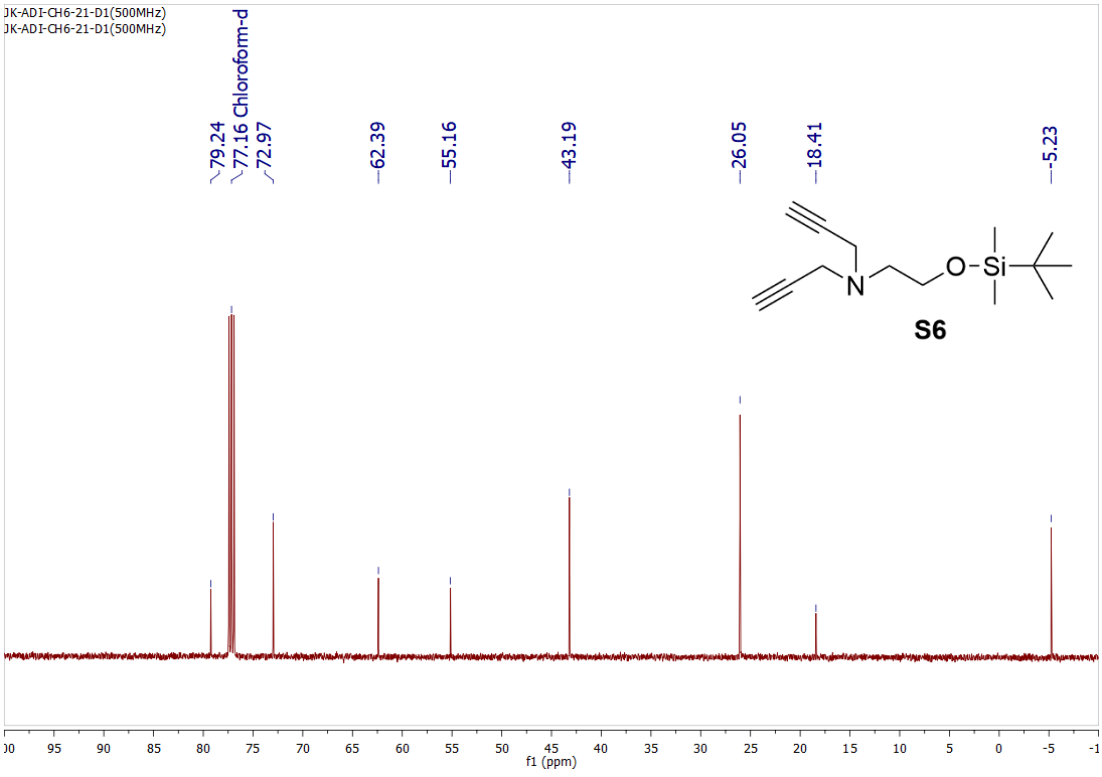
JK-ADI-CH6-21-D1(500MHz)
JK-ADI-CH6-21-D1(500MHz)
79.24
77.16 Chloroform-d
72.97
62.39
55.16
43.19
26.05
18.41
-5.23
S6
f1 (ppm)

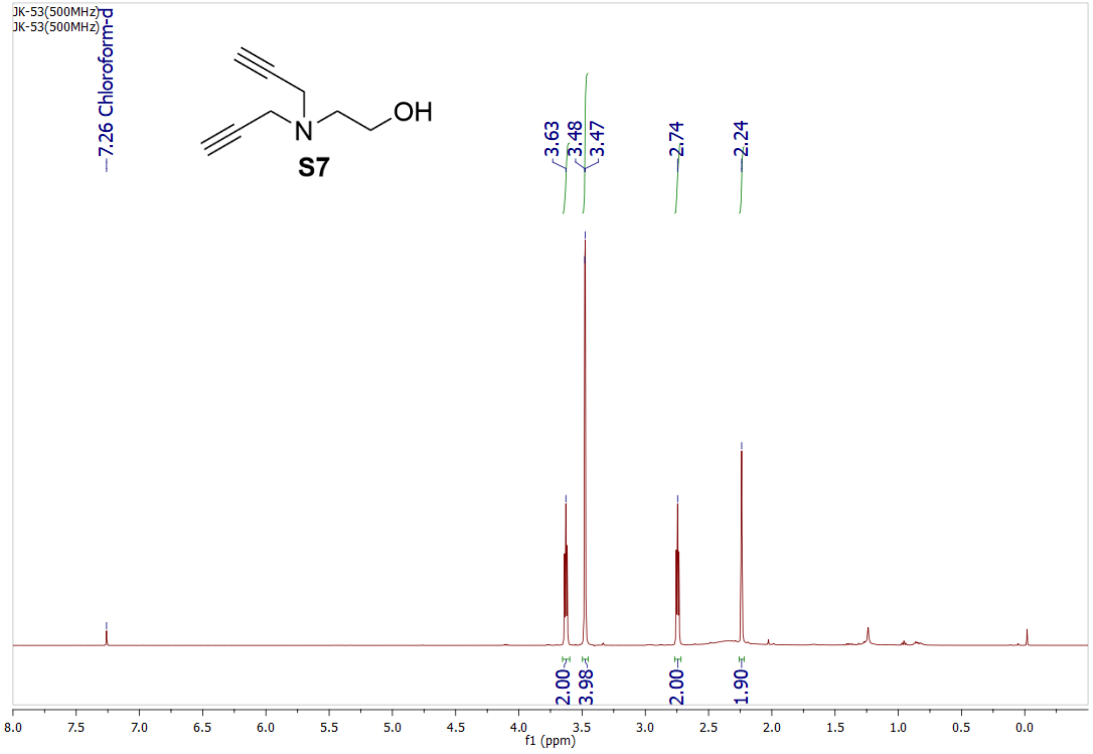
JK-53(500MHz)
JK-53(500MHz)
7.26 Chloroform-d
OH
N
S7
3.63
3.48
3.47
2.74
2.24
2.00
3.98
2.00
1.90
f1 (ppm)

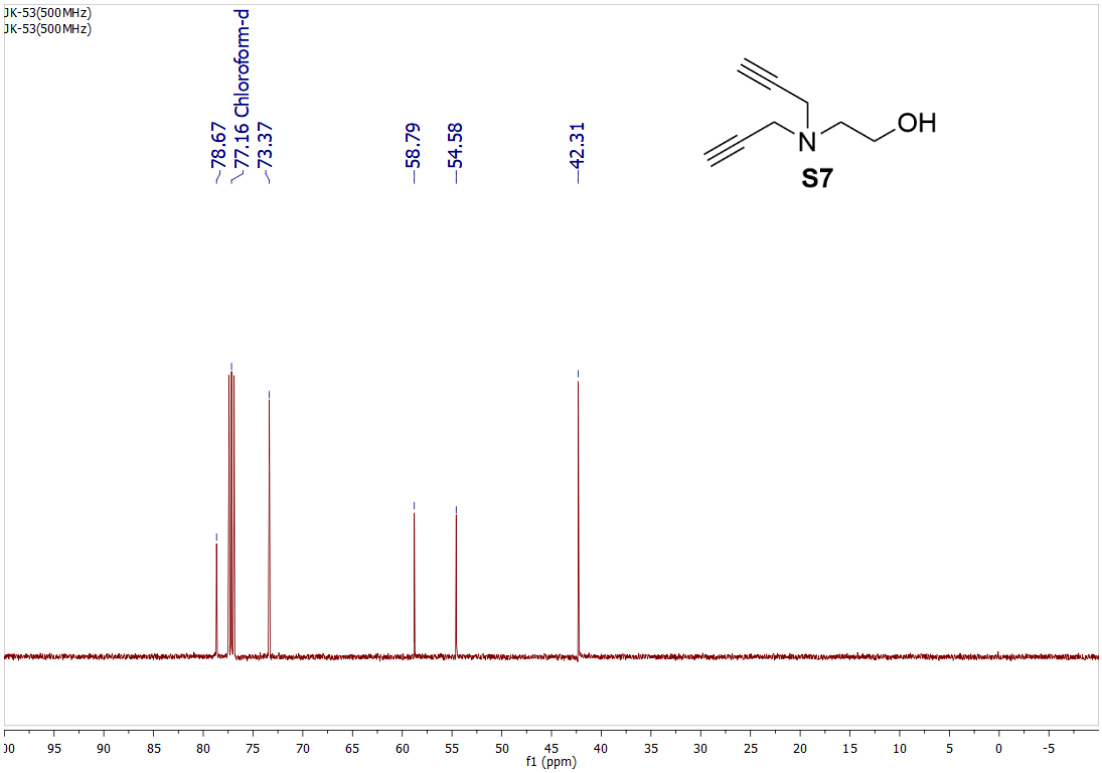
JK-53(500MHz)
JK-53(500MHz)
78.67
77.16 Chloroform-d
73.37
58.79
54.58
42.31
OH
N
S7
f1 (ppm)

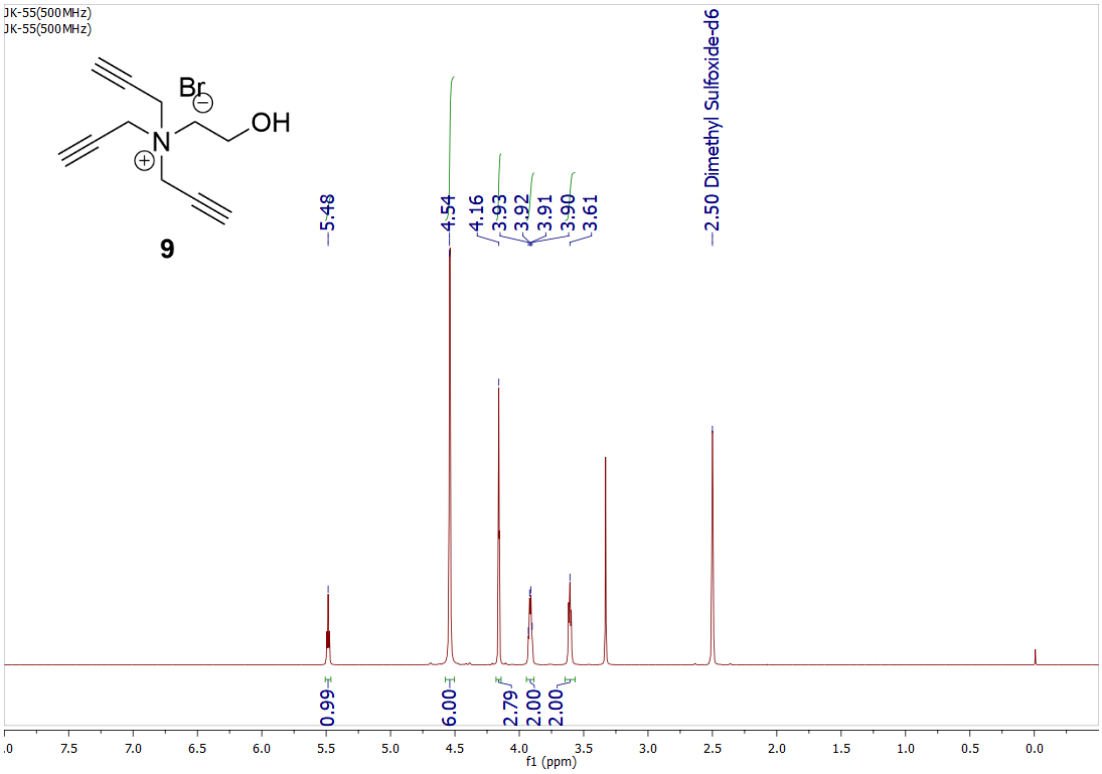
JK-55(500MHz)
JK-55(500MHz)
Br
OH
N
9
5.48
4.54
4.16
3.93
3.92
3.91
3.90
3.61
2.50 Dimethyl Sulfoxide-d6
0.99
6.00
2.79
2.00
2.00
f1 (ppm)

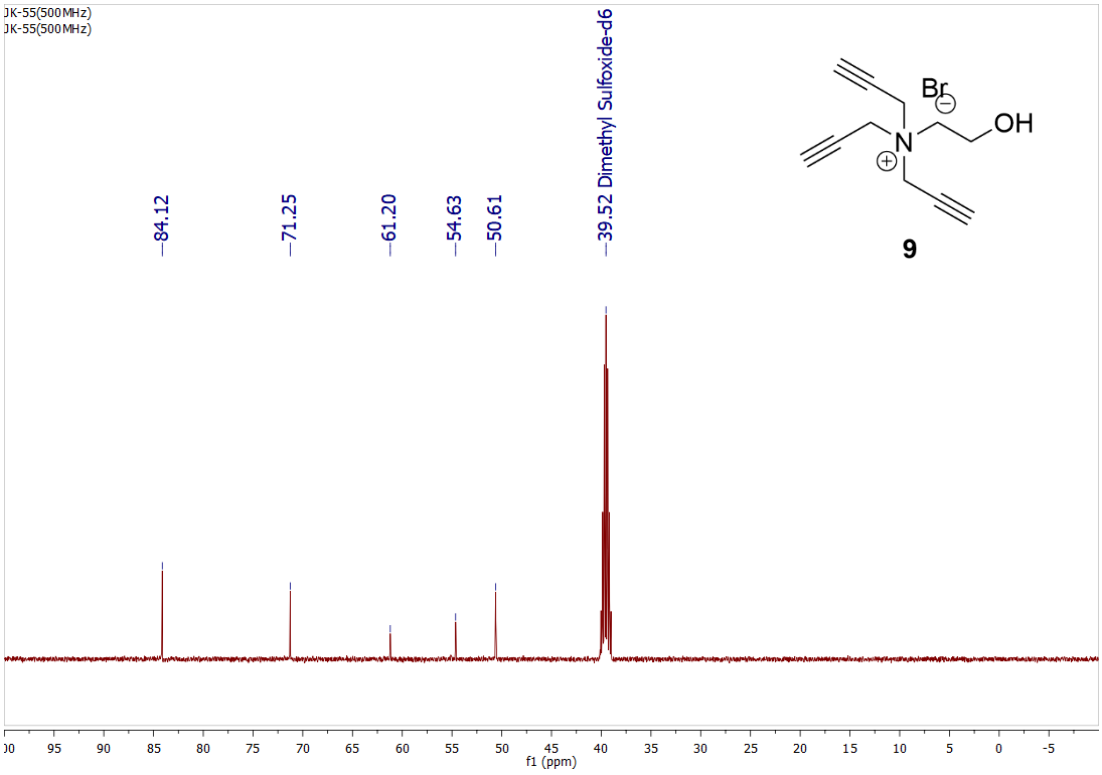
JK-55(500MHz)
JK-55(500MHz)
84.12
71.25
61.20
54.63
50.61
39.52 Dimethyl Sulfoxide-d6
Br
OH
N
9
f1 (ppm)

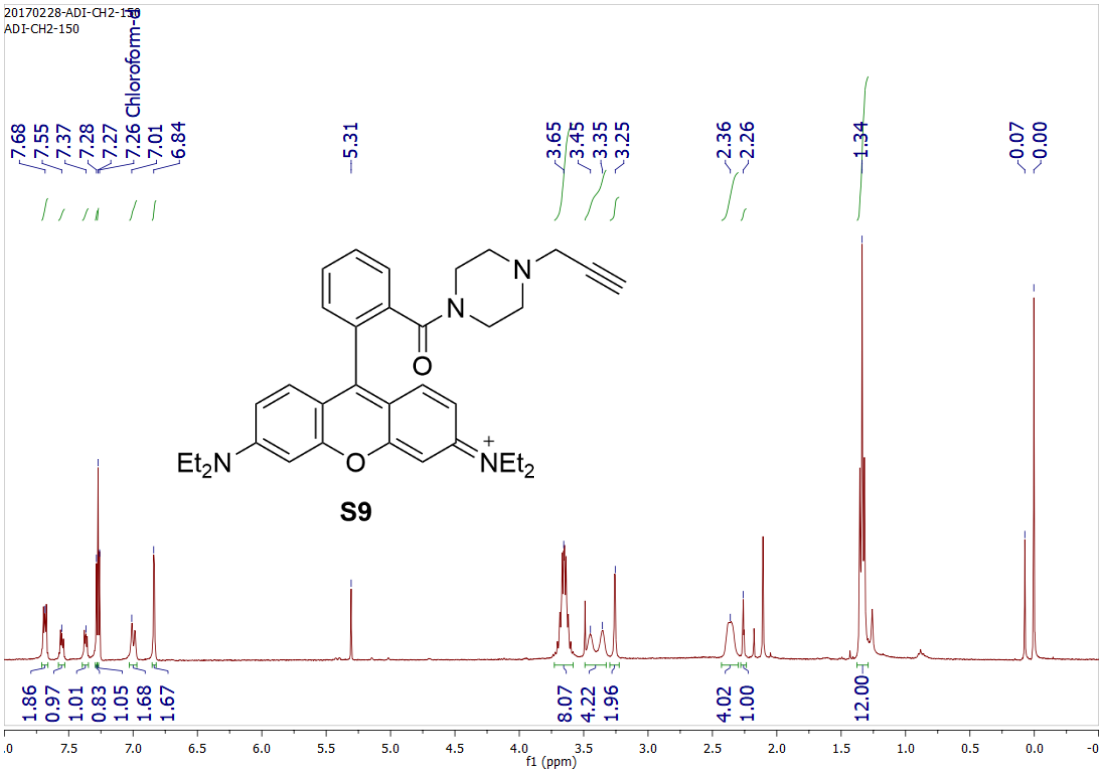
20170228-ADI-CH2-150
ADI-CH2-150
7.68
7.55
7.37
7.28
7.27
7.26 Chloroform-d
7.01
6.84
5.31
3.65
3.45
3.35
3.25
2.36
2.26
1.34
0.07
0.00
N
N
O
Et2N
O
+
NEt2
S9
1.86
0.97
1.01
0.83
1.05
1.68
1.67
8.07
4.22
1.96
4.02
1.00
12.00
f1 (ppm)

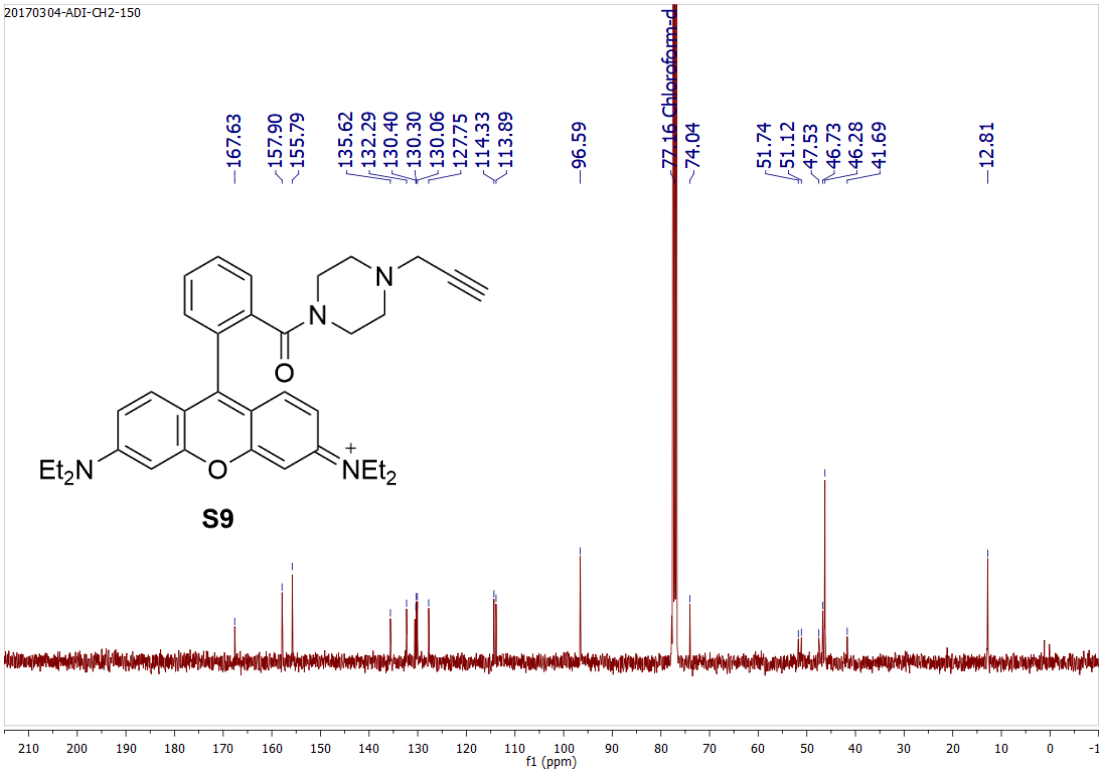
20170304-ADI-CH2-150
167.63
157.90
155.79
135.62
132.29
130.40
130.30
130.06
127.75
114.33
113.89
96.59
77.16 Chloroform-d
74.04
51.74
51.12
47.53
46.73
46.28
41.69
12.81
N
N
O
Et2N
O
+
NEt2
S9
f1 (ppm)

2.6 References

1. Haberkant, P.; Raijmakers, R.; Wildwater, M.; Sachsenheimer, T.; Brugger, B.; Maeda, K.; Houweling, M.; Gavin, A. C.; Schultz, C.; van Meer, G.; Heck, A. J.; Holthuis, J. C., In vivo profiling and visualization of cellular protein-lipid interactions using bifunctional fatty acids. *Angew Chem Int Ed Engl* **2013,** *52* (14), 4033-8.

2. Haberkant, P.; Stein, F.; Hoglinger, D.; Gerl, M. J.; Brugger, B.; Van Veldhoven, P. P.; Krijgsveld, J.; Gavin, A. C.; Schultz, C., Bifunctional Sphingosine for Cell-Based Analysis of Protein-Sphingolipid Interactions. *ACS Chem Biol* **2016,** *11* (1), 222-30.

3. Niphakis, M. J.; Lum, K. M.; Cognetta, A. B., 3rd; Correia, B. E.; Ichu, T. A.; Olucha, J.; Brown, S. J.; Kundu, S.; Piscitelli, F.; Rosen, H.; Cravatt, B. F., A Global Map of Lipid-Binding Proteins and Their Ligandability in Cells. *Cell* **2015,** *161* (7), 1668-80.

4. Das, J., Aliphatic diazirines as photoaffinity probes for proteins: recent developments. *Chem Rev* **2011,** *111* (8), 4405-17.

5. Jao, C. Y.; Roth, M.; Welti, R.; Salic, A., Metabolic labeling and direct imaging of choline phospholipids in vivo. *Proc Natl Acad Sci U S A* **2009,** *106* (36), 15332-7.

6. Jao, C. Y.; Roth, M.; Welti, R.; Salic, A., Biosynthetic labeling and two-color imaging of phospholipids in cells. *ChemBiochem* **2015,** *16* (3), 472-6.

7. Brugger, B.; Erben, G.; Sandhoff, R.; Wieland, F. T.; Lehmann, W. D., Quantitative analysis of biological membrane lipids at the low picomole level by nano-electrospray ionization tandem mass spectrometry. *Proc Natl Acad Sci U S A* **1997,** *94* (6), 2339-44.

8. Baker, P. R. S.; Armando, A. M.; Campbell, J. L.; Quehenberger, O.; Dennis, E. A., Three-dimensional enhanced lipidomics analysis combining UPLC, differential ion mobility spectrometry, and mass spectrometric separation strategies. *J Lipid Res* **2014,** *55* (11), 2432-2442.

9. Nguyen, T.; Francis, M. B., Practical synthetic route to functionalized rhodamine dyes. *Org Lett* **2003,** *5* (18), 3245-8.

10. Shieh, P.; Hangauer, M. J.; Bertozzi, C. R., Fluorogenic azidofluoresceins for biological imaging. *J Am Chem Soc* **2012,** *134* (42), 17428-31.

11. Ejsing, C. S.; Duchoslav, E.; Sampaio, J.; Simons, K.; Bonner, R.; Thiele, C.; Ekroos, K.; Shevchenko, A., Automated identification and quantification of glycerophospholipid molecular species by multiple precursor ion scanning. *Anal Chem* **2006,** *78* (17), 6202-14.

12. Hancock, S. E.; Friedrich, M. G.; Mitchell, T. W.; Truscott, R. J.; Else, P. L., Decreases in Phospholipids Containing Adrenic and Arachidonic Acids Occur in the Human Hippocampus over the Adult Lifespan. *Lipids* **2015,** *50* (9), 861-72.

13. Norris, S. E.; Friedrich, M. G.; Mitchell, T. W.; Truscott, R. J. W.; Else, P. L., Human prefrontal cortex phospholipids containing docosahexaenoic acid increase during normal adult aging, whereas those containing arachidonic acid decrease. *Neurobiol Aging* **2015,** *36* (4), 1659-1669.

14. Sud, M.; Fahy, E.; Cotter, D.; Brown, A.; Dennis, E. A.; Glass, C. K.; Merrill, A. H., Jr.; Murphy, R. C.; Raetz, C. R.; Russell, D. W.; Subramaniam, S., LMSD: LIPID MAPS structure database. *Nucleic Acids Res* **2007,** *35* (Database issue), D527-32.

Chapter 3

β-Diazirine Cholines as Metabolic Labeling Probes for Choline Metabolites

This chapter is adapted with permission from the publication: Dixit, A.; Jose, G. P.; Shanbhag, C.; Tagad, N.; Kalia, J. Metabolic labeling-based chemoproteomics establishes choline metabolites as protein function modulators. *ACS Chem. Biol.* **2022**, *17*, 2272–2283. Copyright 2022 American Chemical Society.

3.1 Introduction

I envisioned using photoaffinity labeling as a method to identify the binding partners of choline metabolites in mammalian cells (Figure 1.7b). Among the many photocrosslinkable groups reported in the literature, I chose diazirines due to their small size, stability in acidic and alkaline conditions and towards nucleophiles, and the shorter lifespan of their subsequent carbenes intermediates.[1-5]

For the success of the proposed strategy depicted in Figure 1.7b, I needed to design a bifunctional choline analog possessing the photocrosslinkable diazirine group and an affinity handle such as an alkyne group, that is amenable to metabolic labeling in mammalian cells. The design of the probe was guided by the structure-activity relationship survey of the nine choline analogs tested in the previous chapter (probes **1**-**9**). I concluded that the alkyl substitutions on the two *N*-methyl groups of choline were well tolerated by the mammalian biosynthetic machinery of choline lipids. These results served as motivation to develop bifunctional choline analogs bearing the diazirine and the alkyne/azido groups on different alkyl substituents on the choline nitrogen. The feasibility of this strategy was supported by the successful metabolic labeling of choline lipids by analogs **5, 6** and **7** wherein two *N*-methyl groups of choline were replaced with longer alkyl groups (Figures 2.8-2.10). Here, I report the development of the first series of bifunctional choline analogs for the evaluation of their metabolic labeling efficiency in mammalian cells and their crosslinking efficiency with cellular proteins.

3.2 Results and Discussion

3.2.1 β-diazirine choline analogs metabolically label choline lipids but are not suitable chemoproteomic probes

We began our metabolic labeling experiments on diazirine choline derivatives with the β-diazirine choline compound, **10** (Figure 3.1). Lipidomics analyses revealed that **10** labeled choline lipids efficiently as demonstrated by the TIC peak intensity of ~1.2E8 units obtained for the **10**-labeled choline lipids isolated from HEK293 cells cultured in its presence (Figure 3.1). Please note that to account for the loss of N_2 incurred during the fragmentation of diazirine compounds while

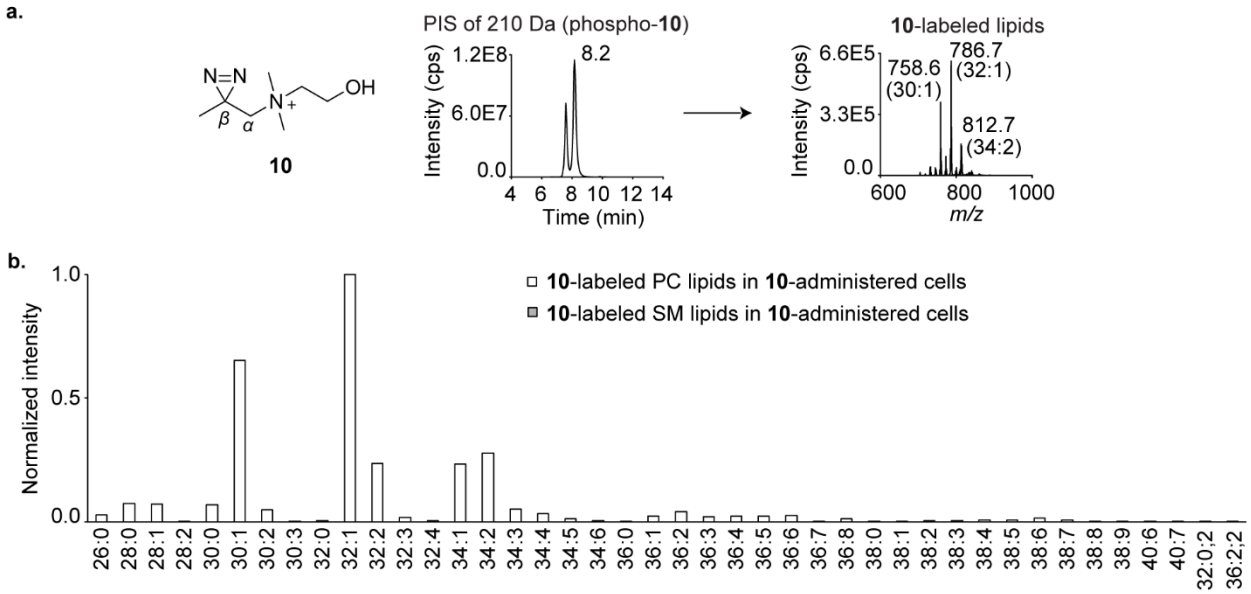

Figure 3.1. Metabolic labeling studies on β-diazirine choline analog **10**. a) The TIC and XIC plots obtained by employing a PIS of 210 Da (the *m/z* for phospho-**10**) on lipids extracted from HEK293 cells cultured for 24 h in the presence of compound **10** (2 mM). b) A bar graph obtained from the LipidView software denoting all **10**-labeled lipids identified from the XIC depicted above. The *y*-axis has been normalized to the most intense peak *i.e.*, lipid 32:1 of the XIC.

performing MS/MS analysis, the PIS analysis performed for all lipids labeled with diazirine derivatives reported in this study (such as compound **10**) employed the daughter ion *m/z* value corresponding to 28 Da less than that for the phospho-derivative of the compound.

We then proceeded to synthesize the bifunctional alkynyl β-diazirine choline compound **11** which was also observed to metabolically label the cellular choline lipids yielding a TIC intensity of ~4.0E6 units (Figure 3.2a). Notably, LipidView analysis of the XICs for the β-diazirine choline analogs **10** and **11** revealed that the most intense **10**- and **11**-labeled PC lipid was 32:1 (Figure 3.1b and 3.2b) as opposed to 34:1 that was the most abundant species for choline lipids labeled with analogs **1**-**9** (Figure 2.4-2.12). Nevertheless, encouraged by these results, we performed in-gel fluorescence experiments that involved treating the lysate of UV-irradiated HEK293 cells cultured in the presence of **11** with the fluorescent azide compound, Alexa Fluor 594 azide, followed by subjecting this reaction mixture to SDS-PAGE. Visualization of the gel under a fluorimager revealed negligible intensity for fluorescently labeled proteins in both the +UV

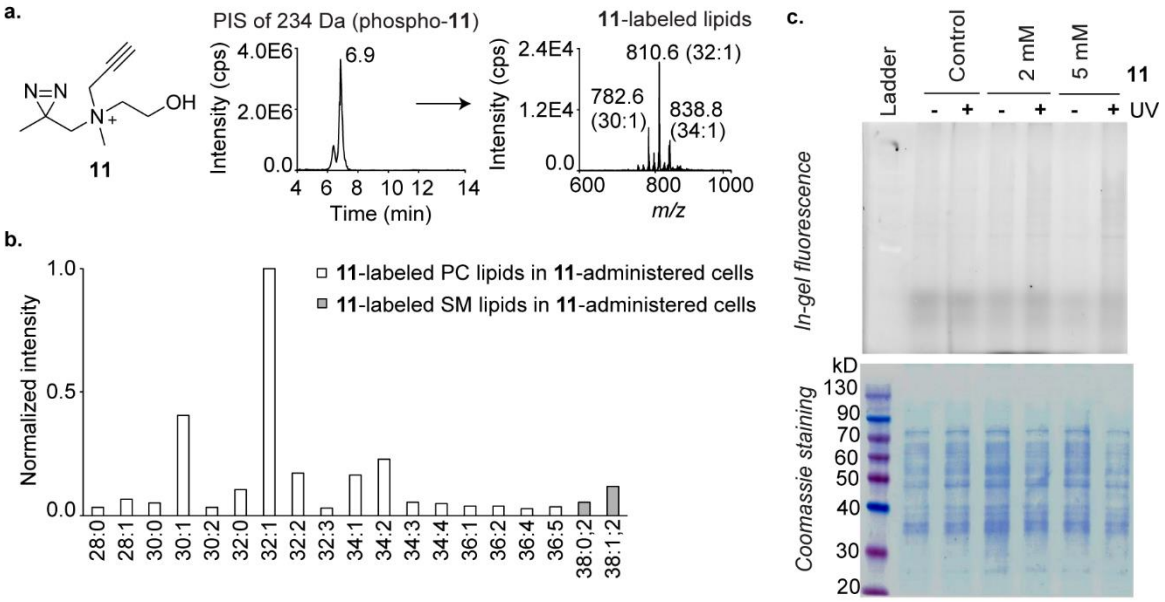

Figure 3.2. Metabolic labeling studies on β-diazirine choline analog **11**. a) The TIC and XIC plots obtained by employing a PIS of 234 Da (the *m/z* for phospho-**11**) on lipids extracted from HEK293 cells cultured for 24 h in the presence of compound **11** (2 mM). b) A bar graph obtained from the LipidView software denoting all **11**-labeled lipids identified from the XIC depicted above. The *y*-axis has been normalized to the most intense peak *i.e.*, lipid 32:1 of the XIC. c) In-gel fluorescence experiments on HEK293 cells metabolically labeled with increasing concentrations of **11**.

samples and the -UV controls (Figure 3.2c) demonstrating that **11** is not a suitable probe for the discovery of the cellular choline-metabolite interacting proteome as it was unable to yield sufficient amounts of crosslinked proteins.

The failure of **11** to yield fluorescently-labeled photocrosslinked proteins was unexpected as our lipidomics experiments convincingly demonstrated that the choline lipids of cells treated with this probe were metabolically labeled with it (Figure 3.2a,b) and prompted us to investigate whether the diazirine group of **11** was UV-reactive or not. UV-irradiation of **11** resulted in a time-dependent change in its ^{1}H-NMR spectrum (Figure 3.3a) establishing that **11** was UV-reactive. We also tested the thermal stability of the diazirine ring on **11** by incubating it at different temperatures followed by dissolving each sample in water and recording the UV absorption spectrum. This experiment showed that the characteristic peak for the diazirine ring was stable at ~330 nm at all the temperature conditions tested (Figure 3.3b). Moreover, ^{1}H-NMR-based stability studies on **11**

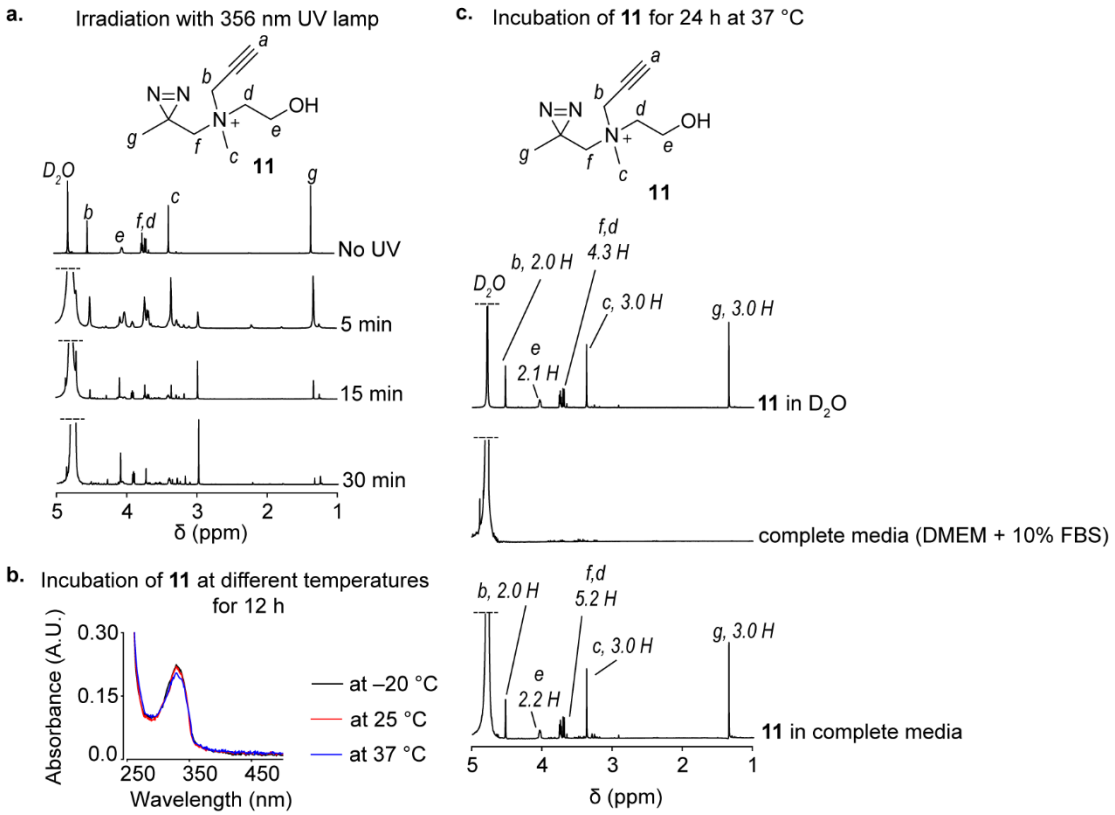

Figure 3.3. Uncaging and stability studies of **11**. a) ^{1}H-NMR traces of solutions of **11** (3.2 mM) in D_2O that were either not irradiated or irradiated for 5 min, 15 min, and 30 min with UV light (356 nm) on ice. The NMR traces show almost complete photolysis of **11** within 30 min as demonstrated by a substantial attenuation of the peak for the protons on the carbon atoms labeled "*g*" in the structure of **11**, as well as those for other peaks. b) The thermal stability of **11** was monitored by incubating it at the depicted temperatures for 12 h under dark followed by recording the UV absorption spectrum of each sample dissolved in water to a concentration of 4.1 mM. c) The ^{1}H-NMR spectra of a solution of **11** in D_2O (top) and in DMEM + D_2O (bottom) after incubation at 37 °C for 12 h under dark with tetramethylsilane (TMS) as the reference. The peaks in the spectra are assigned to the protons in the structure of **11** by annotating them by using the symbols *a-g* and the integral values in terms of the number of protons for each peak is denoted next to it. The ^{1}H-NMR spectrum of a solution of complete media in D_2O (100 µL of complete media added to 600 µL D_2O) is provided in the middle panel.

revealed that it was completely stable at 37 °C in water as well as in DMEM media (Figure 3.3c). These studies ruled out lack of reactivity of the diazirine group of **11** and chemical instability as potential reasons for the lack of protein crosslinking obtained in cells administered with it.

Notably, although **11**-labeled lipids yielded a TIC peak intensity similar to those obtained for **7**, **8** and **9**- labeled lipids (~E6 units; Figures 2.10-2.12), cellular imaging experiments with **11** yielded intense fluorescence signals (Figure 3.4a), in contrast to the low signals obtained with **7**, **8**, and **9** (Figures 2.10-2.12). In fact, these signals were reminiscent of those obtained with **1** (Figure 2.4a; left panel) and engendered the hypothesis that cells cultured in presence of **11** were forming **1**-labeled choline lipids. To test this hypothesis, we subjected lipids isolated from cells treated with

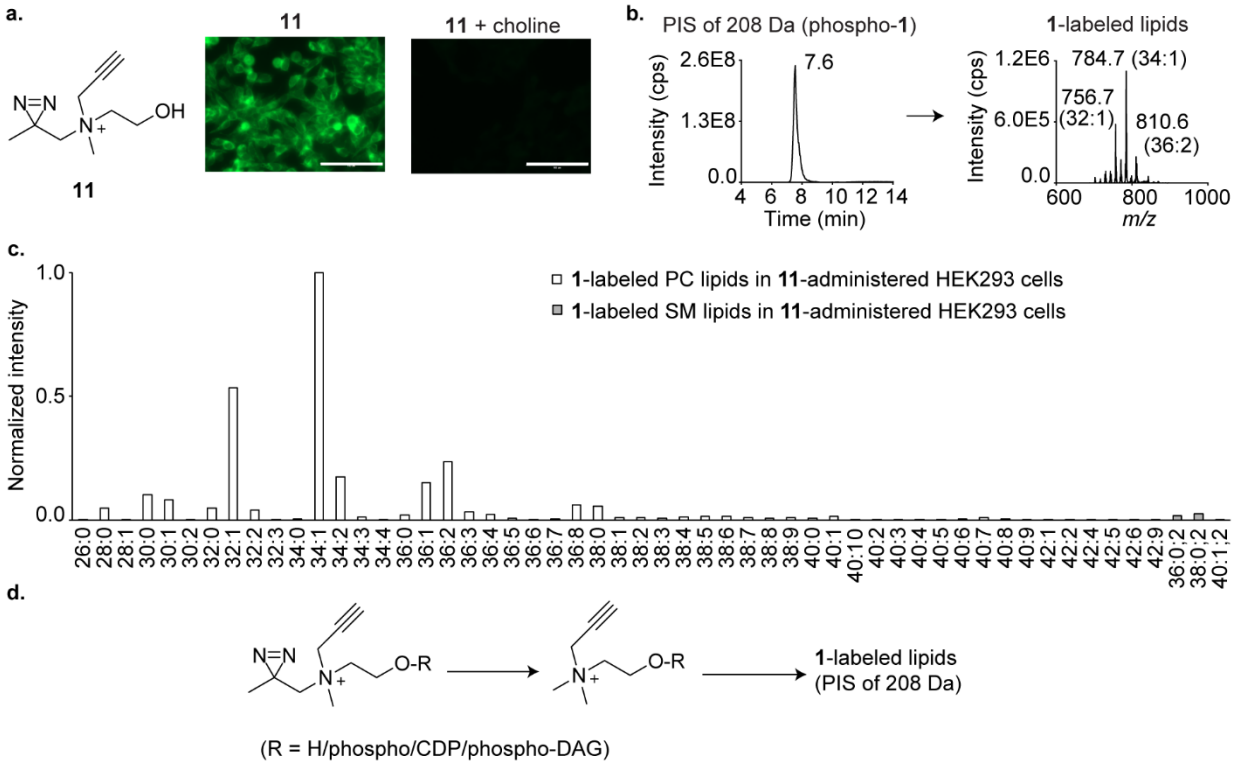

Figure 3.4. Testing the cellular conversion of **11**-labeled metabolites/lipids to **1**-labeled lipids. a) Imaging experiments on **11** (2 mM)-administered HEK293 cells (left), and cells administered with both **11** and choline (2 mM each; right). The scale bars represent 100 µm. b) The TIC and XIC plots obtained by employing a PIS of 208 Da (the *m/z* for phospho-**1**) on lipids extracted from HEK293 cells cultured in the presence of compound **11** (2 mM). c) LipidView analysis of **1**-labeled choline lipids obtained from the HEK293 cells cultured for 24 h in the presence of **11**. The *y*-axis has been normalized to the most intense peak *i.e.*, lipid 34:1 of the XIC depicted above. d) The proposed transformation of **11**-labeled metabolites/lipids into **1**-labeled lipids in HEK293 cells cultured in the presence of **11**. DAG is an abbreviation for diacylglycerol and the phospho-DAG derivatives of **11** represent **11**-labeled PC lipids.

11 to a PIS lipidomics experiment wherein all the parent ions that upon fragmentation yielded phospho-**1** as daughter ions were identified. This experiment yielded a high-intensity peak (~2.6E8 units) on the TIC (Figure 3.4b) for **1**-labeled lipids, thereby supporting our hypothesis. It is important to note that such a transformation can occur either: a) directly from **11** to **1** (indicated as R = H in Figure 3.4d) or, b) from other **11**-labeled Kennedy pathway metabolites (indicated as R = phospho/CDP in Figure 3.4d) into their **1**-labeled counterparts that can be processed further to generate **1**-labeled lipids or, c) directly from **11**-labeled PC lipids (indicated as R = phospho-DAG in Figure 3.4d)) into **1**-labeled PC lipids.

Our discovery that the cellular administration of **11** results in the formation of diazirine-devoid **1**-labeled choline lipids prompted us to investigate whether this treatment also results in the formation of alkyne-devoid **10**-labeled lipids (Figure 3.5a). This speculation was established to be accurate by the results of PIS lipidomics experiments that demonstrated that lipids isolated from

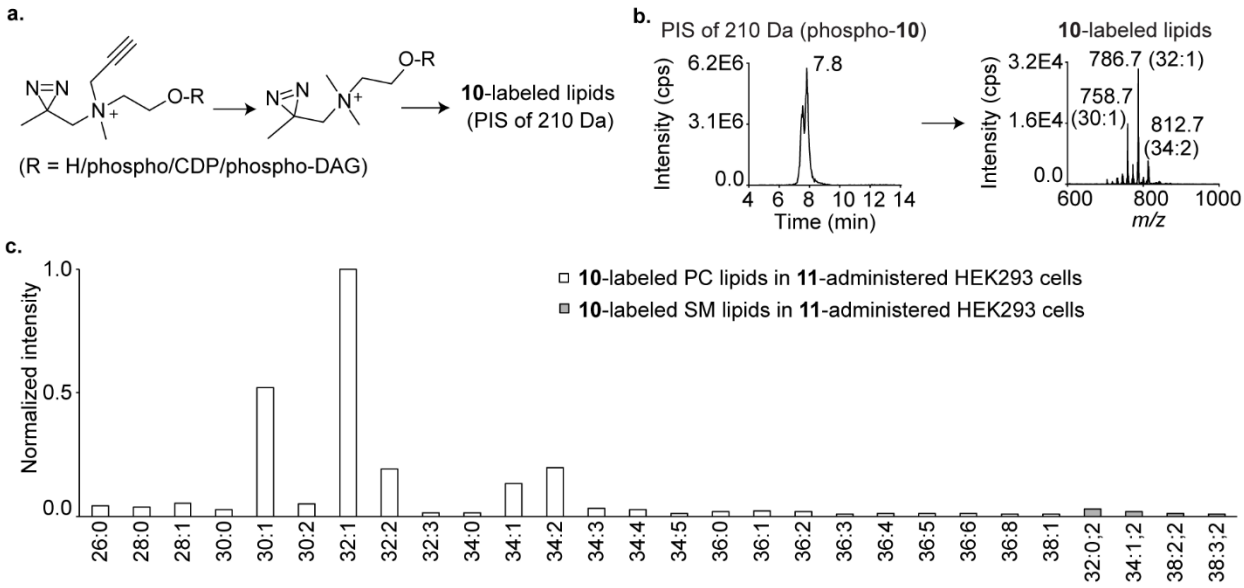

Figure 3.5. Testing the cellular conversion of **11**-labeled metabolites/lipids to **10**-labeled lipids a) The expected transformation of **11**-labeled metabolites/lipids into **10**-labeled lipids in HEK293 cells cultured in the presence of **11**. b) The TIC and XIC plots obtained by employing a PIS of 210 Da (the *m/z* for phospho-**10**) on lipids extracted from HEK293 cells cultured in the presence of compound **11** (2 mM). c) LipidView analysis of **1**-labeled lipids obtained from the HEK293 cells cultured for 24 h in the presence of **11** (2 mM). The *y*-axis has been normalized to the most intense peak *i.e.*, lipid 32:1 of the XIC.

11-treated cells were labeled with **10** (Figure 3.5b-c). Notably, the peak intensity of the TIC obtained for **10**-labeled lipids (~6.2E6 units, Figure 3.5b) were similar to those obtained for **11**-labeled lipids (~4.0E6 units, Figure 3.2a) and two orders of magnitude lower than that for **1**-labeled lipids (~2.6E8 units, Figure 3.4b) demonstrating that propargyl choline (**1**)-labeled lipids are the dominant metabolically labeled choline lipid species obtained upon cellular administration of **11**.

To further consolidate this conclusion, we performed time-course experiments wherein cells were treated with **11** for 4 h, 8 h and 16 h in addition to the standard 24 h treatments performed in the experiments described above. Lipids isolated from these treatments were subjected to PIS lipidomics to characterize choline lipid labeling with **1**, **10** and **11** and the TIC peaks were integrated to provide a semi-quantitative estimate of metabolic labeling (all the corresponding TICs and XICs are provided in Figure A1 of the Appendix). Plotting these area values against the time period of incubation yielded plots depicted in Figure 3.6a that convincingly demonstrated that treatment of HEK293 cells with **11** results in the formation of primarily the diazirine-devoid **1**-labeled lipids and that diazirine-containing **11**- and **10**-labeled lipids are formed in comparatively much lower amounts at all time points tested.

Subjecting two other mammalian cell lines, HeLa and MDA-MB-231, to **11** gave results very similar to the ones obtained with HEK293 cells with **1**-labeled choline lipids being formed in overwhelming abundance as compared to **11**- and **10**-labeled lipids as depicted in Figure 3.6b (Figures A2 and A3 of the Appendix depict the 24 h time point TICs, XICs and LipidView plots for the **11**-, **10**- and **1**-labeled lipids identified in lipids isolated from these two cell lines).

The formation of large amounts of **1**-labeled lipids accounts for the high fluorescence intensity observed in the imaging experiments (Figure 3.4a) whereas the formation of small amounts of **11**-labeled choline metabolites explains the low intensity of the fluorescently labeled crosslinked proteins observed in the in-gel fluorescence experiment (Figure 3.2c). The problem of low protein crosslinking levels observed in cells cultured in presence of **11** is likely aggravated by the presence of similar amounts of choline metabolites labeled with the alkyne-devoid diazirine **10** formed in these cells (Figures 3.5, 3.6a) as they will compete with their **11**-labeled counterparts for the same binding sites on proteins, thereby resulting in a further reduction in the levels of proteins crosslinked to **11**-labeled choline metabolites and lipids.

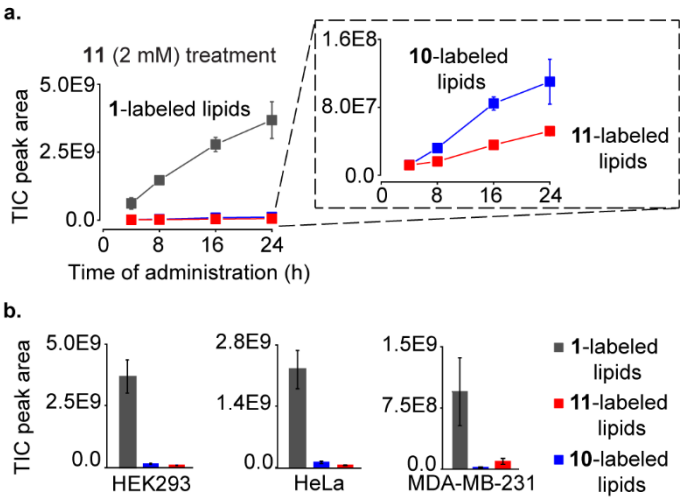

Figure 3.6. Estimate of **1**-, **10**- and **11**-labeled lipids formed from the cellular administration of **11**. a) A plot of the TIC peak areas versus time wherein the areas under the TIC plots were obtained from the PIS for **1**-, **10**-, and **11**- labeled lipids on the lipids extracted from HEK293 cells cultured in presence of **11** (2 mM) for 4, 8, 16, and 24 h. The representative TIC and XIC plots for the aforementioned treatments are depicted in Figure A1 of the Appendix. Each data point is an average of three biological replicates and the error bars represent the standard error values. b) A bar graph representing the TIC peak areas for **1**-, **10**-, and **11**-labeled lipids extracted from HEK293, HeLa and MDA-MB-231 cells cultured for 24 h in the presence of **11** (2 mM). Each peak area value is an average of three biological replicates and the error bars represent the standard error values. The representative TIC and XIC plots for these experiments are depicted in Figures A1-A3 of the Appendix.

Since our first bifunctional choline analog **11** showed unexpected transformation in mammalian cells, therefore, we synthesized two other bifunctional choline analogs, the azido derivative **12** (Figure 3.7) and compound **13** (Figure 3.8) to test whether they undergo similar metabolic transformations in cells. Metabolic labeling experiments with **12** yielded results similar to those observed with **11**—it did not itself label the cellular choline lipids (Figure 3.7a) and instead, yielded azido choline (**2**)-labeled lipids (TIC and XIC depicted in Figure 3.7b-c and LipidView profile in Figure 3.7d) whereas no lipids labeled with the azide-devoid diazirine-containing version of **12** (compound **10**) were detected (Figure 3.7e-f).

We also tested the metabolic incorporation of β-diazirine choline analog **13**, a homolog of **11** containing one additional carbon atom on the diazirine-containing alkyl chain. The cellular

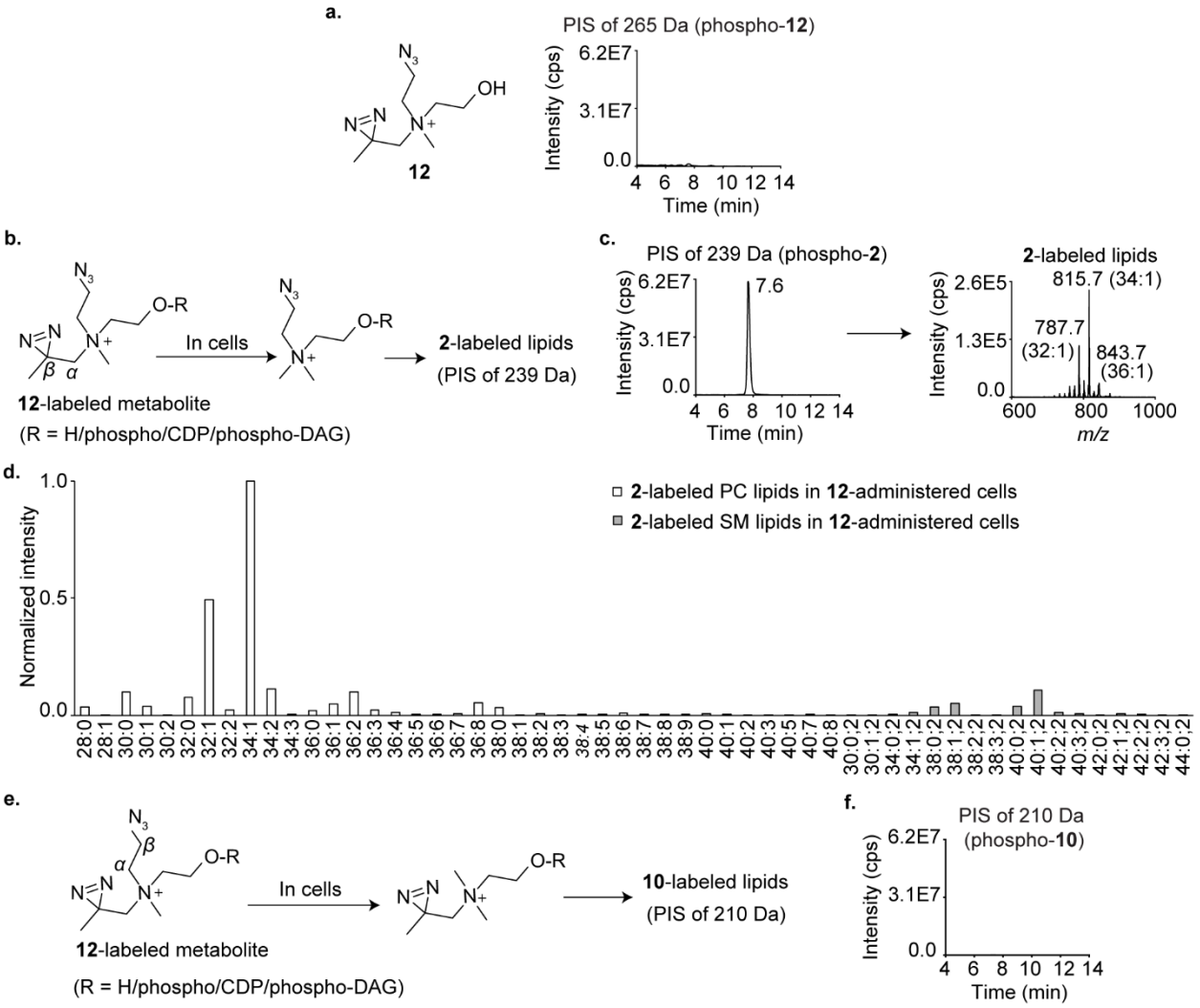

Figure 3.7. Metabolic labeling studies on β-diazirine choline analog **12**. a) The TIC plot obtained by employing a PIS of 265 Da (the *m/z* for phospho-**12**) on lipids extracted from HEK293 cells cultured in the presence of compound **12** (2 mM). The resultant TIC shows no peak for **12**-labeled lipids. b) The expected transformation of **12**-labeled metabolites/lipids into **2**-labeled lipids in HEK293 cells cultured in the presence of **12**. c) The TIC and XIC plots obtained by employing a PIS of 239 Da (the *m/z* for phospho-**2**) on lipids extracted from HEK293 cells cultured in the presence of compound **12** (2 mM). d) LipidView analysis of **2**-labeled choline lipids obtained from the HEK293 cells cultured for 24 h in the presence of **12** (2 mM). The *y*-axis has been normalized to the most intense peak *i.e.*, lipid 34:1 of the XIC. e) The proposed transformation of **12**-labeled metabolites/lipids into the azide-devoid **10**-labeled lipids in HEK293 cells cultured in the presence of **12**. f) The TIC plot obtained by employing a PIS of 210 Da (the *m/z* for phospho-**10**) on lipids extracted from HEK293 cells cultured in the presence of compound **12** (2 mM). The resultant TIC shows no peak for **10**-labeled lipids.

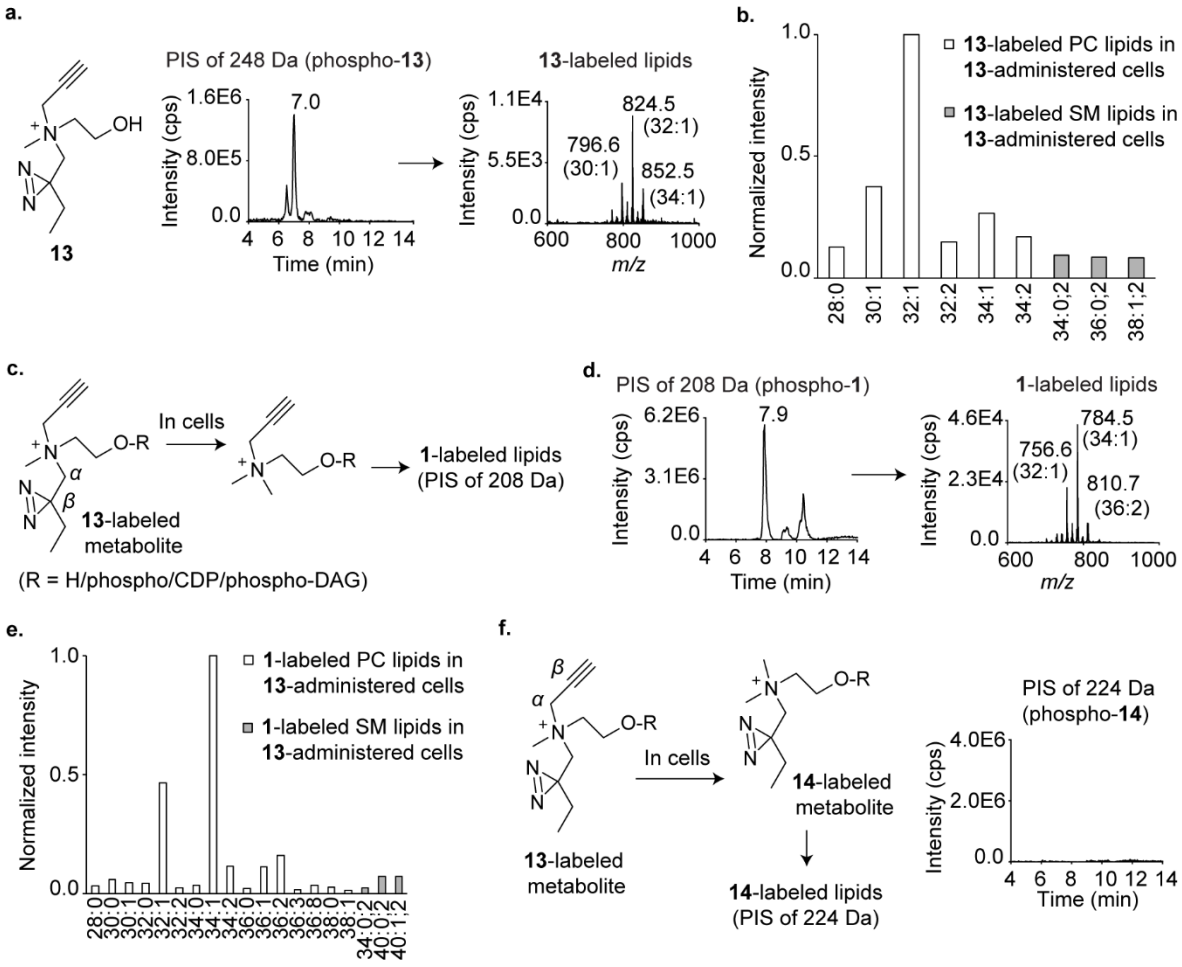

Figure 3.8. Metabolic labeling studies on β-diazirine choline analog **13**. a) The TIC and XIC plots obtained by employing a PIS of 248 Da (the *m/z* for phospho-**13**) on lipids extracted from HEK293 cells cultured in the presence of compound **13** (2 mM). b) LipidView analysis of **13**-labeled choline lipids obtained from the HEK293 cells cultured for 24 h in the presence of **13** (2 mM). The *y*-axis has been normalized to the most intense peak *i.e.*, lipid 32:1 of the XIC. c) The expected transformation of **13**-labeled metabolites/lipids into **1**-labeled lipids in HEK293 cells cultured in the presence of **13**. d) The TIC and XIC plots obtained by employing a PIS of 208 Da (the *m/z* for phospho-**1**) on lipids extracted from HEK293 cells cultured in the presence of compound **13** (2 mM). e) LipidView analysis of **1**-labeled choline lipids obtained from the HEK293 cells cultured for 24 h in the presence of **13** (2 mM). The *y*-axis has been normalized to the most intense peak *i.e.*, lipid 34:1 of the XIC. f) The proposed transformation of **13**-labeled metabolites/lipids into the alkyne-devoid **14**-labeled lipids in HEK293 cells cultured in the presence of **13** (2 mM) and the resultant TIC plot obtained by employing a PIS of 224 Da (the *m/z* for phospho-**14**). The plot shows no peak for **14**-labeled lipids.

administration of **13** was observed to metabolically label choline lipids, albeit with poor efficiency as demonstrated by the TIC obtained by employing a PIS of 248 Da (~1.6E6 units, Figure 3.8a-b) on the lipids extracted from HEK293 cells administered with **13**. Consistent with the results obtained for the choline derivative **12**, we found that **13** was also processed by mammalian cells in a similar fashion, *i.e.*, yielding diazirine-devoid propargyl choline (**1**) lipids as the dominant metabolically labeled choline lipid species (Figure 3.8c-e), whereas lipids labeled with the alkyne-devoid diazirine derivative of **13** (compound **14**) were not detected (Figure 3.8e-f).

Compounds **12** and **13** showed different metabolic labeling efficiencies in mammalian cells—**12** did not show any metabolic labeling of choline lipids by itself and **13** showed weak incorporation into cellular choline lipids (compare TICs in Figures 3.7a and 3.8a), however, both of them showed consistent metabolic transformation into their respective diazirine-devoid choline metabolites (Figures 3.7c and 3.8d) similar to that observed for **11**. Therefore, we hypothesized that the most straightforward explanation for the formation of diazirine containing **10**-labeled choline lipid species, and the diazirine devoid **1**/**2**-labeled lipid species in the cells administered with choline analogs **11**, **12**, and **13** is that the β-diazirine labeled choline metabolites undergo a C_α–C_β bond cleavage in cells (hypothesis shown for **11** in Figure 3.9).

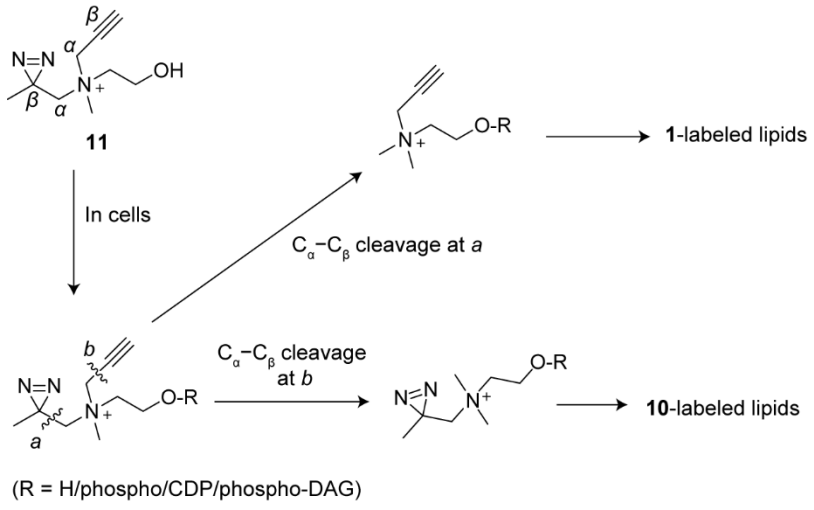

Figure 3.9. The C_α–C_β bond cleavage hypothesis to explain the formation of **1**- and **10**-labeled lipids in **11**-administered cells.

3.2.2 β-diazirine choline-labeled metabolites undergo dealkylation followed by methylation in cells

To test the hypothesis depicted in Figure 3.9, we synthesized a branched alkynyl diazirine choline compound (**15**, Figure 3.10a) containing a methyl substituent on the C_α atom of its diazirine-bearing alkyl substituent and cultured HEK293 cells in its presence for 24 h. If our proposed C_α–C_β bond cleavage mechanism is accurate, culturing HEK293 cells in the presence of **15** should result in the formation of ethyl propargyl choline (**16**)-labeled lipids (Figure 3.10a) that would be

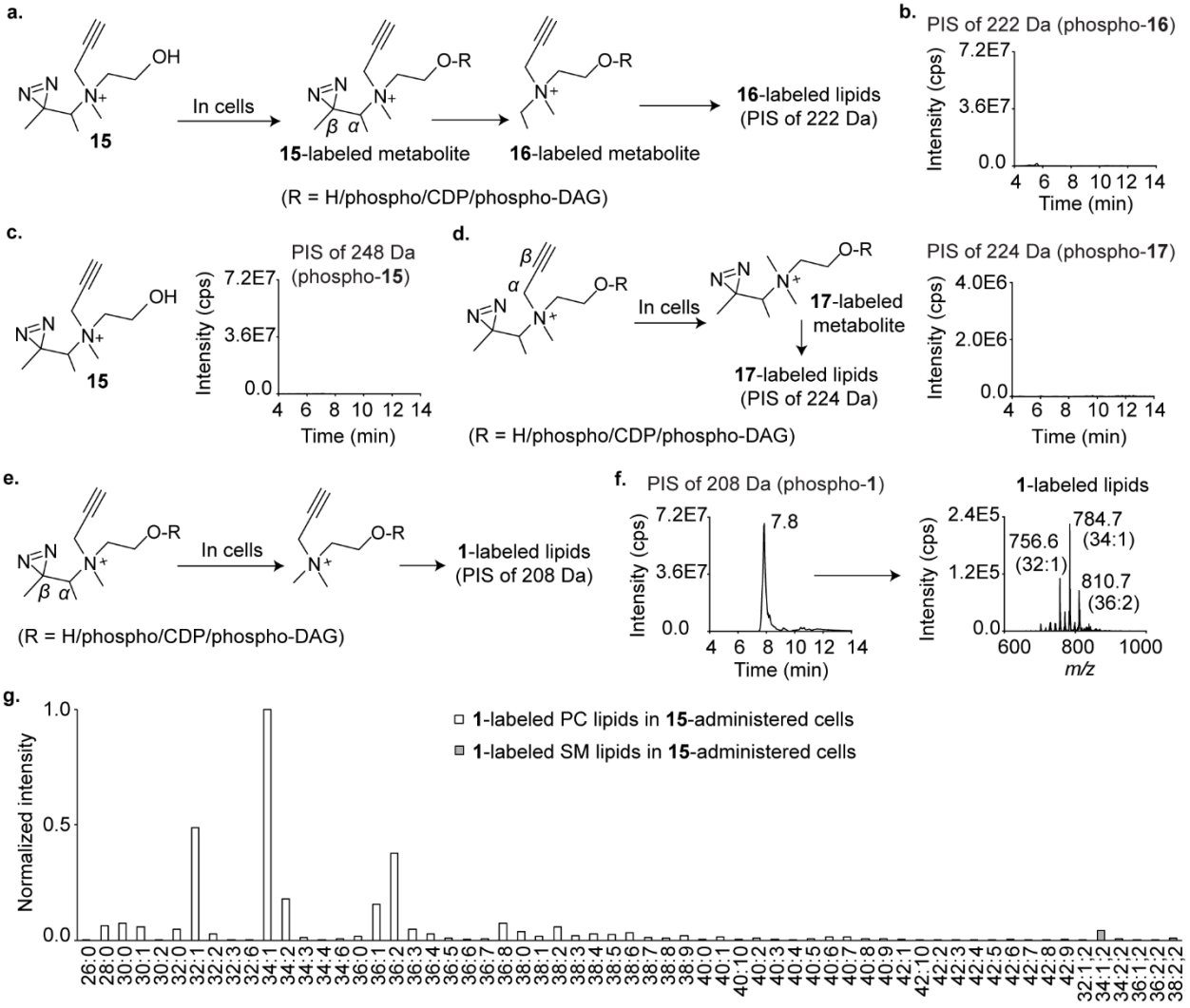

Figure 3.10. Metabolic labeling studies on β-diazirine choline analog **15**. a) A scheme depicting the expected cellular transformation of **15**-labeled choline metabolites/lipids into **16**-labeled lipids as per the route proposed in Figure 3.9. *Legend continued to next page.*

Figure 3.10 legend continued from the last page. b) The resultant TIC obtained by employing a PIS of 222 Da (the *m/z* for phospho-**16**) on lipids extracted from HEK293 cells cultured for 24 h in the presence of compound **15** (2 mM) shows no peak. c) The TIC plot obtained by employing a PIS of 248 Da (the *m/z* for phospho-**15**) on lipids extracted from HEK293 cells cultured in the presence of compound **15** (2 mM). The resultant TIC shows no peak for **15**-labeled lipids. d) Left: The expected cellular transformation of **15**-labeled choline metabolites/lipids into **17**-labeled lipids as per the route proposed in Figure 3.9. Right: The resultant TIC obtained by employing a PIS of 224 Da (the *m/z* for phospho-**17**) on lipids extracted from HEK293 cells cultured for 24 h in the presence of compound **15** (2 mM) shows no peak. e) The unexpected transformation of **15**-labeled choline metabolites/lipids into **1**-labeled lipids. f) The TIC and XIC plots obtained by employing a PIS of 208 Da (the *m/z* for phospho-**1**) on lipids extracted from HEK293 cells cultured in the presence of compound **15** (2 mM). g) LipidView analysis of **1**-labeled choline lipids obtained from the HEK293 cells cultured for 24 h in the presence of **15** (2 mM). The *y*-axis has been normalized to the most intense peak *i.e.*, lipid 34:1 of the XIC.

detected as parent ions in a PIS lipidomics experiment with phospho-**16** (*m*/*z* = 222 Da) as the daughter ion. Contrary to this expectation, our lipidomics experiments revealed that **15**-administered HEK293 cells did not form **16**-labeled choline lipids (Figure 3.10b). Moreover, these cells neither formed **15**-labeled choline lipids (Figure 3.10c), nor the lipids labeled with the other expected C_α–C_β bond cleavage product, the alkyne-devoid diazirine labeled derivative of **15** (compound **17**, Figure 3.10d). Instead, these cells formed propargyl choline (**1**)-labeled lipids (Figure 3.10e-g).

The formation of **1**-labeled lipids in cells administered with **11** as well as those administered with **15** suggested that our hypothesis that β-diazirine choline-labeled metabolites and/or lipids were undergoing C_α–C_β bond cleavage (Figure 3.9) within cells was inaccurate. Instead, these results supported an alternate hypothesis involving the cleavage of the N–C bonds between the choline nitrogen and the α-carbon atom of the *N*-alkyl substituents followed by methylation to form the observed propargyl choline-labeled lipids (as depicted for β-diazirine choline derivatives in Figure 3.11).

To further explore the generality of this phenomenon, we investigated whether native choline metabolites are also cellularly processed in this fashion by culturing HEK293 cells in presence of

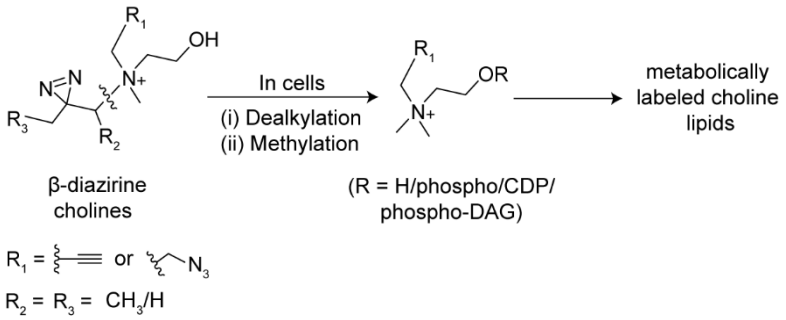

Figure 3.11. A general scheme depicting our dealkylation-methylation hypothesis for the cellular turnover of β-diazirine choline compounds.

deuterated choline (D9 choline) and performing PIS lipidomics on lipids isolated from these cells to detect choline lipids labeled with D6 choline which would be formed as a result of sequential demethylation (removal of a -CD_3 group) followed by methylation (addition of a -CH_3 group) as depicted in Figure 3.12a. These experiments yielded clear signals for choline lipids labeled with D6 choline (left panel; Figure 3.12b) at the same retention time as that for native (H9) choline lipids (right panel; Figure 3.12b) and the TICs for these lipids demonstrated a dose-dependent increase in the labeled peak intensities with respect to the concentrations of D9 choline administered. The TIC peak intensities for D6 choline-labeled lipids were, however, of the order of E5 units which is much lower than those typically observed for the propargyl choline (**1**)-labeled lipids generated by the putative dealkylation followed by methylation of β-diazirine choline metabolites. Indeed, peak intensities of the order of E8 (Figure 3.4b) and E7 (Figure 3.10f) were observed for **1**-labeled lipids in lipids isolated from cells administered with the β-diazirine cholines **11** and **15** respectively. These results demonstrate that although native choline metabolites are also susceptible to dealkylation followed by methylation within mammalian cells, β-diazirine choline-labeled metabolites undergo this transformation much more efficiently.

3.3 Conclusions

In this chapter, we report the synthesis of our first photocrosslinkable alkynyl choline analog **11** that although successfully labeled choline lipids, but was unsuitable for our chemoproteomics workflow as it underwent cellular metabolic transformations to form the undesired diazirine-

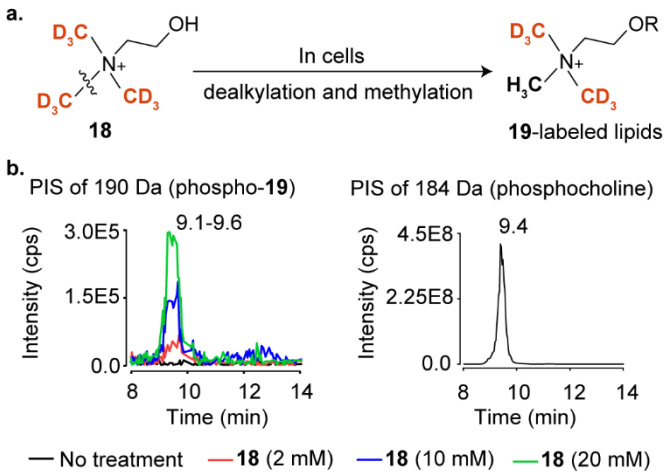

Figure 3.12. Testing the N–C bond cleavage hypothesis on cells administered with D9 choline. a) A scheme depicting the expected generation of D6 labeled (**19**-labeled) choline lipids due to N–C bond cleavage followed by methylation in D9 choline (**18**)-administered cells. b) Left panel: The TIC obtained by employing a PIS of 190 Da (the *m/z* for phospho-**19**) on lipids extracted from HEK293 cells cultured in the presence of specified concentrations of **18**. Right panel: A reference TIC obtained for native choline lipids by employing a PIS of 184 Da for phosphocholine on lipids extracted from HEK293 cells cultured in standard media devoid of unnatural choline analogs.

devoid **1**-labeled metabolites/lipids and alkyne-devoid **10**-labeled metabolites/lipids. Similar results were obtained with other β-diazirine choline analogs **12** and **13**, where upon their cellular administration, large quantities of the diazirine-devoid **2**- and **1**-labeled choline metabolites/lipids were formed respectively. Upon testing our branched β-diazirine choline analog **15**, we found that these metabolic transformations occur via a sequential N–C bond cleavage between the choline nitrogen atom and the α-carbon atom of the *N*-alkyl substituents followed by methylation. Similar results were observed for cellular choline lipids labeled with D9 choline. These results were significant in uncovering a novel metabolic conversion in lipid biology where choline lipid headgroups are susceptible to chemical remodeling via sequential dealkylation and methylation within mammalian cells, however, the identity of the Kennedy pathway intermediate (choline/phosphocholine/CDP-choline/PC lipid) upon which these transformations occur is unknown. Future experiments dedicated towards identification of the Kennedy pathway intermediate and the enzyme(s) responsible for the aforementioned chemical conversion will provide valuable insights into lipid biology.

It is also noteworthy to observe that consistent with the previous results depicted in the LipidView profiles for **1**-**9**-labeled choline lipids (LipidView profiles in Figures 2.4-2.12), the most abundant diazirine-devoid **1**-labeled lipid in cells treated with β-diazirine choline derivatives **11**, **13** and **15** (compare LipidView profiles in Figures 3.4c, 3.8e and 3.10g respectively) and the most abundant diazirine-devoid **2**-labeled lipid in cells treated with analog **12** (Figure 3.7d) was 34:1. Contrary to this trend, however, the most abundant β-diazirine containing **10**-, **11**-, and **13**-labeled choline lipid in their respective treatment was 32:1 (compare LipidView profiles in Figures 3.1b, 3.2b, 3.8b). The reason for the disparity in the selection of the diacyl glycerol chains between the alkynyl/azido choline lipids and the β-diazirine labeled choline lipids by the cellular biosynthetic machinery is unclear.

In conclusion, although the results from the cellular administration of the β-diazirine choline analogs helped us discover a novel cellular choline lipid headgroup remodeling mechanism, none of these probes were adequate for our chemoproteomics application as they are unstable in the cellular milieu. As a result, the we needed to continue our pursuit for a suitable bifunctional choline analog that did not lose integrity in cells.

3.4 Experimental Methods

3.4.1 Materials

Materials used for the experiments performed in this chapter were the same as documented in section 2.4.1. All reactions, work-ups and column purifications involving diazirine compounds were performed under minimal exposure to light. All UV exposure experiments were done by irradiating the sample with the UV light emitted from 5 × 8W UV lamps (λ_{max} = 356 nm, Sankyo-Denki F8T5BLB lamp) and passed through a Magnaflux black light filter (part #519227). D9 choline chloride (compound **18**) was purchased from Cambridge Isotope Laboratories. Complete EDTA-free protease inhibitor cocktail, tris((1-benzyl-4-triazolyl)methyl)amine (TBTA), tris(2-carboxyethyl)phosphine (TCEP), and the Bradford reagent were purchased from Sigma Aldrich. Alexa Fluor 594 azide was purchased from Thermo Fisher Scientific.

3.4.2 Instrumentation and software

Instrumentation and software used for the experiments performed in this chapter were the same as documented in section 2.4.2. The UV-Visible spectroscopy experiments were performed on a Cary 300 UV-Visible spectrophotometer (Agilent) using quartz cuvettes. SDS-PA gels were visualized on a ChemiDoc imaging system (Biorad) for the in-gel fluorescence experiments. Reverse-phase flash chromatographic purifications for compounds **13** and **15** were performed on a Combi Flash Rf^+ chromatography system (Teledyne ISCO).

3.4.3 Synthetic schemes and procedures

Scheme 3.1 Synthesis of diazirine choline **10**

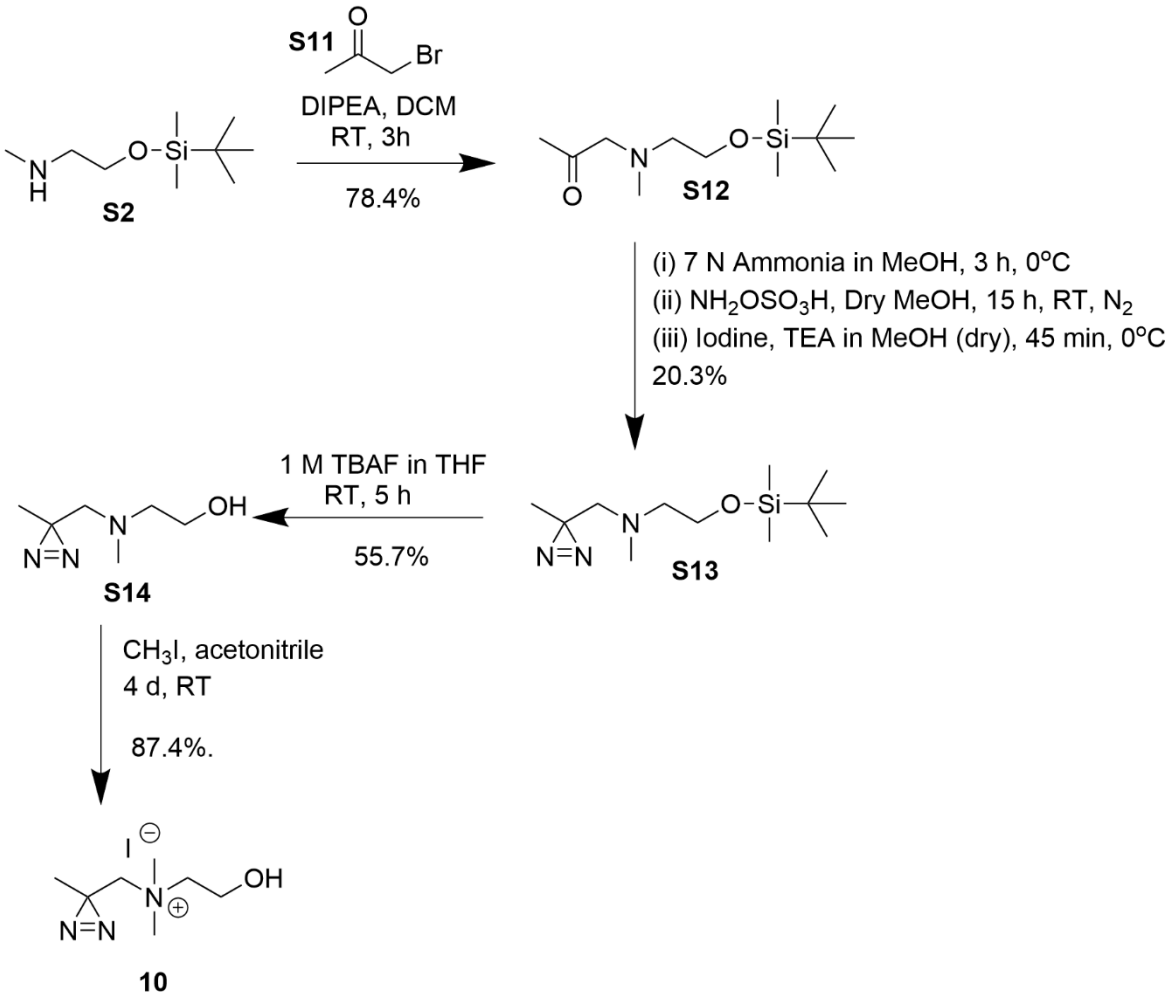

1-((2-((*t*-butyldimethylsilyl)oxy)ethyl)(methyl)amino)propan-2-one (S12)

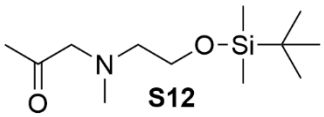

Compound **S11** was synthesized according to a previously reported procedure.[6] **S2** (1.35 g, 7.13 mmol, 1 eq.) and *N*,*N*-diisopropylethylamine (0.46 g, 3.56 mmol, 0.5 eq.) were added to dichloromethane (13 mL) and the mixture was cooled to 0 °C. Subsequently, **S12** (0.488 g, 3.56 mmol, 0.5 eq.) was added dropwise to this solution and the reaction mixture was allowed to warm to room temperature, stirred for 3 h and then washed with saturated sodium bicarbonate solution (2 × 20 mL). The organic extracts were combined, dried over anhydrous sodium sulfate and concentrated under reduced pressure. The resultant residue was subjected to silica gel column chromatography (10% ethyl acetate in hexane) to yield **S12** as a clear yellow liquid (685.6 mg, 78.4%).

^{1}H NMR (500 MHz, $CDCl_3$) δ 3.73 (t, *J* = 5.95 Hz, 2H), 3.30 (s, 2H), 2.58 (t, *J* = 5.95 Hz, 2H), 2.32 (s, 3H), 2.12 (s, 3H), 0.87 (s, 9H), 0.04 (s, 6H).

^{13}C NMR (125 MHz, $CDCl_3$) δ 208.1, 68.3, 61.8, 59.7, 43.7, 27.6, 26.0, 18.4, -5.3.

HRMS (ESI): $C_{12}H_{27}NO_2Si$; Calculated mass, $[M+H]^+$ 246.1884; Observed $[M+H]^+$ 246.1874.

2-((*t*-butyldimethylsilyl)oxy)-*N*-methyl-*N*-((3-methyl-3H-diazirin-3-yl)methyl)ethan-1-amine (S13)

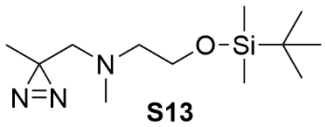

S13

A round-bottomed flask charged with **S12** (648.7 mg, 2.64 mmol, 1 eq.) was subjected to high-vacuum for 30 min and cooled to 0 °C. To this flask, an ice-cold solution of 7 N NH_3 in methanol (15.5 mL, 710 mmol, 268.9 eq.) was added and the mixture was stirred at 0 °C for 3 h. A solution of hydroxylamine-*O*-sulfonic acid (343.7 mg, 3.04 mmol, 1.2 eq.) in anhydrous methanol (15 mL) that was bubbled with nitrogen gas for 30 min, was added dropwise to the aforementioned solution by using a gas-tight syringe under nitrogen atmosphere. The flask was wrapped with Al-foil and stirred at room temperature for 15 h, resulting in the formation of a heterogeneous mixture of a white precipitate and a clear yellow liquid. Subsequently, the excess ammonia was expelled from the reaction mixture by purging it with nitrogen gas for 2 h. The resultant mixture was then filtered through celite and the retentate was washed with diethyl ether (100 mL). The filtrate was reduced to dryness, subjected to high vacuum for 30 min, purged with nitrogen gas, dissolved in anhydrous

methanol (3 mL) and cooled to 0 °C followed by addition of anhydrous triethylamine (552.5µL, 3.96 mmol, 1.5 eq.). After 10 min, iodine beads (737.9 mg, 2.9 mmol, 1.1 eq.) were added and the resultant reaction mixture was stirred at 0 °C for 45 min. Subsequently, the excess iodine was quenched by adding a solution of 10% *w/v* sodium thiosulfate (20 mL) and the mixture was washed with ethyl acetate (1 × 20 mL). The organic layer was separated, dried by adding anhydrous sodium sulfate, concentrated and subjected to silica-gel column chromatography (10% ethyl acetate in hexane) to afford 197.1 mg of **S13** as a yellow liquid (20.3%).

^{1}H NMR (500 MHz, $CDCl_3$) δ 3.69 (t, *J* = 6.2 Hz, 2H), 2.53 (t, *J* = 6.2 Hz, 2H), 2.29 (s, 3H), 2.28 (s, 2H), 1.04 (s, 3H), 0.89 (s, 9H), 0.06 (s, 6H).

^{13}C NMR (125 MHz, $CDCl_3$) δ 62.2, 61.5, 59.7, 43.3, 26.1, 25.2, 18.6, 18.4, -5.2.

HRMS (ESI): $C_{12}H_{27}N_3OSi$; Calculated mass, $[M+H]^+$ 258.1996; Observed $[M+H]^+$ 258.2016.

2-(methyl((3-methyl-3H-diazirin-3-yl)methyl)amino)ethan-1-ol (S14)

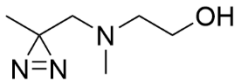

S14

A mixture of **S13** (630.4 mg, 2.44 mmol, 1 eq.) and tetrabutylammonium fluoride (3.86 mL of a 1 M solution in THF, 3.86 mmol, 1.5 eq.) in anhydrous THF (44 mL) was stirred at room temperature for 5 h. Subsequently, the solvent was removed under reduced pressure and the residue was subjected to silica-gel column chromatography (2% methanol in ethyl acetate) to yield **S14** as a yellow liquid (195.4 mg, 55.7%).

^{1}H NMR (500 MHz, $CDCl_3$) δ 3.59 (t, *J* = 5.3 Hz, 2H), 2.55 (t, *J* = 5.3 Hz, 2H), 2.31(s, 2H), 2.29 (s, 3H), 1.06 (s, 3H).

^{13}C NMR (125 MHz, $CDCl_3$) δ 61.7, 59.0, 58.5, 42.0, 24.9, 18.6.

HRMS (ESI): $C_6H_{13}N_3O$; Calculated mass, $[M+Na]^+$ 166.0951; Observed $[M+Na]^+$ 166.0945.

Diazirine choline (10)

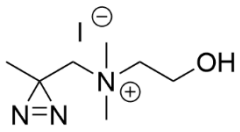

10

To a round-bottomed flask containing acetonitrile (6 mL), **S14** (195.4 mg, 1.36 mmol, 1 eq.) and methyl iodide (254.8 µL, 4.09 mmol, 3 eq.) were added and the resultant mixture was stirred at room temperature for 4 d. The brown precipitate thus obtained was triturated with ice-cold chloroform (10 × 2 mL) and, vacuum dried to afford **10** as a deep-yellow solid (339.3 mg, 87%).

^{1}H NMR (400 MHz, DMSO-d6) δ 5.29 (t, *J* = 4.88 Hz, 1H), 3.83 – 3.79 (m, 2H), 3.59 (s, 2H), 3.51 – 3.48 (m, 2H), 3.20 (s, 6H), 1.28 (s, 3H).

^{13}C NMR (100 MHz, DMSO-d6) δ 70.0, 66.2, 54.8, 51.5, 21.1, 21.0.

HRMS (ESI): $C_7H_{16}N_3O^+$; Calculated mass $[M]^+$ 158.1288; Observed Mass $[M]^+$ 158.1293.

Scheme 3.2 Synthesis of propargyl diazirine choline **11**

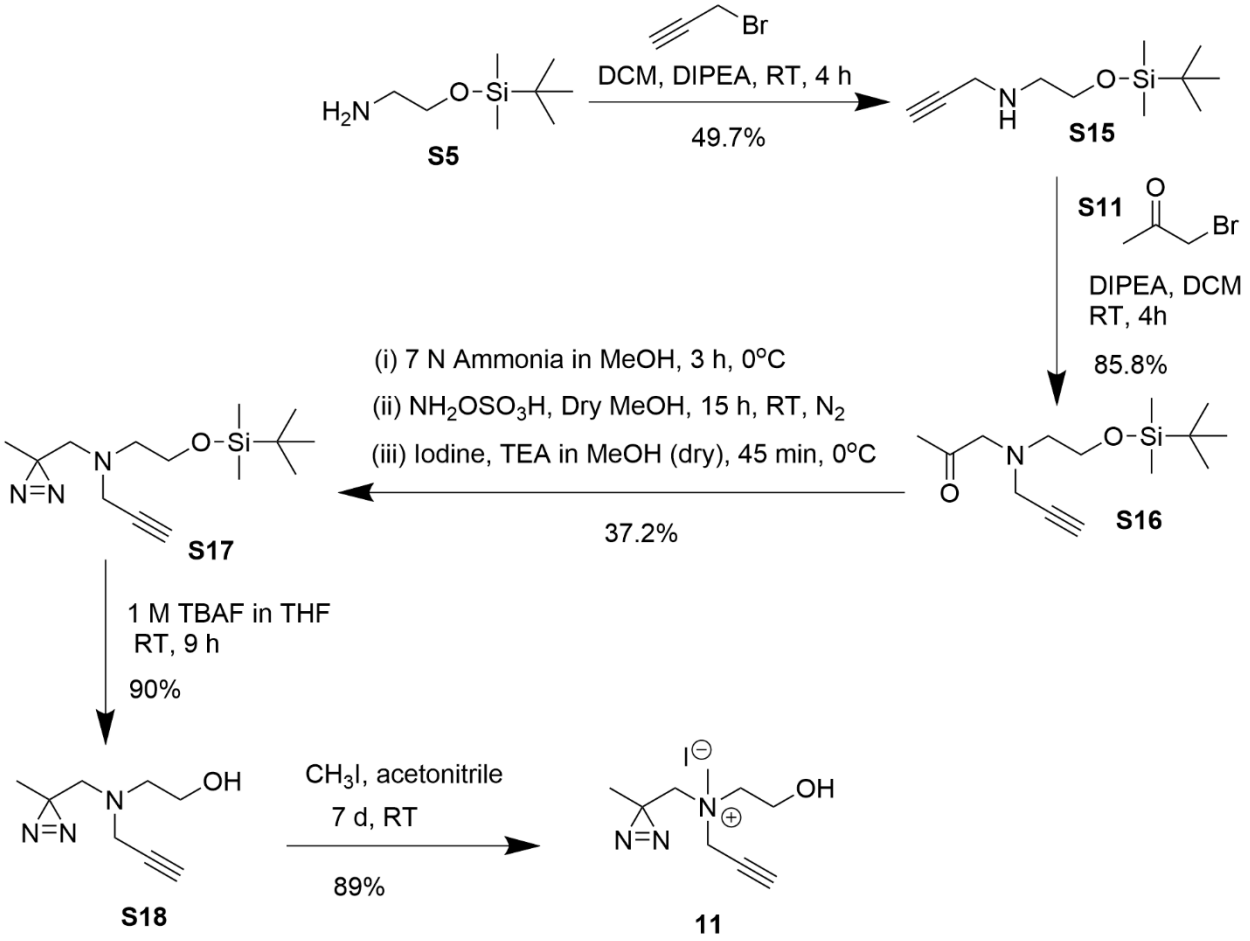

***N*-(2-((*t*-butyldimethylsilyl) oxy)ethyl)prop-2-yn-1-amine (S15)**

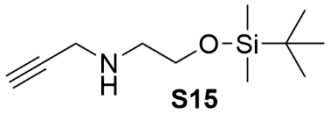

To a round-bottomed flask containing **S5** (15 g, 85.54 mmol, 1 eq.) in dichloromethane (100 mL), *N*,*N*-diisopropylethylamine (7.45 mL, 42.77 mmol, 0.5 eq.) was added and after cooling this solution to 0 °C, a solution of 80% *w*/*w* propargyl bromide in toluene (4.61 mL, 42.77 mmol, 0.5 eq.) in dichloromethane (50 mL) was added dropwise. After stirring the mixture at 0 °C for 30 min, it was warmed up to room temperature and stirred for 4 h. Subsequently, the resulting orange solution was washed with saturated sodium bicarbonate solution (2 × 150 mL), dried by adding anhydrous sodium sulfate, concentrated under reduced pressure and the crude residue was subjected to silica gel column chromatography (30% ethyl acetate in hexane) to yield **S15** as a yellow liquid (4.54 g, 49.7%).

^{1}H NMR (400 MHz, $CDCl_3$) δ 3.73 (t, *J* = 5.2 Hz, 2H), 3.45 (d, *J* = 2.4 Hz, 2H), 2.79 (t, *J* = 5.2 Hz, 2H), 2.20 (t, *J* = 2.4 Hz, 1H), 0.89 (s, 9H), 0.06 (s, 6H).

^{13}C NMR (100 MHz, $CDCl_3$) δ 82.3, 71.4, 62.4, 50.7, 38.3, 26.1, 18.4, -5.2.

HRMS (ESI): $C_{11}H_{23}NOSi$; Calculated mass, $[M]^+$ 213.1549; Observed mass, $[M]^+$ 213.1549.

1-((2-((*t*-butyldimethylsilyl)oxy)ethyl)(prop-2-yn-1-yl)amino)propan-2-one (S16)

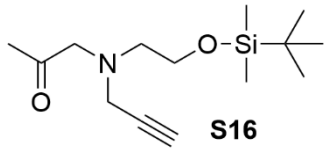

S16

To an ice-cold solution of *N*,*N*-diisopropylethylamine (1.85 mL, 10.59 mmol, 0.5 eq.) and **S15** (4.52 g, 21.18 mmol, 1 eq.) in dichloromethane (51 mL), **S11** (1.45 g, 10.59 mmol, 0.5 eq.) was added dropwise. This mixture was subsequently warmed to room temperature and stirred for 4 h followed by washing with saturated sodium bicarbonate solution (1 × 50 mL). The aqueous layer was given another wash with dichloromethane (1 × 50 mL) and the organic extracts were combined, dried by adding anhydrous sodium sulfate, concentrated under reduced pressure, and subjected to silica gel column chromatography (30% ethyl acetate in hexane) to afford **S16** as a dark-yellow liquid (0.53 g, 85.8%).

^{1}H NMR (400 MHz, $CDCl_3$) δ 3.75 (t, *J* = 6.0 Hz, 2H), 3.52 (d, *J* = 2.4 Hz, 2H), 3.49 (s, 2H), 2.68 (t, *J* = 6.0 Hz, 2H), 2.20 (t, *J* = 2.4 Hz, 1H), 2.14 (s, 3H), 0.88 (s, 9H), 0.05 (s, 6H).

^{13}C NMR (100 MHz, $CDCl_3$) δ 207.4, 78.8, 73.3, 64.5, 62.5, 56.4, 44.2, 27.9, 26.1, 18.5, -5.2.

HRMS (ESI): $C_{14}H_{27}NO_2Si$; Calculated mass, $[M]^+$ 269.1811; Observed mass, $[M]^+$ 269.1811.

***N*-(2-((*t*-butyldimethylsilyl)oxy)ethyl)-*N*-((3-methyl-3H-diazirin-3-yl)methyl)prop-2-yn-1-amine (S17)**

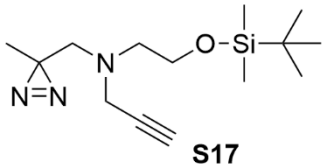

S17

A round-bottomed flask containing **S16** (4.14 g, 15.36 mmol, 1 eq.) was subjected to high-vacuum for 30 min and then cooled on an ice bath. Subsequently, an ice-cold solution of 7 N NH_3 in methanol (109 mL, 768 mmol, 50 eq.) was added to this flask and the resulting mixture was stirred

at 0 °C for 3 h after which, a solution of hydroxylamine-*O*-sulfonic acid (1.99 g, 17.66 mmol, 1.15 eq.) in anhydrous methanol (88 mL) that had been bubbled with nitrogen gas for 30 min, was added to this reaction mixture by using a gas-tight syringe. The resulting solution was warmed to room temperature and stirred for 15 h, resulting in the formation of a heterogeneous mixture containing a white precipitate and a pale-yellow liquid. Subsequently, ammonia was expelled from the reaction mixture by purging with nitrogen gas for 2 h and the mixture was filtered through a celite plug and washed with diethyl ether (100 mL). The filtrate was reduced to dryness, subjected to high vacuum for 30 min and purged with nitrogen gas. Subsequently, anhydrous methanol (18 mL) and anhydrous triethylamine (3.21 mL, 23.04 mmol, 1.5 eq.) were added and the mixture was cooled to 0 °C. After 10 min, iodine beads (4.29 g, 16.89 mmol, 1.1 eq.) were added and the reaction mixture was stirred for 45 min under ice-cold conditions. The excess iodine was then quenched with a 10% *w/v* sodium thiosulfate solution (75 mL) and the solution was washed with ethyl acetate (3 × 75 mL). The organic layers were combined, dried by adding anhydrous sodium sulfate, concentrated and subjected to silica gel column chromatography (2% ethyl acetate in hexane) to afford **S17** (1.61 g, 37.2%) as a yellow liquid.

^{1}H NMR (400 MHz, $CDCl_3$) δ 3.70 (t, *J* = 6.0 Hz, 2H), 3.51 (d, *J* = 2.4 Hz, 2H), 2.64 (t, *J* = 6.0 Hz, 2H), 2.44 (s, 2H), 2.15 (t, *J* = 2.4 Hz, 1H), 1.05 (s, 3H), 0.90 (s, 9H), 0.06 (s, 6H).

^{13}C NMR (100 MHz, $CDCl_3$) δ 78.5, 73.2, 62.0, 58.2, 55.5, 43.4, 26.1, 24.9, 18.5, 18.4, -5.2.

HRMS (ESI): $C_{14}H_{27}N_3OSi$; Calculated mass, $[M]^+$ 281.1923; Observed mass, $[M]^+$ 281.1923.

2-(((3-methyl-3H-diazirin-3-yl)methyl)(prop-2-yn-1-yl)amino)ethan-1-ol (S18)

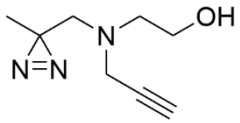

S18

S17 (1.59 g, 5.65 mmol, 1 eq.) and tetrabutylammonium fluoride (8.47 mL of a 1 M solution in THF, 8.47 mmol, 1.5 eq.) were dissolved in anhydrous THF (70 mL) and stirred at room temperature for 9 h. Subsequently, the solvent was evaporated under reduced pressure and the residue was subjected to silica gel column chromatography (20% ethyl acetate in hexane) to afford **S18** (0.85 g, 90%) as a yellow oil.

^{1}H NMR (400 MHz, $CDCl_3$) δ 3.59 (t, *J* = 5.2 Hz, 2H), 3.50 (d, *J* = 2.4 Hz, 2H), 2.69 (t, *J* = 5.2 Hz, 2H), 2.49 (s, 2H), 2.18 (t, *J* = 2.4 Hz, 1H), 1.07 (s, 3H).

^{13}C NMR (100 MHz, $CDCl_3$) δ 73.7, 58.6, 57.1, 55.2, 42.1, 24.6, 18.7.

HRMS (ESI): $C_8H_{13}N_3O$; Calculated mass, $[M\text{-}N_2+H]^+$ 140.1131; Observed mass, $[M\text{-}N_2+H]^+$ 139.9892.

Propargyl diazirine choline (11)

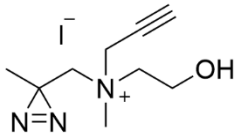

11

To a solution of **S18** (0.44 g, 2.62 mmol, 1 eq.) in acetonitrile (4 mL), methyl iodide (0.25 mL, 4.01 mmol, 1.5 eq.) was added and the mixture was stirred at room temperature for 7 d. Each day, methyl iodide (0.25 mL) was added (total of 1.75 mL, 28.1 mmol, 10.5 eq.) to the reaction mixture. Subsequently, the excess solvent was evaporated under reduced pressure and the dark brown residue was triturated with ice-cold chloroform (4 × 5 mL) and vacuum dried to afford **11** as an orange-brown solid (0.72 g, 89%).

^{1}H NMR (400 MHz, DMSO-d6) δ 5.37 (t, *J* = 4.8 Hz, 1H), 4.64 – 4.53 (m, 2H), 4.09 (t, *J* = 2.4 Hz, 1H), 3.83 (q, *J* = 5.2 Hz, 2H), 3.83 – 3.56 (m, 4H), 3.24 (s, 3H), 1.29 (s, 3H).

^{13}C NMR (100 MHz, DMSO-d6) δ 83.7, 72.0, 68.1, 64.1, 54.7, 52.9, 49.2, 20.8, 20.7.

HRMS (ESI): $C_9H_{16}N_3O^+$; Calculated mass, $[M\text{-}N_2]^+$ 154.1288; Observed mass, $[M\text{-}N_2]^+$ 154.1239.

Scheme 3.3 Synthesis of azido diazirine choline **12**

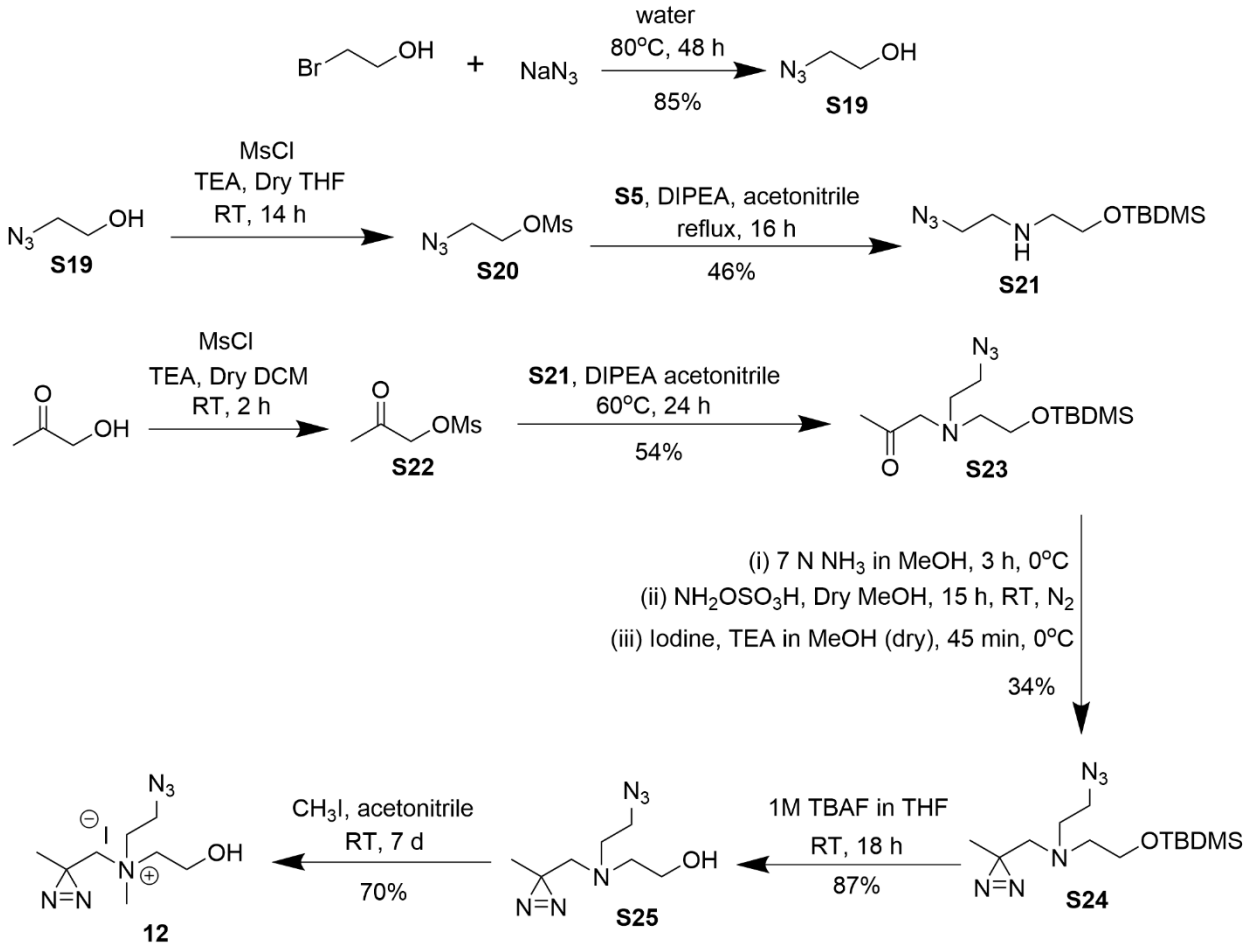

2-azidoethanol (S19)

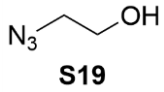

Sodium azide (11.45 g, 176.5 mmol, 1 eq.) was slowly added to an ice-cold solution of 2-bromoethanol (5 mL, 70.5 mmol, 2.5 eq.) in water (10 mL). The solution was then warmed up to room temperature and then heated at 80 °C for 48 h. Subsequently, the reaction mixture was washed with diethyl ether (10 × 10 mL), the organic layers were pooled, dried by adding anhydrous sodium sulfate and concentrated to afford pure **S19** as a colorless oil (85%).

^{1}H NMR (400 MHz, $CDCl_3$) δ 3.77 (t, *J* = 5.2 Hz, 2H), 3.44 (t, *J* = 5.2 Hz, 2H), 2.05 (s, 1H).

^{13}C NMR (100 MHz, $CDCl_3$) δ 61.6, 53.6.

HRMS (ESI): $C_2H_5N_3O$; Calculated mass for $[M]^+$ 87.0436; Observed mass for $[M]^+$ 87.0761.

2-azido-*N*-(2-((*t*-butyldimethylsilyl)oxy)ethyl)ethan-1-amine (S21)

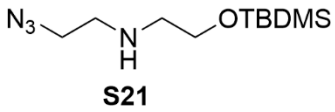

S21

S19 (1.98 g, 22.8 mmol, 1 eq.) was dissolved in dry THF (60 mL) under nitrogen atmosphere and dry triethylamine (6.35 mL, 45.6 mmol, 2 eq.) was added. The resultant mixture was cooled on an ice bath and methanesulfonyl chloride (3.5 mL, 45.6 mmol, 2 eq.) was added. The mixture was stirred at room temperature for 14 h. The reaction mixture was then added to 1 N NaOH (100 mL) and the resultant mixture was washed with dichloromethane (3 × 100 mL), the organic layers were combined, dried by adding anhydrous sodium sulfate, and concentrated under reduced pressure. This concentrated mesylate (**S20**) was treated with a solution of **S5** (4.0 g, 22.8 mmol, 1 eq.) and *N*,*N*-diisopropylethylamine (4 mL, 22.8 mmol, 1 eq.) in acetonitrile (95 mL). The resultant yellow solution was refluxed for 16 h and then the solvent was evaporated under reduced pressure. The concentrated residue was dissolved in ethyl acetate (100 mL), washed with 1 N NaOH (1 ×100 mL) and the organic layer was dried by adding anhydrous sodium sulfate, concentrated and subjected to silica gel column chromatography (50% ethyl acetate in dichloromethane) to afford **S21**(46.2%) as a pale-yellow oil.

^{1}H NMR (400 MHz, $CDCl_3$) δ 3.72 (t, *J* = 5.2 Hz, 2H), 3.42 (t, *J* = 5.6 Hz, 2H), 2.82 (t, *J* = 5.6 Hz, 2H), 2.73 (t, *J* = 5.2 Hz, 2H), 0.90 (s, 9H), 0.06 (s, 6H).

^{13}C NMR (100 MHz, $CDCl_3$) δ 62.5, 51.8, 51.6, 48.6, 26.1, 18.5, -5.1.

HRMS (ESI): $C_{10}H_{24}N_4OSi$; Calculated mass $[M+H]^+$ 245.1792; Observed mass $[M+H]^+$ 245.1803.

1-((2-azidoethyl)(2-((*t*-butyldimethylsilyl)oxy)ethyl)amino)propan-2-one (S23)

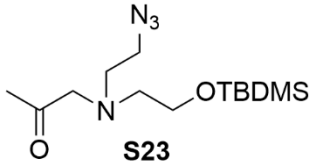

S23

A round-bottomed flask containing hydroxyacetone (1.0 mL, 14.76 mmol, 1 eq.) was subjected to high vacuum, flushed with nitrogen gas and dry dichloromethane (67 mL) and dry triethylamine (4.1 mL, 29.46 mmol, 2 eq.) were added. The flask was then cooled to 0 °C and methanesulfonyl chloride (2.3 mL, 29.46 mmol, 2 eq.) was added dropwise under nitrogen atmosphere. The

resultant reaction mixture was stirred for 2 h at 0 °C and then washed with 1 N NaOH (60 mL). The organic layer was dried by adding anhydrous sodium sulfate and concentrated under reduced pressure. This concentrated mesylate (**S22)** was added to a solution of **S21** (3.6 g, 14.7 mmol, 1 eq.) and *N*,*N*-diisopropylethylamine (2.8 mL, 16.2 mmol, 1.1 eq.) in acetonitrile (70 mL) and the resultant solution was stirred for 24 h at 60 °C. Subsequently, the solvent was evaporated under reduced pressure and saturated sodium bicarbonate solution (70 mL) was added to the concentrated residue. The mixture was transferred to a separating funnel and washed with dichloromethane (3 × 70 mL). The organic layers were pooled, dried by adding anhydrous sodium sulfate, concentrated and subjected to silica gel column chromatography (15% ethyl acetate in hexane) to afford **S23** as a yellow oil (2.30 g, 54%).

^{1}H NMR (400 MHz, $CDCl_3$) δ 3.71(t, *J* = 5.6 Hz, 2H), 3.49 (s, 2H), 3.30 (t, *J* = 6.0 Hz, 2H), 2.85 (t, *J* = 6.0 Hz, 2H), 2.76 (t, *J* = 5.6 Hz, 2H), 2.14 (s, 3H), 0.88 (s, 9H), 0.05 (s, 6H).

^{13}C NMR (100 MHz, $CDCl_3$) δ 208.7, 65.6, 62.4, 56.9, 54.9, 49.9, 27.5, 26.0, 18.4, -5.3.

HRMS (ESI): $C_{13}H_{28}N_4O_2Si$; Calculated mass $[M+H]^+$ 301.2054; Observed mass $[M+H]^+$ 301.2063.

2-azido-*N*-(2-((*t*-butyldimethylsilyl)oxy)ethyl)-*N*-((3-methyl-3H-diazirin-3-yl)methyl)ethan-1-amine (S24)

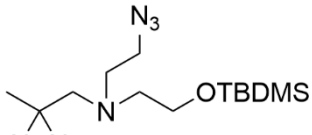

S24

A round-bottomed flask containing **S23** (2.12 g, 7.06 mmol, 1 eq.) was subjected to high-vacuum for 30 min and then cooled to 0 °C. To this mixture, an ice-cold solution of 7 N NH_3 in methanol (50 mL, 353 mmol, 50 eq.) was added and the mixture was stirred at 0 °C for 3 h. Subsequently, a solution of hydroxylamine-*O*-sulfonic acid (1.19 g, 10.59 mmol, 1.5 eq) in anhydrous methanol (41 mL) that had been bubbled with nitrogen gas for 30 min, was added dropwise via a syringe into the aforementioned mixture and the resultant solution was stirred for 15 h at room temperature. Excess ammonia was expelled by purging the mixture with nitrogen gas for 2 h after which a heterogeneous mixture containing a white precipitate and a yellow liquid was observed. The

precipitate was filtered through celite and washed with diethyl ether (100 mL) and the filtrate was concentrated under reduced pressure, kept under high vacuum for 30 min, and purged with nitrogen gas for 30 min. Subsequently, dry methanol (8 mL) and dry triethylamine (1.5 mL, 10.59 mmol, 1.5 eq.) were added and the mixture was cooled to 0 °C. To this flask, iodine beads (1.97 g, 7.77 mmol, 1.1 eq.) were added and the resultant deep-brown colored mixture was stirred for 45 min under ice-cold conditions. Excess iodine was quenched by adding 10% *w/v* sodium thiosulfate solution (20 mL) and the resultant mixture was washed with ethyl acetate (3 × 20 mL). The organic layers were combined, dried by adding anhydrous sodium sulfate, concentrated under reduced pressure to yield a residue that was subjected to silica gel column chromatography (2% ethyl acetate in hexane) to afford **S24** as a yellow liquid (0.77 g, 34%).

^{1}H NMR (400 MHz, $CDCl_3$) δ3.69 (t, *J* = 6.0 Hz, 2H), 3.28 (t, *J* = 6.4 Hz, 2H), 2.77 (t, *J* = 6.0 Hz, 2H), 2.70 (t, *J* = 6.0 Hz, 2H), 2.47 (s, 2H), 1.06 (s, 3H), 0.89 (s, 9H), 0.06 (s, 6H).

^{13}C NMR (100 MHz, $CDCl_3$) δ 61.6, 59.4, 56.4, 54.5, 49.5, 26.0, 25.5, 18.4, 18.3, -5.3.

HRMS (ESI): $C_{13}H_{28}N_6OSi$; Calculated mass $[M+H]^+$ 313.2166; Observed mass $[M+H]^+$ 313.2176.

2-((2-azidoethyl)((3-methyl-3H-diazirin-3-yl)methyl)amino)ethan-1-ol (S25)

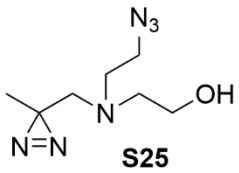

S25

S24 (242 mg, 0.77 mmol, 1 eq.) and tetrabutylammonium fluoride (1.2 mL of a 1 M solution in THF, 1.2 mmol, 1.5 eq.) were added to anhydrous THF (10 mL) and stirred for 18 h at room temperature. Subsequently, the solvent was evaporated under reduced pressure and the residue was subjected to silica gel column chromatography (20% ethyl acetate in dichloromethane) to yield **S25** as a yellow liquid (0.13 g, 87%).

^{1}H NMR (400 MHz, $CDCl_3$) δ 3.61 (q, *J* = 5.2 Hz, 2H), 3.36 (t, *J* = 6.0 Hz, 2H), 2.72 (t, *J* = 6.0 Hz, 2H), 2.68 (t, *J* = 5.2 Hz, 2H), 2.49 (s, 2H), 1.09 (s, 3H).

^{13}C NMR (100 MHz, $CDCl_3$) δ 59.3, 58.7, 56.6, 53.6, 49.4, 25.2, 18.5.

HRMS (ESI): $C_7H_{14}N_6O$; Calculated mass $[M]^+$ 198.1229; Observed mass $[M]^+$ 198.1308.

Azido diazirine choline (12)

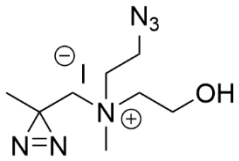

12

To a solution of **S25** (3.27 g, 16.5 mmol, 1 eq.) in acetonitrile (12 mL), methyl iodide (1.96 mL, 31.5 mmol, 1.9 eq.) was added and the mixture was stirred at room temperature for 7 d. Each day, methyl iodide (1.96 mL) was added (total of 13.72 mL, 0.22 mol, 13.3 eq.) to the reaction mixture. Subsequently, the solvent was evaporated under reduced pressure and the crude residue was dissolved in water (20 mL) and washed with diethyl ether (10 × 20 mL). The organic layers were combined, dried by adding anhydrous sodium sulfate, and concentrated under reduced pressure to afford **12** as a viscous yellow liquid (70%).

^{1}H NMR (400 MHz, DMSO-d6) δ 5.33 (t, *J* = 4.4 Hz, 1H), 3.89 (t, *J* = 6.0 Hz, 2H), 3.78 – 3.83 (m, 2H), 3.68 – 3.65 (m, 4H), 3.58 (t, *J* = 5.2 Hz, 2H), 3.24 (s, 3H), 1.28 (s, 3H).

^{13}C NMR (100 MHz, DMSO-d6) δ 68.7, 63.9, 60.9, 54.7, 49.5, 44.0, 21.1, 20.9.

HMRS (ESI): $C_{20}H_{11}N_3O_5$; Calculated mass $[M]^+$ 373.0699; Observed mass $[M+H]^+$ 374.0778.

Scheme 3.4 Synthesis of propargyl ethyl diazirine choline **13**

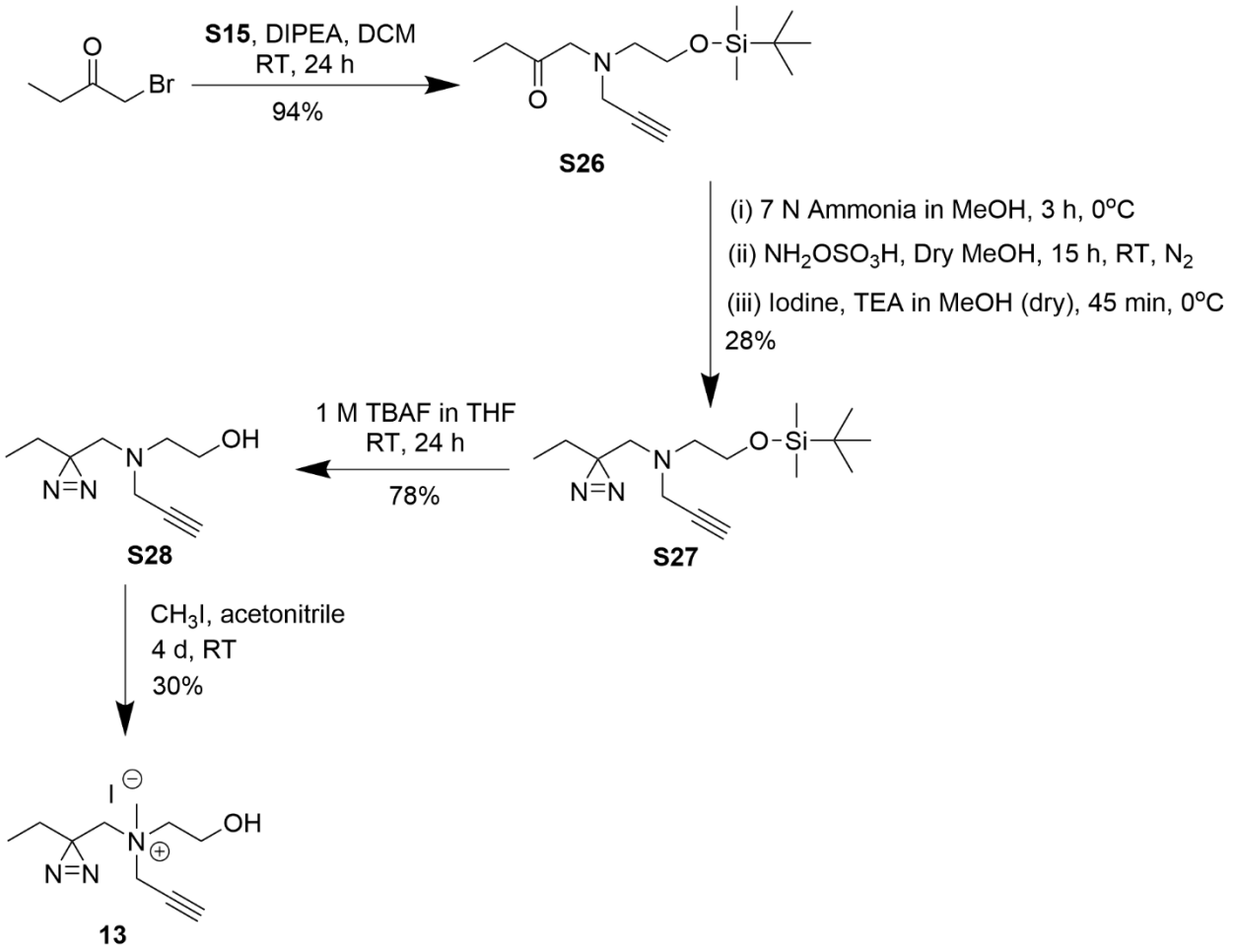

1-((2-((*t*-butyldimethylsilyl)oxy)ethyl)(prop-2-yn-1-yl)amino)butan-2-one (S26)

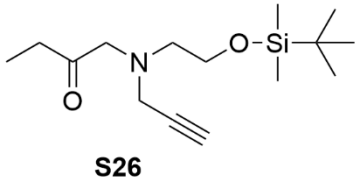

To a round-bottomed flask containing an ice-cold solution of **S15** (3.63 g, 17.88 mmol, 1 eq.) in dichloromethane (15 mL), *N*,*N*-diisopropylethylamine (3.80 mL, 21.84 mmol, 1.2 eq.) was added. To this flask, bromobutan-2-one (3 g, 19.86 mmol, 1.1 eq.) was added dropwise and the resultant mixture was stirred at 0 °C for 30 min and then at room temperature for 12 h. The reaction mixture was further diluted with dichloromethane (50 mL) and washed with a saturated solution of sodium bicarbonate (1 × 50 mL). The aqueous layer was washed with dichloromethane (3 × 50 mL) and all organic layers were combined, dried by adding anhydrous sodium sulfate and concentrated

under reduced pressure. The resultant residue was subjected to silica gel column chromatography (8% ethyl acetate in hexane) to give **S26** as a colorless oil (4.70 g, 94%).

^{1}H NMR (400 MHz, $CDCl_3$) δ 3.75 (t, *J* = 6.0 Hz, 2H), 3.52 (d, *J* = 2.4 Hz, 2H), 3.48 (s, 2H), 2.68 (t, *J* = 6.0 Hz, 2H), 2.47 (q, *J* = 7.6 Hz, 2H), 2.20 (t, *J* = 2.4 Hz, 1H), 1.06 (t, *J* = 7.6 Hz, 3H), 0.88 (s, 9H), 0.05 (s, 6H).

^{13}C NMR (100 MHz, $CDCl_3$) δ 210.1, 78.9, 73.3, 63.4, 62.4, 56.3, 44.1, 33.6, 26.0, 18.4, 7.9, -5.3.

HRMS (ESI): $C_{15}H_{30}NO_2Si$; Calculated for $[M+H]^+$ 284.2046; Observed for $[M+H]^+$, 284.2051

***N*-(2-((*t*-butyldimethylsilyl)oxy)ethyl)-*N*-((3-ethyl-3H-diazirin-3-yl)methyl)prop-2-yn-1-amine (S27)**

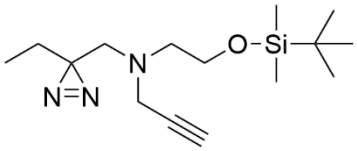

S27

A round-bottomed flask charged with **S26** (0.5 g, 1.76 mmol, 1 eq.) was kept under high vacuum for 30 min and cooled to 0 °C. Subsequently, an ice-cold solution of 7 N NH_3 in methanol (12.5 mL, 87.5 mmol, 50 eq.) was added and the mixture was stirred at 0 °C for 3 h. To this mixture, a solution of hydroxylamine-*O*-sulfonic acid (0.39 g, 3.26 mmol, 1.9 eq.) in anhydrous methanol (5 mL) that had been bubbled with nitrogen gas for 30 min, was added dropwise via a syringe and the reaction mixture was stirred at room temperature for 15 h. Subsequently, excess ammonia was removed by bubbling nitrogen gas for 2 h, and the heterogeneous mixture containing a white precipitate and a yellow solution thus obtained, was filtered on celite and washed with diethyl ether (100 mL). The filtrate was evaporated to dryness, subjected to high vacuum for 30 min and purged with nitrogen gas. Subsequently, dry methanol (15 mL) and dry triethylamine (0.37 mL, 2.65 mmol, 1.5 eq.) were added and the solution was cooled to 0 °C followed by addition of iodine (0.49 g, 1.94 mmol, 1.1 eq.) in small portions and the mixture was stirred at 0 °C for 45 min. Subsequently, ethyl acetate (50 mL) was added and the mixture was washed with 1 N HCl (1 × 50 mL), and a saturated solution of sodium bicarbonate (1 × 50 mL). The organic layer was dried by adding anhydrous sodium sulfate and concentrated under reduced pressure to give a residue which

was subjected to silica gel column chromatography (2% ethyl acetate in hexane) to give **S27** as a pale-yellow oil (0.11 g, 21%).

^{1}H NMR (400 MHz, $CDCl_3$) δ 3.68 (t, *J* = 6.0 Hz, 2H), 3.50 (d, *J* = 2.4 Hz, 2H), 2.63 (t, *J* = 6.0 Hz, 2H), 2.45 (s, 2H), 2.15 (t, *J* = 2.4 Hz, 1H), 1.48 (q, *J* = 8.0 Hz, 2H), 0.89 (s, 9H), 0.69 (t, *J* = 6.0 Hz, 3H), 0.06 (s, 6H).

^{13}C NMR (100 MHz, $CDCl_3$) δ 78.4, 73.0, 61.8, 56.7, 55.4, 43.2, 28.5, 25.9, 24.3, 18.3, 8.0, -5.4.

HRMS (ESI): $C_{15}H_{30}N_3OSi$; Calculated mass $[M+Na]^+$ 296.2158; Observed mass $[M+Na]^+$ 296.2152.

2-(((3-ethyl-3H-diazirin-3-yl)methyl)(prop-2-yn-1-yl)amino)ethan-1-ol (S28)

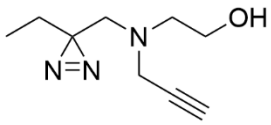

S28

S27 (1.2 g, 4.06 mmol, 1 eq.) and tetrabutylammonium fluoride (6.1 mL of a 1 M solution in THF, 6.09 mmol, 1.5 eq.) was added to dry THF (5 mL) and stirred for 24 h at room temperature. Subsequently, the solvent was removed under reduced pressure and the concentrated residue was subjected to silica gel column chromatography (5% ethyl acetate in dichloromethane) to give **S28** as a colorless oil (0.58 g, 78%).

^{1}H NMR (400 MHz, $CDCl_3$) δ 3.58 (t, *J* = 5.2 Hz, 2H), 3.48 (d, *J* = 2.4 Hz, 2H), 2.68 (t, *J* = 5.2 Hz, 2H), 2.50 (s, 2H), 2.18 (t, *J* = 2.4 Hz, 1H), 1.51 (q, *J* = 7.6 Hz, 2H), 0.70 (t, *J* = 7.6 Hz, 3H).

^{13}C NMR (100 MHz, $CDCl_3$) δ 73.7, 58.7, 55.7, 55.2, 42.2, 28.4, 24.6, 8.2, 0.1.

HRMS (ESI): $C_9H_{15}N_3O$; Calculated mass $[M]^+$ 182.1215; Observed mass $[M]^+$ 182.1289.

Propargyl ethyl diazirine choline (13)

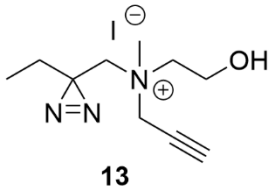

13

To a solution of **S28** (0.56 g, 3.10 mmol, 1 eq.) in acetonitrile (3 mL), methyl iodide (1.15 mL, 18.4 mmol, 6 eq.) was added and the mixture was stirred at room temperature for 4 d. Each day,

methyl iodide (1.15 mL) was added (total of 4.6 mL, 74 mmol, 24 eq.) to the reaction mixture. Subsequently, the solvent was removed by evaporation under reduced pressure and the resultant residue was subjected to reverse phase flash column chromatography by using a Redisep Rf 43 g C18 column with water-acetonitrile as the mobile phase (gradient: 0-20 min (100% water), 20-30 min (100-0% water), 30-35 min (0% water), 35-40 min (0-100% water); flow rate = 5 mL/min) to give pure column fractions containing **13**. These fractions were concentrated under reduced pressure to afford **13** as a colorless liquid (0.3 g, 30%).

^{1}H NMR (400 MHz, D_2O) δ 4.51 (s, 2H), 4.03 – 4.01 (m, 2H), 3.73 (t, *J* = 4.8 Hz, 2H), 3.69 (d, *J* = 5.2 Hz, 2H), 3.35 (s, 3H), 1.85 (q, *J* = 7.6 Hz, 2H), 0.65 (t, *J* = 7.6 Hz, 3H).

^{13}C NMR (100 MHz, DMSO-d6) δ 83.7, 71.9, 70.0, 64.1, 54.7, 52.8, 49.2, 25.2, 24.7, 7.7.

HRMS (ESI): $C_{10}H_{18}N_3O$; Calculated mass $[M]^+$ 196.1444; Observed mass $[M]^+$ 196.1454.

Scheme 3.5 Synthesis of propargyl methyl diazirine choline **15**

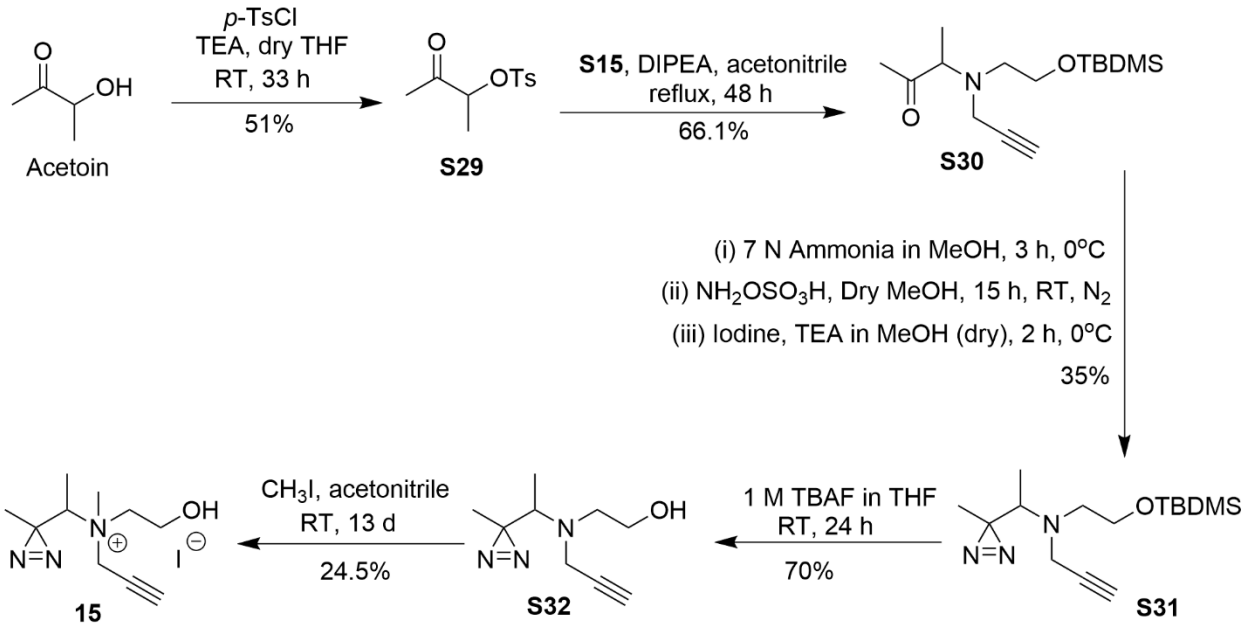

3-oxobutan-2-yl 4-methylbenzenesulfonate (S29)

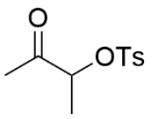

S29

A round-bottomed flask containing a mixture of acetoin (6 g, 68 mmol, 1 eq.) and *p*-toluenesulfonyl chloride was flushed with nitrogen gas and cooled in an ice bath. Dry THF (70 mL) was added and the mixture was stirred on the ice bath for 15 min. Dry triethylamine (18.9 mL, 136 mmol, 2 eq.) was then added and the resultant mixture was allowed to stir at 0 °C for another 10 min and then at room temperature for 33 h. Subsequently, the solvent was removed under reduced pressure and the concentrated residue was dissolved in ethyl acetate (100 mL). This solution was washed with 1 N HCl (1 × 100 mL), saturated solution of sodium bicarbonate (1 × 100 mL), and brine (1 × 100 mL). The organic layer was concentrated under reduced pressure and the residue was subjected to silica gel column chromatography (10% ethyl acetate in hexane) to afford **S29** as a yellow liquid (16.5 g, 51%).

^{1}H-NMR (400Hz, $CDCl_3$) δ 7.81 (d, *J* = 8.4 Hz, 2H), 7.36 (d, *J* = 8.8 Hz, 2H), 4.75 (q, *J* = 6.8 Hz, 1H), 2.46 (s, 3H), 2.21 (s, 3H), 1.34 (d, *J* = 6.8 Hz, 3H).

^{13}C NMR (100 MHz, $CDCl_3$) δ 205.4, 145.5, 133.3, 130.2, 128.0, 81.0, 25.7, 21.8, 17.4.

HRMS (ESI): $C_{11}H_{14}O_4S$; Calculated mass, $[M+H]^+$ 243.0686; Observed mass, $[M+H]^+$ 243.0695.

3-((2-((*t*-butyldimethylsilyl)oxy)ethyl)(prop-2 -yn-1-yl)amino)butan-2-one (S30)

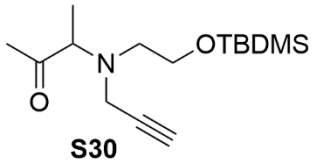

S30

N,*N*-diisopropylethylamine (3.16 mL, 18.15 mmol, 1.1 eq.) was added to a solution of **S15** (4 g, 16.5 mmol, 1 eq.) in acetonitrile (40 mL). To this flask, **S29** (3.52 g, 16.5 mmol, 1 eq.) was added dropwise and the mixture was refluxed for 48 h at room temperature. Subsequently, the solvent was removed under reduced pressure and the concentrated residue was dissolved in dichloromethane (50 mL) and washed with saturated sodium bicarbonate solution (50 mL). The aqueous layer was further washed with dichloromethane (2 × 50 mL). All the organic layers were pooled, dried by adding anhydrous sodium sulfate, and concentrated under reduced pressure. The concentrated residue was subjected to silica gel column chromatography (5% ethyl acetate in hexane) to afford **S30** as a dark yellow liquid (4.67 g, 66.1%).

^{1}H-NMR (400Hz, $CDCl_3$) δ 3.70 (t, *J* = 6.4 Hz, 2H), 3.54 – 3.42 (m, 3H), 2.71 – 2.5 (m, 2H), 2.23 (s, 3H), 2.19 (t, *J* = 2.4 Hz, 1H), 1.18 (d, *J* = 7.2 Hz, 3H), 0.89 (s, 9H), 0.05 (s, 6H).

^{13}C NMR (100 MHz, $CDCl_3$) δ 211.5, 79.8, 72.8, 66.7, 62.1, 52.9, 40.6, 26.7, 25.9, 18.3, 11.6, -5.4.

HRMS (ESI): $C_{15}H_{29}NO_2Si$; Calculated mass, $[M+H]^+$ 284.2040, Observed mass, $[M+H]^+$ 284.2047.

***N*-(2-((*t*-butyldimethylsilyl)oxy)ethyl)-*N*-(1-(3-methyl-3H-diazirin-3-yl)ethyl)prop-2-yn-1-amine (S31)**

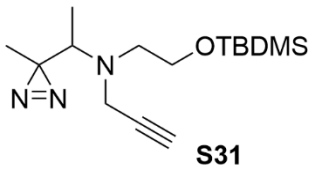

S31

A round-bottomed flask charged with **S30** (2.84 g, 10 mmol, 1 eq.) was kept under high vacuum for 30 min and cooled to 0 °C. Subsequently, an ice-cold solution of 7 N ammonia in methanol (72 mL, 500 mmol, 50 eq.) was added and the mixture was stirred at 0 °C for 3 h. To this flask, a solution of hydroxylamine-*O*-sulfonic acid (1.69 g, 15 mmol, 1.5 eq.) in dry methanol (75 mL) that had been bubbled with nitrogen gas for 30 min, was added dropwise via a syringe and the resultant mixture was stirred for 15 h at room temperature. Subsequently, excess ammonia was purged out by bubbling nitrogen gas for 2 h, and the heterogeneous mixture of a white precipitate and a yellow liquid thus obtained was filtered on celite and washed with diethyl ether (100 mL). The filtrate was evaporated to dryness, kept under high vacuum for 30 min, and was purged with nitrogen gas. To this flask, dry methanol (12 mL) and dry triethylamine (2.1 mL, 15 mmol, 1.5 eq.) were added and the mixture was cooled to 0 °C. After 10 min, iodine (2.79 g, mmol, 1.1 eq.) was added in small portions and the reaction mixture was stirred for 2 h at 0 °C. The reaction was quenched by adding a solution of 10% *w*/*v* sodium thiosulfate (50 mL) and turbid solution thus obtained was washed with ethyl acetate (3 × 50 mL). The organic layers were combined, dried by adding anhydrous sodium sulfate and concentrated under reduced pressure. The resultant residue was subjected to silica gel column chromatography (2% ethyl acetate in hexane) to yield **S31** as a yellow liquid (0.95 g, 35%).

^{1}H-NMR (400Hz, $CDCl_3$) δ3.75 (td, *J* = 6.2 Hz, 2.0 Hz, 2H). 3.65 (dd, *J* = 17.6 Hz, 2.4 Hz, 1H), 3.48 (dd, *J* = 17.2 Hz, 2 Hz, 1H), 2.81 – 2.77 (m, 2H), 2.48 (q, *J* = 6.8 Hz, 1H), 2.14 (t, *J* = 2.4 Hz, 1H), 1.00 (s, 3H), 0.90 (s, 9H), 0.88 (d, *J* = 6.8 Hz, 3H), 0.08 (s, 6H).

^{13}C NMR (100 MHz, $CDCl_3$) δ 79.9, 72.7, 62.4, 59.8, 52.1, 40.3, 28.7, 26.1, 18.5, 17.2, 12.6, -5.2.

HRMS (ESI): $C_{15}H_{29}N_3OSi$; Calculated mass, $[M-N_2+H]^+$ 268.2152; Observed mass, $[M-N_2+H]^+$ 268.2101.

2-((1-(3-methyl-3H-diazirin-3-yl)ethyl)(prop-2-yn-1-yl)amino)ethan-1-ol (S32)

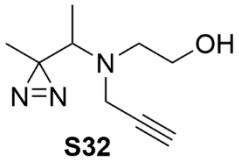

S32

To a solution of **S31** (950 mg, 3.21 mmol, 1 eq.) in dry THF (30 mL), tetrabutylammonium fluoride (4.8 mL of a 1 M solution in THF, 4.8 mmol, 1.5 eq.) was added and the mixture was stirred at room temperature for 24 h to give an orange-colored solution. After removing the solvent under reduced pressure, the residue was subjected to silica gel column chromatography (10% ethyl acetate in dichloromethane) to yield **S32** (583 mg, 70%) as a yellow liquid.

^{1}H-NMR (400Hz, $CDCl_3$) δ 3.66 (q, *J* = 5.2 Hz, 2H), 3.55 (dd, *J* = 17.6 Hz, 2.4 Hz, 1H), 3.45 (dd, *J* = 17.8 Hz, 2.0 Hz, 1H), 2.86 (t, *J* = 5.2 Hz, 2H), 2.63 (q, *J* = 6.8 Hz, 1H), 2.38 (t, *J* = 5.6 Hz, 1H), 2.19 (t, *J* = 2.4 Hz, 1H), 1.03 (s, 3H), 0.89 (d, *J* = 6.8 Hz, 3H).

^{13}C NMR (100 MHz, $CDCl_3$) δ 79.3, 73.3, 59.8, 58.9, 51.6, 38.8, 28.2, 17.7, 12.6.

HRMS (ESI): $C_9H_{15}N_3O$; Calculated mass, $[M+Na]^+$ 204.1107; Observed mass, $[M+Na]^+$ 204.1590.

Propargyl methyl diazirine choline (15)

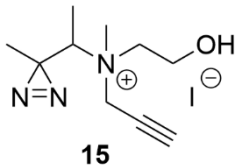

15

To a solution of **S32** (0.39 g, 2.15 mmol, 1 eq.) in acetonitrile (10 mL), methyl iodide (0.27 mL, 4.34 mmol, 2 eq.) was added and the mixture was stirred at room temperature for 13 d. Each day,

methyl iodide (0.27 mL) was added (total of 3.51 mL, 56.4 mmol, 26 eq.) to the reaction mixture. Subsequently, the solvent was evaporated under reduced pressure and the residue was subjected to reverse phase flash column chromatography by using a Redisep Rf 43 g C18 column with water-acetonitrile as the mobile phase (gradient: 0-20 min (100% water), 20-30 min (100-0% water), 30-35 min (0% water), 35-40 min (0-100% water); flow rate = 5 mL/min) to isolate **15**. The fractions containing **15** were concentrated under reduced pressure to yield a colorless oil (0.14 g, 24.5%).

^{1}H NMR (400 MHz, D_2O) δ 4.73 – 4.38 (m, 2H), 4.12 – 4.05 (m, 2H), 3.90 – 3.77 (m, 2H), 3.70 – 3.54 (m, 1H), 3.29 – 3.23 (m, 4H), 1.49 (d, *J* = 6.8 Hz, 3H), 1.28 (s, 3H).

^{13}C NMR (100 MHz, DMSO-d6) δ 83.7, 83.6, 73.1, 73.0, 72.3, 72.1, 61.8, 61.7, 54.9, 54.6, 52.8, 51.5, 51.4, 46.6, 24.4, 24.3, 19.23, 19.22, 11.2, 11.0.

HRMS (ESI): $C_{10}H_{18}N_3O^+$; Calculated mass, $[M]^+$ 196.1444; Observed mass, $[M]^+$ 196.1450.

Note: Compound **15** was purified as a racemic mixture and the H atoms on the CH_2 group between the quaternary nitrogen atom and the triple bonded carbon atom of this compound are diastereotopic resulting in the appearance of sets of two closely spaced peaks in the ^{1}H and ^{13}C NMR spectra.

3.4.4 General procedure for cell culture

Mammalian cells (HEK29/HeLa/MDA-MB-231) were cultured in DMEM medium supplemented with 10% FBS, 100 units/mL penicillin, and 100 µg/mL streptomycin (complete media) in a humidified CO_2 incubator maintaining 5% CO_2 levels and a temperature of 37 °C. All the treatments and incubations of mammalian cells performed in a CO_2 incubator were done in an incubator maintaining 5% CO_2 levels, and a temperature of 37 °C.

3.4.5 Procedure for the characterization of metabolic labeling by cellular imaging

The procedure for imaging metabolically labeled choline lipids that were administered with either compound **11** (2 mM) alone or co-administered with compound **11** and choline chloride (2 mM each) is the same as documented in section 2.4.5.

3.4.6 Procedure for the characterization of metabolic labeling by lipidomics

The procedures for the extraction of lipids from mammalian cells, HPLC method details, the mass-spectrometry details, and the LipidView analyses details are the same as mentioned in section 2.4.6. For detecting ethyl propargyl choline (**16)**-labeled lipids (PIS of 222.1 Da) and D6 choline (**19**)-labeled lipids (PIS of 190.1 Da), the compound parameters that were optimized for the detection of native choline lipids (PIS of 184.1 Da) were used. For all diazirine containing choline lipids, the PIS mass used was 28 Da less than that of the fragment mass of their phosphoryl derivatives to account for the N_2 loss that diazirines characteristically undergo during fragmentation. Compound parameters were separately optimized for detecting the β-diazirine **11**-labeled choline lipids by using a PIS of 234.1 Da and the same parameters were used in all PIS experiments for detecting choline lipids labeled with other β-diazirine analogs **10**, **12**, **13**, **14**, **15**, and **17**.

Table 3.1. Compound parameters used for the PIS of lipids labeled with the choline analogs **10**-**15**

S. No.	Head group	PIS mode mass (Da)	Declustering Potential (volts)	Entrance Potential (volts)	Collision Energy (volts)	Collision cell Exit Potential (volts)
For native, D6 and diazirine-devoid **16**-labeled choline lipids						
1.	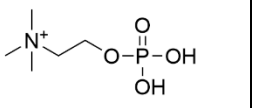 phosphocholine (native lipids)	184.1	110.0	7.8	30.9	5.2
2.	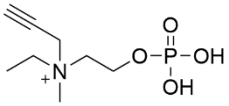 phospho-**16**	222.1				

3.	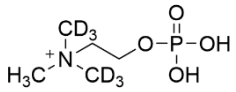 phospho-**19**	190.1	110.0	7.8	30.9	5.2
For β-diazirine choline lipids						
4.	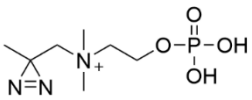 phospho-**10**	210.1 (loss of N_2)	169.3	5.0	53.6	1.1
5.	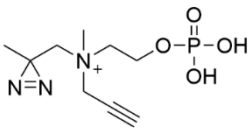 phospho-**11**	234.1 (loss of N_2)				
6.	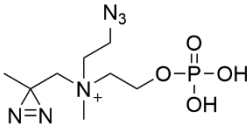 phospho-**12**	265.1 (loss of N_2)				
7.	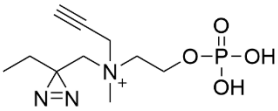 phospho-**13**	248.1 (loss of N_2)				
8.	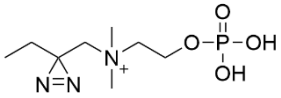 phospho-**14**	224.1 (loss of N_2)				
9.	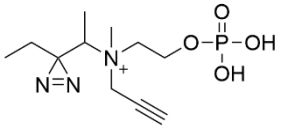 phospho-**15**	248.1 (loss of N_2)				
10.	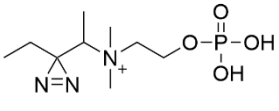 phospho-**17**	224.1 (loss of N_2)				

3.4.7 Metabolic labeling studies on D9 choline 18

For each treatment, 3 million HEK293 cells in 10 mL of complete medium were seeded in two 10 cm culture dishes and incubated in a CO_2 incubator for 24 h. Subsequently, each flask was administered 200 μL of a solution of **18** in PBS (0.1 M, 0.5 M, and 1 M stocks yielding final concentrations of 2 mM, 10 mM, and 20 mM respectively) and after a 24 h-long incubation in a CO_2 incubator, the adhered cells were washed with ice-cold PBS (2 × 5 mL), resuspended in ice-cold PBS (5 mL) and subjected to lipid extraction as per the protocol described in section 2.4.6 above. Cells not treated with **18** served as control. Subsequently, the extracted lipid samples were subjected to LC-MS/MS for the identification of **19**-labeled lipids using a PIS of 190 Da as described in section 3.4.6 and Table 3.1 above. Figure 3.12b shows the dose-dependent increase in the formation of **16**-labeled lipids.

3.4.8 In-gel fluorescence experiments

Gel-based analysis of crosslinked proteins in HEK293 cells: Six 10 cm culture dishes each containing HEK293 cells (10 mL of a 0.2 million cells per mL culture in complete media) were placed in a CO_2 incubator for 12 h. Subsequently, 317 μL and 769 μL of a 65 mM solution of **11** in PBS was administered into two plates each (final concentration of **11** in each plate was 2 mM and 5 mM respectively) and the cultures were allowed to grow in the CO_2 incubator for another 24 h. Two culture dishes that were administered with 317 μL of PBS served as control. After the incubation, cells were washed with ice-cold DMEM containing 10% FBS (1 × 5 mL) and then with ice-cold PBS (2 × 5 mL). Subsequently, cells were overlaid with ice-cold PBS (10 mL) and exposed to 356 nm UV as described in section 3.4.1 above for 30 min on ice. Cells from plates that were overlaid with ice-cold PBS (10 mL) but not exposed to any UV light served as -UV control. After the UV exposure (or no UV exposure), cells were scraped into ice-cold PBS (5 mL) and pelleted by centrifugation (1,000 *g*, 5 min, 4 °C). The resultant cell pellet was resuspended by gentle pipetting in PBS containing EDTA-free protease inhibitor cocktail from Roche (467 μL) and incubated on ice for 30 min. Cells were lysed by probe sonication on ice (8 pulses of 5 sec each with a gap of 5 sec between each pulse, 30% amplitude on a Branson 450 Digital Sonifier), and to the cell lysate (50 μL containing 1 mg/mL protein concentration estimated by employing the Bradford assay), click chemistry reagents were added. Specifically, to this 50 μL cell lysate, 1

μL of a solution of 50 mM $CuSO_4.5H_2O$ in water (final concentration, 0.9 mM), 1 μL of a solution of 50 mM TCEP in PBS (final concentration, 0.9 mM), 3 μL of a solution of 1.7 mM TBTA in 1:4 *t*-butanol:DMSO (final concentration, 0.09 mM), and 1 μL of a 1.25 mM solution of Alexa Fluor 594 azide in DMSO (final concentration, 22 μM) were added and the mixture was incubated for 1 h at room temperature under dark after mixing by pipetting. The click reactions were quenched by heating the samples with 2X SDS loading dye (56 μL) for 5 min at 98 °C and the samples were then subjected to SDS-PAGE analysis (10% gel) followed by fluorescence imaging of the gel on the ChemiDoc gel imaging system. Finally, the gel was stained with coomassie blue and the gel images thus obtained are depicted in Figure 3.2c.

3.5 ^{1}H and ^{13}C-NMR Spectra for the Synthetic Procedures of Analogs 10-15

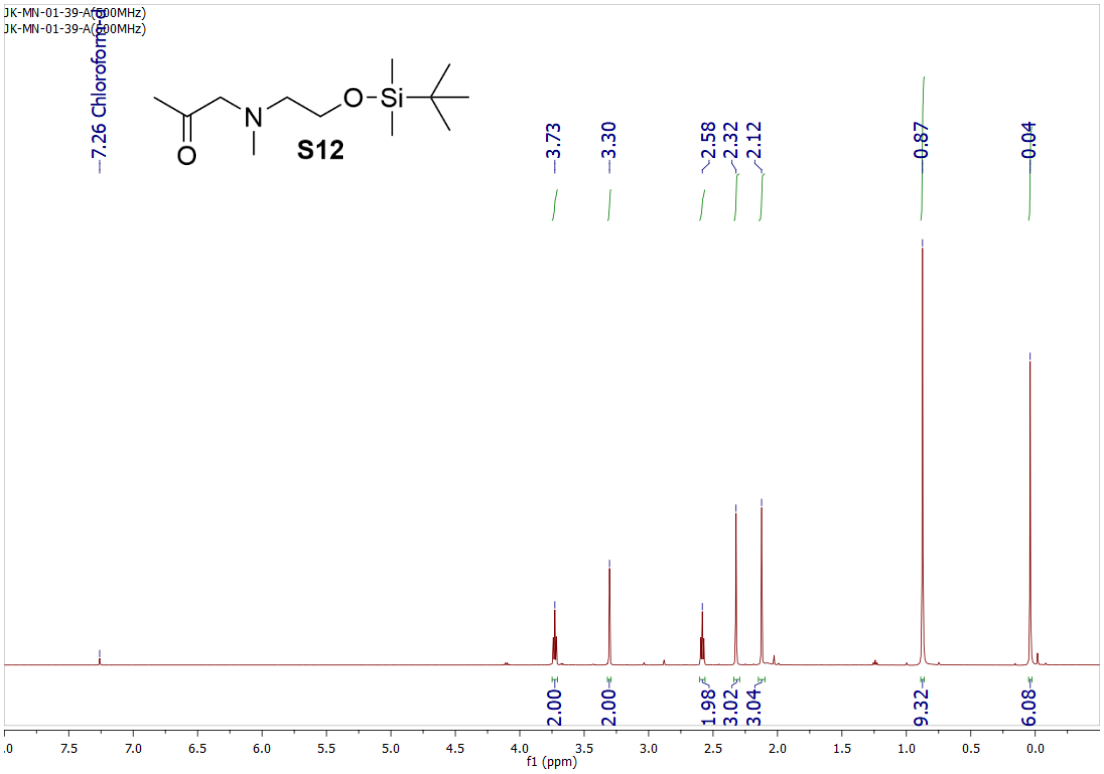

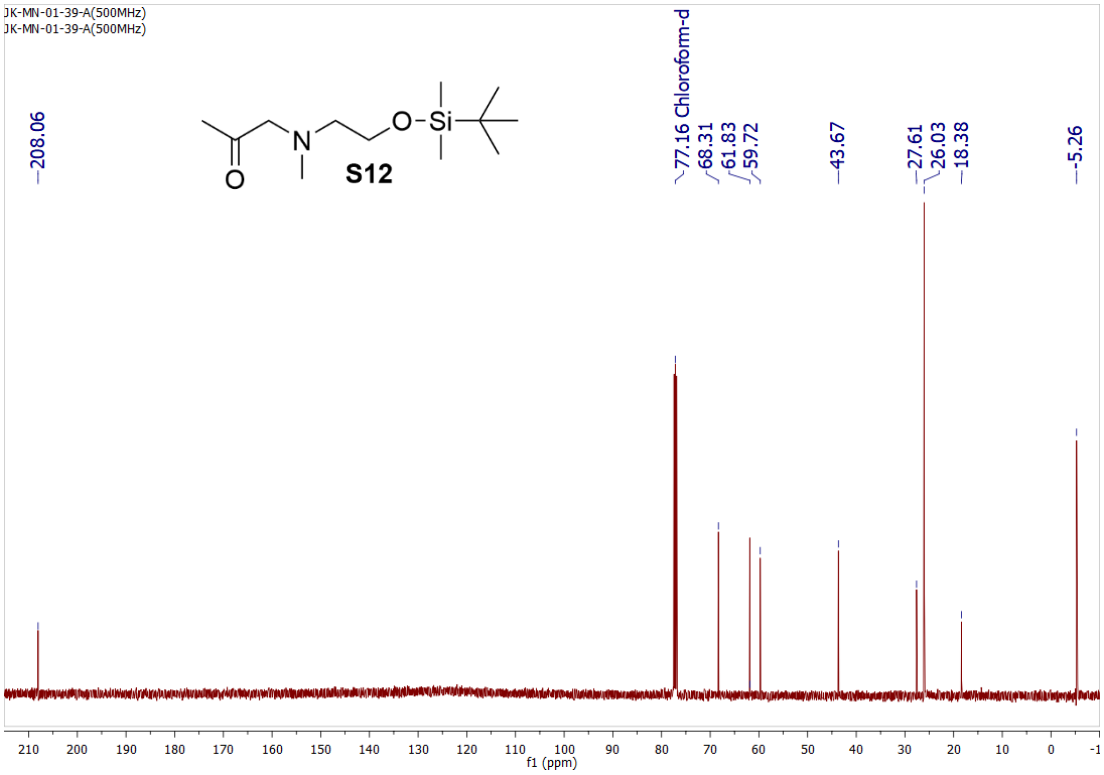

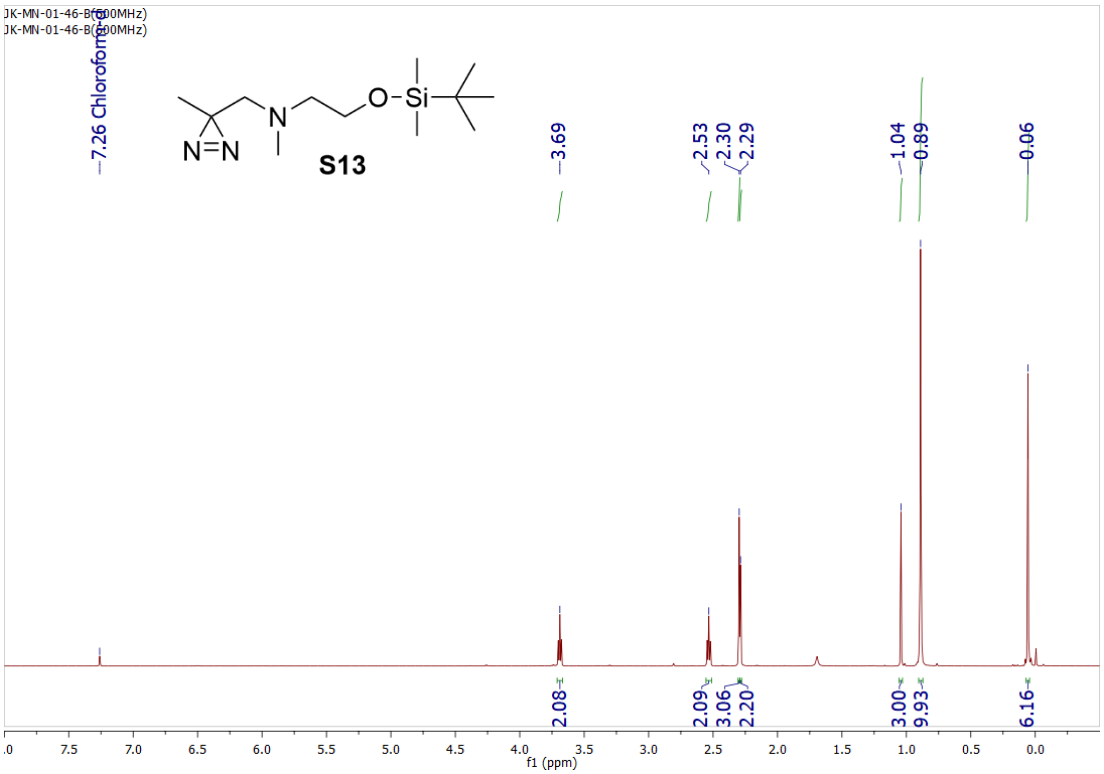
JK-MN-01-46-B(500MHz)
JK-MN-01-46-B(500MHz)
7.26 Chloroform-d
S13
3.69
2.53
2.30
2.29
1.04
0.89
0.06
2.08
2.09
3.06
2.20
3.00
9.93
6.16
f1 (ppm)

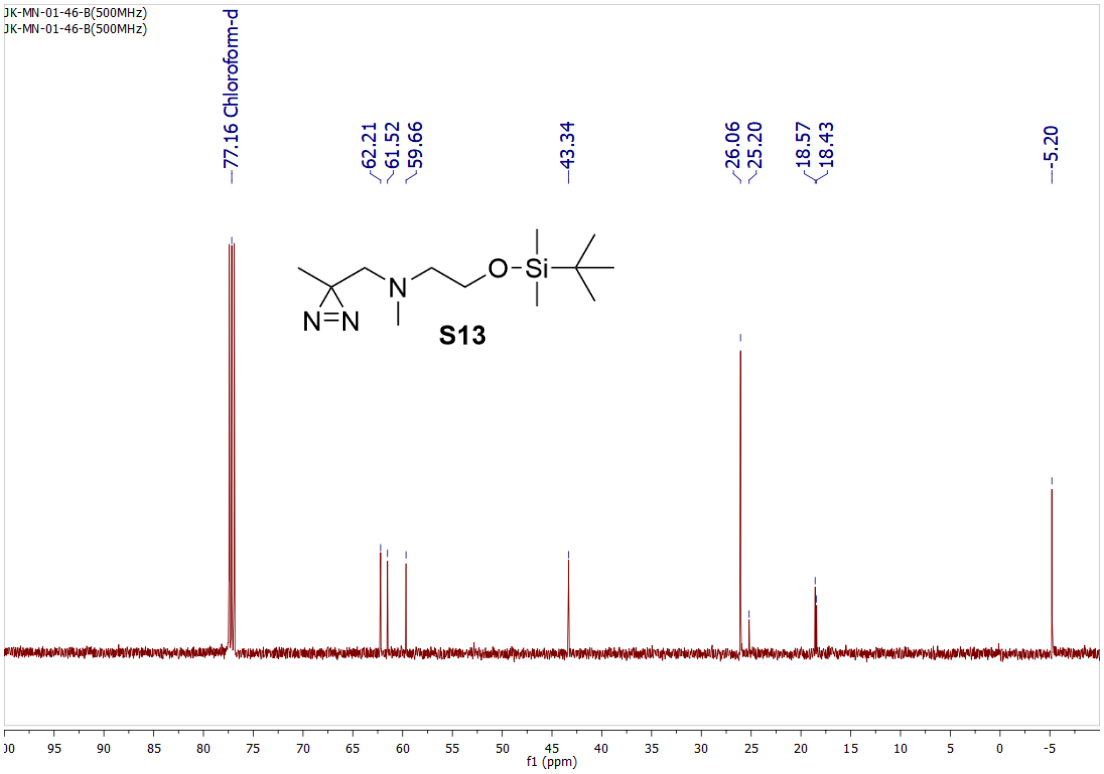
JK-MN-01-46-B(500MHz)
JK-MN-01-46-B(500MHz)
77.16 Chloroform-d
62.21
61.52
59.66
43.34
26.06
25.20
18.57
18.43
-5.20
S13
f1 (ppm)

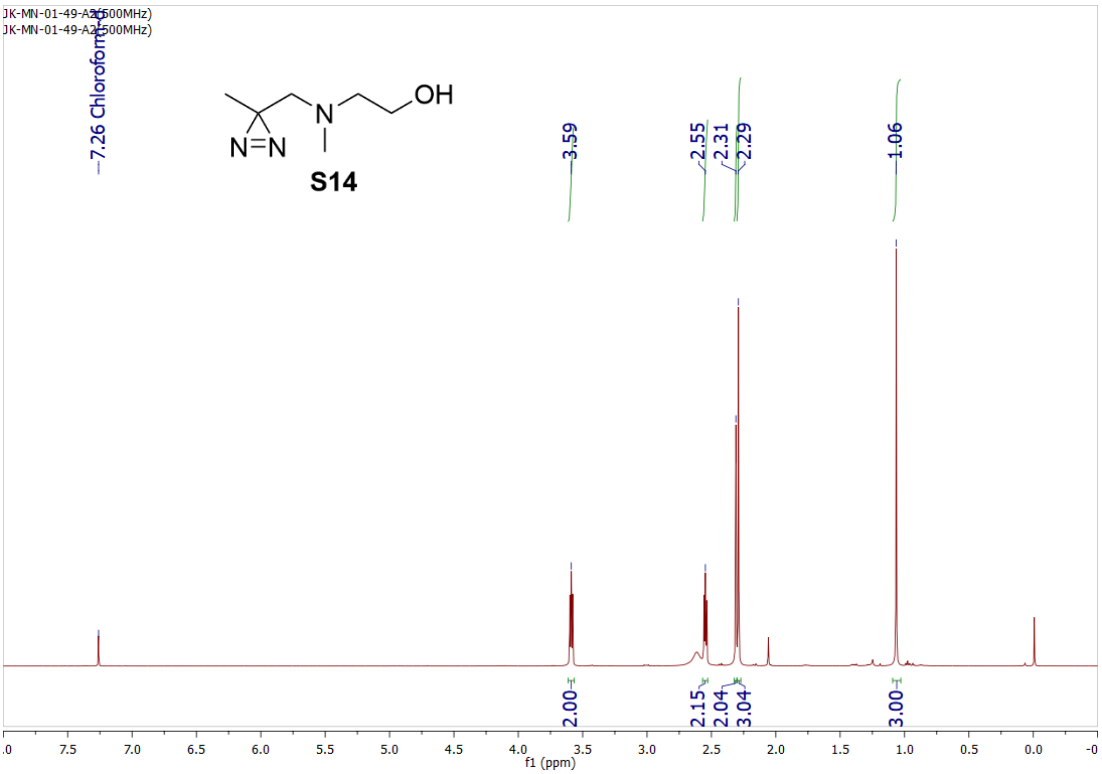
JK-MN-01-49-A2(500MHz)
JK-MN-01-49-A2(500MHz)
7.26 Chloroform-d
3.59
2.55
2.31
2.29
1.06
OH
N
N=N
S14
2.00
2.15
2.04
3.04
3.00
f1 (ppm)

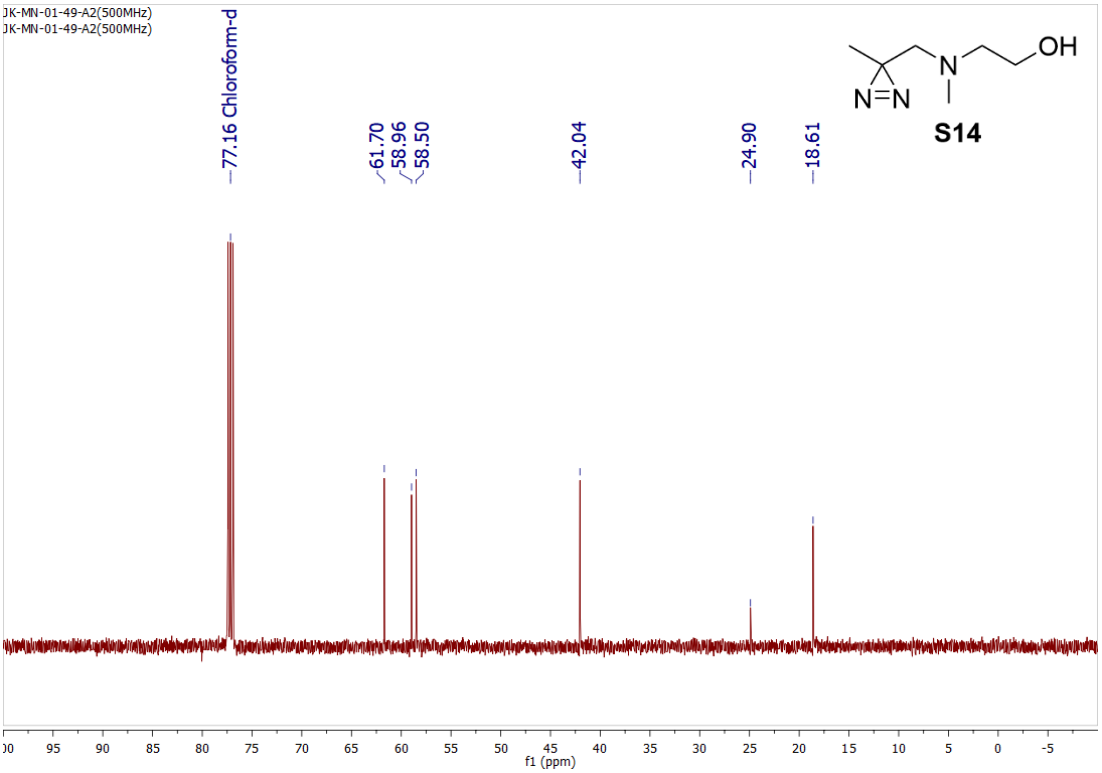
JK-MN-01-49-A2(500MHz)
JK-MN-01-49-A2(500MHz)
77.16 Chloroform-d
61.70
58.96
58.50
42.04
24.90
18.61
OH
N
N=N
S14
f1 (ppm)

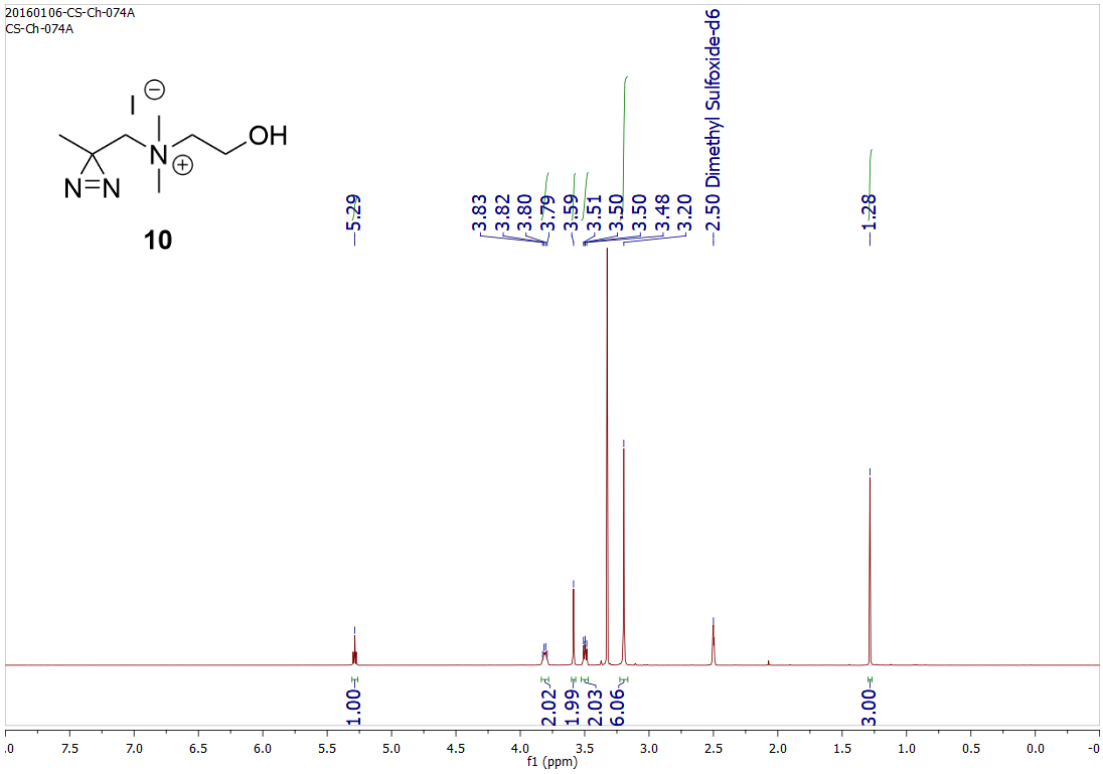
20160106-CS-Ch-074A
CS-Ch-074A
I
OH
N
N=N
10
5.29
3.83
3.82
3.80
3.79
3.59
3.51
3.50
3.50
3.48
3.20
2.50 Dimethyl Sulfoxide-d6
1.28
1.00
2.02
1.99
2.03
6.06
3.00
f1 (ppm)

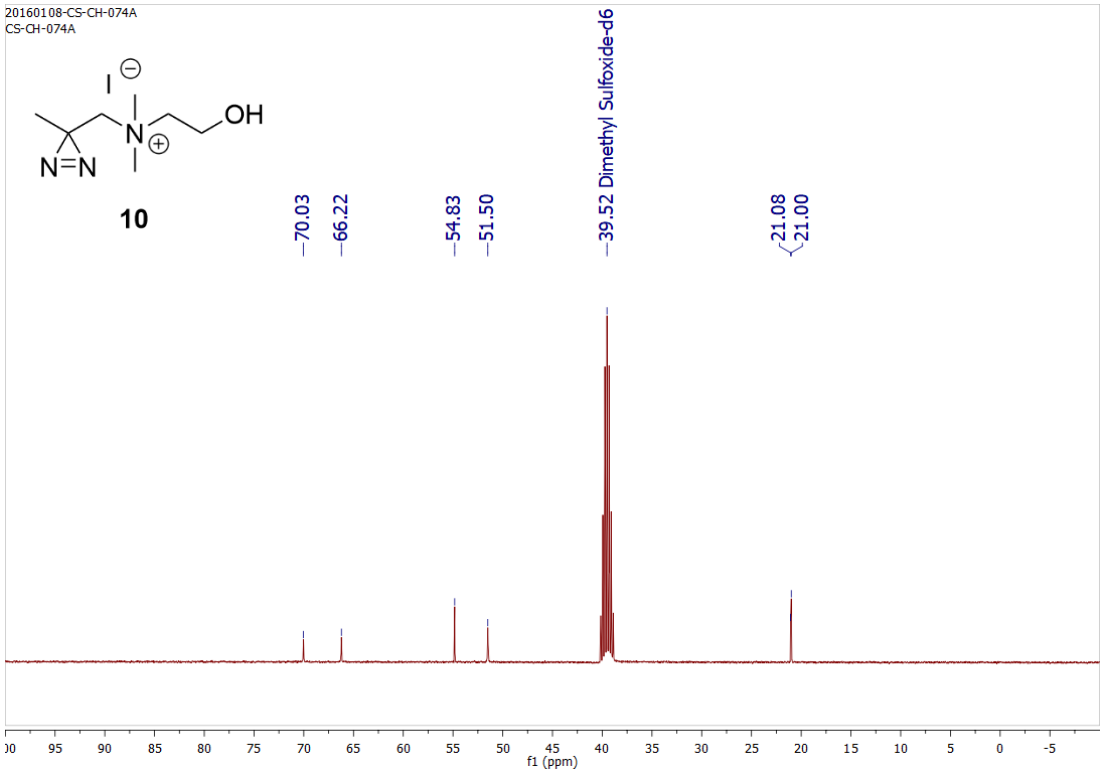
20160108-CS-CH-074A
CS-CH-074A
I
OH
N
N=N
10
70.03
66.22
54.83
51.50
39.52 Dimethyl Sulfoxide-d6
21.08
21.00
f1 (ppm)

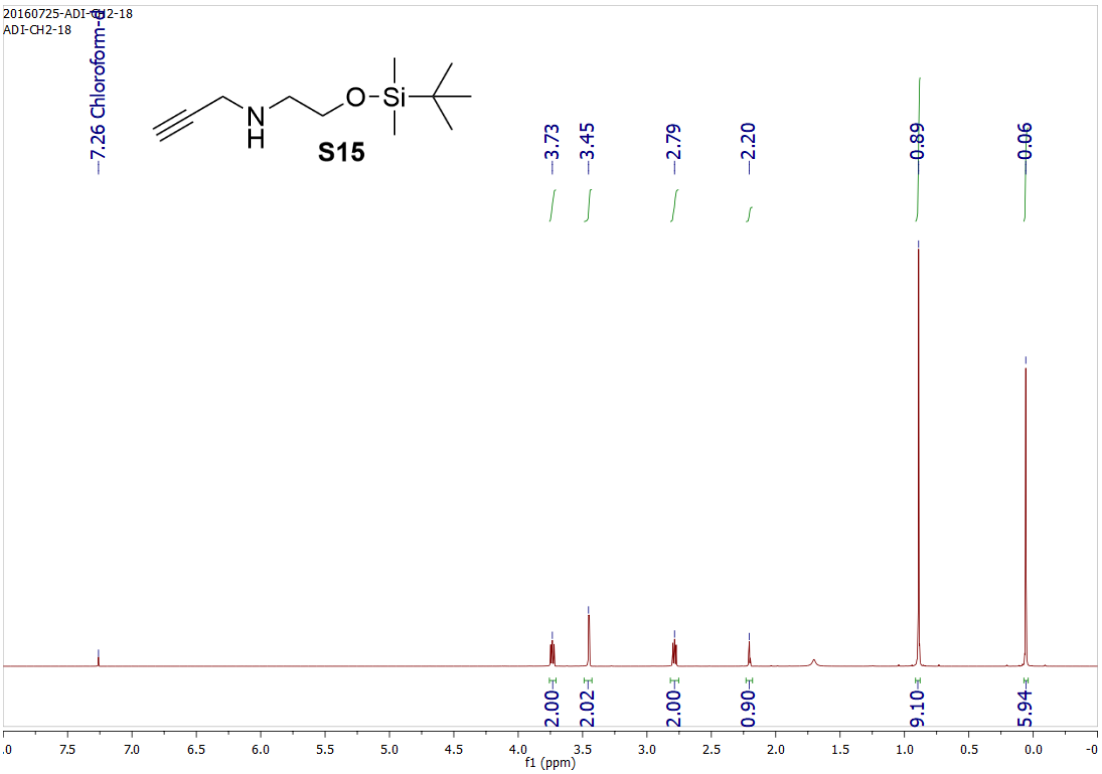
20160725-ADI-CH2-18
ADI-CH2-18
7.26 Chloroform-d
S15
3.73
3.45
2.79
2.20
0.89
0.06
2.00
2.02
2.00
0.90
9.10
5.94
f1 (ppm)

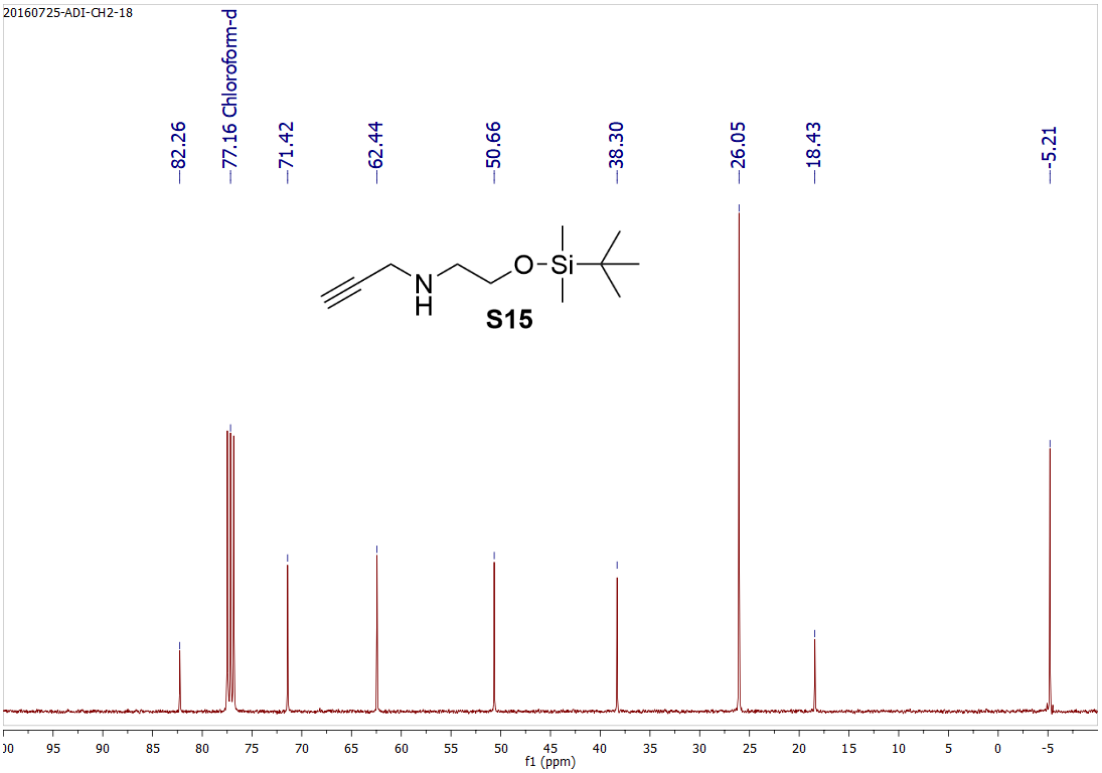
20160725-ADI-CH2-18
82.26
77.16 Chloroform-d
71.42
62.44
50.66
38.30
26.05
18.43
-5.21
S15
f1 (ppm)

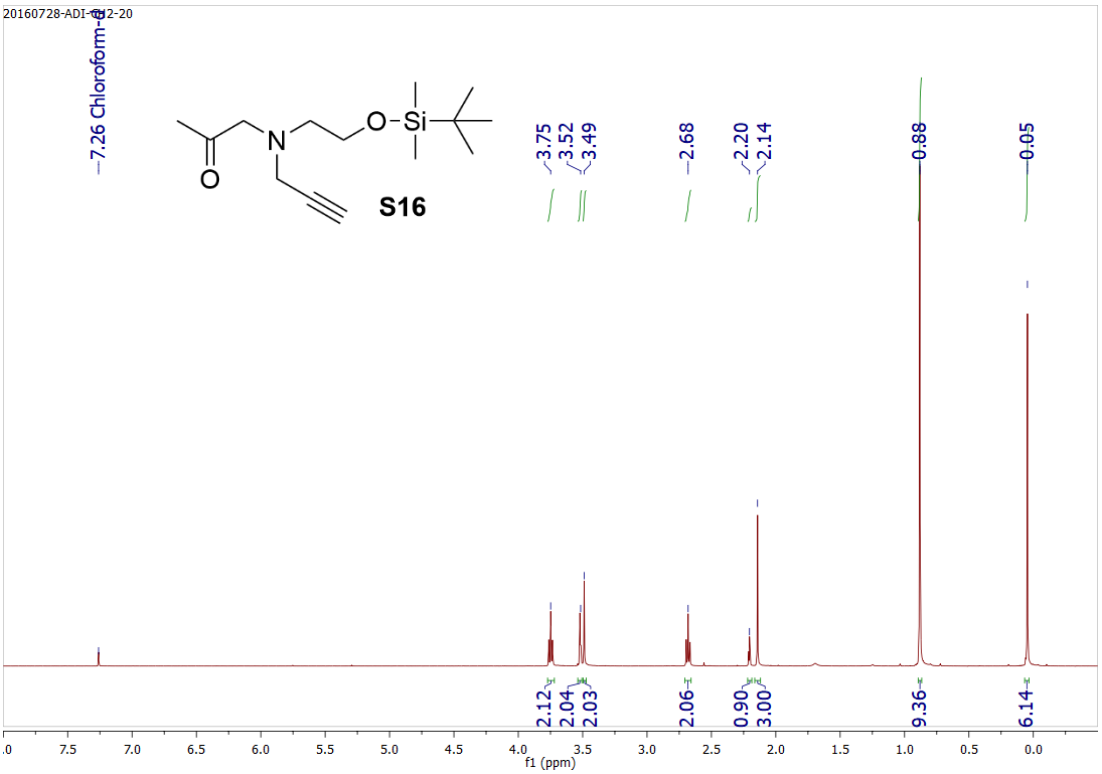
20160728-ADI-CH2-20
7.26 Chloroform-d
3.75
3.52
3.49
2.68
2.20
2.14
0.88
0.05
S16
2.12
2.04
2.03
2.06
0.90
3.00
9.36
6.14
f1 (ppm)

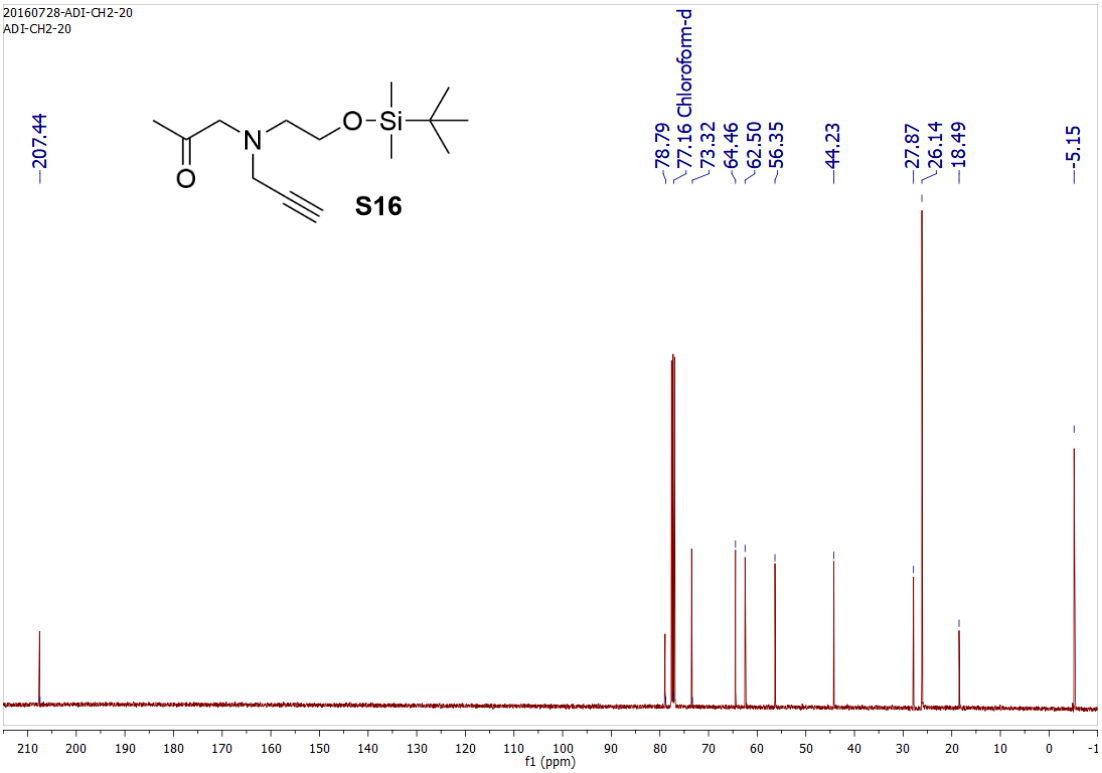
20160728-ADI-CH2-20
ADI-CH2-20
207.44
78.79
77.16 Chloroform-d
73.32
64.46
62.50
56.35
44.23
27.87
26.14
18.49
5.15
S16
f1 (ppm)

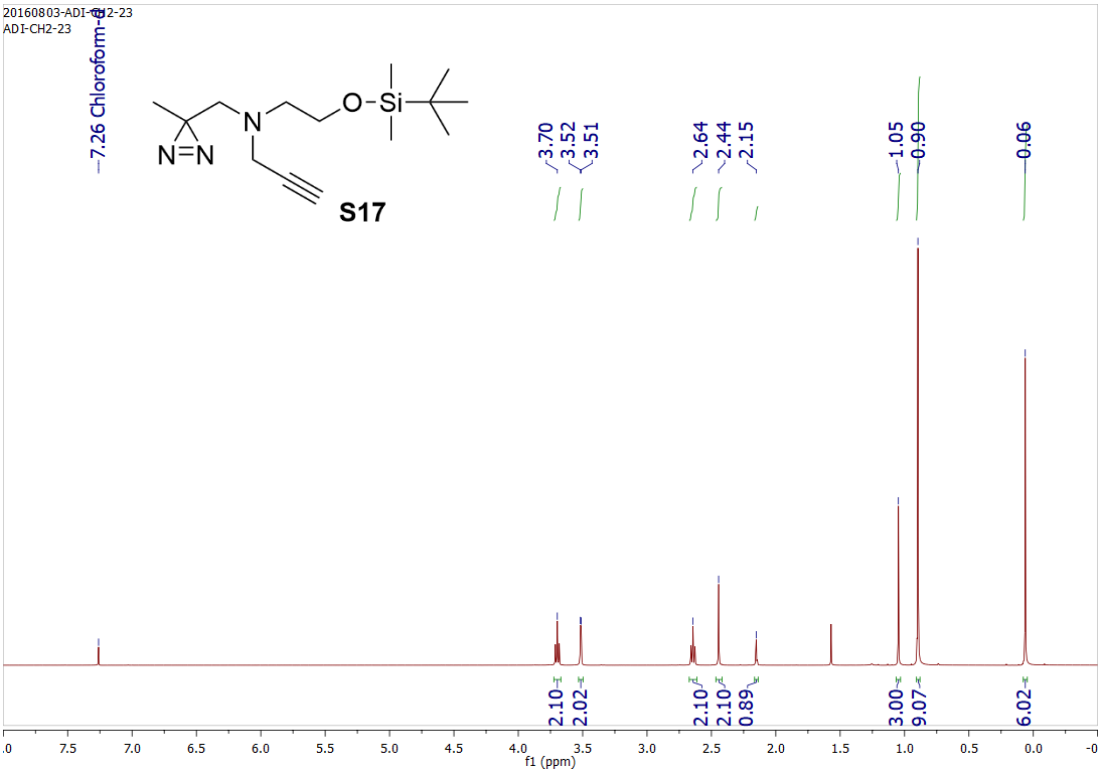
20160803-ADI-CH2-23
ADI-CH2-23
7.26 Chloroform-d
3.70
3.52
3.51
2.64
2.44
2.15
1.05
0.90
0.06
2.10
2.02
2.10
2.10
0.89
3.00
9.07
6.02
f1 (ppm)
S17

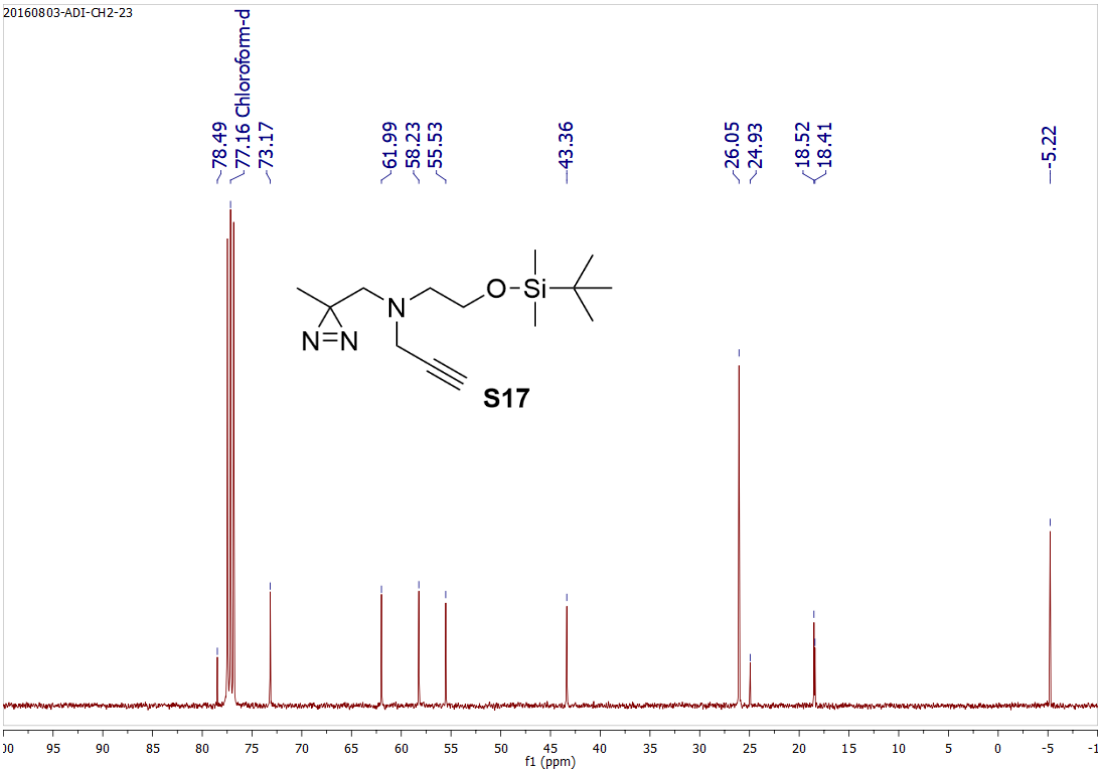
20160803-ADI-CH2-23
78.49
77.16 Chloroform-d
73.17
61.99
58.23
55.53
43.36
26.05
24.93
18.52
18.41
-5.22
f1 (ppm)
S17

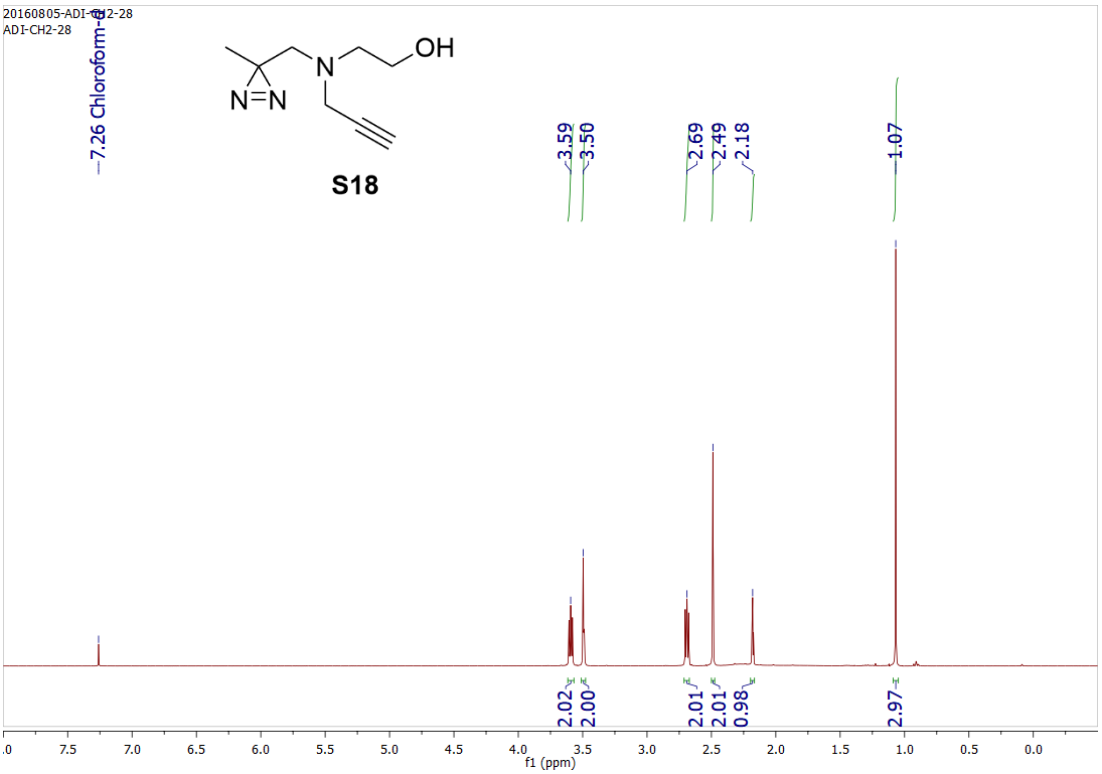
20160805-ADI-CH2-28
ADI-CH2-28
7.26 Chloroform-d
3.59
3.50
2.69
2.49
2.18
1.07
2.02
2.00
2.01
2.01
0.98
2.97
OH
N
N=N
S18
f1 (ppm)

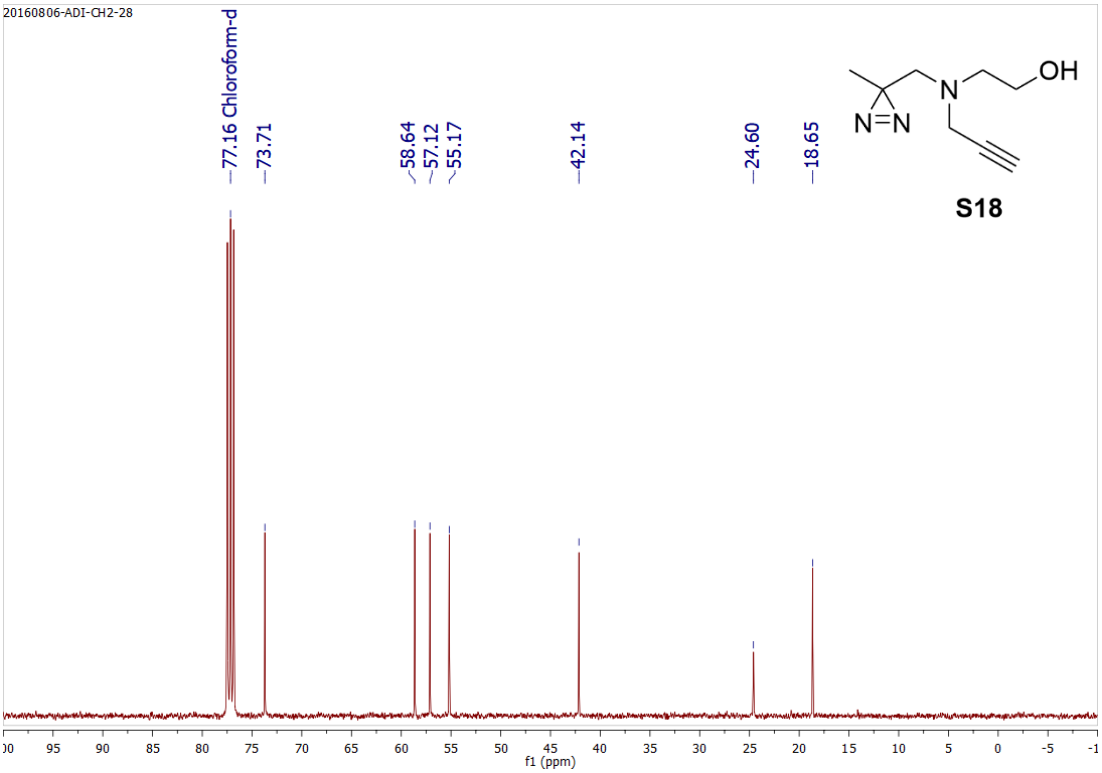
20160806-ADI-CH2-28
77.16 Chloroform-d
73.71
58.64
57.12
55.17
42.14
24.60
18.65
OH
N
N=N
S18
f1 (ppm)

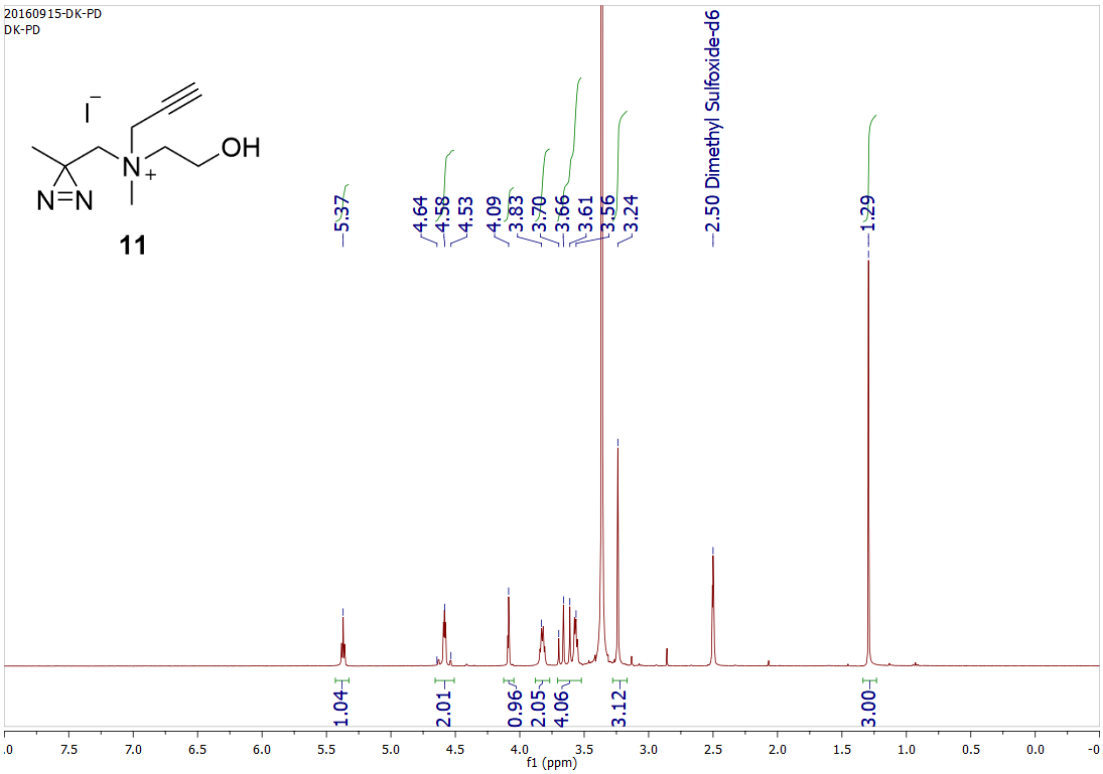
20160915-DK-PD
DK-PD
11
5.37
4.64
4.58
4.53
4.09
3.83
3.70
3.66
3.61
3.56
3.24
2.50 Dimethyl Sulfoxide-d6
1.29
1.04
2.01
0.96
2.05
4.06
3.12
3.00
f1 (ppm)

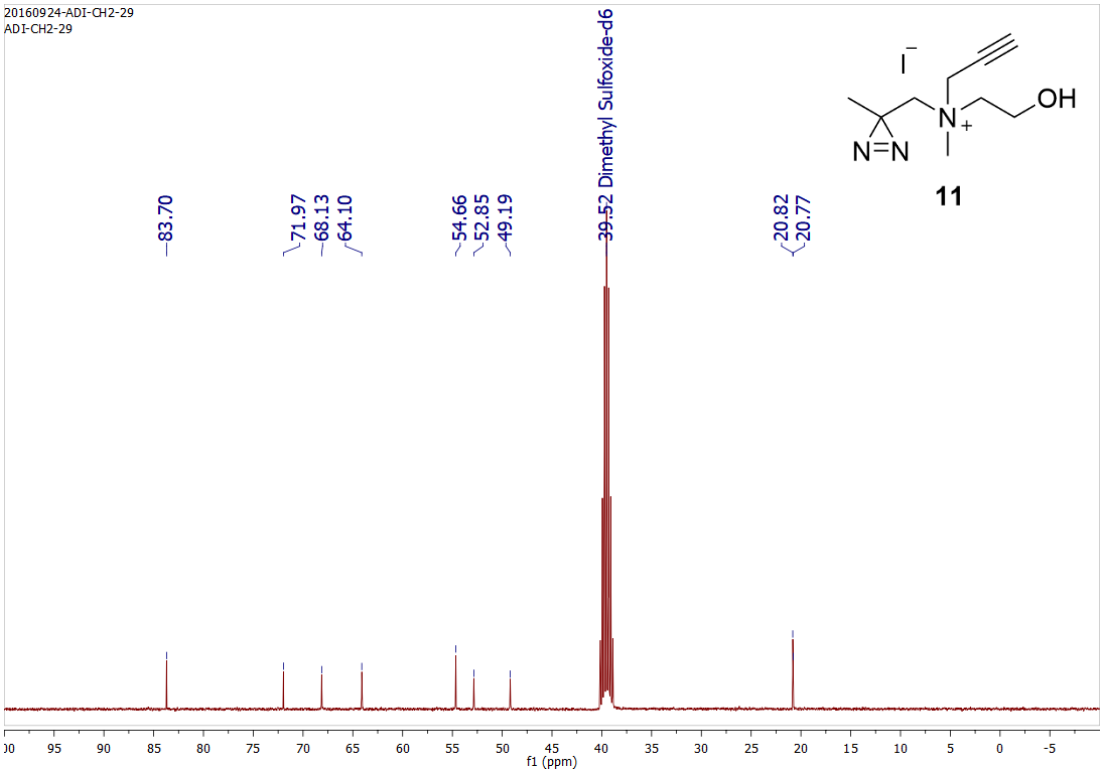
20160924-ADI-CH2-29
ADI-CH2-29
11
83.70
71.97
68.13
64.10
54.66
52.85
49.19
39.52 Dimethyl Sulfoxide-d6
20.82
20.77
f1 (ppm)

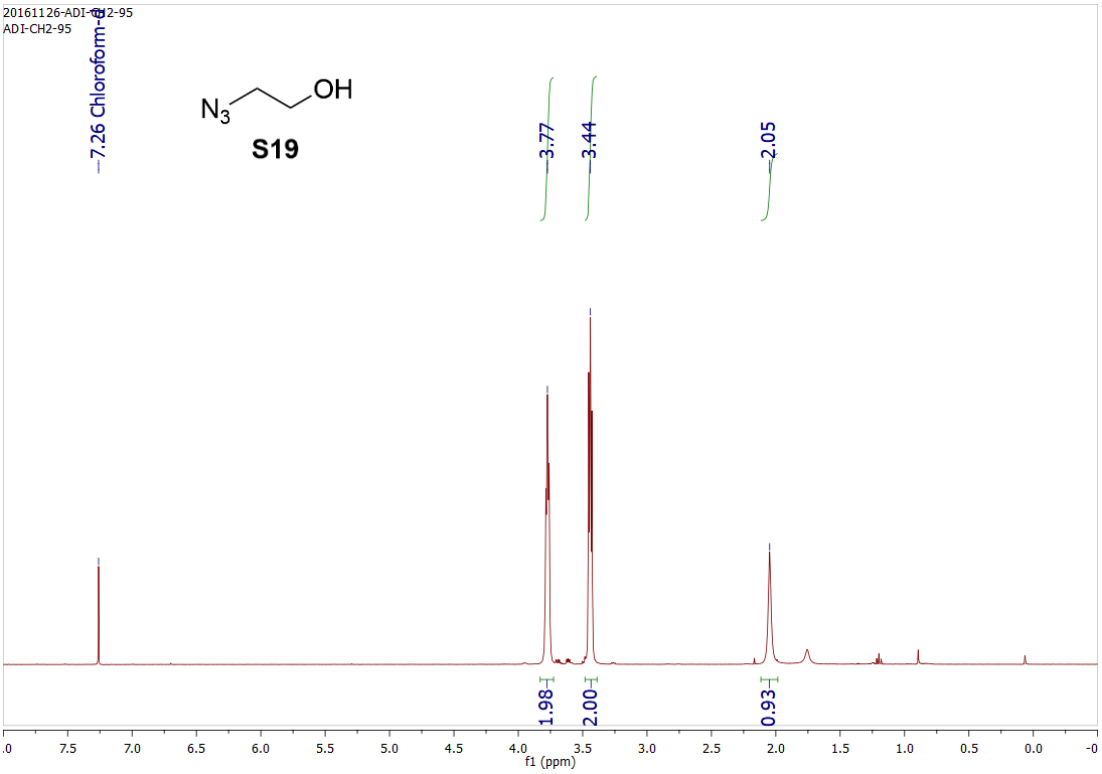
20161126-ADI-CH2-95
ADI-CH2-95
7.26 Chloroform-d
N3
OH
S19
3.77
3.44
2.05
1.98
2.00
0.93
f1 (ppm)

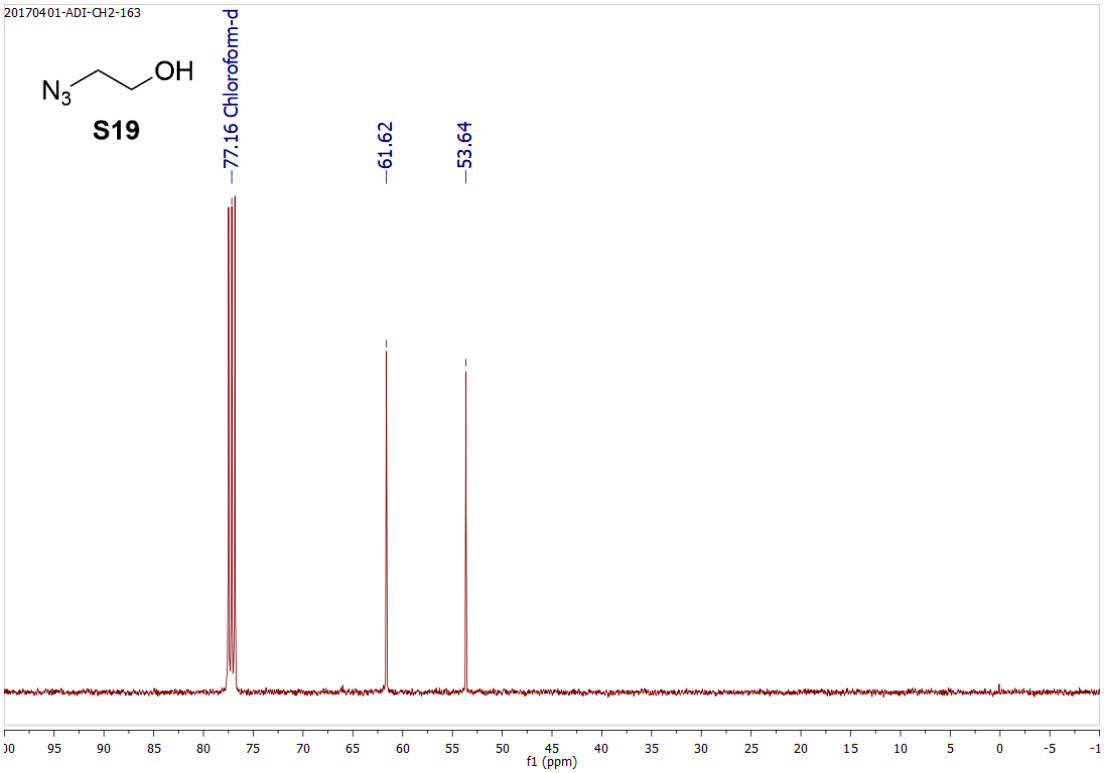
20170401-ADI-CH2-163
N3
OH
S19
77.16 Chloroform-d
61.62
53.64
f1 (ppm)

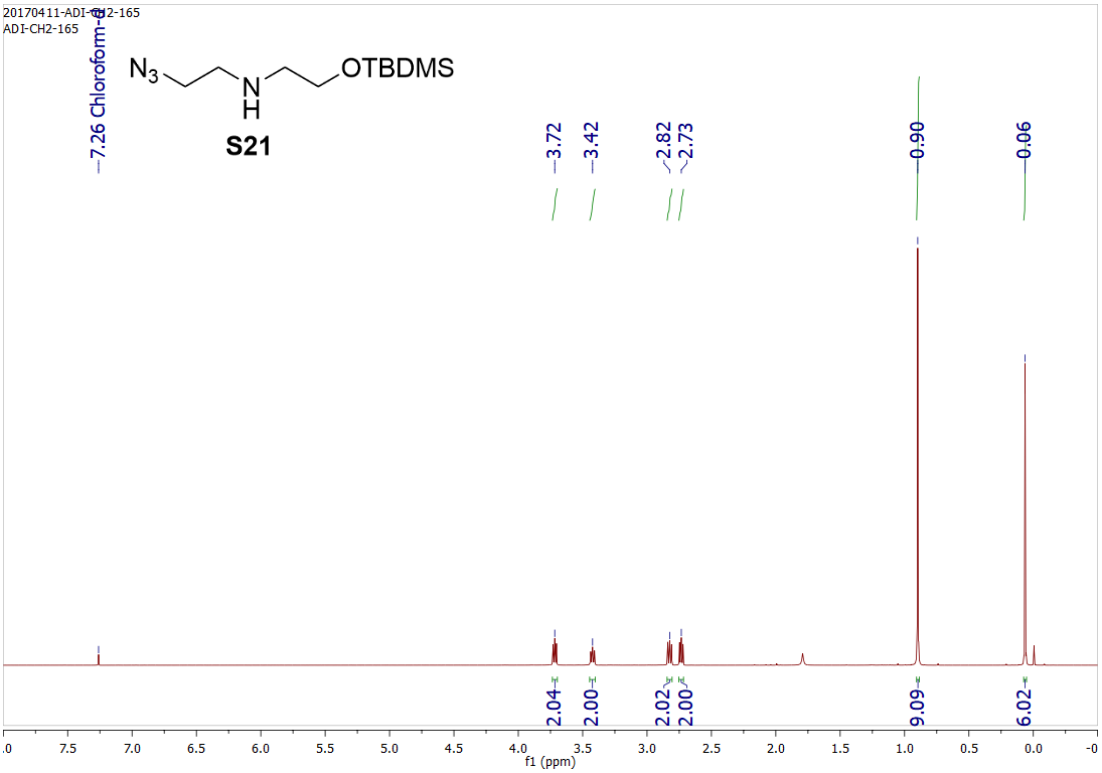
20170411-ADI-CH2-165
ADI-CH2-165
7.26 Chloroform-d
N3
N
H
OTBDMS
S21
3.72
3.42
2.82
2.73
0.90
0.06
2.04
2.00
2.02
2.00
9.09
6.02
f1 (ppm)

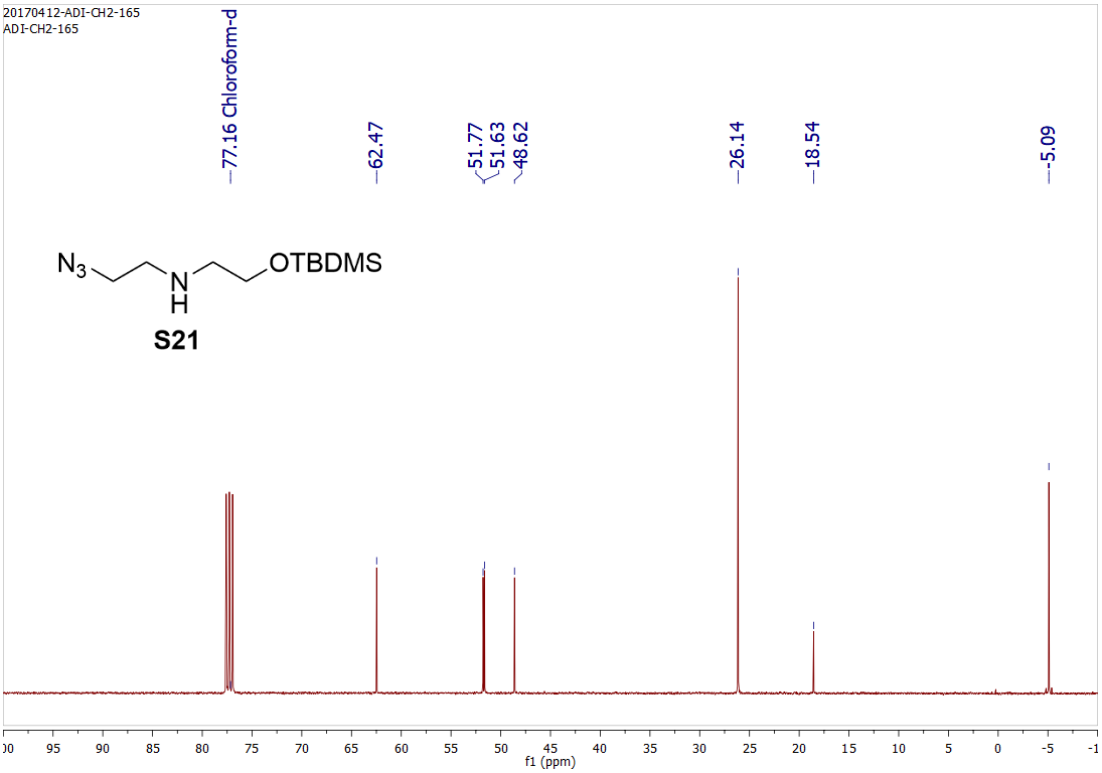
20170412-ADI-CH2-165
ADI-CH2-165
77.16 Chloroform-d
62.47
51.77
51.63
48.62
26.14
18.54
-5.09
N3
N
H
OTBDMS
S21
f1 (ppm)

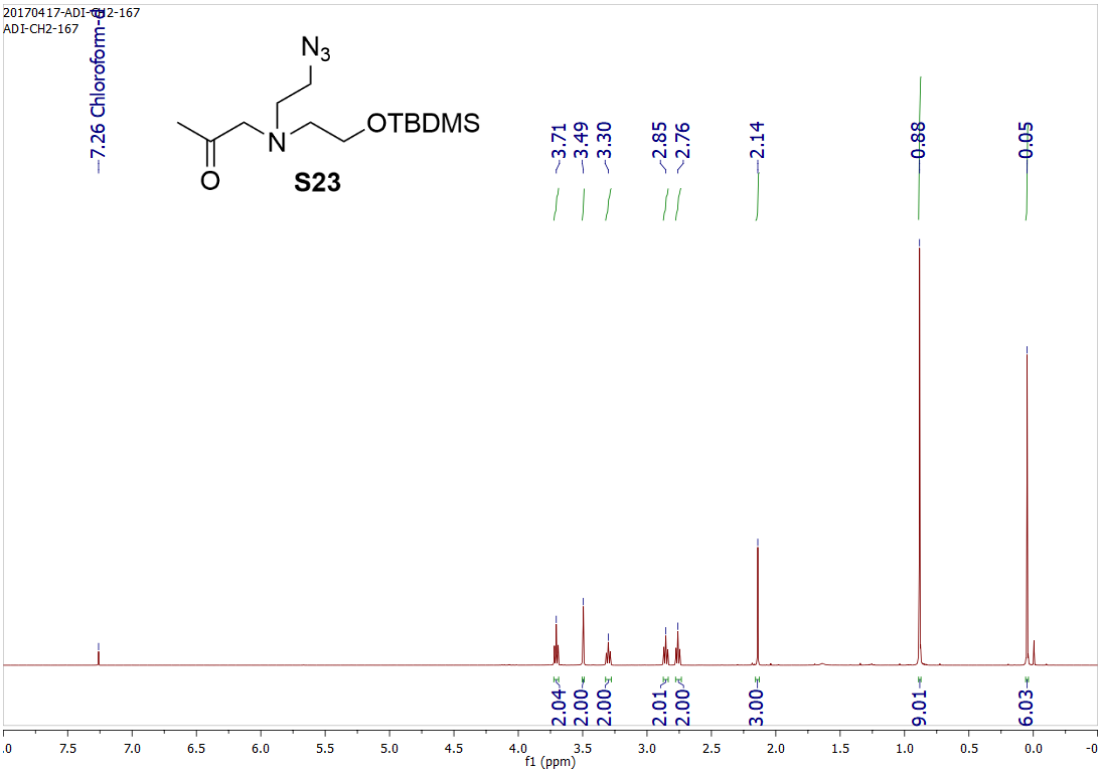
20170417-ADI-CH2-167
ADI-CH2-167
7.26 Chloroform-d
N3
OTBDMS
N
O
S23
3.71
3.49
3.30
2.85
2.76
2.14
0.88
0.05
2.04
2.00
2.00
2.01
2.00
3.00
9.01
6.03
f1 (ppm)

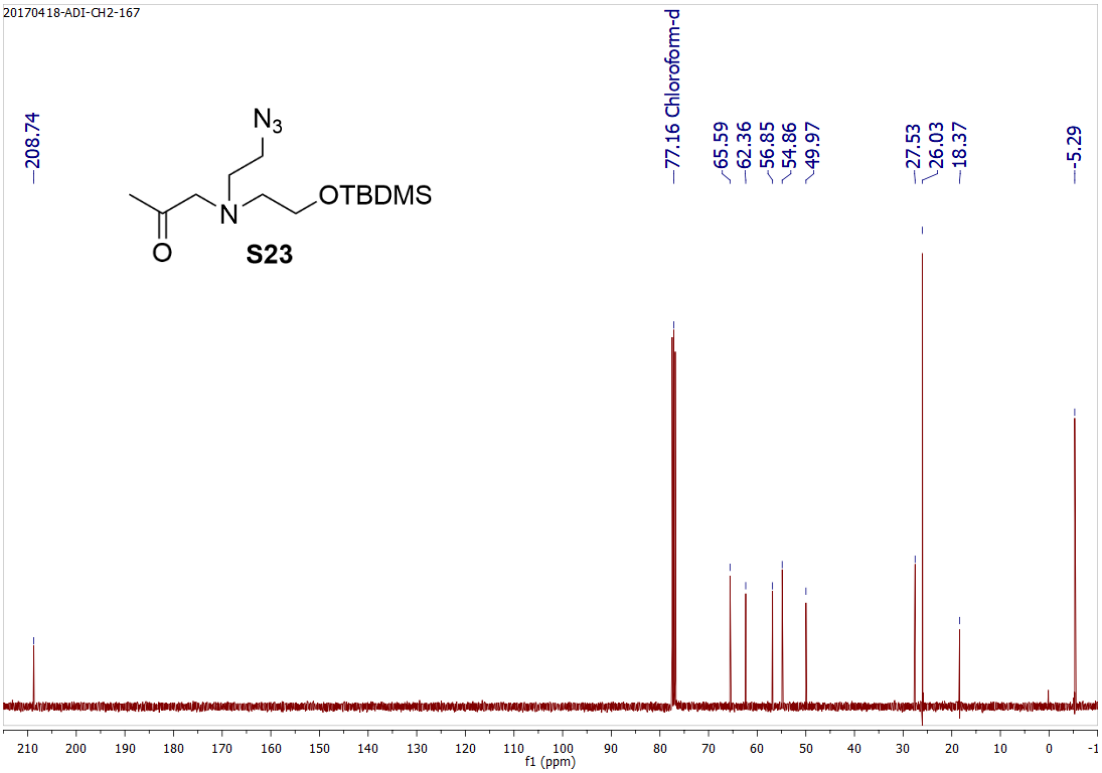
20170418-ADI-CH2-167
208.74
N3
OTBDMS
N
O
S23
77.16 Chloroform-d
65.59
62.36
56.85
54.86
49.97
27.53
26.03
18.37
-5.29
f1 (ppm)

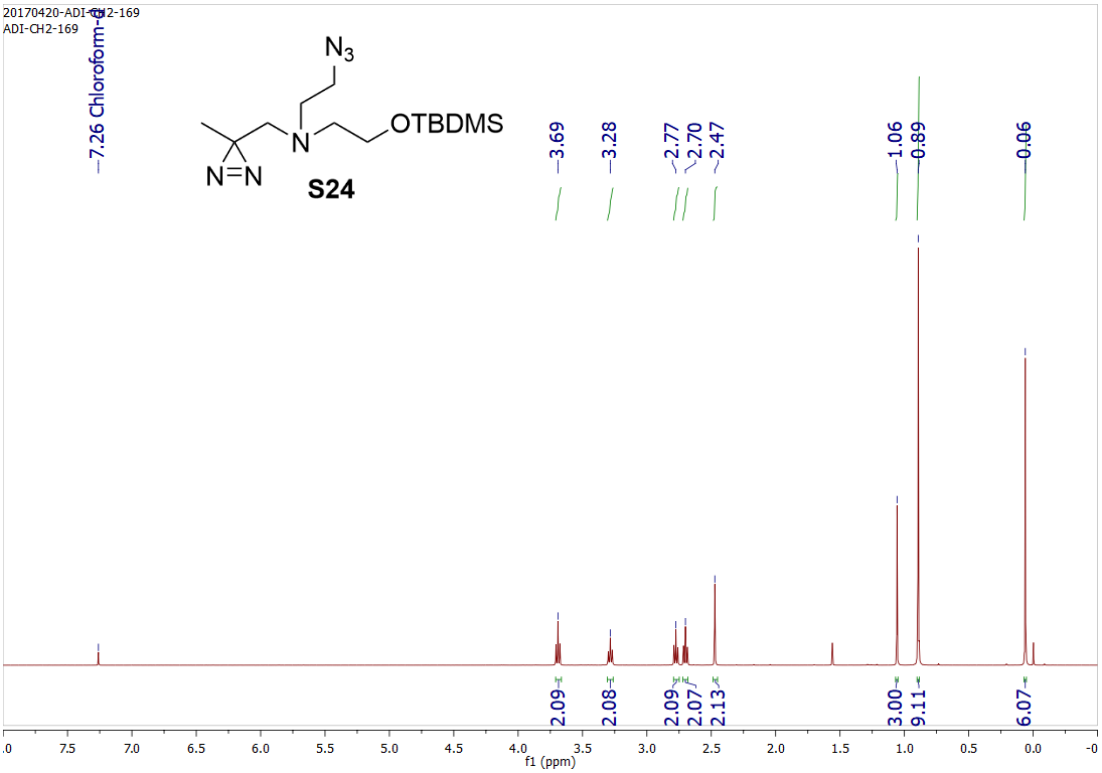
20170420-ADI-CH2-169
ADI-CH2-169
7.26 Chloroform-d
N3
OTBDMS
N
N=N
S24
3.69
3.28
2.77
2.70
2.47
1.06
0.89
0.06
2.09
2.08
2.09
2.07
2.13
3.00
9.11
6.07
f1 (ppm)

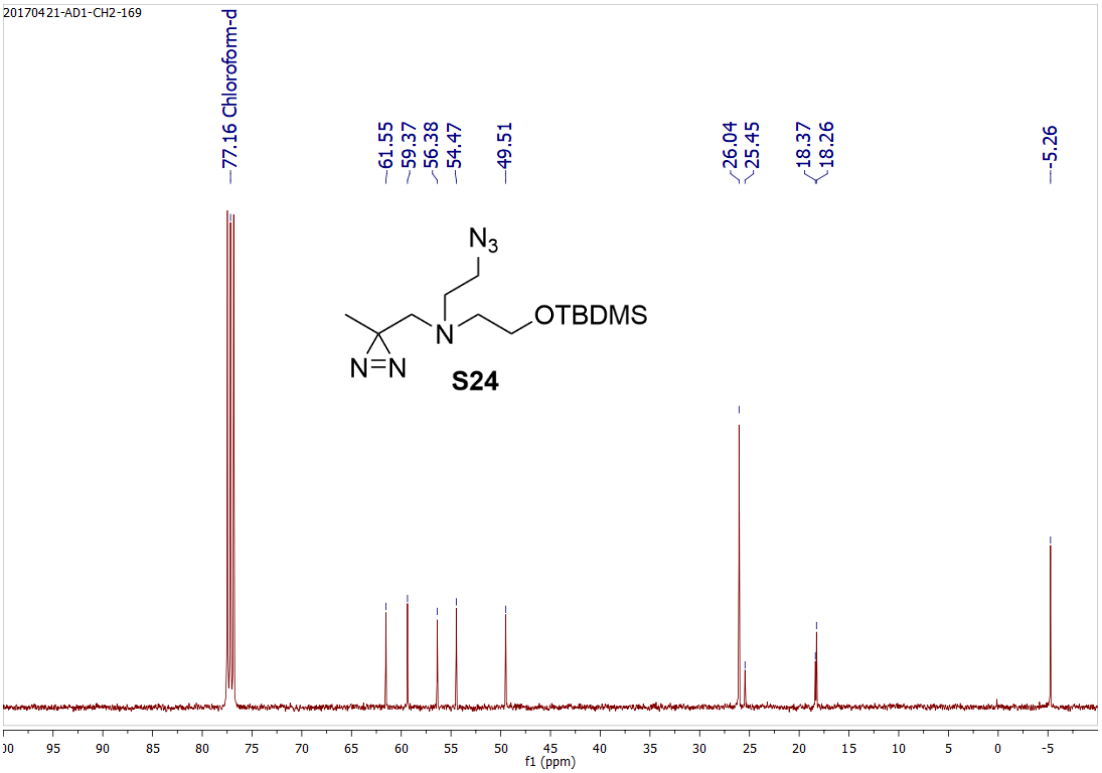
20170421-AD1-CH2-169
77.16 Chloroform-d
61.55
59.37
56.38
54.47
49.51
26.04
25.45
18.37
18.26
-5.26
N3
OTBDMS
N
N=N
S24
f1 (ppm)

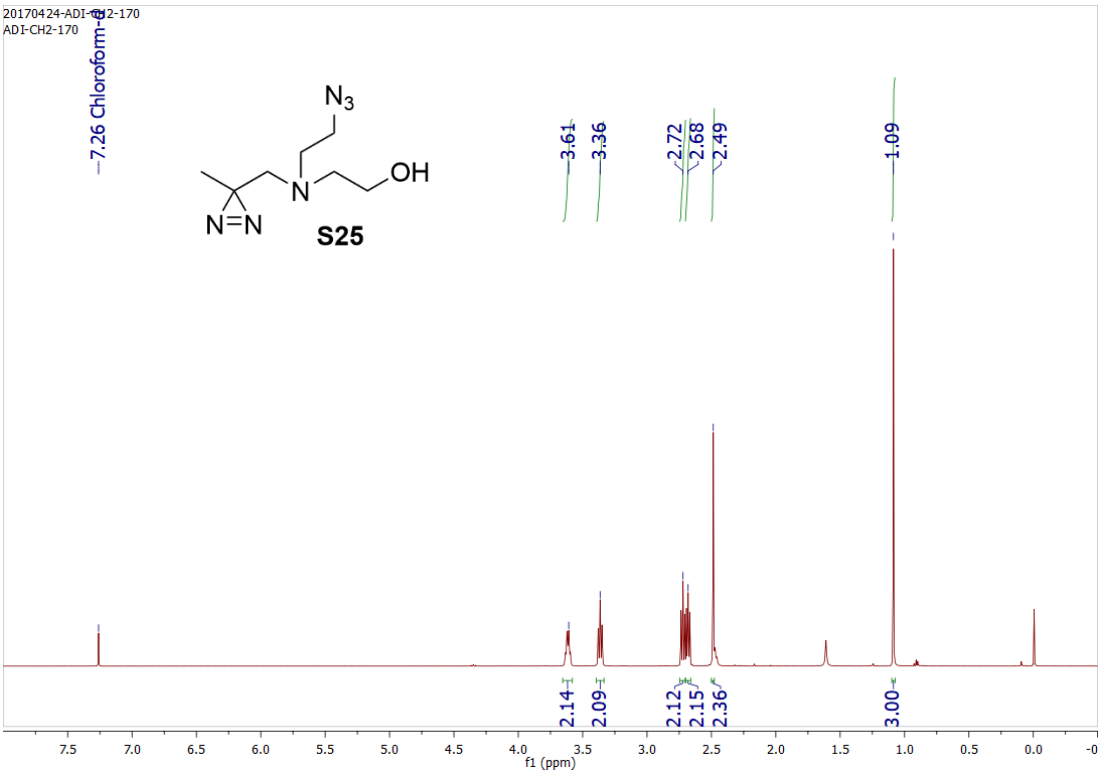
20170424-ADI-CH2-170
ADI-CH2-170
7.26 Chloroform-d
N3
OH
N
N=N
S25
3.61
3.36
2.72
2.68
2.49
1.09
2.14
2.09
2.12
2.15
2.36
3.00
f1 (ppm)

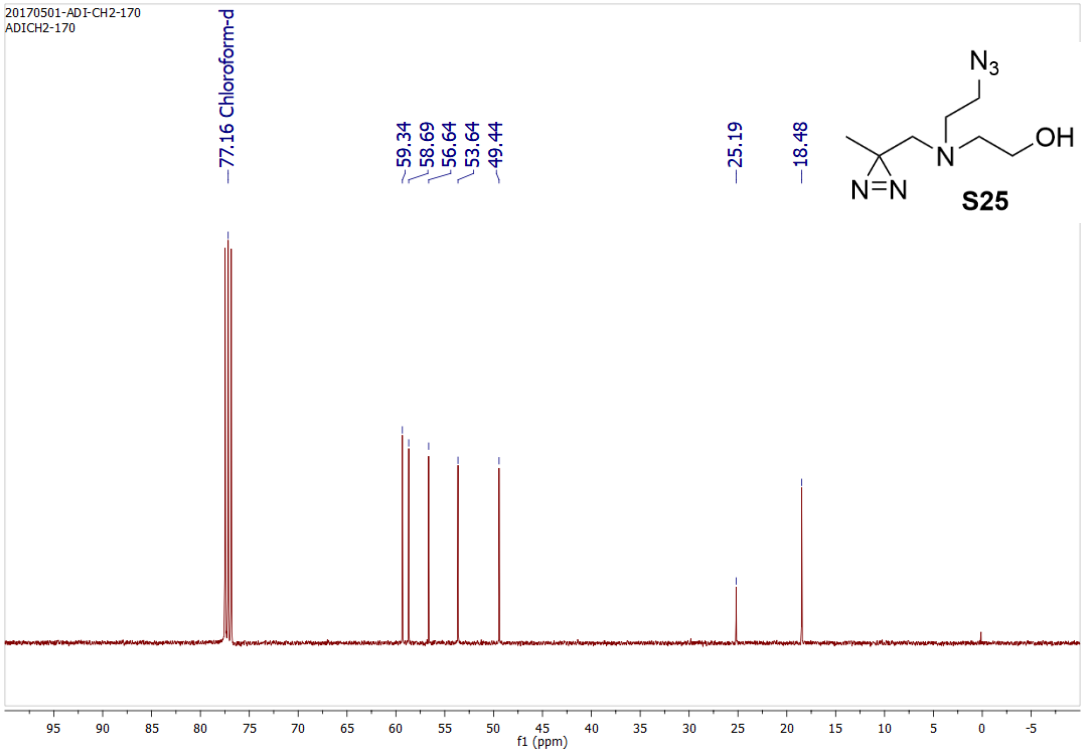
20170501-ADI-CH2-170
ADICH2-170
77.16 Chloroform-d
59.34
58.69
56.64
53.64
49.44
25.19
18.48
N3
OH
N
N=N
S25
f1 (ppm)

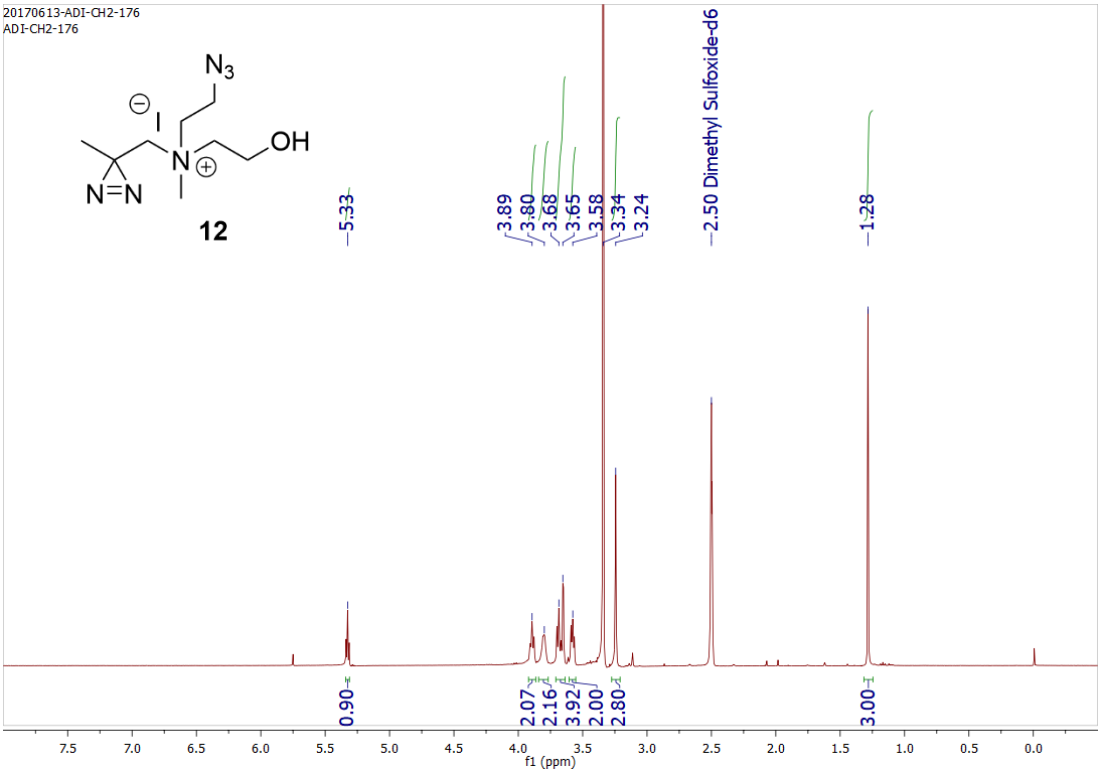
20170613-ADI-CH2-176
ADI-CH2-176
N3
I
OH
N
N=N
12
5.33
3.89
3.80
3.68
3.65
3.58
3.34
3.24
2.50 Dimethyl Sulfoxide-d6
1.28
0.90
2.07
2.16
3.92
2.00
2.80
3.00
f1 (ppm)

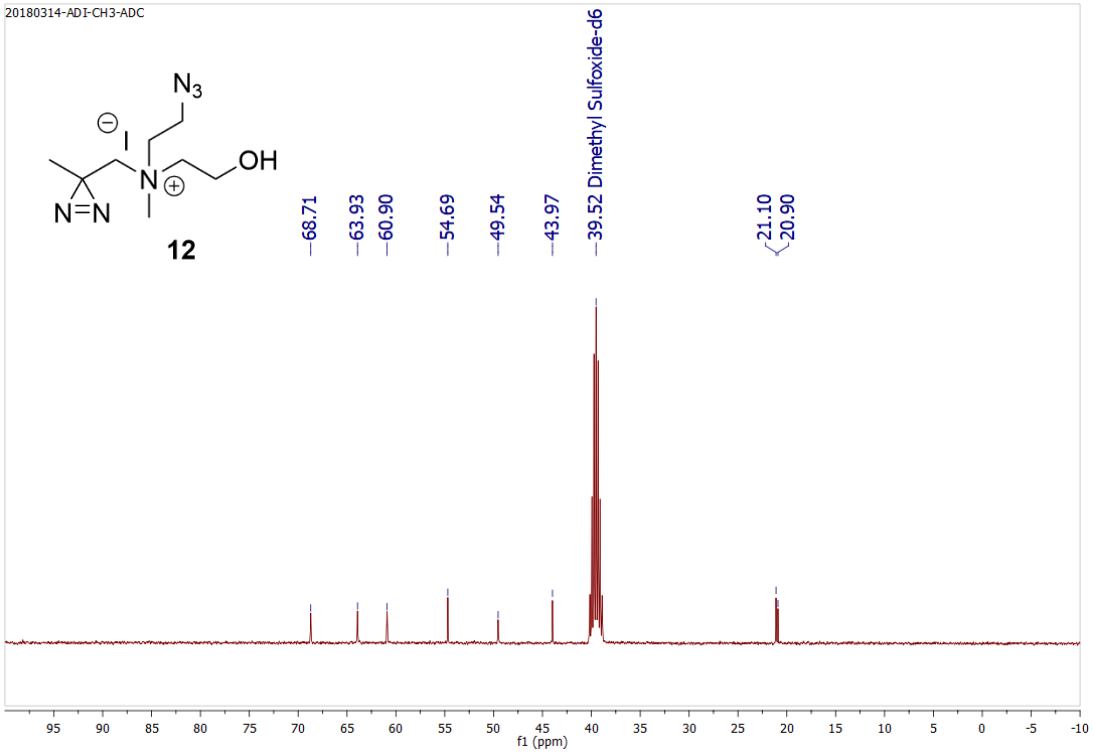
20180314-ADI-CH3-ADC
N3
I
OH
N
N=N
12
68.71
63.93
60.90
54.69
49.54
43.97
39.52 Dimethyl Sulfoxide-d6
21.10
20.90
f1 (ppm)

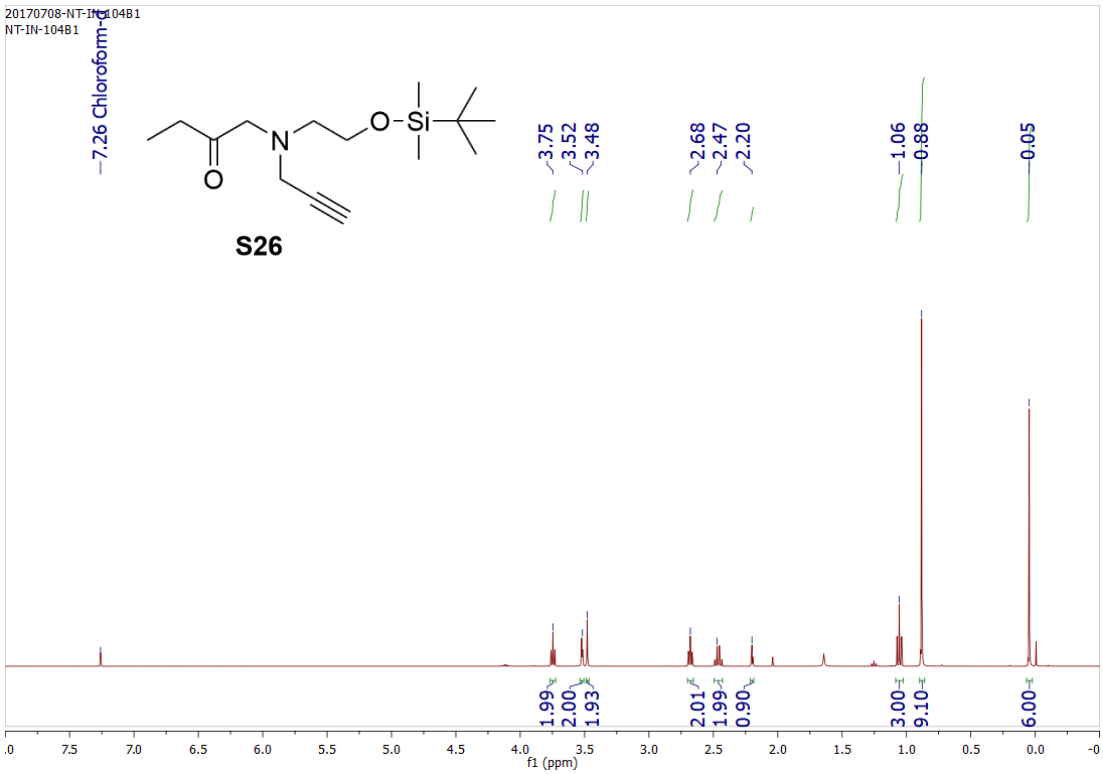
20170708-NT-IN-104B1
NT-IN-104B1
7.26 Chloroform-d
3.75
3.52
3.48
2.68
2.47
2.20
1.06
0.88
0.05
S26
1.99
2.00
1.93
2.01
1.99
0.90
3.00
9.10
6.00
f1 (ppm)

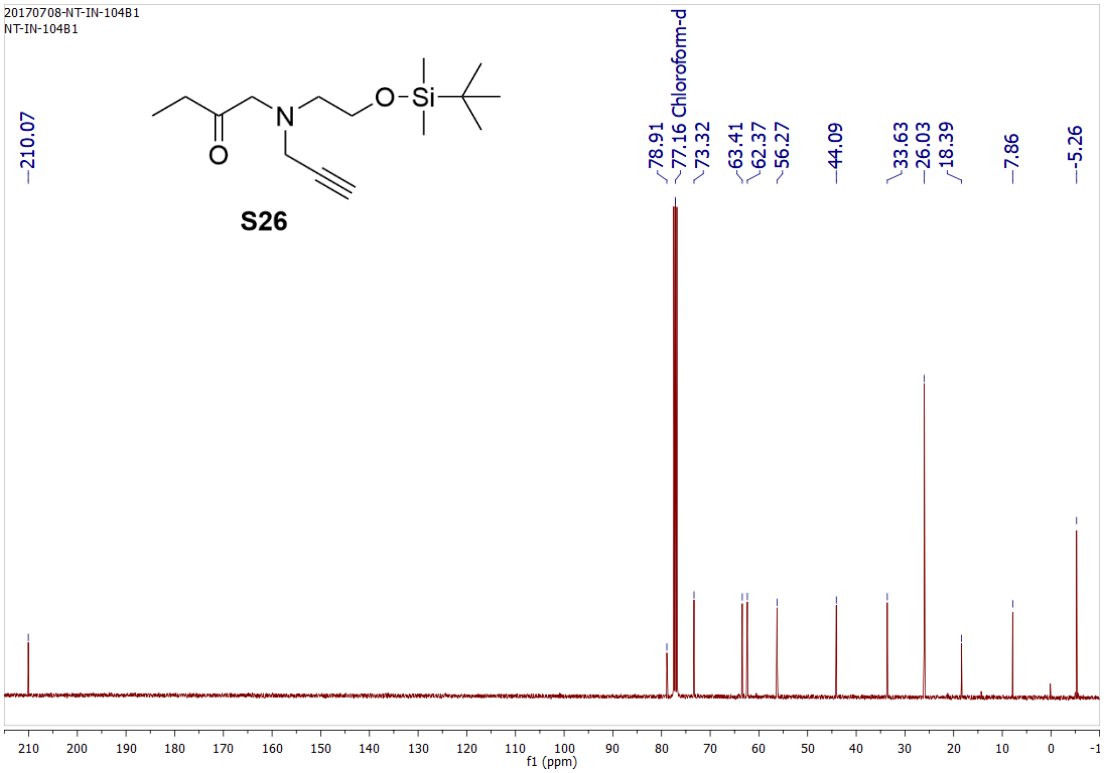
20170708-NT-IN-104B1
NT-IN-104B1
210.07
78.91
77.16 Chloroform-d
73.32
63.41
62.37
56.27
44.09
33.63
26.03
18.39
7.86
-5.26
S26
f1 (ppm)

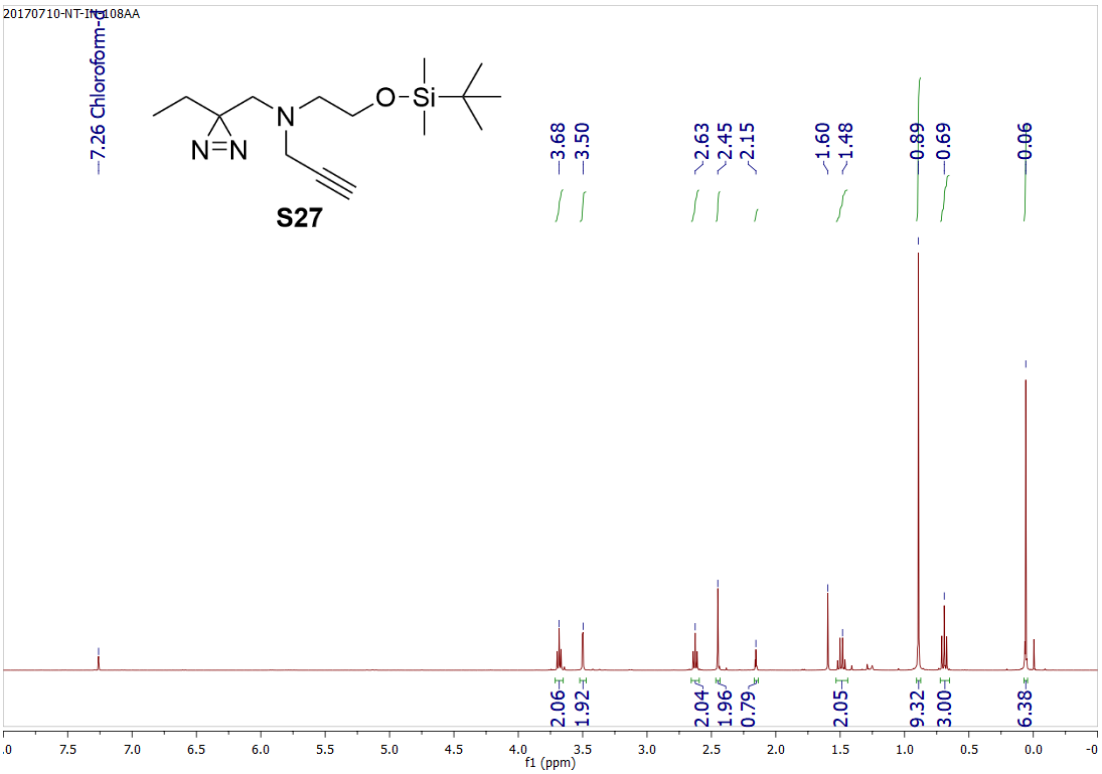
20170710-NT-IN-108AA
7.26 Chloroform-d
3.68
3.50
2.63
2.45
2.15
1.60
1.48
0.89
0.69
0.06
2.06
1.92
2.04
1.96
0.79
2.05
9.32
3.00
6.38
f1 (ppm)
S27

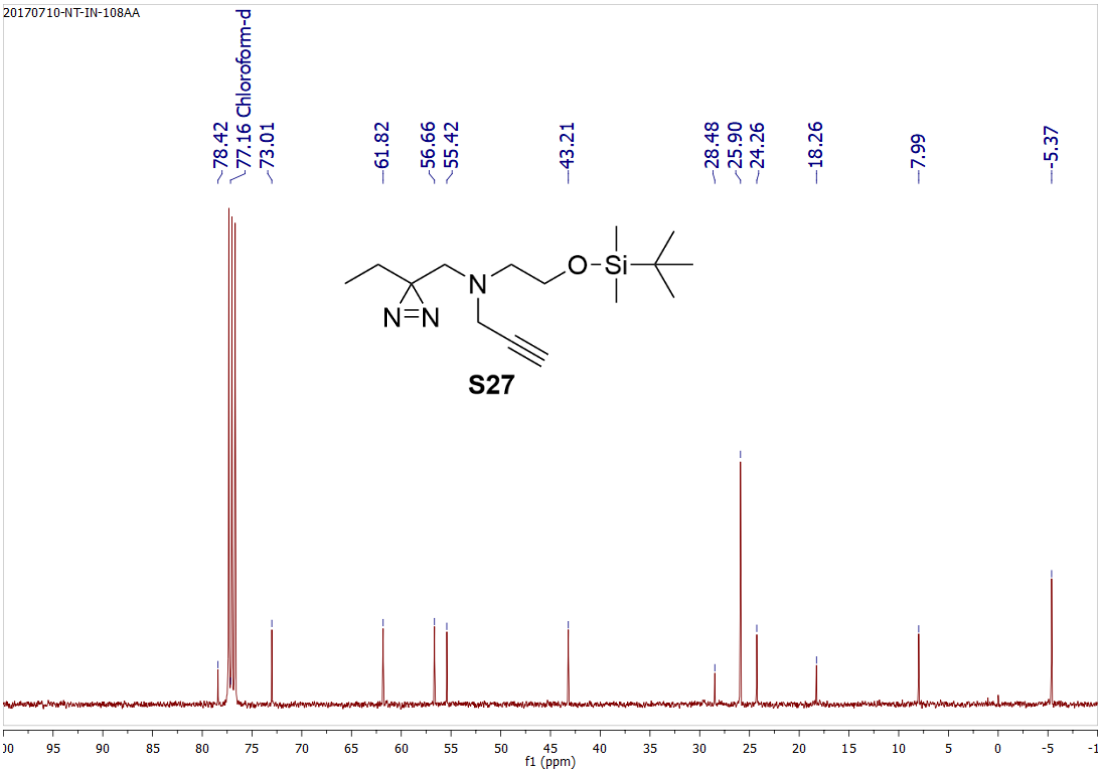
20170710-NT-IN-108AA
78.42
77.16 Chloroform-d
73.01
61.82
56.66
55.42
43.21
28.48
25.90
24.26
18.26
7.99
-5.37
f1 (ppm)
S27

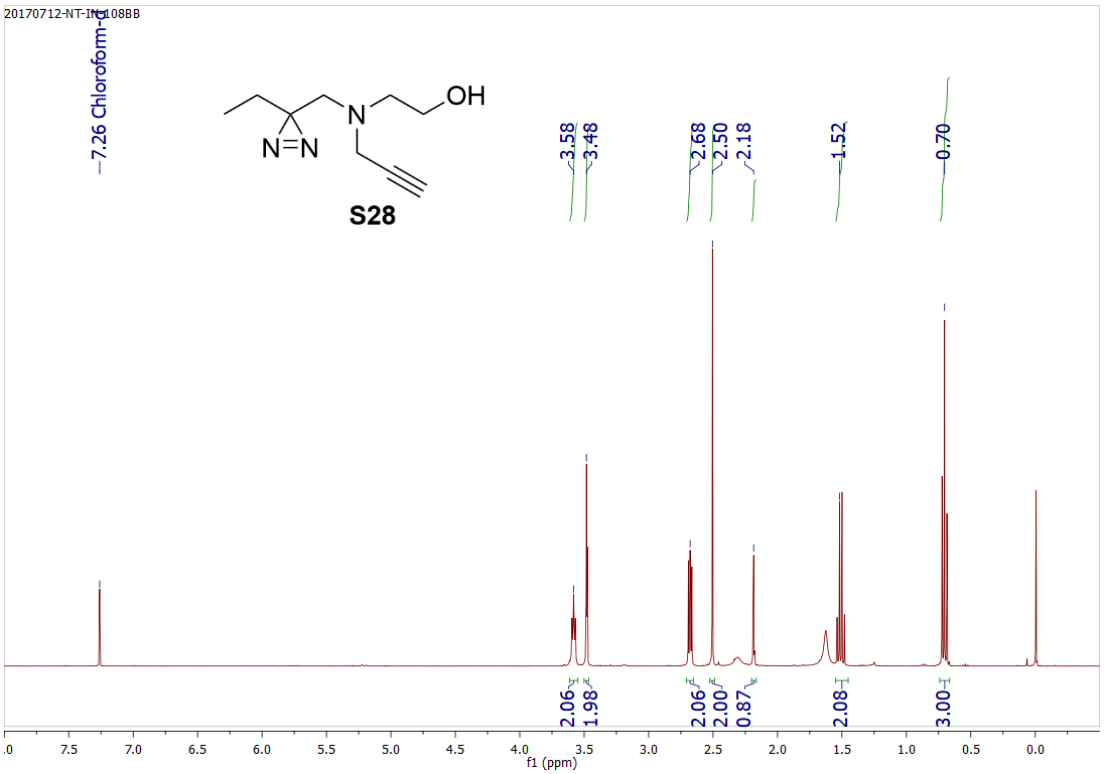
20170712-NT-IN-108BB
7.26 Chloroform-d
3.58
3.48
2.68
2.50
2.18
1.52
0.70
OH
N
N=N
S28
2.06
1.98
2.06
2.00
0.87
2.08
3.00
f1 (ppm)

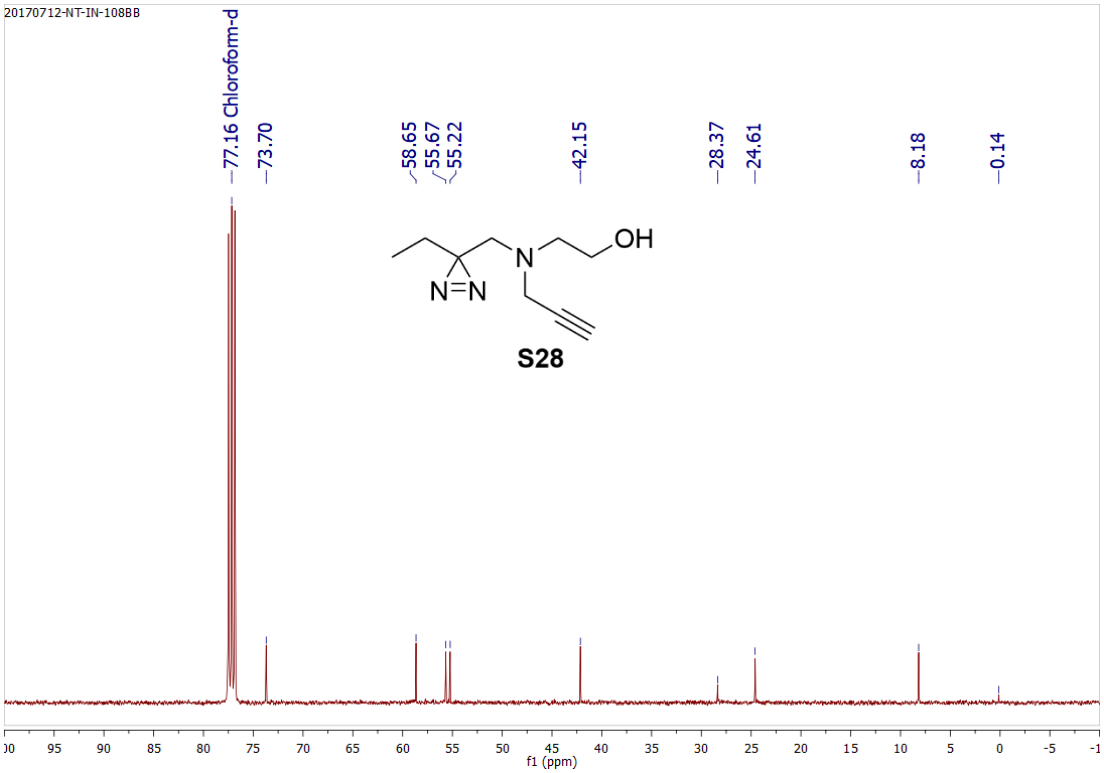
20170712-NT-IN-108BB
77.16 Chloroform-d
73.70
58.65
55.67
55.22
42.15
28.37
24.61
8.18
0.14
OH
N
N=N
S28
f1 (ppm)

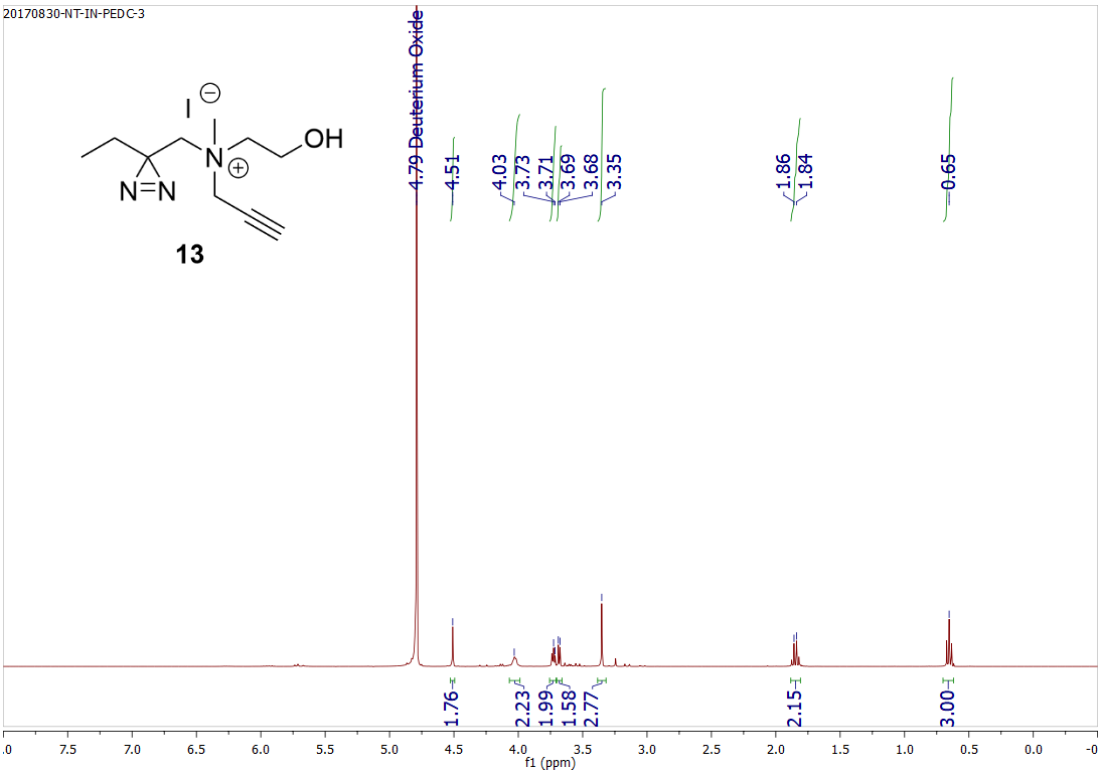
20170830-NT-IN-PEDC-3
I
OH
N
N=N
13
4.79 Deuterium Oxide
4.51
4.03
3.73
3.71
3.69
3.68
3.35
1.86
1.84
0.65
1.76
2.23
1.99
1.58
2.77
2.15
3.00
f1 (ppm)

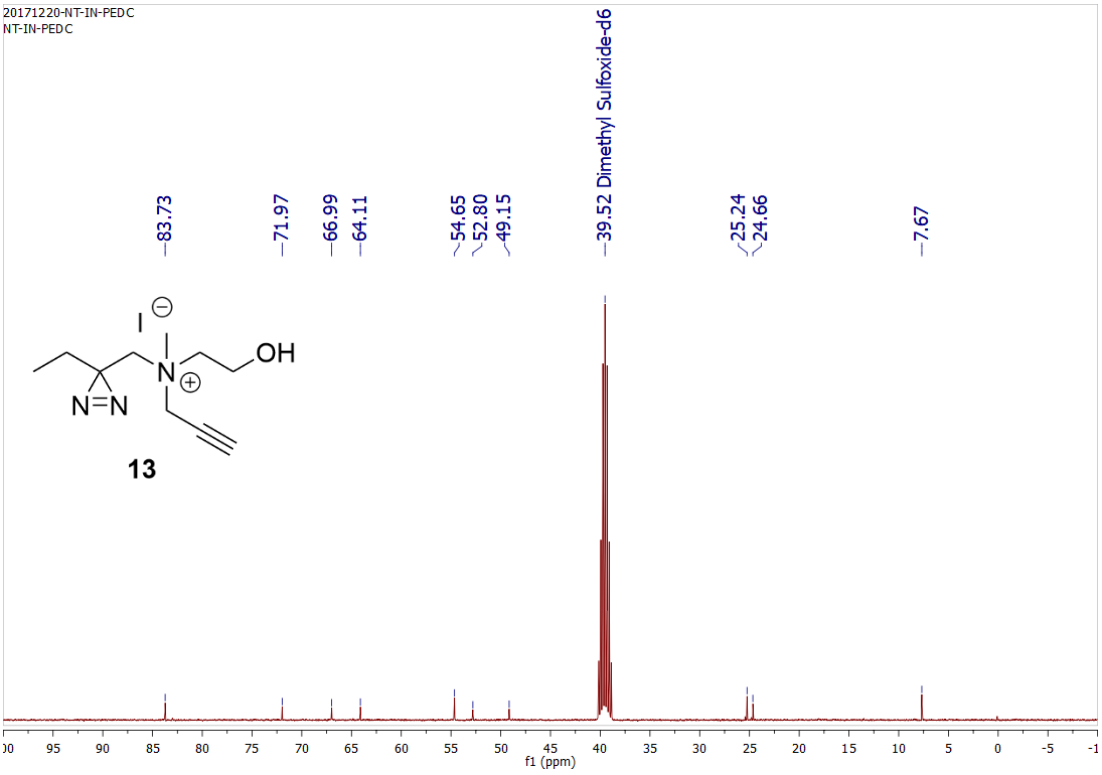
20171220-NT-IN-PEDC
NT-IN-PEDC
83.73
71.97
66.99
64.11
54.65
52.80
49.15
39.52 Dimethyl Sulfoxide-d6
25.24
24.66
7.67
I
OH
N
N=N
13
f1 (ppm)

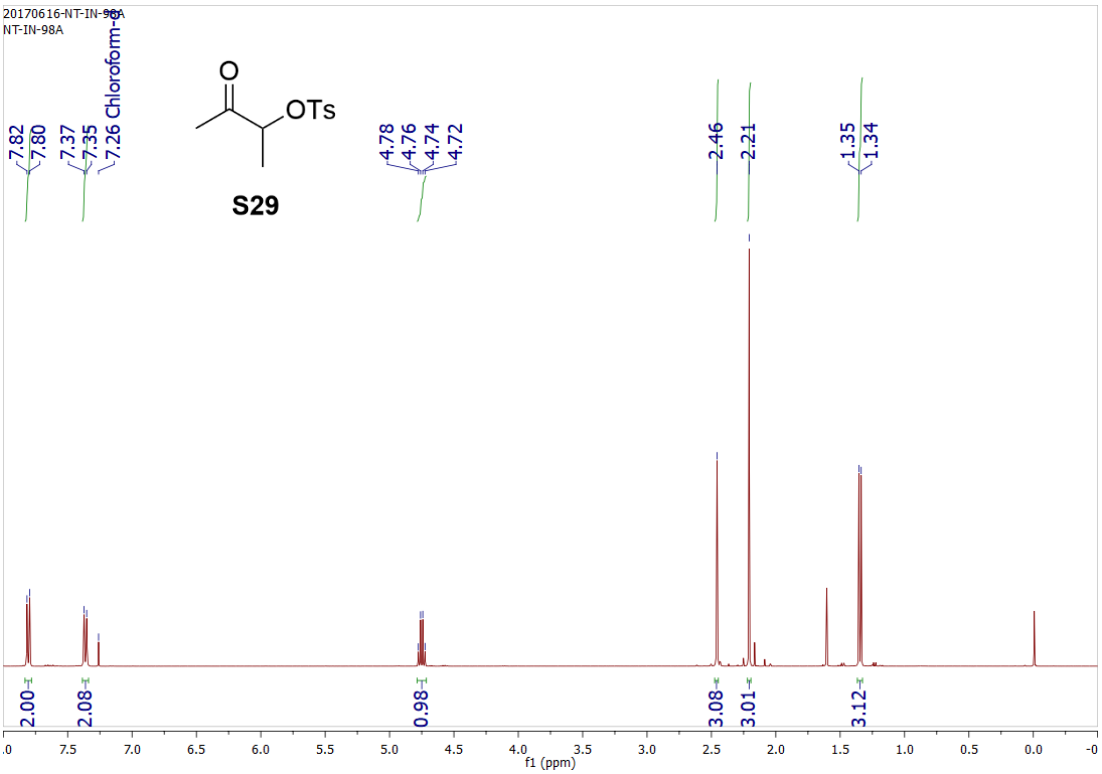
20170616-NT-IN-98A
NT-IN-98A
7.82
7.80
7.37
7.35
7.26 Chloroform-d
O
OTs
S29
4.78
4.76
4.74
4.72
2.46
2.21
1.35
1.34
2.00
2.08
0.98
3.08
3.01
3.12
f1 (ppm)

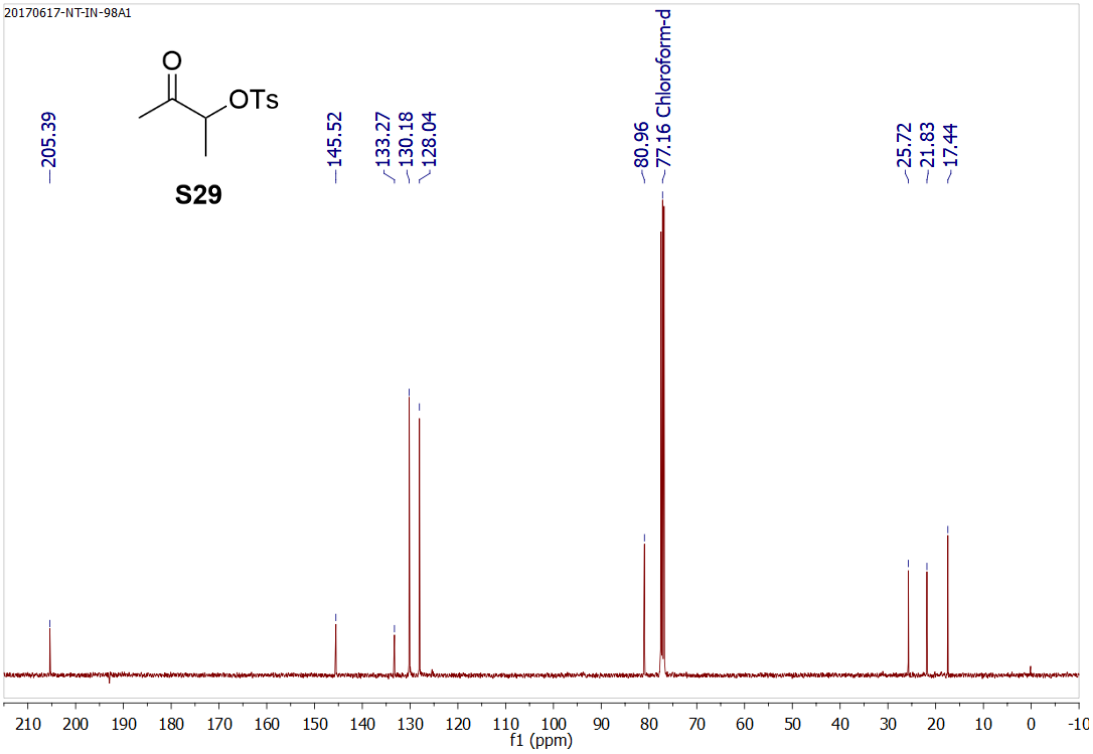
20170617-NT-IN-98A1
O
OTs
S29
205.39
145.52
133.27
130.18
128.04
80.96
77.16 Chloroform-d
25.72
21.83
17.44
f1 (ppm)

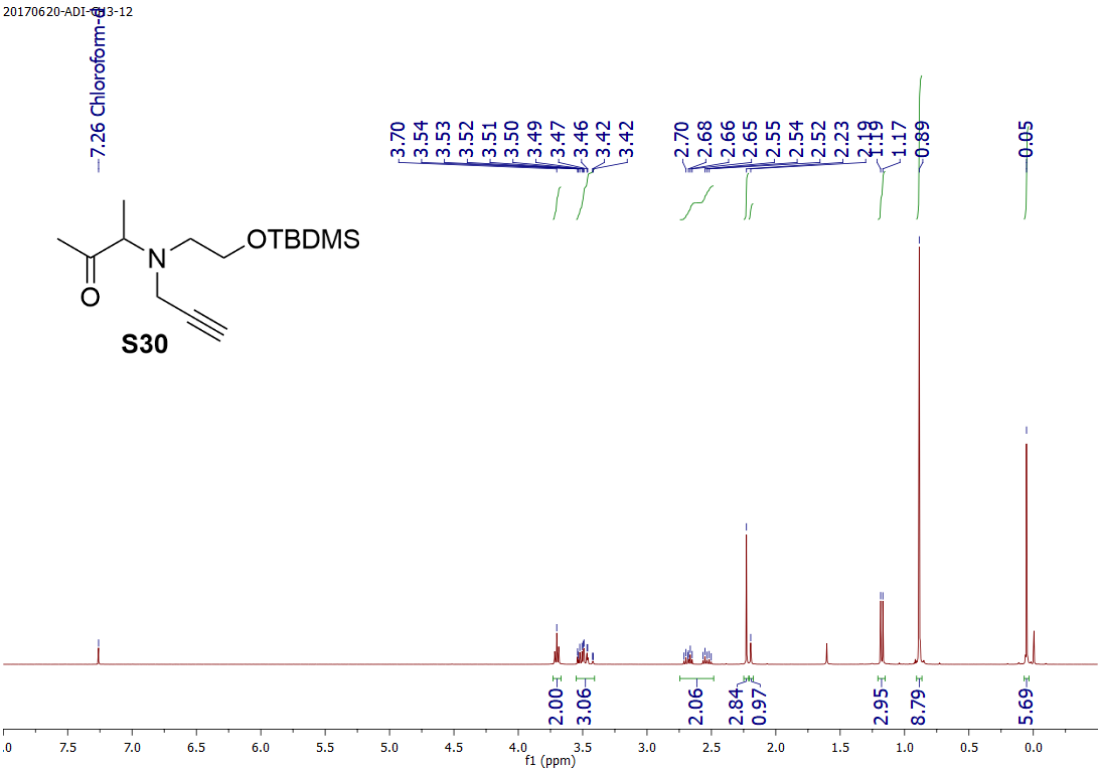
20170620-ADI-CH3-12
7.26 Chloroform-d
OTBDMS
N
O
S30
3.70
3.54
3.53
3.52
3.51
3.50
3.49
3.47
3.46
3.42
3.42
2.70
2.68
2.66
2.65
2.55
2.54
2.52
2.23
1.19
1.17
0.89
0.05
2.00
3.06
2.06
2.84
0.97
2.95
8.79
5.69
f1 (ppm)

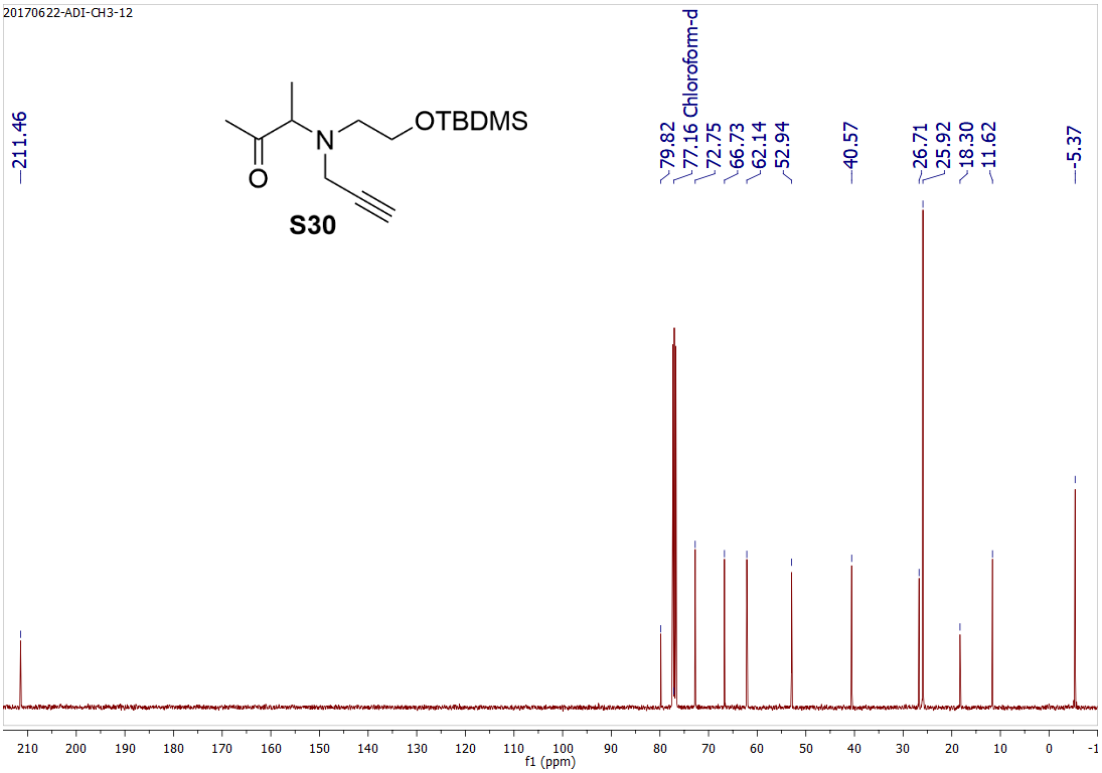
20170622-ADI-CH3-12
211.46
OTBDMS
N
O
S30
79.82
77.16 Chloroform-d
72.75
66.73
62.14
52.94
40.57
26.71
25.92
18.30
11.62
-5.37
f1 (ppm)

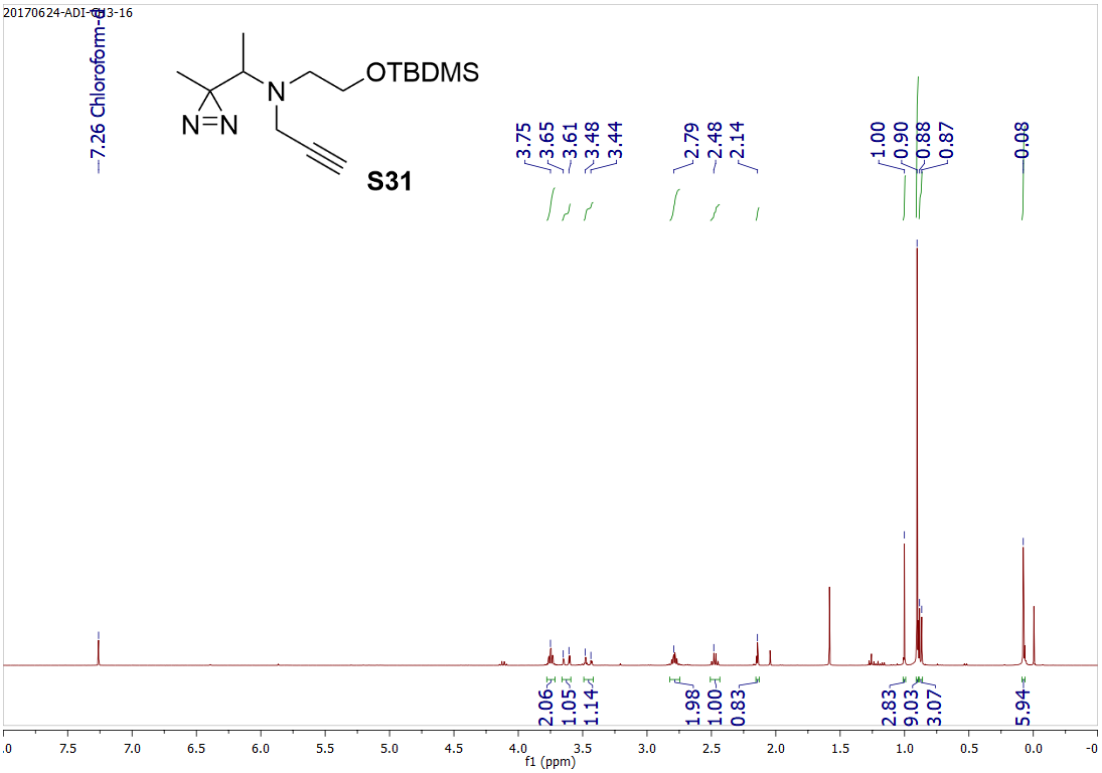
20170624-ADI-CH3-16
7.26 Chloroform-d
OTBDMS
N
N=N
S31
3.75
3.65
3.61
3.48
3.44
2.79
2.48
2.14
1.00
0.90
0.88
0.87
0.08
2.06
1.05
1.14
1.98
1.00
0.83
2.83
9.03
3.07
5.94
f1 (ppm)

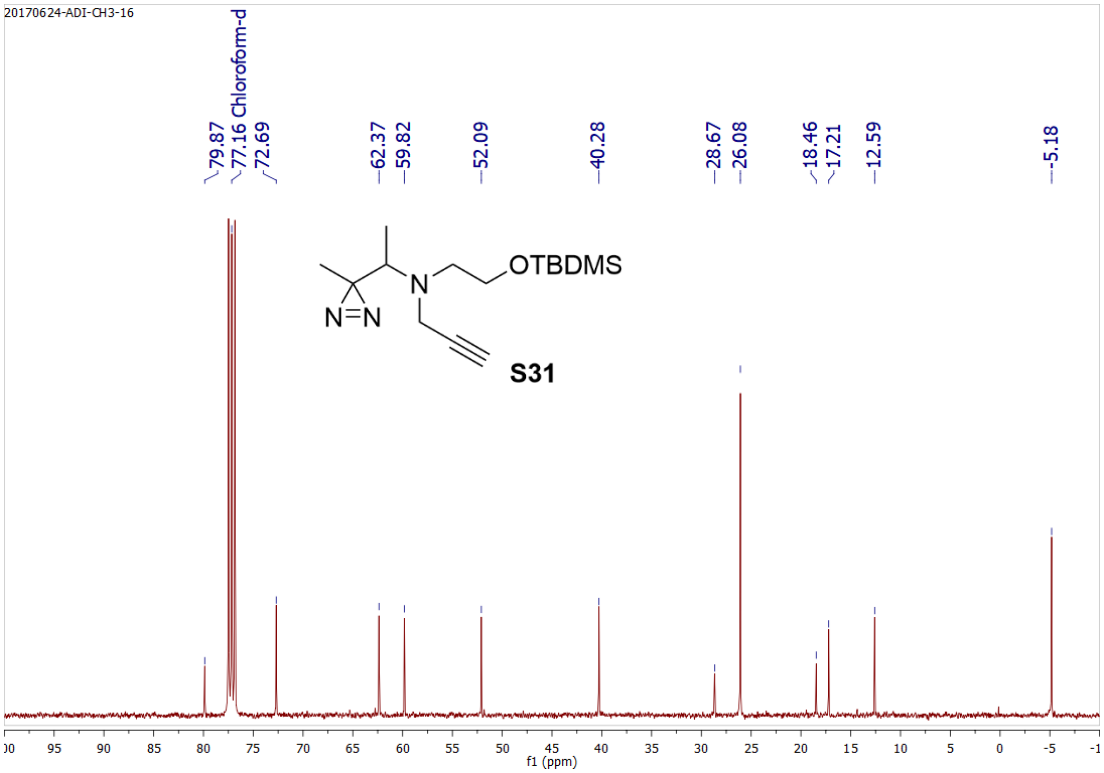
20170624-ADI-CH3-16
79.87
77.16 Chloroform-d
72.69
62.37
59.82
52.09
40.28
28.67
26.08
18.46
17.21
12.59
-5.18
OTBDMS
N
N=N
S31
f1 (ppm)

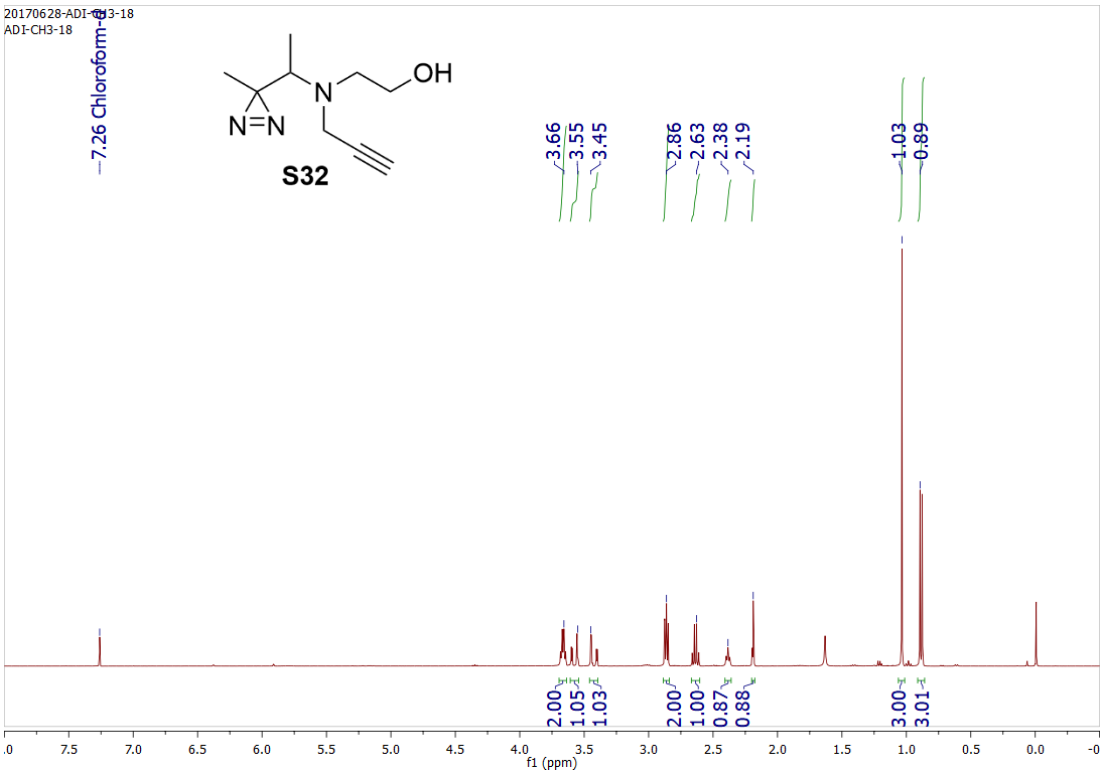
20170628-ADI-CH3-18
ADI-CH3-18
7.26 Chloroform-d
S32
3.66
3.55
3.45
2.86
2.63
2.38
2.19
1.03
0.89
2.00
1.05
1.03
2.00
1.00
0.87
0.88
3.00
3.01
f1 (ppm)

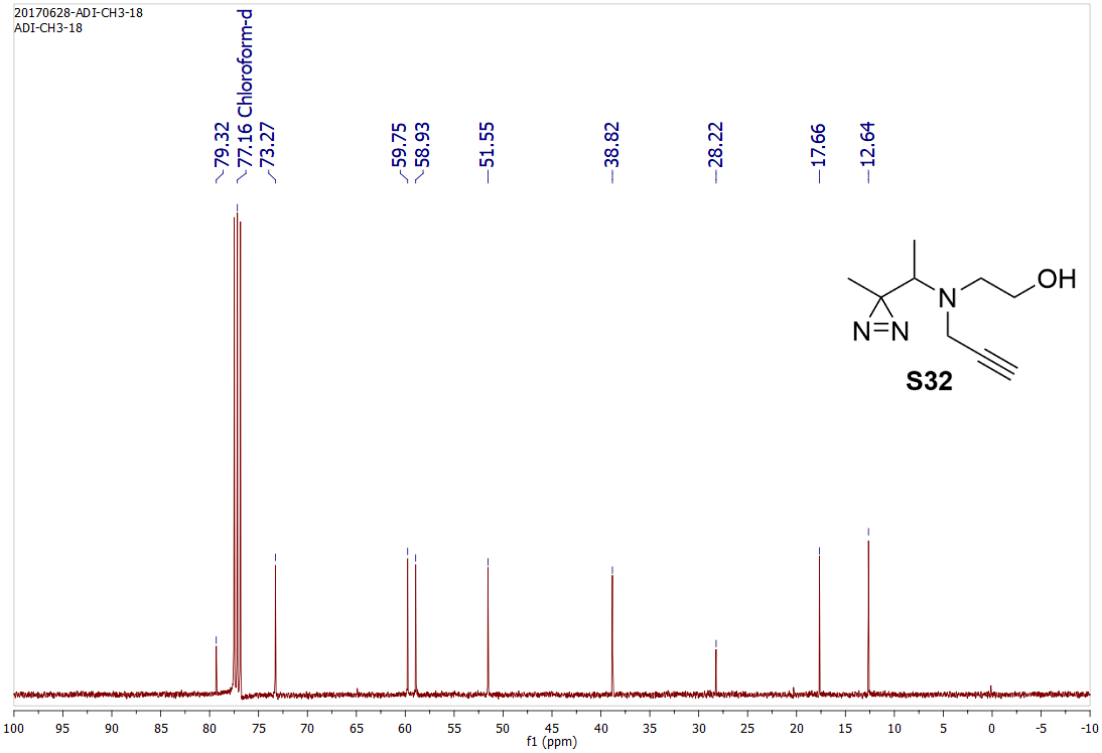
20170628-ADI-CH3-18
ADI-CH3-18
79.32
77.16 Chloroform-d
73.27
59.75
58.93
51.55
38.82
28.22
17.66
12.64
S32
f1 (ppm)

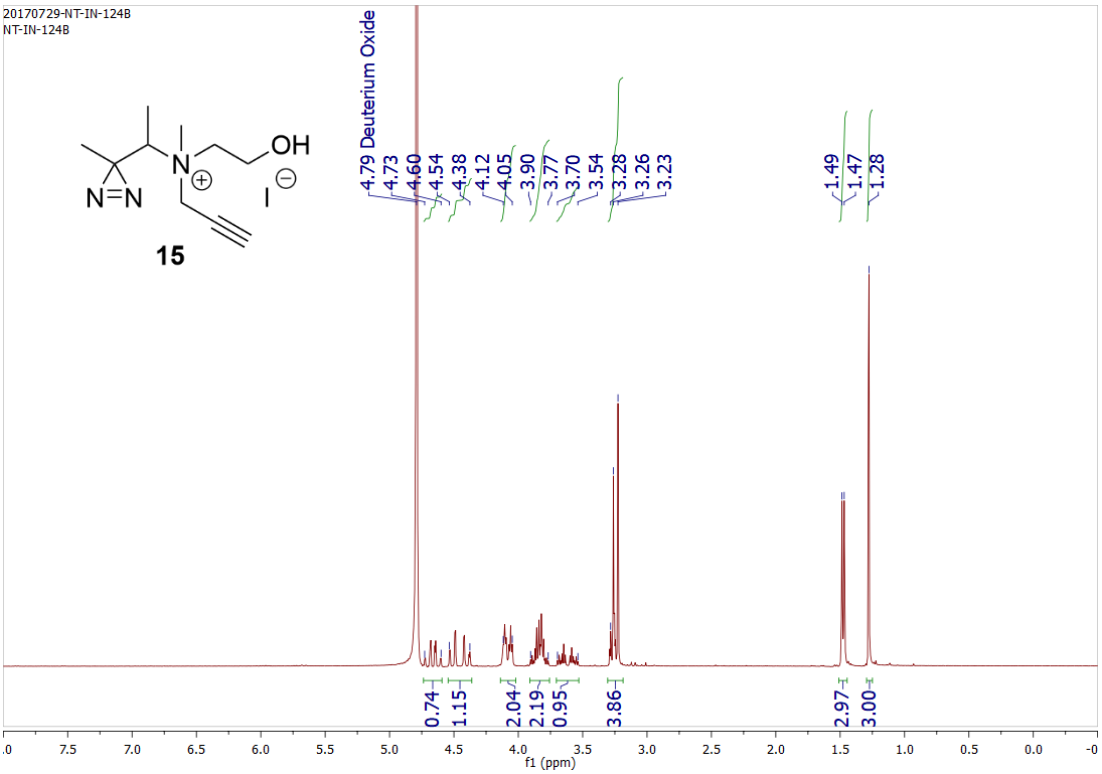
20170729-NT-IN-124B
NT-IN-124B
4.79 Deuterium Oxide
4.73
4.60
4.54
4.38
4.12
4.05
3.90
3.77
3.70
3.54
3.28
3.26
3.23
1.49
1.47
1.28
0.74
1.15
2.04
2.19
0.95
3.86
2.97
3.00
OH
N
I
15
f1 (ppm)

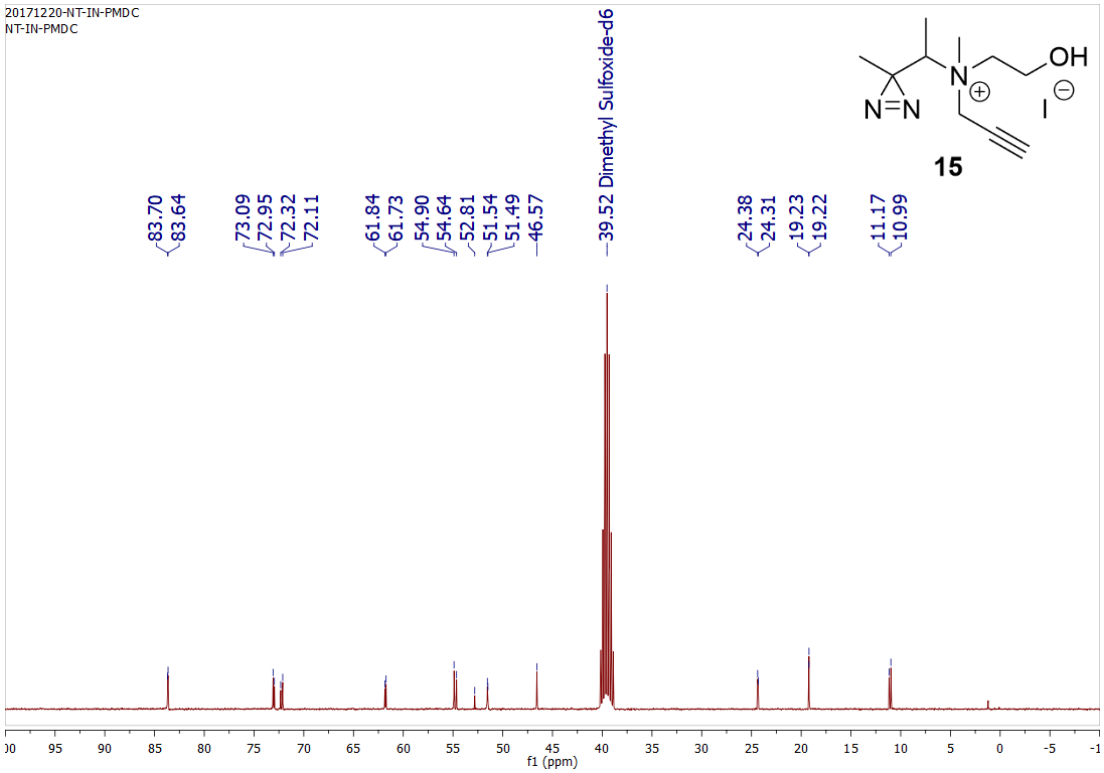
20171220-NT-IN-PMDC
NT-IN-PMDC
39.52 Dimethyl Sulfoxide-d6
83.70
83.64
73.09
72.95
72.32
72.11
61.84
61.73
54.90
54.64
52.81
51.54
51.49
46.57
24.38
24.31
19.23
19.22
11.17
10.99
OH
N
I
15
f1 (ppm)

3.6 References

1. Blencowe, A.; Hayes, W., Development and application of diazirines in biological and synthetic macromolecular systems. *Soft Matter* **2005,** *1* (3), 178-205.

2. Das, J., Aliphatic diazirines as photoaffinity probes for proteins: recent developments. *Chem Rev* **2011,** *111* (8), 4405-17.

3. Dubinsky, L.; Krom, B. P.; Meijler, M. M., Diazirine based photoaffinity labeling. *Bioorg Med Chem* **2012,** *20* (2), 554-70.

4. Smith, R. A.; Knowles, J. R., Letter: Aryldiazirines. Potential reagents for photolabeling of biological receptor sites. *J Am Chem Soc* **1973,** *95* (15), 5072-73.

5. Smith, R. A. G.; Knowles, J. R., The preparation and photolysis of 3-aryl-3H-diazirines. *J Chem Soc, Perkin Trans 2* **1975,** (7), 686-94.

6. Levene, P. A., Bromoacetone. *Org Synth* **1930,** *10*.

Chapter 4

γ-Diazirine Cholines as Metabolic Labeling Probes for Choline Metabolites

This chapter is adapted with permission from the publication: Dixit, A.; Jose, G. P.; Shanbhag, C.; Tagad, N.; Kalia, J. Metabolic labeling-based chemoproteomics establishes choline metabolites as protein function modulators. *ACS Chem. Biol.* **2022**, *17*, 2272–2283. Copyright 2022 American Chemical Society.

4.1 Introduction

Our studies on β-diazirine cholines as described in Chapter 3, provided valuable insights on lipid biology, however, they also established that these compounds were not suitable for choline metabolite-interactome mapping due to their poor cellular photocrosslinking yields. They undergo undesired metabolic conversions and are transformed into other choline derivatives that limit their use as efficient photocrosslinkable probes for the isolation of choline metabolite and lipid-interacting proteins. Since the β-diazirine cholines (compounds **11**-**15**) served as effective substrates for the putative N–C bond cleavage mechanism followed by methylation in cells, I reasoned that γ-diazirine choline analogs may show reduced (or negligible) propensity towards undergoing N–C bond cleavage followed by methylation. In this chapter, I report the evaluation of γ-diazirine containing choline analogs for their metabolic labeling efficiency in mammalian cells and their use as effective photocrosslinkable probes.

4.2 Results and Discussion

4.2.1 γ-diazirine choline analogs are ideal metabolic labeling probes for choline lipids

We synthesized our first and simplest γ-diazirine choline, compound **20** and observed that it showed robust metabolic labeling as demonstrated by the TIC peak intensity of ~6.6E8 units obtained for the **20**-labeled choline lipids isolated from HEK293 cells cultured in its presence (Figure 4.1).

Encouraged by this result, appending a propargyl group to **20** yielded the bifunctional diazirine compound **21** that also metabolically labeled choline lipids efficiently yielding a TIC peak value of ~1.8E7 units for choline lipids metabolically labeled with it (Figure 4.2a). Notably, this TIC peak intensity is more than 4-fold higher than that obtained for the analogous alkynyl β-diazirine choline compound (**11**) that yielded a TIC peak value of ~4.0E6 units (Figure 3.2a) demonstrating that **21** was a more proficient metabolic labeling probe. The LipidView analysis of the XIC depicting the identity of all of the **21**-labeled PC and SM lipids detected is shown in Figure 4.2b. Similar to the PC lipids labeled with the β-diazirine analogs **10**, **11**, and **13**, the most abundant PC lipid labeled with γ-diazirine choline analog **20** is also 32:1 (compare LipidView profiles in

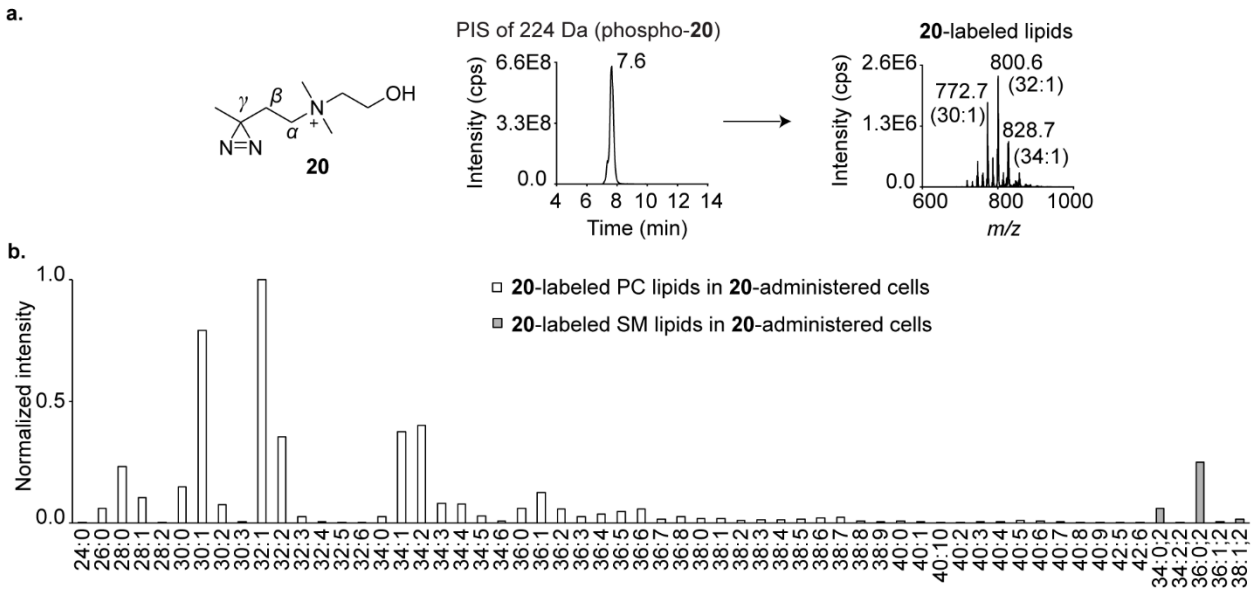

Figure 4.1. Metabolic labeling studies on γ-diazirine choline analog **20**. a) The TIC and XIC plots obtained by employing a PIS of 224 Da (the *m/z* for phospho-**20**) on lipids extracted from HEK293 cells cultured for 24 h in the presence of compound **20** (2 mM). b) A bar graph obtained from the LipidView software denoting all **20**-labeled choline lipids identified from the XIC depicted above. The *y*-axis has been normalized to the most intense peak *i.e.*, lipid 32:1 of the XIC.

Figures 3.1b, 3.2b, 3.8b and Figure 4.1b). Surprisingly, however, the most abundant **21**-labeled PC lipid is 34:1 (Figure 4.2b) that is also the most preferred acyl chain combination for native choline lipids and the choline lipids labeled with analogs **1**-**9** (LipidView profiles in Figures 2.4-2.12). Moreover, as expected from an alkynyl choline analog that yields a TIC peak intensity of <E8 units, poor fluorescence intensity was obtained when cells metabolically labeled with **21** were treated with 5-azido fluorescein under click chemistry conditions (Figure 4.3a) suggesting that unlike compound **11** (Figure 3.4b), this compound does not form large amounts of propargyl choline (**1**)-labeled lipids.

This speculation was demonstrated to be correct by the results of our lipidomics experiments that demonstrated that lipids isolated from cells cultured in the presence of **21** yielded a small peak for **1**-labeled lipids (TIC and XIC in Figure 4.3c and LipidView analysis in Figure 4.3d). Moreover, no detectable amount of choline lipids labeled with the alkyne-devoid diazirine (**20**) was observed in lipids isolated from these cells (Figure 4.4) demonstrating that compound **21** is a more superior

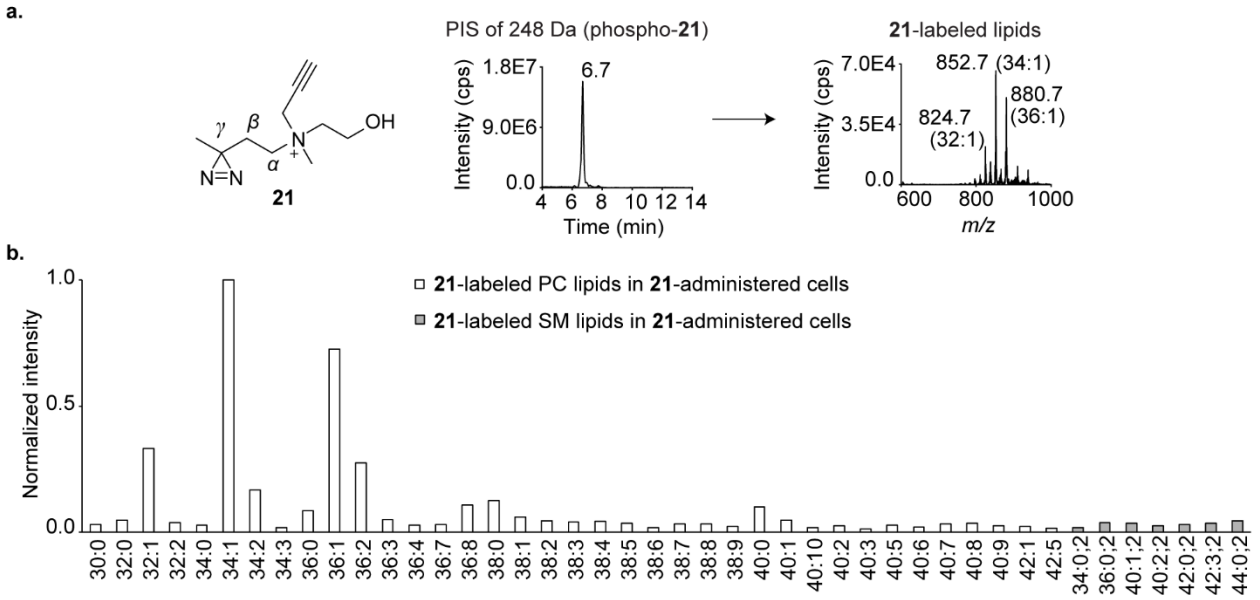

Figure 4.2. Metabolic labeling studies on bifunctional γ-diazirine choline analog **21**. a) The TIC and XIC plots obtained by employing a PIS of 248 Da (the *m/z* for phospho-**21**) on lipids extracted from HEK293 cells cultured for 24 h in the presence of compound **21** (2 mM). b) A bar graph obtained from the LipidView software denoting all **21**-labeled choline lipids identified from the XIC depicted above. The *y*-axis has been normalized to the most intense peak *i.e.*, lipid 34:1 of the XIC.

probe for labeling choline lipids with the diazirine and the alkyne groups as compared to the β-diazirine choline derivatives described in the previous chapter.

We consolidated this conclusion by performing our time course-based experiments where lipids were isolated from HEK293 cells that were administered with **21** for 4 h, 8 h, 16 h, and 24 h and tested for the formation of **1**-, **20**-, and **21**-labeled choline lipids. Plotting the respective TIC peak areas versus the time of administration revealed that at all time points tested, **21**-labeled choline lipids were the dominant metabolically labeled choline lipids in HEK293 cells (Figures 4.5a, 4.5b (left) and Figure A4 of the Appendix). Two other mammalian cell lines (HeLa and MDA-MB-231) were cultured in the presence of **21** for 24 h and tested for the formation of **1**-, **20**-, and **21**-labeled choline lipids. Results for these experiments were similar to the ones that were obtained for HEK293 cells where **21**-labeled choline lipids were the most abundant lipids (Figure 4.5b (middle and right)). Interestingly, although both HEK293 and HeLa cells showed the formation of small amounts of **1**-labeled lipids (see TICs for PIS of 208 Da in Figures A4 and A5b of the

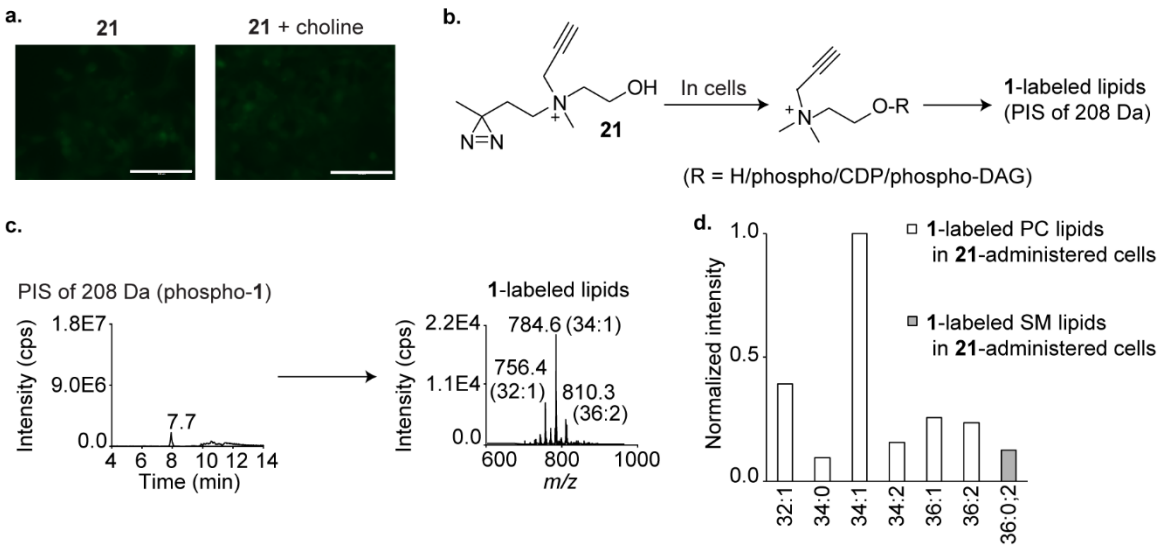

Figure 4.3. Testing the cellular conversion of **21**-labeled metabolites/lipids to **1**-labeled lipids. a) Imaging experiments on **21** (2 mM)-administered HEK293 cells (left), and cells administered with both **21** and choline (2 mM each; right). The scale bars represent 100 µm. b) The expected formation of **1**-labeled lipids in **21**-administered cells. c) The TIC and XIC plots obtained by employing a PIS of 208 Da (the *m/z* for phospho-**1**) on lipids extracted from HEK293 cells cultured in the presence of compound **21** (2 mM). d) LipidView analysis of **1**-labeled choline lipids obtained from the HEK293 cells cultured for 24 h in the presence of **21**. The *y*-axis has been normalized to the most intense peak *i.e.*, lipid 34:1 of the XIC.

Appendix) upon administration of **21** for 24 h, MDA-MB-231 cells did not show the any detectable peaks for **1**-labeled choline lipids (Figure A6b of the Appendix). These results are in stark contrast to those obtained with the cultured alkynyl β- diazirine choline compound **11** wherein the desired **11**-labeled choline lipids were formed in much lower amounts as compared to the diazirine-devoid alkynyl choline (**1**)-labeled lipids (Figure 3.6).

4.2.2 The alkynyl γ-diazirine choline probe 21 enables the discovery of the cellular choline metabolite and lipid-interacting proteome

Efficient metabolic labeling of mammalian choline lipids with the γ-diazirine choline derivative **21** and minimal concomitant labeling with its diazirine/alkyne-devoid derivatives rendered this compound a promising candidate for the discovery of the choline metabolite and lipid-interacting

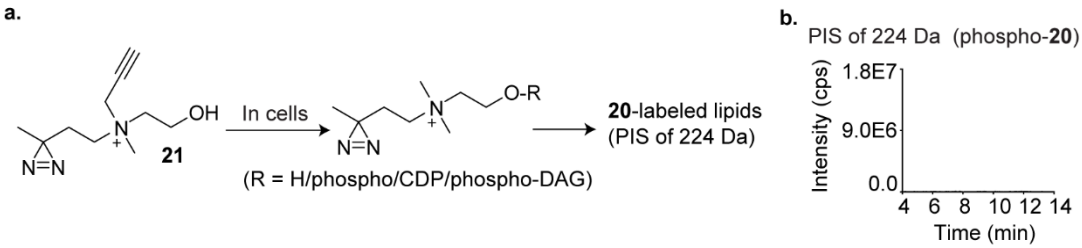

Figure 4.4. Testing the cellular conversion of **21**-labeled metabolites/lipids to **20**-labeled lipids. a) The expected formation of **20**-labeled lipids in **21**-administered cells. b) The TIC plot obtained by employing a PIS of 224 Da (the *m/z* for phospho-**20**) on lipids extracted from HEK293 cells cultured in the presence of compound **21** (2 mM). The resultant TIC shows no peak for **20**-labeled lipids.

proteome of mammalian cells. Encouraged by these results, we next explored the crosslinking efficiency of **21**-labeled choline metabolites to their interacting proteins in cells. UV-irradiating HEK293 cells cultured in the presence of **21** followed by lysing the cells and treating the cell lysate with Alexa Fluor 594 azide under click chemistry conditions yielded a multitude of fluorescently labeled proteins that demonstrated a dose-dependent increase in fluorescence intensities (SDS-PAGE analysis depicted in Figure 4.6a). This result is in contrast to that obtained when compound **11** was similarly tested (bottom panel of Figure 3.2c) wherein negligible fluorescence signal above background was obtained. Not only was the cellular crosslinking dose-dependent, but also UV-irradiation time dependent as revealed by the enhancement of the fluorescence intensities of crosslinked protein bands with increasing UV-exposure time durations (Figure 4.6b).

We next compared compound **21** with our other photocrosslinkable choline analogs. In this pursuit, we cultured HEK293 cells in the presence of the alkynyl diazirine choline compounds **11**, **13** and **15** and the azido diazirine choline compound **12**, as well as the non-photocrosslinkable compound, propargyl choline (**1**), in parallel. After UV-irradiating the cells, they were lysed and the lysates of the cells that were administered with the alkynyl compounds **1**, **11**, **13**, **15** and **21** were treated with the Alexa Fluor 594 azide dye under click chemistry conditions whereas the lysates of cells administered with the azido compound **12** was treated with Alexa Fluor 594 alkyne under click chemistry conditions. SDS-PAGE analysis revealed that only **21**-administered mammalian cells yielded fluorescently labeled proteins (Figure 4.7a) demonstrating that compound **21** was our only metabolic labeling probe capable of efficiently crosslinking choline metabolites and lipids with its

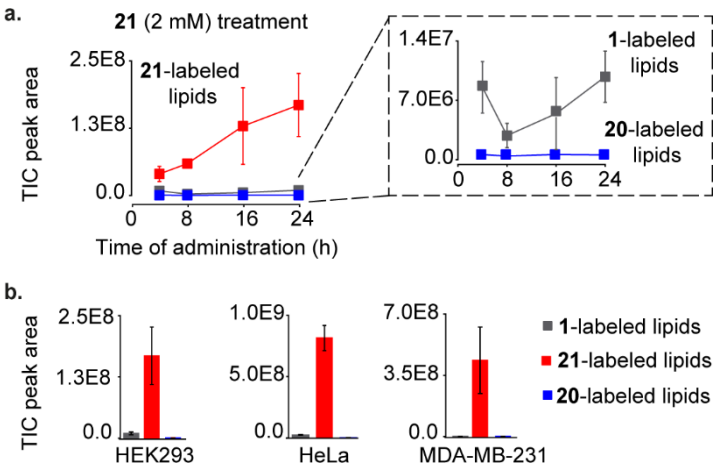

Figure 4.5. Estimate of **1**-, **20**-, and **21**-labeled lipids formed from the cellular administration of **21**. a) A plot of the TIC peak areas versus time wherein the areas under the TIC plots were obtained from the PIS for **1**-, **20**-, and **21**-labeled lipids on the lipids extracted from HEK293 cells cultured in presence of **21** (2 mM) for 4, 8, 16, and 24 h. The representative TIC and XIC plots for the aforementioned treatments are depicted in Figure A4 of the Appendix. Each data point is an average of three biological replicates and the error bars represent the standard error values. b) A bar graph representing the TIC peak areas for **1**-, **20**-, and **21**-labeled lipids extracted from HEK293, HeLa and MDA-MB-231 cells cultured for 24 h in the presence of **21** (2 mM). Each peak area value is an average of three biological replicates and the error bars represent the standard error values. The representative TIC and XIC plots for these experiments are depicted in Figures A4-A6.

interacting proteins. In-gel fluorescence-based choline-competition experiments involving co-administration of choline with **21** revealed a clear attenuation of the intensity of fluorescent bands with increasing choline concentrations (Figure 4.7b) demonstrating that **21** was an effective surrogate for choline. All fluorimager-visualized gels discussed above were stained with coomassie (bottom panels of Figure 4.6 and 4.7) to demonstrate uniformity in protein loading across the different lanes of the individual gels.

The in-gel fluorescence experiments described above established the suitability of **21** for covalently capturing choline metabolite and lipid-interacting proteins of mammalian cells and also demonstrated that after crosslinking, its alkyne tag was amenable to click chemistry-mediated derivatization with azide-labeled compounds. We next employed the optimal UV-irradiation and photocrosslinking conditions that were determined from these studies for performing click

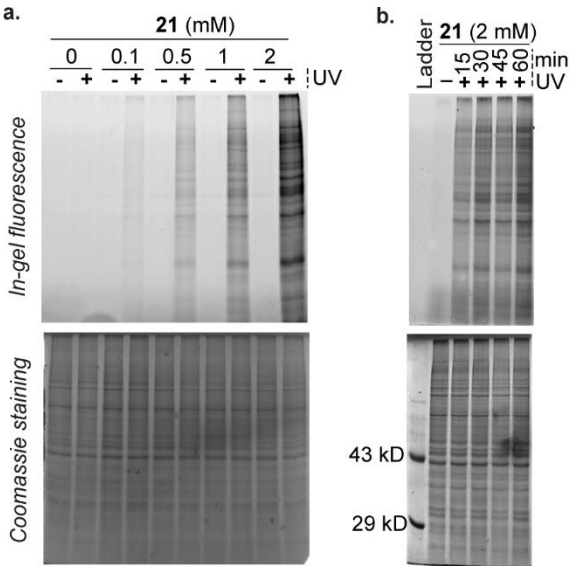

Figure 4.6. Testing the crosslinking efficiency of **21**-labeled choline metabolites in cells. Panels a) and b) represent data obtained from in-gel fluorescence experiments with the fluorimager-captured images depicted on the top and the same gels subsequently stained with Coomassie on the bottom. a) In-gel fluorescence experiments on HEK293 cells cultured in presence of increasing concentrations of **21** for 24 h. b) Evaluation of the time-dependence of UV-irradiation on photocrosslinking efficiency in cells cultured for 24 h in the presence of **21**.

chemistry-based biotinylation followed by enrichment of the crosslinked proteins as this was a critical step of our proposed workflow depicted in Figure 1.7b. These experiments involved metabolically labeling the HEK293 cells with increasing concentrations of **21** (ranging from 0.5 to 2 mM) followed by UV-irradiation and subsequently treating the cells lysates with azido biotin under click chemistry conditions and applying the proteins isolated from this reaction mixture onto an avidin column. These experiments yielded a dose-dependent enrichment of biotinylated proteins as shown in the Western blot against biotin in Figure 4.8a, demonstrating unequivocally that compound **21** was an ideal probe for our application.

Next, we performed proteomics experiments on the choline metabolite and lipid-interacting proteins captured by employing the optimized metabolic labeling, photocrosslinking and biotinylation conditions obtained from the experiments described above. Specifically, we treated the cell lysate of UV-irradiated HEK293 cells cultured in the presence of **21** (2 mM) with azido biotin under click-chemistry conditions and applied the proteins extracted from this reaction

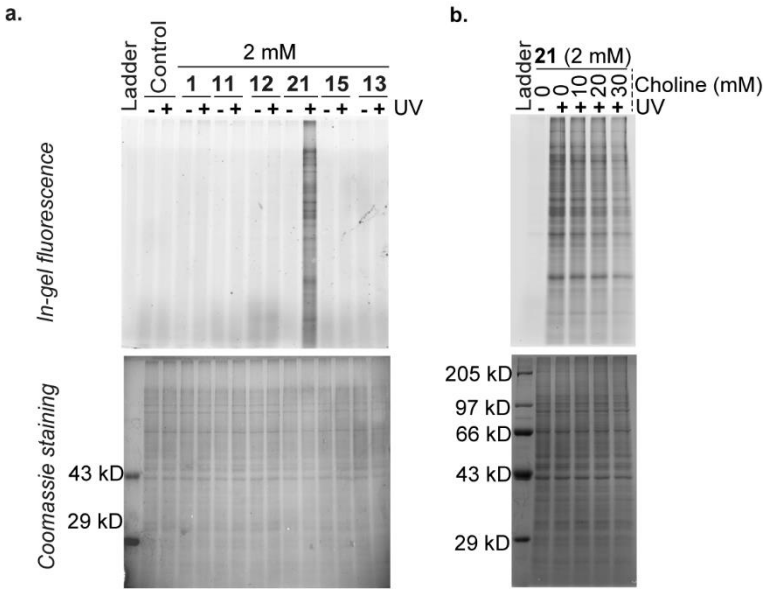

Figure 4.7. Comparing the crosslinking efficiency of **21** with other alkynyl/azido choline derivatives and in presence of choline in cells. Panels a) and b) represent data obtained from in-gel fluorescence experiments with the fluorimager-captured images depicted on the top and the same gels subsequently stained with Coomassie on the bottom. a) Comparison of photocrosslinking efficiency in cells metabolically labeled with the alkynyl choline diazirine probes **11**, **13**, **15** and **21**, and the azido choline diazirine probe, **12**. Propargyl choline (**1**) was used a negative control. d) Competition experiments with choline wherein cells were cultured in presence of both **21** and native choline at the indicated concentrations.

mixture onto an avidin column. We performed these "+UV" experiments on three culture plates and in parallel, we performed the "-UV" experiments on three different culture plates. We submitted the avidin resin containing the captured proteins obtained from these six independent sets of treatments to the Thermo Fisher Centre for Multiplexed Proteomics at the Harvard University for sixplex tandem mass tag (TMT) proteomics. For each sample, the intensities of all the peaks for peptides obtained from individual proteins were added to yield a quantitative estimate of the amount of that protein. The resulting values obtained for the three +UV samples were averaged and divided by the averaged value obtained from the three -UV samples, to yield the enrichment ratio for each protein (the raw data for each of the six samples is provided in Table A1 of the Appendix). This analysis yielded a total of 674 proteins with a minimum enrichment ratio

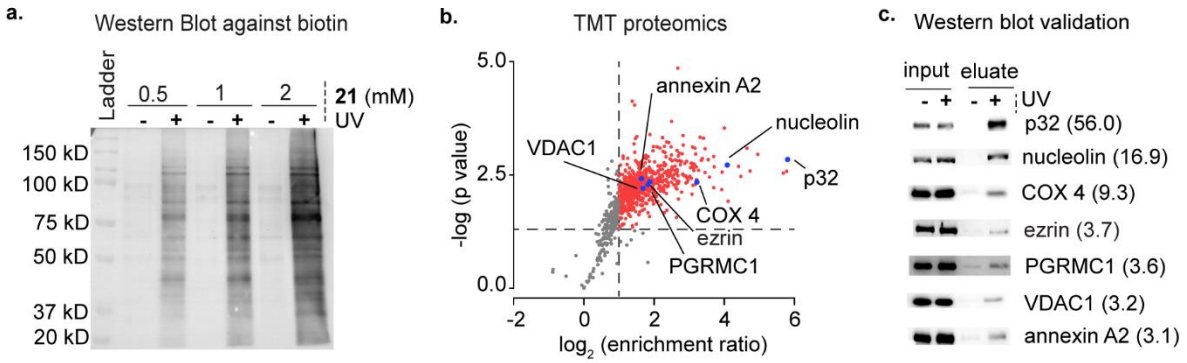

Figure 4.8. Identification of the choline metabolite and lipid-interacting proteome of HEK293 cells by using the γ-diazirine choline analog **21**. a) Western blot characterization of the biotinylation of UV-crosslinked proteins obtained from cells metabolically labeled with **21** enriched on avidin resin. b) A plot depicting the results of our sixplex TMT analysis (three +UV and three -UV samples) on avidin-captured proteins obtained from cells metabolically labeled with **21** after being subjected to biotinylation. The averaged enrichment ratio of the 902 proteins detected is plotted against their respective p-values and high-confidence 674 protein hits that yielded an enrichment ratio of ≥ 2.00 (dotted line parallel to the *y*-axis) and p-value of ≤ 0.05 (dotted line parallel to the *x*-axis) are depicted as either red or blue dots. Only these high-confidence protein hits were considered for the analyses depicted in Figures 4.9-4.11. c) Western blot validation of the enrichment of the seven proteins marked by blue dots in Figure 4.8b blotted by using primary antibodies against the individual proteins with their enrichment ratios depicted within parentheses.

of 2.0 and p value ≤ 0.05 that we annotated as "high-confidence hits" (depicted as red and blue dots in the plot shown in Figure 4.8b). Among these 674 proteins, 225 proteins were quantitated by only 1 unique peptide (Table A1 of the Appendix). Whereas in many proteomics studies only proteins that yield at least two peptide fragments are considered as high-confidence hits, we decided to include these 225 proteins in our list of high-confidence proteins considering that our proteomics experiments were performed in multiple replicates (on three +UV and three -UV samples).

To evaluate the veracity of this proteomics data, we performed Western blotting-based validation experiments on seven of these protein hits (p32, nucleolin, COX 4, ezrin, PGRMC1, VDAC1, and annexin A2) possessing a diverse range of TMT enrichment values (depicted as blue dots in Figure 4.8b). These experiments involved the UV-irradiation (or not) of HEK293 cells metabolically

labeled with **21** followed by treatment with azido biotin and enrichment on avidin resin. The proteins captured on the resin were eluted and probed for each of the seven proteins by Western blotting. The results of these experiments (Figure 4.8c) revealed UV-dependent enrichment of each of these proteins including COX 4 (Figure 4.8c, fourth row from the top) that had yielded only one unique peptide for TMT analysis (Table A1 of the Appendix). These experiments validated the results of proteomic studies and also supported our decision to include proteins quantitated with only one peptide as high-confidence hits.

4.2.3 Choline metabolites and lipids interact with a diverse range of cellular proteins

A survey of the choline metabolite and lipid-binding proteins identified by our chemoproteomic approach described above revealed that these proteins are expressed in a variety of cellular organelles and participate in diverse metabolic pathways (Table A2 of the Appendix). The classification of these proteins with respect to their expression in various organelles and cellular locations (Figure 4.9a) demonstrates that whereas a majority of these proteins (a total of 355 out of 674) are expressed in the cytoplasm, 324 of them are nuclear and 166 are mitochondrial proteins (this list includes proteins that are expressed in multiple locations, Table A2 of the Appendix). Since our approach resulted in the identification of proteins that interact with water soluble choline

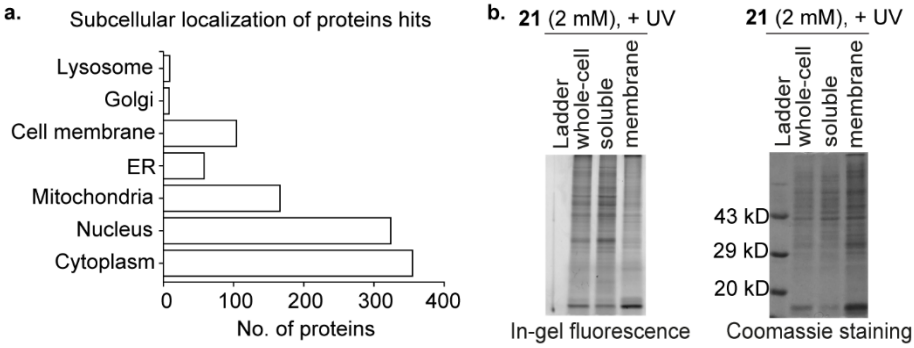

Figure 4.9. Subcellular distribution of our choline metabolite-interacting proteins. a) The subcellular distribution of our 674 high-confidence protein hits as per the UniProt database. "ER" is an abbreviation for the endoplasmic reticulum. The protein-wide list for this analysis is depicted in Table A2 of the Appendix. b) HEK293 cells administered with **21** (2 mM) were UV-irradiated and the cell lysates were fractionated into soluble and membrane proteins by ultracentrifugation. Each fraction was treated with Alexa Fluor 594 azide under standard click chemistry conditions and subjected to SDS-PAGE. The gel was visualized under a fluorescence imager (left) and subsequently stained with coomassie (right).

metabolites (choline, phosphocholine, CDP-choline and GPC) as well as those that bind to the membrane lipids PC and SM, not surprisingly, it consists of both soluble and membrane proteins. Analysis of our hits on the UniProt database revealed that the majority (73%) of these proteins are soluble proteins (Table A2 of the Appendix) and this conclusion was supported by our in-gel fluorescence experiments that yielded many more fluorescently labeled protein bands in the soluble protein fraction as compared to those in the membrane protein fraction (Figure 4.9b).

Although cellular proteins that interact with water-soluble choline metabolites have not been profiled previously, several proteins have been reported to bind to choline lipids, many of which are also present in our list of protein hits. These proteins include ADP/ATP translocase, the cytochrome c oxidase complex proteins COX 2, 4I1, 5A, 5B, 7A2, 7C, and subunits 1 and 2 of the cytochrome bc1 complex whose structures depict PC lipids bound to them.[1-3] Additionally, the chaperone, HSP-90 beta that has been previously reported to bind to PC lipids was also identified in our study.[4] Moreover, 60 of our protein hits were also identified by Yao and co-workers to bind to PC lipids in HeLa cells (Table A3 of the Appendix).[5] Comparison of our protein hits with the PC-interacting yeast mitochondrial proteins identified by de Kroon and co-workers[6] revealed that the mammalian homologs of 10 out of the 47 proteins reported in that study were present in our list of identified proteins (Table A4 of the Appendix). Our identified proteins also include those that are known lipid-binding proteins, but have been previously demonstrated to bind to lipids other than choline lipids. Such proteins include succinate dehydrogenase that binds to phosphatidylethanolamine and cardiolipin,[7] annexin A2 and ezrin that bind to phosphatidylinositol lipids,[8, 9] annexins A1, A5 and A6 that interact with phosphatidylethanolamine and phosphatidylserine lipids[10] and the cardiolipin-binding protein, stomatin-like protein.[11]

Subjecting our protein hits to the PANTHER classification system[12] resulted in their categorization into sixteen functional classes (Table A5 of the Appendix; the ten most abundant classes are depicted in Figure 4.10a). Interestingly, a large number of proteins (106) belong to the metabolite interconversion enzymes category suggesting that choline metabolites may serve as allosteric modulators of these enzymes and regulate the biosynthesis of other metabolites. Proteins belonging to the translational protein and the nucleic acid metabolism categories contribute 86 and 80 proteins respectively to our list (Figure 4.10a Table A5 of the Appendix), several of which are

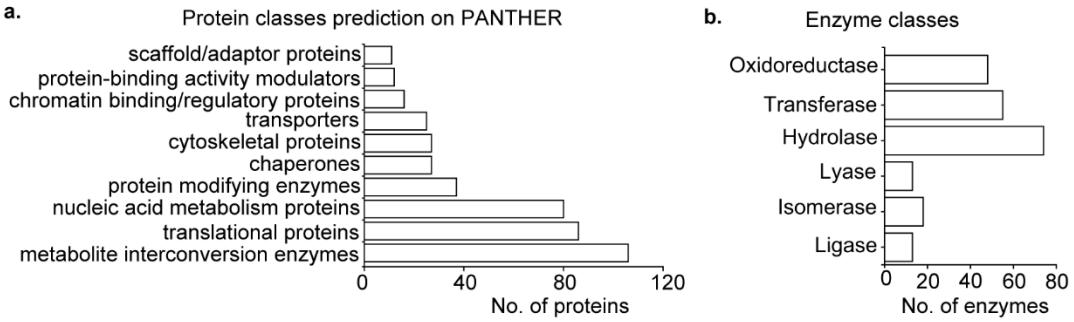

Figure 4.10. The functional classification of the high-confidence protein hits. a) The protein hits classified according to their biochemical functions as per the PANTHER database. b) The classification of the enzyme protein hits according to the UniProt database. The lists of all the proteins in the above analyses are provided in Tables A5 and A6 of the Appendix.

implicated in disease states including the proliferating cell nuclear antigen (PCNA) that is involved in hypothyroidism and is targeted by the drug, liothyronine.[13] Our list contains enzymes belonging to all of the six major enzyme subclasses (Figure 4.10b and Table A6 of the Appendix), and is enriched in enzymes involved in key cellular metabolic pathways. Indeed, our list includes seven of the ten glycolytic enzymes, seven of the eight Kreb's cycle enzymes, and proteins belonging to all five enzyme complexes of the oxidative phosphorylation (OXPHOS) pathway.

4.2.4 Choline metabolite-interacting proteins play important roles in diseases and are attractive drug targets

Analyzing the gene IDs of our protein list via the DAVID resource[14] revealed that a large majority of these proteins (67%) were associated with diseases, including 190 with infectious diseases, 109 with cancer, 128 with metabolic disorders, and 99 with neurological disorders (Figure 4.11a, Table A7 of the Appendix).

As discussed in section 1.3 of Chapter 1, cancer is of special interest with respect to choline metabolite-binding proteins as the levels of choline metabolites are considerably elevated in cancer cells and tumors. Therefore, we were intrigued by our finding that ~55% of the genes encoding for our protein hits are overexpressed in at least five different types of cancer according to the ONCOMINE database[15] (Table A8 of the Appendix). Moreover, several of our protein hits are

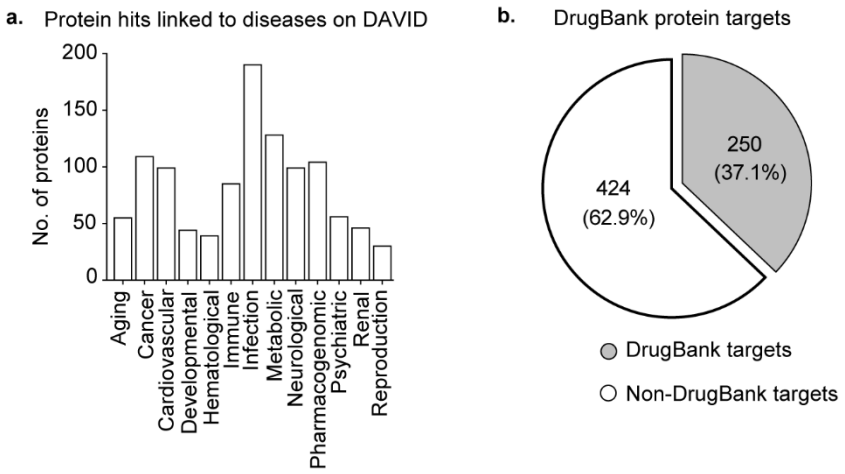

Figure 4.11. The classification of the high-confidence protein hits as per their roles in diseases. a) The protein hits genetically linked to various disease classes as per the DAVID bioinformatics database. b) Pie-chart depicting the assortment of the high-confidence protein hits with respect to their annotation as drug targets according to the DrugBank database. The identity of all the proteins in the above analyses are provided in Tables A7 and A9 of the Appendix.

known anticancer drug targets including PARP1, DNA topoisomerase 2-alpha, GART and isocitrate dehydrogenase 2 that are targeted by the drugs olaparib,[16] doxorubicin,[17] pemetrexed[18] and enasidenib,[19] respectively (Table A9 of the Appendix).

Analysis of our protein hits on the DrugBank database[20] revealed that in addition to cancer, the proteins identified in our study are targets for the therapy of several other diseases as well, with 37.1% (a total of 250 proteins) of them known to serve as drug targets (Figure 4.11b and Table A9 of the Appendix). This percentage is much higher than the percentage of proteins among the entire human proteome pool that are known drug targets (12%),[20, 21] suggesting that choline metabolite-binding proteins are attractive targets for drug development.

4.3 Conclusions

In this chapter, I have described the design of an optimal γ-diazirine choline analog, compound **21** that not only metabolically labeled choline lipids in cells, but also was resistant to chemical remodeling via sequential dealkylation and methylation within mammalian cells. This attribute of

21 was the key factor underlying its success as an effective chemoproteomic probe as it resulted in efficient photocrosslinking yields.

The results of our metabolic labeling experiments strongly suggest that the use of chemical probes for cellular applications should be accompanied by studies focused on determining their metabolic fates. Such investigations are critical for establishing the suitability of the probes for addressing the desired biological questions. For example, if photocrosslinkable probes intended for use in chemoproteomic workflows are transformed into metabolic derivatives that are structurally distinct from the original probes, the results of the ensuing proteomics studies will report on the proteins that interact with these unintended metabolic derivatives rather than with the original probe, rendering the study erroneous.

Interestingly, compound **21** that turned out to be an ideal probe for our chemoproteomic platform has been investigated previously for metabolically labeling choline lipids in mammalian cells.[5] Based on imaging experiments, this previous study concluded that **21** is incapable of labeling choline lipids in HeLa cells. Consistent with this observation, our imaging experiments on HEK293 cells administered with **21** failed to yield fluorescence signals above background (Figure 4.3a). Yet, our lipidomics experiments convincingly demonstrated that **21** metabolically labels choline lipids in HEK293, HeLa and MDA-MB-231 cells (Figure 4.5). These results established the superiority of sensitive lipidomics approaches over standard imaging techniques for characterizing metabolic labeling. Notably however, it was the anomalously high fluorescence intensity obtained from our imaging experiments on the β-diazirine choline compound **11** (Figure 3.4a) that engendered the key hypothesis that cells administered with **11** form **1**-labeled lipids. Consequently, imaging and lipidomics proved to be synergistic in enabling us to identify an optimal alkynyl diazirine choline probe.

Subsequently, we subjected the **21**-labeled HEK293 cells to our chemoproteomics workflow (as depicted in Figure 1.7b) and identified 674 high-confidence choline metabolite and lipid interacting proteins. Further analyses of the high confidence protein hits revealed that the choline metabolite-interacting proteins have diverse subcellular localizations and functions. Notably, several of these proteins were also found to be genetically linked to various diseases including cancer. Finally, we anticipate that these significant findings can open several avenues for

investigating the physiological importance of the choline metabolite-protein interactions by performing functional assays on the various protein hits.

4.4 Experimental Methods

4.4.1 Materials

Materials used for the experiments performed in this chapter were the same as documented in section 3.4.1. Additionally, azido biotin and avidin-agarose resin were purchased from Sigma Aldrich. Alexa 594 alkyne, TMT-sixplex isobaric reagent kit, and ECL Western blotting substrate were purchased from Thermo Fisher Scientific. The Immobilon PVDF membrane (0.45 µm pore size) was purchased from Merck. The manufacturer details for all antibodies used are documented in Table 4.2.

4.4.2 Instrumentation and software

Instrumentation and software used for the experiments performed in this chapter were the same as documented in section 3.4.2. Fluorescent gels were visualized on Typhoon Trio^{+} Variable scanner (GE), and the Western blots were detected for chemiluminescence on either ChemiDoc imaging system (Biorad) or LAS-3000 imager (Fujifilm). All lipidomics experiments were performed on a triple quadrupole mass spectrometer (QTRAP 4500 system from Sciex) equipped with an Exion UHPLC (Sciex). The data for TMT-based proteomics was acquired on an Orbitrap Fusion mass spectrometer (Thermo Fisher Scientific) equipped with a Thermo Easy-nLC 1200 at the Thermo Fisher Centre for Multiplexed Proteomics, Harvard Medical School.

4.4.3 Synthetic schemes and procedures

Scheme 4.1 Synthesis of γ-diazirine choline **20**

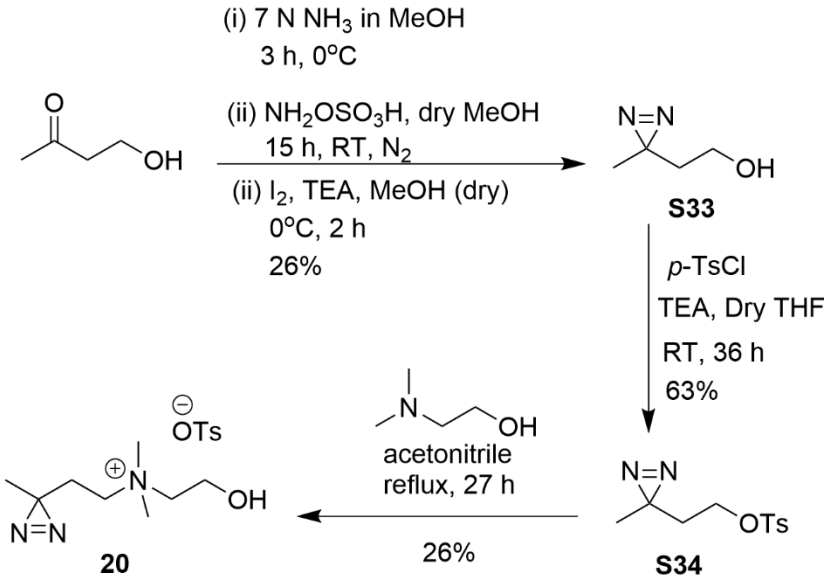

2-(3-methyl-3H-diazirin-3-yl)ethan-1-ol (S33)

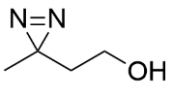

S33

A two-necked round-bottomed flask charged with 4-hydroxy-2-butanone (6.13 g, 69.57 mmol, 1 eq.) was kept under high vacuum for 30 min and then cooled to 0 °C. Subsequently, an ice-cold solution of 7 N NH_3 in methanol (495 mL, 3.47 mol, 50 eq.) was added and the mixture was stirred at 0 °C for 3 h. To this mixture, a solution of hydroxylamine-*O*-sulfonic acid (11.81 g, 104.50 mmol, 1.5 eq.) in anhydrous methanol (80 mL) that was bubbled with nitrogen gas for 30 min, was added dropwise by using a gas-tight syringe and the resultant reaction mixture was warmed to room temperature and stirred for another 15 h. Subsequently, excess ammonia was purged out by bubbling nitrogen gas for 2 h, and the heterogeneous mixture of a white precipitate and a pale-yellow liquid thus obtained was filtered on celite and washed with diethyl ether (100 mL). The filtrate was evaporated to dryness, kept under high vacuum for 30 min and purged with nitrogen gas. To this flask, dry methanol (60 mL) and dry triethylamine (14.56 mL, 104.3 mmol, 1.5 eq.) were added and the mixture was cooled to 0 °C. Subsequently, iodine (19.44 g, 76.62 mmol, 1.1 eq.) was added in small portions and the reaction mixture was stirred for 2 h at 0 °C followed by the addition of ethyl acetate (100 mL) and the mixture was washed with 1 N HCl (1 × 100 mL),

and saturated sodium thiosulfate solution (1 × 100 mL). The organic layer was dried over anhydrous sodium sulfate, concentrated under reduced pressure and the residue was subjected to purification by silica gel column chromatography (30% ethyl acetate in hexane) to give **S33** as a yellow oil (1.83 g, 26%).

^{1}H NMR (400 MHz, $CDCl_3$) δ 3.53 (t, *J* = 6.4 Hz, 2H), 1.63 (t, *J* = 6.4 Hz, 2H), 1.06 (s, 3H).

^{13}C NMR (100 MHz, $CDCl_3$) δ 57.6, 37.0, 24.3, 20.2.

HRMS (ESI): $C_4H_8N_2O$; Calculated mass, $[M+H]^+$ 101.0709; Observed mass, $[M+H]^+$ 101.0711.

2-(3-methyl-3H-diazirin-3-yl)ethyl 4-methylbenzenesulfonate (S34)

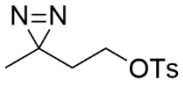

S34

A round-bottomed flask containing a mixture of **S33** (1.6 g, 15.98 mmol, 1 eq.) and *p*-toluenesulfonyl chloride (9.14 g, 47.94 mmol, 3 eq.) was flushed with nitrogen gas and cooled to 0 °C. Subsequently, anhydrous THF (30 mL) was added and the mixture was stirred for 15 min. Dry triethylamine (6.68 mL, 47.94 mmol, 3 eq.) was then added and the reaction n mixture was allowed to stir at 0 °C for another 10 min and then at room temperature for 36 h. Subsequently, THF was removed under reduced pressure and ethyl acetate (50 mL) was added to the concentrated residue. This solution was washed with 1 N HCl (1 × 50 mL), saturated solution of sodium bicarbonate (1 × 50 mL), and concentrated under reduced pressure after being dried by adding anhydrous sodium sulfate. The product was isolated from the concentrated residue using silica gel column chromatography (10% ethyl acetate in hexane) to give **S34** (2.58 g, 63%) as a pale-yellow oil.

^{1}H NMR (400 MHz, $CDCl_3$) δ 7.83 (d, *J* = 8.4 Hz, 2H), 7.37 (d, *J* = 8.4 Hz, 2H), 3.95 (t, *J* = 6.4 Hz, 2H), 2.46 (s, 3H), 1.67 (t, *J* = 6.4 Hz, 2H), 1.00 (s, 3H).

^{13}C NMR (100 MHz, $CDCl_3$) δ 145.5, 133.3, 130.4, 128.4, 65.5, 34.7, 23.8, 22.1, 20.3.

HRMS (ESI): $C_{11}H_{14}N_2O_3S$; Calculated mass, $[M+H]^+$ 255.0798; Observed mass, $[M+H]^+$ 255.0801.

γ-diazirine choline (20)

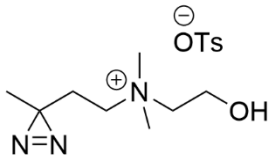

20

An ice-cold solution of **S34** (80 mg, 0.31 mmol, 1 eq.) in acetonitrile (1 mL) was added to an ice-cold solution of *N*,*N*-dimethylaminoethanol (23.4 mg, 0.26 mmol, 3 eq.) dissolved in acetonitrile (1 mL) and after 10 min of stirring, the reaction mixture was refluxed for 27 h followed by removal of the solvent under reduced pressure. The remaining crude residue was triturated with ice-cold diethyl ether (5 × 2 mL) to yield 98 mg of **20** (26%) as dirty-white solid.

^{1}H NMR (500 MHz, CD_3OD) δ 7.72 (d, *J* = 8.2 Hz, 2H), 7.25 (d, *J* = 7.9 Hz, 2H), 3.96 – 3.94 (m, 2H), 3.49 – 3.46 (m, 2H), 3.43 – 3.41 (m, 2H), 3.12 (s, 6H), 2.37 (s, 3H), 1.87 – 1.83 (m, 2H), 1.08 (s, 3H).

^{13}C NMR (175 MHz, CD_3OD) δ 143.6, 141.7, 129.8, 127.0, 66.5, 61.4, 56.8, 52.3, 29.3, 24.4, 21.3, 19.3.

HRMS (ESI): $C_8H_{18}N_3O^+$; Calculated mass, $[M]^+$ 172.1444; Observed mass, $[M]^+$ 172.1444.

Scheme 4.2 Synthesis of propargyl γ-diazirine choline **21**

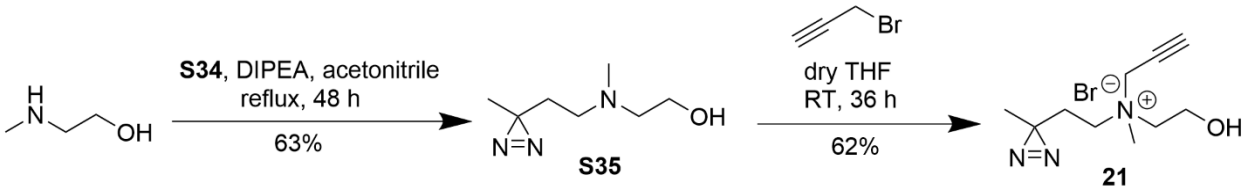

2-(methyl(2-(3-methyl-3H-diazirin-3-yl)ethyl)amino)ethan-1-ol (S35)

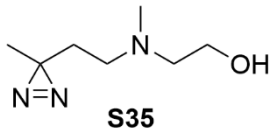

S35

To an ice-cold mixture of *N*-methylaminoethanol (0.44 g, 5.87 mmol, 1.5 eq.) and *N*,*N*-diisopropylethylamine (0.56 g, 4.31 mmol, 1.1 eq.) in acetonitrile (5 mL), a solution of **S34** in acetonitrile (2 mL) was added dropwise. The resultant mixture was stirred under ice-cold conditions for 30 min and then refluxed for 48 h. After this, the solvent was removed under reduced

pressure and the residue was dissolved in dichloromethane (50 mL) and washed with saturated solution of sodium bicarbonate (1 ×50 mL). The resultant aqueous layer was further washed with dichloromethane (3 × 50 mL). The organic layers were pooled, dried by adding anhydrous sodium sulfate, and concentrated under reduced pressure. The concentrated residue was subjected to silica gel column chromatography (1% triethylamine in ethyl acetate) to afford **S35** as a pale-yellow liquid (0.39 g, 63%).

^{1}H NMR (500 MHz, $CDCl_3$) δ 3.56 (t, *J* = 4.0 Hz, 2H), 2.46 (t, *J* = 4.0 Hz, 2H), 2.27 (t, *J* = 6.0 Hz, 2H), 2.18 (s, 3H), 1.55 (t, *J* = 6.0 Hz, 2H), 1.02 (s, 3H).

^{13}C NMR (100 MHz, $CDCl_3$) δ 58.8, 58.5, 52.3, 41.2, 31.9, 25.0, 20.3.

HRMS (ESI): $C_4H_{15}N_3O^+$; Calculated mass, $[M+H]^+$ 158.1288; Observed mass, $[M+H]^+$ 158.1297.

Propargyl γ-diazirine choline (21)

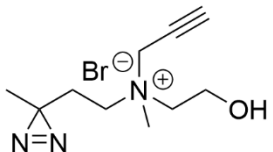

21

To an ice-cold solution of **S35** (368.3 mg, 2.34 mmol, 1.0 eq.) in dry THF (20 mL), a solution of 80% *w*/*w* propargyl bromide in toluene (1.31 mL, 11.71 mmol, 5.0 eq.) was added dropwise. The mixture was stirred at 0 °C for 30 min and then at room temperature for 36 h. The yellow precipitate thus obtained was isolated by decantation followed by trituration with THF (5 × 10 mL), diethyl ether (5 × 25 mL), and ethyl acetate (7 × 25 mL) and dried under vacuum to give **21** as a dirty-white solid (0.65 g, 62%).

^{1}H NMR (400 MHz, DMSO-d6) δ 5.37 (t, *J* = 4.8 Hz, 1H), 4.42 (d, *J* = 2.4 Hz, 2H), 4.10 (t, *J* = 2.4 Hz, 1H), 3.83 – 3.82 (m, 2H), 3.52 – 3.48 (m, 2H), 3.44 – 3.42 (m, 2H), 3.08 (s, 3H), 1.83 – 1.79 (m, 2H), 1.06 (s, 3H).

^{13}C NMR (100 MHz, DMSO-d6) δ 83.3, 72.1, 62.8, 56.8, 54.7, 52.3, 48.6, 27.5, 24.0, 19.0.

HRMS (ESI):$C_{10}H_{18}N_3O^+$, Calculated mass, $[M]^+$ 196.1444; Observed mass, $[M]^+$ 196.1454.

4.4.4 General procedure for cell culture

Mammalian cells (HEK293/HeLa/MDA-MB-231) were cultured exactly as mentioned in section 3.4.4.

4.4.5 Procedure for the characterization of metabolic labeling of 21 by cellular imaging

The procedure for imaging metabolically labeled choline lipids that were administered with either compound **21** (2 mM) alone or co-administered with compound **21** and choline chloride (2 mM each) is the same as documented in section 2.4.5.

4.4.6 Procedure for the characterization of metabolic labeling by lipidomics

The procedures for the extraction of lipids from mammalian cells, HPLC method details, the mass-spectrometry details, and the LipidView analyses details are the same as mentioned in section 2.4.6. For detecting diazirine containing choline lipids, the PIS mass used was 28 Da less than that of the fragment mass of their phosphoryl derivatives to account for the N_2 loss that diazirines characteristically undergo during fragmentation. Compound parameters were separately optimized for detecting the γ-diazirine **21**-labeled choline lipids by using a PIS of 248.1 Da and the same parameters were used to detect **20**-labeled choline lipids.

Table 4.1. Compound parameters used for the PIS of lipids labeled with the γ-choline analogs **20** and **21**

S. No.	Head group	PIS mode mass (Da)	Declustering Potential (volts)	Entrance Potential (volts)	Collision Energy (volts)	Collision cell Exit Potential (volts)
1.	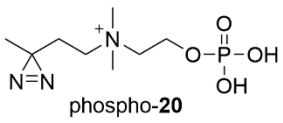 phospho-**20**	224.1 (loss of N_2)	100.0	2.9	43.0	15.0
2	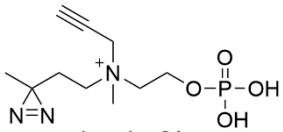 phospho-**21**	248.1 (loss of N_2)				

4.4.7 In-gel fluorescence experiments

(i) Gel-based analysis of crosslinked proteins in HEK293 cells: Six 10 cm culture dishes each containing HEK293 cells (10 mL of a 0.2 million cells per mL culture in complete media) were placed in a CO_2 incubator for 12 h. Subsequently, 317 µL of a 65 mM solution of either **1**, **11**, **12**, **13**, **15**, or **21** in PBS was administered into each flask (final concentration of each of these choline analogs in the flask was 2 mM) and the cultures were allowed to grow in the CO_2 incubator for another 24 h. Cells not treated with any choline analog served as control. After the incubation, cells were washed with ice-cold DMEM containing 10% FBS (1 × 5 mL) and then with ice-cold PBS (2 × 5 mL). Subsequently, cells were overlaid with ice-cold PBS (10 mL) and exposed to 356 nm UV as described in in section 3.4.1 for 30 min on ice. After the UV exposure, cells were scraped into ice-cold PBS (5 mL) and pelleted by centrifugation (1,000 *g*, 5 min, 4 °C). The resultant cell pellet was resuspended by gentle pipetting in PBS containing EDTA-free protease inhibitor cocktail (467 µL) and incubated on ice for 30 min. Cells were lysed by probe sonication on ice (8 pulses of 5 sec each with a gap of 5 sec between each pulse, 30% amplitude on a Branson 450 Digital Sonifier), and to the cell lysate (50 µL containing 1 mg/mL protein concentration estimated by employing the Bradford assay), click chemistry reagents were added. Specifically, to this 50 µL cell lysate, 1 µL of a solution of 50 mM $CuSO_4.5H_2O$ in water (final concentration, 0.9 mM), 1 µL of a solution of 50 mM TCEP in PBS (final concentration, 0.9 mM), 3 µL of a solution of 1.7 mM TBTA in 1:4 *t*-butanol:DMSO (final concentration, 0.09 mM), and 1 µL of a 1.25 mM solution of Alexa Fluor 594 azide in DMSO (final concentration, 22 µM) were added and the mixture was incubated for 1 h at room temperature under dark after mixing by pipetting. For the azido analog **12**, Alexa Fluor 594 azide was replaced with 1 µL of a 1.25 mM solution of Alexa Fluor 594 alkyne in DMSO (final concentration, 22 µM). The click reactions were quenched by heating the samples with 2X SDS loading dye (56 µL) for 5 min at 98 °C and the samples were then subjected to SDS-PAGE analysis (10% gel) followed by fluorescence imaging of the gel by GE Typhoon Trio$^+$ system with 532 nm excitation, and 610 nm (BP30) emission filter. Finally, the gel was stained with coomassie blue and the gel images thus obtained are depicted in Figure 4.7a.

*(ii) UV-irradiation time optimization for crosslinking of **21**-labeled metabolites in HEK293 cells:* Five 10 cm culture dishes each containing HEK293 cells (10 mL of a 0.2 million cells per mL culture in complete media) were placed in a CO_2 incubator for 12 h. Subsequently, 317 µL of a 65

mM solution of **21** in PBS was administered into each flask (final concentration of **21** in each flask was 2 mM) and the cultures were allowed to grow in the CO_2 incubator for another 24 h. After the incubation, cells in each plate were washed with ice-cold DMEM containing 10% FBS (1 × 5 mL) and then with ice-cold PBS (2 × 5 mL). Subsequently, cells were overlaid with ice-cold PBS (10 mL) and each plate was exposed to 356 nm UV as described in section 3.4.1 above for either 0, 15, 30, 45, or 60 min on ice. After the UV light exposure, cells from each plate were lysed and subjected to the in-gel fluorescence protocol described in section 4.4.7(i) above. The in-gel fluorescence and the coomassie stained gel images thus obtained are depicted in Figure 4.6b.

*(iii) Dose dependent crosslinking of **21** in HEK293 cells:* Ten 10 cm culture dishes each containing HEK293 cells (10 mL of a 0.2 million cells per mL culture in complete media) were placed in a CO_2 incubator for 12 h. Subsequently, 15.4 µL, 77 µL, 154 µL, and 317 µL of a 65 mM solution of **21** in PBS was administered into two plates each (final concentration of **21** were 0.1 mM, 0.5 mM, 1 mM, and 2 mM respectively) and the cultures were allowed to grow in the CO_2 incubator for another 24 h. Two flasks containing cells not administered with **21** served as control. After the incubation, the cells were subjected to the in-gel fluorescence protocol described in section 4.4.7(i) above. The in-gel fluorescence and the coomassie stained gel images thus obtained are depicted in Figure 4.6a.

*(iv) Gel-based analysis of crosslinked proteins in HEK293 cells co-treated with **21** and choline:* Four 10 cm culture dishes each containing HEK293 cells (10 mL of a 0.2 million cells per mL culture in complete media) were placed in a CO_2 incubator for 12 h. Subsequently, 317 µL of a 65 mM solution of **21** in PBS was administered into each flask (final concentration of **21** in each flask was 2 mM). Three of these dishes were also simultaneously administered 50 µL of either a 2 M, 4 M or a 6 M solution of choline chloride in PBS (final concentrations of choline in these flasks were 10, 20 and 30 mM respectively). The same volume of PBS was added in the control cell culture dish. After 24 h incubation in a CO_2 incubator, the cells were subjected to the in-gel fluorescence protocol described in section 4.4.7(i) above. The in-gel fluorescence and the coomassie stained gel images thus obtained are depicted in Figure 4.7b.

(v) Membrane protein fractionation of crosslinked proteins in HEK293 cells: Six 10 cm culture dishes each containing HEK293 cells (10 mL of a 0.4 million cells per mL culture in complete

media) were placed in a CO_2 incubator for 12 h. Subsequently, 317 µL of a 65 mM solution of **21** in PBS was added to each flask (final concentration of **21** in each flask was 2 mM) and the cultures were incubated in the CO_2 incubator for another 24 h. After the incubation, the cells were washed with ice-cold DMEM containing 10% FBS (5 mL) and then with ice-cold PBS (2 × 5 mL), and then overlaid with ice-cold PBS (10 mL) before irradiating them with 356 nm UV radiation as described in section 3.4.1 for 30 min on ice. Subsequently, the cells were scraped into ice-cold PBS (5 mL) and pelleted by centrifugation (1,000 *g*, 15 min, 4 °C). The supernatant was decanted and the cell pellet was resuspended in an ice-cold solution of PBS containing EDTA-free protease inhibitor cocktail (3 mL) by gentle pipetting and the cells were lysed using probe sonication as per the protocols described in section 4.4.7(i) above. This cell lysate was centrifuged (180 *g*, 3 min, 4 °C) to remove any unlysed cells and the resultant supernatant was ultracentrifuged (100,000 *g*, 45 min, 4 °C) to separate the soluble proteins from the membrane proteins. The supernatant thus obtained contained the soluble cellular proteins. The membrane fraction pellet was washed with ice-cold PBS (5 × 5 mL), treated with a solution of 1% *w/v* SDS in EDTA-free protease inhibitor cocktail containing PBS (1 mL) and probe sonicated (12 pulses of 5 sec each with a gap of 10 sec between each pulse, 30% amplitude on a Branson 450 Digital Sonifier) to give a clear solution. Proteins in both soluble and membrane fractions were diluted to 1 mg/mL in PBS by employing the Bradford assay followed by subjecting them to click chemistry and in-gel fluorescence SDS-PAGE protocols described in section 4.4.7(i) above. The in-gel fluorescence and the coomassie-stained gel images thus obtained are depicted in Figure 4.9b.

4.4.8 Biotinylation and affinity purification of crosslinked proteins

Three 10 cm culture dishes each containing HEK293 cells (10 mL of a 0.3 million cells per mL culture in complete media) were placed in a CO_2 incubator for 12 h. Subsequently, each dish was administered 317 µL of either a 16.3 mM, 32.5 mM or 65 mM solution of **21** in PBS (final concentrations of **21** were 0.5 mM, 1 mM and 2 mM respectively) and placed in a CO_2 incubator for another 24 h. The cells were then washed with ice-cold DMEM media containing 10% FBS (5 mL) and then with ice-cold PBS (2 × 5 mL), overlaid with ice-cold PBS (10 mL) and exposed to 356 nm UV as described in section 3.4.1 above for 30 min on ice. Cells subjected to the same treatment as described above but not exposed to UV light served as the -UV control. After the +UV or -UV treatments, cells were scraped into ice-cold PBS (5 mL) and pelleted by

centrifugation (1,000 *g*, 5 min, 4 °C). The resultant cell pellets were resuspended by gentle pipetting in PBS containing EDTA-free protease inhibitor cocktail (467 µL) and incubated on ice for 30 min. The cells were lysed by probe sonication on ice (8 pulses of 5 sec each with a gap of 5 sec between each pulse, 30% amplitude on a Branson 450 Digital Sonifier), and the protein concentration in the cell lysate was estimated by employing the Bradford assay. The cell lysate was then subjected to click chemistry reagents as reported previously.[22, 23] Specifically, to a volume of the cell lysate containing 1 mg of protein, was added 20 µL of a solution of 25 mM azido biotin in DMSO (final concentration, 0.5 mM), 20 µL of a solution of 50 mM TCEP in PBS (final concentration, 1 mM), 59 µL of a solution of 1.7 mM TBTA in 1:4 *t*-butanol:DMSO (final concentration, 0.1 mM), and 20 µL of a solution of 50 mM $CuSO_4.5H_2O$ in water (final concentration, 1 mM). The total volume of this reaction mixture was made up to 1 mL by adding PBS. The mixture was then incubated at room temperature for 90 min. Subsequently, the protein was extracted from this reaction mixture by performing methanol-chloroform extraction. Briefly, ice-cold methanol (480 µL) and ice-cold chloroform (160 µL) were added to the reaction mixture and the resultant heterogeneous mixture was vortexed for 1 min. Water (400 µL at room temperature) was then added to this mixture followed by vortexing for 1 min and the mixture was centrifuged (14,000 *g*, 5 min, room temperature) to achieve phase separation between an aqueous layer on the top and an organic layer at the bottom with a cloudy layer of protein at the interface of the two layers. The aqueous layer at the top was removed by aspiration and to the remaining cloudy layer of protein and the lower organic layer, ice-cold methanol (300 µL) was added followed by vortexing for 1 min. Subsequently, the proteins were pelleted by centrifugation (14,000 *g*, 5 min at room temperature) and the supernatant was aspirated off. To the resulting pellet was added ice-cold methanol (480 µL) and ice-cold chloroform (160 µL) and the mixture was subjected to methanol-chloroform extraction exactly as mentioned above and the pellet thus obtained was resuspended in 1% *w/v* SDS in PBS (800 µL) by vortexing for 2 min, probe sonicated at room temperature (6 pulses of 5 sec each with a gap of 5 sec between each pulse, 60% amplitude on a Branson 450 Digital Sonifier) and incubated at 37 °C for 15 min (with shaking at 1,400 rpm on an Eppendorf Thermomixer). The resulting solution was centrifuged (2,000 *g*, 5 min at room temperature) to separate any insoluble material and the supernatant was transferred to a centrifuge tube and diluted with PBS to a final volume of 4 mL so that the final SDS concentration was

reduced to 0.2% *w/v*. This solution was set aside and avidin-agarose resin (200 µL of a 50% *v/v* suspension in glycerol) was washed with PBS at room temperature. Specifically, the resin was resuspended in PBS (500 µL) by gentle pipetting and the resulting suspension was centrifuged (400 *g*, 5 min at room temperature) and the supernatant was aspirated off. The pellet containing avidin-agarose resin was washed again by resuspension in PBS (500 µL) by gentle pipetting and centrifugation (400 *g*, 5 min at room temperature) followed by removal of the supernatant. The pellet thus obtained contained washed avidin-agarose resin that was further resuspended in 100 µL PBS and this suspension was transferred to the aforementioned 4 mL solution of methanol-chloroform extracted proteins dissolved in 0.2% *w/v* SDS in PBS. This mixture was incubated for 2 h at room temperature with constant rotation (10 rpm) on a 360° vertical rotating mixer (Biobase). Subsequently, the resin was spun down from the suspension (400 *g*, 5 min at room temperature) and the supernatant was removed. The resin was then washed with 0.2% *w/v* SDS solution in PBS (10 × 1 mL) and then with PBS (3 × 1 mL) as per the procedure described above that was used to wash the avidin-agarose resin with PBS. To elute the proteins bound to the resin, it was treated with 2X SDS loading dye (100 µL) and incubated at room temperature for 15 min, then heated at 98 °C for 5 min. This mixture was briefly centrifuged (5,000 *g*, 1 min at room temperature) and the supernatant was collected as the desired eluate. This eluate was separated by SDS-PAGE (10% gel) followed by electrophoretically transferring the proteins to a PVDF membrane. The membrane was then treated with 5% *w/v* BSA solution in PBS for 1 h at room temperature, incubated with anti-biotin antibody (details in Table 4.2) for 3 h at room temperature. Subsequently, the membrane was washed three times with PBST and incubated with shaking in PBST for 10 min after each wash and then it was incubated in anti-mouse IgG conjugated to HRP (details in Table 4.2) for 2 h at room temperature. Finally, the membrane was washed with PBST three times with intermittent 10 min incubations in PBST with shaking. To visualize the proteins present in the eluate, the blot was developed using the ECL kit as per the instructions in manufacturer's protocol and imaged for chemiluminescence using ChemiDoc imaging system (Biorad). The blot thus obtained is depicted in Figure 4.8a.

4.4.9 Sample preparation for quantitative proteomics (TMT) and target validation by Western blotting

For protein identification, the same procedure for the isolation of crosslinked proteins as described in section 4.4.8 above was followed except that instead of three 10 cm culture dishes, six culture dishes were administered with a final concentration of 2 mM of **21** (three +UV and three -UV experiments), and the avidin column-bound proteins were not eluted. Instead, the protein-bound avidin-agarose resin thus obtained was subjected to the sixplex tandem mass tag (TMT) analysis on the three +UV and the three -UV samples (experimental details below in section 4.4.10) that yielded a list of 902 proteins that were identified in all the six samples (data in Table A1 of the Appendix). For each sample, the raw intensities of all the peaks for peptides obtained from individual proteins were added to yield a quantitative estimate of the amount of that protein. The resulting values obtained for the three +UV samples were averaged and divided by the averaged value obtained from the three -UV samples, to yield the enrichment ratio for each protein (the raw data for each of the six samples is provided in Table A1 of the Appendix). Unpaired two-tailed *t*-test was done on the raw intensity values obtained for each protein from the set of three +UV and the set of three -UV samples. The 674 proteins that gave the enrichment ratio (+UV/-UV) of ≥ 2 and p-value ≤ 0.05 were deemed "high-confidence" protein hits (entries marked in red in Table A1 of the Appendix). The volcano plot for -log(p-value) *vs* $\log_2$ (enrichment ratio) for all the 902 proteins is depicted in Figure 4.8b. Seven proteins from the list of high confidence protein hits (p32, nucleolin, COX 4, ezrin, PGRMC1, VDAC1, and annexin A2) were selected for the validation by Western blot. For validation of the aforementioned proteins, the same procedure for the avidin-enrichment of the crosslinked proteins as described above in section 4.4.8 was followed except that the experiments were performed on one 10 cm culture dish administered with a final concentration of 2 mM of **21**. Instead of blotting against anti-biotin as was done in the procedure described in section 4.4.8, the BSA blocked membrane was incubated with either of the following primary antibodies: anti-p32, anti-nucleolin, anti-COX 4, anti-ezrin, anti-PGRMC1, anti-VDAC1, or anti-annexin A2 followed by incubation with the secondary antibody conjugated to HRP. The details of the primary antibodies and the secondary antibodies conjugated to HRP are described in Table 4.2 below. The blot was developed using the ECL kit as per the instructions in

manufacturer's protocol and imaged for chemiluminescence using LAS-3000 imager (Fujifilm). The blot thus obtained is depicted in Figure 4.8c.

Table 4.2. Details of antibodies used for Western blot experiments

S. No.	Antibody	Manufacturer	Dilution used	Data Figure
1.	Anti-p32	Abcam	1:1000	Figure 4.8c
2.	Anti-nucleolin	Abcam	1:1000	Figure 4.8c
3.	Anti-COX 4	Cell Signaling Technology	1:1000	Figure 4.8c
4.	Anti-ezrin	Abcam	1:1000	Figure 4.8c
5.	Anti-PGRMC1	Cell Signaling Technology	1:1000	Figure 4.8c
6.	Anti-VDAC1	Abcam	1:1000	Figure 4.8c
7.	Anti-annexin A2	Abcam	1:1000	Figure 4.8c
8.	Anti-biotin	Santa Cruz	1:4000	Figure 4.8a
9.	Goat-anti rabbit IgG conjugated to HRP	Abcam	1:10000	Figure 4.8c
10.	Goat anti-mouse IgG conjugated to HRP	Abcam	1:10000	Figures 4.8a and 4.8c

4.4.10 Quantitative proteomics (TMT) experiments

(i) *On-bead digestion:* The avidin-agarose resin containing the enriched proteins (obtained as described in section 4.4.9 above) was washed three times with 50 mM Tris-HCl buffer at pH 8.0 followed by resuspension in a solution of 1 M urea in 50 mM Tris-HCl at pH 8.0. The initial protein digestion was performed with trypsin (5 ng/µL) at 37 °C for 1 h. After the initial trypsin digestion, samples were centrifuged briefly and the supernatant was collected. The beads were further washed three times with a solution of 1 M urea in 50 mM Tris-HCl at pH 8.0. All the bead washes were pooled in the same tube and digested overnight at room temperature by incubating in

trypsin (5 ng/µL). Digested peptides were reduced with 5 mM DTT followed by alkylation with 15 mM iodoacetamide, quenching alkylation with 10 mM DTT and finally quenching the digestion process with TFA. Acidified digested peptides were desalted over C_{18}STAGE tips. Desalted peptides were reconstituted with 200 mM EPPS buffer at pH 8.0 and labeled with sixplex tandem mass tag (TMT) reagents. The sixplex labeling reactions were performed for 2 h at room temperature. Modification of tyrosine residue with TMT was reversed by the addition of 0.5% hydroxylamine for 15 min and the reaction was quenched with 0.5% TFA. Samples were combined at a 1:1:1:1:1:1 ratio and the resultant sample was further desalted using a STAGE tip and reconstituted with 5% acetonitrile + 5% formic acid for mass spectrometric analysis.

(ii) Liquid chromatography-MS3 spectrometry (LC-MS3): The labeled peptide sample obtained from the section 4.4.10(i) was analyzed with an LC-MS3 data collection strategy on an Orbitrap Fusion mass spectrometer equipped with a Thermo Easy-nLC 1200 for online sample handling and peptide separations.[24] The resuspended peptide from the previous step was loaded onto a 100 µm inner diameter fused-silica micro capillary with a needle tip pulled to an internal diameter less than 5 µm. The column was packed in-house to a length of 35 cm with a C_{18} reverse phase resin (GP118 resin 1.8 µm, 120 Å, Sepax Technologies). The peptides were separated using a 180 min linear gradient from 3% to 25% buffer B (100% acetonitrile + 0.125% formic acid) equilibrated with buffer A (3% acetonitrile + 0.125% formic acid) at a flow rate of 600 nL/min across the column. The scan sequence for the Fusion Orbitrap began with an MS1 spectrum (Orbitrap analysis, resolution 120,000, 400−1400 *m/z* scan range, AGC target 2×10^5, maximum injection time 100 ms, dynamic exclusion of 90 seconds). The "Top10" precursors were selected for MS2 analysis, which consisted of CID (quadrupole isolation set at 0.5 Da and ion trap analysis, AGC 8×10^3, collision Energy 35%, maximum injection time 150 ms). The top ten precursors from each MS2 scan were selected for MS3 analysis (synchronous precursor selection), in which precursors were fragmented by HCD prior to Orbitrap analysis (collision Energy 55%, max AGC 1×10^5, maximum injection time 150 msec, isolation window 2.5 Da, resolution 60,000).

(iii) LC-MS3 data analysis: A suite of in-house software tools were used to for .RAW file processing and controlling peptide and protein level false discovery rates, assembling proteins from peptides, and protein quantification from peptides as previously described. MS/MS spectra were searched against a UniProt Human database with both the forward and reverse sequences.

Database search criteria are as follows: tryptic with two missed cleavages, a precursor mass tolerance of 50 ppm, fragment ion mass tolerance of 1.0 Da, static alkylation of cysteine (57.02146 Da), static TMT labeling of lysine residues and *N*-termini of peptides (229.162932 Da), and variable oxidation of methionine (15.99491 Da). TMT reporter ion intensities were measured using a 0.003 Da window around the theoretical *m*/*z* for each reporter ion in the MS3 scan. Peptide spectral matches with poor quality MS3 spectra were excluded from quantitation (<100 summed signal-to-noise across 10 channels and <0.5 precursor isolation specificity).

4.4.11 Analysis of the high-confidence proteins obtained from proteomics studies

To identify the subcellular localization of all the 674 high-confidence protein hits, their corresponding UniProt IDs were submitted to the retrieve/ID mapping feature of the UniProt database. The proteins were characterized into seven categories: lysosome, golgi, ER, cell membrane, mitochondria, nucleus, and cytoplasm and the total number of proteins in each location were counted manually. The list thus obtained is provided in the Table A2 of the Appendix and a graph summarizing this data is depicted in the Figure 4.9a. The total number of proteins among the seven categories was higher than 674 because of multiple annotations for several proteins. The same UniProt database was used to characterize these 674 high-confidence proteins as membrane or soluble. Proteins that possessed known or predicted transmembrane domains were labeled as membrane proteins and the remaining ones were considered soluble. The resulting data is depicted in Table A2 of the Appendix. Using the same retrieve/ID mapping feature, the 674 UniProt IDs were also sorted for subclasses of enzymes namely, oxidoreductases, transferases, hydrolases, lyases, isomerases, and ligases. The number of proteins belonging to each enzyme subclass were counted manually and a plot summarizing this data is depicted in Figure 4.10b of the main text and the protein-wise list thus obtained is provided in Table A6 of the Appendix. The retrieve/ID mapping tool on UniProt database was also used to categorize proteins as DrugBank targets (data depicted in Figure 4.11b and Table A9 of the Appendix).

In addition to this analysis, the UniProt IDs of the 674 protein hits were also submitted to the PANTHER classification system resulting in the classification of 449 of these proteins into sixteen functional classes—translational proteins, cytoskeletal proteins, receptors, nucleic acid metabolism proteins, transfer/carrier proteins, chaperones, adaptors, transporters, metabolite

interconversion enzymes, protein modifying enzymes, membrane traffic proteins, protein-binding activity modulators, calcium-binding proteins, intercellular signal molecules, gene-specific transcriptional regulators, and chromatin binding/regulatory proteins. The list thus obtained is depicted in Table A5 of the Appendix and a plot summarizing the data on the ten most abundant protein classes is depicted in Figure 4.10a of the main text.

The gene IDs of the 674 high-confidence protein hits were analyzed by the DAVID Bioinformatics Database to categorize proteins that are genetically liked to the following disease classes—aging, cancer, cardiovascular, developmental, hematological, immune, infection, metabolic, neurological, pharmacogenomic, psychiatric, renal, and reproduction (Table A7 of the Appendix and Figure 4.11a).

To determine whether the mRNAs of our 674 high-confidence protein hits are known to be overexpressed in any type of cancer, the corresponding gene IDs of each of the high-confidence protein hits were manually submitted to the Oncomine database and the results of this analysis are summarized in Table A8 of the Appendix.

4.5 ^{1}H and ^{13}C-NMR Spectra for the Synthetic Procedures of Analogs 20 and 21

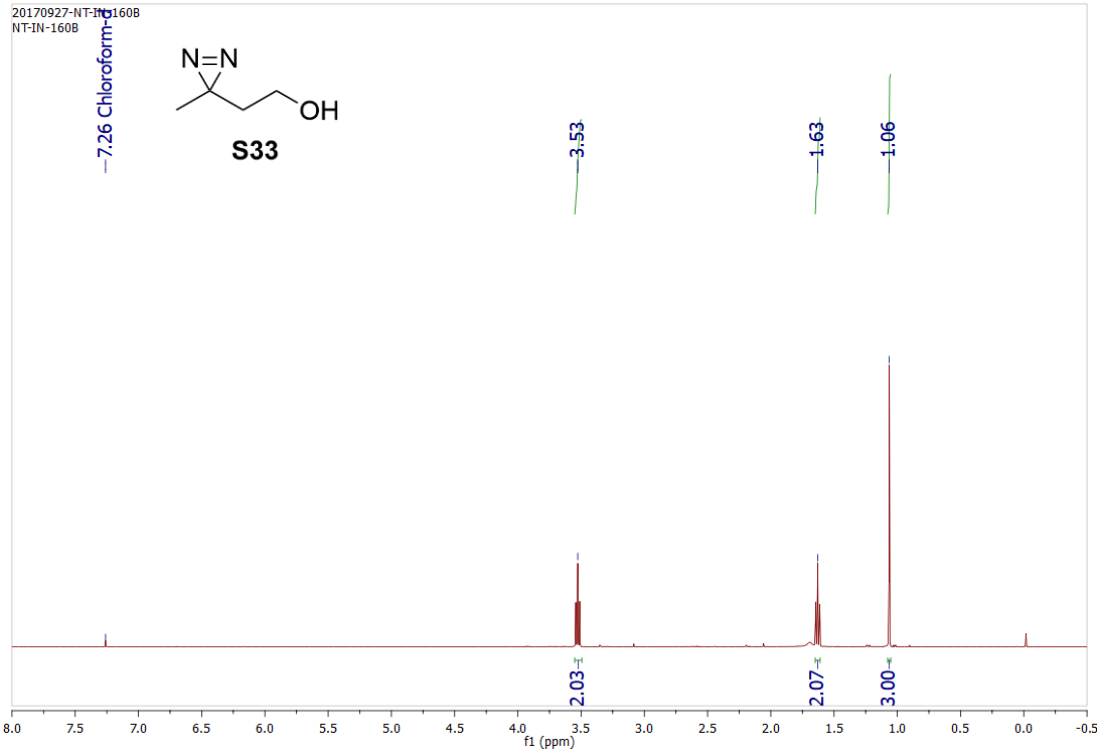

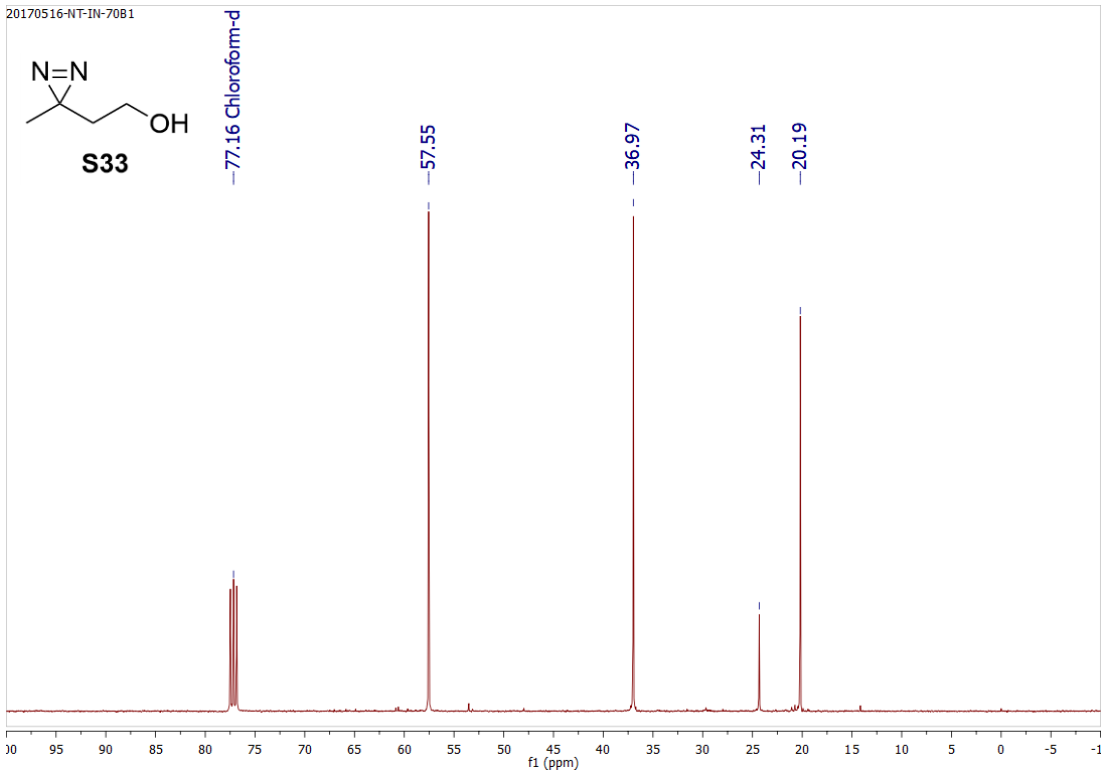

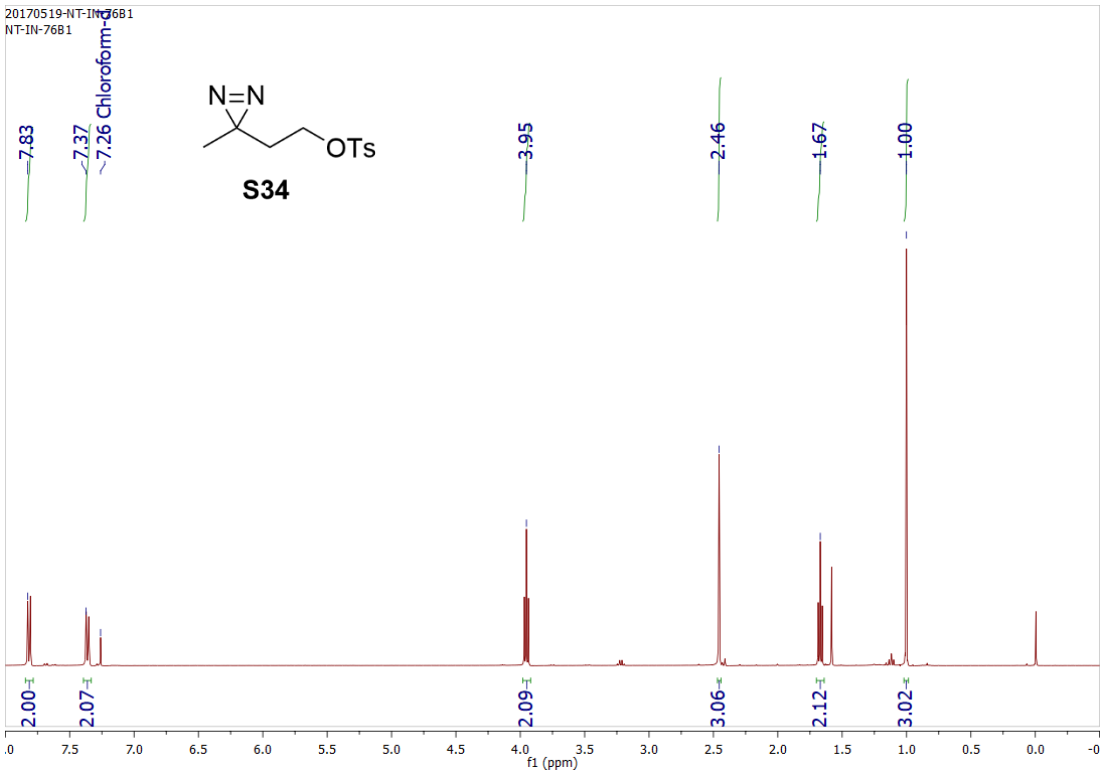
20170519-NT-IN-76B1
NT-IN-76B1
7.83
7.37
7.26 Chloroform-d
N=N
OTs
S34
3.95
2.46
1.67
1.00
2.00
2.07
2.09
3.06
2.12
3.02
f1 (ppm)

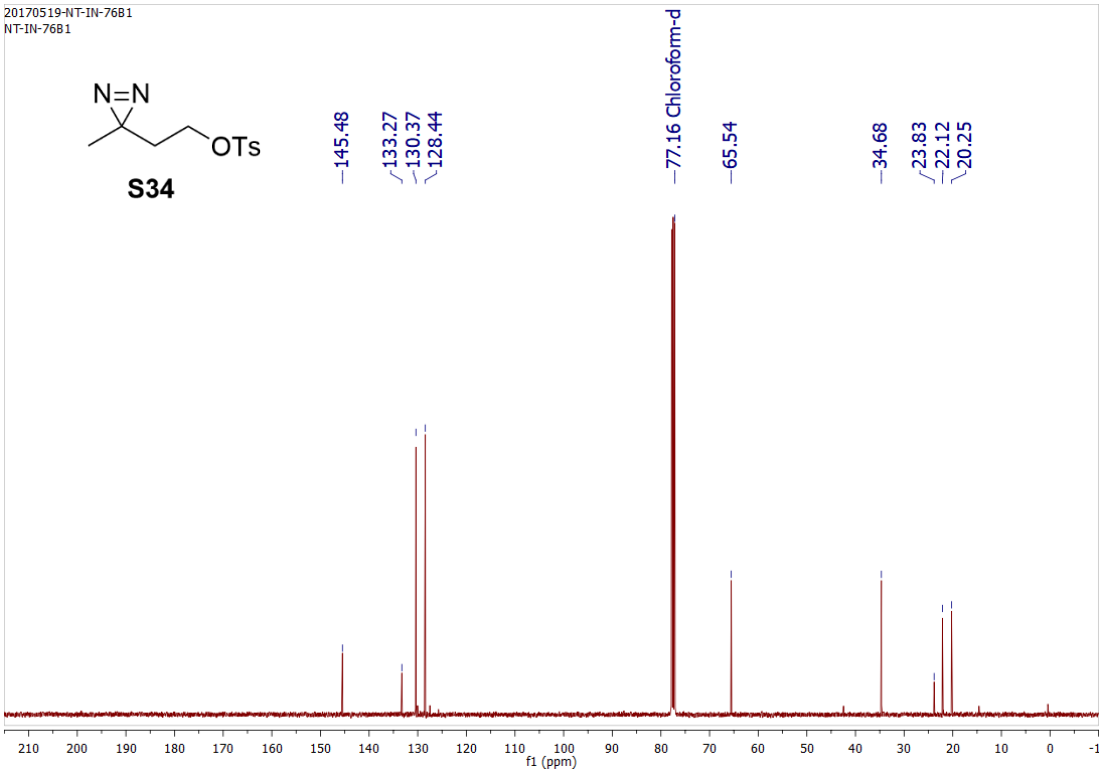
20170519-NT-IN-76B1
NT-IN-76B1
N=N
OTs
S34
145.48
133.27
130.37
128.44
77.16 Chloroform-d
65.54
34.68
23.83
22.12
20.25
f1 (ppm)

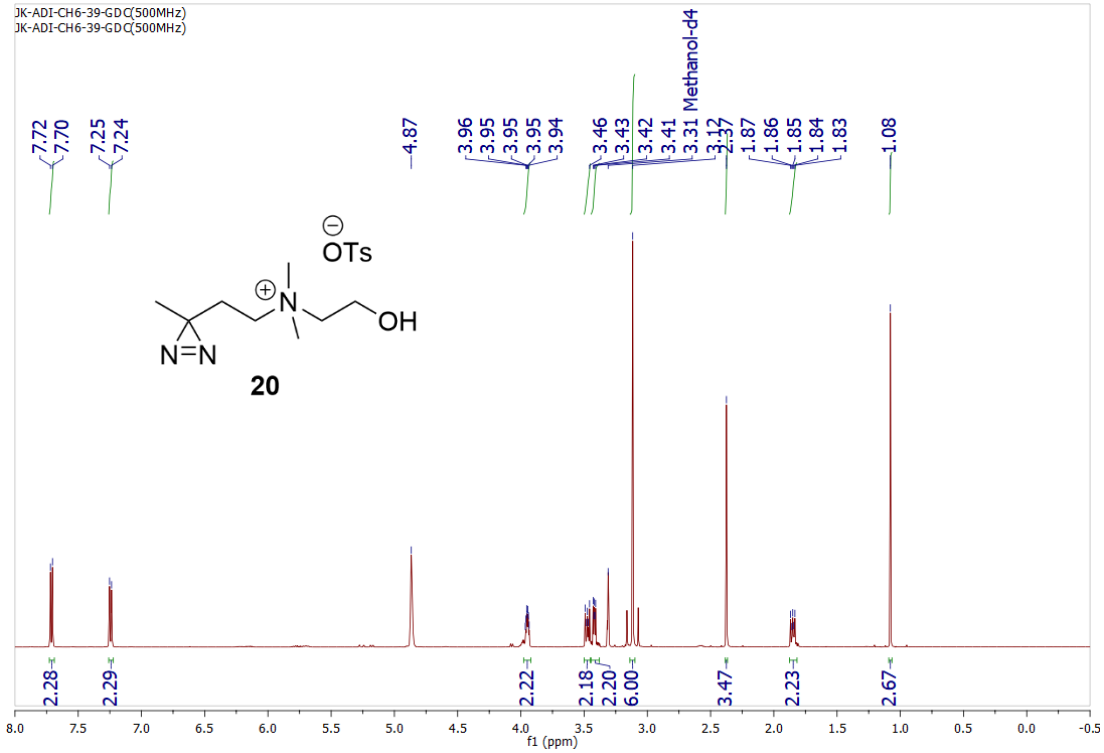
JK-ADI-CH6-39-GDC(500MHz)
JK-ADI-CH6-39-GDC(500MHz)
7.72
7.70
7.25
7.24
4.87
3.96
3.95
3.95
3.95
3.94
3.46
3.43
3.42
3.41
3.31 Methanol-d4
3.12
2.37
1.87
1.86
1.85
1.84
1.83
1.08
OTs
N
OH
N=N
20
2.28
2.29
2.22
2.18
2.20
6.00
3.47
2.23
2.67
f1 (ppm)

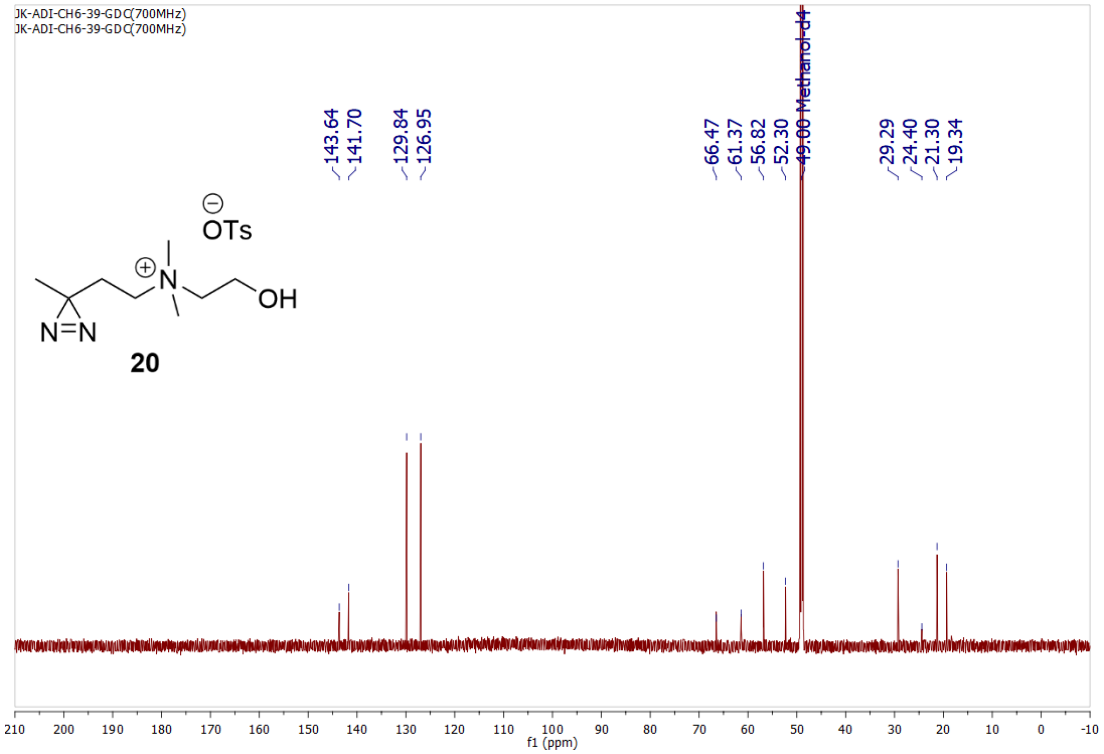
JK-ADI-CH6-39-GDC(700MHz)
JK-ADI-CH6-39-GDC(700MHz)
143.64
141.70
129.84
126.95
66.47
61.37
56.82
52.30
49.00 Methanol-d4
29.29
24.40
21.30
19.34
OTs
N
OH
N=N
20
f1 (ppm)

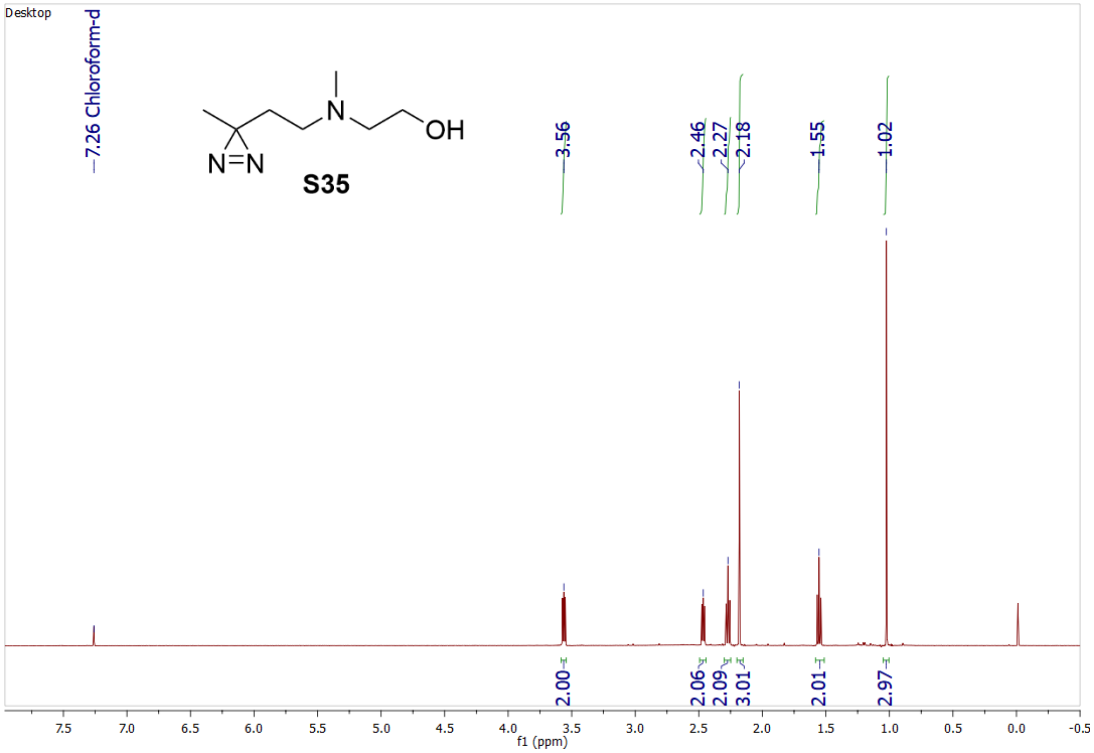
Desktop
7.26 Chloroform-d
N
OH
N=N
S35
3.56
2.46
2.27
2.18
1.55
1.02
2.00
2.06
2.09
3.01
2.01
2.97
f1 (ppm)

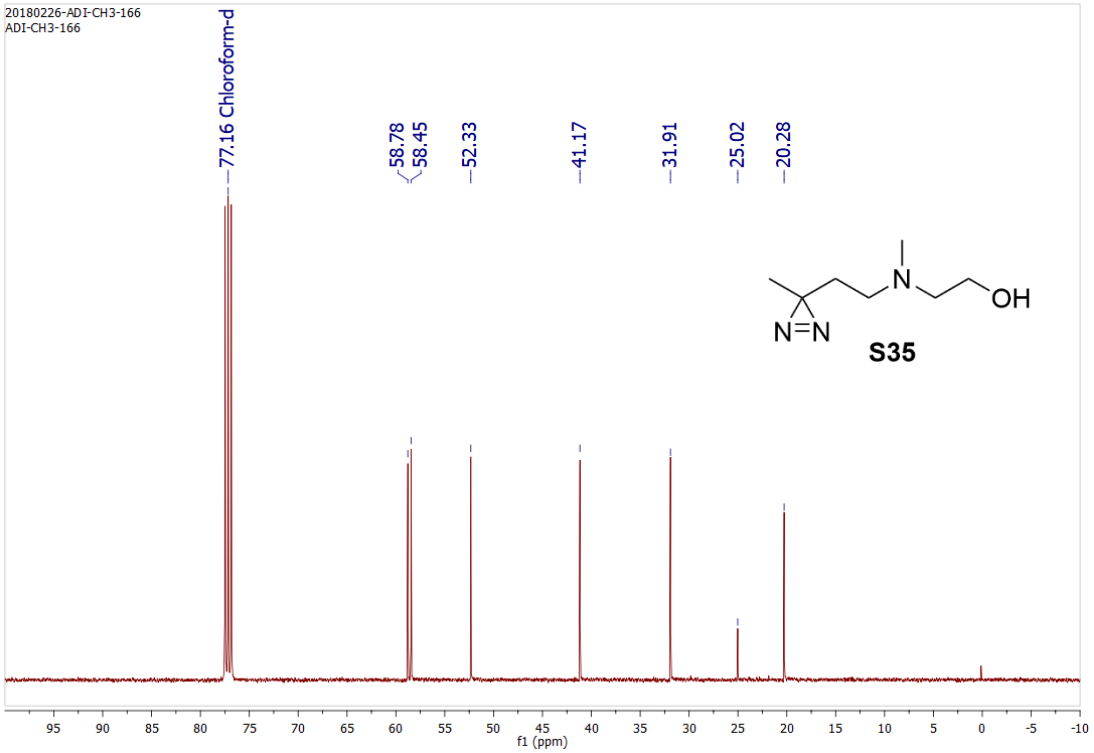
20180226-ADI-CH3-166
ADI-CH3-166
77.16 Chloroform-d
58.78
58.45
52.33
41.17
31.91
25.02
20.28
N
OH
N=N
S35
f1 (ppm)

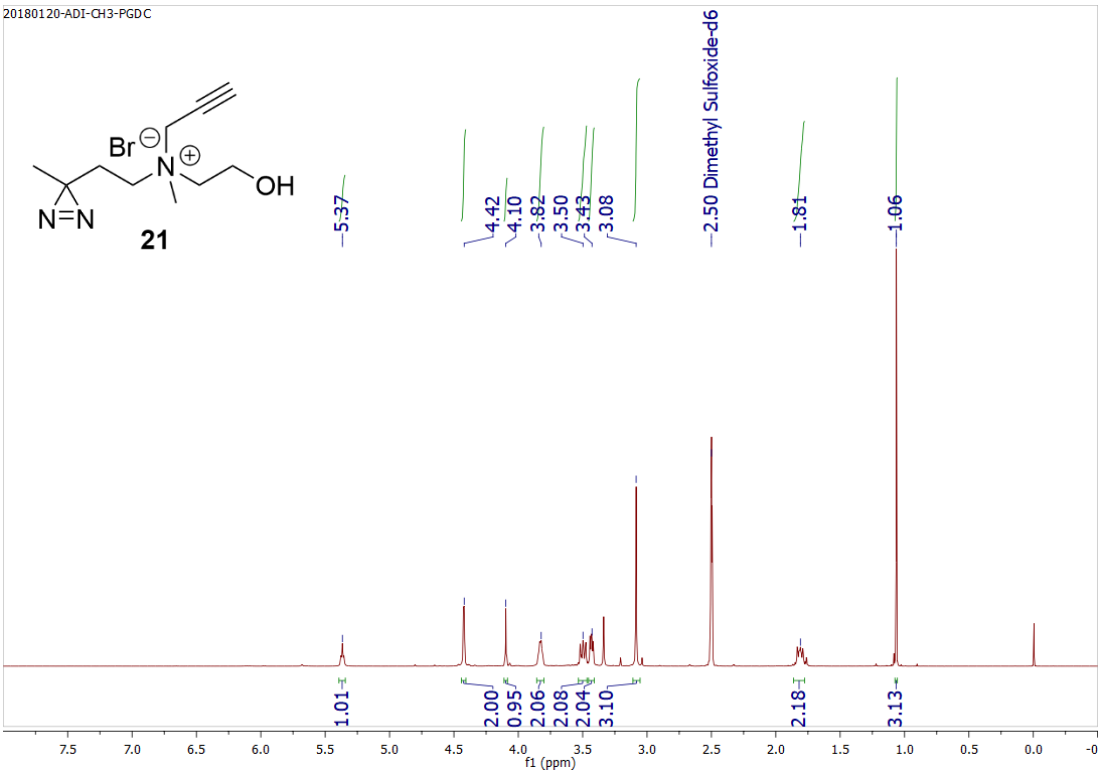
20180120-ADI-CH3-PGDC
Br
N
OH
N=N
21
5.37
4.42
4.10
3.82
3.50
3.43
3.08
2.50 Dimethyl Sulfoxide-d6
1.81
1.06
1.01
2.00
0.95
2.06
2.08
2.04
3.10
2.18
3.13
f1 (ppm)

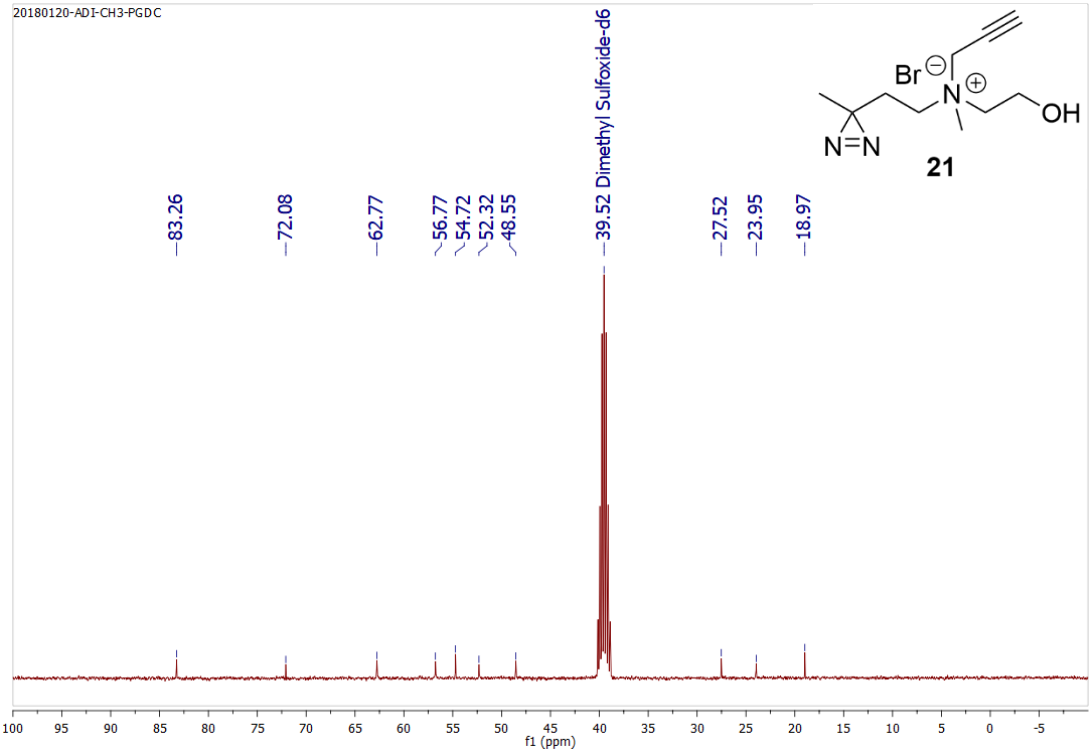
20180120-ADI-CH3-PGDC
Br
N
OH
N=N
21
83.26
72.08
62.77
56.77
54.72
52.32
48.55
39.52 Dimethyl Sulfoxide-d6
27.52
23.95
18.97
f1 (ppm)

4.6 References

1. Pebay-Peyroula, E.; Dahout-Gonzalez, C.; Kahn, R.; Trezeguet, V.; Lauquin, G. J.; Brandolin, G., Structure of mitochondrial ADP/ATP carrier in complex with carboxyatractyloside. *Nature* **2003,** *426* (6962), 39-44.

2. Shinzawa-Itoh, K.; Aoyama, H.; Muramoto, K.; Terada, H.; Kurauchi, T.; Tadehara, Y.; Yamasaki, A.; Sugimura, T.; Kurono, S.; Tsujimoto, K.; Mizushima, T.; Yamashita, E.; Tsukihara, T.; Yoshikawa, S., Structures and physiological roles of 13 integral lipids of bovine heart cytochrome c oxidase. *EMBO J* **2007,** *26* (6), 1713-25.

3. Lange, C.; Nett, J. H.; Trumpower, B. L.; Hunte, C., Specific roles of protein-phospholipid interactions in the yeast cytochrome bc1 complex structure. *EMBO J* **2001,** *20* (23), 6591-600.

4. Zhang, M.; Wang, D.; Li, P.; Sun, C.; Xu, R.; Geng, Z.; Xu, W.; Dai, Z., Interaction of Hsp90 with phospholipid model membranes. *Biochim Biophys Acta Biomembr* **2018,** *1860* (2), 611-16.

5. Wang, D.; Du, S.; Cazenave-Gassiot, A.; Ge, J.; Lee, J. S.; Wenk, M. R.; Yao, S. Q., Global Mapping of Protein-Lipid Interactions by Using Modified Choline-Containing Phospholipids Metabolically Synthesized in Live Cells. *Angew Chem Int Ed Engl* **2017,** *56* (21), 5829-33.

6. Gubbens, J.; Ruijter, E.; de Fays, L. E.; Damen, J. M.; de Kruijff, B.; Slijper, M.; Rijkers, D. T.; Liskamp, R. M.; de Kroon, A. I., Photocrosslinking and click chemistry enable the specific detection of proteins interacting with phospholipids at the membrane interface. *Chem Biol* **2009,** *16* (1), 3-14.

7. Yankovskaya, V.; Horsefield, R.; Tornroth, S.; Luna-Chavez, C.; Miyoshi, H.; Leger, C.; Byrne, B.; Cecchini, G.; Iwata, S., Architecture of succinate dehydrogenase and reactive oxygen species generation. *Science* **2003,** *299* (5607), 700-04.

8. Gokhale, N. A.; Abraham, A.; Digman, M. A.; Gratton, E.; Cho, W., Phosphoinositide specificity of and mechanism of lipid domain formation by annexin A2-p11 heterotetramer. *J Biol Chem* **2005,** *280* (52), 42831-40.

9. Barret, C.; Roy, C.; Montcourrier, P.; Mangeat, P.; Niggli, V., Mutagenesis of the phosphatidylinositol 4,5-bisphosphate (PIP(2)) binding site in the NH(2)-terminal domain of ezrin correlates with its altered cellular distribution. *J Cell Biol* **2000,** *151* (5), 1067-80.

10. Lizarbe, M. A.; Barrasa, J. I.; Olmo, N.; Gavilanes, F.; Turnay, J., Annexin-phospholipid interactions. Functional implications. *Int J Mol Sci* **2013,** *14* (2), 2652-83.

11. Christie, D. A.; Lemke, C. D.; Elias, I. M.; Chau, L. A.; Kirchhof, M. G.; Li, B.; Ball, E. H.; Dunn, S. D.; Hatch, G. M.; Madrenas, J., Stomatin-like protein 2 binds cardiolipin and regulates mitochondrial biogenesis and function. *Mol Cell Biol* **2011,** *31* (18), 3845-56.

12. Thomas, P. D.; Kejariwal, A.; Campbell, M. J.; Mi, H.; Diemer, K.; Guo, N.; Ladunga, I.; Ulitsky-Lazareva, B.; Muruganujan, A.; Rabkin, S.; Vandergriff, J. A.; Doremieux, O., PANTHER: a browsable database of gene products organized by biological function, using curated protein family and subfamily classification. *Nucleic Acids Res* **2003,** *31* (1), 334-41.

13. Punchihewa, C.; Inoue, A.; Hishiki, A.; Fujikawa, Y.; Connelly, M.; Evison, B.; Shao, Y.; Heath, R.; Kuraoka, I.; Rodrigues, P.; Hashimoto, H.; Kawanishi, M.; Sato, M.; Yagi, T.; Fujii, N., Identification of small molecule proliferating cell nuclear antigen (PCNA) inhibitor that disrupts interactions with PIP-box proteins and inhibits DNA replication. *J Biol Chem* **2012,** *287* (17), 14289-300.

14. Huang da, W.; Sherman, B. T.; Lempicki, R. A., Systematic and integrative analysis of large gene lists using DAVID bioinformatics resources. *Nat Protoc* **2009,** *4* (1), 44-57.

15. Rhodes, D. R.; Yu, J.; Shanker, K.; Deshpande, N.; Varambally, R.; Ghosh, D.; Barrette, T.; Pander, A.; Chinnaiyan, A. M., ONCOMINE: A Cancer Microarray Database and Integrated Data-Mining Platform. *Neoplasia* **2004,** *6* (1), 1-6.

16. Verhagen, C. V.; de Haan, R.; Hageman, F.; Oostendorp, T. P.; Carli, A. L.; O'Connor, M. J.; Jonkers, J.; Verheij, M.; van den Brekel, M. W.; Vens, C., Extent of radiosensitization by the PARP inhibitor olaparib depends on its dose, the radiation dose and the integrity of the homologous recombination pathway of tumor cells. *Radiother Oncol* **2015,** *116* (3), 358-65.

17. Pommier, Y.; Leo, E.; Zhang, H.; Marchand, C., DNA topoisomerases and their poisoning by anticancer and antibacterial drugs. *Chem Biol* **2010,** *17* (5), 421-33.

18. Joerger, M.; Omlin, A.; Cerny, T.; Fruh, M., The role of pemetrexed in advanced non small-cell lung cancer: special focus on pharmacology and mechanism of action. *Curr Drug Targets* **2010,** *11* (1), 37-47.

19. Medeiros, B. C.; Fathi, A. T.; DiNardo, C. D.; Pollyea, D. A.; Chan, S. M.; Swords, R., Isocitrate dehydrogenase mutations in myeloid malignancies. *Leukemia* **2017,** *31* (2), 272-81.

20. Wishart, D. S.; Knox, C.; Guo, A. C.; Shrivastava, S.; Hassanali, M.; Stothard, P.; Chang, Z.; Woolsey, J., DrugBank: a comprehensive resource for in silico drug discovery and exploration. *Nucleic Acids Res* **2006,** *34* (Database issue), D668-72.

21. Overington, J. P.; Al-Lazikani, B.; Hopkins, A. L., How many drug targets are there? *Nat Rev Drug Discov* **2006,** *5* (12), 993-96.

22. Haberkant, P.; Raijmakers, R.; Wildwater, M.; Sachsenheimer, T.; Brugger, B.; Maeda, K.; Houweling, M.; Gavin, A. C.; Schultz, C.; van Meer, G.; Heck, A. J.; Holthuis, J. C., In vivo profiling and visualization of cellular protein-lipid interactions using bifunctional fatty acids. *Angew Chem Int Ed Engl* **2013,** *52* (14), 4033-38.

23. Niphakis, M. J.; Lum, K. M.; Cognetta, A. B., 3rd; Correia, B. E.; Ichu, T. A.; Olucha, J.; Brown, S. J.; Kundu, S.; Piscitelli, F.; Rosen, H.; Cravatt, B. F., A Global Map of Lipid-Binding Proteins and Their Ligandability in Cells. *Cell* **2015,** *161* (7), 1668-80.

24. McAlister, G. C.; Nusinow, D. P.; Jedrychowski, M. P.; Wuhr, M.; Huttlin, E. L.; Erickson, B. K.; Rad, R.; Haas, W.; Gygi, S. P., MultiNotch MS3 enables accurate, sensitive, and multiplexed detection of differential expression across cancer cell line proteomes. *Anal Chem* **2014,** *86* (14), 7150-58.

Chapter 5

Functional Studies Aimed at Determining the Role of Choline Metabolites in Protein Function

This chapter is adapted with permission from the publication: Dixit, A.; Jose, G. P.; Shanbhag, C.; Tagad, N.; Kalia, J. Metabolic labeling-based chemoproteomics establishes choline metabolites as protein function modulators. *ACS Chem. Biol.* **2022**, *17*, 2272–2283. Copyright 2022 American Chemical Society.

5.1 Introduction

Chemoproteomics is a powerful tool that can be used to uncover the interaction landscape of a cellular metabolite. This technology not only enables identification of novel metabolite-interacting partners, but also opens several avenues for further investigations on validation of these binding interactions using orthogonal methods and interrogations on the significance of these metabolite-protein interactions on the function of the protein. Several traditional methods are used to orthogonally validate the binding between the metabolite and its target protein such as surface plasmon resonance (SPR), isothermal titration calorimetry (ITC), and X-ray crystallography.

SPR is one of the popular spectroscopic methods to detect the binding between ligand and proteins. It measures the change in the refractive index of the medium that is present in close proximity to a metal chip made of gold or silver. This chip is immobilized with a protein of interest and upon perfusing the aqueous solution containing the metabolite over this chip, the refractive index of the medium changes when the metabolite binds to the immobilized protein. This change in the refractive index is then used to monitor the real time association and dissociation rates of the protein-metabolite complex.[1] SPR has been extensively used in screening the libraries of drugs for binding with protein targets, to probe DNA-protein, and protein-protein interactions.[2-4] Gestwicki and co-workers used SPR to validate the binding kinetics between maltose binding protein and its known endogenous agonists such as maltose, maltotetraose and maltotriose.[5] Despite offering a label-free and a sensitive method for quantitative detection of protein-metabolite interactions, SPR's use is limited because of the requirement of expensive metal chips.

Another important method to validate the binding between protein and a metabolite is ITC wherein the heat released or absorbed as a result of a binding event is measured. The accuracy of the result however, is reliant on the yield and purity of the purified protein. Even small impurities can generate erroneous results.[6, 7] Techniques such as X-ray crystallography are deeply insightful as it provides a high-resolution snapshot of the structure of the protein bound to a metabolite or a drug, however, this technique requires crystallization of a purified protein-metabolite complex that is a slow and cumbersome process.[8]

The aforementioned methods for target validation undeniably provide valuable information on the binding events. For example, SPR and ITC can provide information on binding affinities and

stoichiometry of the protein-metabolite complex, and X-ray crystallography can reveal the residues of the protein that bind with the ligand, however, all these methods require sophisticated equipment that need dedicated training and expertise to operate. Modern methodologies such as cellular thermal shift assay (CETSA)[9] or drug affinity responsive target stability (DARTS)[10] overcome these limitations as they do not require any specialized equipment.

CETSA exploits the difference in the thermal melting temperatures of an unbound protein and the metabolite-bound protein complex as the latter shows resistance towards heat-mediated denaturation. It has been gaining prominence in validating several known small molecule-protein interactions and also to discover novel metabolite partners for soluble as well as membrane proteins.[9, 11, 12] In an alternate approach, Brett Lomenick *et al.* used limited proteolysis to ascertain the binding of a metabolite/small molecule with a protein.[10] Binding of a metabolite/small molecule with a protein makes the assembly resistant from protease digestion. Lomenick *et al* utilized this additional stability of a protein-metabolite complex towards proteolysis to distinguish it from the unbound protein in an assay called DARTS and validated several known protein-small molecule interactions and discovered many novel ones.[10, 13] Both CETSA and DARTS are advantageous as they are high-throughput and can be performed in purified protein samples or cell lysates.

In the previous chapter, we used a chemoproteomics-based workflow (depicted in Figure 1.7b) to obtain a protein-wide list of the choline metabolites and lipid-binding partners in HEK293 cells. We also performed validation on seven proteins from this list bearing different enrichment ratios by following the same workflow and detecting each of the seven proteins in the UV-treated enriched protein samples by performing Western blots against them (Figure 4.8c). The overarching goal of our study, however, was to evaluate the functional significance of the choline metabolite-protein interactions. Towards this goal, we decided to characterize the interaction of choline metabolites and lipids with the most enriched protein in our list, p32. In this chapter, we report DARTS-based assays to orthogonally validate the binding between choline metabolites and p32. Next, we performed ELISA-based binding studies to discern the role of these interaction towards the function of p32. In addition to p32, we also determined the effect of choline metabolites on the function of five other enzymes from our list of protein hits by performing enzymatic assays on them.

5.2 Results and Discussion

5.2.1 Phosphocholine profoundly modulates p32 function

We decided to pursue functional studies on the p32 protein not only because it was our most enriched protein hit (enrichment ratio of 56; Figure 4.8b and Table A1 of the Appendix) but also because of its fascinating functional characteristics and its important role in cancer progression. Also known as HABP1, p33 and gC1qR, p32 is a multifunctional protein that demonstrates a remarkably diverse expression profile within mammalian cells—it is expressed in multiple locations including the mitochondrial matrix, the plasma membrane, the nucleus, the endoplasmic reticulum and the cytosol, and it is also a secreted protein.[14, 15] At these various locations, p32 performs diverse functions including acting as a facilitator of mitochondrial mRNA translation,[16, 17] orchestrating cell attachment and migration by binding to extracellular matrix (ECM) components such as hyaluronic acid (HA) at the plasma membrane,[18] and contributing to HIV infectivity by binding to the HIV Tat protein within the nucleus.[19] Moreover, p32 is overexpressed in malignant tumors found in various organs including lungs, breast and ovary[14] and p32 expressed on the surface of cancer cells plays an important role in cancer progression by contributing to lamellipodia formation which is required for cell migration.[20] The levels of plasma membrane-expressed p32, in particular, are dramatically enhanced in cancer cells as compared to healthy cells and they correlate with the degree of cancer progression suggesting that cell surface p32 levels can serve both as a diagnostic marker for the disease as well as a target for anti-cancer drugs.[14] In fact, the tumor homing cyclic peptide Lyp-1 that has shown considerable promise as an anticancer as well as a tumor-imaging agent is recruited to cancer cells via its specific binding to p32 expressed on the surface of these cells before being internalized upon which it induces apoptosis.[21, 22] Moreover, the treatment of various cancer cell lines with antibodies against p32 has been demonstrated to inhibit cell migration and administration of this antibody into a xenograft mouse model resulted in reduced tumorigenesis, demonstrating the tremendous potential of p32-binding agents for cancer therapy development.[23]

Recombinant production of p32 was necessary to be able to perform functional studies on it. The plasmid encoding the *N*-terminal 6X-Histidine-tagged p32 (henceforth known as His-p32) was generously provided by Prof. Tambet Teesalu (University of Tartu, Estonia). *E. coli* BL21 (DE3)

cells were transformed with this plasmid and the resultant transformants were induced for the production of His-p32 by culturing them in LB broth supplemented with isopropyl β-D-1-thiogalactopyranoside (IPTG). The SDS-PAGE analysis showing the overexpressed protein band for His-p32 in IPTG induced BL21(DE3) cells is shown in Figure 5.1a. The overexpressed protein was then purified by lysing the cells and subjecting the lysate to Ni-NTA resin-based affinity chromatography (Figure 5.1b).

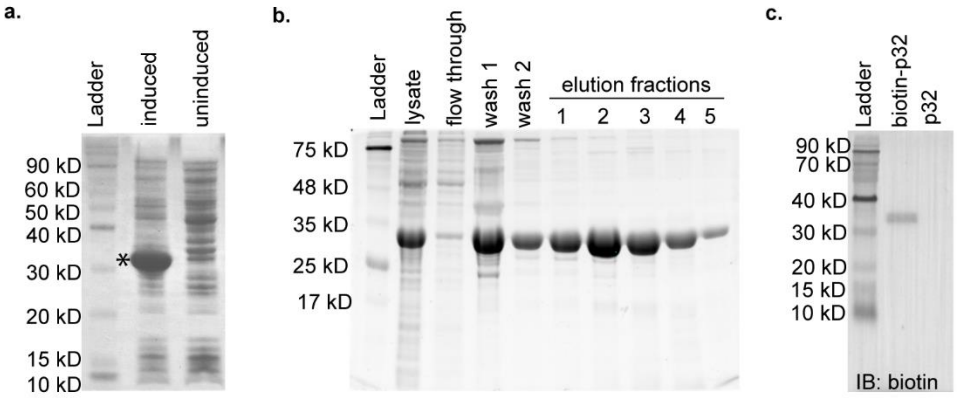

Figure 5.1. Recombinant production and biotinylation of His-p32. a) SDS-PAGE analysis for His-p32 overexpression in IPTG induced BL21 (DE3) cells. The overexpressed His-p32 band is indicated by the asterisk mark. b) An SDS-PAGE analysis of the Ni-NTA purification of His-p32. c) Detection of biotinylated-p32 (loaded in the second lane) using Western blot against biotin. The third lane was loaded with purified p32 that was not subjected to biotinylation.

After purification, our studies on recombinantly produced His-p32 began with investigating its binding to individual choline metabolites and lipids by performing the DARTS experiments.[10] These experiments involved the treatment of His-p32 with the protease cocktail, pronase,[24] in presence of choline metabolites followed by SDS-PAGE analysis to evaluate whether they protect His-p32 from proteolysis or not. The results of these experiments are shown in Figure 5.2 wherein the gel lanes marked "+" represent samples containing choline metabolites/lipids at the indicated concentrations and those marked "-" denote control samples wherein these metabolites/lipids were replaced with equimolar concentrations of either NaCl (for choline, CDP-choline and GPC that were used in their chloride salt forms), or $CaCl_2$ (for phosphocholine which was used in its calcium salt form), or with equal volume of DMSO (for PC and SM lipids that were employed in their

DMSO-solubilized forms). A comparison of the intensity of the bands for the intact uncleaved His-p32 protein in pronase-treated samples (lanes 3-12 from the left) of the gels depicted in Figures 5.2 a,c,d,e and f reveal that at all the tested choline metabolite/lipid concentrations (the "+" lanes), the extent of cleavage of His-p32 was similar to that in their absence (the corresponding control lanes denoted by "-"). In contrast, in the presence of 25 and 50 mM phosphocholine, pronase-mediated cleavage of p32 was substantially lower as compared to that in controls wherein

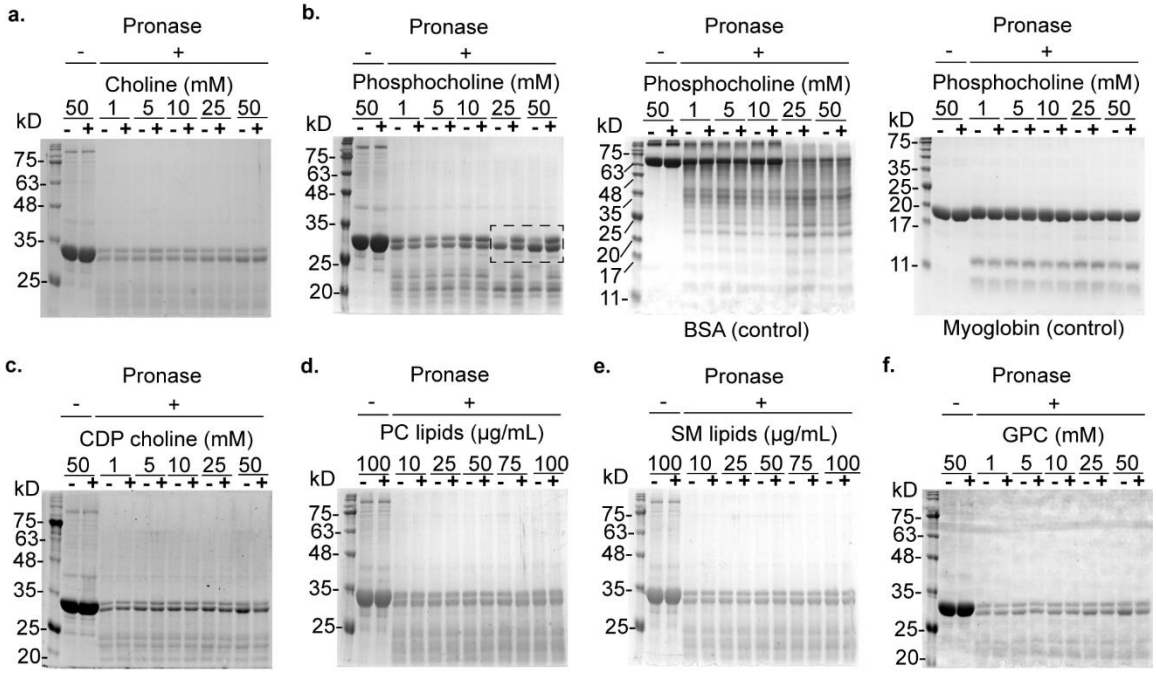

Figure 5.2. DARTS analysis of the binding of choline metabolites to p32.All images depicted are those of Coomassie-stained gels. Pronase was added at a dilution of 1:300 (*w/w*) relative to p32 and proteolysis reactions were performed for 30 min. Experiments with choline (a), phosphocholine (b), CDP choline (c) and GPC (f) were performed with 1-50 mM concentrations of these metabolites (lanes marked "+"), whereas those with PC (d) and SM (e) were performed with DMSO-solubilized lipids (10-100 µg/mL). The metabolite-devoid negative controls (lanes marked "–") for experiments with choline, CDP choline and GPC contained NaCl instead of the choline metabolites, and those for phosphocholine (used in its calcium salt form) contained $CaCl_2$ instead of phosphocholine. The "–" lanes for the PC and SM experiments contained DMSO (vehicle). The enhanced proteolytic efficiency of pronase observed in the presence of 25 and 50 mM $CaCl_2$ (the "–" lanes within the dotted rectangle in b) as compared to the other "–" lanes in the same gel corresponding to lower $CaCl_2$ levels, is expected as pronase activity is catalyzed by Ca^{2+}.[24]

phosphocholine was replaced with equimolar amounts of $CaCl_2$ as demonstrated by a much more intense band for intact p32 in the "+" lanes as compared to those in the "-" lanes (highlighted by a dotted rectangle in Figure 5.2b). In contrast to these results with His-p32, identical experiments on the bovine serum albumin (BSA) and myoglobin proteins demonstrated negligible phosphocholine-mediated protection against protease cleavage (similar intensities for the intact protein bands in the "+" and the "-" lanes of the SDS-PAGE analysis images depicted in the middle and the right panels of Figure 5.2b). These results demonstrate that the protective effect of phosphocholine towards the susceptibility of p32 to undergo proteolysis is due the specific binding of phosphocholine to p32.

DARTS assay enabled us to discover that phosphocholine specifically binds to p32. We next wanted to characterize the effect of choline metabolites and lipids on the function of p32. Towards this goal, we studied their effect on the binding of p32 with its cellular interacting partners by performing ELISA. These experiments entailed producing biotinylated p32 that was achieved by subjecting the purified His-p32 to an amine-reactive biotinylating agent–biotin *N*-hydroxysuccinimide ester. The biotinylated-p32 was purified from its reaction mixture by employing size-exclusion chromatography and the resultant protein was characterized by a single band near 34 kD as observed on the Western Blot against biotin (Figure 5.1c).

For the ELISA experiments, the biotinylated-p32 was incubated with surface-immobilized p32-interacting partners in solutions containing physiologically relevant concentrations of choline/phosphocholine/CDP choline/GPC/PC/SM followed by estimation of bound biotinylated p32. Experiments with phosphocholine were performed with 5 mM phosphocholine considering that intracellular levels as high as 9 mM of this metabolite have been measured[25] whereas those for other choline metabolites were performed with 1 mM metabolite concentrations as they are known to be present at micromolar concentrations in mammalian cells with GPC levels reaching as high as 0.6 mM in MDA-MB-231 cancer cells and 1 mM in metastatic prostate cancer PC-3 cells.[25, 26]

We first focused on the p32-HA complex that is formed on the surface of cancer cells and has an important role in tumor cell adhesion.[14, 18, 27] The results of our ELISA experiments revealed that phosphocholine inhibits the binding between p32 and HA in a competitive fashion (Figure 5.3a,

left panel), whereas choline, CDP-choline, GPC, PC and SM did not show significant modulation of p32-HA binding (Figure 5.3a, middle and right panels). These observations support the results of the DARTS experiments described above that suggested that phosphocholine is the only choline metabolite that binds to p32. The inhibitory activity of phosphocholine on the binding of p32 to HA motivated us to investigate whether this inhibition can result in attenuation of cell migration in cancer cells, akin to that demonstrated by extracellularly administered anti-p32 antibodies alluded to above.[23] Cell migration assays based on the transwell migration approach on the MDA-MB-231 cancer cells that has been previously shown to express p32 on its cell surface[21] demonstrated that the number of migrated cells were 33% lower when 1 mM phosphocholine was

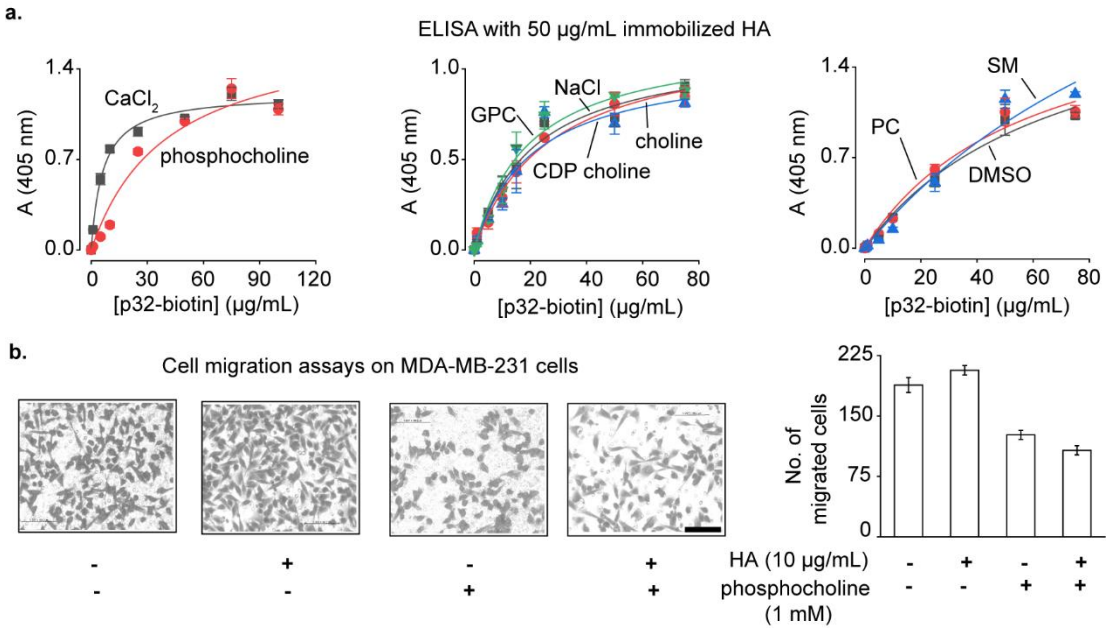

Figure 5.3. Studies on the modulation of p32 binding to HA by choline metabolites. a) Characterization of the effect of choline metabolites on the binding of p32 to HA via ELISA. The metabolite/salt concentrations employed in the ELISAs were as follows: 1 mM choline/CDP choline/GPC/NaCl, 5 mM phosphocholine/$CaCl_2$, and 100 µg/mL PC/SM. b) Transwell cell migration assays on MDA-MB-231 cells to study the effect of phosphocholine on cancer cell migration. The migrated cells were fixed and stained with crystal violet and visualized under a light microscope at 20× magnification (left panel). The scale bars represent 100.2 µm. The migration was quantified by counting the number of cells from each treatment. The bar graph represents the average value from three biological replicates and the error bars represent the standard error of the mean (right).

extracellularly present in the media (third bar from the left in the bar graph in Figure 5.3b) as compared to control experiments with regular media not containing phosphocholine (first bar in Figure 5.3b). Substantial inhibition of cell migration was also observed when 1 mM phosphocholine was introduced into media supplemented with HA. Indeed, the number of migrated cells were 48% lower in phosphocholine-containing HA-supplemented media as compared to HA-supplemented media not containing phosphocholine (fourth and second bars respectively in Figure 5.3b). These experiments demonstrate that phosphocholine can inhibit cancer cell migration when administered extracellularly.

We wanted to employ ELISA to probe the interaction between p32 with its binding partners other than HA in presence of choline metabolites. On the surface of cancer cells, in addition to HA, p32 is known to bind to the tumor homing peptide, Lyp-1, leading to the peptide's cellular internalization enabling it to trigger apoptosis.[21, 22] Our ELISA experiments revealed that phosphocholine profoundly inhibits the binding of Lyp-1 to p32 (Figure 5.4, left panel). In comparison, as observed with the HA experiments, other choline metabolites demonstrated minimal modulation of p32-Lyp-1 binding (Figure 5.4, middle panel) whereas the PC and SM lipids demonstrated moderate inhibition (Figure 5.4, right panel).

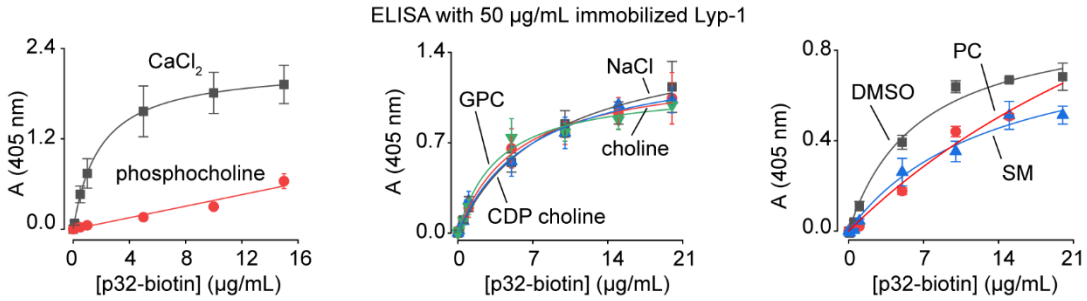

Figure 5.4. Characterization of the effect of choline metabolites on the binding of p32 to Lyp-1 via ELISA. The metabolite/salt concentrations employed in the ELISAs were as follows: 1 mM choline/CDP choline/GPC/NaCl, 5 mM phosphocholine/$CaCl_2$, and 100 µg/mL PC/SM.

In addition to its important role in cancer, p32 regulates viral infectivity in mammalian cells.[19, 28-31] The role of p32 in HIV-1 infectivity involves its binding to the acetylated HIV-1 Tat protein resulting in the recruitment of p32 to the HIV-1 promoter where it inhibits splicing enabling the production of full-length transcripts that are believed to be required for the production of infectious virions.[19] An 18 amino acids-long stretch spanning residues 36-53 of the Tat protein acetylated at Lys41, Lys50 and Lys51 forms the functionally critical region of the acetylated Tat protein[32] and a peptide possessing this sequence has been previously demonstrated to recapitulate the binding of the acetylated Tat protein to p32, thereby acting as a faithful surrogate of the full-length Tat protein for this binding interaction.[19] These experiments (Figure 5.5) revealed that phosphocholine potently inhibits the binding of p32 to the acetylated Tat peptide whereas GPC, CDP choline and choline demonstrate moderate inhibitory effects and the PC and SM lipids demonstrate negligible modulation of this interaction.

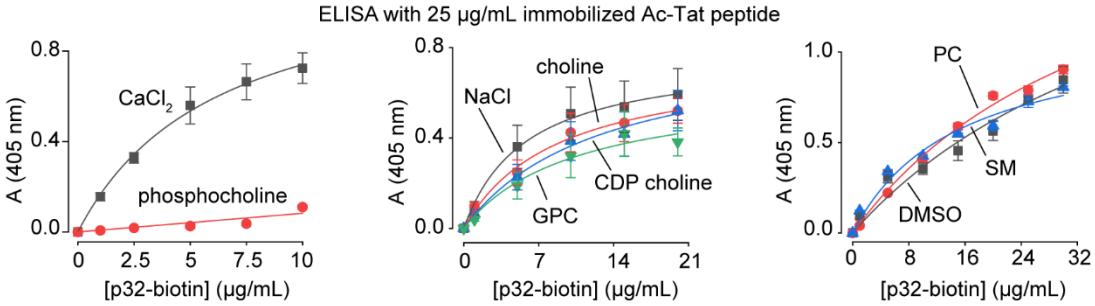

Figure 5.5. Characterization of the effect of choline metabolites on the binding of p32 to acetylated-Tat peptide via ELISA. The metabolite/salt concentrations employed in the ELISAs were as follows: 1 mM choline/CDP choline/GPC/NaCl, 5 mM phosphocholine/$CaCl_2$, and 100 µg/mL PC/SM.

Another protein that p32 binds to within mammalian cells is the monocyte chemoattractant protein-1 (MCP1), a chemokine that plays an important role in recruiting monocytes to the site of infection. Indeed, it has been demonstrated that p32 serves as a pro-inflammatory agent by binding to MCP1 with nanomolar affinity and slowing down its rapid cellular degradation leading to an increase in its cellular levels.[33] Our studies (Figure 5.6) reveal that phosphocholine inhibits the binding of p32 with MCP1 in a competitive fashion and choline also demonstrates moderate inhibitory properties towards p32-MCP1 binding.

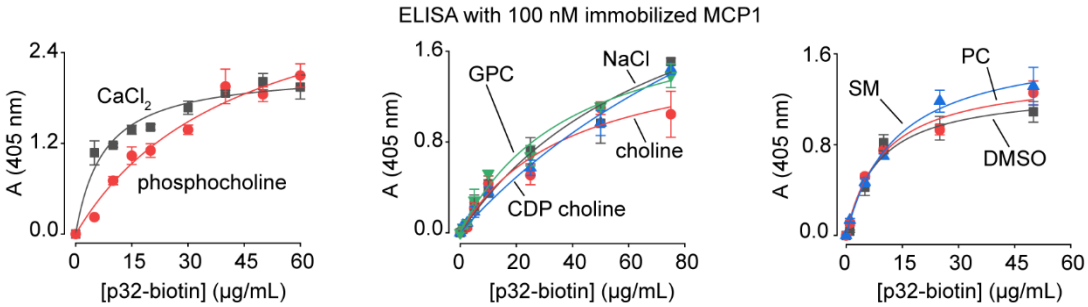

Figure 5.6. Characterization of the effect of choline metabolites on the binding of p32 to MCP1 via ELISA. The metabolite/salt concentrations employed in the ELISAs were as follows: 1 mM choline/CDP choline/GPC/NaCl, 5 mM phosphocholine/$CaCl_2$, and 100 μg/mL PC/SM.

The observation that phosphocholine disrupts an array of p32-ligand interactions demonstrates that it is a general modulator of p32 function. Since phosphocholine is present at elevated levels in cancer cells, its modulation of p32 function is likely an important contributor to the roles of this protein in disease progression.

5.2.2 Choline metabolites modulate the activity of cellular enzymes

In addition to p32, we also evaluated the effect of choline metabolites on the function of another protein hit of ours that plays an important role in cancer progression, the lactate dehydrogenase (LDH) enzyme, which yielded an enrichment ratio of 2.5 for LDH-B chain and the ratio of 2.08 for LDH-A chain in our TMT proteomics dataset (Table A1 of the Appendix). LDH is a cytosolic enzyme that converts pyruvate to lactate using NADH as a cofactor (Figure 5.7a) and it is overexpressed in almost all types of cancer and LDH inhibitors are promising anticancer agents.[34] At constant NADH concentrations, we observed that the apparent K_m value for pyruvate was reduced ~5-fold in presence of 1 mM choline, whereas it was halved in the presence of the same concentrations of CDP-choline and GPC (Figure 5.7b,c). The presence of these three metabolites also caused an attenuation of the K_m values of the enzyme in assays wherein the concentration of pyruvate was kept constant whereas that of NADH was altered, with the largest effect seen with choline (a ~4-fold reduction, Figure 5.7b,d). These results suggest that choline, CDP choline and GPC facilitate the binding of pyruvate and NADH to LDH via an allosteric effect.

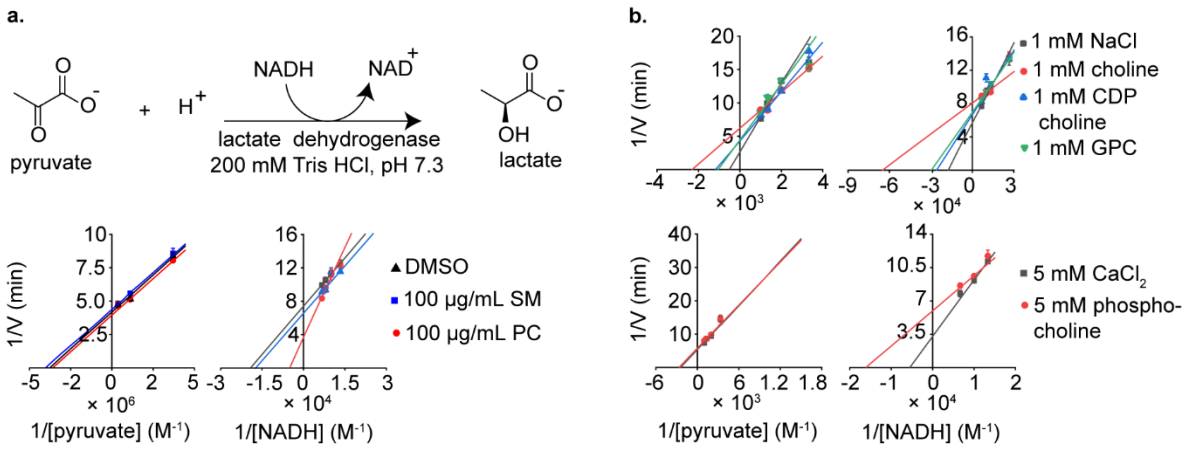

c.

Variable pyruvate, constant NADH

Metabolite/Control	K_m app (M)	K_m metabolite / K_m control	V_{max} (min^{-1})	V_{max} metabolite / V_{max} control
DMSO (control)	$(2.95 \pm 0.4) \times 10^{-7}$	1	0.24 ± 0.01	1
PC	$(3.09 \pm 0.3) \times 10^{-7}$	1.05 ± 0.2	0.23 ± 0.01	0.95 ± 0.1
SM	$(2.76 \pm 0.3) \times 10^{-7}$	0.94 ± 0.2	0.25 ± 0.01	1.06 ± 0.1
1 mM NaCl (control)	$(1.93 \pm 0.5) \times 10^{-3}$	1	0.38 ± 0.1	1
1 mM choline	$(4.34 \pm 0.6) \times 10^{-4}$	0.22 ± 0.1	0.16 ± 0.01	0.43 ± 0.2
1 mM CDP choline	$(8.51 \pm 1.1) \times 10^{-4}$	0.44 ± 0.1	0.23 ± 0.03	0.61 ± 0.2
1 mM GPC	$(9.60 \pm 1.8) \times 10^{-4}$	0.50 ± 0.2	0.23 ± 0.05	0.60 ± 0.3
5 mM $CaCl_2$ (control)	$(4.09 \pm 1.2) \times 10^{-4}$	1	0.19 ± 0.03	1
5 mM phosphocholine	$(3.77 \pm 0.6) \times 10^{-4}$	0.92 ± 0.3	0.17 ± 0.01	0.94 ± 0.2

d.

Variable NADH, constant pyruvate

Metabolite/Control	K_m app (M)	K_m metabolite / K_m control	V_{max} (min^{-1})	V_{max} metabolite / V_{max} control
DMSO (control)	$(5.22 \pm 0.4) \times 10^{-5}$	1	0.14 ± 0.00	1
PC	$(1.95 \pm 0.5) \times 10^{-4}$	3.73 ± 0.9	0.27 ± 0.07	2.01 ± 0.5
SM	$(5.79 \pm 1.1) \times 10^{-5}$	1.11 ± 0.2	0.15 ± 0.02	1.13 ± 0.1
1 mM NaCl (control)	$(5.75 \pm 0.7) \times 10^{-5}$	1	0.18 ± 0.01	1
1 mM choline	$(1.54 \pm 0.7) \times 10^{-5}$	0.27 ± 0.1	0.12 ± 0.01	0.69 ± 0.1
1 mM CDP choline	$(3.85 \pm 0.7) \times 10^{-5}$	0.67 ± 0.1	0.15 ± 0.01	0.84 ± 0.1
1 mM GPC	$(3.37 \pm 0.1) \times 10^{-5}$	0.59 ± 0.1	0.14 ± 0.00	0.80 ± 0.1
5 mM $CaCl_2$ (control)	$(1.82 \pm 0.2) \times 10^{-4}$	1	0.31 ± 0.05	1
5 mM phosphocholine	$(6.22 \pm 2.3) \times 10^{-5}$	0.34 ± 0.1	0.17 ± 0.03	0.54 ± 0.1

Figure 5.7. Characterizing the effect of choline metabolites on the activity of lactate dehydrogenase. a) The enzymatic reaction of lactate dehydrogenase. b) Double reciprocal plots generated by calculating the initial velocity of each enzyme-catalyzed reaction in the presence of the designated choline metabolites or in the presence of salt/vehicle solvent instead of the metabolites. *Figure legend continued to the next page.*

Figure 5.7 legend continued from the previous page. Specifically, whereas assays performed with choline, CDP choline and GPC contained 1 mM concentrations of these metabolites (used in their chloride salt forms), in the corresponding metabolite-devoid experiments, these metabolites were replaced with 1 mM NaCl. Assays with phosphocholine were performed in the presence of 5 mM phosphocholine (used as phosphocholine chloride calcium salt), whereas the corresponding metabolite-devoid experiments contained 5 mM $CaCl_2$. PC and SM were introduced into the assays in their DMSO-solubilized forms and the corresponding negative controls contained an identical volume of the DMSO vehicle. c) and d) Table depicting the value of K_m and V_{max} of the enzymatic reactions.

We also characterized the effect of choline metabolites and lipids on four of our other enzyme hits—the Kreb's cycle enzyme, citrate synthase, the glycolytic enzyme, glyceraldehyde 3-phosphate dehydrogenase (GAPDH), malic enzyme and glutamic dehydrogenase. Our assays on citrate synthase (Figure 5.8) revealed that at constant acetyl CoA concentrations, the apparent K_m value for oxaloacetic acid was reduced by ~2.6-fold in presence of 100 μg/mL PC lipids whereas the soluble choline metabolites did not have any effects on the activity of this enzyme. Assays on malic enzyme revealed a ~2 fold-attenuation of the K_m values of $NADP^+$ in the presence of GPC, phosphocholine and PC, and a similar attenuation of the K_m value of malate in presence of GPC (Figure 5.9). GAPDH (Figure 5.10) and glutamate dehydrogenase (Figure 5.11) were tested and they demonstrated negligible alterations in their kinetic parameters in presence of choline metabolites and lipids.

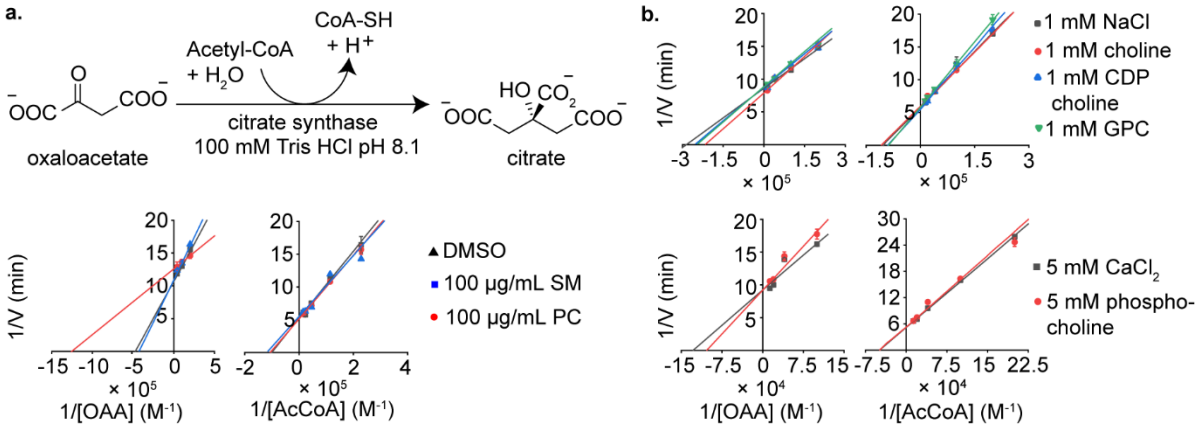

c.

Variable AcCoA, constant oxaloacetate

Metabolite/Control	K_m app (M)	K_m metabolite / K_m control	V_{max} (min^{-1})	V_{max} metabolite / V_{max} control
DMSO (control)	(1.14 ± 0.1) × 10^{-5}	1	0.19 ± 0.01	1
PC	(1.07 ± 0.03) × 10^{-5}	0.94 ± 0.1	0.19 ± 0.002	1.00 ± 0.05
SM	(9.60 ± 2.1) × 10^{-6}	0.84 ± 0.2	0.18 ± 0.03	0.94 ± 0.16
1 mM NaCl (control)	(9.84 ± 0.1) × 10^{-6}	1	0.17 ± 0.001	1
1 mM choline	(9.25 ± 0.3) × 10^{-6}	0.94 ± 0.04	0.17 ± 0.003	0.95 ± 0.02
1 mM CDP choline	(1.09 ± 0.04) × 10^{-5}	1.11 ± 0.1	0.18 ± 0.003	1.01 ± 0.02
1 mM GPC	(1.12 ± 0.04) × 10^{-5}	1.14 ± 0.04	0.17 ± 0.001	0.97 ± 0.01
5 mM $CaCl_2$ (control)	(2.06 ± 0.005) × 10^{-5}	1	0.20 ± 0.004	1
5 mM phosphocholine	(2.05 ± 0.09) × 10^{-5}	1.00 ± 0.1	0.19 ± 0.01	0.96 ± 0.06

d.

Variable oxaloacetate, constant AcCoA

Metabolite/Control	K_m app (M)	K_m metabolite / K_m control	V_{max} (min^{-1})	V_{max} metabolite / V_{max} control
DMSO (control)	(2.11 ± 0.2) × 10^{-6}	1	0.093 ± 0.002	1
PC	(7.97 ± 0.7) × 10^{-7}	0.38 ± 0.1	0.079 ± 0.001	0.86 ± 0.02
SM	(2.34 ± 0.4) × 10^{-6}	1.11 ± 0.2	0.092 ± 0.004	0.99 ± 0.1
1 mM NaCl (control)	(3.20 ± 0.2) × 10^{-6}	1	0.116 ± 0.003	1
1 mM choline	(4.62 ± 0.4) × 10^{-6}	1.32 ± 0.2	0.124 ± 0.01	1.07 ± 0.1
1 mM CDP choline	(3.95 ± 0.6) × 10^{-6}	1.13 ± 0.2	0.115 ± 0.01	0.99 ± 0.1
1 mM GPC	(4.05 ± 0.2) × 10^{-6}	1.16 ± 0.1	0.114 ± 0.002	0.98 ± 0.03
5 mM $CaCl_2$ (control)	(7.79 ± 1.4) × 10^{-6}	1	0.109 ± 0.01	1
5 mM phosphocholine	(9.68 ± 1.9) × 10^{-6}	1.24 ± 0.3	0.109 ± 0.01	0.99 ± 0.1

Figure 5.8. Characterizing the activity of citrate synthase in presence of choline metabolites and lipids. a) The enzymatic reaction of citrate synthase. b) Double reciprocal plots generated by calculating the initial velocity of each enzyme-catalyzed reaction in the presence of the designated choline metabolites or in the presence of salt/vehicle solvent instead of the metabolites. *Figure legend continued to the next page.*

Figure 5.8 legend continued from the previous page. Specifically, whereas assays performed with choline, CDP choline and GPC contained 1 mM concentrations of these metabolites, in the corresponding metabolite-devoid experiments, these metabolites were replaced with 1 mM NaCl. Assays with phosphocholine were performed in the presence of 5 mM phosphocholine (used as phosphocholine chloride calcium salt), whereas the corresponding metabolite-devoid experiments contained 5 mM $CaCl_2$. PC and SM were introduced into the assays in their DMSO-solubilized forms and the corresponding negative controls contained an identical volume of the DMSO vehicle. c) and d) Table depicting the value of K_m and V_{max} of the enzymatic reactions.

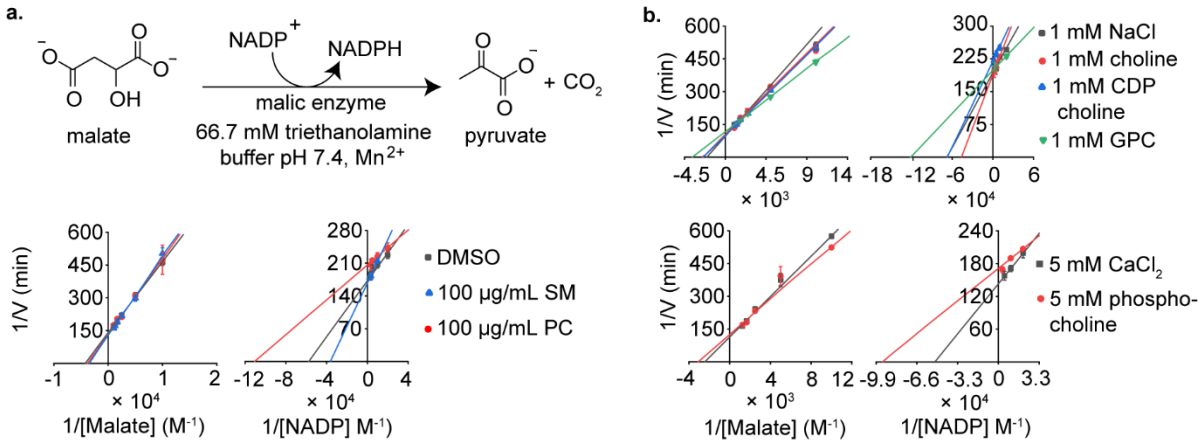

c.

Variable malate, constant NADP+

Metabolite/Control	K_m app (M)	K_m metabolite / K_m control	V_{max} (min^{-1})	V_{max} metabolite / V_{max} control
DMSO (control)	$(2.38 \pm 0.05) \times 10^{-4}$	1	$(7.25 \pm 0.09) \times 10^{-3}$	1
PC	$(2.62 \pm 0.2) \times 10^{-4}$	1.10 ± 0.08	$(7.53 \pm 0.3) \times 10^{-3}$	1.04 ± 0.04
SM	$(2.89 \pm 0.09) \times 10^{-4}$	1.22 ± 0.05	$(7.95 \pm 0.2) \times 10^{-3}$	1.10 ± 0.03
1 mM NaCl (control)	$(4.92 \pm 0.2) \times 10^{-4}$	1	$(1.05 \pm 0.02) \times 10^{-2}$	1
1 mM choline	$(3.94 \pm 0.3) \times 10^{-4}$	0.80 ± 0.06	$(9.54 \pm 0.7) \times 10^{-3}$	0.91 ± 0.07
1 mM CDP choline	$(4.10 \pm 0.07) \times 10^{-4}$	0.83 ± 0.03	$(1.00 \pm 0.02) \times 10^{-2}$	0.95 ± 0.04
1 mM GPC	$(2.74 \pm 0.06) \times 10^{-4}$	0.56 ± 0.02	$(8.59 \pm 0.2) \times 10^{-3}$	0.82 ± 0.03
5 mM $CaCl_2$(control)	$(4.11 \pm 0.1) \times 10^{-4}$	1	$(8.88 \pm 0.5) \times 10^{-3}$	1
5 mM phosphocholine	$(3.24 \pm 0.3) \times 10^{-4}$	0.79 ± 0.07	$(7.94 \pm 0.6) \times 10^{-3}$	0.89 ± 0.08

d.

Variable NADP+, constant malate

Metabolite/Control	K_m app (M)	K_m metabolite / K_m control	V_{max} (min^{-1})	V_{max} metabolite / V_{max} control
DMSO (control)	$(1.74 \pm 0.3) \times 10^{-5}$	1	$(5.81 \pm 0.08) \times 10^{-3}$	1
PC	$(9.02 \pm 1.3) \times 10^{-6}$	0.52 ± 0.1	$(4.85 \pm 0.05) \times 10^{-3}$	0.83 ± 0.01
SM	$(2.76 \pm 0.02) \times 10^{-5}$	1.59 ± 0.23	$(5.95 \pm 0.01) \times 10^{-3}$	1.02 ± 0.01
1 mM NaCl (control)	$(1.48 \pm 0.2) \times 10^{-5}$	1	$(5.22 \pm 0.1) \times 10^{-3}$	1
1 mM choline	$(2.15 \pm 0.1) \times 10^{-5}$	1.46 ± 0.21	$(5.30 \pm 0.05) \times 10^{-3}$	1.02 ± 0.02
1 mM CDP choline	$(1.49 \pm 0.3) \times 10^{-5}$	1.01 ± 0.22	$(4.58 \pm 0.09) \times 10^{-3}$	0.88 ± 0.02
1 mM GPC	$(8.28 \pm 0.6) \times 10^{-6}$	0.56 ± 0.08	$(5.05 \pm 0.04) \times 10^{-3}$	0.97 ± 0.02
5 mM $CaCl_2$ (control)	$(1.95 \pm 0.06) \times 10^{-5}$	1	$(6.98 \pm 0.05) \times 10^{-3}$	1
5 mM phosphocholine	$(1.06 \pm 0.2) \times 10^{-5}$	0.55 ± 0.09	$(5.85 \pm 0.2) \times 10^{-3}$	0.84 ± 0.02

Figure 5.9. Characterizing the activity of malic enzyme in presence of choline metabolites and lipids. a) The enzymatic reaction of malic enzyme. b) Double reciprocal plots generated by calculating the initial velocity of each enzyme-catalyzed reaction in the presence of the designated choline metabolites or in the presence of salt/vehicle solvent instead of the metabolites. d) Table depicting the value of K_m and V_{max} of the enzymatic reactions. *Figure legend continued to the next page.*

Figure 5.9 legend continued from the previous page. Specifically, whereas assays performed with choline, CDP choline and GPC contained 1 mM concentrations of these metabolites, in the corresponding metabolite-devoid experiments, these metabolites were replaced with 1 mM NaCl. Assays with phosphocholine were performed in the presence of 5 mM phosphocholine (used as phosphocholine chloride calcium salt), whereas the corresponding metabolite-devoid experiments contained 5 mM $CaCl_2$. PC and SM were introduced into the assays in their DMSO-solubilized forms

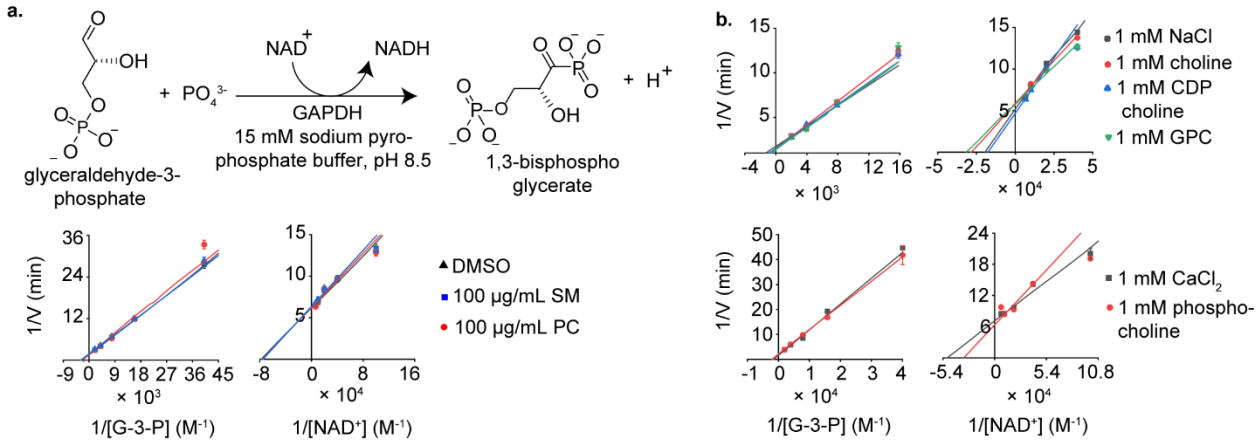

c. Variable glyceraldehyde-3-phosphate, constant NAD^+ (control)

Metabolite/Control	K_m app (M)	K_m metabolite / K_m control	V_{max} (min^{-1})	V_{max} metabolite / V_{max} control
DMSO (control)	$(4.19 \pm 0.2) \times 10^{-4}$	1	0.64 ± 0.01	1
PC	$(4.69 \pm 0.5) \times 10^{-4}$	1.12 ± 0.11	0.70 ± 0.09	1.08 ± 0.15
SM	$(3.41 \pm 0.1) \times 10^{-4}$	0.81 ± 0.02	0.54 ± 0.02	0.84 ± 0.03
1 mM NaCl (control)	$(3.29 \pm 0.4) \times 10^{-4}$	1	0.58 ± 0.07	1
1 mM choline	$(4.35 \pm 0.1) \times 10^{-4}$	1.32 ± 0.17	0.65 ± 0.05	1.14 ± 0.15
1 mM CDP choline	$(4.05 \pm 0.2) \times 10^{-4}$	1.23 ± 0.16	0.66 ± 0.05	1.15 ± 0.16
1 mM GPC	$(4.75 \pm 1.2) \times 10^{-4}$	1.44 ± 0.41	0.76 ± 0.23	1.32 ± 0.43
1 mM $CaCl_2$(control)	$(6.02 \pm 0.5) \times 10^{-4}$	1	0.58 ± 0.08	1
1 mM phosphocholine	$(5.17 \pm 0.2) \times 10^{-4}$	0.86 ± 0.07	0.53 ± 0.02	0.90 ± 0.13

d. Variable NAD^+, constant glyceraldehyde-3-phosphate

Metabolite/Control	K_m app (M)	K_m metabolite / K_m control	V_{max} (min^{-1})	V_{max} metabolite / V_{max} control
DMSO (control)	$(1.83 \pm 0.3) \times 10^{-5}$	1	0.17 ± 0.01	1
PC	$(1.60 \pm 0.2) \times 10^{-5}$	0.87 ± 0.15	0.17 ± 0.01	1.00 ± 0.06
SM	$(1.86 \pm 0.3) \times 10^{-5}$	1.02 ± 0.22	0.16 ± 0.01	0.97 ± 0.05
1 mM NaCl (control)	$(4.99 \pm 0.9) \times 10^{-5}$	1	0.19 ± 0.01	1
1 mM choline	$(3.53 \pm 0.6) \times 10^{-5}$	0.71 ± 0.18	0.17 ± 0.01	0.91 ± 0.16
1 mM CDP choline	$(5.63 \pm 0.8) \times 10^{-5}$	1.13 ± 0.27	0.21 ± 0.02	1.12 ± 0.20
1 mM GPC	$(3.14 \pm 0.4) \times 10^{-5}$	0.63 ± 0.14	0.17 ± 0.01	0.91 ± 0.16
1 mM $CaCl_2$ (control)	$(2.02 \pm 0.3) \times 10^{-5}$	1	0.14 ± 0.01	1
1 mM phosphocholine	$(3.13 \pm 0.4) \times 10^{-5}$	1.55 ± 0.32	0.16 ± 0.02	1.12 ± 0.16

Figure 5.10. Characterizing the activity of GAPDH in presence of choline metabolites and lipids. a) The enzymatic reaction of GAPDH. b) Double reciprocal plots generated by calculating the initial velocity of each enzyme-catalyzed reaction in the presence of the designated choline metabolites or in the presence of salt/vehicle solvent instead of the metabolites. *Figure legend continued to the next page.*

Figure 5.10 legend continued from the previous page. Specifically, whereas assays performed with choline, CDP choline and GPC contained 1 mM concentrations of these metabolites, in the corresponding metabolite-devoid experiments, these metabolites were replaced with 1 mM NaCl. Assays with phosphocholine were also performed in the presence of 1 mM phosphocholine (used as phosphocholine chloride calcium salt), whereas the corresponding metabolite-devoid experiments contained 1 mM $CaCl_2$. PC and SM were introduced into the assays in their DMSO-solubilized forms and the corresponding negative controls contained an identical volume of the DMSO vehicle. c) and d) Table depicting the value of K_m and V_{max} of the enzymatic reactions.

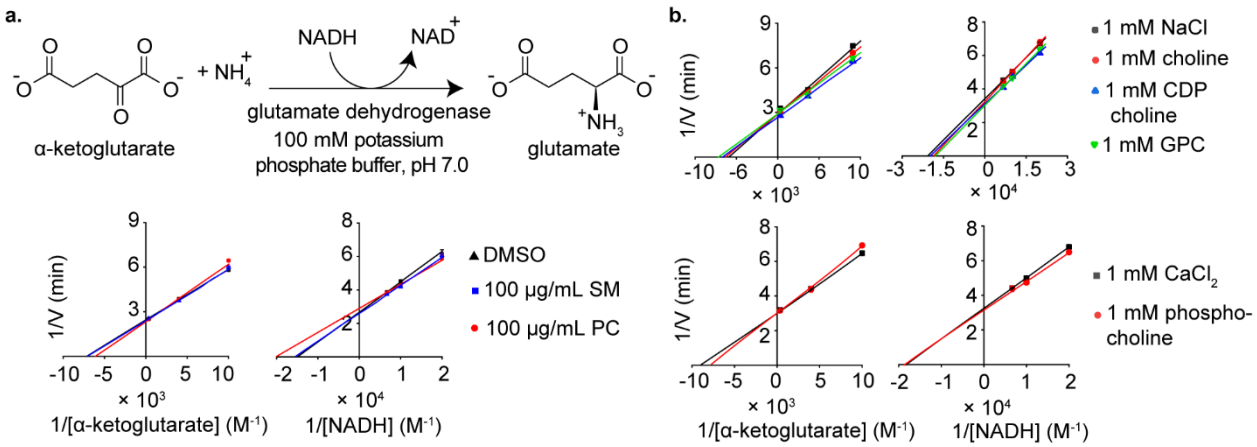

c. Variable α-ketoglutarate, constant NADH

Metabolite/Control	K_m app (M)	K_m metabolite / K_m control	V_{max} (min^{-1})	V_{max} metabolite / V_{max} control
DMSO (control)	$(1.40 \pm 0.1) \times 10^{-4}$	1	0.41 ± 0.01	1
PC	$(1.63 \pm 0.1) \times 10^{-4}$	1.17 ± 0.1	0.42 ± 0.01	1.05 ± 0.1
SM	$(1.41 \pm 0.1) \times 10^{-4}$	1.01 ± 0.1	0.41 ± 0.01	1.01 ± 0.1
1 mM NaCl (control)	$(1.54 \pm 0.1) \times 10^{-4}$	1	0.35 ± 0.03	1
1 mM choline	$(1.45 \pm 0.1) \times 10^{-4}$	0.94 ± 0.1	0.35 ± 0.01	1.01 ± 0.1
1 mM CDP choline	$(1.36 \pm 0.1) \times 10^{-4}$	0.89 ± 0.1	0.37 ± 0.01	1.09 ± 0.1
1 mM GPC	$(1.27 \pm 0.1) \times 10^{-4}$	0.82 ± 0.1	0.34 ± 0.02	0.99 ± 0.1
1 mM $CaCl_2$ (control)	$(1.11 \pm 0.01) \times 10^{-4}$	1	0.33 ± 0.01	1
1 mM phosphocholine	$(1.28 \pm 0.1) \times 10^{-4}$	1.15 ± 0.04	0.33 ± 0.01	1.01 ± 0.1

d. Variable NADH, constant α-ketoglutarate

Metabolite/Control	K_m app (M)	K_m metabolite / K_m control	V_{max} (min^{-1})	V_{max} metabolite / V_{max} control
DMSO (control)	$(6.70 \pm 0.5 \times 10^{-5}$	1	0.37 ± 0.01	1
PC	$(4.95 \pm 0.7) \times 10^{-5}$	0.74 ± 0.11	0.35 ± 0.02	0.93 ± 0.1
SM	$(6.43 \pm 0.7) \times 10^{-5}$	0.96 ± 0.13	0.39 ± 0.03	1.04 ± 0.1
1 mM NaCl (control)	$(4.83 \pm 0.1) \times 10^{-5}$	1	0.29 ± 0.01	1
1 mM choline	$(5.39 \pm 0.1) \times 10^{-5}$	1.12 ± 0.02	0.31 ± 0.01	1.05 ± 0.1
1 mM CDP choline	$(5.06 \pm 0.5) \times 10^{-5}$	1.05 ± 0.11	0.32 ± 0.02	1.11 ± 0.1
1 mM GPC	$(5.56 \pm 0.2) \times 10^{-5}$	1.15 ± 0.05	0.33 ± 0.01	1.13 ± 0.1
1 mM $CaCl_2$ (control)	$(5.49 \pm 0.2) \times 10^{-5}$	1	0.31 ± 0.01	1
1 mM phosphocholine	$(5.38 \pm 0.5) \times 10^{-5}$	0.98 ± 0.09	0.32 ± 0.02	1.04 ± 0.1

Figure 5.11. Characterizing the activity of glutamate dehydrogenase in presence of choline metabolites and lipids. a) The enzymatic reaction of glutamate dehydrogenase. b) Double reciprocal plots generated by calculating the initial velocity of each enzyme-catalyzed reaction in the presence of the designated choline metabolites or in the presence of salt/vehicle solvent instead of the metabolites. *Figure legend continued to the next page.*

Figure 5.11 legend continued from the previous page. Specifically, whereas assays performed with choline, CDP choline and GPC contained 1 mM concentrations of these metabolites, in the corresponding metabolite-devoid experiments, these metabolites were replaced with 1 mM NaCl. Assays with phosphocholine were performed in the presence of 1 mM phosphocholine (used as phosphocholine chloride calcium salt), whereas the corresponding metabolite-devoid experiments contained 1 mM $CaCl_2$. PC and SM were introduced into the assays in their DMSO-solubilized forms and the corresponding negative controls contained an identical volume of the DMSO vehicle. c) and d) Table depicting the value of K_m and V_{max} of the enzymatic reactions.

5.3 Conclusions

In summary, we attempted to elucidate the roles of choline metabolites in addition to their roles as biosynthetic precursors to PC and SM lipids by performing functional assays on the choline metabolite and lipid-interacting proteins from the list that we had obtained in the last chapter. Towards this end, we first validated the specific interaction of phosphocholine with p32 by performing DARTS assays. These results from an orthogonal workflow increased the confidence in our chemoproteomics results. Next, ELISA experiments showed that phosphocholine acts as a general modulator of p32 at physiological concentrations by demonstrating that it inhibits the interaction between p32 and several of its cellular binding partners.

Next, I tested the activity of five enzymes in presence of choline metabolites and lipids, and demonstrated that three out of them showed modulation in the latter's presence: a) phosphocholine modulated the anticancer therapy target, LDH, and b) other choline metabolites and lipids modulated the activity of citrate synthase and malic enzyme. Contrary to the aforementioned enzymes, however, GAPDH and glutamate dehydrogenase did not alter their function in presence of choline metabolites and lipids. Collectively, these results strongly emphasize the importance of complementing interactome mapping studies with functional experiments to interrogate the physiological significance of the identified interactions. Finally, to interrogate the functional relevance of the interactions of choline metabolites and lipids with other protein hits that our chemoproteomic approach has identified, we anticipate that performing orthogonal binding experiments such as ELISA and DARTS assays may be necessary.

5.4 Experimental Methods

5.4.1 Materials

Lyp-1 peptide was purchased from Anaspec, MCP1 from R&D systems, and the sodium salt of HA from Merck. Acetylated Tat (Ac-Tat) peptide (aa 36 to 53 with the lysine residues at 41, 50 and 51 positions acetylated) was purchased from Grey Matter Research Foundation Pvt. Ltd. Streptavidin conjugated to HRP, biotin *N*-hydroxysuccinimide ester, ECL kit, and Zeba spin desalting columns were purchased from Thermo Fisher Scientific. Recombinant lactate dehydrogenase, citrate synthase, GAPDH, malic enzyme, glutamate dehydrogenase, choline chloride, phosphocholine chloride calcium salt tetrahydrate, CDP choline sodium salt hydrate, PC and SM lipids from chicken egg yolk, pronase and the metabolites used for the enzymatic assays and DARTS assays were purchased from Sigma Aldrich. Vivaspin spin concentrators (5 kDa molecular weight cut off) were purchased from GE life sciences. Transwell migration chambers (8 µm pore size) were purchased from Corning. Ni-NTA resin was purchased from Qiagen. Anti-biotin and goat anti-mouse IgG conjugated to HRP antibodies were purchased from Santa Cruz Biotechnology and Abcam respectively.

5.4.2 Instrumentation and software

The enzyme assays were performed on a Perkin Elmer Lambda25 UV-Vis spectrophotometer. The absorbance for the ELISA assays were recorded on an iMark microtiter plate reader (Biorad). The images for cell migration assay were acquired on a Zeiss Axio Vert.A1 microscope. SDS-PA gels and the chemiluminescence from the Western Blots were visualized on a ChemiDoc imaging system (Biorad).

5.4.3 Recombinant production of His-p32

A plasmid containing the gene encoding for the *N*-terminus 6X-His tagged p32 protein in the pET15b vector was used to transform *E. coli* BL21 (DE3) cells. LB broth cultures (1 L) containing ampicillin (100 µg/mL) were inoculated with the transformed *E. coli* BL21 (DE3) cells and induced with IPTG (0.5 mM) on reaching an O.D. (600 nm) of 0.4-0.6 at 37 °C. The induced culture was pelleted (6,000 rpm, 10 min at room temperature) after 6 h of growth and the supernatant was discarded. The efficiency of the induction was evaluated by performing SDS-

PAGE analysis (Figure 5.1a). Consistent with the previous reports,[35] although the molecular weight of His-p32 is 26.1 kDa, we observed that it gave a band at ~34 kDa. To purify the protein, the cell pellet was resuspended by vigorous vortexing in 20 mL of HEPES buffer (20 mM at pH 7.6) containing 0.5 M NaCl, 1.5 mM $MgCl_2$, 1 mM DTT, 0.1% (*v/v*) TritonX-100, and 20% (*v/v*) glycerol (henceforth known as lysis buffer). The resuspended cells were lysed via probe sonication on ice (150 pulses of 2 sec each with a gap of 3 sec between each pulse, 30% amplitude on a Branson 450 Digital Sonifier) followed by centrifugation at 15,500 *g* at 4 °C for 30 min and the resulting supernatant was retained. A column packed with 1.5 mL of Ni-NTA resin was washed with 20 mL of lysis buffer at 4 °C and the aforementioned cell lysate containing overexpressed His-p32 was applied to the resin at 4 °C. After collecting the flow-through, the column was washed twice with 5 mL of sodium phosphate buffer (50 mM at pH 6.0) containing 0.3 M NaCl, 10 mM imidazole, and 0.05% Tween-20 at 4 °C. The bound protein was eluted by applying 25 mL of sodium phosphate buffer (50 mM at pH 6.0) containing 0.3 M NaCl, 300 mM imidazole and 0.05% Tween-20 at 4 °C and the eluted fractions were collected as 5 mL aliquots. The collected fractions were characterized by subjecting 10 µL of each fraction to SDS-PAGE (Figure 5.1b). The fractions that contained the required His-p32 (fraction numbers 1-5) were combined and used for further processing as described in sections 5.4.4 and 5.4.5 below.

5.4.4 Testing the binding of choline metabolites with His-p32 using DARTS

The fractions containing His-p32 obtained as described in the section 5.4.3 above were combined and dialyzed against Tris HCl buffer (50 mM at pH 8.0 containing 150 mM NaCl). Subsequently, the dialyzed protein was concentrated by using 5 kDa molecular weight cutoff Vivaspin spin concentrators, and quantified by measuring the absorbance of the concentrated protein solution at 280 nm. A solution of 3.13 mg/mL His-p32 in Tris HCl buffer (50 mM at pH 8.0 containing 150 mM NaCl) was supplemented with EDTA-free protease inhibitor cocktail (from a 10X stock solution in water), 50 mM NaF (from a stock solution of 500 mM in water), 1 mM PMSF (from a stock solution of 100 mM in ethanol), and 1% *v/v* NP-40 (stock solution of 10% *v/v* in water). This protein solution was used to test the binding of His-p32 with choline metabolites and lipids by employing drug affinity responsive target stability (DARTS) assays.[10] To perform these assays, 40 µL binding reaction mixture samples (the "+" samples) were constituted that contained 2.5 mg/mL His-p32 (32 µL of the aforementioned 3.13 mg/mL stock solution was added), 10 mM $CaCl_2$ (2

µL of a 200 mM stock solution in water was added), and 1-50 mM choline/ CDP-choline/GPC/phosphocholine (a 50 mM metabolite stock solution was used for achieving the final concentrations of 1 mM and 5 mM in the samples, whereas a 500 mM stock solution in water was used for achieving concentrations of 10 mM, 25 mM, and 50 mM). These samples were incubated at 25 °C for 4 h with shaking at 600 rpm in an Eppendorf Thermomixer. In the control "-" samples for choline, CDP choline and GPC, these metabolites were replaced with NaCl at concentrations identical to those for the metabolites in the corresponding "+" samples. In the control "-" samples for phosphocholine, the metabolite was replaced with $CaCl_2$. To test the binding of His-p32 with 10-100 µg/mL PC and SM, these lipids were added from their 1 mg/mL stocks in DMSO to yield the final concentrations of 10 µg/mL, 25 µg/mL, 50 µg/mL, 75 µg/mL or 100 µg/mL. In the corresponding vehicle controls, instead of the lipid stock solutions, equal volume of DMSO was added. To each of these 40 µL reaction mixtures, 4 µL of an 83.3 ng/µL stock of pronase (stock solution made in 50 mM Tris-HCl buffer at pH 8.0 containing 50 mM NaCl and 10 mM $CaCl_2$) was added, and the mixture was incubated at 25 °C for 30 min without shaking (final pronase: protein *w/w* ratio in each sample was 1:300). To the control samples, instead of this pronase stock solution, 4 µL of 50 mM Tris-HCl buffer at pH 8.0 containing 50 mM NaCl and 10 mM $CaCl_2$ was added. The proteolysis reaction was quenched by adding 2X SDS-loading buffer (44 µL) in each sample and heating the resultant mixture at 75 °C for 10 min. The samples were then centrifuged (8,000 *g*, 3 min at room temperature) and the supernatants (15 µL) were subjected to SDS-PAGE (12% gel) and stained with Coomassie. To test the binding of 1-50 mM phosphocholine with other proteins, the experiment described above was repeated with the 3.13 mg/mL stock solution of BSA and myoglobin instead of His-p32. The gel images thus obtained are depicted in Figure 5.2a-f.

5.4.5 Biotinylation of His-p32

The fractions containing His-p32 obtained as described in section 5.4.3 above were combined and dialyzed against PBS. Subsequently, the dialyzed protein was concentrated by using 5 kDa molecular weight cutoff Vivaspin spin concentrators and quantified by measuring the absorbance of the concentrated protein solution at 280 nm. Biotinylation was performed by adding a solution of biotin *N*-hydroxysuccinimide ester in DMSO (950 nmol, 47 µL, 20 eq.) to a solution of His-p32 in PBS (47.5 nmol, 470 µL, 1 eq.). After incubating for 2 h at room temperature, the reaction

mixture was desalted by using Zeba spin 7 kDa molecular weight cutoff desalting columns and the protein solution was then subjected to Western blotting against the anti-biotin antibody to characterize biotinylation. Specifically, the desalted protein solution was subjected to SDS-PAGE (12% gel) followed by electrophoretically transferring the protein to a PVDF membrane. The membrane was incubated in 5% *w/v* BSA solution in PBS for 1 h at room temperature and then in anti-biotin antibody (1:4000 *v/v* dilution in PBST) for 3 h at room temperature. Subsequently, the membrane was washed three times with PBST and incubated with shaking in PBST for 10 min after each wash and then it was incubated in anti-mouse IgG conjugated to HRP (1:10000 *v/v* dilution in PBST) for 2 h at room temperature. Finally, the membrane was washed with PBST three times with intermittent 10 min incubations in PBST with shaking. To visualize the biotinylated His-p32, the blot was developed using the ECL kit as per the manufacturer's protocol and imaged for chemiluminescence using the ChemiDoc imaging system as depicted in Figure 5.1c.

5.4.6 Probing the binding between p32 and its ligands, Lyp-1, HA, Ac-Tat peptide and MCP1 using ELISA

The stock solutions of the ligands were made in PBS at the following concentrations: Ac-Tat peptide (5 mg/mL), MCP1 (11.5 mM), Lyp-1 (2 mg/mL) and HA (10 mg/mL). These solutions were diluted into the sodium carbonate-bicarbonate buffer (50 mM, pH 9.6) to achieve their respective working concentrations (25 µg/mL for Ac-Tat, 100 nM for MCP1 and 50 µg/mL for both Lyp-1 and HA) and 100 µL of each of these solutions were added to 96 well-plates and incubated for 12 h at 4 °C to immobilize the ligands. Subsequently, each well was washed with PBS (300 µL/well × 3) and blocked with 5% (*w/v*) skimmed milk solution in PBS (300 µL/well) for 2 h at room temperature. The skimmed milk solution was then aspirated off and the wells were washed three times with 0.05% (*v/v*) PBST (300 µL/well) before introducing solutions (100 µL/well) containing different concentrations of biotinylated His-p32 in PBS (as indicated by the data points of the ELISA plots depicted in Figures 5.3-5.6) and choline metabolites (at concentrations mentioned in the legends of Figures 5.3-5.6). Wells administered with 100 µL of PBS instead of biotinylated His-p32 served as blank. Subsequently, the plates were incubated at room temperature for 2 h following which, the solutions were aspirated off and the wells were washed three times with PBST (300 µL/well). The bound biotinylated-p32 was detected by

incubation in a solution containing HRP conjugated to streptavidin diluted to a ratio of 1:5000 *v/v* in 5% *w/v* BSA in PBS (100 µL/well) for 2 h at room temperature. The unbound protein was washed off with PBST (300 µL/well × 3) and the wells were incubated in 100 µL of the substrate solution containing 1.82 mM ABTS (2,2'-azino-bis(3-ethylbenzothiazoline-6-sulfonic acid)) and 0.03% *w/w* hydrogen peroxide solution (diluted from a 30% *w/w* stock) in citrate-phosphate buffer (100 mM, pH 5.0) for 15 min at room temperature under dark. The reaction was stopped by adding sulfuric acid (625 mM, 100 µL/well) and the intensity of the resulting blue-green color was immediately quantified by measuring the absorbance at 405 nm by using an iMark microplate reader (Biorad). The readings obtained from the blank wells containing immobilized Lyp-1/HA/MCP1/Ac-Tat peptide, but not administered with biotinylated p32 were subtracted from those obtained from the experimental samples and these blank-subtracted values were used to generate a saturation binding curve (Figures 5.3-5.6). Each value is an average of at least three technical replicates.

5.4.7 Transwell cell migration assays on MDA-MB-231 cells

Transwell cell migration assays were performed to investigate the effect of phosphocholine on the migration of the HA-treated and untreated MDA-MB-231 cells by making slight modifications to the previously reported methods.[23, 36] Four 6 cm culture dishes each containing MDA-MB-231 cells (5 mL of a 0.3 million cells per mL culture in serum free DMEM) were taken. One of these four dishes was administered 2.5 µL of a 20 mg/mL solution of HA in water (final concentration of HA in the dish was 10 µg/mL), another was administered 100 µL of a 50 mM solution of phosphocholine in water (the final concentration of phosphocholine in the dish was 1 mM), the third dish was administered both of the aforementioned solutions, and the fourth dish (the control) was administered 100 µL of water. Subsequently, all four dishes were incubated at 37 °C in a CO_2 incubator for 24 h after which, cells from each plate were trypsinized (1.5 min, 37 °C), resuspended into 4 mL of complete media by gently pipetting up and down, and pelleted down by centrifugation (300 *g*, 3 min, 25 °C). The supernatant was discarded and the resultant cell pellet was resuspended into 4 mL of serum free DMEM by gently pipetting up and down. This cell-suspension was centrifuged (300 *g*, 3 min, 25 °C) and the resultant pellet was resuspended in 1 mL of serum free DMEM and the cell density of this cellular resuspension was measured by using a hemocytometer. Subsequently, for each treatment, the volume of the cellular resuspension in serum free DMEM

equivalent to 0.4 million cells was taken into a microfuge tube and mixed with serum free DMEM such that the total volume amounted to 1 mL (the final cell density in serum free DMEM was 0.4 million cells per mL). To this mixture was added either a 10 μL solution of 20 mg/mL stock of HA in water (final concentration of HA in the microfuge tube was 10 μg/mL), or 10 μL of a 100 mM solution of phosphocholine in water (final concentration of phosphocholine in the tube was 1 mM), or both the aforementioned solutions, or 20 μL water, and the resultant mixture was resuspended by gentle pipetting. Subsequently, 250 μL of each of the aforementioned cell suspensions (a total of 10^5 cells) were transferred to the upper chambers of transwell migration inserts (8 μm pore size) and these inserts were placed in separate wells of a 24-well plate each containing 700 μL of DMEM supplemented with 10% FBS as a chemoattractant. The cells were allowed to migrate to the other side of the porous membrane of the transwell insert in a CO_2 incubator at 37°C for 24 h. After the incubation, the serum free DMEM inside the transwell inserts were discarded by aspiration and each transwell insert was then washed twice by dipping in a beaker containing PBS. Subsequently, the cells were fixed by introducing the inserts into wells containing 700 μL of 4% *w/v* paraformaldehyde solution (PFA) in PBS. The upper chambers of the inserts were filled with 250 μL of 4% *w/v* PFA in PBS, and this assembly was incubated at room temperature for 20 min. After fixation, each transwell insert was washed twice by dipping in a beaker containing PBS. The non-migrated cells from the upper surface of each transwell insert were removed by gently wiping with a cotton swab. Subsequently, the migrated cells present on the other side of the membrane were stained by incubating the inserts in 700 μL of a 0.1% *w/v* crystal violet solution (made in 20% methanol in water) for 20 min at room temperature. After the incubation, the excess staining solution was removed by gently dabbing the insert on a tissue paper followed by washing it off by dipping in a beaker containing PBS twice. Subsequently, these transwell inserts were air dried for 30 min at room temperature and the migrated cells that were stained with crystal violet were visualized under a 20× objective by using an inverted light microscope (Zeiss Axio Vert.A1). For each treatment, five images were captured from non-overlapping fields (representative images are depicted in Figure 5.3b left panel) and the number of cells were manually counted by using the multi-point tool on the ImageJ software (NIH) on each image. These experiments were performed in triplicate. Each data point depicted in the bar graph in Figure 5.3b (right panel) is an average of at least fifteen images across the three biological replicates.

5.4.8 Investigations on the effects of choline metabolites on the function of enzymes

(i) Lactate dehydrogenase (LDH): Enzymatic assays on rabbit muscle LDH were performed at 25 °C in a quartz cuvette by using a UV-Vis spectrophotometer as per a procedure described previously.[37] The stock solutions of choline, CDP choline, GPC and sodium chloride (20 mM each), phosphocholine and calcium chloride (100 mM each), sodium pyruvate and NADH were made in 0.2 M Tris-HCl buffer at pH 7.3 and the stock solutions of PC and SM lipids (2.5 mg/mL each) were made in DMSO. All enzyme assays were performed in 0.2 M Tris-HCl buffer at pH 7.3. To generate kinetic plots with varying NADH and constant pyruvate concentrations, the final concentrations of reaction components in the kinetic runs were as follows: LDH: 0.06 U/mL (from a stock of 1.2 units/mL in 0.2 M Tris-HCl buffer at pH 7.3), sodium pyruvate: 1 mM (from a stock of 20 mM in 0.2 M Tris-HCl buffer at pH 7.3), and choline metabolite/lipid or control: as depicted in Figure 5.7b. The enzymatic reactions were initiated by adding NADH (37.5 µM-150 µM from a stock of 3 mM in 0.2 M Tris-HCl buffer at pH 7.3) to the cuvette. To generate kinetic plots with varying pyruvate and constant NADH concentrations, the final concentrations of reaction components in the kinetic runs were as follows: LDH: 0.06 U/mL, choline metabolite/lipid or control: as depicted in Figure 5.7b, and sodium pyruvate: 300 µM-1 mM (from a stock solution of 20 mM in 0.2 M Tris-HCl buffer at pH 7.3). The enzymatic reactions were initiated by adding NADH (150 µM from a stock solution of 3 mM in 0.2 M Tris-HCl buffer at pH 7.3). The velocity of the enzymatic reaction was monitored by recording the rate of decrease in the absorbance of NADH at 340 nm and the K_m and V_{max} values were obtained from the double reciprocal plots that were generated by using the initial velocity of the reactions. The kinetic runs corresponding to each reaction were repeated at least three times.

(ii) Citrate Synthase (CS): Enzymatic assays on porcine heart CS were performed at 25 °C in a quartz cuvette and by using a UV-Vis spectrophotometer (Perkin Elmer Lambda 25) as per a procedure described previously.[38] The stock solutions of choline, CDP choline, GPC and sodium chloride (20 mM each), acetyl-CoA (1 mM), and phosphocholine and calcium chloride (100 mM each) were made in water. The 0.5 mM stock of 5,5'-dithiobis-(2-nitrobenzoic acid) or DTNB was made in 0.5 M Tris-HCl buffer at pH 8.1 and the 2 mM stock of oxaloacetic acid was made in 0.1 M triethanolamine-HCl buffer at pH 8.0 containing 1 mM EDTA (henceforth known as buffer A), and that of the CS enzyme was made in 0.1 M Tris-HCl buffer at pH 7.0. The stock solutions of

PC and SM lipids were made in DMSO at 2.5 mg/mL. All enzyme assays were performed in 0.1 M Tris-HCl buffer at pH 8.1. To generate kinetic plots with varying acetyl-CoA and constant oxaloacetic acid concentrations, the final concentrations of reaction components in the kinetic runs were as follows: DTNB: 100 µM (from a stock solution of 0.5 mM in 0.5 M Tris-HCl buffer at pH 8.1), oxaloacetic acid: 100 µM (from a stock solution of 2 mM in buffer A), choline metabolite/lipid or control: as depicted in Figure 5.8b, and acetyl-CoA: 5 µM–75 µM (from a stock solution of 1 mM in water). The enzymatic reactions were initiated by adding CS enzyme (194 ng/mL from a stock of 3.87 µg/mL in 0.1 M Tris -HCl buffer at pH 7.0) to the cuvette. To generate kinetic plots with varying oxaloacetic acid and constant acetyl-CoA concentrations, the final concentrations of reaction components in the kinetic runs were as follows: acetyl-CoA: 50 µM (from a stock solution of 1 mM in water), DTNB: 100 µM (from a stock solution of 0.5 mM in 0.5 M Tris-HCl buffer at pH 8.1), choline metabolite/lipid or control: as depicted in Figure 5.8b, and oxaloacetic acid: 5 µM–75 µM (from a stock solution of 1 mM in buffer A). The enzymatic reactions were initiated by adding CS enzyme (194 ng/mL from a stock of 3.87 µg/mL in 0.1 M Tris-HCl buffer at pH 7.0) to the cuvette. The velocity of the enzymatic reaction was monitored by recording the rate of increase in the absorbance at 412 nm which was a result of reduction of DTNB by enzymatically liberated CoA-SH. The K_m and V_{max} values were obtained from the double reciprocal plots that were generated by using the initial velocity of the reactions. The kinetic runs corresponding to each reaction condition were repeated at least three times.

(iii) Glyceraldehyde-3-phosphate dehydrogenase (GAPDH): Enzymatic assays on rabbit muscle GAPDH were performed at 25 °C in a quartz cuvette by using a UV-Vis spectrophotometer by making slight modifications to the procedures described previously.[39, 40] The stock solutions of PC and SM lipids (2.5 mg/mL) were made in DMSO, and those of choline, CDP choline, GPC, sodium chloride , phosphocholine, calcium chloride were made in 15 mM sodium pyrophosphate buffer at pH 8.5 containing 30 mM sodium arsenate (henceforth known as buffer B) at 30 mM. Stock solution of DL-glyceraldehyde-3-phosphate (G-3-P; 7.6 mM), and NAD^+ (4.5 mM) were also made in buffer B. All enzyme assays were performed in buffer B containing 3.3 mM DTT (added from a stock of 100 mM in buffer B). To generate kinetic plots with varying G-3-P and constant NAD^+ concentrations, the final concentrations of reaction components in the kinetic runs were as follows: GAPDH: 0.38 U/mL (added from a stock of 11.4 units/mL in buffer B), NAD^+: 150 µM

(added from a stock of 4.5 mM in buffer B), and choline metabolite/lipid or control: as depicted in Figure 5.10b. The enzymatic reactions were initiated by adding G-3-P (63.3 µM-500 µM from a stock of 7.6 mM in buffer B) to the cuvette. To generate kinetic plots with varying NAD^+ and constant G-3-P concentrations, the final concentrations of reaction components in the kinetic runs were as follows: GAPDH: 0.38 U/mL (added from a stock of 11.4 units/mL in buffer B), choline metabolite/lipid or control: as depicted in Figure 5.10b, and NAD^+: 25 µM-150 µM (from a stock solution of 4.5 mM in buffer B). The enzymatic reactions were initiated by adding G-3-P (126.6 µM from a stock solution of 7.6 mM in buffer B). The velocity of the enzymatic reaction was monitored by recording the rate of increase in the absorbance of NADH at 340 nm and the K_m and V_{max} values were obtained from the double reciprocal plots that were generated by using the initial velocity of the reactions. The kinetic runs corresponding to each reaction were repeated at least three times.

(iv) *Malic enzyme (ME):* Enzymatic assays on chicken liver ME were performed at 25 °C in a 96-well plate by using a microtiter plate reader as per a procedure described previously.[41] The stock solutions of choline, CDP choline, GPC, and sodium chloride were made in water at 20 mM. The stocks solution for phosphocholine and calcium chloride were made in water at 150 mM, and those of PC and SM lipids were made in DMSO at 2.5 mg/mL. All enzyme assays were performed in 66.7 mM triethanolamine-HCl buffer at pH 7.4. To generate kinetic plots with varying malic acid and constant $NADP^+$ concentrations, the final concentrations of reaction components in the kinetic runs were as follows: manganese (II) chloride: 5 mM (from a stock solution of 0.1 M in water), $NADP^+$: 300 µM (from a stock solution of 6 mM in water), choline metabolite/lipid or control: as depicted in Figure 5.9b, and malic acid: 100 µM-1 mM (from a stock of 20 mM in water). The enzymatic reactions were initiated by adding ME (0.033 U/mL from a stock solution of 1 U/mL in 50 mM Tris-HCl buffer at pH 7.5) to the 96-well plate. To generate kinetic plots with varying $NADP^+$ and constant malic acid concentrations, the final concentrations of reaction components in the kinetic runs were as follows: manganese (II) chloride: 5 mM (from a stock solution of 0.1 M in water), malic acid: 800 µM (from a stock of 20 mM in water), choline metabolite/lipid or control: as depicted in Figure 5.9b, and $NADP^+$: 5 µM-500 µM (from a stock solution of 6 mM in water). The enzymatic reactions were initiated by adding ME (0.033 U/mL from a stock solution of 1 U/mL in 50 mM Tris-HCl buffer at pH 7.5) to the 96-well plate. The velocity of the enzymatic

reaction was monitored by recording the rate of increase in the absorbance of NADPH at 340 nm and the K_m and V_{max} values were obtained from the double reciprocal plots that were generated by using the initial velocity of the reactions. The kinetic runs corresponding to each reaction were repeated at least three times.

(v) Glutamate dehydrogenase (GLUD1): Enzymatic assays on bovine liver GLUD1 were performed at 25 °C in a quartz cuvette by using a UV-Vis spectrophotometer as per the procedure described previously.[42] The stock solutions of choline, CDP choline, phosphocholine, GPC, sodium chloride and calcium chloride were made in water at 30 mM, and those of PC and SM lipids were made in DMSO at 2.5 mg/mL. All enzyme assays were performed in 100 mM potassium phosphate buffer at pH 7.0. To generate kinetic plots with varying α-ketoglutarate (α-KG) and constant NADH concentrations, the final concentrations of reaction components in the kinetic runs were as follows: ammonium chloride: 50 mM (from a stock solution of 1.5 M in water), NADH: 150 µM (from a stock solution of 5 mM in water), choline metabolite/lipid or control: as depicted in Figure 5.11b, and α-KG: 100 µM-3 mM (from a stock of 90 mM in water). The enzymatic reactions were initiated by adding GLUD1 (0.16 U/mL from a stock solution of 24 U/mL in 100 mM potassium phosphate buffer at pH 7.0) to the cuvette. To generate kinetic plots with varying NADH and constant α-KG concentrations, the final concentrations of reaction components in the kinetic runs were as follows: ammonium chloride: 50 mM (from a stock solution of 1.5 M in water), α-KG: 250 µM (from a stock solution of 7.5 mM in water), choline metabolite/lipid or control: as depicted in Figure 5.11b, and NADH: 50 µM-100 µM (from a stock of 5 mM in water). The enzymatic reactions were initiated by adding GLUD1 (0.16 U/mL from a stock solution of 24 U/mL in 100 mM potassium phosphate buffer at pH 7.0) to the cuvette. The velocity of the enzymatic reaction was monitored by recording the rate of decrease in the absorbance of NADH at 340 nm and the K_m and V_{max} values were obtained from the double reciprocal plots that were generated by using the initial velocity of the reactions. The kinetic runs corresponding to each reaction were repeated at least three times.

5.5 References

1. Patching, S. G., Surface plasmon resonance spectroscopy for characterisation of membrane protein-ligand interactions and its potential for drug discovery. *Biochim Biophys Acta* **2014,** *1838* (1 Pt A), 43-55.

2. Neumann, T.; Junker, H. D.; Schmidt, K.; Sekul, R., SPR-based fragment screening: advantages and applications. *Curr Top Med Chem* **2007,** *7* (16), 1630-42.

3. Teh, H. F.; Peh, W. Y. X.; Su, X. D.; Thomsen, J. S., Characterization of protein-DNA interactions using surface plasmon resonance spectroscopy with various assay schemes. *Biochemistry* **2007,** *46* (8), 2127-35.

4. Madeira, A.; Ohman, E.; Nilsson, A.; Sjogren, B.; Andren, P. E.; Svenningsson, P., Coupling surface plasmon resonance to mass spectrometry to discover novel protein-protein interactions. *Nat Protoc* **2009,** *4* (7), 1023-37.

5. Gestwicki, J. E.; Hsieh, H. V.; Pitner, J. B., Using receptor conformational change to detect low molecular weight analytes by surface plasmon resonance. *Anal Chem* **2001,** *73* (23), 5732-37.

6. Ladbury, J. E.; Chowdhry, B. Z., Sensing the heat: the application of isothermal titration calorimetry to thermodynamic studies of biomolecular interactions. *Chem Biol* **1996,** *3* (10), 791-801.

7. Yang, G. X.; Li, X.; Snyder, M., Investigating metabolite-protein interactions: an overview of available techniques. *Methods* **2012,** *57* (4), 459-66.

8. Palmer, R. A.; Niwa, H., X-ray crystallographic studies of protein-ligand interactions. *Biochem Soc Trans* **2003,** *31* (Pt 5), 973-79.

9. Martinez Molina, D.; Jafari, R.; Ignatushchenko, M.; Seki, T.; Larsson, E. A.; Dan, C.; Sreekumar, L.; Cao, Y.; Nordlund, P., Monitoring drug target engagement in cells and tissues using the cellular thermal shift assay. *Science* **2013,** *341* (6141), 84-87.

10. Brett, L.; Hao, R.; Jonai, N.; Chin, R. M.; Aghajan, M.; Warburton, S.; Wang, J.; Wu, R. P.; Gomez, F.; Loo, J. A.; Wohlschlegel, J. A.; Vondriska, T. M.; Pelletier, J.; Herschman, H. R.;

Clardy, J.; Clarke, C. F.; Huang, J.,Target identification using drug affinity responsive target stability (DARTS). *Proc Natl Acad Sci U S A* **2009,** *106* (51), 21984-89.

11. Kawatkar, A.; Schefter, M.; Hermansson, N. O.; Snijder, A.; Dekker, N.; Brown, D. G.; Lundback, T.; Zhang, A. X.; Castaldi, M. P., CETSA beyond Soluble Targets: a Broad Application to Multipass Transmembrane Proteins. *ACS Chem Biol* **2019,** *14* (9), 1913-20.

12. Almqvist, H.; Axelsson, H.; Jafari, R.; Dan, C.; Mateus, A.; Haraldsson, M.; Larsson, A.; Martinez Molina, D.; Artursson, P.; Lundback, T.; Nordlund, P., CETSA screening identifies known and novel thymidylate synthase inhibitors and slow intracellular activation of 5-fluorouracil. *Nat Commun* **2016,** *7*, 11040.

13. Chin, R. M.; Fu, X.; Pai, M. Y.; Vergnes, L.; Hwang, H.; Deng, G.; Diep, S.; Lomenick, B.; Meli, V. S.; Monsalve, G. C.; Hu, E.; Whelan, S. A.; Wang, J. X.; Jung, G.; Solis, G. M.; Fazlollahi, F.; Kaweeteerawat, C.; Quach, A.; Nili, M.; Krall, A. S.; Godwin, H. A.; Chang, H. R.; Faull, K. F.; Guo, F.; Jiang, M.; Trauger, S. A.; Saghatelian, A.; Braas, D.; Christofk, H. R.; Clarke, C. F.; Teitell, M. A.; Petrascheck, M.; Reue, K.; Jung, M. E.; Frand, A. R.; Huang, J., The metabolite alpha-ketoglutarate extends lifespan by inhibiting ATP synthase and TOR. *Nature* **2014,** *510* (7505), 397-401.

14. Saha, P.; Datta, K., Multi-functional, multicompartmental hyaluronan-binding protein 1 (HABP1/p32/gC1qR): implication in cancer progression and metastasis. *Oncotarget* **2018,** *9* (12), 10784-807.

15. Ghebrehiwet, B.; Geisbrecht, B. V.; Xu, X.; Savitt, A. G.; Peerschke, E. I. B., The C1q Receptors: Focus on gC1qR/p33 (C1qBP, p32, HABP-1)(1). *Semin Immunol* **2019,** *45*, 101338.

16. Yagi, M.; Uchiumi, T.; Takazaki, S.; Okuno, B.; Nomura, M.; Yoshida, S.; Kanki, T.; Kang, D., p32/gC1qR is indispensable for fetal development and mitochondrial translation: importance of its RNA-binding ability. *Nucleic Acids Res* **2012,** *40* (19), 9717-37.

17. Fogal, V.; Richardson, A. D.; Karmali, P. P.; Scheffler, I. E.; Smith, J. W.; Ruoslahti, E., Mitochondrial p32 protein is a critical regulator of tumor metabolism via maintenance of oxidative phosphorylation. *Mol Cell Biol* **2010,** *30* (6), 1303-18.

18. Deb, T. B.; Datta, K., Molecular cloning of human fibroblast hyaluronic acid-binding protein confirms its identity with P-32, a protein co-purified with splicing factor SF2. Hyaluronic acid-binding protein as P-32 protein, co-purified with splicing factor SF2. *J Biol Chem* **1996,** *271* (4), 2206-12.

19. Berro, R.; Kehn, K.; de la Fuente, C.; Pumfery, A.; Adair, R.; Wade, J.; Colberg-Poley, A. M.; Hiscott, J.; Kashanchi, F., Acetylated Tat regulates human immunodeficiency virus type 1 splicing through its interaction with the splicing regulator p32. *J Virol* **2006,** *80* (7), 3189-204.

20. Kim, K. B.; Yi, J. S.; Nguyen, N.; Lee, J. H.; Kwon, Y. C.; Ahn, B. Y.; Cho, H.; Kim, Y. K.; Yoo, H. J.; Lee, J. S.; Ko, Y. G., Cell-surface receptor for complement component C1q (gC1qR) is a key regulator for lamellipodia formation and cancer metastasis. *J Biol Chem* **2011,** *286* (26), 23093-101.

21. Fogal, V.; Zhang, L.; Krajewski, S.; Ruoslahti, E., Mitochondrial/cell-surface protein p32/gC1qR as a molecular target in tumor cells and tumor stroma. *Cancer Res* **2008,** *68* (17), 7210-18.

22. Song, N.; Zhao, L.; Zhu, M.; Zhao, J., Recent progress in LyP-1-based strategies for targeted imaging and therapy. *Drug Deliv* **2019,** *26* (1), 363-75.

23. Kim, B. C.; Hwang, H. J.; An, H. T.; Lee, H.; Park, J. S.; Hong, J.; Ko, J.; Kim, C.; Lee, J. S.; Ko, Y. G., Antibody neutralization of cell-surface gC1qR/HABP1/SF2-p32 prevents lamellipodia formation and tumorigenesis. *Oncotarget* **2016,** *7* (31), 49972-85.

24. Narahashi, Y.; Yanagita, M., Studies on proteolytic enzymes (pronase) of *Streptomyces griseus* K-1. I. Nature and properties of the proteolytic enzyme system. *J Biochem* **1967,** *62* (6), 633-41.

25. Mori, N.; Wildes, F.; Takagi, T.; Glunde, K.; Bhujwalla, Z. M., The Tumor Microenvironment Modulates Choline and Lipid Metabolism. *Front Oncol* **2016,** *6*, 262.

26. Ackerstaff, E.; Pflug, B. R.; Nelson, J. B.; Bhujwalla, Z. M., Detection of increased choline compounds with proton nuclear magnetic resonance spectroscopy subsequent to malignant transformation of human prostatic epithelial cells. *Cancer Res* **2001,** *61* (9), 3599-603.

27. Gupta, S.; Datta, K., Possible role of hyaluronectin on cell adhesion in rat histiocytoma. *Exp Cell Res* **1991,** *195* (2), 386-94.

28. Liu, Z.; Kato, A.; Oyama, M.; Kozuka-Hata, H.; Arii, J.; Kawaguchi, Y., Role of Host Cell p32 in Herpes Simplex Virus 1 De-Envelopment during Viral Nuclear Egress. *J Virol* **2015,** *89* (17), 8982-98.

29. Kittlesen, D. J.; Chianese-Bullock, K. A.; Yao, Z. Q.; Braciale, T. J.; Hahn, Y. S., Interaction between complement receptor gC1qR and hepatitis C virus core protein inhibits T-lymphocyte proliferation. *J Clin Invest* **2000,** *106* (10), 1239-49.

30. Wang, Y.; Yang, Y.; Wu, S.; Pan, S.; Zhou, C.; Ma, Y.; Ru, Y.; Dong, S.; He, B.; Zhang, C.; Cao, Y., p32 is a novel target for viral protein ICP34.5 of herpes simplex virus type 1 and facilitates viral nuclear egress. *J Biol Chem* **2014,** *289* (52), 35795-805.

31. Van Scoy, S.; Watakabe, I.; Krainer, A. R.; Hearing, J., Human p32: a coactivator for Epstein-Barr virus nuclear antigen-1-mediated transcriptional activation and possible role in viral latent cycle DNA replication. *Virol* **2000,** *275* (1), 145-57.

32. Calnan, B. J.; Biancalana, S.; Hudson, D.; Frankel, A. D., Analysis of arginine-rich peptides from the HIV Tat protein reveals unusual features of RNA-protein recognition. *Genes Dev* **1991,** *5* (2), 201-10.

33. Anders, E.; Nebel, D.; Westman, J.; Herwald, H.; Nilsson, B. O.; Svensson, D., Globular C1q receptor (p33) binds and stabilizes pro-inflammatory MCP-1: a novel mechanism for regulation of MCP-1 production and function. *Biochem J* **2018,** *475* (4), 775-86.

34. Feng, Y.; Xiong, Y.; Qiao, T.; Li, X.; Jia, L.; Han, Y., Lactate dehydrogenase A: A key player in carcinogenesis and potential target in cancer therapy. *Cancer Med* **2018,** *7* (12), 6124-36.

35. Kaul, R.; Saha, P.; Saradhi, M.; Prasad, R. L.; Chatterjee, S.; Ghosh, I.; Tyagi, R. K.; Datta, K., Overexpression of hyaluronan-binding protein 1 (HABP1/p32/gC1qR) in HepG2 cells leads to increased hyaluronan synthesis and cell proliferation by up-regulation of cyclin D1 in AKT-dependent pathway. *J Biol Chem* **2012,** *287* (23), 19750-64.

36. Ghose, S.; Biswas, S.; Datta, K.; Tyagi, R. K., Dynamic Hyaluronan drives liver endothelial cells towards angiogenesis. *BMC Cancer* **2018,** *18* (1), 648.

37. Baskakov, I.; Bolen, D. W., Time-Dependent Effects of Trimethylamine-N-Oxide/Urea on Lactate Dehydrogenase Activity: An Unexplored Dimension of the Adaptation Paradigm. *Biophys J* **1998,** *74* (5), 2658-65.

38. Matsuoka, Y.; Srere, P. A., Kinetic studies of citrate synthase from rat kidney and rat brain. *J Biol Chem* **1973,** *248* (23), 8022-30.

39. Krebs, E. G., Glyceraldehyde-3-phosphate Dehydrogenase from Yeast. *Meth Enzymol* **1955,** *1*.

40. Velick, S., Glyceraldehyde-3-Phosphate Dehydrogenase from Muscle. *Meth Enzymol* **1955**, 401.

41. Chang, G. G.; Huang, T. M.; Wang, J. K.; Lee, H. J.; Chou, W. Y.; Meng, C. L., Kinetic mechanism of the cytosolic malic enzyme from human breast cancer cell line. *Arch Biochem Biophys* **1992,** *296* (2), 468-73.

42. King, K. S.; Frieden, C., The Purification and Physical Properties of Glutamate Dehydrogenase from Rat Liver. *J Biol Chem* **1970,** *245* (17), 4391-96.

Conclusions and Future Directions

The objective of this study was the elucidation of the roles of choline metabolites in mammalian cellular physiology outside of their well-known functions as metabolic intermediates. To address this question, a sequential three-tier work flow consisting of the following components was employed in this thesis: a) metabolic labeling studies to identify a photocrosslinkable choline analog for labeling choline metabolites in mammalian cells, b) establishing a chemoproteomic platform utilizing this analog for the discovery of the mammalian choline metabolite-interacting proteome, and c) studies focused on characterizing the effect of choline metabolites on the function of proteins identified via this platform.

In order to identify a photocrosslinkable choline analog that is accepted as a surrogate to native choline in cells, structure-activity relationship studies targeted at exploring the promiscuity of the Kennedy pathway were warranted. Consequently, in Chapter 2 of this thesis, we tested several choline analogs that were structurally more elaborate than native choline for their metabolic incorporation into the Kennedy pathway. Surprisingly, we found that all of them successfully labeled mammalian choline lipids, thereby revealing the remarkable levels of promiscuity in the mammalian lipidic biosynthetic machinery. This discovery encouraged us to test the bifunctional β-diazirine choline analogs for their metabolic incorporation in Chapter 3. Although metabolic labeling studies on these analogs revealed their successful incorporation into the Kennedy pathway, our UV crosslinking-based experiments demonstrated that these analogs were unsuitable for the discovery of the mammalian choline metabolite-interacting proteome. In our pursuit of understanding these unexpected results, we unveiled a novel choline lipid headgroup remodeling mechanism involving sequential dealkylation and methylation. I anticipate that our discoveries from Chapter 3 shall encourage future studies focused on unraveling the biochemical basis of this mechanism and characterizing its ramifications on lipid homeostasis. Towards elucidating the biochemical mechanism, I envision that identification of the dealkylated intermediates is imperative and that can be achieved by performing LC-MS/MS-based metabolomics studies.

Chapter 4 describes the development of a γ-diazirine choline analog that showed successful incorporation into the Kennedy pathway and was utilized to discover 674 proteins that interacted with choline metabolites and lipids in cells. Survey of these protein hits revealed that many of

them are targets for known drugs. It would be interesting to study the role of the choline metabolites on the drug-protein interfaces.

In Chapter 5, we studied the role of choline metabolites on the function of six different proteins that were identified from our chemoproteomics analysis. Our studies on p32 revealed that phosphocholine is a potent modulator of various aspects of p32 function. These results have important implications in cancer biology not only because p32 plays important roles in cancer progression and is an attractive target for anti-cancer drugs, but also because cancer is accompanied by a marked elevation in the cellular phosphocholine levels. The discovery of phosphocholine binding sites on p32 will be valuable in discerning the mechanism of modulation of p32 by phosphocholine. To this end, the development of a photocrosslinkable analog of phosphocholine to reveal the binding sites on p32 can be deemed as a suitable strategy.

In summary, the work described herein provides insights into choline lipid biology and sheds light on the physiological relevance of choline metabolites outside of their well-established roles as intermediates in the cellular choline lipid biosynthetic pathway. We anticipate that the results of our experiments on the p32 protein will encourage studies focused on interrogating the functional relevance of the interactions of choline metabolites and lipids on other protein hits that our chemoproteomic approach has identified. A detailed understanding of the mechanisms underlying the functional modulation of proteins by choline metabolites and lipids will not only contribute to our understanding of cellular physiology but will also engender efforts focused on targeting these metabolite/lipid-protein interfaces by small molecules for therapeutic purposes.

Appendix

This chapter is adapted with permission from the publication: Dixit, A.; Jose, G. P.; Shanbhag, C.; Tagad, N.; Kalia, J. Metabolic labeling-based chemoproteomics establishes choline metabolites as protein function modulators. *ACS Chem. Biol.* **2022**, *17*, 2272–2283. Copyright 2022 American Chemical Society.

A.1 TIC, XIC and LipidView Plots for the Lipidomics Experiments Performed in Figure 3.6

This section depicts the lipidomics data that was aquired and processed to generate plots in Figure 3.6. It contains:

1. The representative TIC and XIC plots (Figure A1 below) from PIS experiments for detecting **1**-, **10**-, and **11**-labeled lipids in the lipid samples extracted from HEK293 cells that were administered with compound **11** for 4 h, 8 h, 16 h, and 24 h. The area under the TIC peaks was used to generate semi-quantitaive plots in Figure 3.6a and Figure 3.6b (left panel).
2. The representative TIC and XIC plots (Figures A2 and A3 below) from PIS experiments for detecting **1**-, **10**-, and **11**-labeled lipids in the lipid samples extracted from HeLa cells and MDA-MB-231 cells that were administered with compound **11** for 24 h. The area under the TIC peaks was used to generate Figure 3.6b (middle and right panel).

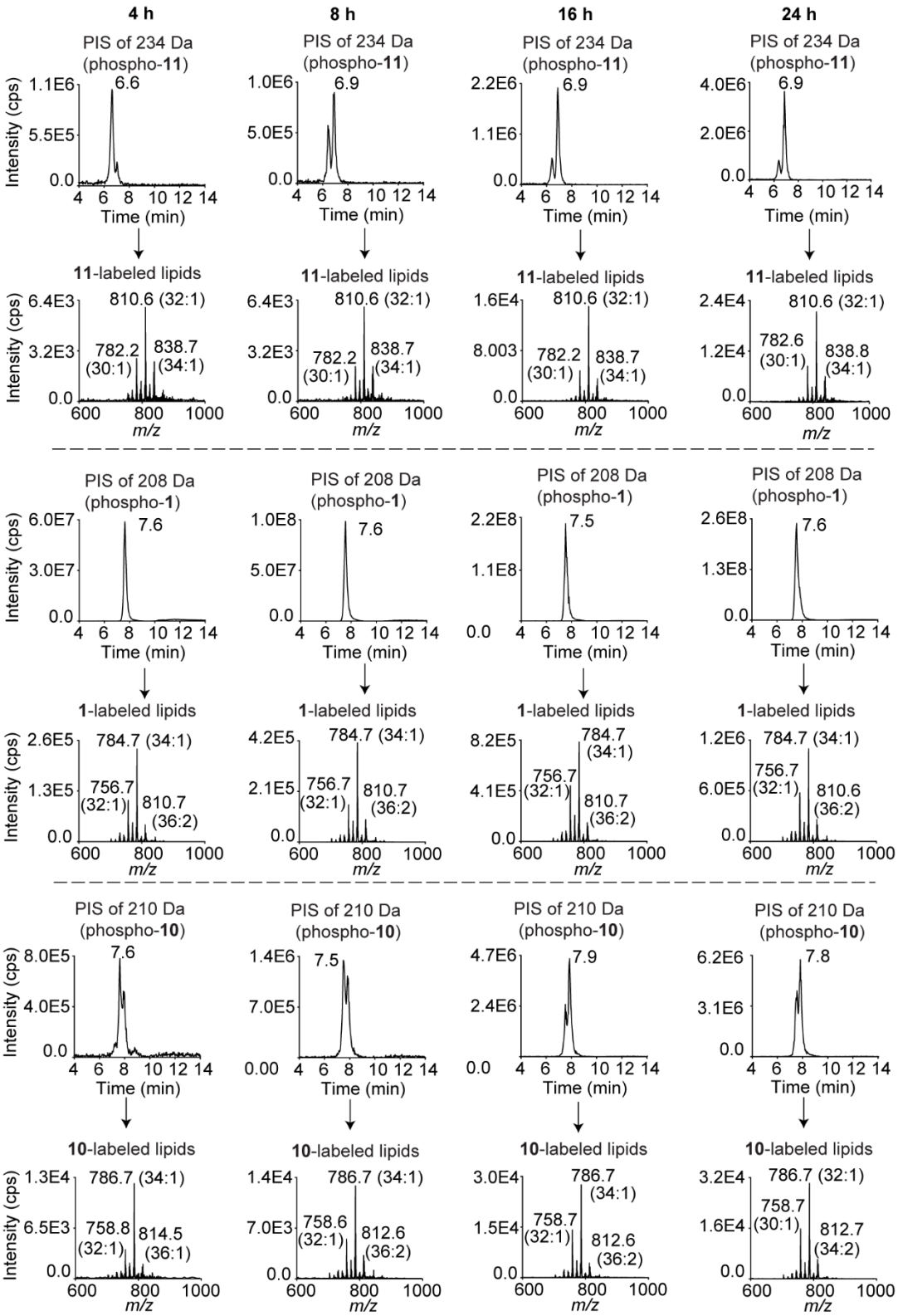

Figure A1. Kinetics for the formation of the metabolically labeled choline lipids produced in HEK293 cells cultured in presence of **11**. *Legend continued in the next page.*

Figure A1 legend continued from the last page. Lipids extracted from HEK293 cells that were administered with **11** (2 mM) for 4 h, 8 h, 16 h, and 24 h were subjected to LC-MS/MS and analyzed for the formation of **11**-, **1**-, and **10**-labeled lipids by employing a PIS of 234 Da, 208 Da, and 210 Da respectively. Each chromatogram is representative of at least three biological replicates. The area under the TIC peaks were manually calculated using the Analyst software to generate the plots in Figure 3.6a and 3.6b (left).

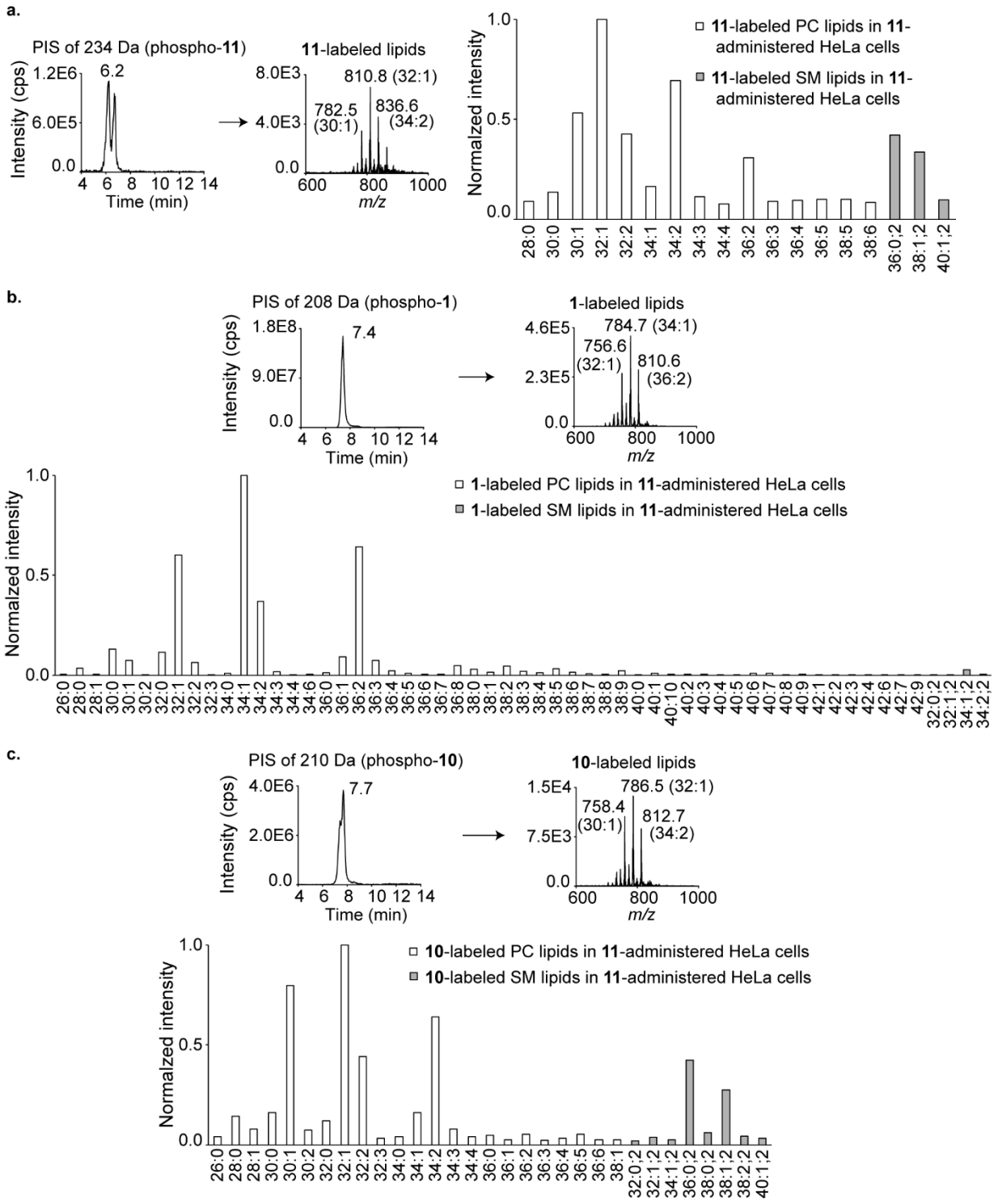

Figure A2. Characterization of the metabolically labeled choline lipids produced in HeLa cells cultured in presence of **11**. *Legend continued in the next page.*

Figure A2 legend continued from the last page. a) Left: Lipids extracted from HeLa cells that were cultured in presence of **11** (2 mM) for 24 h were subjected to LC-MS/MS and analyzed for the formation of **11**-labeled lipids by employing a PIS of 234 Da. The area under the peak on the TIC was manually calculated using the Analyst software to generate the plot on Figure 3.6b (middle). Right: A bar graph obtained from the LipidView software denoting all the **11**-labeled choline lipids identified from the XIC on the left panel. The *y*-axis has been normalized to the most intense peak *i.e.*, lipid 32:1 of the XIC. b) Top: Lipids extracted from HeLa cells that were cultured in presence of **11** (2 mM) for 24 h were subjected to LC-MS/MS and analyzed for the formation of **1**-labeled lipids by employing a PIS of 208 Da. The area under the peak on the TIC was manually calculated using the Analyst software to generate the plot on Figure 3.6b (middle). Bottom: A bar graph obtained from the LipidView software denoting all **1**-labeled choline lipids identified from the XIC on the top panel. The *y*-axis has been normalized to the most intense peak *i.e.*, lipid 34:1 of the XIC. c) Top: Lipids extracted from HeLa cells that were cultured in presence of **11** (2 mM) for 24 h were subjected to LC-MS/MS and analyzed for the formation of **10**-labeled lipids by employing a PIS of 210 Da. The area under the TIC peaks were manually calculated using the Analyst software to generate the plot on Figure 3.6b (middle). Bottom: A bar graph obtained from the LipidView software denoting all **10**-labeled choline lipids identified from the XIC on the top panel. The *y*-axis has been normalized to the most intense peak *i.e.*, lipid 32:1 of the XIC.

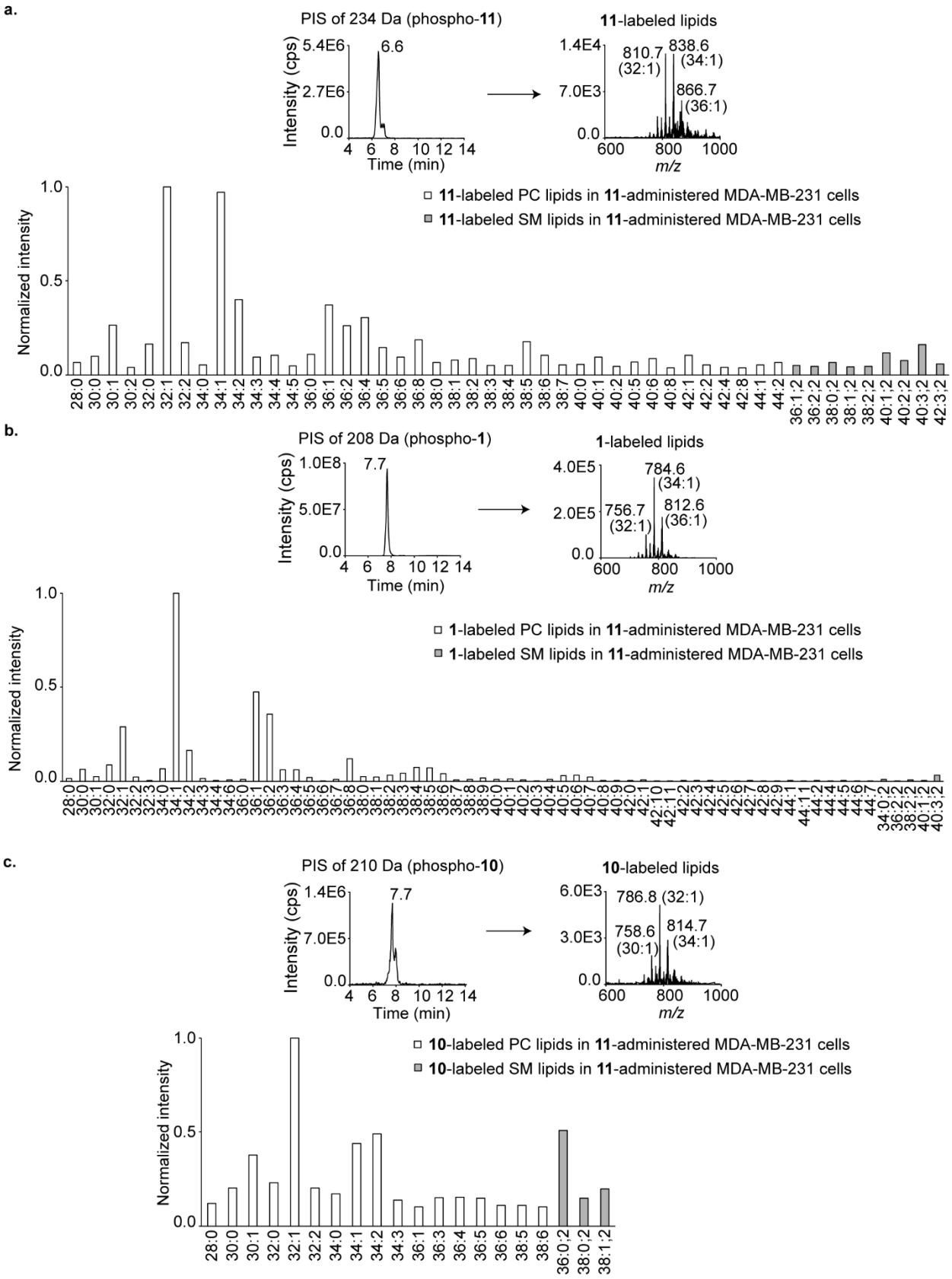

Figure A3. *Legend continued in the next page.*

Figure A3 legend continued from the last page. Characterization of the metabolically labeled choline lipids produced in MDA-MB-231 cells cultured in presence of **11**. a) Top: Lipids extracted from MDA-MB-231 cells that were cultured in presence of **11** (2 mM) for 24 h were subjected to LC-MS/MS and analyzed for the formation of **11**-labeled lipids by employing a PIS of 234 Da. The area under the peak on the TIC was manually calculated using the Analyst software to generate the plot on Figure 3.6b (right). Bottom: A bar graph obtained from the LipidView software denoting all the **11**-labeled choline lipids identified from the XIC on the top panel. The *y*-axis has been normalized to the most intense peak *i.e.*, lipid 32:1 of the XIC. b) Top: Lipids extracted from MDA-MB-23 cells that were cultured in presence of **11** (2 mM) for 24 h were subjected to LC-MS/MS and analyzed for the formation of **1**-labeled lipids by employing a PIS of 208 Da. The area under the peak on the TIC was manually calculated using the Analyst software to generate the plot on Figure 3.6b (right). Bottom: A bar graph obtained from the LipidView software denoting all **1**-labeled choline lipids identified from the XIC on the top panel. The *y*-axis has been normalized to the most intense peak *i.e.*, lipid 34:1 of the XIC. c) Top: Lipids extracted from MDA-MB-23 cells that were cultured in presence of **11** (2 mM) for 24 h were subjected to LC-MS/MS and analyzed for the formation of **10**-labeled lipids by employing a PIS of 210 Da. The area under the TIC peaks were manually calculated using the Analyst software to generate the plot on Figure 3.6b (right). Bottom: A bar graph obtained from the LipidView software denoting all **10**-labeled choline lipids identified from the XIC on the top panel. The *y*-axis has been normalized to the most intense peak *i.e.*, lipid 32:1 of the XIC.

A.2 TIC, XIC and LipidView Plots for the Lipidomics Experiments Performed in Figure 4.5

This section depicts the data that was acquired and processed to generate plots in Figure 4.5. It contains:

1. The representative TIC and XIC plots (Figure A4 below) from PIS experiments for detecting **1**-, **20**-, and **21**-labeled lipids in the lipid samples extracted from HEK293 cells that were administered with compound **21** for 4 h, 8 h, 16 h, and 24 h. The area under the TIC peaks was used to generate semi-quantitative plots in Figure 4.5a and Figure 4.5b (left).

2. The representative TIC and XIC plots (Figure A5 and A6 below) from PIS experiments for detecting **1**-, **20**-, and **21**-labeled lipids in the lipid samples extracted from HeLa cells and MDA-MB-231 cells that were administered with compound **21** for 24 h. The area under the TIC peaks was used to generate Figure 4.5b (middle and right panel).

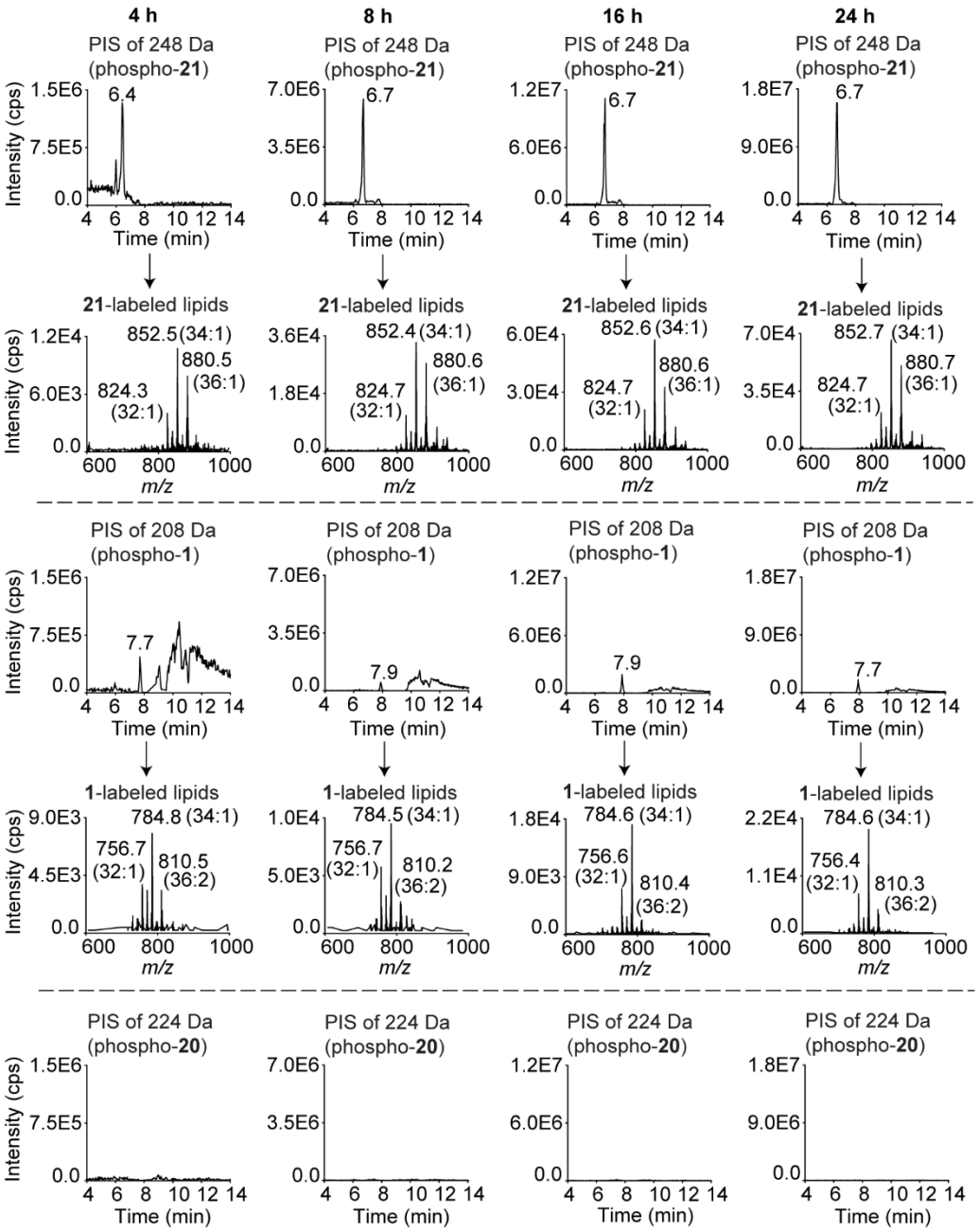

Figure A4. Kinetics for the formation of the metabolically labeled choline lipids in HEK293 cells cultured in presence of **21**. Lipids extracted from HEK293 cells that were administered with **21** (2 mM) for 4 h, 8 h, 16 h, and 24 h were subjected to LC-MS/MS and analyzed for the formation of **21-**, **1-**, and **20**-labeled lipids by employing a PIS of 248 Da, 208 Da, and 224 Da respectively. Each chromatogram is representative of three biological replicates. The area under the TIC peaks was manually calculated using the Analyst software to generate the plot on Figure 4.5a and 4.5b (left).

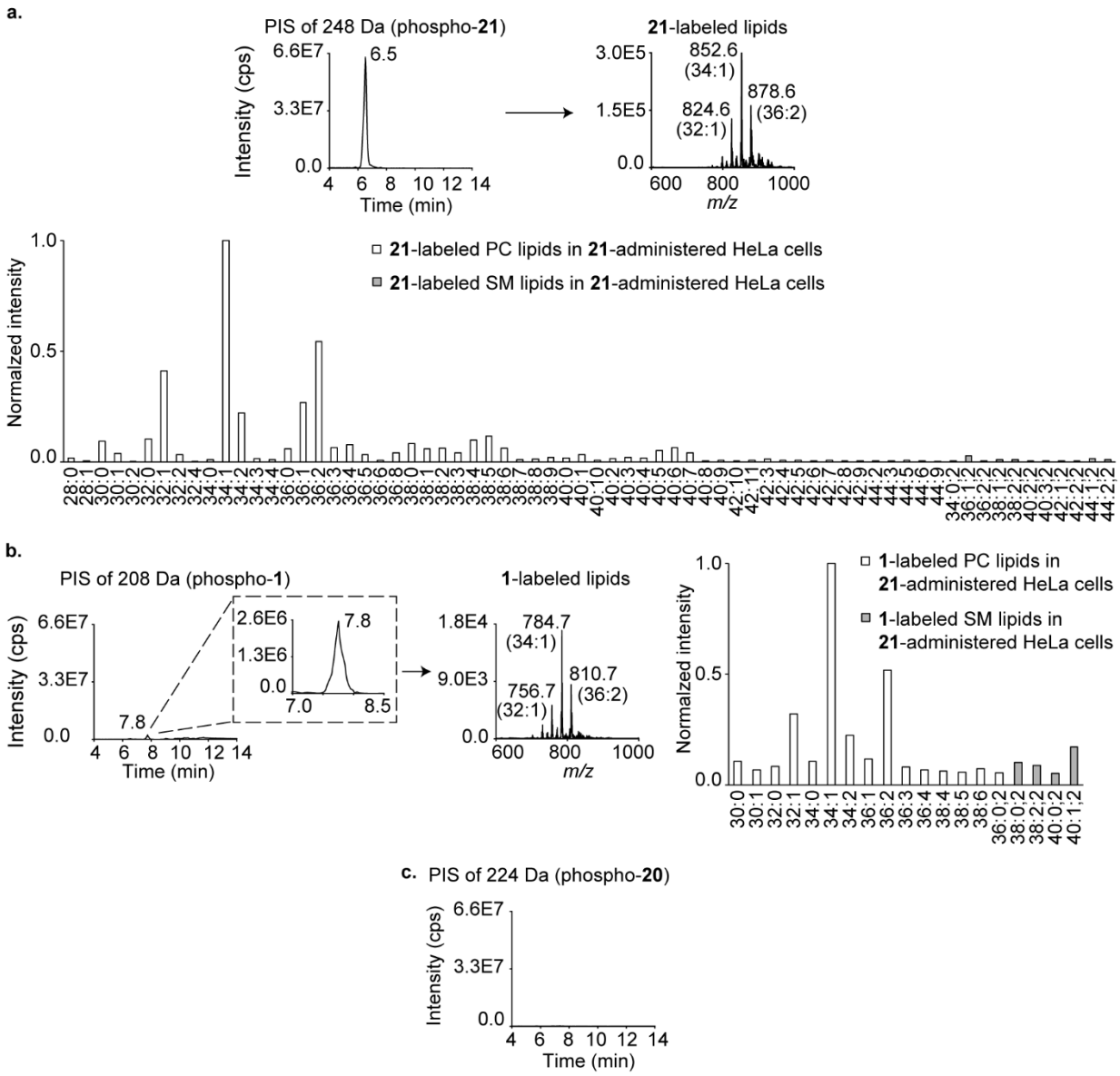

Figure A5. Characterization of the metabolically labeled choline lipids produced in HeLa cells cultured in presence of **21**. a) Top: Lipids extracted from HeLa cells cultured in presence of **21** (2 mM) for 24 h were subjected to LC-MS/MS and analyzed for the formation of **21**-labeled lipids by employing a PIS of 248 Da. The area under the TIC peaks were manually calculated using the Analyst software to generate the plot on Figure 4.5b (middle). Bottom: A bar graph obtained from the LipidView software denoting all **21**-labeled PC and SM lipids identified from the XIC in the top panel. The *y*-axis has been normalized to the most intense peak *i.e.*, lipid 34:1 of the XIC. b) Left: Lipids extracted from HeLa cells cultured for 24 h in presence of **21** (2 mM) were subjected to LC-MS/MS and analyzed for the formation of **1**-labeled lipids by employing a PIS of 208 Da. *Figure legend continued to the next page.*

Figure A5 legend continued from the last page. The area under the peak on the TIC was manually calculated using the Analyst software to generate the plot on Figure 4.5b (middle). Right: A bar graph obtained from the LipidView software denoting all **1**-labeled PC and SM lipids identified from the XIC in the left panel. The *y*-axis has been normalized to the most intense peak *i.e.*, lipid 34:1 of the XIC. c) Lipids extracted from HeLa cells cultured for 24 h in presence of **21** (2 mM) were subjected to LC-MS/MS and analyzed for the formation of **20**-labeled lipids by employing a PIS of 224 Da. The resultant TIC shows no peak for **20**-labeled lipids.

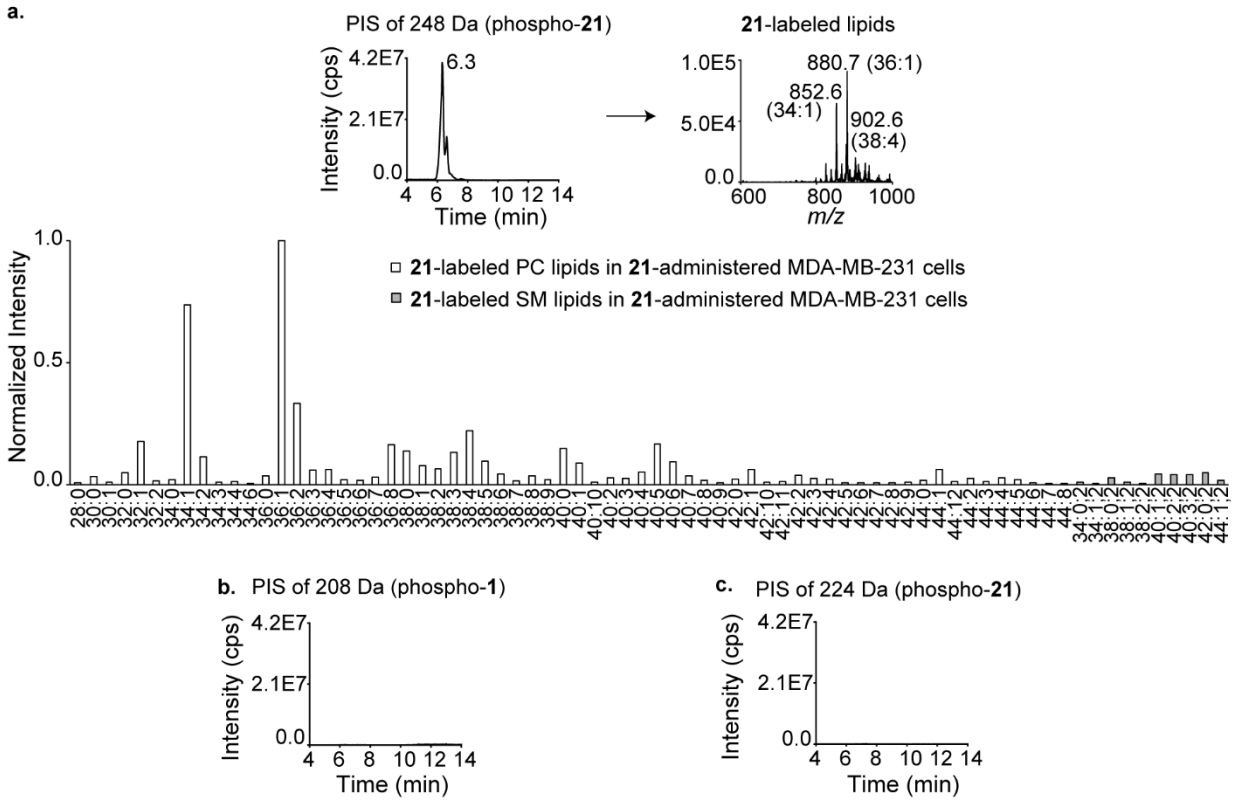

Figure A6. Characterization of the metabolically labeled choline lipids produced in MDA-MB-231 cells cultured in presence of **21**. a) Top: Lipids extracted from MDA-MB-231 cells cultured for 24 h in presence of **21** (2 mM) were subjected to LC-MS/MS and analyzed for the formation of **21**-labeled lipids by employing a PIS of 248 Da. The area under the TIC peaks were manually calculated using the Analyst software to generate the plot on Figure 4.5b (right). Bottom: LipidView analysis of **21**-labeled PC and SM lipids identified from the XIC in the top panel. The *y*-axis has been normalized to the most intense peak *i.e.*, lipid 36:1 of the XIC. b) Lipids extracted from MDA-MB-231 cells cultured for 24 h in presence of **21** (2 mM) were subjected to LC-MS/MS and analyzed for the formation of **1**-labeled lipids by employing a PIS of 208 Da. The resultant TIC shows no peak for **1**-labeled lipids. c) Lipids extracted from MDA-MB-231 cells cultured for 24 h in presence of **21** (2 mM) were subjected to LC-MS/MS and analyzed for the formation of **20**-labeled lipids by employing a PIS of 224 Da. The resultant TIC shows no peak for **20**-labeled lipids.

A.3 Data for Figures 4.8-4.11

This section contains tables depicting the raw proteomics data and the lists of protein hits classified with respect to parameters including expression and functional profiles, involvement in diseases and roles as drug targets.

Table A1. The list of 902 proteins identified from the sixplex TMT experiment with the 674 "high-confidence" protein hits (enrichment ratio ≥ 2 and p value ≤ 0.05) written in red. The remainder proteins that did not meet the aforementioned criteria are written in black. This table was used to generate the plot for -log (p-value) versus $\log_2$ (enrichment ratio) that is depicted in Figure 4.8b.

					Summed Intensity									
S.No.	**UniProt ID**	**Gene ID**	**Protein Name**	**Quantified peptides**	**A1 (-UV)**	**A2 (-UV)**	**A3 -UV)**	**Avg. (-UV)**	**A4 (+UV)**	**A5 (+UV)**	**A6 (+UV)**	**Avg. (+UV)**	**Enrichment Ratio = Avg. (+UV) / Avg.(-UV)**	**p value**
1	Q07021	C1QBP	Complement component 1 Q subcomponent-binding protein (or p32), mitochondrial	9	58.55	65.55	22.20	48.77	2051.48	3154.55	2987.13	2731.05	56.00	1.45E-03
2	P20671	HIST1H2AD	Histone H2A type 1-D	5	29.96	33.98	14.68	26.21	1022.22	1585.50	1712.61	1440.11	54.95	2.64E-03
3	Q71UI9	H2AFV	Histone H2A.V	2	35.86	41.34	14.23	30.47	1096.84	1756.34	1845.65	1566.28	51.40	2.89E-03
4	Q01105	SET	Protein SET	6	86.89	76.38	43.81	69.03	1695.70	2177.85	2550.42	2141.32	31.02	1.12E-03
5	P67809	YBX1	Nuclease-sensitive element-binding protein 1	1	37.36	28.93	17.39	27.89	566.42	728.19	935.93	743.51	26.66	2.61E-03
6	P14406	COX7A2	Cytochrome c oxidase subunit 7A2, mitochondrial	1	20.40	22.34	7.10	16.61	328.85	456.12	464.00	416.32	25.06	8.18E-04
7	Q13765-2	NACA	Isoform 2 of Nascent polypeptide-associated complex subunit alpha	2	23.33	21.36	16.75	20.48	322.20	484.01	559.60	455.27	22.23	3.43E-03
8	Q14978-2	NOLC1	Isoform Beta of Nucleolar and coiled-body phosphoprotein 1	3	50.64	42.03	27.52	40.07	659.77	1052.35	837.81	849.98	21.21	2.05E-03
9	P62158	CALM1	Calmodulin	1	5.87	13.82	4.36	8.01	78.94	164.74	171.41	138.36	17.26	1.21E-02
10	P19338	NCL	Nucleolin	25	1645.69	1160.74	664.19	1156.87	14590.60	21988.20	22395.20	19658.00	16.99	1.92E-03
11	P14314	PRKCSH	Glucosidase 2 subunit beta	2	43.54	46.43	35.39	41.79	564.38	730.17	716.20	670.25	16.04	2.94E-04
12	P05387	RPLP2	60S acidic ribosomal protein P2	5	117.77	114.71	70.62	101.03	1160.08	1576.66	1919.55	1552.10	15.36	2.74E-03
13	P35637	FUS	RNA-binding protein FUS	1	40.98	58.11	25.16	41.42	447.74	606.34	839.54	631.21	15.24	6.67E-03
14	P43307	SSR1	Translocon-associated protein subunit alpha	1	52.70	53.68	34.23	46.87	460.02	657.95	726.92	614.96	13.12	2.10E-03

15	P61604	HSPE1	10 kDa heat shock protein, mitochondrial	2	62.97	61.17	40.86	55.00	542.76	645.28	955.78	714.61	12.99	6.07E-03
16	Q5QNW6-2	HIST2H2BF	Isoform 2 of Histone H2B type 2-F	6	425.44	355.30	129.81	303.52	3117.49	4095.61	4612.71	3941.94	12.99	1.24E-03
17	P11177	PDHB	Pyruvate dehydrogenase E1 component subunit beta, mitochondrial	4	212.43	199.30	110.63	174.12	1481.13	2274.63	2499.76	2085.17	11.98	3.54E-03
18	O60888-2	CUTA	Isoform A of Protein CutA	1	21.38	12.73	11.47	15.20	142.52	175.03	213.51	177.02	11.65	1.46E-03
19	Q92804	TAF15	TATA-binding protein-associated factor 2N	2	115.75	135.65	54.78	102.06	899.71	1042.67	1414.17	1118.85	10.96	2.81E-03
20	Q13247	SRSF6	Serine/arginine-rich splicing factor 6	1	85.79	81.26	74.16	80.40	745.82	1048.20	848.24	880.75	10.95	8.41E-04
21	O60812	HNRNPCL1	Heterogeneous nuclear ribonucleoprotein C-like 1	1	49.74	47.73	19.63	39.04	345.40	454.44	445.61	415.15	10.64	4.89E-04
22	Q9BRL6	SRSF8	Serine/arginine-rich splicing factor 8	1	16.16	17.00	10.34	14.50	117.42	174.02	160.55	150.66	10.39	1.38E-03
23	Q15287	RNPS1	RNA-binding protein with serine-rich domain 1	1	7.22	13.05	4.79	8.36	67.26	100.31	87.50	85.02	10.17	1.51E-03
24	P23396	RPS3	40S ribosomal protein S3	16	1455.87	1023.61	486.01	988.50	9232.43	8826.55	11387.00	9815.33	9.93	4.69E-04
25	Q12849	GRSF1	G-rich sequence factor 1	3	69.70	68.10	40.51	59.44	430.76	600.05	688.04	572.95	9.64	2.51E-03
26	P13073	COX4I1	Cytochrome c oxidase subunit 4 isoform 1, mitochondrial	1	25.59	29.26	14.85	23.23	158.71	217.85	274.57	217.04	9.34	4.54E-03
27	P30048	PRDX3	Thioredoxin-dependent peroxide reductase, mitochondrial	5	549.05	651.80	273.66	491.50	3427.14	4476.32	5759.43	4554.30	9.27	4.02E-03
28	P39687	ANP32A	Acidic leucine-rich nuclear phosphoprotein 32 family member A	3	200.33	195.67	146.90	180.96	1323.16	1625.56	2043.24	1663.99	9.20	2.10E-03
29	Q16629	SRSF7	Serine/arginine-rich splicing factor 7	4	129.40	157.24	68.56	118.40	857.09	1210.34	1166.67	1078.03	9.11	1.10E-03
30	Q16836-2	HADH	Isoform 2 of Hydroxyacyl-coenzyme A dehydrogenase, mitochondrial	1	42.33	50.90	22.07	38.43	250.35	352.47	440.78	347.86	9.05	5.13E-03
31	P13995	MTHFD2	Bifunctional methylenetetrahydrofolate dehydrogenase/cyclohydrolase, mitochondrial	1	17.37	21.01	9.19	15.85	116.30	149.27	161.37	142.31	8.98	8.13E-04
32	P07910	HNRNPC	Heterogeneous nuclear ribonucleoproteins C1/C2	8	441.65	549.33	286.52	425.83	2890.21	4059.96	4365.32	3771.83	8.86	1.84E-03
33	Q13243	SRSF5	Serine/arginine-rich splicing factor 5	1	32.30	25.58	19.39	25.76	167.51	249.71	261.42	226.21	8.78	2.54E-03
34	P38159	RBMX	RNA-binding motif protein, X chromosome	6	281.18	258.25	117.18	218.87	1454.73	2000.89	2259.77	1905.13	8.70	2.26E-03
35	Q14257	RCN2	Reticulocalbin-2	5	106.47	97.21	56.15	86.61	513.29	818.68	907.00	746.32	8.62	5.38E-03
36	P10809	HSPD1	60 kDa heat shock protein, mitochondrial	27	2308.09	2261.48	1001.00	1856.86	12278.30	17228.50	18453.70	15986.83	8.61	1.87E-03
37	P06748	NPM1	Nucleophosmin	11	1012.40	1036.27	537.47	862.05	6018.70	8239.58	7875.99	7378.09	8.56	7.69E-04
38	P06454	PTMA	Prothymosin alpha	1	49.96	29.05	33.50	37.50	203.67	389.61	358.61	317.30	8.46	8.43E-03
39	P27797	CALR	Calreticulin	4	306.77	358.56	182.36	282.57	1808.37	2594.83	2754.89	2386.03	8.44	2.10E-03
40	P35659	DEK	Protein DEK	6	373.15	389.40	239.00	333.85	2149.44	3190.67	3060.80	2800.30	8.39	1.73E-03
41	Q9UJZ1	STOML2	Stomatin-like protein 2, mitochondrial	2	30.75	42.13	25.55	32.81	196.12	300.09	325.41	273.88	8.35	3.77E-03
42	Q9H3G5	CPVL	Probable serine carboxypeptidase CPVL	1	47.23	56.37	29.05	44.22	304.49	348.60	449.05	367.38	8.31	1.76E-03

43	P22695	UQCRC2	Cytochrome b-c1 complex subunit 2, mitochondrial	9	271.25	306.82	156.72	244.93	1538.25	2131.73	2376.71	2015.56	8.23	2.19E-03
44	Q6DN03	HIST2H2BC	Putative histone H2B type 2-C	2	28.14	27.22	21.29	25.55	153.41	215.77	253.47	207.55	8.12	3.40E-03
45	P38117	ETFB	Electron transfer flavoprotein subunit beta	10	542.88	587.09	313.94	481.30	2711.09	4008.52	4576.05	3765.22	7.82	4.18E-03
46	Q9NYK5-2	MRPL39	Isoform 2 of 39S ribosomal protein L39, mitochondrial	3	103.38	105.35	57.89	88.87	514.62	693.83	851.31	686.59	7.73	3.72E-03
47	Q4G0N4	NADK2	NAD kinase 2, mitochondrial	2	97.48	108.04	57.19	87.57	507.35	677.66	838.38	674.46	7.70	3.74E-03
48	P82979	SARNP	SAP domain-containing ribonucleoprotein	1	68.58	85.43	41.14	65.05	351.37	543.10	597.34	497.27	7.64	4.66E-03
49	P84103	SRSF3	Serine/arginine-rich splicing factor 3	3	308.35	320.13	232.90	287.13	1744.31	2601.46	2212.31	2186.03	7.61	1.59E-03
50	P04181	OAT	Ornithine aminotransferase, mitochondrial	10	370.98	398.49	233.15	334.21	1907.41	2572.38	3122.88	2534.22	7.58	3.45E-03
51	O75475	PSIP1	PC4 and SFRS1-interacting protein	3	175.56	200.69	91.04	155.76	824.68	1274.02	1404.19	1167.63	7.50	4.79E-03
52	Q9NP92	MRPS30	28S ribosomal protein S30, mitochondrial	2	56.78	57.70	32.46	48.98	265.88	408.61	421.96	365.48	7.46	3.34E-03
53	P08670	VIM	Vimentin	13	603.85	622.69	369.12	531.89	3022.32	4230.96	4473.53	3908.94	7.35	1.78E-03
54	P09622	DLD	Dihydrolipoyl dehydrogenase, mitochondrial	11	850.71	905.38	416.91	724.33	3867.71	5629.60	6203.30	5233.54	7.23	3.31E-03
55	P67936	TPM4	Tropomyosin alpha-4 chain	5	216.72	203.19	155.57	191.83	1132.91	1415.30	1549.72	1365.98	7.12	6.99E-04
56	P62995	TRA2B	Transformer-2 protein homolog beta	2	117.77	144.27	72.18	111.40	692.42	897.99	777.76	789.39	7.09	4.29E-04
57	P07197	NEFM	Neurofilament medium polypeptide	2	84.83	94.28	42.69	73.93	394.56	538.94	627.53	520.34	7.04	3.06E-03
58	Q13685	AAMP	Angio-associated migratory cell protein	1	14.22	13.00	7.51	11.58	67.41	79.76	94.88	80.69	6.97	1.09E-03
59	O75947	ATP5H	ATP synthase subunit d, mitochondrial	2	37.39	50.98	19.03	35.80	168.21	263.65	308.24	246.70	6.89	7.58E-03
60	P20674	COX5A	Cytochrome c oxidase subunit 5A, mitochondrial	2	89.94	82.50	40.21	70.88	386.72	511.40	563.47	487.20	6.87	1.60E-03
61	Q92552	MRPS27	28S ribosomal protein S27, mitochondrial	4	290.32	339.13	183.99	271.15	1455.92	1841.05	2175.91	1824.29	6.73	1.88E-03
62	P06576	ATP5B	ATP synthase subunit beta, mitochondrial	15	1170.09	986.28	441.59	865.99	4532.03	6333.88	6276.84	5714.25	6.60	1.54E-03
63	J3KN67	TPM3	Tropomyosin alpha-3 chain	4	145.44	123.88	73.40	114.24	641.52	727.62	886.80	751.98	6.58	1.05E-03
64	Q7Z2W9	MRPL21	39S ribosomal protein L21, mitochondrial	2	56.36	61.64	28.91	48.97	229.48	352.20	376.95	319.54	6.53	4.42E-03
65	P54105	CLNS1A	Methylosome subunit pICln	1	23.83	20.88	14.10	19.61	92.42	132.18	156.91	127.17	6.49	4.80E-03
66	Q9H2U2-2	PPA2	Isoform 2 of Inorganic pyrophosphatase 2, mitochondrial	1	53.34	47.83	34.96	45.38	193.91	304.43	383.28	293.87	6.48	1.08E-02
67	Q99623	PHB2	Prohibitin-2	1	17.24	16.47	9.52	14.41	74.52	101.32	103.38	93.08	6.46	1.21E-03
68	Q92688	ANP32B	Acidic leucine-rich nuclear phosphoprotein 32 family member B	5	235.03	228.36	152.42	205.27	1021.21	1300.89	1627.73	1316.61	6.41	3.30E-03
69	O14561	NDUFAB1	Acyl carrier protein, mitochondrial	1	8.40	4.27	5.63	6.10	39.89	38.71	38.47	39.02	6.39	1.40E-05
70	Q7Z4V5	HDGFRP2	Hepatoma-derived growth factor-related protein 2	1	13.79	6.57	10.11	10.16	53.14	64.17	76.69	64.67	6.37	1.56E-03
71	P49006	MARCKSL1	MARCKS-related protein	1	24.15	23.30	12.96	20.14	99.75	120.76	161.37	127.29	6.32	4.37E-03

72	P24666	ACP1	Low molecular weight phosphotyrosine protein phosphatase	4	107.76	108.73	69.14	95.21	525.86	530.63	747.48	601.32	6.32	2.42E-03
73	Q8NAB5		Putative uncharacterized protein FLJ35645 PE	1	50.76	49.59	29.86	43.40	224.79	286.87	309.15	273.60	6.30	9.17E-04
74	P13804	ETFA	Electron transfer flavoprotein subunit alpha, mitochondrial	4	304.97	340.63	161.40	269.00	1218.05	1807.24	2058.50	1694.60	6.30	5.02E-03
75	Q07955-2	SRSF1	Isoform ASF-2 of Serine/arginine-rich splicing factor 1	7	368.43	338.70	226.78	311.30	1468.16	2225.93	2185.51	1959.87	6.30	2.73E-03
76	Q00059	TFAM	Transcription factor A, mitochondrial	5	549.01	557.70	271.28	459.33	2031.73	3037.12	3588.84	2885.90	6.28	6.46E-03
77	P29966	MARCKS	Myristoylated alanine-rich C-kinase substrate	4	265.71	233.04	126.27	208.34	1028.51	1274.92	1591.85	1298.43	6.23	2.93E-03
78	P62979	RPS27A	Ubiquitin-40S ribosomal protein S27a	4	259.84	165.04	210.93	211.94	778.48	1279.35	1902.39	1320.07	6.23	2.74E-02
79	Q5SSJ5	HP1BP3	Heterochromatin protein 1-binding protein 3	1	40.23	32.60	27.67	33.50	142.47	247.77	226.71	205.65	6.14	6.02E-03
80	Q9UKM9	RALY	RNA-binding protein Raly	2	45.17	39.05	28.05	37.42	181.19	238.63	261.42	227.08	6.07	1.47E-03
81	P35269	GTF2F1	General transcription factor IIF subunit 1	1	16.86	18.66	12.80	16.11	77.63	98.13	116.68	97.48	6.05	2.04E-03
82	O75439	PMPCB	Mitochondrial-processing peptidase subunit beta	4	389.95	384.93	220.67	331.85	1534.66	2099.56	2344.00	1992.74	6.00	2.51E-03
83	P09001	MRPL3	39S ribosomal protein L3, mitochondrial	1	132.59	150.90	81.22	121.57	547.39	745.36	888.31	727.02	5.98	3.90E-03
84	Q8NI60	ADCK3	Chaperone activity of bc1 complex-like, mitochondrial	1	39.45	53.19	24.20	38.95	179.97	231.35	280.24	230.52	5.92	3.14E-03
85	O14773	TPP1	Tripeptidyl-peptidase 1	1	20.71	18.90	12.12	17.24	72.93	108.51	123.67	101.70	5.90	5.21E-03
86	P30042	C21orf33	ES1 protein homolog, mitochondrial	2	218.88	216.49	122.58	185.98	797.08	1147.19	1271.28	1071.85	5.76	3.68E-03
87	Q9NUJ1	ABHD10	Mycophenolic acid acyl-glucuronide esterase, mitochondrial	1	29.22	27.48	16.76	24.49	110.83	153.59	155.20	139.87	5.71	1.55E-03
88	P36542	ATP5C1	ATP synthase subunit gamma, mitochondrial	5	198.75	210.10	98.51	169.12	755.49	1031.02	1107.77	964.76	5.70	2.12E-03
89	O95831	AIFM1	Apoptosis-inducing factor 1, mitochondrial	7	432.08	458.53	238.53	376.38	1652.23	2442.61	2341.53	2145.46	5.70	2.36E-03
90	Q15293	RCN1	Reticulocalbin-1	2	77.63	71.32	44.30	64.42	283.04	383.70	428.95	365.23	5.67	2.46E-03
91	Q8IYB3	SRRM1	Serine/arginine repetitive matrix protein 1	2	233.87	312.49	189.44	245.27	1238.13	1516.22	1407.63	1387.33	5.66	2.08E-04
92	O75390	CS	Citrate synthase, mitochondrial	10	1011.87	1071.57	536.07	873.17	3598.10	5333.16	5882.05	4937.77	5.66	4.58E-03
93	Q9UII2	ATPIF1	ATPase inhibitor, mitochondrial	3	180.52	151.11	82.65	138.09	641.24	817.16	881.32	779.91	5.65	1.15E-03
94	Q13428-4	TCOF1	Isoform 4 of Treacle protein	3	70.59	73.92	45.39	63.30	299.47	403.55	362.09	355.04	5.61	7.62E-04
95	P27824	CANX	Calnexin	4	363.35	444.05	227.31	344.90	1431.43	2166.04	2135.00	1910.82	5.54	3.22E-03
96	Q9BTT0	ANP32E	Acidic leucine-rich nuclear phosphoprotein 32 family member E	1	91.18	87.66	50.71	76.52	351.33	413.08	495.39	419.93	5.49	1.42E-03
97	Q9Y3B9	RRP15	RRP15-like protein	1	63.84	77.86	44.34	62.02	259.31	367.61	393.96	340.30	5.49	2.77E-03
98	Q08170	SRSF4	Serine/arginine-rich splicing factor 4	4	212.64	197.10	125.18	178.31	868.33	1104.25	894.29	955.62	5.36	6.10E-04
99	Q15459	SF3A1	Splicing factor 3A subunit 1	2	88.17	110.16	59.70	86.01	343.63	499.30	532.33	458.42	5.33	3.42E-03
100	Q7L0Y3	TRMT10C	Mitochondrial ribonuclease P protein 1	1	41.20	42.66	21.01	34.96	134.85	195.80	225.70	185.45	5.31	5.52E-03

101	P10515	DLAT	Dihydrolipoyllysine-residue acetyltransferase component of pyruvate dehydrogenase complex, mitochondrial	9	605.05	635.00	338.14	526.07	2163.86	2957.47	3236.02	2785.78	5.30	2.51E-03
102	Q13283	G3BP1	Ras GTPase-activating protein-binding protein 1	1	15.61	10.26	10.28	12.05	48.08	63.65	79.00	63.58	5.28	4.80E-03
103	Q13595	TRA2A	Transformer-2 protein homolog alpha	2	44.08	40.20	27.99	37.42	146.32	226.06	210.47	194.28	5.19	3.23E-03
104	Q9BZE1	MRPL37	39S ribosomal protein L37, mitochondrial	3	92.49	97.59	53.43	81.17	304.56	441.83	514.62	420.34	5.18	5.80E-03
105	P10606	COX5B	Cytochrome c oxidase subunit 5B, mitochondrial	1	56.37	59.23	25.81	47.14	189.22	255.11	285.62	243.32	5.16	2.97E-03
106	Q9Y266	NUDC	Nuclear migration protein nudC	2	110.85	71.30	74.77	85.64	286.78	607.44	429.27	441.16	5.15	1.91E-02
107	Q96RP9-2	GFM1	Isoform 2 of Elongation factor G, mitochondrial	1	58.93	55.25	34.43	49.54	186.08	279.70	297.61	254.47	5.14	4.43E-03
108	P62805	HIST1H4A	Histone H4	5	538.36	452.43	195.10	395.30	1849.04	2281.85	1958.57	2029.82	5.13	5.95E-04
109	O94925	GLS	Glutaminase kidney isoform, mitochondrial	3	113.51	122.48	59.74	98.58	367.28	498.33	646.81	504.14	5.11	8.15E-03
110	P25705	ATP5A1	ATP synthase subunit alpha, mitochondrial	17	1642.06	1671.16	847.22	1386.81	5260.05	7868.37	8146.82	7091.75	5.11	3.99E-03
111	O43615	TIMM44	Mitochondrial import inner membrane translocase subunit TIM44	3	155.62	153.12	94.30	134.35	507.95	735.06	814.86	685.96	5.11	4.23E-03
112	Q13242	SRSF9	Serine/arginine-rich splicing factor 9	3	124.81	153.84	89.32	122.66	479.11	668.30	718.28	621.90	5.07	2.67E-03
113	Q8NC51	SERBP1	Plasminogen activator inhibitor 1 RNA-binding protein	4	304.67	243.48	151.97	233.38	966.51	1274.06	1305.85	1182.14	5.07	1.26E-03
114	Q9C0C9	UBE2O	Ubiquitin-conjugating enzyme E2 O	1	8.91	7.50	10.22	8.88	34.99	49.94	49.06	44.66	5.03	1.88E-03
115	Q14444	CAPRIN1	Caprin-1	5	261.80	285.31	183.42	243.51	1050.50	1161.27	1416.43	1209.40	4.97	1.02E-03
116	Q99733	NAP1L4	Nucleosome assembly protein 1-like 4	2	60.65	45.14	33.03	46.27	165.08	254.56	268.54	229.39	4.96	5.38E-03
117	P04844	RPN2	Dolichyl-diphosphooligosaccharide--protein glycosyltransferase subunit 2	4	207.52	192.17	111.23	170.31	664.69	922.45	937.26	841.46	4.94	1.99E-03
118	P49321-3	NASP	Isoform 3 of Nuclear autoantigenic sperm protein	4	184.70	182.53	119.79	162.34	645.44	815.27	941.99	800.90	4.93	1.96E-03
119	Q05519	SRSF11	Serine/arginine-rich splicing factor 11	1	47.29	57.14	27.83	44.09	172.15	236.63	242.45	217.08	4.92	2.00E-03
120	P25788	PSMA3	Proteasome subunit alpha type-3	1	55.89	43.00	35.97	44.95	170.48	232.31	259.49	220.76	4.91	2.86E-03
121	P09429	HMGB1	High mobility group protein B1	3	287.37	280.28	194.50	254.05	1064.90	1253.05	1419.12	1245.69	4.90	7.43E-04
122	P82933	MRPS9	28S ribosomal protein S9, mitochondrial	1	51.46	54.29	32.79	46.18	162.80	248.05	268.34	226.40	4.90	5.48E-03
123	Q5JPH6	EARS2	Probable glutamate--tRNA ligase, mitochondrial	1	25.87	25.88	25.80	25.85	79.31	174.66	125.70	126.56	4.90	2.16E-02
124	P46087-4	NOP2	Isoform 4 of Putative ribosomal RNA methyltransferase NOP2	4	174.50	176.17	131.38	160.68	577.96	921.58	848.10	782.55	4.87	4.14E-03
125	P49411	TUFM	Elongation factor Tu, mitochondrial	19	1655.84	1712.20	886.75	1418.26	5556.53	7407.74	7757.22	6907.16	4.87	1.70E-03
126	Q9Y371-2	SH3GLB1	Isoform 2 of Endophilin-B1	1	32.13	30.10	19.66	27.30	104.69	119.89	172.91	132.50	4.85	7.48E-03
127	Q5JRX3-2	PITRM1	Isoform 2 of Presequence protease, mitochondrial	4	90.22	88.83	50.50	76.52	261.62	412.23	439.99	371.28	4.85	6.61E-03

128	Q3ZCQ8-2	TIMM50	Isoform 2 of Mitochondrial import inner membrane translocase subunit TIM50	1	26.55	28.27	16.58	23.80	95.06	127.38	119.29	113.91	4.79	9.67E-04
129	P45973	CBX5	Chromobox protein homolog 5	1	56.18	65.04	32.30	51.17	177.93	250.56	299.08	242.52	4.74	6.35E-03
130	O75027-2	ABCB7	Isoform 2 of ATP-binding cassette sub-family B member 7, mitochondrial	2	106.82	122.16	54.05	94.34	357.26	443.09	539.99	446.78	4.74	3.40E-03
131	P30084	ECHS1	Enoyl-CoA hydratase, mitochondrial	3	256.98	195.92	99.77	184.22	776.69	915.24	922.11	871.34	4.73	4.77E-04
132	P55809	OXCT1	Succinyl-CoA:3-ketoacid coenzyme A transferase 1, mitochondrial	1	66.39	70.58	42.61	59.86	207.09	318.55	321.97	282.54	4.72	4.54E-03
133	P38646	HSPA9	Stress-70 protein, mitochondrial	24	2213.44	2279.77	1248.88	1914.03	7069.83	9851.28	10168.90	9030.00	4.72	2.38E-03
134	P50213	IDH3A	Isocitrate dehydrogenase [NAD] subunit alpha, mitochondrial	5	298.04	309.98	211.99	273.34	963.87	1456.35	1400.73	1273.65	4.66	3.24E-03
135	Q9NSE4	IARS2	Isoleucine--tRNA ligase, mitochondrial	12	845.02	862.93	487.98	731.98	2526.04	3611.58	3959.51	3365.71	4.60	4.20E-03
136	Q9UKV3	ACIN1	Apoptotic chromatin condensation inducer in the nucleus	1	22.83	25.46	14.07	20.79	80.75	114.03	91.65	95.48	4.59	1.98E-03
137	P0C7P4	UQCRFS1P1	Putative cytochrome b-c1 complex subunit Rieske-like protein 1	1	40.74	60.34	29.42	43.50	138.79	193.72	264.38	198.96	4.57	1.43E-02
138	P08621	SNRNP70	U1 small nuclear ribonucleoprotein 70 kDa	2	176.18	124.09	71.38	123.88	402.64	624.32	665.23	564.07	4.55	7.18E-03
139	Q96EY4	TMA16	Translation machinery-associated protein 16	1	38.91	31.98	23.56	31.49	110.41	138.87	180.33	143.20	4.55	5.78E-03
140	Q08945	SSRP1	FACT complex subunit SSRP1	6	547.47	476.69	336.97	453.71	1550.90	2240.60	2363.80	2051.77	4.52	3.57E-03
141	Q01844-5	EWSR1	Isoform 5 of RNA-binding protein EWS	1	74.73	98.95	41.91	71.86	296.17	278.67	395.42	323.42	4.50	3.25E-03
142	P55209	NAP1L1	Nucleosome assembly protein 1-like 1	4	378.48	358.55	206.33	314.45	1274.89	1339.21	1625.70	1413.27	4.49	8.09E-04
143	Q9H9J2	MRPL44	39S ribosomal protein L44, mitochondrial	2	118.85	121.27	86.25	108.79	380.52	525.39	557.75	487.89	4.48	2.43E-03
144	P28331-2	NDUFS1	Isoform 2 of NADH-ubiquinone oxidoreductase 75 kDa subunit, mitochondrial	4	298.67	324.94	162.59	262.06	871.30	1241.39	1411.25	1174.65	4.48	5.47E-03
145	P24752	ACAT1	Acetyl-CoA acetyltransferase, mitochondrial	5	330.72	360.43	190.79	293.98	977.09	1449.93	1507.60	1311.54	4.46	4.45E-03
146	Q16891	IMMT	Mitochondrial inner membrane protein	4	323.48	395.82	264.65	327.98	1146.70	1581.46	1623.65	1450.60	4.42	2.03E-03
147	P68431	HIST1H3A	Histone H3.1	3	539.88	500.63	235.13	425.21	1365.16	2151.07	2125.62	1880.62	4.42	6.12E-03
148	P30044	PRDX5	Peroxiredoxin-5, mitochondrial	2	135.68	130.48	77.35	114.50	380.60	543.28	591.55	505.14	4.41	4.19E-03
149	Q9H1E3	NUCKS1	Nuclear ubiquitous casein and cyclin-dependent kinase substrate 1	2	74.51	157.58	105.76	112.62	402.98	604.98	465.42	491.12	4.36	4.20E-03
150	P53597	SUCLG1	Succinyl-CoA ligase [ADP/GDP-forming] subunit alpha, mitochondrial	2	78.71	92.59	46.07	72.45	229.29	344.96	373.52	315.92	4.36	6.21E-03
151	Q8TCS8	PNPT1	Polyribonucleotide nucleotidyltransferase 1, mitochondrial	2	292.13	302.11	142.95	245.73	820.88	1129.72	1262.40	1071.00	4.36	4.20E-03
152	P14625	HSP90B1	Endoplasmin	21	2530.01	2676.68	1423.34	2210.01	7499.83	10597.70	10769.90	9622.48	4.35	2.83E-03
153	O60783	MRPS14	28S ribosomal protein S14, mitochondrial	1	62.76	63.07	33.23	53.02	176.55	244.54	267.85	229.65	4.33	3.73E-03
154	P55786	NPEPPS	Puromycin-sensitive aminopeptidase	16	1625.71	1381.94	986.12	1331.26	4775.90	5702.64	6818.49	5765.68	4.33	2.01E-03

155	Q96EY1	DNAJA3	DnaJ homolog subfamily A member 3, mitochondrial	3	121.38	135.92	68.41	108.57	381.55	473.36	554.92	469.94	4.33	2.61E-03
156	P30405	PPIF	Peptidyl-prolyl cis-trans isomerase F, mitochondrial	1	110.87	120.06	61.28	97.40	277.54	470.22	509.22	418.99	4.30	1.21E-02
157	P35268	RPL22	60S ribosomal protein L22	2	231.97	206.54	105.42	181.31	596.04	791.01	932.29	773.11	4.26	4.85E-03
158	P08865	RPSA	40S ribosomal protein SA	2	63.47	54.04	36.38	51.30	187.08	224.17	242.01	217.76	4.25	7.64E-04
159	O95202	LETM1	LETM1 and EF-hand domain-containing protein 1, mitochondrial	6	492.20	577.61	287.69	452.50	1443.64	2059.21	2244.85	1915.90	4.23	4.70E-03
160	Q9HAV7	GRPEL1	GrpE protein homolog 1, mitochondrial	4	260.96	304.68	197.33	254.32	809.55	1180.95	1235.68	1075.39	4.23	3.94E-03
161	P40926	MDH2	Malate dehydrogenase, mitochondrial	16	1796.49	1946.47	920.35	1554.44	4976.12	6987.55	7715.00	6559.56	4.22	4.71E-03
162	P42166	TMPO	Lamina-associated polypeptide 2, isoform alpha	3	119.81	142.57	71.74	111.37	351.20	507.30	545.80	468.10	4.20	4.81E-03
163	O75312	ZNF259	Zinc finger protein ZPR1	1	34.56	34.52	20.70	29.93	86.82	128.56	161.65	125.67	4.20	1.24E-02
164	Q9P015	MRPL15	39S ribosomal protein L15, mitochondrial	1	30.73	23.28	10.45	21.49	63.81	99.43	106.83	90.02	4.19	9.22E-03
165	Q13185	CBX3	Chromobox protein homolog 3	1	109.43	104.34	59.60	91.12	287.38	358.30	491.77	379.15	4.16	9.68E-03
166	Q6P1L8	MRPL14	39S ribosomal protein L14, mitochondrial	2	84.91	82.57	49.53	72.33	210.09	333.57	350.92	298.19	4.12	7.85E-03
167	P43487	RANBP1	Ran-specific GTPase-activating protein	2	241.51	196.19	146.67	194.79	630.81	828.87	937.77	799.15	4.10	3.00E-03
168	P42126	ECI1	Enoyl-CoA delta isomerase 1, mitochondrial	1	51.87	63.82	28.10	47.93	140.54	211.79	232.68	195.00	4.07	7.84E-03
169	P35232	PHB	Prohibitin	10	688.87	743.81	394.92	609.20	1856.81	2700.64	2861.62	2473.02	4.06	4.83E-03
170	P23528	CFL1	Cofilin-1	7	602.47	561.47	388.54	517.49	1850.61	1947.09	2485.72	2094.47	4.05	1.63E-03
171	P31930	UQCRC1	Cytochrome b-c1 complex subunit 1, mitochondrial	5	241.85	220.82	118.02	193.56	542.60	880.93	910.52	778.02	4.02	9.23E-03
172	Q9NVV4-2	MTPAP	Isoform 2 of Poly(A) RNA polymerase, mitochondrial	1	32.45	37.20	22.13	30.59	96.90	115.91	155.60	122.80	4.01	6.68E-03
173	P62750	RPL23A	60S ribosomal protein L23a	2	222.36	166.33	94.63	161.11	533.74	649.19	756.23	646.38	4.01	2.81E-03
174	P61978-3	HNRNPK	Isoform 3 of Heterogeneous nuclear ribonucleoprotein K	15	1350.64	1313.90	723.36	1129.30	3521.20	4950.56	4966.77	4479.51	3.97	3.00E-03
175	P48735	IDH2	Isocitrate dehydrogenase [NADP], mitochondrial	3	120.45	129.16	81.38	110.33	330.77	493.43	486.54	436.91	3.96	4.06E-03
176	P09651	HNRNPA1	Heterogeneous nuclear ribonucleoprotein A1	6	490.33	558.32	260.45	436.37	1138.48	1986.03	2058.90	1727.80	3.96	1.39E-02
177	P16402	HIST1H1D	Histone H1.3	5	315.80	1111.24	414.06	613.70	1959.13	2461.61	2868.58	2429.77	3.96	7.48E-03
178	P62304	SNRPE	Small nuclear ribonucleoprotein E	2	131.01	129.49	64.10	108.20	374.78	454.01	454.62	427.80	3.95	7.54E-04
179	P31942	HNRNPH3	Heterogeneous nuclear ribonucleoprotein H3	3	269.92	297.30	155.83	241.02	717.08	1046.83	1084.06	949.32	3.94	4.70E-03
180	P22626	HNRNPA2B1	Heterogeneous nuclear ribonucleoproteins A2/B1	13	1590.62	1387.56	621.39	1199.86	3583.07	5264.45	5286.98	4711.50	3.93	5.28E-03
181	P58546	MTPN	Myotrophin	1	30.54	23.65	21.79	25.33	84.65	100.69	112.20	99.18	3.92	9.32E-04
182	Q5BKZ1	ZNF326	DBIRD complex subunit ZNF326	1	57.46	61.10	31.41	49.99	145.43	221.98	219.19	195.53	3.91	5.54E-03

183	P08559-4	PDHA1	Isoform 4 of Pyruvate dehydrogenase E1 component subunit alpha, somatic form, mitochondrial	5	148.25	151.74	97.21	132.40	374.79	580.74	595.92	517.15	3.91	6.35E-03
184	Q9BYD3	MRPL4	39S ribosomal protein L4, mitochondrial	1	33.42	33.23	16.43	27.69	78.01	108.12	138.22	108.11	3.90	1.17E-02
185	P00367	GLUD1	Glutamate dehydrogenase 1, mitochondrial	7	536.49	535.30	369.81	480.53	1466.21	2070.96	2062.59	1866.59	3.88	2.62E-03
186	Q9Y5B9	SUPT16H	FACT complex subunit SPT16	2	106.89	100.52	68.75	92.06	262.47	381.66	425.43	356.52	3.87	6.18E-03
187	P49755	TMED10	Transmembrane emp24 domain-containing protein 10	1	149.54	167.64	87.96	135.05	402.69	559.38	602.21	521.42	3.86	4.08E-03
188	P30419	NMT1	Glycylpeptide N-tetradecanoyltransferase 1	2	55.45	47.41	33.57	45.48	136.99	174.96	211.54	174.50	3.84	4.54E-03
189	P61956	SUMO2	Small ubiquitin-related modifier 2	1	143.27	122.23	86.09	117.20	356.75	449.10	531.84	445.90	3.80	3.50E-03
190	Q09028	RBBP4	Histone-binding protein RBBP4	5	397.61	409.30	241.12	349.34	1056.00	1407.72	1517.37	1327.03	3.80	2.81E-03
191	P37108	SRP14	Signal recognition particle 14 kDa protein	1	104.24	106.75	60.11	90.37	262.00	389.93	376.57	342.83	3.79	4.32E-03
192	Q16625	OCLN	Occludin	1	11.80	16.62	7.86	12.09	32.93	48.31	56.31	45.85	3.79	9.92E-03
193	P31040	SDHA	Succinate dehydrogenase [ubiquinone] flavoprotein subunit, mitochondrial	4	235.14	235.34	140.83	203.77	525.65	858.31	910.37	764.78	3.75	1.08E-02
194	Q99714	HSD17B10	3-hydroxyacyl-CoA dehydrogenase type-2	3	166.16	145.43	89.02	133.54	368.84	559.19	574.70	500.91	3.75	6.33E-03
195	Q9P032	NDUFAF4	NADH dehydrogenase [ubiquinone] 1 alpha subcomplex assembly factor 4	1	38.80	43.35	26.23	36.13	94.05	146.90	164.98	135.31	3.75	1.06E-02
196	P00403	MT-CO2	Cytochrome c oxidase subunit 2	1	113.26	128.14	67.11	102.84	283.38	420.61	450.55	384.85	3.74	6.69E-03
197	O75489	NDUFS3	NADH dehydrogenase [ubiquinone] iron-sulfur protein 3, mitochondrial	6	504.16	603.97	298.86	469.00	1377.88	1797.09	2061.13	1745.37	3.72	4.26E-03
198	P42704	LRPPRC	Leucine-rich PPR motif-containing protein, mitochondrial	32	3341.53	3570.11	2082.52	2998.05	9035.83	11348.40	12980.00	11121.41	3.71	2.76E-03
199	O75367	H2AFY	Core histone macro-H2A.1	10	1250.56	1257.92	620.15	1042.88	2861.90	4443.85	4275.73	3860.49	3.70	6.62E-03
200	Q96GA3	LTV1	Protein LTV1 homolog	1	9.17	11.06	11.92	10.72	31.43	42.49	44.77	39.56	3.69	2.35E-03
201	O15355	PPM1G	Protein phosphatase 1G	4	231.37	210.74	162.02	201.37	667.16	735.20	823.67	742.01	3.68	4.07E-04
202	O60637	TSPAN3	Tetraspanin-3	1	46.03	47.42	34.02	42.49	118.99	180.41	169.62	156.34	3.68	4.21E-03
203	P15311	EZR	Ezrin	8	683.50	614.57	375.54	557.87	1594.10	2131.28	2419.88	2048.42	3.67	4.54E-03
204	P49821	NDUFV1	NADH dehydrogenase [ubiquinone] flavoprotein 1, mitochondrial	1	71.57	64.30	39.00	58.29	159.86	219.60	260.98	213.48	3.66	7.43E-03
205	Q96EY7	PTCD3	Pentatricopeptide repeat domain-containing protein 3, mitochondrial	3	146.11	122.47	100.82	123.13	297.83	622.21	430.89	450.31	3.66	2.62E-02
206	Q15185	PTGES3	Prostaglandin E synthase 3	2	158.70	132.78	87.92	126.47	388.08	474.85	519.85	460.93	3.64	1.59E-03
207	P11021	HSPA5	78 kDa glucose-regulated protein	16	2093.69	2145.85	1217.20	1818.91	5390.17	7154.89	7260.66	6601.91	3.63	2.12E-03
208	Q04837	SSBP1	Single-stranded DNA-binding protein, mitochondrial	7	656.67	914.38	237.33	602.80	1725.76	2289.08	2533.00	2182.61	3.62	7.00E-03
209	P62280	RPS11	40S ribosomal protein S11	6	903.37	747.92	493.78	715.02	2096.96	2527.41	3136.11	2586.83	3.62	4.47E-03

210	O14979	HNRNPDL	Heterogeneous nuclear ribonucleoprotein D-like	5	633.80	739.16	350.38	574.45	1592.63	2255.90	2380.07	2076.20	3.61	5.16E-03
211	P26440	IVD	Isovaleryl-CoA dehydrogenase, mitochondrial	2	163.69	153.49	84.58	133.92	337.70	528.64	585.00	483.78	3.61	1.14E-02
212	O76021	RSL1D1	Ribosomal L1 domain-containing protein 1	5	367.04	360.60	200.72	309.45	851.09	1255.08	1232.41	1112.86	3.60	4.80E-03
213	Q07666	KHDRBS1	KH domain-containing, RNA-binding, signal transduction-associated protein 1	2	239.59	238.07	116.84	198.17	513.01	801.45	821.21	711.89	3.59	8.81E-03
214	P47914	RPL29	60S ribosomal protein L29	1	49.50	38.96	27.23	38.56	112.54	134.89	167.39	138.28	3.59	4.38E-03
215	P32969	RPL9	60S ribosomal protein L9	1	18.59	20.19	13.08	17.28	48.53	63.86	73.22	61.87	3.58	4.04E-03
216	P04179	SOD2	Superoxide dismutase [Mn], mitochondrial	4	415.36	463.74	246.10	375.07	1060.96	1399.25	1550.97	1337.06	3.56	3.78E-03
217	O00264	PGRMC1	Membrane-associated progesterone receptor component 1	2	161.16	196.05	108.24	155.15	426.67	577.19	654.96	552.94	3.56	5.16E-03
218	P54727	RAD23B	UV excision repair protein RAD23 homolog B	1	13.31	18.15	8.57	13.34	43.39	45.36	53.74	47.50	3.56	1.25E-03
219	O43837	IDH3B	Isocitrate dehydrogenase [NAD] subunit beta, mitochondrial	2	101.88	89.76	64.80	85.48	226.37	328.30	357.76	304.15	3.56	6.10E-03
220	P08574	CYC1	Cytochrome c1, heme protein, mitochondrial	1	80.81	73.89	36.90	63.86	143.59	253.57	282.98	226.71	3.55	2.17E-02
221	Q6UWP8	SBSN	Suprabasin	1	12.21	9.44	20.87	14.17	105.64	29.04	16.01	50.23	3.54	2.70E-01
222	P61163	ACTR1A	Alpha-centractin	1	39.95	29.46	18.44	29.28	79.82	105.87	125.42	103.71	3.54	6.99E-03
223	P00505	GOT2	Aspartate aminotransferase, mitochondrial	8	658.00	716.35	385.00	586.45	1574.85	2311.14	2342.58	2076.19	3.54	5.33E-03
224	Q15365	PCBP1	Poly(rC)-binding protein 1	4	407.75	351.15	254.99	337.96	974.21	1123.06	1461.23	1186.17	3.51	4.92E-03
225	Q06787	FMR1	Fragile X mental retardation protein 1	1	65.10	39.97	24.42	43.16	123.54	170.70	158.03	150.76	3.49	4.28E-03
226	Q15388	TOMM20	Mitochondrial import receptor subunit TOM20 homolog	1	96.08	125.95	72.05	98.03	276.86	373.02	375.52	341.80	3.49	2.49E-03
227	P62851	RPS25	40S ribosomal protein S25	4	706.10	662.60	371.12	579.94	1426.42	2067.09	2545.68	2013.06	3.47	1.36E-02
228	Q13123	IK	Protein Red	1	23.23	28.29	16.83	22.78	61.66	87.52	87.96	79.05	3.47	3.77E-03
229	Q9NVI7-2	ATAD3A	Isoform 2 of ATPase family AAA domain-containing protein 3A	10	841.07	884.63	469.49	731.73	1894.61	2787.90	2894.69	2525.73	3.45	6.40E-03
230	P05386	RPLP1	60S acidic ribosomal protein P1	1	219.45	173.37	110.01	167.61	467.31	583.14	682.32	577.59	3.45	4.19E-03
231	P30041	PRDX6	Peroxiredoxin-6	2	326.05	218.04	162.16	235.42	701.11	843.25	878.02	807.46	3.43	1.39E-03
232	P62913	RPL11	60S ribosomal protein L11	3	587.80	488.67	316.73	464.40	1272.73	1621.12	1884.64	1592.83	3.43	4.36E-03
233	Q15061	WDR43	WD repeat-containing protein 43	1	118.14	122.97	76.23	105.78	297.18	377.06	413.66	362.63	3.43	2.37E-03
234	Q14498	RBM39	RNA-binding protein 39	2	148.62	173.43	99.35	140.47	385.82	523.18	535.46	481.49	3.43	2.93E-03
235	P05388	RPLP0	60S acidic ribosomal protein P0	10	1282.31	1131.33	692.33	1035.32	2921.37	3673.37	4050.47	3548.40	3.43	2.61E-03
236	Q07065	CKAP4	Cytoskeleton-associated protein 4	6	435.23	440.02	240.99	372.08	1017.11	1365.52	1428.19	1270.27	3.41	3.34E-03
237	P02545	LMNA	Prelamin-A/C	5	570.27	499.24	279.08	449.53	1124.38	1833.84	1640.67	1532.96	3.41	9.12E-03
238	Q99873	PRMT1	Protein arginine N-methyltransferase 1	8	1295.04	1140.31	689.82	1041.72	2769.46	3450.28	4433.28	3551.01	3.41	8.26E-03

239	P0CW22	RPS17L	40S ribosomal protein S17-like	2	102.08	81.16	53.59	78.94	228.63	265.87	312.12	268.87	3.41	2.44E-03
240	Q9NYF8	BCLAF1	Bcl-2-associated transcription factor 1	2	210.57	201.08	123.02	178.22	561.76	693.29	562.76	605.93	3.40	1.17E-03
241	P63241-2	EIF5A	Isoform 2 of Eukaryotic translation initiation factor 5A-1	5	1125.60	881.96	632.40	879.99	2626.55	2936.60	3399.61	2987.59	3.40	1.37E-03
242	P48047	ATP5O	ATP synthase subunit O, mitochondrial	1	10.72	11.55	27.83	16.70	43.08	69.24	57.71	56.68	3.39	1.31E-02
243	Q9UQ80	PA2G4	Proliferation-associated protein 2G4	6	691.10	606.55	393.24	563.63	1556.90	1999.39	2181.30	1912.53	3.39	2.79E-03
244	P36957	DLST	Dihydrolipoyllysine-residue succinyltransferase component of 2-oxoglutarate dehydrogenase complex, mitochondrial	4	232.31	218.36	136.93	195.87	493.09	747.74	750.77	663.86	3.39	6.63E-03
245	P21912	SDHB	Succinate dehydrogenase [ubiquinone] iron-sulfur subunit, mitochondrial	4	499.98	586.63	253.63	446.75	1086.54	1572.98	1881.75	1513.76	3.39	1.33E-02
246	P23786	CPT2	Carnitine O-palmitoyltransferase 2, mitochondrial	4	312.15	298.45	171.35	260.65	673.93	935.58	1039.68	883.06	3.39	6.13E-03
247	P11387	TOP1	DNA topoisomerase 1	2	110.37	125.36	60.19	98.64	253.99	367.86	374.33	332.06	3.37	5.95E-03
248	P27348	YWHAQ	14-3-3 protein theta	6	305.07	256.67	194.95	252.23	757.27	794.67	993.28	848.41	3.36	1.72E-03
249	P29692-2	EEF1D	Isoform 2 of Elongation factor 1-delta	4	327.32	283.27	181.97	264.19	695.45	909.59	1050.53	885.19	3.35	5.15E-03
250	Q9Y277-2	VDAC3	Isoform 2 of Voltage-dependent anion-selective channel protein 3	6	581.77	643.78	328.23	517.93	1276.38	1871.55	2050.45	1732.79	3.35	8.65E-03
251	P50502	ST13	Hsc70-interacting protein	2	449.70	380.49	245.76	358.65	952.69	1198.72	1446.06	1199.16	3.34	5.54E-03
252	P78316	NOP14	Nucleolar protein 14	1	32.85	35.94	21.71	30.17	78.36	117.63	105.48	100.49	3.33	4.75E-03
253	P18754-2	RCC1	Isoform 2 of Regulator of chromosome condensation	2	125.46	128.00	108.64	120.70	329.63	472.64	402.92	401.73	3.33	2.53E-03
254	Q6UB35	MTHFD1L	Monofunctional C1-tetrahydrofolate synthase, mitochondrial	11	809.17	846.86	463.27	706.43	1827.79	2437.75	2779.08	2348.21	3.32	5.68E-03
255	P62899-2	RPL31	Isoform 2 of 60S ribosomal protein L31	1	23.06	21.33	9.96	18.12	52.62	57.36	70.51	60.16	3.32	3.38E-03
256	Q01081	U2AF1	Splicing factor U2AF 35 kDa subunit	2	143.82	126.97	72.68	114.49	297.73	370.37	471.20	379.77	3.32	8.33E-03
257	P82675	MRPS5	28S ribosomal protein S5, mitochondrial	1	89.28	85.46	45.03	73.25	193.25	283.25	252.39	242.96	3.32	4.79E-03
258	P61081	UBE2M	NEDD8-conjugating enzyme Ubc12	1	69.19	84.32	48.28	67.27	182.19	218.21	268.20	222.87	3.31	4.52E-03
259	Q12931	TRAP1	Heat shock protein 75 kDa, mitochondrial	17	2607.21	2819.19	1403.40	2276.60	5732.47	8034.79	8821.58	7529.61	3.31	6.89E-03
260	Q9BYC9	MRPL20	39S ribosomal protein L20, mitochondrial	1	32.42	34.47	21.81	29.57	65.03	104.90	123.39	97.77	3.31	1.81E-02
261	P20700	LMNB1	Lamin-B1	13	882.56	975.11	534.59	797.42	2088.09	2890.20	2928.68	2635.66	3.31	3.82E-03
262	Q12874	SF3A3	Splicing factor 3A subunit 3	4	425.03	435.45	240.13	366.87	913.91	1295.85	1416.85	1208.87	3.30	6.86E-03
263	P51116	FXR2	Fragile X mental retardation syndrome-related protein 2	1	68.44	59.32	32.15	53.30	146.43	172.79	205.72	174.98	3.28	3.91E-03
264	P61981	YWHAG	14-3-3 protein gamma	3	326.46	296.79	221.95	281.74	785.44	944.55	1040.94	923.64	3.28	1.35E-03
265	P45880-1	VDAC2	Isoform 1 of Voltage-dependent anion-selective channel protein 2	9	1275.19	1370.68	716.88	1120.92	2850.99	3795.14	4348.72	3664.95	3.27	6.20E-03
266	Q00839	HNRNPU	Heterogeneous nuclear ribonucleoprotein U	17	3240.42	3227.22	1611.13	2692.92	7081.00	9653.35	9573.05	8769.13	3.26	3.74E-03

267	Q9Y305-4	ACOT9	Isoform 4 of Acyl-coenzyme A thioesterase 9, mitochondrial	1	110.39	115.42	70.05	98.62	243.58	323.52	391.93	319.68	3.24	8.10E-03
268	P50579	METAP2	Methionine aminopeptidase 2	1	43.59	30.07	33.11	35.59	90.73	125.16	129.39	115.09	3.23	3.53E-03
269	Q15366-2	PCBP2	Isoform 2 of Poly(rC)-binding protein 2	6	1111.87	993.45	605.34	903.55	2362.70	2918.94	3454.89	2912.18	3.22	4.59E-03
270	Q9NYY8	FASTKD2	FAST kinase domain-containing protein 2	1	20.61	26.58	14.37	20.52	48.75	68.54	81.00	66.09	3.22	1.05E-02
271	P51991	HNRNPA3	Heterogeneous nuclear ribonucleoprotein A3	8	957.23	993.02	474.42	808.22	2229.68	2756.12	2819.88	2601.89	3.22	2.02E-03
272	O75821	EIF3G	Eukaryotic translation initiation factor 3 subunit G	2	77.08	69.10	44.30	63.50	164.91	209.74	238.39	204.35	3.22	3.93E-03
273	P21796	VDAC1	Voltage-dependent anion-selective channel protein 1	3	436.40	466.60	250.23	384.41	943.86	1349.68	1413.43	1235.66	3.21	6.26E-03
274	Q8WY22	BRI3BP	BRI3-binding protein	1	17.77	16.82	14.15	16.25	32.73	79.10	44.81	52.21	3.21	6.12E-02
275	P32322	PYCR1	Pyrroline-5-carboxylate reductase 1, mitochondrial	2	91.95	113.48	61.85	89.10	212.27	319.62	326.54	286.14	3.21	7.83E-03
276	P25398	RPS12	40S ribosomal protein S12	4	617.04	500.87	332.33	483.41	1216.80	1537.62	1887.63	1547.35	3.20	7.22E-03
277	P18583-9	SON	Isoform I of Protein SON	1	9.17	10.86	7.76	9.26	24.42	29.67	34.79	29.63	3.20	2.87E-03
278	P23368	ME2	NAD-dependent malic enzyme, mitochondrial	1	83.68	92.65	51.21	75.85	188.82	270.89	266.02	241.91	3.19	4.85E-03
279	Q9Y4L1	HYOU1	Hypoxia up-regulated protein 1	4	230.18	264.08	135.27	209.85	516.61	723.51	766.47	668.86	3.19	5.99E-03
280	P62195	PSMC5	26S protease regulatory subunit 8	1	63.85	51.60	36.28	50.58	106.55	177.56	198.95	161.02	3.18	1.91E-02
281	P43897	TSFM	Elongation factor Ts, mitochondrial	1	29.62	31.69	16.69	26.00	58.51	94.00	95.64	82.72	3.18	1.20E-02
282	P05141	SLC25A5	ADP/ATP translocase 2	2	404.89	419.24	205.72	343.28	768.46	1169.79	1336.23	1091.49	3.18	1.47E-02
283	P26038	MSN	Moesin	1	26.20	28.51	18.31	24.34	62.27	86.61	83.11	77.33	3.18	2.95E-03
284	O43847-2	NRD1	Isoform 2 of Nardilysin	2	154.87	149.73	99.56	134.72	335.84	415.49	529.84	427.05	3.17	7.73E-03
285	P23284	PPIB	Peptidyl-prolyl cis-trans isomerase B	4	598.00	716.52	346.83	553.78	1319.09	1930.15	1998.50	1749.25	3.16	7.81E-03
286	P11310-2	ACADM	Isoform 2 of Medium-chain specific acyl-CoA dehydrogenase, mitochondrial	1	67.53	68.93	40.55	59.00	133.38	213.56	208.93	185.29	3.14	1.02E-02
287	Q15691	MAPRE1	Microtubule-associated protein RP/EB family member 1	1	48.67	42.41	22.58	37.89	99.01	128.41	129.39	118.94	3.14	3.09E-03
288	P51148-2	RAB5C	Isoform 2 of Ras-related protein Rab-5C	2	166.69	197.29	101.71	155.23	404.30	490.52	566.98	487.27	3.14	3.74E-03
289	P36776	LONP1	Lon protease homolog, mitochondrial	4	142.24	130.98	85.69	119.64	256.27	416.09	451.58	374.65	3.13	1.51E-02
290	P62820	RAB1A	Ras-related protein Rab-1A	3	807.92	922.12	474.23	734.76	1852.87	2409.96	2633.08	2298.64	3.13	4.30E-03
291	P07355-2	ANXA2	Isoform 2 of Annexin A2	8	812.24	787.79	592.79	730.94	1819.00	2368.51	2667.15	2284.89	3.13	3.82E-03
292	P08758	ANXA5	Annexin A5	4	249.95	252.07	160.11	220.71	602.51	678.46	787.48	689.48	3.12	1.60E-03
293	O14950	MYL12B	Myosin regulatory light chain 12B	1	40.21	30.80	24.60	31.87	87.51	96.17	114.55	99.41	3.12	1.81E-03
294	Q96EP5	DAZAP1	DAZ-associated protein 1	1	31.90	34.98	24.16	30.35	76.73	98.27	108.71	94.57	3.12	2.97E-03
295	P13693	TPT1	Translationally-controlled tumor protein	1	163.49	116.13	87.75	122.45	305.28	424.91	413.46	381.22	3.11	4.20E-03

296	Q13838-2	DDX39B	Isoform 2 of Spliceosome RNA helicase DDX39B	10	1149.88	1185.79	597.33	977.67	2447.97	3304.99	3360.29	3037.75	3.11	4.23E-03
297	Q9BUJ2	HNRNPUL1	Heterogeneous nuclear ribonucleoprotein U-like protein 1	2	74.94	91.36	49.56	71.96	175.08	239.97	251.55	222.20	3.09	4.92E-03
298	Q9Y3T9	NOC2L	Nucleolar complex protein 2 homolog	1	60.20	61.10	34.67	51.99	125.81	182.94	171.76	160.17	3.08	5.17E-03
299	P07237	P4HB	Protein disulfide-isomerase	11	1260.87	1413.67	718.16	1130.90	2706.93	3770.09	3963.57	3480.20	3.08	6.12E-03
300	P60903	S100A10	Protein S100-A10	1	168.60	186.80	105.09	153.50	329.25	515.23	571.80	472.09	3.08	1.46E-02
301	P62826	RAN	GTP-binding nuclear protein Ran	5	819.94	723.67	469.48	671.03	1684.10	2163.58	2343.14	2063.61	3.08	3.34E-03
302	Q9P2K3-3	RCOR3	Isoform 3 of REST corepressor 3	1	11.94	11.80	6.13	9.96	24.24	34.24	33.25	30.58	3.07	5.14E-03
303	Q5JTZ9	AARS2	Alanine--tRNA ligase, mitochondrial	1	24.31	24.60	16.97	21.96	49.97	77.29	74.96	67.41	3.07	7.50E-03
304	Q9Y6E0	STK24	Serine/threonine-protein kinase 24	1	64.88	51.20	37.67	51.25	127.75	152.85	191.18	157.26	3.07	6.14E-03
305	P05455	SSB	Lupus La protein	4	225.24	215.93	147.47	196.21	486.51	573.05	743.88	601.15	3.06	7.01E-03
306	Q16555	DPYSL2	Dihydropyrimidinase-related protein 2	2	119.36	122.36	79.15	106.96	258.75	355.39	365.27	326.47	3.05	3.94E-03
307	P12956	XRCC6	X-ray repair cross-complementing protein 6	15	2756.74	2372.92	1578.68	2236.11	5275.02	7274.11	7904.26	6817.80	3.05	6.10E-03
308	P30040	ERP29	Endoplasmic reticulum resident protein 29	2	104.47	95.37	53.67	84.50	194.74	294.76	282.86	257.45	3.05	7.97E-03
309	Q13151	HNRNPA0	Heterogeneous nuclear ribonucleoprotein A0	3	308.18	292.69	216.39	272.42	624.48	972.22	881.14	825.95	3.03	6.84E-03
310	P55884-2	EIF3B	Isoform 2 of Eukaryotic translation initiation factor 3 subunit B	4	377.95	348.97	210.93	312.62	825.47	933.82	1081.97	947.09	3.03	2.18E-03
311	Q96T88-2	UHRF1	Isoform 2 of E3 ubiquitin-protein ligase UHRF1	3	141.97	145.27	76.12	121.12	288.76	394.36	417.14	366.75	3.03	5.70E-03
312	P52597	HNRNPF	Heterogeneous nuclear ribonucleoprotein F	5	470.49	503.66	277.55	417.23	985.57	1311.85	1491.86	1263.09	3.03	6.72E-03
313	Q12797	ASPH	Aspartyl/asparaginyl beta-hydroxylase	1	23.54	29.91	15.17	22.87	55.67	72.77	79.19	69.21	3.03	4.86E-03
314	P63104	YWHAZ	14-3-3 protein zeta/delta	7	448.12	357.71	261.55	355.79	920.97	1085.50	1220.38	1075.62	3.02	2.12E-03
315	P55010	EIF5	Eukaryotic translation initiation factor 5	3	177.95	135.96	100.22	138.04	349.54	436.42	465.82	417.26	3.02	2.54E-03
316	P24534	EEF1B2	Elongation factor 1-beta	4	655.52	502.80	323.28	493.87	1147.65	1491.21	1838.05	1492.30	3.02	1.07E-02
317	Q16795	NDUFA9	NADH dehydrogenase [ubiquinone] 1 alpha subcomplex subunit 9, mitochondrial	4	218.11	211.33	107.77	179.07	360.33	618.13	644.22	540.89	3.02	2.06E-02
318	P07737	PFN1	Profilin-1	7	1344.18	1076.39	583.95	1001.51	2641.53	3083.08	3347.14	3023.92	3.02	2.63E-03
319	A4D1E9	GTPBP10	GTP-binding protein 10	1	22.28	18.73	11.38	17.46	38.26	61.43	58.35	52.68	3.02	1.14E-02
320	Q9NQ55-3	PPAN	Isoform 3 of Suppressor of SWI4 1 homolog	1	140.57	141.55	93.80	125.31	294.26	420.66	416.81	377.24	3.01	4.76E-03
321	P62258	YWHAE	14-3-3 protein epsilon	10	1645.27	1504.23	936.12	1361.87	3648.37	3961.95	4682.45	4097.59	3.01	1.88E-03
322	P51649-2	ALDH5A1	Isoform 2 of Succinate-semialdehyde dehydrogenase, mitochondrial	3	111.73	129.57	85.58	108.96	259.24	358.05	365.67	327.65	3.01	3.93E-03
323	Q99729-2	HNRNPAB	Isoform 2 of Heterogeneous nuclear ribonucleoprotein A/B	3	405.84	468.50	237.34	370.56	842.41	1259.19	1211.41	1104.34	2.98	7.84E-03
324	Q14676	MDC1	Mediator of DNA damage checkpoint protein 1	1	63.95	63.74	50.46	59.38	154.74	217.02	159.04	176.93	2.98	4.64E-03

325	Q8NE71	ABCF1	ATP-binding cassette sub-family F member 1	1	28.53	27.28	18.48	24.76	56.92	73.78	90.41	73.71	2.98	8.58E-03
326	P49458	SRP9	Signal recognition particle 9 kDa protein	1	72.47	67.59	42.23	60.77	141.67	189.57	210.70	180.65	2.97	5.95E-03
327	Q16543	CDC37	Hsp90 co-chaperone Cdc37	2	211.70	193.50	135.73	180.31	459.40	530.17	617.34	535.64	2.97	2.25E-03
328	P28838	LAP3	Cytosol aminopeptidase	1	13.44	7.57	6.95	9.32	18.61	34.63	29.75	27.66	2.97	2.38E-02
329	Q9NTK5	OLA1	Obg-like ATPase 1	3	241.69	256.42	148.04	215.38	536.14	640.69	740.72	639.18	2.97	3.40E-03
330	O43809	NUDT21	Cleavage and polyadenylation specificity factor subunit 5	1	31.54	35.86	20.71	29.37	65.50	98.15	97.70	87.11	2.97	7.87E-03
331	Q9UDR5	AASS	Alpha-aminoadipic semialdehyde synthase, mitochondrial	1	78.97	89.98	49.91	72.95	163.26	226.71	258.57	216.18	2.96	9.29E-03
332	P61247	RPS3A	40S ribosomal protein S3a	8	911.53	779.82	522.03	737.80	1778.83	2238.78	2538.67	2185.43	2.96	4.35E-03
333	P52292	KPNA2	Importin subunit alpha-1	4	360.59	336.62	229.93	309.05	746.61	893.43	1100.77	913.60	2.96	5.40E-03
334	Q15181	PPA1	Inorganic pyrophosphatase	2	119.27	93.90	62.87	92.01	202.94	287.99	324.67	271.87	2.95	1.05E-02
335	Q06265-2	EXOSC9	Isoform 2 of Exosome complex component RRP45	1	32.19	32.85	17.63	27.56	66.02	88.47	89.61	81.37	2.95	4.18E-03
336	P16435	POR	NADPH--cytochrome P450 reductase	1	62.29	73.94	45.86	60.70	137.24	199.54	200.33	179.04	2.95	6.19E-03
337	P50914	RPL14	60S ribosomal protein L14	3	244.34	209.51	115.71	189.85	454.70	573.03	652.01	559.91	2.95	5.84E-03
338	P25789	PSMA4	Proteasome subunit alpha type-4	1	167.76	145.49	94.96	136.07	313.07	428.89	460.04	400.67	2.94	5.96E-03
339	P31943	HNRNPH1	Heterogeneous nuclear ribonucleoprotein H	9	959.85	1030.86	547.18	845.96	2012.27	2744.42	2711.93	2489.54	2.94	4.34E-03
340	O00567	NOP56	Nucleolar protein 56	6	528.06	636.59	325.21	496.62	1220.08	1543.41	1606.57	1456.69	2.93	3.10E-03
341	Q14103	HNRNPD	Heterogeneous nuclear ribonucleoprotein D0	4	258.57	329.98	198.63	262.40	658.51	793.50	855.42	769.15	2.93	1.87E-03
342	P46777	RPL5	60S ribosomal protein L5	7	449.21	311.67	199.06	319.98	739.43	1043.96	1025.52	936.30	2.93	7.28E-03
343	P22087	FBL	rRNA 2'-O-methyltransferase fibrillarin	4	767.23	820.69	475.98	687.97	1572.20	2265.54	2195.45	2011.06	2.92	5.69E-03
344	P33316	DUT	Deoxyuridine 5'-triphosphate nucleotidohydrolase, mitochondrial	1	145.01	134.34	86.23	121.86	281.53	338.77	448.18	356.16	2.92	1.09E-02
345	Q16881	TXNRD1	Thioredoxin reductase 1, cytoplasmic	1	18.05	19.95	13.74	17.25	42.65	52.18	56.25	50.36	2.92	1.71E-03
346	P15880	RPS2	40S ribosomal protein S2	6	935.27	781.41	494.81	737.17	1732.68	2195.03	2525.05	2150.92	2.92	5.83E-03
347	P12236	SLC25A6	ADP/ATP translocase 3	11	2651.66	2251.98	1019.34	1974.33	5150.25	6074.22	6049.49	5757.99	2.92	2.81E-03
348	Q99798	ACO2	Aconitate hydratase, mitochondrial	10	815.47	850.30	474.43	713.40	1578.12	2216.92	2424.14	2073.06	2.91	8.45E-03
349	Q1KMD3	HNRNPUL2	Heterogeneous nuclear ribonucleoprotein U-like protein 2	1	20.77	27.17	12.04	19.99	49.38	57.09	67.74	58.07	2.90	5.25E-03
350	Q16630-2	CPSF6	Isoform 2 of Cleavage and polyadenylation specificity factor subunit 6	1	44.28	40.64	28.49	37.80	83.34	132.65	113.00	109.66	2.90	8.92E-03
351	P62318	SNRPD3	Small nuclear ribonucleoprotein Sm D3	2	108.14	99.33	55.03	87.50	205.42	272.72	282.28	253.47	2.90	4.75E-03
352	Q92747	ARPC1A	Actin-related protein 2/3 complex subunit 1A	1	93.20	86.50	70.02	83.24	190.35	288.03	244.19	240.85	2.89	5.61E-03
353	Q02790	FKBP4	Peptidyl-prolyl cis-trans isomerase FKBP4	4	335.14	273.10	178.92	262.38	623.66	784.76	867.41	758.61	2.89	4.25E-03

354	Q9BXP5	SRRT	Serrate RNA effector molecule homolog	6	324.52	329.23	207.32	287.02	634.39	915.82	933.69	827.97	2.88	6.69E-03
355	P30101	PDIA3	Protein disulfide-isomerase A3	11	1070.66	1179.71	615.34	955.24	2138.19	2921.78	3206.11	2755.36	2.88	7.72E-03
356	Q8TAA3	PSMA8	Proteasome subunit alpha type-7-like	1	26.17	21.75	14.64	20.85	49.35	62.64	68.29	60.09	2.88	3.88E-03
357	Q08J23	NSUN2	tRNA (cytosine(34)-C(5))-methyltransferase	1	107.78	95.84	69.64	91.09	209.44	263.31	313.90	262.22	2.88	6.02E-03
358	Q6PI48	DARS2	Aspartate--tRNA ligase, mitochondrial	2	175.41	190.95	102.38	156.25	351.23	462.61	531.44	448.42	2.87	7.83E-03
359	Q96AG4	LRRC59	Leucine-rich repeat-containing protein 59	6	611.97	806.08	383.51	600.52	1347.81	1883.81	1920.84	1717.49	2.86	7.30E-03
360	P11388-4	TOP2A	Isoform 4 of DNA topoisomerase 2-alpha	7	656.40	584.09	425.20	555.23	1230.18	1948.99	1583.64	1587.60	2.86	9.13E-03
361	O75306	NDUFS2	NADH dehydrogenase [ubiquinone] iron-sulfur protein 2, mitochondrial	2	102.42	120.13	65.46	96.00	218.99	296.61	306.66	274.09	2.86	5.13E-03
362	O00483	NDUFA4	NADH dehydrogenase [ubiquinone] 1 alpha subcomplex subunit 4	1	106.77	131.65	53.14	97.19	205.58	296.77	328.45	276.93	2.85	1.45E-02
363	P31949	S100A11	Protein S100-A11	1	36.46	41.89	39.93	39.43	106.05	105.16	125.69	112.30	2.85	4.51E-04
364	Q8IYU8	MICU2	Calcium uptake protein 2, mitochondrial	1	38.69	62.68	26.66	42.68	91.36	133.67	139.07	121.37	2.84	1.30E-02
365	Q9UMS4	PRPF19	Pre-mRNA-processing factor 19	10	1497.95	1620.05	942.78	1353.59	3029.06	4236.32	4275.67	3847.02	2.84	5.58E-03
366	P60033	CD81	CD81 antigen	1	47.76	51.13	31.84	43.58	111.83	118.05	140.59	123.49	2.83	1.64E-03
367	O94979-8	SEC31A	Isoform 8 of Protein transport protein Sec31A	1	17.30	21.17	21.96	20.14	33.42	64.08	73.06	56.85	2.82	3.85E-02
368	Q15417	CNN3	Calponin-3	3	202.76	267.78	140.71	203.75	478.84	572.19	673.22	574.75	2.82	5.21E-03
369	P62244	RPS15A	40S ribosomal protein S15a	1	144.25	115.20	76.20	111.88	257.04	321.22	368.45	315.57	2.82	5.75E-03
370	P62753	RPS6	40S ribosomal protein S6	5	511.89	411.15	269.14	397.39	912.00	1192.70	1255.94	1120.21	2.82	4.71E-03
371	Q03252	LMNB2	Lamin-B2	1	48.73	49.23	29.95	42.63	95.29	136.56	126.23	119.36	2.80	5.30E-03
372	P78347	GTF2I	General transcription factor II-I	2	85.36	86.87	45.63	72.62	161.70	214.23	232.61	202.85	2.79	6.64E-03
373	P62834	RAP1A	Ras-related protein Rap-1A	1	177.95	219.90	108.29	168.71	372.93	486.85	553.71	471.16	2.79	8.17E-03
374	P56537	EIF6	Eukaryotic translation initiation factor 6	2	143.76	132.19	83.85	119.93	252.21	375.25	376.38	334.61	2.79	8.91E-03
375	Q14739	LBR	Lamin-B receptor	6	978.78	1026.62	606.41	870.60	1893.60	2512.54	2858.11	2421.42	2.78	7.63E-03
376	Q9P258	RCC2	Protein RCC2	4	265.56	217.29	158.74	213.86	404.38	652.38	727.47	594.74	2.78	2.05E-02
377	Q5RKV6	EXOSC6	Exosome complex component MTR3	1	28.53	25.44	15.70	23.22	54.23	67.45	71.88	64.52	2.78	3.26E-03
378	Q08380	LGALS3BP	Galectin-3-binding protein	2	48.83	42.78	40.11	43.91	102.44	133.10	130.35	121.97	2.78	1.52E-03
379	P52907	CAPZA1	F-actin-capping protein subunit alpha-1	1	77.92	69.53	55.01	67.48	151.58	204.35	205.97	187.30	2.78	3.28E-03
380	O15371	EIF3D	Eukaryotic translation initiation factor 3 subunit D	2	178.68	175.07	117.10	156.95	361.10	431.67	513.87	435.55	2.78	4.53E-03
381	Q99497	PARK7	Protein DJ-1	2	543.93	299.10	316.85	386.63	897.59	1199.32	1117.95	1071.62	2.77	4.62E-03
382	P25786-2	PSMA1	Isoform Long of Proteasome subunit alpha type-1	1	78.45	72.85	42.64	64.65	136.98	188.27	212.19	179.15	2.77	9.93E-03
383	P62316	SNRPD2	Small nuclear ribonucleoprotein Sm D2	2	71.89	81.94	58.09	70.64	153.54	216.51	217.03	195.70	2.77	4.87E-03

384	Q9UBM7	DHCR7	7-dehydrocholesterol reductase	2	356.87	390.67	242.95	330.16	847.39	926.25	964.94	912.86	2.76	4.99E-04
385	Q9UGP8	SEC63	Translocation protein SEC63 homolog	1	51.98	61.50	33.60	49.03	110.07	141.23	155.25	135.52	2.76	5.25E-03
386	P62263	RPS14	40S ribosomal protein S14	2	119.50	111.76	62.82	98.03	207.63	285.84	319.01	270.83	2.76	9.96E-03
387	P22061-2	PCMT1	Isoform 2 of Protein-L-isoaspartate(D-aspartate) O-methyltransferase	1	16.22	11.24	6.30	11.26	29.12	34.71	29.14	30.99	2.75	4.44E-03
388	Q13423	NNT	NAD(P) transhydrogenase, mitochondrial	10	817.40	814.32	486.72	706.15	1523.89	1965.93	2317.75	1935.86	2.74	8.45E-03
389	P25205	MCM3	DNA replication licensing factor MCM3	6	567.88	525.89	357.70	483.82	1048.75	1408.37	1519.37	1325.50	2.74	5.69E-03
390	Q2TAY7	SMU1	WD40 repeat-containing protein SMU1	3	160.24	143.23	63.30	122.26	302.82	357.58	342.94	334.45	2.74	3.39E-03
391	Q13263	TRIM28	Transcription intermediary factor 1-beta	13	2035.96	2049.93	1225.73	1770.54	3990.84	5160.29	5361.88	4837.67	2.73	3.76E-03
392	P60953-1	CDC42	Isoform 1 of Cell division control protein 42 homolog	3	169.12	167.53	102.09	146.25	382.87	377.30	438.27	399.48	2.73	1.00E-03
393	Q9UBT2	UBA2	SUMO-activating enzyme subunit 2	1	91.16	83.09	76.09	83.45	141.80	324.98	215.78	227.52	2.73	5.42E-02
394	Q9BRT9	GINS4	DNA replication complex GINS protein SLD5	1	10.82	7.83	9.76	9.47	25.61	26.77	24.95	25.78	2.72	9.13E-05
395	Q92945	KHSRP	Far upstream element-binding protein 2	9	984.85	991.87	568.00	848.24	1752.78	2461.47	2709.00	2307.75	2.72	1.02E-02
396	Q9H773	DCTPP1	dCTP pyrophosphatase 1	1	49.93	49.24	33.34	44.17	99.03	129.96	131.31	120.10	2.72	3.05E-03
397	P41250	GARS	Glycine--tRNA ligase	3	262.23	208.09	158.21	209.51	455.16	548.63	703.83	569.21	2.72	1.02E-02
398	Q9NVH1	DNAJC11	DnaJ homolog subfamily C member 11	2	114.99	114.92	69.92	99.94	209.31	299.60	305.06	271.32	2.71	7.65E-03
399	Q9BVP2	GNL3	Guanine nucleotide-binding protein-like 3	4	129.97	154.22	79.55	121.24	269.75	361.34	355.88	328.99	2.71	4.91E-03
400	Q13435	SF3B2	Splicing factor 3B subunit 2	5	647.63	664.01	344.97	552.20	1199.37	1682.42	1599.04	1493.61	2.70	6.59E-03
401	P62888	RPL30	60S ribosomal protein L30	3	285.35	238.33	142.78	222.15	493.24	633.46	672.46	599.72	2.70	5.34E-03
402	Q9Y230	RUVBL2	RuvB-like 2	1	34.42	34.52	27.93	32.29	76.55	92.89	91.79	87.08	2.70	6.57E-04
403	P14678-3	SNRPB	Isoform SM-B1 of Small nuclear ribonucleoprotein-associated proteins B and B'	2	408.43	425.62	198.75	344.26	699.55	1000.88	1080.52	926.98	2.69	1.31E-02
404	Q5BJF2	TMEM97	Transmembrane protein 97	2	27.27	26.07	16.06	23.13	51.15	66.07	69.63	62.28	2.69	4.23E-03
405	P49721	PSMB2	Proteasome subunit beta type-2	2	206.34	198.05	136.47	180.29	416.29	476.62	560.35	484.42	2.69	2.99E-03
406	P53007	SLC25A1	Tricarboxylate transport protein, mitochondrial	3	465.20	512.08	261.82	413.03	801.62	1196.10	1331.53	1109.75	2.69	1.69E-02
407	P61204	ARF3	ADP-ribosylation factor 3	1	152.60	191.18	89.24	144.34	335.85	371.82	455.73	387.80	2.69	6.27E-03
408	P68036-3	UBE2L3	Isoform 3 of Ubiquitin-conjugating enzyme E2 L3	1	123.98	77.24	71.79	91.00	204.70	251.03	273.53	243.09	2.67	4.36E-03
409	P05091	ALDH2	Aldehyde dehydrogenase, mitochondrial	1	34.81	29.54	19.60	27.98	54.12	77.06	92.76	74.65	2.67	1.81E-02
410	P32119	PRDX2	Peroxiredoxin-2	4	750.16	637.21	470.96	619.44	1389.62	1622.21	1941.00	1650.94	2.67	4.52E-03
411	P12004	PCNA	Proliferating cell nuclear antigen	5	297.39	244.33	171.76	237.83	501.41	654.94	745.01	633.79	2.66	7.73E-03
412	O96008	TOMM40	Mitochondrial import receptor subunit TOM40 homolog	2	107.59	84.75	31.77	74.71	217.15	191.75	187.01	198.64	2.66	7.01E-03

413	O75400	PRPF40A	Pre-mRNA-processing factor 40 homolog A	2	267.18	316.95	187.99	257.37	579.07	749.84	713.01	680.64	2.64	2.72E-03
414	P40939	HADHA	Trifunctional enzyme subunit alpha, mitochondrial	11	919.09	773.86	452.16	715.04	1487.26	2102.91	2073.78	1887.98	2.64	8.53E-03
415	P19404	NDUFV2	NADH dehydrogenase [ubiquinone] flavoprotein 2, mitochondrial	1	26.48	28.53	20.07	25.03	49.39	72.41	76.20	66.00	2.64	9.45E-03
416	P18077	RPL35A	60S ribosomal protein L35a	6	592.51	493.58	285.77	457.28	884.95	1267.06	1462.96	1204.99	2.64	1.77E-02
417	Q9Y6C9	MTCH2	Mitochondrial carrier homolog 2	3	286.51	301.12	162.59	250.08	498.97	697.92	776.56	657.82	2.63	1.21E-02
418	P60660-2	MYL6	Isoform Smooth muscle of Myosin light polypeptide 6	2	193.03	186.46	115.00	164.83	351.94	435.82	509.66	432.47	2.62	6.74E-03
419	Q14566	MCM6	DNA replication licensing factor MCM6	2	146.36	136.89	84.67	122.64	260.86	340.58	363.36	321.60	2.62	5.51E-03
420	P62249	RPS16	40S ribosomal protein S16	2	194.59	175.46	105.02	158.36	318.44	426.02	500.86	415.11	2.62	1.25E-02
421	P30046	DDT	D-dopachrome decarboxylase	1	21.14	16.82	14.34	17.43	35.07	50.59	51.37	45.68	2.62	7.57E-03
422	Q06055-2	ATP5G2	Isoform 2 of ATP synthase F(0) complex subunit C2, mitochondrial	1	191.12	188.20	116.59	165.30	258.36	486.01	554.53	432.97	2.62	4.48E-02
423	P46109	CRKL	Crk-like protein	1	34.40	32.71	19.83	28.98	59.16	81.30	87.13	75.86	2.62	8.39E-03
424	P07686	HEXB	Beta-hexosaminidase subunit beta	3	146.25	147.31	77.51	123.69	262.71	365.66	342.97	323.78	2.62	6.74E-03
425	Q71U36	TUBA1A	Tubulin alpha-1A chain	1	254.93	237.28	136.32	209.51	464.39	531.24	649.37	548.34	2.62	6.64E-03
426	P62266	RPS23	40S ribosomal protein S23	3	266.52	210.18	140.12	205.60	419.69	572.98	618.79	537.15	2.61	9.26E-03
427	P51149	RAB7A	Ras-related protein Rab-7a	4	483.22	552.16	294.56	443.31	940.45	1201.61	1331.50	1157.85	2.61	6.68E-03
428	P24928	POLR2A	DNA-directed RNA polymerase II subunit RPB1	1	28.51	31.54	36.29	32.11	55.50	115.24	80.63	83.79	2.61	4.16E-02
429	Q04637-9	EIF4G1	Isoform 9 of Eukaryotic translation initiation factor 4 gamma 1	6	371.93	318.04	220.45	303.47	669.51	802.36	903.53	791.80	2.61	3.81E-03
430	P13796	LCP1	Plastin-2	3	497.51	434.03	301.68	411.07	891.19	1057.54	1260.02	1069.58	2.60	5.58E-03
431	P63173	RPL38	60S ribosomal protein L38	2	135.08	120.31	70.58	108.66	218.31	280.41	349.18	282.63	2.60	1.50E-02
432	Q9UNE7	STUB1	E3 ubiquitin-protein ligase CHIP	1	54.41	61.93	39.49	51.94	105.18	136.05	163.62	134.95	2.60	1.02E-02
433	O95456	PSMG1	Proteasome assembly chaperone 1	1	16.87	15.56	15.52	15.98	41.81	38.84	43.88	41.51	2.60	7.53E-05
434	Q9UJS0-2	SLC25A13	Isoform 2 of Calcium-binding mitochondrial carrier protein Aralar2	4	202.72	218.81	112.42	177.98	349.51	504.15	532.75	462.13	2.60	1.25E-02
435	P60900	PSMA6	Proteasome subunit alpha type-6	1	97.10	70.43	59.59	75.71	163.31	201.68	224.42	196.47	2.60	4.56E-03
436	Q9NR30	DDX21	Nucleolar RNA helicase 2	15	2323.13	2266.99	1237.42	1942.51	4054.25	5546.65	5521.90	5040.93	2.60	6.95E-03
437	P25325	MPST	3-mercaptopyruvate sulfurtransferase	2	96.04	94.19	52.36	80.86	161.51	229.51	238.38	209.80	2.59	1.02E-02
438	P14174	MIF	Macrophage migration inhibitory factor	1	117.70	103.62	70.23	97.18	216.43	262.98	276.88	252.10	2.59	2.56E-03
439	Q5JWF2	GNAS	Guanine nucleotide-binding protein G(s) subunit alpha isoforms XLas	1	239.88	288.88	163.35	230.70	490.68	607.61	696.95	598.41	2.59	6.29E-03
440	Q9Y265	RUVBL1	RuvB-like 1	6	490.04	462.08	288.65	413.59	849.97	1140.43	1227.86	1072.75	2.59	7.21E-03
441	O43390	HNRNPR	Heterogeneous nuclear ribonucleoprotein R	20	4235.88	4215.83	2090.20	3513.97	6984.02	10128.50	10230.50	9114.34	2.59	1.20E-02
442	P33993	MCM7	DNA replication licensing factor MCM7	2	110.92	102.74	58.12	90.60	190.65	245.09	269.03	234.92	2.59	7.08E-03

443	P49770	EIF2B2	Translation initiation factor eIF-2B subunit beta	1	9.90	11.40	17.12	12.81	25.35	33.71	40.45	33.17	2.59	1.41E-02
444	P37802	TAGLN2	Transgelin-2	5	629.98	519.48	328.62	492.69	1039.53	1297.11	1490.99	1275.88	2.59	7.66E-03
445	P26368	U2AF2	Splicing factor U2AF 65 kDa subunit	4	701.92	778.73	412.46	631.04	1275.92	1747.95	1862.74	1628.87	2.58	9.17E-03
446	Q8NBS9	TXNDC5	Thioredoxin domain-containing protein 5	2	50.36	66.91	43.04	53.44	99.18	171.19	143.12	137.83	2.58	1.88E-02
447	Q00325	SLC25A3	Phosphate carrier protein, mitochondrial	8	937.76	940.13	489.32	789.07	1484.07	2253.32	2367.51	2034.97	2.58	1.68E-02
448	P08238	HSP90AB1	Heat shock protein HSP 90-beta	14	2671.03	2154.53	1343.18	2056.25	4485.09	5384.06	6002.15	5290.43	2.57	5.26E-03
449	Q96SB4-3	SRPK1	Isoform 1 of SRSF protein kinase 1	1	155.42	156.67	88.00	133.36	287.75	360.14	379.30	342.40	2.57	4.35E-03
450	Q9P2R7	SUCLA2	Succinyl-CoA ligase [ADP-forming] subunit beta, mitochondrial	1	100.10	112.91	59.91	90.97	195.81	262.54	242.25	233.53	2.57	4.95E-03
451	P39656	DDOST	Dolichyl-diphosphooligosaccharide--protein glycosyltransferase 48 kDa subunit	3	284.11	346.40	173.82	268.11	554.27	740.55	769.39	688.07	2.57	7.56E-03
452	Q9BVA1	TUBB2B	Tubulin beta-2B chain	13	1400.32	943.81	606.11	983.41	2344.33	2525.95	2696.45	2522.24	2.56	3.62E-03
453	P52565	ARHGDIA	Rho GDP-dissociation inhibitor 1	2	240.85	225.09	126.94	197.62	397.54	530.28	592.76	506.86	2.56	1.03E-02
454	P34932	HSPA4	Heat shock 70 kDa protein 4	6	580.13	518.86	370.79	489.93	999.35	1379.15	1378.25	1252.25	2.56	5.65E-03
455	Q15084-2	PDIA6	Isoform 2 of Protein disulfide-isomerase A6	4	262.06	287.09	153.53	234.23	469.64	653.47	672.03	598.38	2.55	8.90E-03
456	Q9H9B4	SFXN1	Sideroflexin-1	1	42.74	54.57	32.84	43.38	83.87	134.81	113.71	110.80	2.55	1.37E-02
457	P14618	PKM	Pyruvate kinase PKM	22	3454.10	2596.67	1678.79	2576.52	5763.20	6824.45	7134.91	6574.19	2.55	3.74E-03
458	Q9H583	HEATR1	HEAT repeat-containing protein 1	1	11.70	14.32	16.96	14.32	17.27	47.45	44.83	36.52	2.55	8.56E-02
459	Q02543	RPL18A	60S ribosomal protein L18a	7	1709.39	1185.24	755.34	1216.66	2531.72	3159.03	3613.08	3101.28	2.55	1.07E-02
460	P47755	CAPZA2	F-actin-capping protein subunit alpha-2	1	50.22	49.48	33.40	44.37	94.02	119.56	125.55	113.04	2.55	3.49E-03
461	Q06830	PRDX1	Peroxiredoxin-1	6	1588.35	1443.67	872.03	1301.35	2746.21	3318.12	3865.10	3309.81	2.54	6.75E-03
462	Q9NVU7	SDAD1	Protein SDA1 homolog	1	100.23	103.13	53.77	85.71	187.54	226.43	239.85	217.94	2.54	4.12E-03
463	P61960-2	UFM1	Isoform 2 of Ubiquitin-fold modifier 1	1	12.60	15.31	11.11	13.01	26.93	32.07	40.16	33.05	2.54	7.72E-03
464	P11142	HSPA8	Heat shock cognate 71 kDa protein	23	3742.37	3221.13	1859.59	2941.03	6425.28	7792.32	8125.82	7447.81	2.53	4.16E-03
465	Q15717	ELAVL1	ELAV-like protein 1	6	737.95	809.13	426.11	657.73	1313.65	1895.87	1775.78	1661.77	2.53	9.20E-03
466	P54886	ALDH18A1	Delta-1-pyrroline-5-carboxylate synthase	14	1480.10	1721.22	845.46	1348.93	2629.34	3672.49	3911.01	3404.28	2.52	1.21E-02
467	Q9BZZ5	API5	Apoptosis inhibitor 5	1	68.94	66.02	36.49	57.15	113.16	155.94	163.52	144.21	2.52	9.79E-03
468	P26599-3	PTBP1	Isoform 3 of Polypyrimidine tract-binding protein 1	7	905.09	930.73	463.53	766.45	1514.63	2255.06	2024.17	1931.29	2.52	1.19E-02
469	Q02880	TOP2B	DNA topoisomerase 2-beta	5	201.17	181.95	120.88	168.00	316.97	508.55	444.16	423.23	2.52	1.41E-02
470	Q9H0D6	XRN2	5'-3' exoribonuclease 2	1	51.03	55.64	32.46	46.38	92.00	130.37	127.73	116.70	2.52	7.86E-03
471	P17812	CTPS1	CTP synthase 1	2	68.37	63.96	44.25	58.86	116.52	155.03	172.74	148.10	2.52	7.99E-03

472	Q99797	MIPEP	Mitochondrial intermediate peptidase	1	92.46	99.65	71.33	87.81	160.36	243.99	258.03	220.80	2.51	1.37E-02
473	Q9Y3D3	MRPS16	28S ribosomal protein S16, mitochondrial	1	56.93	43.02	32.17	44.04	74.76	126.28	130.31	110.45	2.51	2.61E-02
474	P61758	VBP1	Prefoldin subunit 3	1	24.05	22.53	16.16	20.91	40.11	52.39	64.80	52.43	2.51	1.38E-02
475	P07900-2	HSP90AA1	Isoform 2 of Heat shock protein HSP 90-alpha	24	4731.50	4079.96	2494.54	3768.67	8180.94	9536.70	10624.40	9447.35	2.51	4.25E-03
476	P27695	APEX1	DNA-(apurinic or apyrimidinic site) lyase	1	77.79	74.51	43.97	65.43	141.70	156.24	193.91	163.95	2.51	6.48E-03
477	P07195	LDHB	L-lactate dehydrogenase B chain	9	1727.95	1335.64	804.86	1289.48	2938.54	3337.36	3402.98	3226.29	2.50	3.12E-03
478	Q8TDD1-2	DDX54	Isoform 2 of ATP-dependent RNA helicase DDX54	1	45.80	43.87	24.11	37.93	75.91	107.76	100.75	94.80	2.50	8.76E-03
479	B5ME19	EIF3CL	Eukaryotic translation initiation factor 3 subunit C-like protein	4	283.56	261.90	167.71	237.72	500.28	605.41	675.34	593.68	2.50	4.58E-03
480	P30837	ALDH1B1	Aldehyde dehydrogenase X, mitochondrial	3	151.17	158.44	91.29	133.63	276.49	357.65	363.13	332.42	2.49	4.83E-03
481	O00541	PES1	Pescadillo homolog	3	158.23	158.35	100.00	138.86	259.56	405.29	371.39	345.42	2.49	1.27E-02
482	P30050	RPL12	60S ribosomal protein L12	5	886.05	784.86	550.97	740.63	1527.30	1958.43	2023.83	1836.52	2.48	4.04E-03
483	P68363	TUBA1B	Tubulin alpha-1B chain	22	4887.75	3861.09	2337.76	3695.53	8635.86	8622.11	10218.40	9158.79	2.48	3.89E-03
484	Q9UBB4	ATXN10	Ataxin-10	1	39.77	46.33	27.92	38.01	79.23	101.32	101.92	94.16	2.48	3.66E-03
485	Q9UBQ5	EIF3K	Eukaryotic translation initiation factor 3 subunit K	1	63.32	60.27	41.35	54.98	109.33	133.99	164.64	135.99	2.47	9.64E-03
486	P12277	CKB	Creatine kinase B-type	8	482.98	371.84	245.15	366.66	811.84	912.04	996.01	906.63	2.47	3.42E-03
487	Q13148	TARDBP	TAR DNA-binding protein 43	2	157.55	154.83	72.63	128.34	251.29	353.49	346.85	317.21	2.47	1.19E-02
488	Q92598	HSPH1	Heat shock protein 105 kDa	4	517.20	460.54	271.58	416.44	874.08	1020.95	1189.79	1028.27	2.47	6.51E-03
489	P28066	PSMA5	Proteasome subunit alpha type-5	1	54.84	48.05	34.03	45.64	106.35	127.39	104.15	112.63	2.47	2.23E-03
490	P00492	HPRT1	Hypoxanthine-guanine phosphoribosyltransferase	2	157.06	172.63	94.09	141.26	316.52	321.33	404.25	347.37	2.46	5.21E-03
491	O60271	SPAG9	C-Jun-amino-terminal kinase-interacting protein 4	2	88.29	88.10	60.29	78.89	164.89	190.90	224.95	193.58	2.45	4.35E-03
492	P60866-2	RPS20	Isoform 2 of 40S ribosomal protein S20	1	205.47	188.97	114.70	169.72	310.18	442.31	490.87	414.45	2.44	1.58E-02
493	P50395	GDI2	Rab GDP dissociation inhibitor beta	4	329.01	300.18	186.29	271.83	562.91	665.54	762.86	663.77	2.44	5.62E-03
494	Q15050	RRS1	Ribosome biogenesis regulatory protein homolog	1	11.79	16.87	16.92	15.19	30.13	41.43	39.71	37.09	2.44	4.97E-03
495	Q8IY81	FTSJ3	pre-rRNA processing protein FTSJ3	4	307.78	359.90	187.82	285.17	573.18	756.58	758.33	696.03	2.44	6.75E-03
496	P18124	RPL7	60S ribosomal protein L7	6	970.67	772.23	418.28	720.39	1340.77	1844.18	2079.59	1754.85	2.44	1.89E-02
497	Q9Y6B6	SAR1B	GTP-binding protein SAR1b	1	68.85	56.46	38.09	54.46	97.43	144.48	155.67	132.53	2.43	1.74E-02
498	P18669	PGAM1	Phosphoglycerate mutase 1	3	148.53	129.36	80.66	119.52	247.83	299.92	323.97	290.57	2.43	4.80E-03
499	Q13162	PRDX4	Peroxiredoxin-4	3	444.96	417.91	260.98	374.62	737.20	961.84	1030.79	909.94	2.43	7.13E-03
500	P27635	RPL10	60S ribosomal protein L10	4	790.82	661.81	404.68	619.10	1258.62	1511.43	1740.53	1503.53	2.43	7.90E-03
501	Q96HC4	PDLIM5	PDZ and LIM domain protein 5	1	102.00	70.13	51.29	74.47	131.88	190.86	219.42	180.72	2.43	2.33E-02

502	Q08257	CRYZ	Quinone oxidoreductase	3	309.17	597.00	309.90	405.36	747.34	1202.84	997.06	982.41	2.42	2.39E-02
503	Q9UBE0	SAE1	SUMO-activating enzyme subunit 1	1	207.87	188.18	129.61	175.22	368.09	434.14	471.47	424.56	2.42	2.87E-03
504	P62917	RPL8	60S ribosomal protein L8	5	721.26	568.81	335.64	541.90	1091.25	1390.87	1456.74	1312.95	2.42	8.31E-03
505	P13797	PLS3	Plastin-3	17	2811.54	2417.52	1470.56	2233.21	4699.65	5420.44	6078.64	5399.58	2.42	4.91E-03
506	Q92841	DDX17	Probable ATP-dependent RNA helicase DDX17	17	2430.46	2610.80	1267.13	2102.80	4134.48	5402.52	5694.68	5077.23	2.41	9.56E-03
507	Q9BWF3	RBM4	RNA-binding protein 4	2	187.70	205.89	111.49	168.36	329.86	448.80	439.95	406.20	2.41	7.71E-03
508	P07437	TUBB	Tubulin beta chain	2	414.81	307.51	227.98	316.77	608.69	736.68	945.90	763.76	2.41	1.63E-02
509	Q9NZI8	IGF2BP1	Insulin-like growth factor 2 mRNA-binding protein 1	6	472.42	407.17	235.81	371.80	701.01	920.68	1051.09	890.93	2.40	1.39E-02
510	P47756-2	CAPZB	Isoform 2 of F-actin-capping protein subunit beta	1	151.94	123.60	91.25	122.26	241.57	297.76	339.06	292.79	2.39	6.84E-03
511	Q5VTE0	EEF1A1P5	Putative elongation factor 1-alpha-like 3	14	3332.41	2236.10	1379.39	2315.97	4720.30	6120.87	5754.36	5531.84	2.39	1.03E-02
512	Q96DI7	SNRNP40	U5 small nuclear ribonucleoprotein 40 kDa protein	1	49.14	44.81	28.87	40.94	77.50	109.07	106.59	97.72	2.39	8.73E-03
513	O95433	AHSA1	Activator of 90 kDa heat shock protein ATPase homolog 1	1	18.35	23.21	16.61	19.39	37.39	49.59	51.54	46.17	2.38	5.24E-03
514	P02786	TFRC	Transferrin receptor protein 1	6	300.31	309.90	270.97	293.73	622.51	792.40	682.60	699.17	2.38	1.37E-03
515	Q15424-3	SAFB	Isoform 3 of Scaffold attachment factor B1	3	601.86	802.76	430.35	611.66	1262.59	1510.71	1591.44	1454.91	2.38	4.48E-03
516	P52948	NUP98	Nuclear pore complex protein Nup98-Nup96	1	84.28	73.31	41.86	66.48	122.01	176.73	175.53	158.09	2.38	1.43E-02
517	O60264	SMARCA5	SWI/SNF-related matrix-associated actin-dependent regulator of chromatin subfamily A member 5	3	320.79	330.94	200.74	284.16	524.79	722.07	779.65	675.50	2.38	1.12E-02
518	Q07020	RPL18	60S ribosomal protein L18	3	315.72	296.73	154.98	255.81	489.21	647.98	684.70	607.30	2.37	1.10E-02
519	O43242	PSMD3	26S proteasome non-ATPase regulatory subunit 3	2	209.48	188.08	122.48	173.35	342.68	429.83	455.77	409.43	2.36	5.39E-03
520	P43243	MATR3	Matrin-3	15	1875.76	2079.99	1104.26	1686.67	3210.73	4589.85	4142.53	3981.04	2.36	1.03E-02
521	Q92769	HDAC2	Histone deacetylase 2	1	82.86	80.07	48.11	70.34	138.67	171.04	187.25	165.65	2.35	6.25E-03
522	Q9Y262	EIF3L	Eukaryotic translation initiation factor 3 subunit L	2	84.96	89.94	58.86	77.92	156.27	183.60	210.57	183.48	2.35	4.58E-03
523	P15954	COX7C	Cytochrome c oxidase subunit 7C, mitochondrial	1	26.04	33.50	22.81	27.45	52.35	75.42	66.08	64.62	2.35	7.41E-03
524	P23246	SFPQ	Splicing factor, proline- and glutamine-rich	10	1917.72	2102.43	1101.78	1707.31	2995.86	4812.05	4242.54	4016.82	2.35	2.02E-02
525	Q9Y2X3	NOP58	Nucleolar protein 58	1	83.89	80.04	41.57	68.50	130.85	187.20	165.29	161.11	2.35	1.21E-02
526	P10599	TXN	Thioredoxin	3	784.61	668.98	532.02	661.87	1378.64	1567.64	1717.06	1554.45	2.35	1.86E-03
527	P09972	ALDOC	Fructose-bisphosphate aldolase C	1	34.37	28.55	23.23	28.72	60.96	62.79	78.21	67.32	2.34	3.70E-03
528	P62829	RPL23	60S ribosomal protein L23	3	694.86	629.50	410.60	578.32	1115.11	1372.79	1578.24	1355.38	2.34	8.15E-03
529	Q16658	FSCN1	Fascin	2	105.27	88.85	59.36	84.49	167.74	206.29	219.68	197.90	2.34	5.28E-03
530	Q12873-3	CHD3	Isoform 3 of Chromodomain-helicase-DNA-binding protein 3	1	11.74	11.11	12.47	11.77	12.36	37.62	32.51	27.50	2.34	1.11E-01

531	P55265-4	ADAR	Isoform 4 of Double-stranded RNA-specific adenosine deaminase	1	117.94	140.36	83.26	113.85	205.49	294.64	294.13	264.75	2.33	1.13E-02
532	Q12905	ILF2	Interleukin enhancer-binding factor 2	7	1025.80	1044.30	569.48	879.86	1663.35	2334.58	2137.45	2045.13	2.32	9.93E-03
533	P49720	PSMB3	Proteasome subunit beta type-3	1	75.23	64.70	33.32	57.75	122.11	138.40	141.83	134.11	2.32	5.46E-03
534	O95394-4	PGM3	Isoform 3 of Phosphoacetylglucosamine mutase	2	127.96	118.28	87.74	111.33	213.77	256.31	303.60	257.89	2.32	6.89E-03
535	P62495	ETF1	Eukaryotic peptide chain release factor subunit 1	3	267.33	255.08	141.16	221.19	454.46	510.18	569.54	511.39	2.31	5.10E-03
536	P55072	VCP	Transitional endoplasmic reticulum ATPase	6	1079.91	963.46	572.44	871.94	1653.78	2039.76	2334.72	2009.42	2.30	1.04E-02
537	P62906	RPL10A	60S ribosomal protein L10a	2	121.51	105.96	86.53	104.67	194.04	257.86	269.27	240.39	2.30	6.00E-03
538	P06733	ENO1	Alpha-enolase	16	3106.58	2573.90	1792.24	2490.91	4893.91	6213.02	6015.40	5707.44	2.29	4.57E-03
539	P20073	ANXA7	Annexin A7	1	49.66	38.60	35.16	41.14	83.69	84.93	113.76	94.13	2.29	7.88E-03
540	Q14974	KPNB1	Importin subunit beta-1	6	794.76	726.25	480.88	667.30	1304.78	1510.42	1760.60	1525.27	2.29	6.19E-03
541	P61019	RAB2A	Ras-related protein Rab-2A	1	16.18	14.35	9.07	13.20	21.79	30.90	37.75	30.14	2.28	2.91E-02
542	P62241	RPS8	40S ribosomal protein S8	7	881.67	730.35	449.62	687.21	1204.04	1650.91	1844.88	1566.61	2.28	1.82E-02
543	P12268	IMPDH2	Inosine-5'-monophosphate dehydrogenase 2	2	146.98	140.87	85.17	124.34	242.30	287.23	319.84	283.13	2.28	6.02E-03
544	P05198	EIF2S1	Eukaryotic translation initiation factor 2 subunit 1	1	80.43	56.37	34.46	57.09	139.22	121.09	129.51	129.94	2.28	6.96E-03
545	Q96AE4-2	FUBP1	Isoform 2 of Far upstream element-binding protein 1	1	101.83	103.01	67.62	90.82	167.17	242.11	210.84	206.71	2.28	9.28E-03
546	Q96P70	IPO9	Importin-9	1	101.49	113.77	62.80	92.68	198.19	206.66	227.75	210.87	2.28	2.61E-03
547	P09211	GSTP1	Glutathione S-transferase P	5	893.03	690.96	448.38	677.46	1281.62	1593.38	1743.55	1539.52	2.27	9.99E-03
548	P33991	MCM4	DNA replication licensing factor MCM4	2	143.01	108.11	74.29	108.47	243.94	240.07	254.96	246.32	2.27	2.47E-03
549	P08107	HSPA1A	Heat shock 70 kDa protein 1A/1B	21	4406.77	3590.58	2111.84	3369.73	6776.20	8085.62	8094.36	7652.06	2.27	5.92E-03
550	Q93009	USP7	Ubiquitin carboxyl-terminal hydrolase 7	2	375.31	368.11	228.65	324.02	644.89	739.60	817.78	734.09	2.27	4.05E-03
551	Q8N163-2	CCAR2	Isoform 2 of Cell cycle and apoptosis regulator protein 2	2	34.86	41.24	24.14	33.41	60.30	78.97	87.47	75.58	2.26	1.11E-02
552	Q9BYT8	NLN	Neurolysin, mitochondrial	1	35.28	33.51	20.10	29.63	56.31	71.39	73.36	67.02	2.26	6.58E-03
553	P38919	EIF4A3	Eukaryotic initiation factor 4A-III	6	813.83	785.44	461.73	687.00	1273.87	1647.67	1738.31	1553.28	2.26	8.83E-03
554	O75083	WDR1	WD repeat-containing protein 1	2	154.73	164.29	112.24	143.75	234.90	373.51	366.18	324.86	2.26	1.93E-02
555	P04083	ANXA1	Annexin A1	3	236.00	195.96	189.77	207.24	390.59	491.97	521.69	468.08	2.26	3.50E-03
556	P60891	PRPS1	Ribose-phosphate pyrophosphokinase 1	2	159.04	145.04	90.49	131.52	241.62	308.34	341.08	297.01	2.26	1.00E-02
557	P63244	GNB2L1	Guanine nucleotide-binding protein subunit beta-2-like 1	9	794.96	666.24	455.80	639.00	1169.17	1493.24	1665.56	1442.66	2.26	1.03E-02
558	P30086	PEBP1	Phosphatidylethanolamine-binding protein 1	3	113.74	96.87	75.35	95.32	167.65	229.71	245.04	214.13	2.25	1.05E-02
559	P60174	TPI1	Triosephosphate isomerase	11	2425.16	2125.49	1443.44	1998.03	3820.13	4623.95	5010.33	4484.80	2.24	5.46E-03
560	Q16531	DDB1	DNA damage-binding protein 1	11	915.97	854.29	581.55	783.94	1412.03	1907.89	1956.06	1758.66	2.24	8.48E-03

561	P83881	RPL36A	60S ribosomal protein L36a	2	328.30	294.28	206.88	276.49	517.63	651.61	687.70	618.98	2.24	5.59E-03
562	Q8TED0	UTP15	U3 small nucleolar RNA-associated protein 15 homolog	1	131.02	157.50	87.33	125.28	227.02	320.42	293.43	280.29	2.24	1.09E-02
563	Q9H6D7	HAUS4	HAUS augmin-like complex subunit 4	2	132.72	177.91	157.38	156.00	289.36	418.54	337.21	348.37	2.23	8.52E-03
564	P08240	SRPR	Signal recognition particle receptor subunit alpha	1	180.22	196.45	97.31	157.99	282.44	367.72	408.23	352.80	2.23	1.55E-02
565	O00505	KPNA3	Importin subunit alpha-4	2	224.63	218.60	139.90	194.37	378.20	428.90	493.83	433.64	2.23	5.19E-03
566	P22392-2	NME2	Isoform 3 of Nucleoside diphosphate kinase B	11	1456.57	1229.26	697.54	1127.79	2122.87	2734.70	2667.24	2508.27	2.22	9.65E-03
567	P04075-2	ALDOA	Isoform 2 of Fructose-bisphosphate aldolase A	14	2276.91	1833.61	1339.44	1816.65	3409.95	4196.22	4500.80	4035.66	2.22	6.31E-03
568	P49189	ALDH9A1	4-trimethylaminobutyraldehyde dehydrogenase	4	290.91	271.43	175.79	246.04	445.92	557.90	634.23	546.02	2.22	1.00E-02
569	P62277	RPS13	40S ribosomal protein S13	4	486.10	371.74	216.75	358.20	714.63	850.53	818.13	794.43	2.22	7.77E-03
570	P26373	RPL13	60S ribosomal protein L13	3	312.47	384.00	265.00	320.49	601.54	758.47	770.57	710.20	2.22	3.78E-03
571	Q15758	SLC1A5	Neutral amino acid transporter B(0)	2	71.27	89.20	54.33	71.60	133.17	163.94	178.67	158.59	2.22	6.56E-03
572	Q9H8H0	NOL11	Nucleolar protein 11	2	130.64	148.60	90.19	123.14	233.09	287.52	295.70	272.10	2.21	4.70E-03
573	P62937	PPIA	Peptidyl-prolyl cis-trans isomerase A	8	1956.36	1608.25	1015.44	1526.68	3094.18	3347.91	3669.01	3370.37	2.21	4.56E-03
574	Q9BVJ6	UTP14A	U3 small nucleolar RNA-associated protein 14 homolog A	2	175.37	180.87	92.12	149.45	259.00	353.92	376.41	329.78	2.21	1.73E-02
575	P43246	MSH2	DNA mismatch repair protein Msh2	2	43.77	36.04	31.02	36.94	67.35	87.33	89.86	81.52	2.21	5.15E-03
576	P48643	CCT5	T-complex protein 1 subunit epsilon	9	1459.60	1147.03	655.34	1087.32	2082.42	2489.32	2620.67	2397.47	2.20	1.00E-02
577	P40616	ARL1	ADP-ribosylation factor-like protein 1	1	99.53	59.17	40.19	66.30	110.96	148.79	178.46	146.07	2.20	3.83E-02
578	P48556	PSMD8	26S proteasome non-ATPase regulatory subunit 8	2	248.98	229.68	147.62	208.76	362.13	471.25	546.15	459.84	2.20	1.53E-02
579	O15042	U2SURP	U2 snRNP-associated SURP motif-containing protein	1	41.17	53.47	34.97	43.20	77.55	119.08	88.60	95.08	2.20	1.87E-02
580	Q10713	PMPCA	Mitochondrial-processing peptidase subunit alpha	3	150.06	202.93	231.96	194.98	449.45	491.38	342.66	427.83	2.19	9.84E-03
581	Q99459	CDC5L	Cell division cycle 5-like protein	5	477.06	532.95	283.08	431.03	774.23	1009.24	1049.82	944.43	2.19	1.10E-02
582	Q13509	TUBB3	Tubulin beta-3 chain	14	3144.51	1876.76	1010.80	2010.69	4615.36	4208.43	4391.12	4404.97	2.19	1.92E-02
583	P13010	XRCC5	X-ray repair cross-complementing protein 5	13	4470.19	3632.49	2442.15	3514.94	6242.02	8278.90	8536.29	7685.74	2.19	1.11E-02
584	Q9BQG0-2	MYBBP1A	Isoform 2 of Myb-binding protein 1A	10	760.59	854.59	521.87	712.35	1226.43	1637.94	1800.77	1555.05	2.18	1.30E-02
585	P25787	PSMA2	Proteasome subunit alpha type-2	1	17.84	21.36	12.06	17.09	30.65	38.57	42.57	37.27	2.18	1.04E-02
586	O00231-2	PSMD11	Isoform 2 of 26S proteasome non-ATPase regulatory subunit 11	2	87.34	97.41	75.96	86.90	154.13	189.86	223.83	189.27	2.18	8.27E-03
587	P26641	EEF1G	Elongation factor 1-gamma	8	1283.65	1093.43	739.12	1038.73	1934.72	2282.77	2567.59	2261.69	2.18	7.30E-03
588	Q8TEX9-2	IPO4	Isoform 2 of Importin-4	1	31.41	28.49	19.28	26.39	58.16	59.28	54.65	57.36	2.17	1.38E-03
589	P11216	PYGB	Glycogen phosphorylase, brain form	1	14.68	14.41	12.06	13.72	26.27	31.18	31.96	29.80	2.17	1.22E-03
590	P68371	TUBB4B	Tubulin beta-4B chain	4	277.11	188.82	103.77	189.90	399.45	413.59	424.02	412.35	2.17	1.17E-02

591	P09110	ACAA1	3-ketoacyl-CoA thiolase, peroxisomal	1	14.23	12.82	9.01	12.02	20.94	25.88	31.38	26.07	2.17	1.44E-02
592	P09874	PARP1	Poly [ADP-ribose] polymerase 1	26	4057.69	3297.07	2032.20	3128.99	5307.03	8048.23	6971.26	6775.51	2.17	2.13E-02
593	P53004	BLVRA	Biliverdin reductase A	1	93.58	91.88	60.22	81.89	141.09	189.98	200.79	177.29	2.16	1.11E-02
594	P00390	GSR	Glutathione reductase, mitochondrial	2	262.24	223.45	155.37	213.69	349.87	503.75	533.60	462.40	2.16	1.86E-02
595	P40925-3	MDH1	Isoform 3 of Malate dehydrogenase, cytoplasmic	5	390.06	424.95	269.03	361.35	691.28	798.63	843.71	777.87	2.15	3.11E-03
596	P37837	TALDO1	Transaldolase	3	1079.48	956.49	596.10	877.36	1575.38	1965.03	2124.81	1888.41	2.15	9.80E-03
597	P83731	RPL24	60S ribosomal protein L24	2	430.06	341.07	223.45	331.53	579.51	729.18	830.91	713.20	2.15	1.56E-02
598	P49207	RPL34	60S ribosomal protein L34	2	379.71	272.21	206.24	286.05	494.43	628.39	723.08	615.30	2.15	1.68E-02
599	P18206	VCL	Vinculin	2	144.82	118.57	79.02	114.14	178.55	315.09	242.13	245.26	2.15	4.03E-02
600	P22102	GART	Trifunctional purine biosynthetic protein adenosine-3	2	181.02	147.75	95.40	141.39	255.22	296.35	359.84	303.80	2.15	1.45E-02
601	O94776	MTA2	Metastasis-associated protein MTA2	4	359.98	367.83	223.68	317.16	533.00	722.54	788.31	681.28	2.15	1.54E-02
602	P78371	CCT2	T-complex protein 1 subunit beta	13	2220.05	1883.76	1269.87	1791.23	3189.28	4018.30	4327.21	3844.93	2.15	9.47E-03
603	P17844	DDX5	Probable ATP-dependent RNA helicase DDX5	15	1878.17	2010.95	1068.52	1652.55	2767.92	3890.19	3976.09	3544.73	2.15	1.79E-02
604	Q86XP3	DDX42	ATP-dependent RNA helicase DDX42	2	629.92	547.27	339.67	505.62	822.81	1176.39	1254.26	1084.49	2.14	2.17E-02
605	Q9BSJ8-2	ESYT1	Isoform 2 of Extended synaptotagmin-1	2	78.89	71.82	34.49	61.74	118.97	133.42	143.74	132.04	2.14	1.06E-02
606	P84098	RPL19	60S ribosomal protein L19	3	699.81	555.14	358.72	537.89	948.11	1246.62	1249.83	1148.19	2.13	1.23E-02
607	Q53GQ0	HSD17B12	Estradiol 17-beta-dehydrogenase 12	1	92.38	87.89	57.56	79.27	115.80	183.10	208.72	169.20	2.13	3.92E-02
608	P50990	CCT8	T-complex protein 1 subunit theta	17	2668.19	2317.06	1441.42	2142.22	3756.09	4738.53	5187.33	4560.65	2.13	1.23E-02
609	Q7RTV0	PHF5A	PHD finger-like domain-containing protein 5A	1	109.96	141.04	87.47	112.82	203.13	265.82	250.85	239.93	2.13	6.53E-03
610	P60842	EIF4A1	Eukaryotic initiation factor 4A-I	12	2046.81	1448.84	876.37	1457.34	2721.92	3091.79	3479.24	3097.65	2.13	1.52E-02
611	P51610-4	HCFC1	Isoform 4 of Host cell factor 1	2	137.61	134.93	77.98	116.84	201.72	267.96	274.83	248.17	2.12	1.24E-02
612	Q15008	PSMD6	26S proteasome non-ATPase regulatory subunit 6	2	274.38	285.07	197.77	252.41	420.27	629.41	557.46	535.71	2.12	1.35E-02
613	O00487	PSMD14	26S proteasome non-ATPase regulatory subunit 14	1	76.45	78.15	48.54	67.71	120.54	168.39	140.33	143.09	2.11	1.11E-02
614	Q8TDN6	BRIX1	Ribosome biogenesis protein BRX1 homolog	5	620.68	680.50	333.09	544.76	899.70	1296.59	1256.78	1151.02	2.11	2.16E-02
615	O76003	GLRX3	Glutaredoxin-3	1	48.89	50.16	38.28	45.78	75.25	108.01	106.38	96.55	2.11	1.09E-02
616	P62854	RPS26	40S ribosomal protein S26	4	534.05	388.24	248.98	390.42	657.43	857.02	953.71	822.72	2.11	2.27E-02
617	P13639	EEF2	Elongation factor 2	20	3780.96	3109.82	2132.81	3007.86	5808.55	6237.06	6943.11	6329.57	2.10	4.65E-03
618	P45974	USP5	Ubiquitin carboxyl-terminal hydrolase 5	2	61.37	52.07	41.41	51.62	90.70	109.12	126.00	108.61	2.10	8.24E-03
619	P41091	EIF2S3	Eukaryotic translation initiation factor 2 subunit 3	2	61.06	57.83	47.02	55.31	90.67	139.36	119.00	116.34	2.10	1.44E-02
620	Q9UHG3	PCYOX1	Prenylcysteine oxidase 1	3	149.14	152.46	90.50	130.70	199.52	319.70	304.73	274.65	2.10	2.83E-02

621	P04406	GAPDH	Glyceraldehyde-3-phosphate dehydrogenase	10	1871.44	1253.37	902.23	1342.35	2387.00	3147.63	2926.56	2820.40	2.10	1.51E-02
622	O14776	TCERG1	Transcription elongation regulator 1	1	33.45	35.18	18.53	29.05	50.70	69.71	62.69	61.03	2.10	1.40E-02
623	P43304	GPD2	Glycerol-3-phosphate dehydrogenase, mitochondrial	1	91.96	101.25	64.01	85.74	144.93	192.21	201.95	179.69	2.10	1.08E-02
624	P62701	RPS4X	40S ribosomal protein S4, X isoform	10	2617.07	2095.17	1379.23	2030.49	3586.23	4471.40	4705.67	4254.43	2.10	1.09E-02
625	Q9BZE4	GTPBP4	Nucleolar GTP-binding protein 1	4	717.70	741.22	428.12	629.01	1051.48	1543.54	1352.71	1315.91	2.09	1.72E-02
626	Q00526	CDK3	Cyclin-dependent kinase 3	2	207.04	227.05	100.41	178.17	323.95	398.84	394.62	372.47	2.09	1.36E-02
627	P43490	NAMPT	Nicotinamide phosphoribosyltransferase	2	232.52	203.08	137.67	191.09	327.82	420.10	450.37	399.43	2.09	1.08E-02
628	O95373	IPO7	Importin-7	6	262.93	251.41	166.24	226.86	431.68	451.67	538.65	474.00	2.09	5.28E-03
629	Q92900	UPF1	Regulator of nonsense transcripts 1	2	122.78	102.76	64.88	96.81	157.76	223.05	225.97	202.26	2.09	1.97E-02
630	P36551	CPOX	Coproporphyrinogen-III oxidase, mitochondrial	1	95.35	95.45	52.44	81.08	139.74	178.80	189.29	169.28	2.09	1.32E-02
631	P52888	THOP1	Thimet oligopeptidase	1	79.89	65.13	54.84	66.62	117.46	141.87	157.21	138.85	2.08	6.15E-03
632	P51532	SMARCA4	Transcription activator BRG1	3	190.39	180.39	103.42	158.07	279.61	346.59	359.80	328.67	2.08	9.98E-03
633	P13667	PDIA4	Protein disulfide-isomerase A4	17	3055.16	3277.66	1662.06	2664.96	4394.75	6177.47	6050.41	5540.88	2.08	1.98E-02
634	Q9H857	NT5DC2	5'-nucleotidase domain-containing protein 2	3	607.25	606.86	346.64	520.25	844.99	1127.20	1272.43	1081.54	2.08	2.12E-02
635	P00338-3	LDHA	Isoform 3 of L-lactate dehydrogenase A chain	8	2364.56	2002.04	1298.64	1888.41	3267.91	4072.04	4436.40	3925.45	2.08	1.19E-02
636	P54855	UGT2B15	UDP-glucuronosyltransferase 2B15	1	13.05	20.25	12.91	15.40	17.71	37.64	40.30	31.88	2.07	9.38E-02
637	P50991	CCT4	T-complex protein 1 subunit delta	10	1420.36	1237.72	740.87	1132.98	2034.44	2436.86	2557.10	2342.80	2.07	9.29E-03
638	Q9BWD1	ACAT2	Acetyl-CoA acetyltransferase, cytosolic	1	24.02	20.23	14.63	19.63	35.06	43.59	43.09	40.58	2.07	5.71E-03
639	Q16527	CSRP2	Cysteine and glycine-rich protein 2	1	13.27	15.30	10.53	13.03	24.31	27.92	28.58	26.94	2.07	1.92E-03
640	Q8N1G4	LRRC47	Leucine-rich repeat-containing protein 47	2	125.77	104.99	66.43	99.06	189.61	207.25	217.37	204.74	2.07	5.30E-03
641	O00299	CLIC1	Chloride intracellular channel protein 1	2	288.47	283.66	187.31	253.15	482.22	512.72	571.25	522.06	2.06	3.07E-03
642	Q9NYU2	UGGT1	UDP-glucose:glycoprotein glucosyltransferase 1	2	187.04	181.17	107.80	158.67	259.83	357.82	362.90	326.85	2.06	1.62E-02
643	P00558	PGK1	Phosphoglycerate kinase 1	13	2216.67	1835.87	1205.23	1752.59	3336.61	3693.39	3797.10	3609.03	2.06	4.71E-03
644	Q8TAQ2	SMARCC2	SWI/SNF complex subunit SMARCC2	1	18.01	19.76	12.35	16.70	27.85	35.65	39.63	34.38	2.06	1.27E-02
645	P62424	RPL7A	60S ribosomal protein L7a	4	558.94	462.93	263.34	428.40	709.34	929.83	1001.16	880.11	2.05	2.17E-02
646	O15144	ARPC2	Actin-related protein 2/3 complex subunit 2	1	148.23	126.70	82.48	119.14	213.45	264.16	256.38	244.66	2.05	7.34E-03
647	P22234-2	PAICS	Isoform 2 of Multifunctional protein ADE2	3	222.27	203.60	151.12	192.33	343.89	397.49	442.22	394.54	2.05	4.70E-03
648	Q9ULX3	NOB1	RNA-binding protein NOB1	1	21.30	18.84	12.20	17.45	27.87	39.37	40.04	35.76	2.05	1.88E-02
649	P33992	MCM5	DNA replication licensing factor MCM5	5	279.34	275.63	183.62	246.19	396.58	548.08	567.80	504.15	2.05	1.45E-02
650	Q04760	GLO1	Lactoylglutathione lyase	2	283.83	171.20	76.94	177.32	406.14	338.10	340.54	361.59	2.04	4.47E-02

651	Q96GQ7	DDX27	Probable ATP-dependent RNA helicase DDX27	2	198.38	193.27	110.55	167.40	261.51	408.02	353.76	341.09	2.04	2.78E-02
652	Q12906-7	ILF3	Isoform 7 of Interleukin enhancer-binding factor 3	19	2937.27	2769.01	1363.60	2356.63	3975.77	5314.48	5112.60	4800.95	2.04	1.98E-02
653	Q2NL82	TSR1	Pre-rRNA-processing protein TSR1 homolog	1	14.13	14.23	9.60	12.65	20.57	32.88	23.86	25.77	2.04	3.01E-02
654	Q9BY77	POLDIP3	Polymerase delta-interacting protein 3	1	40.41	48.66	28.90	39.32	67.59	91.75	79.83	79.72	2.03	1.10E-02
655	P13489	RNH1	Ribonuclease inhibitor	2	121.13	96.01	69.57	95.57	180.58	207.94	192.68	193.73	2.03	4.33E-03
656	Q96I24	FUBP3	Far upstream element-binding protein 3	2	74.62	74.12	49.18	65.97	115.13	155.06	130.64	133.61	2.03	9.20E-03
657	P50454	SERPINH1	Serpin H1	2	90.81	86.12	59.81	78.91	128.11	184.00	166.11	159.41	2.02	1.35E-02
658	Q99832	CCT7	T-complex protein 1 subunit eta	9	1408.20	1214.71	785.78	1136.23	1891.38	2371.27	2618.93	2293.86	2.02	1.48E-02
659	Q9UIG0	BAZ1B	Tyrosine-protein kinase BAZ1B	1	114.75	104.51	62.23	93.83	154.28	212.73	200.75	189.25	2.02	1.65E-02
660	Q16822	PCK2	Phosphoenolpyruvate carboxykinase [GTP], mitochondrial	1	30.72	29.17	20.88	26.92	40.86	62.31	59.64	54.27	2.02	2.10E-02
661	Q86W42	THOC6	THO complex subunit 6 homolog	1	42.92	48.96	30.23	40.70	72.54	81.63	91.84	82.00	2.01	6.23E-03
662	Q9NVP1	DDX18	ATP-dependent RNA helicase DDX18	7	780.59	849.56	500.25	710.13	1136.46	1624.88	1524.22	1428.52	2.01	1.72E-02
663	Q53GS9	USP39	U4/U6.U5 tri-snRNP-associated protein 2	1	32.47	29.02	17.97	26.49	42.79	57.60	59.33	53.24	2.01	1.73E-02
664	O60506	SYNCRIP	Heterogeneous nuclear ribonucleoprotein Q	7	1252.42	1151.18	655.74	1019.78	1643.96	2272.50	2232.29	2049.58	2.01	1.99E-02
665	Q7L2E3-2	DHX30	Isoform 2 of Putative ATP-dependent RNA helicase DHX30	4	334.41	380.32	262.67	325.80	573.88	695.02	688.13	652.34	2.00	3.31E-03
666	A0FGR8-6	ESYT2	Isoform 6 of Extended synaptotagmin-2	1	38.74	36.95	25.70	33.80	55.96	76.13	70.88	67.65	2.00	9.70E-03
667	P62136-2	PPP1CA	Isoform 2 of Serine/threonine-protein phosphatase PP1-alpha catalytic subunit	1	117.34	121.56	64.61	101.17	170.98	223.73	210.82	201.85	2.00	1.42E-02
668	Q96HJ9-2	C7orf55	Isoform 2 of UPF0562 protein C7orf55	1	11.75	17.88	8.49	12.70	20.74	29.75	25.50	25.33	1.99	2.90E-02
669	Q15427	SF3B4	Splicing factor 3B subunit 4	1	71.95	69.43	39.09	60.16	83.93	147.64	127.36	119.64	1.99	5.09E-02
670	P49589-3	CARS	Isoform 3 of Cysteine--tRNA ligase, cytoplasmic	1	107.70	96.51	56.79	87.00	141.83	178.86	197.74	172.81	1.99	1.90E-02
671	Q6P5S2	C6orf58	UPF0762 protein C6orf58	1	62.01	46.00	34.06	47.36	42.59	106.56	132.95	94.04	1.99	1.71E-01
672	P18621-3	RPL17	Isoform 3 of 60S ribosomal protein L17	3	848.18	982.19	596.99	809.12	1296.98	1832.93	1683.45	1604.45	1.98	1.53E-02
673	Q9Y3E5	PTRH2	Peptidyl-tRNA hydrolase 2, mitochondrial	2	184.13	218.95	113.15	172.08	261.08	382.02	380.08	341.06	1.98	2.90E-02
674	Q9H4A4	RNPEP	Aminopeptidase B	1	18.11	13.88	13.59	15.19	26.25	29.88	34.05	30.06	1.98	5.22E-03
675	P54577	YARS	Tyrosine--tRNA ligase, cytoplasmic	3	447.81	428.14	244.88	373.61	637.63	772.46	805.11	738.40	1.98	1.15E-02
676	P34897	SHMT2	Serine hydroxymethyltransferase, mitochondrial	21	2554.31	3157.05	1501.73	2404.36	3720.98	5220.07	5250.93	4730.66	1.97	2.92E-02
677	P03905	MT-ND4	NADH-ubiquinone oxidoreductase chain 4	1	38.32	58.31	23.39	40.01	74.72	76.02	84.47	78.40	1.96	2.21E-02
678	Q9UNM6-2	PSMD13	Isoform 2 of 26S proteasome non-ATPase regulatory subunit 13	3	295.95	281.29	175.38	250.87	424.64	490.38	559.78	491.60	1.96	1.15E-02
679	P08133	ANXA6	Annexin A6	1	56.10	40.33	44.64	47.02	74.91	89.76	111.12	91.93	1.95	1.76E-02

680	Q14683	SMC1A	Structural maintenance of chromosomes protein 1A	3	395.25	442.51	240.77	359.51	597.99	737.57	770.68	702.08	1.95	1.32E-02
681	Q9H993	C6orf211	UPF0364 protein C6orf211	1	18.37	15.21	13.40	15.66	26.51	32.97	32.26	30.58	1.95	4.00E-03
682	P55196-5	MLLT4	Isoform 5 of Afadin	1	40.45	32.96	22.49	31.97	45.76	67.28	74.09	62.38	1.95	3.84E-02
683	P46779-3	RPL28	Isoform 3 of 60S ribosomal protein L28	3	746.86	550.28	363.00	553.38	867.89	1153.54	1212.31	1077.91	1.95	2.69E-02
684	Q9Y3F4	STRAP	Serine-threonine kinase receptor-associated protein	3	392.57	401.38	233.46	342.47	608.90	655.11	735.90	666.63	1.95	7.97E-03
685	P49736	MCM2	DNA replication licensing factor MCM2	7	1005.31	821.97	630.83	819.37	1274.35	1666.31	1841.91	1594.19	1.95	1.78E-02
686	P15170-3	GSPT1	Isoform 3 of Eukaryotic peptide chain release factor GTP-binding subunit ERF3A	1	40.76	40.39	30.26	37.14	65.43	78.98	71.49	71.97	1.94	2.62E-03
687	P62857	RPS28	40S ribosomal protein S28	1	119.97	124.16	82.15	108.76	181.81	204.55	244.01	210.12	1.93	1.09E-02
688	Q9H307	PNN	Pinin	1	108.08	18.20	28.59	51.62	55.55	147.78	95.72	99.68	1.93	2.85E-01
689	Q96PK6	RBM14	RNA-binding protein 14	11	1637.30	1910.80	804.22	1450.77	2239.53	2924.71	3230.99	2798.41	1.93	3.84E-02
690	P61803	DAD1	Dolichyl-diphosphooligosaccharide--protein glycosyltransferase subunit DAD1	1	75.65	88.73	46.49	70.29	113.01	143.28	150.34	135.54	1.93	1.83E-02
691	P04843	RPN1	Dolichyl-diphosphooligosaccharide--protein glycosyltransferase subunit 1	13	2583.48	2824.25	1566.82	2324.85	3455.36	5129.57	4827.06	4470.66	1.92	2.90E-02
692	Q8N7H5	PAF1	RNA polymerase II-associated factor 1 homolog	1	27.49	19.05	17.31	21.28	33.17	43.82	45.55	40.84	1.92	1.72E-02
693	P67775	PPP2CA	Serine/threonine-protein phosphatase 2A catalytic subunit alpha isoform	2	287.27	260.61	170.06	239.31	377.68	449.23	550.76	459.22	1.92	2.32E-02
694	P23921	RRM1	Ribonucleoside-diphosphate reductase large subunit	4	380.68	322.55	201.34	301.52	481.19	601.75	652.16	578.36	1.92	1.94E-02
695	Q8N3U4-2	STAG2	Isoform 2 of Cohesin subunit SA-2	1	137.40	123.16	77.48	112.68	173.87	233.51	240.76	216.04	1.92	2.06E-02
696	O95197	RTN3	Reticulon-3	1	124.94	93.27	77.72	98.64	153.31	200.00	213.79	189.03	1.92	1.70E-02
697	Q15019-2	2-Sep	Isoform 2 of Septin-2	4	443.43	372.82	245.30	353.85	557.83	741.09	730.01	676.31	1.91	1.77E-02
698	Q00765	REEP5	Receptor expression-enhancing protein 5	2	78.79	96.91	68.12	81.27	117.08	158.38	190.49	155.31	1.91	3.17E-02
699	P17987	TCP1	T-complex protein 1 subunit alpha	10	1632.57	1362.93	937.94	1311.15	2100.90	2714.88	2692.69	2502.82	1.91	1.39E-02
700	P52272	HNRNPM	Heterogeneous nuclear ribonucleoprotein M	18	3761.81	3707.06	1748.26	3072.38	4488.79	6992.84	6103.96	5861.86	1.91	4.76E-02
701	Q14008-3	CKAP5	Isoform 3 of Cytoskeleton-associated protein 5	1	100.60	85.81	56.99	81.13	133.61	155.44	174.62	154.56	1.90	1.36E-02
702	P06744-2	GPI	Isoform 2 of Glucose-6-phosphate isomerase	7	796.49	652.41	470.14	639.68	970.72	1401.48	1279.07	1217.09	1.90	2.22E-02
703	P12814-4	ACTN1	Isoform 4 of Alpha-actinin-1	8	1698.65	1476.95	988.41	1388.00	2205.22	2691.44	3018.95	2638.54	1.90	1.67E-02
704	Q01780	EXOSC10	Exosome component 10	1	165.67	175.12	96.30	145.69	200.52	302.36	327.07	276.65	1.90	4.66E-02
705	P04080	CSTB	Cystatin-B	1	40.07	51.89	27.03	39.66	55.16	89.36	81.15	75.22	1.90	4.73E-02
706	P11940	PABPC1	Polyadenylate-binding protein 1	5	556.79	461.48	293.38	437.21	692.97	858.22	933.96	828.38	1.89	2.03E-02
707	O75694	NUP155	Nuclear pore complex protein Nup155	1	35.52	35.06	25.39	31.99	54.57	63.38	63.67	60.54	1.89	3.04E-03

708	Q08211	DHX9	ATP-dependent RNA helicase A	24	3333.92	3821.53	1941.43	3032.29	4658.72	6357.45	6174.30	5730.16	1.89	2.58E-02
709	Q13310-3	PABPC4	Isoform 3 of Polyadenylate-binding protein 4	6	527.85	467.00	311.24	435.36	648.50	904.99	910.36	821.29	1.89	2.32E-02
710	O43707	ACTN4	Alpha-actinin-4	10	1356.10	1275.55	716.38	1116.01	1716.79	2053.26	2545.54	2105.20	1.89	3.44E-02
711	O14744	PRMT5	Protein arginine N-methyltransferase 5	3	357.71	354.62	235.93	316.09	531.11	568.48	686.86	595.48	1.88	1.06E-02
712	P39023	RPL3	60S ribosomal protein L3	6	1220.97	1031.71	588.25	946.98	1474.33	1913.70	1952.74	1780.26	1.88	2.63E-02
713	O00151	PDLIM1	PDZ and LIM domain protein 1	1	82.66	64.59	45.90	64.38	98.04	118.49	145.85	120.79	1.88	3.19E-02
714	P60709	ACTB	Actin, cytoplasmic 1	11	1125.77	877.88	478.52	827.39	1403.49	1733.18	1507.89	1548.19	1.87	2.73E-02
715	Q7KZF4	SND1	Staphylococcal nuclease domain-containing protein 1	5	302.43	257.73	183.01	247.72	389.86	491.70	508.43	463.33	1.87	1.33E-02
716	O00410-3	IPO5	Isoform 3 of Importin-5	8	802.75	681.41	425.19	636.45	1133.78	1121.77	1305.63	1187.06	1.87	1.20E-02
717	P19623	SRM	Spermidine synthase	2	283.81	250.26	166.50	233.52	368.02	468.01	470.00	435.34	1.86	1.41E-02
718	P56134	ATP5J2	ATP synthase subunit f, mitochondrial	1	43.74	54.87	20.34	39.65	63.67	80.60	77.41	73.89	1.86	4.01E-02
719	Q8WWM7-3	ATXN2L	Isoform 3 of Ataxin-2-like protein	2	173.54	161.42	98.73	144.56	212.37	256.30	338.51	269.06	1.86	4.63E-02
720	P14866	HNRNPL	Heterogeneous nuclear ribonucleoprotein L	13	2549.09	2762.44	1350.69	2220.74	3575.34	4630.62	4189.79	4131.92	1.86	2.34E-02
721	O43175	PHGDH	D-3-phosphoglycerate dehydrogenase	9	1723.62	1481.62	1044.47	1416.57	2158.16	2805.09	2939.84	2634.36	1.86	1.76E-02
722	Q9NTI5	PDS5B	Sister chromatid cohesion protein PDS5 homolog B	1	33.18	36.40	24.16	31.25	49.41	69.27	55.39	58.02	1.86	1.81E-02
723	Q96JJ7	TMX3	Protein disulfide-isomerase TMX3	1	107.90	128.48	68.76	101.71	160.90	201.60	202.14	188.22	1.85	1.76E-02
724	Q15393	SF3B3	Splicing factor 3B subunit 3	8	658.69	686.58	394.39	579.89	870.17	1185.88	1156.14	1070.73	1.85	2.32E-02
725	Q9NW13	RBM28	RNA-binding protein 28	1	60.48	40.44	75.45	58.79	121.44	132.10	71.88	108.48	1.85	7.85E-02
726	Q14980	NUMA1	Nuclear mitotic apparatus protein 1	2	114.19	117.67	73.67	101.84	160.49	216.76	185.58	187.61	1.84	1.64E-02
727	Q9H0A0	NAT10	N-acetyltransferase 10	2	82.24	91.47	78.74	84.15	118.38	196.51	149.98	154.96	1.84	3.70E-02
728	Q01518	CAP1	Adenylyl cyclase-associated protein 1	5	626.90	498.65	304.62	476.72	752.47	912.66	968.39	877.84	1.84	2.44E-02
729	P14735	IDE	Insulin-degrading enzyme	2	145.34	122.64	78.04	115.34	169.93	216.43	249.95	212.10	1.84	3.37E-02
730	P68402	PAFAH1B2	Platelet-activating factor acetylhydrolase IB subunit beta	1	50.19	48.16	40.60	46.32	66.63	89.84	98.46	84.98	1.83	1.77E-02
731	P78417	GSTO1	Glutathione S-transferase omega-1	2	143.32	122.52	89.76	118.53	194.63	213.46	244.06	217.38	1.83	9.61E-03
732	Q9UQE7	SMC3	Structural maintenance of chromosomes protein 3	8	632.32	612.41	375.32	540.02	805.26	1060.10	1104.90	990.09	1.83	2.25E-02
733	P48147	PREP	Prolyl endopeptidase	1	50.11	47.62	25.88	41.20	66.69	69.91	89.46	75.36	1.83	3.11E-02
734	P26639	TARS	Threonine--tRNA ligase, cytoplasmic	8	988.16	831.68	542.62	787.49	1243.33	1453.90	1620.10	1439.11	1.83	1.86E-02
735	Q9Y617	PSAT1	Phosphoserine aminotransferase	4	747.44	619.66	406.24	591.12	870.14	1115.26	1255.00	1080.13	1.83	3.12E-02
736	O75844	ZMPSTE24	CAAX prenyl protease 1 homolog	2	338.32	389.12	229.89	319.11	444.48	616.19	687.64	582.77	1.83	3.76E-02
737	Q12907	LMAN2	Vesicular integral-membrane protein VIP36	2	303.93	344.40	206.44	284.92	417.50	582.55	555.97	518.68	1.82	2.34E-02

738	Q8WXF1	PSPC1	Paraspeckle component 1	4	1203.87	1197.08	657.78	1019.58	1443.01	2222.33	1883.29	1849.54	1.81	4.55E-02
739	Q9Y3I0	RTCB	tRNA-splicing ligase RtcB homolog	3	251.21	261.03	163.39	225.21	327.91	412.39	484.70	408.34	1.81	2.90E-02
740	Q8NBJ5	COLGALT1	Procollagen galactosyltransferase 1	1	45.34	62.29	35.48	47.70	63.87	103.26	92.34	86.49	1.81	5.15E-02
741	Q9NY33	DPP3	Dipeptidyl peptidase 3	1	24.51	28.62	16.54	23.22	36.72	42.45	47.08	42.08	1.81	1.53E-02
742	P11586	MTHFD1	C-1-tetrahydrofolate synthase, cytoplasmic	6	759.87	660.27	479.29	633.14	928.02	1273.06	1237.42	1146.17	1.81	2.00E-02
743	Q15029	EFTUD2	116 kDa U5 small nuclear ribonucleoprotein component	7	831.61	828.12	494.55	718.09	1071.06	1377.07	1442.33	1296.82	1.81	2.24E-02
744	Q92481-2	TFAP2B	Isoform 2 of Transcription factor AP-2-beta	1	23.84	21.70	14.79	20.11	31.84	36.23	40.82	36.30	1.80	1.27E-02
745	P10768	ESD	S-formylglutathione hydrolase	1	143.17	131.84	68.94	114.65	178.28	212.51	229.90	206.90	1.80	2.89E-02
746	Q71UM5	RPS27L	40S ribosomal protein S27-like	1	141.82	110.46	66.44	106.24	171.74	200.89	201.50	191.37	1.80	2.37E-02
747	Q9BXJ9	NAA15	N-alpha-acetyltransferase 15, NatA auxiliary subunit	2	118.98	106.61	69.09	98.23	155.20	169.94	205.52	176.89	1.80	2.05E-02
748	P55060	CSE1L	Exportin-2	7	912.75	804.43	516.07	744.41	1174.86	1285.73	1552.14	1337.58	1.80	2.20E-02
749	P29401-2	TKT	Isoform 2 of Transketolase	10	1376.89	1213.83	849.80	1146.84	1661.65	2224.25	2276.52	2054.14	1.79	2.25E-02
750	Q13724	MOGS	Mannosyl-oligosaccharide glucosidase	3	245.22	241.22	149.66	212.03	304.15	405.68	429.39	379.74	1.79	2.76E-02
751	Q9NZ01	TECR	Very-long-chain enoyl-CoA reductase	1	24.60	27.19	13.00	21.60	32.82	40.97	42.16	38.65	1.79	3.16E-02
752	Q92973	TNPO1	Transportin-1	1	53.03	50.55	28.76	44.11	69.48	75.16	92.15	78.93	1.79	2.77E-02
753	P23526	AHCY	Adenosylhomocysteinase	3	551.01	450.87	318.37	440.08	659.14	833.16	866.30	786.20	1.79	2.05E-02
754	Q9NSD9	FARSB	Phenylalanine--tRNA ligase beta subunit	2	339.45	289.76	177.25	268.82	406.02	504.41	530.04	480.15	1.79	2.58E-02
755	P12532-2	CKMT1A	Isoform 2 of Creatine kinase U-type, mitochondrial	2	297.45	311.19	173.01	260.55	344.09	510.60	537.24	463.98	1.78	5.29E-02
756	P48444	ARCN1	Coatomer subunit delta	1	46.84	43.03	26.67	38.85	55.78	68.88	82.55	69.07	1.78	3.79E-02
757	Q92599	8-Sep	Septin-8	1	345.29	284.56	210.77	280.21	391.26	519.96	578.56	496.59	1.77	3.29E-02
758	Q9Y3U8	RPL36	60S ribosomal protein L36	2	170.54	133.59	66.33	123.49	208.55	204.97	242.22	218.58	1.77	4.39E-02
759	O00232	PSMD12	26S proteasome non-ATPase regulatory subunit 12	1	235.01	232.63	129.14	198.92	298.96	353.27	403.86	352.03	1.77	2.96E-02
760	O00425	IGF2BP3	Insulin-like growth factor 2 mRNA-binding protein 3	3	220.93	240.49	107.79	189.74	280.58	352.32	374.04	335.64	1.77	4.35E-02
761	P49368	CCT3	T-complex protein 1 subunit gamma	9	1490.32	1460.59	876.49	1275.80	1903.74	2383.58	2473.21	2253.51	1.77	2.15E-02
762	Q99643	SDHC	Succinate dehydrogenase cytochrome b560 subunit, mitochondrial	1	102.86	124.76	45.79	91.14	138.85	179.16	163.65	160.55	1.76	5.76E-02
763	P21964	COMT	Catechol O-methyltransferase	1	45.26	46.20	34.34	41.94	65.69	90.59	64.48	73.59	1.75	2.74E-02
764	Q9UNX4	WDR3	WD repeat-containing protein 3	1	89.33	100.63	56.92	82.29	113.73	159.94	159.20	144.29	1.75	3.69E-02
765	Q9H8H3	METTL7A	Methyltransferase-like protein 7A	1	47.73	55.97	32.99	45.56	66.52	76.94	94.55	79.33	1.74	3.32E-02
766	P52209	PGD	6-phosphogluconate dehydrogenase, decarboxylating	2	409.35	400.06	327.59	379.00	608.26	672.70	694.55	658.50	1.74	1.58E-03

767	Q15738	NSDHL	Sterol-4-alpha-carboxylate 3-dehydrogenase, decarboxylating	1	22.00	20.04	18.80	20.28	31.95	44.63	29.08	35.22	1.74	3.73E-02
768	P61619	SEC61A1	Protein transport protein Sec61 subunit alpha isoform 1	1	232.66	284.06	163.40	226.71	333.39	408.58	438.27	393.41	1.74	2.36E-02
769	Q86VP6	CAND1	Cullin-associated NEDD8-dissociated protein 1	5	525.51	482.35	311.93	439.93	653.12	761.49	871.97	762.19	1.73	2.38E-02
770	P54136	RARS	Arginine--tRNA ligase, cytoplasmic	1	81.01	77.35	51.00	69.79	101.29	120.12	140.29	120.56	1.73	2.60E-02
771	Q92499	DDX1	ATP-dependent RNA helicase DDX1	4	851.65	773.16	507.37	710.73	1004.89	1303.40	1370.31	1226.20	1.73	2.82E-02
772	P46940	IQGAP1	Ras GTPase-activating-like protein IQGAP1	4	451.76	448.31	307.86	402.64	624.84	666.81	790.72	694.12	1.72	1.33E-02
773	P46782	RPS5	40S ribosomal protein S5	5	1604.89	1332.75	937.83	1291.82	1938.20	2252.50	2489.77	2226.82	1.72	2.04E-02
774	Q14157-5	UBAP2L	Isoform 5 of Ubiquitin-associated protein 2-like	2	192.87	134.58	74.74	134.06	171.49	243.09	278.47	231.02	1.72	1.05E-01
775	M0QYS1	RPL13A	60S ribosomal protein L13a (Fragment)	4	2161.33	1443.69	815.17	1473.40	2180.10	2665.12	2767.02	2537.41	1.72	6.82E-02
776	Q13200	PSMD2	26S proteasome non-ATPase regulatory subunit 2	3	287.90	294.17	168.04	250.04	372.85	437.56	476.99	429.13	1.72	2.47E-02
777	Q8TCT9-2	HM13	Isoform 2 of Minor histocompatibility antigen H13	1	196.88	254.83	115.19	188.97	260.51	341.52	369.97	324.00	1.71	6.06E-02
778	P08195-4	SLC3A2	Isoform 4 of 4F2 cell-surface antigen heavy chain	1	31.78	50.04	25.81	35.88	44.67	73.57	66.31	61.51	1.71	8.65E-02
779	P12270	TPR	Nucleoprotein TPR	2	90.61	89.21	51.61	77.14	114.80	155.23	126.49	132.17	1.71	3.49E-02
780	P35580-4	MYH10	Isoform 4 of Myosin-10	2	331.14	284.93	200.40	272.16	421.33	462.06	515.29	466.22	1.71	1.45E-02
781	P30153	PPP2R1A	Serine/threonine-protein phosphatase 2A 65 kDa regulatory subunit A alpha isoform	3	320.71	354.67	221.12	298.83	427.66	541.77	566.02	511.82	1.71	2.20E-02
782	P40227	CCT6A	T-complex protein 1 subunit zeta	7	605.79	549.79	385.55	513.71	731.25	911.10	996.96	879.77	1.71	2.33E-02
783	P46060	RANGAP1	Ran GTPase-activating protein 1	2	39.02	80.28	29.47	49.59	85.18	85.88	83.53	84.86	1.71	8.67E-02
784	O43808	SLC25A17	Peroxisomal membrane protein PMP34	1	51.19	51.90	24.67	42.59	57.58	81.15	79.47	72.73	1.71	6.22E-02
785	Q99460	PSMD1	26S proteasome non-ATPase regulatory subunit 1	2	287.97	262.55	184.82	245.11	342.19	423.86	489.12	418.39	1.71	3.01E-02
786	Q9UHD8	9-Sep	Septin-9	1	101.01	83.09	56.90	80.33	113.30	149.73	148.03	137.02	1.71	3.15E-02
787	P61927	RPL37	60S ribosomal protein L37	1	49.60	40.71	24.86	38.39	47.31	65.23	83.63	65.39	1.70	1.01E-01
788	Q02809	PLOD1	Procollagen-lysine,2-oxoglutarate 5-dioxygenase 1	2	380.14	372.68	201.97	318.26	419.50	614.84	591.40	541.91	1.70	5.76E-02
789	O75533	SF3B1	Splicing factor 3B subunit 1	7	1413.89	1635.26	926.44	1325.20	1868.12	2377.73	2511.19	2252.35	1.70	3.19E-02
790	Q13155	AIMP2	Aminoacyl tRNA synthase complex-interacting multifunctional protein 2	1	205.68	208.26	173.22	195.72	269.61	363.14	364.47	332.41	1.70	1.49E-02
791	P35998	PSMC2	26S protease regulatory subunit 7	1	30.00	35.29	21.58	28.95	41.02	57.25	49.20	49.16	1.70	3.04E-02
792	Q9ULV4-3	CORO1C	Isoform 3 of Coronin-1C	1	174.41	160.53	91.37	142.10	200.17	248.23	274.73	241.04	1.70	4.26E-02
793	P42224	STAT1	Signal transducer and activator of transcription 1-alpha/beta	1	40.57	37.45	29.47	35.83	47.79	64.32	70.05	60.72	1.69	2.88E-02
794	Q16851	UGP2	UTP--glucose-1-phosphate uridylyltransferase	1	13.63	14.38	10.70	12.90	18.99	23.67	22.89	21.85	1.69	8.16E-03
795	O75534-3	CSDE1	Isoform 3 of Cold shock domain-containing protein E1	3	411.13	361.79	244.95	339.29	527.50	561.59	623.37	570.82	1.68	1.51E-02

796	P30566	ADSL	Adenylosuccinate lyase	1	148.54	131.48	94.37	124.79	192.12	201.96	235.29	209.79	1.68	1.47E-02
797	Q9BVI4	NOC4L	Nucleolar complex protein 4 homolog	1	94.50	101.71	54.98	83.73	123.34	154.66	143.71	140.57	1.68	2.97E-02
798	P48059-3	LIMS1	Isoform 3 of LIM and senescent cell antigen-like-containing domain protein 1	1	23.89	17.18	16.01	19.03	27.61	30.32	37.83	31.92	1.68	3.02E-02
799	Q9HAV4	XPO5	Exportin-5	1	75.33	70.86	50.16	65.45	91.86	100.44	136.34	109.55	1.67	4.82E-02
800	Q8NCA5	FAM98A	Protein FAM98A	1	41.90	48.86	25.19	38.65	58.87	66.85	68.26	64.66	1.67	2.68E-02
801	Q86YP4-3	GATAD2A	Isoform 3 of Transcriptional repressor p66-alpha	1	38.07	38.53	26.90	34.50	48.89	62.26	61.01	57.39	1.66	1.61E-02
802	Q9UHB9	SRP68	Signal recognition particle subunit SRP68	1	38.12	32.97	26.59	32.56	45.69	57.77	59.01	54.16	1.66	1.62E-02
803	Q9HCE1	MOV10	Putative helicase MOV-10	1	29.74	24.23	20.09	24.69	33.26	47.99	41.86	41.04	1.66	3.28E-02
804	Q96TA1	FAM129B	Niban-like protein 1	1	57.00	48.71	39.16	48.29	60.57	92.62	87.23	80.14	1.66	4.63E-02
805	P14868	DARS	Aspartate--tRNA ligase, cytoplasmic	2	190.32	182.79	109.64	160.92	222.09	269.81	309.19	267.03	1.66	4.21E-02
806	P56192	MARS	Methionine--tRNA ligase, cytoplasmic	5	382.73	387.72	234.57	335.00	470.13	584.02	608.23	554.13	1.65	2.92E-02
807	Q13813-2	SPTAN1	Isoform 2 of Spectrin alpha chain, non-erythrocytic 1	4	180.80	205.14	127.55	171.16	238.71	310.59	298.90	282.73	1.65	2.51E-02
808	P07099	EPHX1	Epoxide hydrolase 1	2	321.82	396.20	183.69	300.57	383.34	565.31	539.89	496.18	1.65	8.12E-02
809	P16615	ATP2A2	Sarcoplasmic/endoplasmic reticulum calcium ATPase 2	2	87.33	97.50	60.86	81.90	112.11	130.67	161.95	134.91	1.65	4.35E-02
810	P28482	MAPK1	Mitogen-activated protein kinase 1	2	411.67	352.23	236.61	333.50	439.73	586.19	616.92	547.61	1.64	4.62E-02
811	Q13867	BLMH	Bleomycin hydrolase	1	33.53	42.36	27.01	34.30	55.14	56.53	57.15	56.28	1.64	8.06E-03
812	Q8IXB1	DNAJC10	DnaJ homolog subfamily C member 10	1	107.79	109.72	61.01	92.84	137.35	161.55	157.68	152.19	1.64	2.80E-02
813	P37268	FDFT1	Squalene synthase	1	18.16	23.10	12.15	17.80	25.65	28.31	33.20	29.05	1.63	4.35E-02
814	P36578	RPL4	60S ribosomal protein L4	12	2166.24	1727.35	998.64	1630.74	2172.10	2835.88	2973.43	2660.47	1.63	7.07E-02
815	Q14166	TTLL12	Tubulin--tyrosine ligase-like protein 12	3	196.02	174.95	112.39	161.12	220.20	262.82	305.03	262.68	1.63	4.43E-02
816	Q9UKN8	GTF3C4	General transcription factor 3C polypeptide 4	2	139.65	178.30	94.46	137.47	203.69	230.06	234.43	222.73	1.62	3.08E-02
817	P53618	COPB1	Coatomer subunit beta	1	43.73	44.21	39.84	42.59	59.68	72.67	74.66	69.00	1.62	5.71E-03
818	P49915	GMPS	GMP synthase [glutamine-hydrolyzing]	1	32.44	35.13	26.55	31.37	47.60	54.58	49.83	50.67	1.62	4.10E-03
819	Q14137	BOP1	Ribosome biogenesis protein BOP1	9	1418.38	1569.59	975.34	1321.10	1770.01	2312.88	2306.88	2129.92	1.61	3.31E-02
820	P49916	LIG3	DNA ligase 3	1	124.61	108.25	64.50	99.12	136.09	189.33	153.69	159.70	1.61	6.37E-02
821	P22314	UBA1	Ubiquitin-like modifier-activating enzyme 1	19	3335.07	2957.97	2042.98	2778.67	3775.09	4550.09	5033.70	4452.96	1.60	3.43E-02
822	O14980	XPO1	Exportin-1	2	101.78	119.31	137.98	119.69	193.17	190.25	191.66	191.69	1.60	2.36E-03
823	Q12788	TBL3	Transducin beta-like protein 3	1	84.90	110.38	65.21	86.83	128.99	148.92	136.60	138.17	1.59	2.30E-02
824	P62736	ACTA2	Actin, aortic smooth muscle	18	5895.34	3978.06	1546.10	3806.50	6747.45	5849.46	5562.04	6052.98	1.59	1.61E-01

825	P51659	HSD17B4	Peroxisomal multifunctional enzyme type 2	2	145.19	145.38	89.76	126.78	169.44	226.90	208.28	201.54	1.59	4.07E-02
826	O43670-4	ZNF207	Isoform 4 of Zinc finger protein 207	3	260.47	204.88	128.05	197.80	235.23	364.04	343.88	314.38	1.59	1.03E-01
827	O00571	DDX3X	ATP-dependent RNA helicase DDX3X	12	1625.08	1539.16	954.53	1372.92	1801.92	2276.22	2442.22	2173.45	1.58	4.83E-02
828	Q14258	TRIM25	E3 ubiquitin/ISG15 ligase TRIM25	1	143.80	133.26	90.57	122.54	161.90	198.47	221.08	193.82	1.58	3.97E-02
829	P41252	IARS	Isoleucine--tRNA ligase, cytoplasmic	3	434.13	365.43	256.47	352.01	462.09	546.74	653.27	554.03	1.57	5.59E-02
830	Q96HS1	PGAM5	Serine/threonine-protein phosphatase PGAM5, mitochondrial	3	399.03	379.02	329.15	369.07	470.51	627.75	641.39	579.89	1.57	2.28E-02
831	Q96I59	NARS2	Probable asparagine--tRNA ligase, mitochondrial	1	102.10	195.15	80.28	125.84	203.18	196.42	193.53	197.71	1.57	1.12E-01
832	Q14247-2	CTTN	Isoform 2 of Src substrate cortactin	4	343.43	593.80	308.41	415.21	625.28	692.15	638.17	651.86	1.57	6.21E-02
833	Q14152	EIF3A	Eukaryotic translation initiation factor 3 subunit A	8	960.34	842.86	529.83	777.68	1013.49	1261.68	1385.73	1220.30	1.57	5.86E-02
834	Q99426	TBCB	Tubulin-folding cofactor B	1	121.32	106.30	113.84	113.82	138.75	183.45	213.30	178.50	1.57	4.29E-02
835	Q8TEM1	NUP210	Nuclear pore membrane glycoprotein 210	1	107.05	128.01	66.09	100.39	125.43	177.24	167.93	156.86	1.56	7.98E-02
836	P04040	CAT	Catalase	1	40.94	42.06	26.48	36.49	53.05	60.37	57.49	56.97	1.56	1.98E-02
837	O43776	NARS	Asparagine--tRNA ligase, cytoplasmic	2	144.42	121.07	87.92	117.80	165.27	173.13	212.19	183.53	1.56	3.98E-02
838	Q9UM54	MYO6	Unconventional myosin-VI	3	408.83	413.88	272.99	365.23	512.40	555.24	631.22	566.29	1.55	2.53E-02
839	P19525	EIF2AK2	Interferon-induced, double-stranded RNA-activated protein kinase	1	98.44	94.64	62.80	85.29	104.36	143.47	148.27	132.03	1.55	5.95E-02
840	P31948	STIP1	Stress-induced-phosphoprotein 1	20	4751.34	3632.20	2574.84	3652.79	4731.77	6059.50	6161.14	5650.80	1.55	6.23E-02
841	Q9P2J5	LARS	Leucine--tRNA ligase, cytoplasmic	3	204.88	221.48	136.47	187.61	252.92	282.10	334.67	289.90	1.55	4.44E-02
842	Q9P035	PTPLAD1	Very-long-chain (3R)-3-hydroxyacyl-[acyl-carrier protein] dehydratase 3	5	815.06	1020.58	494.13	776.59	1039.86	1210.48	1337.02	1195.79	1.54	7.55E-02
843	Q5VYK3	ECM29	Proteasome-associated protein ECM29 homolog	1	103.34	76.95	69.48	83.26	114.75	152.18	117.48	128.14	1.54	4.71E-02
844	Q96GX9	APIP	Methylthioribulose-1-phosphate dehydratase	1	76.25	61.17	50.94	62.78	84.14	96.10	109.22	96.49	1.54	3.09E-02
845	Q9GZL7	WDR12	Ribosome biogenesis protein WDR12	1	26.57	38.52	26.13	30.41	39.18	59.07	41.09	46.45	1.53	1.00E-01
846	Q92878-2	RAD50	Isoform 2 of DNA repair protein RAD50	1	86.36	86.25	60.68	77.76	97.61	131.50	126.98	118.70	1.53	3.98E-02
847	Q9Y679	AUP1	Ancient ubiquitous protein 1	1	21.84	26.28	16.04	21.39	23.91	35.38	38.30	32.53	1.52	1.03E-01
848	Q15233	NONO	Non-POU domain-containing octamer-binding protein	17	2784.57	2079.74	819.85	1894.72	2675.03	3334.49	2602.99	2870.84	1.52	1.91E-01
849	Q00341	HDLBP	Vigilin	2	253.81	219.09	137.45	203.45	244.41	311.12	366.25	307.26	1.51	1.03E-01
850	O60568	PLOD3	Procollagen-lysine,2-oxoglutarate 5-dioxygenase 3	1	87.06	87.67	43.97	72.90	78.13	125.35	126.35	109.94	1.51	1.60E-01
851	P35579	MYH9	Myosin-9	12	1100.65	1190.11	819.73	1036.83	1420.64	1517.46	1750.63	1562.91	1.51	2.39E-02
852	P53396	ACLY	ATP-citrate synthase	5	826.37	772.96	553.60	717.64	911.53	1091.45	1239.10	1080.69	1.51	4.52E-02
853	Q01082	SPTBN1	Spectrin beta chain, non-erythrocytic 1	6	607.92	640.96	381.57	543.48	659.34	874.40	899.95	811.23	1.49	7.45E-02

854	Q14690	PDCD11	Protein RRP5 homolog	3	256.52	309.07	181.88	249.16	298.03	416.95	394.83	369.94	1.48	8.06E-02
855	P21333	FLNA	Filamin-A	34	4220.82	3511.35	2748.19	3493.45	4610.51	5313.85	5625.33	5183.23	1.48	3.15E-02
856	Q96KP4	CNDP2	Cytosolic non-specific dipeptidase	1	109.83	81.94	58.03	83.27	94.40	127.21	147.45	123.02	1.48	1.38E-01
857	Q13642	FHL1	Four and a half LIM domains protein 1	4	664.52	598.04	387.22	549.93	717.13	795.80	913.26	808.73	1.47	6.28E-02
858	P78344	EIF4G2	Eukaryotic translation initiation factor 4 gamma 2	1	85.45	77.47	60.37	74.43	93.93	118.06	116.22	109.41	1.47	3.10E-02
859	Q14204	DYNC1H1	Cytoplasmic dynein 1 heavy chain 1	1	64.49	72.66	49.63	62.26	91.22	80.75	101.43	91.13	1.46	3.27E-02
860	Q02878	RPL6	60S ribosomal protein L6	10	3210.46	2469.79	1458.39	2379.55	2784.40	3800.52	3862.30	3482.41	1.46	1.48E-01
861	P61313	RPL15	60S ribosomal protein L15	6	1432.60	1293.26	783.50	1169.79	1258.98	1961.43	1901.27	1707.23	1.46	1.47E-01
862	O43143	DHX15	Putative pre-mRNA-splicing factor ATP-dependent RNA helicase DHX15	7	975.09	1286.76	703.66	988.50	1253.46	1567.11	1504.44	1441.67	1.46	7.95E-02
863	P47897	QARS	Glutamine--tRNA ligase	4	399.81	361.14	238.67	333.21	433.29	510.00	510.89	484.73	1.45	5.10E-02
864	P57088	TMEM33	Transmembrane protein 33	1	134.68	142.57	80.81	119.35	149.83	173.87	193.23	172.31	1.44	8.37E-02
865	Q86X55	CARM1	Histone-arginine methyltransferase CARM1	1	620.85	154.04	156.53	310.47	313.45	445.51	583.52	447.49	1.44	4.74E-01
866	P05166-2	PCCB	Isoform 2 of Propionyl-CoA carboxylase beta chain, mitochondrial	1	72.39	79.69	57.81	69.96	74.98	104.77	122.77	100.84	1.44	1.15E-01
867	P58107	EPPK1	Epiplakin	2	209.85	188.57	145.53	181.32	228.99	267.15	284.23	260.12	1.43	3.44E-02
868	P78527	PRKDC	DNA-dependent protein kinase catalytic subunit	6	596.27	613.37	422.63	544.09	618.95	892.50	807.28	772.91	1.42	8.66E-02
869	P46781	RPS9	40S ribosomal protein S9	9	3599.90	3083.43	1715.16	2799.50	3328.57	4160.53	4437.24	3975.45	1.42	1.46E-01
870	Q96QK1	VPS35	Vacuolar protein sorting-associated protein 35	1	28.90	52.84	34.81	38.85	46.09	73.22	44.92	54.74	1.41	2.46E-01
871	P31939	ATIC	Bifunctional purine biosynthesis protein PURH	7	1132.44	899.73	651.55	894.57	1049.61	1337.23	1390.96	1259.27	1.41	1.05E-01
872	O75340	PDCD6	Programmed cell death protein 6	1	26.22	23.27	11.38	20.29	27.58	29.18	27.30	28.02	1.38	1.66E-01
873	Q92624	APPBP2	Amyloid protein-binding protein 2	1	291.02	302.52	165.77	253.10	311.11	441.27	292.88	348.42	1.38	2.11E-01
874	P26640	VARS	Valine--tRNA ligase	2	104.48	86.99	65.30	85.59	100.57	120.73	128.79	116.70	1.36	9.20E-02
875	Q14697	GANAB	Neutral alpha-glucosidase AB	1	79.02	78.67	45.60	67.76	75.24	110.49	91.34	92.36	1.36	1.78E-01
876	P07814	EPRS	Bifunctional glutamate/proline--tRNA ligase	12	1118.67	1111.45	843.48	1024.53	1231.30	1432.68	1513.23	1392.40	1.36	4.07E-02
877	P53621-2	COPA	Isoform 2 of Coatomer subunit alpha	1	77.65	83.36	56.13	72.38	89.24	87.65	116.43	97.77	1.35	1.12E-01
878	Q96TA2	YME1L1	ATP-dependent zinc metalloprotease YME1L1	1	36.26	51.18	34.10	40.51	53.22	54.34	54.83	54.13	1.34	6.49E-02
879	P26196	DDX6	Probable ATP-dependent RNA helicase DDX6	4	730.07	672.84	369.23	590.71	626.18	838.48	891.61	785.42	1.33	2.32E-01
880	Q8IY67-2	RAVER1	Isoform 2 of Ribonucleoprotein PTB-binding 1	4	288.82	247.80	133.16	223.26	222.09	307.79	354.30	294.73	1.32	3.03E-01
881	P46776	RPL27A	60S ribosomal protein L27a	4	1089.97	937.96	543.45	857.13	963.13	1171.72	1251.44	1128.76	1.32	2.14E-01
882	Q01432-4	AMPD3	Isoform 2 of AMP deaminase 3	1	825.16	807.91	427.47	686.84	857.01	1076.34	770.62	901.32	1.31	2.47E-01

883	Q00610	CLTC	Clathrin heavy chain 1	5	714.82	673.09	507.05	631.65	726.54	807.55	935.98	823.35	1.30	9.49E-02
884	P08243	ASNS	Asparagine synthetase [glutamine-hydrolyzing]	12	3607.39	3147.00	1882.94	2879.11	3103.37	3825.47	4303.59	3744.14	1.30	2.37E-01
885	O75643	SNRNP200	U5 small nuclear ribonucleoprotein 200 kDa helicase	14	1715.48	2023.16	1457.91	1732.18	2048.68	2318.64	2225.29	2197.54	1.27	6.24E-02
886	Q14697-2	GANAB	Isoform 2 of Neutral alpha-glucosidase AB	25	6388.58	6215.35	3483.08	5362.34	5327.07	7564.98	6654.88	6515.64	1.22	3.70E-01
887	Q9Y2W1	THRAP3	Thyroid hormone receptor-associated protein 3	1	186.46	176.11	112.95	158.51	147.47	242.83	180.42	190.24	1.20	4.30E-01
888	Q9UDX5	MTFP1	Mitochondrial fission process protein 1	1	30.87	37.69	11.85	26.81	37.41	35.78	23.27	32.16	1.20	5.81E-01
889	Q7L5N1	COPS6	COP9 signalosome complex subunit 6	1	39.39	30.20	58.08	42.56	38.55	57.26	49.99	48.60	1.14	5.73E-01
890	Q9Y490	TLN1	Talin-1	2	112.20	92.33	61.82	88.78	88.74	101.57	112.70	101.00	1.14	4.93E-01
891	P46977	STT3A	Dolichyl-diphosphooligosaccharide--protein glycosyltransferase subunit STT3A	3	1030.09	1344.14	763.93	1046.05	979.80	1171.98	1353.81	1168.53	1.12	5.72E-01
892	Q9BZV3	IMPG2	Interphotoreceptor matrix proteoglycan 2	1	659.43	955.97	417.51	677.63	790.01	754.84	695.39	746.75	1.10	6.85E-01
893	Q96RQ3	MCCC1	Methylcrotonoyl-CoA carboxylase subunit alpha, mitochondrial	6	686.46	840.22	426.95	651.21	570.83	721.80	810.19	700.94	1.08	7.39E-01
894	P07478	PRSS2	Trypsin-2	2	119.00	96.41	92.62	102.67	94.79	132.97	98.23	108.66	1.06	7.05E-01
895	P49327	FASN	Fatty acid synthase	25	4172.06	3549.54	2888.39	3536.66	3091.44	3640.07	3969.16	3566.89	1.01	9.50E-01
896	Q9BT22	ALG1	Chitobiosyldiphosphodolichol beta-mannosyltransferase	3	241.83	254.60	192.29	229.58	195.28	243.73	254.91	231.30	1.01	9.51E-01
897	Q6P2Q9	PRPF8	Pre-mRNA-processing-splicing factor 8	28	5507.39	6034.88	3545.00	5029.09	4395.13	5452.01	5249.51	5032.22	1.00	9.97E-01
898	P11498	PC	Pyruvate carboxylase, mitochondrial	18	2075.86	2241.57	1137.97	1818.47	1420.94	1808.08	2007.15	1745.39	0.96	8.58E-01
899	Q13085-4	ACACA	Isoform 4 of Acetyl-CoA carboxylase 1	2	57.57	51.12	42.64	50.45	43.22	40.24	46.05	43.17	0.86	1.92E-01
900	Q6KCM7-3	SLC25A25	Isoform 3 of Calcium-binding mitochondrial carrier protein SCaMC-2	1	23.05	166.69	203.70	131.15	87.85	127.96	61.19	92.33	0.70	5.43E-01
901	P02042	HBD	Hemoglobin subunit delta	2	75.59	550.53	687.63	437.92	288.47	356.92	69.80	238.40	0.54	3.85E-01
902	P69905	HBA1	Hemoglobin subunit alpha	1	23.41	444.02	505.93	324.45	293.59	224.82	7.58	175.33	0.54	4.41E-01

Table A2. The table contains the list of 674 high-confidence protein hits categorized according to their subcellular localization and their localization in membrane and soluble compartments as per the UniProt database (this list includes protein expressed at multiple locations). This table was used to generate the plot depicted in Figure 4.9a.

S. No.	UniProt ID	Protein Name	Cytoplasm	Nucleus	Mitochondria	ER	Cell membrane	Golgi	Lysosome	Membrane	Soluble
1	Q07021	Complement component 1 Q subcomponent-binding protein (or p32), mitochondrial	1	1	1		1			1	
2	P20671	Histone H2A type 1-D		1							1
3	Q71UI9	Histone H2A.V		1							1
4	Q01105	Protein SET	1	1		1					1
5	P67809	Nuclease-sensitive element-binding protein 1	1	1							1
6	P14406	Cytochrome c oxidase subunit 7A2, mitochondrial			1					1	
7	Q13765-2	Isoform 2 of Nascent polypeptide-associated complex subunit alpha	1	1							1
8	Q14978-2	Isoform Beta of Nucleolar and coiled-body phosphoprotein 1	1	1							1
9	P62158	Calmodulin	1	1			1			1	
10	P19338	Nucleolin	1	1							1
11	P14314	Glucosidase 2 subunit beta				1					1
12	P05387	60S acidic ribosomal protein P2	1								1
13	P35637	RNA-binding protein FUS		1							1
14	P43307	Translocon-associated protein subunit alpha				1				1	
15	P61604	10 kDa heat shock protein, mitochondrial			1						1
16	Q5QNW6-2	Isoform 2 of Histone H2B type 2-F		1							1
17	P11177	Pyruvate dehydrogenase E1 component subunit beta, mitochondrial			1						1
18	O60888-2	Isoform A of Protein CutA					1			1	
19	Q92804	TATA-binding protein-associated factor 2N	1	1							1
20	Q13247	Serine/arginine-rich splicing factor 6		1							1
21	O60812	Heterogeneous nuclear ribonucleoprotein C-like 1		1							1
22	Q9BRL6	Serine/arginine-rich splicing factor 8		1							1
23	Q15287	RNA-binding protein with serine-rich domain 1	1	1							1
24	P23396	40S ribosomal protein S3	1	1	1					1	
25	Q12849	G-rich sequence factor 1			1						1
26	P13073	Cytochrome c oxidase subunit 4 isoform 1, mitochondrial			1					1	
27	P30048	Thioredoxin-dependent peroxide reductase, mitochondrial	1		1						1
28	P39687	Acidic leucine-rich nuclear phosphoprotein 32 family member A	1	1		1					1
29	Q16629	Serine/arginine-rich splicing factor 7	1	1							1
30	Q16836-2	Isoform 2 of Hydroxyacyl-coenzyme A dehydrogenase, mitochondrial			1						1
31	P13995	Bifunctional methylenetetrahydrofolate dehydrogenase/cyclohydrolase, mitochondrial			1						1
32	P07910	Heterogeneous nuclear ribonucleoproteins C1/C2		1							1
33	Q13243	Serine/arginine-rich splicing factor 5		1							1
34	P38159	RNA-binding motif protein, X chromosome		1							1
35	Q14257	Reticulocalbin-2				1					1
36	P10809	60 kDa heat shock protein, mitochondrial			1						1
37	P06748	Nucleophosmin	1	1							1
38	P06454	Prothymosin alpha		1							1

39	P27797	Calreticulin	1			1	1			1	
40	P35659	Protein DEK		1							1
41	Q9UJZ1	Stomatin-like protein 2, mitochondrial	1		1		1			1	
42	Q9H3G5	Probable serine carboxypeptidase CPVL									1
43	P22695	Cytochrome b-c1 complex subunit 2, mitochondrial			1					1	
44	Q6DN03	Putative histone H2B type 2-C		1							1
45	P38117	Electron transfer flavoprotein subunit beta			1						1
46	Q9NYK5-2	Isoform 2 of 39S ribosomal protein L39, mitochondrial			1						1
47	Q4G0N4	NAD kinase 2, mitochondrial			1						1
48	P82979	SAP domain-containing ribonucleoprotein		1							1
49	P84103	Serine/arginine-rich splicing factor 3	1	1							1
50	P04181	Ornithine aminotransferase, mitochondrial			1						1
51	O75475	PC4 and SFRS1-interacting protein		1							1
52	Q9NP92	28S ribosomal protein S30, mitochondrial			1						1
53	P08670	Vimentin	1	1							1
54	P09622	Dihydrolipoyl dehydrogenase, mitochondrial		1	1						1
55	P67936	Tropomyosin alpha-4 chain	1								1
56	P62995	Transformer-2 protein homolog beta		1							1
57	P07197	Neurofilament medium polypeptide	1								1
58	Q13685	Angio-associated migratory cell protein	1				1			1	
59	O75947	ATP synthase subunit d, mitochondrial			1					1	
60	P20674	Cytochrome c oxidase subunit 5A, mitochondrial			1					1	
61	Q92552	28S ribosomal protein S27, mitochondrial	1		1						1
62	P06576	ATP synthase subunit beta, mitochondrial			1					1	
63	J3KN67	Tropomyosin alpha-3 chain	1								1
64	Q7Z2W9	39S ribosomal protein L21, mitochondrial			1						1
65	P54105	Methylosome subunit pICln	1	1							1
66	Q9H2U2-2	Isoform 2 of Inorganic pyrophosphatase 2, mitochondrial			1						1
67	Q99623	Prohibitin-2	1	1	1					1	
68	Q92688	Acidic leucine-rich nuclear phosphoprotein 32 family member B	1	1							1
69	O14561	Acyl carrier protein, mitochondrial			1						1
70	Q7Z4V5	Hepatoma-derived growth factor-related protein 2		1							1
71	P49006	MARCKS-related protein	1				1			1	
72	P24666	Low molecular weight phosphotyrosine protein phosphatase	1								1
73	Q8NAB5	Putative uncharacterized protein FLJ35645 PE									1
74	P13804	Electron transfer flavoprotein subunit alpha, mitochondrial			1						1
75	Q07955-2	Isoform ASF-2 of Serine/arginine-rich splicing factor 1	1	1							1
76	Q00059	Transcription factor A, mitochondrial			1						1
77	P29966	Myristoylated alanine-rich C-kinase substrate	1				1			1	
78	P62979	Ubiquitin-40S ribosomal protein S27a	1	1							1
79	Q5SSJ5	Heterochromatin protein 1-binding protein 3		1							1
80	Q9UKM9	RNA-binding protein Raly		1							1
81	P35269	General transcription factor IIF subunit 1		1							1
82	O75439	Mitochondrial-processing peptidase subunit beta			1						1
83	P09001	39S ribosomal protein L3, mitochondrial			1						1
84	Q8NI60	Chaperone activity of bc1 complex-like, mitochondrial			1		1			1	
85	O14773	Tripeptidyl-peptidase 1							1		1
86	P30042	ES1 protein homolog, mitochondrial			1						1
87	Q9NUJ1	Mycophenolic acid acyl-glucuronide esterase, mitochondrial			1						1
88	P36542	ATP synthase subunit gamma, mitochondrial			1					1	
89	O95831	Apoptosis-inducing factor 1, mitochondrial	1	1	1					1	
90	Q15293	Reticulocalbin-1				1					1
91	Q8IYB3	Serine/arginine repetitive matrix protein 1		1							1
92	O75390	Citrate synthase, mitochondrial			1						1

93	Q9UII2	ATPase inhibitor, mitochondrial			1						1
94	Q13428-4	Isoform 4 of Treacle protein		1							1
95	P27824	Calnexin				1				1	
96	Q9BTT0	Acidic leucine-rich nuclear phosphoprotein 32 family member E	1	1							1
97	Q9Y3B9	RRP15-like protein									1
98	Q08170	Serine/arginine-rich splicing factor 4		1							1
99	Q15459	Splicing factor 3A subunit 1		1							1
100	Q7L0Y3	Mitochondrial ribonuclease P protein 1			1						1
101	P10515	Dihydrolipoyllysine-residue acetyltransferase component of pyruvate dehydrogenase complex, mitochondrial			1						1
102	Q13283	Ras GTPase-activating protein-binding protein 1	1								1
103	Q13595	Transformer-2 protein homolog alpha	1								1
104	Q9BZE1	39S ribosomal protein L37, mitochondrial			1						1
105	P10606	Cytochrome c oxidase subunit 5B, mitochondrial			1					1	
106	Q9Y266	Nuclear migration protein nudC	1	1							1
107	Q96RP9-2	Isoform 2 of Elongation factor G, mitochondrial			1						1
108	P62805	Histone H4		1							1
109	O94925	Glutaminase kidney isoform, mitochondrial	1		1						1
110	P25705	ATP synthase subunit alpha, mitochondrial			1		1			1	
111	O43615	Mitochondrial import inner membrane translocase subunit TIM44			1					1	
112	Q13242	Serine/arginine-rich splicing factor 9		1							1
113	Q8NC51	Plasminogen activator inhibitor 1 RNA-binding protein	1	1							1
114	Q9C0C9	Ubiquitin-conjugating enzyme E2 O	1	1							1
115	Q14444	Caprin-1	1				1			1	
116	Q99733	Nucleosome assembly protein 1-like 4	1	1							1
117	P04844	Dolichyl-diphosphooligosaccharide--protein glycosyltransferase subunit 2				1				1	
118	P49321-3	Isoform 3 of Nuclear autoantigenic sperm protein	1	1							1
119	Q05519	Serine/arginine-rich splicing factor 11		1							1
120	P25788	Proteasome subunit alpha type-3	1	1							1
121	P09429	High mobility group protein B1	1	1			1			1	
122	P82933	28S ribosomal protein S9, mitochondrial			1						1
123	Q5JPH6	Probable glutamate--tRNA ligase, mitochondrial			1						1
124	P46087-4	Isoform 4 of Putative ribosomal RNA methyltransferase NOP2		1							1
125	P49411	Elongation factor Tu, mitochondrial			1						1
126	Q9Y371-2	Isoform 2 of Endophilin-B1	1		1			1		1	
127	Q5JRX3-2	Isoform 2 of Presequence protease, mitochondrial			1						1
128	Q3ZCQ8-2	Isoform 2 of Mitochondrial import inner membrane translocase subunit TIM50		1	1					1	
129	P45973	Chromobox protein homolog 5		1							1
130	O75027-2	Isoform 2 of ATP-binding cassette sub-family B member 7, mitochondrial			1					1	
131	P30084	Enoyl-CoA hydratase, mitochondrial			1						1
132	P55809	Succinyl-CoA:3-ketoacid coenzyme A transferase 1, mitochondrial			1						1
133	P38646	Stress-70 protein, mitochondrial		1	1						1
134	P50213	Isocitrate dehydrogenase [NAD] subunit alpha, mitochondrial			1						1
135	Q9NSE4	Isoleucine--tRNA ligase, mitochondrial			1						1
136	Q9UKV3	Apoptotic chromatin condensation inducer in the nucleus		1							1
137	P0C7P4	Putative cytochrome b-c1 complex subunit Rieske-like protein 1					1			1	
138	P08621	U1 small nuclear ribonucleoprotein 70 kDa		1							1
139	Q96EY4	Translation machinery-associated protein 16		1							1
140	Q08945	FACT complex subunit SSRP1		1							1
141	Q01844-5	Isoform 5 of RNA-binding protein EWS	1	1			1			1	
142	P55209	Nucleosome assembly protein 1-like 1	1	1							1
143	Q9H9J2	39S ribosomal protein L44, mitochondrial			1						1
144	P28331-2	Isoform 2 of NADH-ubiquinone oxidoreductase 75 kDa subunit, mitochondrial			1					1	
145	P24752	Acetyl-CoA acetyltransferase, mitochondrial			1						1

146	Q16891	Mitochondrial inner membrane protein			1					1	
147	P68431	Histone H3.1		1							1
148	P30044	Peroxiredoxin-5, mitochondrial	1		1						1
149	Q9H1E3	Nuclear ubiquitous casein and cyclin-dependent kinase substrate 1		1							1
150	P53597	Succinyl-CoA ligase [ADP/GDP-forming] subunit alpha, mitochondrial			1						1
151	Q8TCS8	Polyribonucleotide nucleotidyltransferase 1, mitochondrial	1		1					1	
152	P14625	Endoplasmin				1					1
153	O60783	28S ribosomal protein S14, mitochondrial			1						1
154	P55786	Puromycin-sensitive aminopeptidase	1	1							1
155	Q96EY1	DnaJ homolog subfamily A member 3, mitochondrial	1		1		1			1	
156	P30405	Peptidyl-prolyl cis-trans isomerase F, mitochondrial			1						1
157	P35268	60S ribosomal protein L22	1	1							1
158	P08865	40S ribosomal protein SA	1	1			1			1	
159	O95202	LETM1 and EF-hand domain-containing protein 1, mitochondrial			1					1	
160	Q9HAV7	GrpE protein homolog 1, mitochondrial			1						1
161	P40926	Malate dehydrogenase, mitochondrial			1						1
162	P42166	Lamina-associated polypeptide 2, isoform alpha		1							1
163	O75312	Zinc finger protein ZPR1	1	1							1
164	Q9P015	39S ribosomal protein L15, mitochondrial			1						1
165	Q13185	Chromobox protein homolog 3		1							1
166	Q6P1L8	39S ribosomal protein L14, mitochondrial			1						1
167	P43487	Ran-specific GTPase-activating protein	1	1							1
168	P42126	Enoyl-CoA delta isomerase 1, mitochondrial			1						1
169	P35232	Prohibitin		1	1					1	
170	P23528	Cofilin-1	1	1			1			1	
171	P31930	Cytochrome b-c1 complex subunit 1, mitochondrial			1					1	
172	Q9NVV4-2	Isoform 2 of Poly(A) RNA polymerase, mitochondrial	1		1						1
173	P62750	60S ribosomal protein L23a	1	1							1
174	P61978-3	Isoform 3 of Heterogeneous nuclear ribonucleoprotein K	1	1							1
175	P48735	Isocitrate dehydrogenase [NADP], mitochondrial			1						1
176	P09651	Heterogeneous nuclear ribonucleoprotein A1	1	1							1
177	P16402	Histone H1.3		1							1
178	P62304	Small nuclear ribonucleoprotein E	1	1							1
179	P31942	Heterogeneous nuclear ribonucleoprotein H3		1							1
180	P22626	Heterogeneous nuclear ribonucleoproteins A2/B1	1	1							1
181	P58546	Myotrophin	1	1							1
182	Q5BKZ1	DBIRD complex subunit ZNF326		1							1
183	P08559-4	Isoform 4 of Pyruvate dehydrogenase E1 component subunit alpha, somatic form, mitochondrial			1						1
184	Q9BYD3	39S ribosomal protein L4, mitochondrial			1						1
185	P00367	Glutamate dehydrogenase 1, mitochondrial			1						1
186	Q9Y5B9	FACT complex subunit SPT16		1							1
187	P49755	Transmembrane emp24 domain-containing protein 10				1	1	1		1	
188	P30419	Glycylpeptide N-tetradecanoyltransferase 1	1				1			1	
189	P61956	Small ubiquitin-related modifier 2		1							1
190	Q09028	Histone-binding protein RBBP4		1							1
191	P37108	Signal recognition particle 14 kDa protein	1								1
192	Q16625	Occludin					1			1	
193	P31040	Succinate dehydrogenase [ubiquinone] flavoprotein subunit, mitochondrial			1					1	
194	Q99714	3-hydroxyacyl-CoA dehydrogenase type-2			1						1
195	Q9P032	NADH dehydrogenase [ubiquinone] 1 alpha subcomplex assembly factor 4			1		1			1	
196	P00403	Cytochrome c oxidase subunit 2			1					1	
197	O75489	NADH dehydrogenase [ubiquinone] iron-sulfur protein 3, mitochondrial			1						1
198	P42704	Leucine-rich PPR motif-containing protein, mitochondrial		1	1						1

199	O75367	Core histone macro-H2A.1		1							1
200	Q96GA3	Protein LTV1 homolog	1	1							1
201	O15355	Protein phosphatase 1G	1				1			1	
202	O60637	Tetraspanin-3					1			1	
203	P15311	Ezrin	1				1			1	
204	P49821	NADH dehydrogenase [ubiquinone] flavoprotein 1, mitochondrial			1					1	
205	Q96EY7	Pentatricopeptide repeat domain-containing protein 3, mitochondrial			1						1
206	Q15185	Prostaglandin E synthase 3	1								1
207	P11021	78 kDa glucose-regulated protein	1			1					1
208	Q04837	Single-stranded DNA-binding protein, mitochondrial			1						1
209	P62280	40S ribosomal protein S11	1	1			1			1	
210	O14979	Heterogeneous nuclear ribonucleoprotein D-like	1	1							1
211	P26440	Isovaleryl-CoA dehydrogenase, mitochondrial			1						1
212	O76021	Ribosomal L1 domain-containing protein 1		1							1
213	Q07666	KH domain-containing, RNA-binding, signal transduction-associated protein 1	1	1			1			1	
214	P47914	60S ribosomal protein L29	1				1			1	
215	P32969	60S ribosomal protein L9	1	1			1				1
216	P04179	Superoxide dismutase [Mn], mitochondrial			1						1
217	O00264	Membrane-associated progesterone receptor component 1			1	1				1	
218	P54727	UV excision repair protein RAD23 homolog B	1	1							1
219	O43837	Isocitrate dehydrogenase [NAD] subunit beta, mitochondrial			1						1
220	P08574	Cytochrome c1, heme protein, mitochondrial			1					1	
221	P61163	Alpha-centractin	1								1
222	P00505	Aspartate aminotransferase, mitochondrial			1		1			1	
223	Q15365	Poly(rC)-binding protein 1	1	1							1
224	Q06787	Fragile X mental retardation protein 1	1	1			1			1	
225	Q15388	Mitochondrial import receptor subunit TOM20 homolog			1					1	
226	P62851	40S ribosomal protein S25	1	1							1
227	Q13123	Protein Red	1	1							1
228	Q9NVI7-2	Isoform 2 of ATPase family AAA domain-containing protein 3A			1					1	
229	P05386	60S acidic ribosomal protein P1	1								1
230	P30041	Peroxiredoxin-6	1						1		1
231	P62913	60S ribosomal protein L11	1	1							1
232	Q15061	WD repeat-containing protein 43		1							1
233	Q14498	RNA-binding protein 39		1							1
234	P05388	60S acidic ribosomal protein P0	1	1							1
235	Q07065	Cytoskeleton-associated protein 4	1			1	1			1	
236	P02545	Prelamin-A/C		1							1
237	Q99873	Protein arginine N-methyltransferase 1	1	1							1
238	P0CW22	40S ribosomal protein S17-like	1	1			1			1	
239	Q9NYF8	Bcl-2-associated transcription factor 1	1	1							1
240	P63241-2	Isoform 2 of Eukaryotic translation initiation factor 5A-1	1	1		1				1	
241	P48047	ATP synthase subunit O, mitochondrial			1					1	
242	Q9UQ80	Proliferation-associated protein 2G4	1	1							1
243	P36957	Dihydrolipoyllysine-residue succinyltransferase component of 2-oxoglutarate dehydrogenase complex, mitochondrial		1	1						1
244	P21912	Succinate dehydrogenase [ubiquinone] iron-sulfur subunit, mitochondrial			1					1	
245	P23786	Carnitine O-palmitoyltransferase 2, mitochondrial			1					1	
246	P11387	DNA topoisomerase 1		1							1
247	P27348	14-3-3 protein theta	1								1
248	P29692-2	Isoform 2 of Elongation factor 1-delta		1							1
249	Q9Y277-2	Isoform 2 of Voltage-dependent anion-selective channel protein 3			1					1	
250	P50502	Hsc70-interacting protein	1								1
251	P78316	Nucleolar protein 14		1							1

252	P18754-2	Isoform 2 of Regulator of chromosome condensation	1	1							1
253	Q6UB35	Monofunctional C1-tetrahydrofolate synthase, mitochondrial			1						1
254	P62899-2	Isoform 2 of 60S ribosomal protein L31	1				1			1	
255	Q01081	Splicing factor U2AF 35 kDa subunit		1							1
256	P82675	28S ribosomal protein S5, mitochondrial			1						1
257	P61081	NEDD8-conjugating enzyme Ubc12	1	1							1
258	Q12931	Heat shock protein 75 kDa, mitochondrial			1					1	
259	Q9BYC9	39S ribosomal protein L20, mitochondrial			1						1
260	P20700	Lamin-B1		1						1	
261	Q12874	Splicing factor 3A subunit 3		1							1
262	P51116	Fragile X mental retardation syndrome-related protein 2	1								1
263	P61981	14-3-3 protein gamma	1								1
264	P45880-1	Isoform 1 of Voltage-dependent anion-selective channel protein 2			1					1	
265	Q00839	Heterogeneous nuclear ribonucleoprotein U	1	1			1			1	
266	Q9Y305-4	Isoform 4 of Acyl-coenzyme A thioesterase 9, mitochondrial			1						1
267	P50579	Methionine aminopeptidase 2	1								1
268	Q15366-2	Isoform 2 of Poly(rC)-binding protein 2	1	1							1
269	Q9NYY8	FAST kinase domain-containing protein 2			1						1
270	P51991	Heterogeneous nuclear ribonucleoprotein A3		1							1
271	O75821	Eukaryotic translation initiation factor 3 subunit G	1	1							1
272	P21796	Voltage-dependent anion-selective channel protein 1			1		1			1	
273	P32322	Pyrroline-5-carboxylate reductase 1, mitochondrial			1						1
274	P25398	40S ribosomal protein S12	1								1
275	P18583-9	Isoform I of Protein SON		1							1
276	P23368	NAD-dependent malic enzyme, mitochondrial			1						1
277	Q9Y4L1	Hypoxia up-regulated protein 1				1					1
278	P62195	26S protease regulatory subunit 8	1	1							1
279	P43897	Elongation factor Ts, mitochondrial			1						1
280	P05141	ADP/ATP translocase 2			1					1	
281	P26038	Moesin	1				1			1	
282	O43847-2	Isoform 2 of Nardilysin	1		1		1			1	
283	P23284	Peptidyl-prolyl cis-trans isomerase B				1					1
284	P11310-2	Isoform 2 of Medium-chain specific acyl-CoA dehydrogenase, mitochondrial			1						1
285	Q15691	Microtubule-associated protein RP/EB family member 1	1					1			1
286	P51148-2	Isoform 2 of Ras-related protein Rab-5C					1			1	
287	P36776	Lon protease homolog, mitochondrial			1						1
288	P62820	Ras-related protein Rab-1A	1			1	1	1		1	
289	P07355-2	Isoform 2 of Annexin A2					1			1	
290	P08758	Annexin A5	1				1			1	
291	O14950	Myosin regulatory light chain 12B	1								1
292	Q96EP5	DAZ-associated protein 1	1	1							1
293	P13693	Translationally-controlled tumor protein	1								1
294	Q13838-2	Isoform 2 of Spliceosome RNA helicase DDX39B	1	1							1
295	Q9BUJ2	Heterogeneous nuclear ribonucleoprotein U-like protein 1		1							1
296	Q9Y3T9	Nucleolar complex protein 2 homolog		1							1
297	P07237	Protein disulfide-isomerase				1	1			1	
298	P60903	Protein S100-A10				1	1			1	
299	P62826	GTP-binding nuclear protein Ran	1	1							1
300	Q9P2K3-3	Isoform 3 of REST corepressor 3		1							1
301	Q5JTZ9	Alanine--tRNA ligase, mitochondrial			1						1
302	Q9Y6E0	Serine/threonine-protein kinase 24	1	1			1			1	
303	P05455	Lupus La protein		1							1
304	Q16555	Dihydropyrimidinase-related protein 2	1				1			1	
305	P12956	X-ray repair cross-complementing protein 6		1							1

306	P30040	Endoplasmic reticulum resident protein 29				1					1
307	Q13151	Heterogeneous nuclear ribonucleoprotein A0		1							1
308	P55884-2	Isoform 2 of Eukaryotic translation initiation factor 3 subunit B	1								1
309	Q96T88-2	Isoform 2 of E3 ubiquitin-protein ligase UHRF1		1							1
310	P52597	Heterogeneous nuclear ribonucleoprotein F		1							1
311	Q12797	Aspartyl/asparaginyl beta-hydroxylase				1				1	
312	P63104	14-3-3 protein zeta/delta	1								1
313	P55010	Eukaryotic translation initiation factor 5	1				1			1	
314	P24534	Elongation factor 1-beta	1								1
315	Q16795	NADH dehydrogenase [ubiquinone] 1 alpha subcomplex subunit 9, mitochondrial			1						1
316	P07737	Profilin-1	1								1
317	A4D1E9	GTP-binding protein 10		1							1
318	Q9NQ55-3	Isoform 3 of Suppressor of SWI4 1 homolog		1							1
319	P62258	14-3-3 protein epsilon	1	1							1
320	P51649-2	Isoform 2 of Succinate-semialdehyde dehydrogenase, mitochondrial			1						1
321	Q99729-2	Isoform 2 of Heterogeneous nuclear ribonucleoprotein A/B	1	1							1
322	Q14676	Mediator of DNA damage checkpoint protein 1		1							1
323	Q8NE71	ATP-binding cassette sub-family F member 1	1	1							1
324	P49458	Signal recognition particle 9 kDa protein	1								1
325	Q16543	Hsp90 co-chaperone Cdc37	1								1
326	P28838	Cytosol aminopeptidase	1								1
327	Q9NTK5	Obg-like ATPase 1	1	1							1
328	O43809	Cleavage and polyadenylation specificity factor subunit 5		1							1
329	Q9UDR5	Alpha-aminoadipic semialdehyde synthase, mitochondrial			1						1
330	P61247	40S ribosomal protein S3a	1	1							1
331	P52292	Importin subunit alpha-1	1	1							1
332	Q15181	Inorganic pyrophosphatase	1								1
333	Q06265-2	Isoform 2 of Exosome complex component RRP45	1	1							1
334	P16435	NADPH--cytochrome P450 reductase				1				1	
335	P50914	60S ribosomal protein L14	1				1			1	
336	P25789	Proteasome subunit alpha type-4	1	1							1
337	P31943	Heterogeneous nuclear ribonucleoprotein H		1							1
338	O00567	Nucleolar protein 56	1	1							1
339	Q14103	Heterogeneous nuclear ribonucleoprotein D0	1	1							1
340	P46777	60S ribosomal protein L5	1	1							1
341	P22087	rRNA 2'-O-methyltransferase fibrillarin		1							1
342	P33316	Deoxyuridine 5'-triphosphate nucleotidohydrolase, mitochondrial		1	1						1
343	Q16881	Thioredoxin reductase 1, cytoplasmic	1	1							1
344	P15880	40S ribosomal protein S2	1	1			1			1	
345	P12236	ADP/ATP translocase 3			1					1	
346	Q99798	Aconitate hydratase, mitochondrial			1						1
347	Q1KMD3	Heterogeneous nuclear ribonucleoprotein U-like protein 2		1							1
348	Q16630-2	Isoform 2 of Cleavage and polyadenylation specificity factor subunit 6	1	1							1
349	P62318	Small nuclear ribonucleoprotein Sm D3	1	1							1
350	Q92747	Actin-related protein 2/3 complex subunit 1A	1	1							1
351	Q02790	Peptidyl-prolyl cis-trans isomerase FKBP4	1	1	1						1
352	Q9BXP5	Serrate RNA effector molecule homolog	1	1							1
353	P30101	Protein disulfide-isomerase A3				1					1
354	Q8TAA3	Proteasome subunit alpha type-7-like		1							1
355	Q08J23	tRNA (cytosine(34)-C(5))-methyltransferase	1	1	1						1
356	Q6PI48	Aspartate--tRNA ligase, mitochondrial			1						1
357	Q96AG4	Leucine-rich repeat-containing protein 59		1		1				1	
358	P11388-4	Isoform 4 of DNA topoisomerase 2-alpha	1	1							1
359	O75306	NADH dehydrogenase [ubiquinone] iron-sulfur protein 2, mitochondrial			1					1	

360	O00483	NADH dehydrogenase [ubiquinone] 1 alpha subcomplex subunit 4			1					1	
361	P31949	Protein S100-A11	1	1							1
362	Q8IYU8	Calcium uptake protein 2, mitochondrial			1						1
363	Q9UMS4	Pre-mRNA-processing factor 19	1	1							1
364	P60033	CD81 antigen					1			1	
365	O94979-8	Isoform 8 of Protein transport protein Sec31A	1			1	1			1	
366	Q15417	Calponin-3	1								1
367	P62244	40S ribosomal protein S15a	1	1			1			1	
368	P62753	40S ribosomal protein S6	1	1		1	1			1	
369	Q03252	Lamin-B2		1						1	
370	P78347	General transcription factor II-I	1	1							1
371	P62834	Ras-related protein Rap-1A	1				1			1	
372	P56537	Eukaryotic translation initiation factor 6	1	1							1
373	Q14739	Lamin-B receptor	1	1		1				1	
374	Q9P258	Protein RCC2	1	1			1			1	
375	Q5RKV6	Exosome complex component MTR3	1	1							1
376	Q08380	Galectin-3-binding protein									1
377	P52907	F-actin-capping protein subunit alpha-1	1								1
378	O15371	Eukaryotic translation initiation factor 3 subunit D	1								1
379	Q99497	Protein DJ-1	1	1	1	1	1			1	
380	P25786-2	Isoform Long of Proteasome subunit alpha type-1	1	1							1
381	P62316	Small nuclear ribonucleoprotein Sm D2	1	1							1
382	Q9UBM7	7-dehydrocholesterol reductase				1				1	
383	Q9UGP8	Translocation protein SEC63 homolog				1					1
384	P62263	40S ribosomal protein S14	1	1			1			1	
385	P22061-2	Isoform 2 of Protein-L-isoaspartate(D-aspartate) O-methyltransferase	1								1
386	Q13423	NAD(P) transhydrogenase, mitochondrial			1					1	
387	P25205	DNA replication licensing factor MCM3		1							1
388	Q2TAY7	WD40 repeat-containing protein SMU1	1	1							1
389	Q13263	Transcription intermediary factor 1-beta		1							1
390	P60953-1	Isoform 1 of Cell division control protein 42 homolog	1				1			1	
391	Q9BRT9	DNA replication complex GINS protein SLD5	1	1							1
392	Q92945	Far upstream element-binding protein 2	1	1							1
393	Q9H773	dCTP pyrophosphatase 1	1	1	1						1
394	P41250	Glycine--tRNA ligase	1		1						1
395	Q9NVH1	DnaJ homolog subfamily C member 11			1					1	
396	Q9BVP2	Guanine nucleotide-binding protein-like 3		1							1
397	Q13435	Splicing factor 3B subunit 2		1							1
398	P62888	60S ribosomal protein L30	1	1			1			1	
399	Q9Y230	RuvB-like 2	1	1			1			1	
400	P14678-3	Isoform SM-B1 of Small nuclear ribonucleoprotein-associated proteins B and B'	1	1							1
401	Q5BJF2	Transmembrane protein 97		1		1	1		1	1	
402	P49721	Proteasome subunit beta type-2	1	1							1
403	P53007	Tricarboxylate transport protein, mitochondrial			1					1	
404	P61204	ADP-ribosylation factor 3	1					1			1
405	P68036-3	Isoform 3 of Ubiquitin-conjugating enzyme E2 L3	1	1							1
406	P05091	Aldehyde dehydrogenase, mitochondrial			1						1
407	P32119	Peroxiredoxin-2	1								1
408	P12004	Proliferating cell nuclear antigen		1							1
409	O96008	Mitochondrial import receptor subunit TOM40 homolog			1					1	
410	O75400	Pre-mRNA-processing factor 40 homolog A		1							1
411	P40939	Trifunctional enzyme subunit alpha, mitochondrial			1					1	
412	P19404	NADH dehydrogenase [ubiquinone] flavoprotein 2, mitochondrial			1					1	
413	P18077	60S ribosomal protein L35a	1				1			1	

414	Q9Y6C9	Mitochondrial carrier homolog 2			1					1	
415	P60660-2	Isoform Smooth muscle of Myosin light polypeptide 6	1				1			1	
416	Q14566	DNA replication licensing factor MCM6		1							1
417	P62249	40S ribosomal protein S16	1	1			1			1	
418	P30046	D-dopachrome decarboxylase	1								1
419	Q06055-2	Isoform 2 of ATP synthase F(0) complex subunit C2, mitochondrial			1					1	
420	P46109	Crk-like protein	1	1			1			1	
421	P07686	Beta-hexosaminidase subunit beta							1		1
422	Q71U36	Tubulin alpha-1A chain	1								1
423	P62266	40S ribosomal protein S23	1			1					1
424	P51149	Ras-related protein Rab-7a							1	1	
425	P24928	DNA-directed RNA polymerase II subunit RPB1	1	1							1
426	Q04637-9	Isoform 9 of Eukaryotic translation initiation factor 4 gamma 1	1								1
427	P13796	Plastin-2					1			1	
428	P63173	60S ribosomal protein L38	1								1
429	Q9UNE7	E3 ubiquitin-protein ligase CHIP	1	1							1
430	O95456	Proteasome assembly chaperone 1	1			1					1
431	Q9UJS0-2	Isoform 2 of Calcium-binding mitochondrial carrier protein Aralar2			1					1	
432	P60900	Proteasome subunit alpha type-6	1	1							1
433	Q9NR30	Nucleolar RNA helicase 2	1	1	1						1
434	P25325	3-mercaptopyruvate sulfurtransferase	1		1						1
435	P14174	Macrophage migration inhibitory factor	1								1
436	Q5JWF2	Guanine nucleotide-binding protein G(s) subunit alpha isoforms XLas					1			1	
437	Q9Y265	RuvB-like 1	1	1			1			1	
438	O43390	Heterogeneous nuclear ribonucleoprotein R	1	1							1
439	P33993	DNA replication licensing factor MCM7	1								1
440	P49770	Translation initiation factor eIF-2B subunit beta	1								1
441	P37802	Transgelin-2	1								1
442	P26368	Splicing factor U2AF 65 kDa subunit	1								1
443	Q8NBS9	Thioredoxin domain-containing protein 5				1					1
444	Q00325	Phosphate carrier protein, mitochondrial			1					1	
445	P08238	Heat shock protein HSP 90-beta	1	1			1			1	
446	Q96SB4-3	Isoform 1 of SRSF protein kinase 1	1	1							1
447	Q9P2R7	Succinyl-CoA ligase [ADP-forming] subunit beta, mitochondrial			1						1
448	P39656	Dolichyl-diphosphooligosaccharide--protein glycosyltransferase 48 kDa subunit				1				1	
449	Q9BVA1	Tubulin beta-2B chain	1							1	
450	P52565	Rho GDP-dissociation inhibitor 1	1								1
451	P34932	Heat shock 70 kDa protein 4	1								1
452	Q15084-2	Isoform 2 of Protein disulfide-isomerase A6				1	1			1	
453	Q9H9B4	Sideroflexin-1			1					1	
454	P14618	Pyruvate kinase PKM	1	1							1
455	Q02543	60S ribosomal protein L18a	1				1			1	
456	P47755	F-actin-capping protein subunit alpha-2	1				1			1	
457	Q06830	Peroxiredoxin-1	1								1
458	Q9NVU7	Protein SDA1 homolog		1							1
459	P61960-2	Isoform 2 of Ubiquitin-fold modifier 1	1	1							1
460	P11142	Heat shock cognate 71 kDa protein	1	1			1			1	
461	Q15717	ELAV-like protein 1	1								1
462	P54886	Delta-1-pyrroline-5-carboxylate synthase			1					1	
463	Q9BZZ5	Apoptosis inhibitor 5	1	1							1
464	P26599-3	Isoform 3 of Polypyrimidine tract-binding protein 1		1							1
465	Q02880	DNA topoisomerase 2-beta	1	1							1
466	Q9H0D6	5'-3' exoribonuclease 2		1							1
467	P17812	CTP synthase 1	1				1			1	

468	Q99797	Mitochondrial intermediate peptidase			1						1
469	Q9Y3D3	28S ribosomal protein S16, mitochondrial			1						1
470	P61758	Prefoldin subunit 3	1	1							1
471	P07900-2	Isoform 2 of Heat shock protein HSP 90-alpha	1	1			1			1	
472	P27695	DNA-(apurinic or apyrimidinic site) lyase	1	1		1					1
473	P07195	L-lactate dehydrogenase B chain	1								1
474	Q8TDD1-2	Isoform 2 of ATP-dependent RNA helicase DDX54		1							1
475	B5ME19	Eukaryotic translation initiation factor 3 subunit C-like protein	1								1
476	P30837	Aldehyde dehydrogenase X, mitochondrial			1						1
477	O00541	Pescadillo homolog		1							1
478	P30050	60S ribosomal protein L12	1	1			1			1	
479	P68363	Tubulin alpha-1B chain	1								1
480	Q9UBB4	Ataxin-10	1								1
481	Q9UBQ5	Eukaryotic translation initiation factor 3 subunit K	1	1							1
482	P12277	Creatine kinase B-type	1								1
483	Q13148	TAR DNA-binding protein 43	1	1							1
484	Q92598	Heat shock protein 105 kDa	1								1
485	P28066	Proteasome subunit alpha type-5	1	1							1
486	P00492	Hypoxanthine-guanine phosphoribosyltransferase	1								1
487	O60271	C-Jun-amino-terminal kinase-interacting protein 4	1						1	1	
488	P60866-2	Isoform 2 of 40S ribosomal protein S20	1								1
489	P50395	Rab GDP dissociation inhibitor beta	1				1			1	
490	Q15050	Ribosome biogenesis regulatory protein homolog		1							1
491	Q8IY81	pre-rRNA processing protein FTSJ3		1							1
492	P18124	60S ribosomal protein L7	1	1			1			1	
493	Q9Y6B6	GTP-binding protein SAR1b				1		1		1	
494	P18669	Phosphoglycerate mutase 1	1				1			1	
495	Q13162	Peroxiredoxin-4	1			1					1
496	P27635	60S ribosomal protein L10	1	1		1	1			1	
497	Q96HC4	PDZ and LIM domain protein 5	1								1
498	Q08257	Quinone oxidoreductase	1								1
499	Q9UBE0	SUMO-activating enzyme subunit 1		1							1
500	P62917	60S ribosomal protein L8	1								1
501	P13797	Plastin-3	1								1
502	Q92841	Probable ATP-dependent RNA helicase DDX17	1	1							1
503	Q9BWF3	RNA-binding protein 4	1	1							1
504	P07437	Tubulin beta chain	1								1
505	Q9NZI8	Insulin-like growth factor 2 mRNA-binding protein 1	1	1							1
506	P47756-2	Isoform 2 of F-actin-capping protein subunit beta	1								1
507	Q5VTE0	Putative elongation factor 1-alpha-like 3	1								1
508	Q96DI7	U5 small nuclear ribonucleoprotein 40 kDa protein		1							1
509	O95433	Activator of 90 kDa heat shock protein ATPase homolog 1	1			1					1
510	P02786	Transferrin receptor protein 1					1			1	
511	Q15424-3	Isoform 3 of Scaffold attachment factor B1		1							1
512	P52948	Nuclear pore complex protein Nup98-Nup96		1						1	
513	O60264	SWI/SNF-related matrix-associated actin-dependent regulator of chromatin subfamily A member 5		1							1
514	Q07020	60S ribosomal protein L18	1			1					1
515	O43242	26S proteasome non-ATPase regulatory subunit 3	1	1			1			1	
516	P43243	Matrin-3		1							1
517	Q92769	Histone deacetylase 2	1	1							1
518	Q9Y262	Eukaryotic translation initiation factor 3 subunit L	1								1
519	P15954	Cytochrome c oxidase subunit 7C, mitochondrial			1					1	
520	P23246	Splicing factor, proline- and glutamine-rich		1							1

521	Q9Y2X3	Nucleolar protein 58		1							1
522	P10599	Thioredoxin	1	1							1
523	P09972	Fructose-bisphosphate aldolase C	1								1
524	P62829	60S ribosomal protein L23	1	1						1	
525	Q16658	Fascin	1								1
526	P55265-4	Isoform 4 of Double-stranded RNA-specific adenosine deaminase	1	1							1
527	Q12905	Interleukin enhancer-binding factor 2	1	1							1
528	P49720	Proteasome subunit beta type-3	1	1							1
529	O95394-4	Isoform 3 of Phosphoacetylglucosamine mutase	1								1
530	P62495	Eukaryotic peptide chain release factor subunit 1	1								1
531	P55072	Transitional endoplasmic reticulum ATPase	1	1		1					1
532	P62906	60S ribosomal protein L10a	1	1			1			1	
533	P06733	Alpha-enolase	1				1			1	
534	P20073	Annexin A7	1	1		1	1			1	
535	Q14974	Importin subunit beta-1	1	1							1
536	P61019	Ras-related protein Rab-2A				1		1		1	
537	P62241	40S ribosomal protein S8	1				1			1	
538	P12268	Inosine-5'-monophosphate dehydrogenase 2	1	1							1
539	P05198	Eukaryotic translation initiation factor 2 subunit 1	1								1
540	Q96AE4-2	Isoform 2 of Far upstream element-binding protein 1		1							1
541	Q96P70	Importin-9	1	1							1
542	P09211	Glutathione S-transferase P	1	1	1						1
543	P33991	DNA replication licensing factor MCM4	1	1							1
544	P08107	Heat shock 70 kDa protein 1A/1B	1	1							1
545	Q93009	Ubiquitin carboxyl-terminal hydrolase 7	1	1							1
546	Q8N163-2	Isoform 2 of Cell cycle and apoptosis regulator protein 2	1	1							1
547	Q9BYT8	Neurolysin, mitochondrial	1		1						1
548	P38919	Eukaryotic initiation factor 4A-III	1	1							1
549	O75083	WD repeat-containing protein 1	1								1
550	P04083	Annexin A1	1	1			1			1	
551	P60891	Ribose-phosphate pyrophosphokinase 1	1								1
552	P63244	Guanine nucleotide-binding protein subunit beta-2-like 1	1	1			1			1	
553	P30086	Phosphatidylethanolamine-binding protein 1	1								1
554	P60174	Triosephosphate isomerase	1								1
555	Q16531	DNA damage-binding protein 1	1	1							1
556	P83881	60S ribosomal protein L36a	1								1
557	Q8TED0	U3 small nucleolar RNA-associated protein 15 homolog		1							1
558	Q9H6D7	HAUS augmin-like complex subunit 4	1								1
559	P08240	Signal recognition particle receptor subunit alpha				1				1	
560	O00505	Importin subunit alpha-4	1	1							1
561	P22392-2	Isoform 3 of Nucleoside diphosphate kinase B	1	1							1
562	P04075-2	Isoform 2 of Fructose-bisphosphate aldolase A	1								1
563	P49189	4-trimethylaminobutyraldehyde dehydrogenase	1								1
564	P62277	40S ribosomal protein S13	1	1			1			1	
565	P26373	60S ribosomal protein L13	1	1		1	1			1	
566	Q15758	Neutral amino acid transporter B(0)					1			1	
567	Q9H8H0	Nucleolar protein 11		1							1
568	P62937	Peptidyl-prolyl cis-trans isomerase A	1								1
569	Q9BVJ6	U3 small nucleolar RNA-associated protein 14 homolog A		1							1
570	P43246	DNA mismatch repair protein Msh2		1							1
571	P48643	T-complex protein 1 subunit epsilon	1								1
572	P40616	ADP-ribosylation factor-like protein 1					1	1		1	
573	P48556	26S proteasome non-ATPase regulatory subunit 8	1	1							1
574	O15042	U2 snRNP-associated SURP motif-containing protein		1							1

575	Q10713	Mitochondrial-processing peptidase subunit alpha			1					1	
576	Q99459	Cell division cycle 5-like protein	1	1							1
577	Q13509	Tubulin beta-3 chain	1								1
578	P13010	X-ray repair cross-complementing protein 5		1							1
579	Q9BQG0-2	Isoform 2 of Myb-binding protein 1A	1	1							1
580	P25787	Proteasome subunit alpha type-2	1	1							1
581	O00231-2	Isoform 2 of 26S proteasome non-ATPase regulatory subunit 11	1	1							1
582	P26641	Elongation factor 1-gamma	1	1			1			1	
583	Q8TEX9-2	Isoform 2 of Importin-4	1	1							1
584	P11216	Glycogen phosphorylase, brain form	1				1		1	1	
585	P68371	Tubulin beta-4B chain	1								1
586	P09110	3-ketoacyl-CoA thiolase, peroxisomal									1
587	P09874	Poly [ADP-ribose] polymerase 1		1							1
588	P53004	Biliverdin reductase A	1								1
589	P00390	Glutathione reductase, mitochondrial	1		1						1
590	P40925-3	Isoform 3 of Malate dehydrogenase, cytoplasmic	1								1
591	P37837	Transaldolase	1								1
592	P83731	60S ribosomal protein L24	1			1	1			1	
593	P49207	60S ribosomal protein L34	1			1					1
594	P18206	Vinculin					1			1	
595	P22102	Trifunctional purine biosynthetic protein adenosine-3	1								1
596	O94776	Metastasis-associated protein MTA2		1							1
597	P78371	T-complex protein 1 subunit beta	1								1
598	P17844	Probable ATP-dependent RNA helicase DDX5	1	1							1
599	Q86XP3	ATP-dependent RNA helicase DDX42	1	1							1
600	Q9BSJ8-2	Isoform 2 of Extended synaptotagmin-1				1	1			1	
601	P84098	60S ribosomal protein L19	1	1			1			1	
602	Q53GQ0	Estradiol 17-beta-dehydrogenase 12				1				1	
603	P50990	T-complex protein 1 subunit theta	1								1
604	Q7RTV0	PHD finger-like domain-containing protein 5A		1							1
605	P60842	Eukaryotic initiation factor 4A-I	1				1			1	
606	P51610-4	Isoform 4 of Host cell factor 1	1	1							1
607	Q15008	26S proteasome non-ATPase regulatory subunit 6	1	1						1	
608	O00487	26S proteasome non-ATPase regulatory subunit 14	1	1							1
609	Q8TDN6	Ribosome biogenesis protein BRX1 homolog		1							1
610	O76003	Glutaredoxin-3	1								1
611	P62854	40S ribosomal protein S26	1			1					1
612	P13639	Elongation factor 2	1	1							1
613	P45974	Ubiquitin carboxyl-terminal hydrolase 5	1						1		1
614	P41091	Eukaryotic translation initiation factor 2 subunit 3	1								1
615	Q9UHG3	Prenylcysteine oxidase 1							1		1
616	P04406	Glyceraldehyde-3-phosphate dehydrogenase	1	1							1
617	O14776	Transcription elongation regulator 1		1							1
618	P43304	Glycerol-3-phosphate dehydrogenase, mitochondrial			1						1
619	P62701	40S ribosomal protein S4, X isoform	1								1
620	Q9BZE4	Nucleolar GTP-binding protein 1	1	1							1
621	Q00526	Cyclin-dependent kinase 3		1							1
622	P43490	Nicotinamide phosphoribosyltransferase	1	1							1
623	O95373	Importin-7	1	1							1
624	Q92900	Regulator of nonsense transcripts 1	1	1							1
625	P36551	Coproporphyrinogen-III oxidase, mitochondrial			1						1
626	P52888	Thimet oligopeptidase	1								1
627	P51532	Transcription activator BRG1	1								1
628	P13667	Protein disulfide-isomerase A4				1					1

629	Q9H857	5'-nucleotidase domain-containing protein 2									1
630	P00338-3	Isoform 3 of L-lactate dehydrogenase A chain	1								1
631	P50991	T-complex protein 1 subunit delta	1								1
632	Q9BWD1	Acetyl-CoA acetyltransferase, cytosolic	1								1
633	Q16527	Cysteine and glycine-rich protein 2		1							1
634	Q8N1G4	Leucine-rich repeat-containing protein 47									1
635	O00299	Chloride intracellular channel protein 1	1	1			1			1	
636	Q9NYU2	UDP-glucose:glycoprotein glucosyltransferase 1				1					1
637	P00558	Phosphoglycerate kinase 1	1								1
638	Q8TAQ2	SWI/SNF complex subunit SMARCC2		1							1
639	P62424	60S ribosomal protein L7a	1	1			1			1	
640	O15144	Actin-related protein 2/3 complex subunit 2	1	1							1
641	P22234-2	Isoform 2 of Multifunctional protein ADE2	1				1			1	
642	Q9ULX3	RNA-binding protein NOB1		1							1
643	P33992	DNA replication licensing factor MCM5	1	1							1
644	Q04760	Lactoylglutathione lyase	1	1			1			1	
645	Q96GQ7	Probable ATP-dependent RNA helicase DDX27		1							1
646	Q12906-7	Isoform 7 of Interleukin enhancer-binding factor 3	1	1							1
647	Q2NL82	Pre-rRNA-processing protein TSR1 homolog		1							1
648	Q9BY77	Polymerase delta-interacting protein 3		1							1
649	P13489	Ribonuclease inhibitor	1								1
650	Q96I24	Far upstream element-binding protein 3		1							1
651	P50454	Serpin H1				1					1
652	Q99832	T-complex protein 1 subunit eta	1								1
653	Q9UIG0	Tyrosine-protein kinase BAZ1B		1							1
654	Q16822	Phosphoenolpyruvate carboxykinase [GTP], mitochondrial			1						1
655	Q86W42	THO complex subunit 6 homolog		1							1
656	Q9NVP1	ATP-dependent RNA helicase DDX18		1							1
657	Q53GS9	U4/U6.U5 tri-snRNP-associated protein 2		1							1
658	O60506	Heterogeneous nuclear ribonucleoprotein Q	1	1		1					1
659	Q7L2E3-2	Isoform 2 of Putative ATP-dependent RNA helicase DHX30	1		1						1
660	A0FGR8-6	Isoform 6 of Extended synaptotagmin-2				1	1			1	
661	P62136-2	Isoform 2 of Serine/threonine-protein phosphatase PP1-alpha catalytic subunit	1	1							1
662	Q96HJ9-2	Isoform 2 of UPF0562 protein C7orf55			1						1
663	P49589-3	Isoform 3 of Cysteine--tRNA ligase, cytoplasmic	1								1
664	P18621-3	Isoform 3 of 60S ribosomal protein L17	1	1							1
665	Q9Y3E5	Peptidyl-tRNA hydrolase 2, mitochondrial			1						1
666	Q9H4A4	Aminopeptidase B					1			1	
667	P54577	Tyrosine--tRNA ligase, cytoplasmic	1								1
668	P34897	Serine hydroxymethyltransferase, mitochondrial	1	1	1					1	
669	P03905	NADH-ubiquinone oxidoreductase chain 4			1					1	
670	Q9UNM6-2	Isoform 2 of 26S proteasome non-ATPase regulatory subunit 13	1	1							1
671	P08133	Annexin A6	1								1
672	Q14683	Structural maintenance of chromosomes protein 1A		1							1
673	Q9H993	UPF0364 protein C6orf211									
674	P55196-5	Isoform 5 of Afadin								1	
		Total	**355**	**324**	**166**	**58**	**104**	**8**	**9**	**179**	**493**
		% proteins								**26.6**	**73.1**

Table A3. A list of our high-confidence protein hits (HEK293 cell proteins) that were also identified in HeLa cells as PC lipid-binding proteins by Yao and co-workers (reference number 6 cited in Chapter 4).

S. No.	UniProt ID	Gene ID	Protein Description
1	Q07021	C1QBP	Complement component 1 Q subcomponent-binding protein, mitochondrial
2	P14314	GLU2B	Glucosidase 2 subunit beta
3	P10809	CH60	60 kDa heat shock protein, mitochondrial
4	P27797	CALR	60 kDa heat shock protein, mitochondrial
5	P22695	QCR2	Cytochrome b-c1 complex subunit 2, mitochondrial
6	P06576	ATPB	ATP synthase subunit beta, mitochondrial
7	Q99623	PHB2	Prohibitin-2
8	P13804	ETFA	Electron transfer flavoprotein subunit alpha, mitochondrial
9	Q5SSJ5	HP1B3	Heterochromatin protein 1-binding protein 3
10	O95831	AIFM1	Apoptosis-inducing factor 1, mitochondrial
11	O75390	CISY	Citrate synthase, mitochondrial
12	P27824	CALX	Calnexin
13	O43615	TIM44	Mitochondrial import inner membrane translocase subunit TIM44
14	P04844	RPN2	Dolichyl-diphosphooligosaccharide--protein glycosyltransferase subunit 2
15	Q3ZCQ8-2	TIM50	Isoform 2 of Mitochondrial import inner membrane translocase subunit TIM50
16	P14625	ENPL	Endoplasmin
17	O95202	LETM1	LETM1 and EF-hand domain-containing protein 1, mitochondrial
18	P40926	MDHM	Malate dehydrogenase, mitochondrial
19	P42166	LAP2A	Lamina-associated polypeptide 2, isoform alpha
20	P31930	QCR1	Cytochrome b-c1 complex subunit 1, mitochondrial
21	P49755	TMEDA	Transmembrane emp24 domain-containing protein 10
22	Q09028	RBBP4	Histone-binding protein RBBP4
23	P00403	COX2	Cytochrome c oxidase subunit 2
24	P11021	GRP78	78 kDa glucose-regulated protein
25	O00264	PGRC1	Membrane-associated progesterone receptor component 1
26	P08574	CY1	Cytochrome c1, heme protein, mitochondrial
27	Q9NVI7-2	ATD3A	Isoform 2 of ATPase family AAA domain-containing protein 3A
28	Q07065	CKAP4	Cytoskeleton-associated protein 4
29	P36957	ODO2	Dihydrolipoyllysine-residue succinyltransferase component of 2-oxoglutarate dehydrogenase complex, mitochondrial
30	P20700	LMNB1	Lamin-B1
31	P21796	VDAC1	Voltage-dependent anion-selective channel protein 1
32	P05141	ADT2	ADP/ATP translocase 2
33	P07237	PDIA1	Protein disulfide-isomerase
34	Q12797	ASPH	Aspartyl/asparaginyl beta-hydroxylase
35	P62258	1433E	14-3-3 protein epsilon
36	P16435	NCPR	NADPH--cytochrome P450 reductase

37	P22087	FBRL	rRNA 2'-O-methyltransferase fibrillarin
38	P12236	ADT3	ADP/ATP translocase 3
39	Q96AG4	LRC59	Leucine-rich repeat-containing protein 59
40	P11388-4	TOP2A	Isoform 4 of DNA topoisomerase 2-alpha
41	Q03252	LMNB2	Lamin-B2
42	O96008	TOM40	Mitochondrial import receptor subunit TOM40 homolog
43	P40939	ECHA	Trifunctional enzyme subunit alpha, mitochondrial
44	Q9Y6C9	MTCH2	Mitochondrial carrier homolog 2
45	P39656	OST48	Dolichyl-diphosphooligosaccharide--protein glycosyltransferase 48 kDa subunit
46	P34932	HSP74	Heat shock 70 kDa protein 4
47	Q9H9B4	SFXN1	Sideroflexin-1
48	P02786	TFR1	Transferrin receptor protein 1
49	Q14974	IMB1	Importin subunit beta-1
50	Q93009	UBP7	Ubiquitin carboxyl-terminal hydrolase 7
51	P04083	ANXA1	Annexin A1
52	Q15758	AAAT	Neutral amino acid transporter B(0)
53	Q9BQG0-2	MBB1A	Isoform 2 of Myb-binding protein 1A
54	P83731	RL24	60S ribosomal protein L24
55	Q53GQ0	DHB12	Estradiol 17-beta-dehydrogenase 12
56	P45974	UBP5	Ubiquitin carboxyl-terminal hydrolase 5
57	Q9UHG3	PCYOX	Prenylcysteine oxidase 1
58	Q92900	RENT1	Regulator of nonsense transcripts 1
59	P13667	PDIA4	Protein disulfide-isomerase A4
60	Q9NVP1	DDX18	ATP-dependent RNA helicase DDX18

Table A4. A list of our high-confidence protein hits (HEK293 cell proteins) that are homologs of the yeast PC lipid-binding mitochondrial proteins identified by de Kroon and co-workers (reference number 7 cited in Chapter 4).

S. No.	UniProt ID	Gene ID	Protein Description
1	P10809	CH60	60 kDa heat shock protein, mitochondrial
2	P22695	QCR2	Cytochrome b-c1 complex subunit 2, mitochondrial
3	P06576	ATPB	ATP synthase subunit beta, mitochondrial
4	Q99623	PHB2	Prohibitin-2
5	P00403	COX2	Cytochrome c oxidase subunit 2
6	P08574	CY1	Cytochrome c1, heme protein, mitochondrial
7	P36957	ODO2	Dihydrolipoyllysine-residue succinyltransferase component of 2-oxoglutarate dehydrogenase complex, mitochondrial
8	P21796	VDAC1	Voltage-dependent anion-selective channel protein 1
9	P62258	1433E	14-3-3 protein epsilon
10	P22087	FBRL	rRNA 2'-O-methyltransferase fibrillarin

Table A5. The list of 674 high-confidence protein hits categorized according to their protein class as per the PANTHER classification system. This table was used to generate the plot depicted in Figure 4.10a.

S. No.	UniProt ID	Protein Name	Protein Class Category
1	Q9Y3D3	28S ribosomal protein S16, mitochondrial (MRP-S16) (S16mt) (Mitochondrial small ribosomal subunit protein bS16m)	Translational Protein
2	Q9Y262	Eukaryotic translation initiation factor 3 subunit L (eIF3l) (Eukaryotic translation initiation factor 3 subunit 6-interacting protein) (Eukaryotic translation initiation factor 3 subunit E-interacting protein)	Translational Protein
3	Q9UBQ5	Eukaryotic translation initiation factor 3 subunit K (eIF3k) (Eukaryotic translation initiation factor 3 subunit 12) (Muscle-specific gene M9 protein) (PLAC-24) (eIF-3 p25) (eIF-3 p28)	Translational Protein
4	Q9P015	39S ribosomal protein L15, mitochondrial (L15mt) (MRP-L15) (Mitochondrial large ribosomal subunit protein uL15m)	Translational Protein
5	Q9NSE4	Isoleucine--tRNA ligase, mitochondrial (EC 6.1.1.5) (Isoleucyl-tRNA synthetase) (IleRS)	Translational Protein
6	Q9NP92	39S ribosomal protein S30, mitochondrial (MRP-S30) (S30mt) (Mitochondrial large ribosomal subunit protein mL65) (Mitochondrial large ribosomal subunit protein mS30) (Programmed cell death protein 9)	Translational Protein
7	Q9BZE1	39S ribosomal protein L37, mitochondrial (L37mt) (MRP-L37) (39S ribosomal protein L2, mitochondrial) (L2mt) (MRP-L2) (Mitochondrial large ribosomal subunit protein mL37)	Translational Protein
8	Q9BYD3	39S ribosomal protein L4, mitochondrial (L4mt) (MRP-L4) (Mitochondrial large ribosomal subunit protein uL4m)	Translational Protein
9	Q9BYC9	39S ribosomal protein L20, mitochondrial (L20mt) (MRP-L20) (Mitochondrial large ribosomal subunit protein bL20m)	Translational Protein
10	Q92552	28S ribosomal protein S27, mitochondrial (MRP-S27) (S27mt) (Mitochondrial ribosomal protein S27) (Mitochondrial small ribosomal subunit protein mS27)	Translational Protein
11	Q8NE71	ATP-binding cassette sub-family F member 1 (ATP-binding cassette 50) (TNF-alpha-stimulated ABC protein)	Translational Protein
12	Q8N1G4	Leucine-rich repeat-containing protein 47	Translational Protein
13	Q7Z2W9	39S ribosomal protein L21, mitochondrial (L21mt) (MRP-L21) (Mitochondrial large ribosomal subunit protein bL21m)	Translational Protein
14	Q6PI48	Aspartate--tRNA ligase, mitochondrial (EC 6.1.1.12) (Aspartyl-tRNA synthetase) (AspRS)	Translational Protein
15	Q6P1L8	39S ribosomal protein L14, mitochondrial (L14mt) (MRP-L14) (39S ribosomal protein L32, mitochondrial) (L32mt) (MRP-L32) (Mitochondrial large ribosomal subunit protein uL14m)	Translational Protein
16	Q5VTE0	Putative elongation factor 1-alpha-like 3 (EF-1-alpha-like 3) (Eukaryotic elongation factor 1 A-like 3) (eEF1A-like 3) (Eukaryotic translation elongation factor 1 alpha-1 pseudogene 5)	Translational Protein
17	Q5JTZ9	Alanine--tRNA ligase, mitochondrial (EC 6.1.1.7) (Alanyl-tRNA synthetase) (AlaRS)	Translational Protein
18	Q5JPH6	Probable glutamate--tRNA ligase, mitochondrial (EC 6.1.1.17) (Glutamyl-tRNA synthetase) (GluRS)	Translational Protein
19	Q15717	ELAV-like protein 1 (Hu-antigen R) (HuR)	Translational Protein
20	Q15050	Ribosome biogenesis regulatory protein homolog	Translational Protein
21	Q07020	60S ribosomal protein L18 (Large ribosomal subunit protein eL18)	Translational Protein
22	Q06787	Synaptic functional regulator FMR1 (Fragile X mental retardation protein 1) (FMRP) (Protein FMR-1)	Translational Protein
23	Q02543	60S ribosomal protein L18a (Large ribosomal subunit protein eL20)	Translational Protein
24	P84098	60S ribosomal protein L19 (Large ribosomal subunit protein eL19)	Translational Protein
25	P83881	60S ribosomal protein L36a (60S ribosomal protein L44) (Cell growth-inhibiting gene 15 protein) (Cell migration-inducing gene 6 protein) (Large ribosomal subunit protein eL42)	Translational Protein
26	P83731	60S ribosomal protein L24 (60S ribosomal protein L30) (Large ribosomal subunit protein eL24)	Translational Protein
27	P82933	28S ribosomal protein S9, mitochondrial (MRP-S9) (S9mt) (Mitochondrial small ribosomal subunit protein uS9m)	Translational Protein
28	P82675	28S ribosomal protein S5, mitochondrial (MRP-S5) (S5mt) (Mitochondrial small ribosomal subunit protein uS5m)	Translational Protein
29	P63173	60S ribosomal protein L38 (Large ribosomal subunit protein eL38)	Translational Protein
30	P62917	60S ribosomal protein L8 (Large ribosomal subunit protein uL2)	Translational Protein
31	P62913	60S ribosomal protein L11 (CLL-associated antigen KW-12) (Large ribosomal subunit protein uL5)	Translational Protein
32	P62906	60S ribosomal protein L10a (CSA-19) (Large ribosomal subunit protein uL1) (Neural precursor cell expressed developmentally down-regulated protein 6) (NEDD-6)	Translational Protein
33	P62888	60S ribosomal protein L30 (Large ribosomal subunit protein eL30)	Translational Protein
34	P62854	40S ribosomal protein S26 (Small ribosomal subunit protein eS26)	Translational Protein
35	P62851	40S ribosomal protein S25 (Small ribosomal subunit protein eS25)	Translational Protein
36	P62829	60S ribosomal protein L23 (60S ribosomal protein L17) (Large ribosomal subunit protein uL14)	Translational Protein
37	P62753	40S ribosomal protein S6 (Phosphoprotein NP33) (Small ribosomal subunit protein eS6)	Translational Protein
38	P62750	60S ribosomal protein L23a (Large ribosomal subunit protein uL23)	Translational Protein
39	P62701	40S ribosomal protein S4, X isoform (SCR10) (Single copy abundant mRNA protein) (Small ribosomal subunit protein eS4)	Translational Protein
40	P62495	Eukaryotic peptide chain release factor subunit 1 (Eukaryotic release factor 1) (eRF1) (Protein Cl1) (TB3-1)	Translational Protein

41	P62424	60S ribosomal protein L7a (Large ribosomal subunit protein eL8) (PLA-X polypeptide) (Surfeit locus protein 3)	Translational Protein
42	P62280	40S ribosomal protein S11 (Small ribosomal subunit protein uS17)	Translational Protein
43	P62277	40S ribosomal protein S13 (Small ribosomal subunit protein uS15)	Translational Protein
44	P62266	40S ribosomal protein S23 (Small ribosomal subunit protein uS12)	Translational Protein
45	P62263	40S ribosomal protein S14 (Small ribosomal subunit protein uS11)	Translational Protein
46	P62249	40S ribosomal protein S16 (Small ribosomal subunit protein uS9)	Translational Protein
47	P62244	40S ribosomal protein S15a (Small ribosomal subunit protein uS8)	Translational Protein
48	P62241	40S ribosomal protein S8 (Small ribosomal subunit protein eS8)	Translational Protein
49	P61247	40S ribosomal protein S3a (Small ribosomal subunit protein eS1) (v-fos transformation effector protein) (Fte-1)	Translational Protein
50	P56537	Eukaryotic translation initiation factor 6 (eIF-6) (B(2)GCN homolog) (B4 integrin interactor) (CAB) (p27(BBP))	Translational Protein
51	P55010	Eukaryotic translation initiation factor 5 (eIF-5)	Translational Protein
52	P54577	Tyrosine--tRNA ligase, cytoplasmic (EC 6.1.1.1) (Tyrosyl-tRNA synthetase) (TyrRS) [Cleaved into: Tyrosine--tRNA ligase, cytoplasmic, N-terminally processed]	Translational Protein
53	P51116	Fragile X mental retardation syndrome-related protein 2	Translational Protein
54	P50914	60S ribosomal protein L14 (CAG-ISL 7) (Large ribosomal subunit protein eL14)	Translational Protein
55	P49770	Translation initiation factor eIF-2B subunit beta (S20I15) (S20III15) (eIF-2B GDP-GTP exchange factor subunit beta)	Translational Protein
56	P49411	Elongation factor Tu, mitochondrial (EF-Tu) (P43)	Translational Protein
57	P49207	60S ribosomal protein L34 (Large ribosomal subunit protein eL34)	Translational Protein
58	P47914	60S ribosomal protein L29 (Cell surface heparin-binding protein HIP) (Large ribosomal subunit protein eL29)	Translational Protein
59	P46777	60S ribosomal protein L5 (Large ribosomal subunit protein uL18)	Translational Protein
60	P43897	Elongation factor Ts, mitochondrial (EF-Ts) (EF-TsMt)	Translational Protein
61	P41250	Glycine--tRNA ligase (EC 6.1.1.14) (Diadenosine tetraphosphate synthetase) (Ap4A synthetase) (EC 2.7.7.-) (Glycyl-tRNA synthetase) (GlyRS) (Glycyl-tRNA synthetase 1)	Translational Protein
62	P41091	Eukaryotic translation initiation factor 2 subunit 3 (EC 3.6.5.3) (Eukaryotic translation initiation factor 2 subunit gamma X) (eIF-2-gamma X) (eIF-2gX)	Translational Protein
63	P35268	60S ribosomal protein L22 (EBER-associated protein) (EAP) (Epstein-Barr virus small RNA-associated protein) (Heparin-binding protein HBp15) (Large ribosomal subunit protein eL22)	Translational Protein
64	P32969	60S ribosomal protein L9 (Large ribosomal subunit protein uL6)	Translational Protein
65	P30050	60S ribosomal protein L12 (Large ribosomal subunit protein uL11)	Translational Protein
66	P27635	60S ribosomal protein L10 (Laminin receptor homolog) (Large ribosomal subunit protein uL16) (Protein QM) (Ribosomal protein L10) (Tumor suppressor QM)	Translational Protein
67	P26373	60S ribosomal protein L13 (Breast basic conserved protein 1) (Large ribosomal subunit protein eL13)	Translational Protein
68	P25398	40S ribosomal protein S12 (Small ribosomal subunit protein eS12)	Translational Protein
69	P24534	Elongation factor 1-beta (EF-1-beta)	Translational Protein
70	P23396	40S ribosomal protein S3 (EC 4.2.99.18) (Small ribosomal subunit protein uS3)	Translational Protein
71	P18124	60S ribosomal protein L7 (Large ribosomal subunit protein uL30)	Translational Protein
72	P18077	60S ribosomal protein L35a (Cell growth-inhibiting gene 33 protein) (Large ribosomal subunit protein eL33)	Translational Protein
73	P15880	40S ribosomal protein S2 (40S ribosomal protein S4) (Protein LLRep3) (Small ribosomal subunit protein uS5)	Translational Protein
74	P13639	Elongation factor 2 (EF-2)	Translational Protein
75	P09001	39S ribosomal protein L3, mitochondrial (L3mt) (MRP-L3) (Mitochondrial large ribosomal subunit protein uL3m)	Translational Protein
76	P08865	40S ribosomal protein SA (37 kDa laminin receptor precursor) (37LRP) (37/67 kDa laminin receptor) (LRP/LR) (67 kDa laminin receptor) (67LR) (Colon carcinoma laminin-binding protein) (Laminin receptor 1) (LamR) (Laminin-binding protein precursor p40) (LBP/p40) (Multidrug resistance-associated protein MGr1-Ag) (NEM/1CHD4) (Small ribosomal subunit protein uS2)	Translational Protein
77	P05388	60S acidic ribosomal protein P0 (60S ribosomal protein L10E) (Large ribosomal subunit protein uL10)	Translational Protein
78	P05387	60S acidic ribosomal protein P2 (Large ribosomal subunit protein P2) (Renal carcinoma antigen NY-REN-44)	Translational Protein
79	P05386	60S acidic ribosomal protein P1 (Large ribosomal subunit protein P1)	Translational Protein
80	P05198	Eukaryotic translation initiation factor 2 subunit 1 (Eukaryotic translation initiation factor 2 subunit alpha) (eIF-2-alpha) (eIF-2A) (eIF-2alpha)	Translational Protein
81	O76021	Ribosomal L1 domain-containing protein 1 (CATX-11) (Cellular senescence-inhibited gene protein) (Protein PBK1)	Translational Protein
82	O75821	Eukaryotic translation initiation factor 3 subunit G (eIF3g) (Eukaryotic translation initiation factor 3 RNA-binding subunit) (eIF-3 RNA-binding subunit) (Eukaryotic translation initiation factor 3 subunit 4) (eIF-3-delta) (eIF3 p42) (eIF3 p44)	Translational Protein
83	O60783	28S ribosomal protein S14, mitochondrial (MRP-S14) (S14mt) (Mitochondrial small ribosomal subunit protein uS14m)	Translational Protein
84	O15371	Eukaryotic translation initiation factor 3 subunit D (eIF3d) (Eukaryotic translation initiation factor 3 subunit 7) (eIF-3-zeta) (eIF3 p66)	Translational Protein
85	O00487	26S proteasome non-ATPase regulatory subunit 14 (EC 3.4.19.-) (26S proteasome regulatory subunit RPN11) (26S proteasome-associated PAD1 homolog 1)	Translational Protein
86	B5ME19	Eukaryotic translation initiation factor 3 subunit C-like protein	Translational Protein
87	Q9Y266	Nuclear migration protein nudC (Nuclear distribution protein C homolog)	Cytoskeletal protein
88	Q9BVA1	Tubulin beta-2B chain	Cytoskeletal protein
89	Q96HC4	PDZ and LIM domain protein 5 (Enigma homolog) (Enigma-like PDZ and LIM domains protein)	Cytoskeletal protein
90	Q92747	Actin-related protein 2/3 complex subunit 1A (SOP2-like protein)	Cytoskeletal protein

91	Q71U36	Tubulin alpha-1A chain (Alpha-tubulin 3) (Tubulin B-alpha-1) (Tubulin alpha-3 chain) [Cleaved into: Detyrosinated tubulin alpha-1A chain]	Cytoskeletal protein
92	Q16658	Fascin (55 kDa actin-bundling protein) (Singed-like protein) (p55)	Cytoskeletal protein
93	Q16527	Cysteine and glycine-rich protein 2 (Cysteine-rich protein 2) (CRP2) (LIM domain only protein 5) (LMO-5) (Smooth muscle cell LIM protein) (SmLIM)	Cytoskeletal protein
94	Q15691	Microtubule-associated protein RP/EB family member 1 (APC-binding protein EB1) (End-binding protein 1) (EB1)	Cytoskeletal protein
95	Q15417	Calponin-3 (Calponin, acidic isoform)	Cytoskeletal protein
96	Q13509	Tubulin beta-3 chain (Tubulin beta-4 chain) (Tubulin beta-III)	Cytoskeletal protein
97	P68371	Tubulin beta-4B chain (Tubulin beta-2 chain) (Tubulin beta-2C chain)	Cytoskeletal protein
98	P68363	Tubulin alpha-1B chain (Alpha-tubulin ubiquitous) (Tubulin K-alpha-1) (Tubulin alpha-ubiquitous chain) [Cleaved into: Detyrosinated tubulin alpha-1B chain]	Cytoskeletal protein
99	P67936	Tropomyosin alpha-4 chain (TM30p1) (Tropomyosin-4)	Cytoskeletal protein
100	P61163	Alpha-centractin (Centractin) (ARP1) (Actin-RPV) (Centrosome-associated actin homolog)	Cytoskeletal protein
101	P52907	F-actin-capping protein subunit alpha-1 (CapZ alpha-1)	Cytoskeletal protein
102	P47755	F-actin-capping protein subunit alpha-2 (CapZ alpha-2)	Cytoskeletal protein
103	P37802	Transgelin-2 (Epididymis tissue protein Li 7e) (SM22-alpha homolog)	Cytoskeletal protein
104	P26038	Moesin (Membrane-organizing extension spike protein)	Cytoskeletal protein
105	P23528	Cofilin-1 (18 kDa phosphoprotein) (p18) (Cofilin, non-muscle isoform)	Cytoskeletal protein
106	P15311	Ezrin (Cytovillin) (Villin-2) (p81)	Cytoskeletal protein
107	P13797	Plastin-3 (T-plastin)	Cytoskeletal protein
108	P13796	Plastin-2 (L-plastin) (LC64P) (Lymphocyte cytosolic protein 1) (LCP-1)	Cytoskeletal protein
109	P13693	Translationally-controlled tumor protein (TCTP) (Fortilin) (Histamine-releasing factor) (HRF) (p23)	Cytoskeletal protein
110	P07737	Profilin-1 (Epididymis tissue protein Li 184a) (Profilin I)	Cytoskeletal protein
111	P07437	Tubulin beta chain (Tubulin beta-5 chain)	Cytoskeletal protein
112	O75083	WD repeat-containing protein 1 (Actin-interacting protein 1) (AIP1) (NORI-1)	Cytoskeletal protein
113	O14950	Myosin regulatory light chain 12B (MLC-2A) (MLC-2) (Myosin regulatory light chain 2-B, smooth muscle isoform) (Myosin regulatory light chain 20 kDa) (MLC20) (Myosin regulatory light chain MRLC2) (SHUJUN-1)	Cytoskeletal protein
114	O00264	Membrane-associated progesterone receptor component 1 (mPR) (Dap1) (IZA)	Receptor
115	Q9Y2X3	Nucleolar protein 58 (Nucleolar protein 5)	Nucleic acid metabolism protein
116	Q9UMS4	Pre-mRNA-processing factor 19 (EC 2.3.2.27) (Nuclear matrix protein 200) (PRP19/PSO4 homolog) (hPso4) (RING-type E3 ubiquitin transferase PRP19) (Senescence evasion factor)	Nucleic acid metabolism protein
117	Q9NZI8	Insulin-like growth factor 2 mRNA-binding protein 1 (IGF2 mRNA-binding protein 1) (IMP-1) (IMP1) (Coding region determinant-binding protein) (CRD-BP) (IGF-II mRNA-binding protein 1) (VICKZ family member 1) (Zipcode-binding protein 1) (ZBP-1)	Nucleic acid metabolism protein
118	Q9NYF8	Bcl-2-associated transcription factor 1 (Btf) (BCLAF1 and THRAP3 family member 1)	Nucleic acid metabolism protein
119	Q9H9J2	39S ribosomal protein L44, mitochondrial (L44mt) (MRP-L44) (EC 3.1.26.-) (Mitochondrial large ribosomal subunit protein mL44)	Nucleic acid metabolism protein
120	Q9H0D6	5'-3' exoribonuclease 2 (EC 3.1.13.-) (DHM1-like protein) (DHP protein)	Nucleic acid metabolism protein
121	Q9BY77	Polymerase delta-interacting protein 3 (46 kDa DNA polymerase delta interaction protein) (p46) (S6K1 Aly/REF-like target) (SKAR)	Nucleic acid metabolism protein
122	Q9BWF3	RNA-binding protein 4 (Lark homolog) (hLark) (RNA-binding motif protein 4) (RNA-binding motif protein 4a)	Nucleic acid metabolism protein
123	Q9BVJ6	U3 small nucleolar RNA-associated protein 14 homolog A (Antigen NY-CO-16) (Serologically defined colon cancer antigen 16)	Nucleic acid metabolism protein
124	Q9BRL6	Serine/arginine-rich splicing factor 8 (Pre-mRNA-splicing factor SRP46) (Splicing factor SRp46) (Splicing factor, arginine/serine-rich 2B)	Nucleic acid metabolism protein
125	Q96I24	Far upstream element-binding protein 3 (FUSE-binding protein 3)	Nucleic acid metabolism protein
126	Q92945	Far upstream element-binding protein 2 (FUSE-binding protein 2) (KH type-splicing regulatory protein) (KSRP) (p75)	Nucleic acid metabolism protein
127	Q92804	TATA-binding protein-associated factor 2N (68 kDa TATA-binding protein-associated factor) (TAF(II)68) (TAFII68) (RNA-binding protein 56)	Nucleic acid metabolism protein
128	Q8TED0	U3 small nucleolar RNA-associated protein 15 homolog	Nucleic acid metabolism protein
129	Q8TDN6	Ribosome biogenesis protein BRX1 homolog (Brix domain-containing protein 2)	Nucleic acid metabolism protein
130	Q8NC51	Plasminogen activator inhibitor 1 RNA-binding protein (PAI1 RNA-binding protein 1) (PAI-RBP1) (SERPINE1 mRNA-binding protein 1)	Nucleic acid metabolism protein
131	Q8IYB3	Serine/arginine repetitive matrix protein 1 (SR-related nuclear matrix protein of 160 kDa) (SRm160) (Ser/Arg-related nuclear matrix protein)	Nucleic acid metabolism protein
132	Q8IY81	pre-rRNA 2'-O-ribose RNA methyltransferase FTSJ3 (EC 2.1.1.-) (Protein ftsJ homolog 3) (Putative rRNA methyltransferase 3)	Nucleic acid metabolism protein
133	Q7L0Y3	tRNA methyltransferase 10 homolog C (HBV pre-S2 trans-regulated protein 2) (Mitochondrial ribonuclease P protein 1)	Nucleic acid metabolism protein
134	Q5RKV6	Exosome complex component MTR3 (Exosome component 6) (mRNA transport regulator 3 homolog) (hMtr3) (p11)	Nucleic acid metabolism protein
135	Q16629	Serine/arginine-rich splicing factor 7 (Splicing factor 9G8) (Splicing factor, arginine/serine-rich 7)	Nucleic acid metabolism protein
136	Q16625	Occludin	Nucleic acid metabolism protein
137	Q16531	DNA damage-binding protein 1 (DDB p127 subunit) (DNA damage-binding protein a) (DDBa) (Damage-specific DNA-binding protein 1) (HBV X-associated protein 1) (XAP-1) (UV-damaged DNA-binding factor) (UV-damaged DNA-binding protein 1) (UV-DDB 1) (XPE-binding factor) (XPE-BF) (Xeroderma pigmentosum group E-complementing protein) (XPCe)	Nucleic acid metabolism protein
138	Q15459	Splicing factor 3A subunit 1 (SF3a120) (Spliceosome-associated protein 114) (SAP 114)	Nucleic acid metabolism protein
139	Q15365	Poly(rC)-binding protein 1 (Alpha-CP1) (Heterogeneous nuclear ribonucleoprotein E1) (hnRNP E1) (Nucleic acid-binding protein SUB2.3)	Nucleic acid metabolism protein

140	Q15287	RNA-binding protein with serine-rich domain 1 (SR-related protein LDC2)	Nucleic acid metabolism protein
141	Q14566	DNA replication licensing factor MCM6 (EC 3.6.4.12) (p105MCM)	Nucleic acid metabolism protein
142	Q14444	Caprin-1 (Cell cycle-associated protein 1) (Cytoplasmic activation- and proliferation-associated protein 1) (GPI-anchored membrane protein 1) (GPI-anchored protein p137) (GPI-p137) (p137GPI) (Membrane component chromosome 11 surface marker 1) (RNA granule protein 105)	Nucleic acid metabolism protein
143	Q13435	Splicing factor 3B subunit 2 (Pre-mRNA-splicing factor SF3b 145 kDa subunit) (SF3b145) (Spliceosome-associated protein 145) (SAP 145)	Nucleic acid metabolism protein
144	Q13283	Ras GTPase-activating protein-binding protein 1 (G3BP-1) (EC 3.6.4.12) (EC 3.6.4.13) (ATP-dependent DNA helicase VIII) (hDH VIII) (GAP SH3 domain-binding protein 1)	Nucleic acid metabolism protein
145	Q13247	Serine/arginine-rich splicing factor 6 (Pre-mRNA-splicing factor SRP55) (Splicing factor, arginine/serine-rich 6)	Nucleic acid metabolism protein
146	Q13243	Serine/arginine-rich splicing factor 5 (Delayed-early protein HRS) (Pre-mRNA-splicing factor SRP40) (Splicing factor, arginine/serine-rich 5)	Nucleic acid metabolism protein
147	Q13242	Serine/arginine-rich splicing factor 9 (Pre-mRNA-splicing factor SRp30C) (Splicing factor, arginine/serine-rich 9)	Nucleic acid metabolism protein
148	Q12874	Splicing factor 3A subunit 3 (SF3a60) (Spliceosome-associated protein 61) (SAP 61)	Nucleic acid metabolism protein
149	Q12849	G-rich sequence factor 1 (GRSF-1)	Nucleic acid metabolism protein
150	Q08J23	RNA cytosine C(5)-methyltransferase NSUN2 (EC 2.1.1.-)	Nucleic acid metabolism protein
151	Q08170	Serine/arginine-rich splicing factor 4 (Pre-mRNA-splicing factor SRP75) (SRP001LB) (Splicing factor, arginine/serine-rich 4)	Nucleic acid metabolism protein
152	Q07666	KH domain-containing, RNA-binding, signal transduction-associated protein 1 (GAP-associated tyrosine phosphoprotein p62) (Src-associated in mitosis 68 kDa protein) (Sam68) (p21 Ras GTPase-activating protein-associated p62) (p68)	Nucleic acid metabolism protein
153	Q05519	Serine/arginine-rich splicing factor 11 (Arginine-rich 54 kDa nuclear protein) (p54) (Splicing factor, arginine/serine-rich 11)	Nucleic acid metabolism protein
154	Q04837	Single-stranded DNA-binding protein, mitochondrial (Mt-SSB) (MtSSB) (PWP1-interacting protein 17)	Nucleic acid metabolism protein
155	Q02880	DNA topoisomerase 2-beta (EC 5.6.2.2) (DNA topoisomerase II, beta isozyme)	Nucleic acid metabolism protein
156	Q01081	Splicing factor U2AF 35 kDa subunit (U2 auxiliary factor 35 kDa subunit) (U2 small nuclear RNA auxiliary factor 1) (U2 snRNP auxiliary factor small subunit)	Nucleic acid metabolism protein
157	P84103	Serine/arginine-rich splicing factor 3 (Pre-mRNA-splicing factor SRP20) (Splicing factor, arginine/serine-rich 3)	Nucleic acid metabolism protein
158	P78347	General transcription factor II-I (GTFII-I) (TFII-I) (Bruton tyrosine kinase-associated protein 135) (BAP-135) (BTK-associated protein 135) (SRF-Phox1-interacting protein) (SPIN) (Williams-Beuren syndrome chromosomal region 6 protein)	Nucleic acid metabolism protein
159	P78316	Nucleolar protein 14 (Nucleolar complex protein 14)	Nucleic acid metabolism protein
160	P62318	Small nuclear ribonucleoprotein Sm D3 (Sm-D3) (snRNP core protein D3)	Nucleic acid metabolism protein
161	P62316	Small nuclear ribonucleoprotein Sm D2 (Sm-D2) (snRNP core protein D2)	Nucleic acid metabolism protein
162	P62304	Small nuclear ribonucleoprotein E (snRNP-E) (Sm protein E) (Sm-E) (SmE)	Nucleic acid metabolism protein
163	P54727	UV excision repair protein RAD23 homolog B (HR23B) (hHR23B) (XP-C repair-complementing complex 58 kDa protein) (p58)	Nucleic acid metabolism protein
164	P52597	Heterogeneous nuclear ribonucleoprotein F (hnRNP F) (Nucleolin-like protein mcs94-1) [Cleaved into: Heterogeneous nuclear ribonucleoprotein F, N-terminally processed]	Nucleic acid metabolism protein
165	P51532	Transcription activator BRG1 (EC 3.6.4.-) (ATP-dependent helicase SMARCA4) (BRG1-associated factor 190A) (BAF190A) (Mitotic growth and transcription activator) (Protein BRG-1) (Protein brahma homolog 1) (SNF2-beta) (SWI/SNF-related matrix-associated actin-dependent regulator of chromatin subfamily A member 4)	Nucleic acid metabolism protein
166	P49458	Signal recognition particle 9 kDa protein (SRP9)	Nucleic acid metabolism protein
167	P43246	DNA mismatch repair protein Msh2 (hMSH2) (MutS protein homolog 2)	Nucleic acid metabolism protein
168	P37108	Signal recognition particle 14 kDa protein (SRP14) (18 kDa Alu RNA-binding protein)	Nucleic acid metabolism protein
169	P35637	RNA-binding protein FUS (75 kDa DNA-pairing protein) (Oncogene FUS) (Oncogene TLS) (POMp75) (Translocated in liposarcoma protein)	Nucleic acid metabolism protein
170	P35269	General transcription factor IIF subunit 1 (General transcription factor IIF 74 kDa subunit) (Transcription initiation factor IIF subunit alpha) (TFIIF-alpha) (Transcription initiation factor RAP74)	Nucleic acid metabolism protein
171	P33993	DNA replication licensing factor MCM7 (EC 3.6.4.12) (CDC47 homolog) (P1.1-MCM3)	Nucleic acid metabolism protein
172	P33992	DNA replication licensing factor MCM5 (EC 3.6.4.12) (CDC46 homolog) (P1-CDC46)	Nucleic acid metabolism protein
173	P33991	DNA replication licensing factor MCM4 (EC 3.6.4.12) (CDC21 homolog) (P1-CDC21)	Nucleic acid metabolism protein
174	P31943	Heterogeneous nuclear ribonucleoprotein H (hnRNP H) [Cleaved into: Heterogeneous nuclear ribonucleoprotein H, N-terminally processed]	Nucleic acid metabolism protein
175	P31942	Heterogeneous nuclear ribonucleoprotein H3 (hnRNP H3) (Heterogeneous nuclear ribonucleoprotein 2H9) (hnRNP 2H9)	Nucleic acid metabolism protein
176	P25205	DNA replication licensing factor MCM3 (EC 3.6.4.12) (DNA polymerase alpha holoenzyme-associated protein P1) (P1-MCM3) (RLF subunit beta) (p102)	Nucleic acid metabolism protein
177	P24928	DNA-directed RNA polymerase II subunit RPB1 (RNA polymerase II subunit B1) (EC 2.7.7.6) (DNA-directed RNA polymerase II subunit A) (DNA-directed RNA polymerase III largest subunit) (RNA-directed RNA polymerase II subunit RPB1) (EC 2.7.7.48)	Nucleic acid metabolism protein
178	P23246	Splicing factor, proline- and glutamine-rich (100 kDa DNA-pairing protein) (hPOMp100) (DNA-binding p52/p100 complex, 100 kDa subunit) (Polypyrimidine tract-binding protein-associated-splicing factor) (PSF) (PTB-associated-splicing factor)	Nucleic acid metabolism protein
179	P22087	rRNA 2'-O-methyltransferase fibrillarin (EC 2.1.1.-) (34 kDa nucleolar scleroderma antigen) (Histone-glutamine methyltransferase) (U6 snRNA 2'-O-methyltransferase fibrillarin)	Nucleic acid metabolism protein
180	P13010	X-ray repair cross-complementing protein 5	Nucleic acid metabolism protein
181	P12956	X-ray repair cross-complementing protein 6	Nucleic acid metabolism protein
182	P12004	Proliferating cell nuclear antigen (PCNA) (Cyclin)	Nucleic acid metabolism protein
183	P11387	DNA topoisomerase 1 (EC 5.6.2.1) (DNA topoisomerase I)	Nucleic acid metabolism protein

184	P09874	Poly [ADP-ribose] polymerase 1 (PARP-1) (EC 2.4.2.30) (ADP-ribosyltransferase diphtheria toxin-like 1) (ARTD1) (DNA ADP-ribosyltransferase PARP1) (EC 2.4.2.-) (NAD(+) ADP-ribosyltransferase 1) (ADPRT 1) (Poly[ADP-ribose] synthase 1) (Protein poly-ADP-ribosyltransferase PARP1) (EC 2.4.2.-)	Nucleic acid metabolism protein
185	P08621	U1 small nuclear ribonucleoprotein 70 kDa (U1 snRNP 70 kDa) (U1-70K) (snRNP70)	Nucleic acid metabolism protein
186	P05455	Lupus La protein (La autoantigen) (La ribonucleoprotein) (Sjoegren syndrome type B antigen) (SS-B)	Nucleic acid metabolism protein
187	O60506	Heterogeneous nuclear ribonucleoprotein Q (hnRNP Q) (Glycine- and tyrosine-rich RNA-binding protein) (GRY-RBP) (NS1-associated protein 1) (Synaptotagmin-binding, cytoplasmic RNA-interacting protein)	Nucleic acid metabolism protein
188	O60264	SWI/SNF-related matrix-associated actin-dependent regulator of chromatin subfamily A member 5 (SWI/SNF-related matrix-associated actin-dependent regulator of chromatin A5) (EC 3.6.4.-) (Sucrose nonfermenting protein 2 homolog) (hSNF2H)	Nucleic acid metabolism protein
189	O43809	Cleavage and polyadenylation specificity factor subunit 5 (Cleavage and polyadenylation specificity factor 25 kDa subunit) (CPSF 25 kDa subunit) (Cleavage factor Im complex 25 kDa subunit) (CFIm25) (Nucleoside diphosphate-linked moiety X motif 21) (Nudix motif 21) (Nudix hydrolase 21) (Pre-mRNA cleavage factor Im 68 kDa subunit)	Nucleic acid metabolism protein
190	O43390	Heterogeneous nuclear ribonucleoprotein R (hnRNP R)	Nucleic acid metabolism protein
191	O15042	U2 snRNP-associated SURP motif-containing protein (140 kDa Ser/Arg-rich domain protein) (U2-associated protein SR140)	Nucleic acid metabolism protein
192	O14776	Transcription elongation regulator 1 (TATA box-binding protein-associated factor 2S) (Transcription factor CA150)	Nucleic acid metabolism protein
193	O00567	Nucleolar protein 56 (Nucleolar protein 5A)	Nucleic acid metabolism protein
194	O00541	Pescadillo homolog	Nucleic acid metabolism protein
195	O14561	Acyl carrier protein, mitochondrial (ACP) (CI-SDAP) (NADH-ubiquinone oxidoreductase 9.6 kDa subunit)	Transfer/carrier protein
196	P05141	ADP/ATP translocase 2 (ADP,ATP carrier protein 2) (ADP,ATP carrier protein, fibroblast isoform) (Adenine nucleotide translocator 2) (ANT 2) (Solute carrier family 25 member 5) [Cleaved into: ADP/ATP translocase 2, N-terminally processed]	Transfer/carrier protein
197	P12236	ADP/ATP translocase 3 (ADP,ATP carrier protein 3) (ADP,ATP carrier protein, isoform T2) (ANT 2) (Adenine nucleotide translocator 3) (ANT 3) (Solute carrier family 25 member 6) [Cleaved into: ADP/ATP translocase 3, N-terminally processed]	Transfer/carrier protein
198	Q9NVH1	DnaJ homolog subfamily C member 11	Chaperone
199	Q99832	T-complex protein 1 subunit eta (TCP-1-eta) (CCT-eta) (HIV-1 Nef-interacting protein) [Cleaved into: T-complex protein 1 subunit eta, N-terminally processed]	Chaperone
200	Q96EY1	DnaJ homolog subfamily A member 3, mitochondrial (DnaJ protein Tid-1) (hTid-1) (Hepatocellular carcinoma-associated antigen 57) (Tumorous imaginal discs protein Tid56 homolog)	Chaperone
201	Q8NBS9	Thioredoxin domain-containing protein 5 (Endoplasmic reticulum resident protein 46) (ER protein 46) (ERp46) (Thioredoxin-like protein p46)	Chaperone
202	Q16543	Hsp90 co-chaperone Cdc37 (Hsp90 chaperone protein kinase-targeting subunit) (p50Cdc37) [Cleaved into: Hsp90 co-chaperone Cdc37, N-terminally processed]	Chaperone
203	Q15185	Prostaglandin E synthase 3 (EC 5.3.99.3) (Cytosolic prostaglandin E2 synthase) (cPGES) (Hsp90 co-chaperone) (Progesterone receptor complex p23) (Telomerase-binding protein p23)	Chaperone
204	Q12931	Heat shock protein 75 kDa, mitochondrial (HSP 75) (TNFR-associated protein 1) (Tumor necrosis factor type 1 receptor-associated protein) (TRAP-1)	Chaperone
205	Q02790	Peptidyl-prolyl cis-trans isomerase FKBP4 (PPIase FKBP4) (EC 5.2.1.8) (51 kDa FK506-binding protein) (FKBP51) (52 kDa FK506-binding protein) (52 kDa FKBP) (FKBP-52) (59 kDa immunophilin) (p59) (FK506-binding protein 4) (FKBP-4) (FKBP59) (HSP-binding immunophilin) (HBI) (Immunophilin FKBP52) (Rotamase) [Cleaved into: Peptidyl-prolyl cis-trans isomerase FKBP4, N-terminally processed]	Chaperone
206	P78371	T-complex protein 1 subunit beta (TCP-1-beta) (CCT-beta)	Chaperone
207	P62937	Peptidyl-prolyl cis-trans isomerase A (PPIase A) (EC 5.2.1.8) (Cyclophilin A) (Cyclosporin A-binding protein) (Rotamase A) [Cleaved into: Peptidyl-prolyl cis-trans isomerase A, N-terminally processed]	Chaperone
208	P61758	Prefoldin subunit 3 (HIBBJ46) (von Hippel-Lindau-binding protein 1) (VBP-1) (VHL-binding protein 1)	Chaperone
209	P61604	10 kDa heat shock protein, mitochondrial (Hsp10) (10 kDa chaperonin) (Chaperonin 10) (CPN10) (Early-pregnancy factor) (EPF)	Chaperone
210	P50991	T-complex protein 1 subunit delta (TCP-1-delta) (CCT-delta) (Stimulator of TAR RNA-binding)	Chaperone
211	P50990	T-complex protein 1 subunit theta (TCP-1-theta) (CCT-theta) (Chaperonin containing T-complex polypeptide 1 subunit 8) (Renal carcinoma antigen NY-REN-15)	Chaperone
212	P48643	T-complex protein 1 subunit epsilon (TCP-1-epsilon) (CCT-epsilon)	Chaperone
213	P30405	Peptidyl-prolyl cis-trans isomerase F, mitochondrial (PPIase F) (EC 5.2.1.8) (Cyclophilin D) (CyP-D) (CypD) (Cyclophilin F) (Mitochondrial cyclophilin) (CyP-M) (Rotamase F)	Chaperone
214	P30101	Protein disulfide-isomerase A3 (EC 5.3.4.1) (58 kDa glucose-regulated protein) (58 kDa microsomal protein) (p58) (Disulfide isomerase ER-60) (Endoplasmic reticulum resident protein 57) (ER protein 57) (ERp57) (Endoplasmic reticulum resident protein 60) (ER protein 60) (ERp60)	Chaperone
215	P27824	Calnexin (IP90) (Major histocompatibility complex class I antigen-binding protein p88) (p90)	Chaperone
216	P27797	Calreticulin (CRP55) (Calregulin) (Endoplasmic reticulum resident protein 60) (ERp60) (HACBP) (grp60)	Chaperone
217	P23284	Peptidyl-prolyl cis-trans isomerase B (PPIase B) (EC 5.2.1.8) (CYP-S1) (Cyclophilin B) (Rotamase B) (S-cyclophilin) (SCYLP)	Chaperone
218	P14625	Endoplasmin (94 kDa glucose-regulated protein) (GRP-94) (Heat shock protein 90 kDa beta member 1) (Tumor rejection antigen 1) (gp96 homolog)	Chaperone
219	P13667	Protein disulfide-isomerase A4 (EC 5.3.4.1) (Endoplasmic reticulum resident protein 70) (ER protein 70) (ERp70) (Endoplasmic reticulum resident protein 72) (ER protein 72) (ERp-72) (ERp72)	Chaperone
220	P08238	Heat shock protein HSP 90-beta (HSP 90) (Heat shock 84 kDa) (HSP 84) (HSP84)	Chaperone
221	P07237	Protein disulfide-isomerase (PDI) (EC 5.3.4.1) (Cellular thyroid hormone-binding protein) (Prolyl 4-hydroxylase subunit beta) (p55)	Chaperone
222	P06748	Nucleophosmin (NPM) (Nucleolar phosphoprotein B23) (Nucleolar protein NO38) (Numatrin)	Chaperone
223	O95456	Proteasome assembly chaperone 1 (PAC-1) (Chromosome 21 leucine-rich protein) (C21-LRP) (Down syndrome critical region protein 2)	Chaperone

224	O95433	Activator of 90 kDa heat shock protein ATPase homolog 1 (AHA1) (p38)	Chaperone
225	Q9UGP8	Translocation protein SEC63 homolog	Adaptor
226	Q96AG4	Leucine-rich repeat-containing protein 59 (Ribosome-binding protein p34) (p34) [Cleaved into: Leucine-rich repeat-containing protein 59, N-terminally processed]	Adaptor
227	Q5SSJ5	Heterochromatin protein 1-binding protein 3 (Protein HP1-BP74)	Adaptor
228	Q5BKZ1	DBIRD complex subunit ZNF326 (Zinc finger protein 326) (Zinc finger protein interacting with mRNPs and DBC1)	Adaptor
229	P63104	14-3-3 protein zeta/delta (Protein kinase C inhibitor protein 1) (KCIP-1)	Adaptor
230	P62258	14-3-3 protein epsilon (14-3-3E)	Adaptor
231	P61981	14-3-3 protein gamma (Protein kinase C inhibitor protein 1) (KCIP-1) [Cleaved into: 14-3-3 protein gamma, N-terminally processed]	Adaptor
232	P46109	Crk-like protein	Adaptor
233	P43487	Ran-specific GTPase-activating protein (Ran-binding protein 1) (RanBP1)	Adaptor
234	P27348	14-3-3 protein theta (14-3-3 protein T-cell) (14-3-3 protein tau) (Protein HS1)	Adaptor
235	O60271	C-Jun-amino-terminal kinase-interacting protein 4 (JIP-4) (JNK-interacting protein 4) (Cancer/testis antigen 89) (CT89) (Human lung cancer oncogene 6 protein) (HLC-6) (JNK-associated leucine-zipper protein) (JLP) (Mitogen-activated protein kinase 8-interacting protein 4) (Proliferation-inducing protein 6) (Protein highly expressed in testis) (PHET) (Sperm surface protein) (Sperm-associated antigen 9) (Sperm-specific protein) (Sunday driver 1)	Adaptor
236	Q9Y6C9	Mitochondrial carrier homolog 2 (Met-induced mitochondrial protein)	Transporter
237	Q9UJZ1	Stomatin-like protein 2, mitochondrial (SLP-2) (EPB72-like protein 2) (Paraprotein target 7) (Paratarg-7)	Transporter
238	Q9HAV7	GrpE protein homolog 1, mitochondrial (HMGE) (Mt-GrpE#1)	Transporter
239	Q9H9B4	Sideroflexin-1	Transporter
240	Q96P70	Importin-9 (Imp9) (Ran-binding protein 9) (RanBP9)	Transporter
241	Q15758	Neutral amino acid transporter B(0) (ATB(0)) (Baboon M7 virus receptor) (RD114/simian type D retrovirus receptor) (Sodium-dependent neutral amino acid transporter type 2) (Solute carrier family 1 member 5)	Transporter
242	Q15388	Mitochondrial import receptor subunit TOM20 homolog (Mitochondrial 20 kDa outer membrane protein) (Outer mitochondrial membrane receptor Tom20)	Transporter
243	Q14974	Importin subunit beta-1 (Importin-90) (Karyopherin subunit beta-1) (Nuclear factor p97) (Pore targeting complex 97 kDa subunit) (PTAC97)	Transporter
244	Q00325	Phosphate carrier protein, mitochondrial (Phosphate transport protein) (PTP) (Solute carrier family 25 member 3)	Transporter
245	P54105	Methylosome subunit pICln (Chloride channel, nucleotide sensitive 1A) (Chloride conductance regulatory protein ICln) (I(Cln)) (Chloride ion current inducer protein) (ClCI) (Reticulocyte pICln)	Transporter
246	P53007	Tricarboxylate transport protein, mitochondrial (Citrate transport protein) (CTP) (Solute carrier family 25 member 1) (Tricarboxylate carrier protein)	Transporter
247	P52948	Nuclear pore complex protein Nup98-Nup96 (EC 3.4.21.-) [Cleaved into: Nuclear pore complex protein Nup98 (98 kDa nucleoporin) (Nucleoporin Nup98) (Nup98); Nuclear pore complex protein Nup96 (96 kDa nucleoporin) (Nucleoporin Nup96) (Nup96)]	Transporter
248	P52292	Importin subunit alpha-1 (Karyopherin subunit alpha-2) (RAG cohort protein 1) (SRP1-alpha)	Transporter
249	P48047	ATP synthase subunit O, mitochondrial (ATP synthase peripheral stalk subunit OSCP) (Oligomycin sensitivity conferral protein) (OSCP)	Transporter
250	P36542	ATP synthase subunit gamma, mitochondrial (ATP synthase F1 subunit gamma) (F-ATPase gamma subunit)	Transporter
251	P25705	ATP synthase subunit alpha, mitochondrial (ATP synthase F1 subunit alpha)	Transporter
252	P21796	Voltage-dependent anion-selective channel protein 1 (VDAC-1) (hVDAC1) (Outer mitochondrial membrane protein porin 1) (Plasmalemmal porin) (Porin 31HL) (Porin 31HM)	Transporter
253	P06576	ATP synthase subunit beta, mitochondrial (EC 7.1.2.2) (ATP synthase F1 subunit beta)	Transporter
254	O96008	Mitochondrial import receptor subunit TOM40 homolog (Protein Haymaker) (Translocase of outer membrane 40 kDa subunit homolog) (p38.5)	Transporter
255	O95373	Importin-7 (Imp7) (Ran-binding protein 7) (RanBP7)	Transporter
256	O95202	Mitochondrial proton/calcium exchanger protein (Leucine zipper-EF-hand-containing transmembrane protein 1)	Transporter
257	O75947	ATP synthase subunit d, mitochondrial (ATPase subunit d) (ATP synthase peripheral stalk subunit d)	Transporter
258	O43615	Mitochondrial import inner membrane translocase subunit TIM44	Transporter
259	O00505	Importin subunit alpha-4 (Importin alpha Q2) (Qip2) (Karyopherin subunit alpha-3) (SRP1-gamma)	Transporter
260	O00299	Chloride intracellular channel protein 1 (Chloride channel ABP) (Nuclear chloride ion channel 27) (NCC27) (Regulatory nuclear chloride ion channel protein) (hRNCC)	Transporter
261	Q9UII2	ATPase inhibitor, mitochondrial (ATP synthase F1 subunit epsilon) (Inhibitor of F(1)F(o)-ATPase) (IF(1)) (IF1)	Metabolite interconversion enzyme
262	Q9UHG3	Prenylcysteine oxidase 1 (EC 1.8.3.5) (Prenylcysteine lyase)	Metabolite interconversion enzyme
263	Q9UDR5	Alpha-aminoadipic semialdehyde synthase, mitochondrial (LKR/SDH) [Includes: Lysine ketoglutarate reductase (LKR) (LOR) (EC 1.5.1.8); Saccharopine dehydrogenase (SDH) (EC 1.5.1.9)]	Metabolite interconversion enzyme
264	Q9UBM7	7-dehydrocholesterol reductase (7-DHC reductase) (EC 1.3.1.21) (Delta7-sterol reductase) (Sterol Delta(7)-reductase) (Sterol reductase SR-2)	Metabolite interconversion enzyme
265	Q9P2R7	Succinate--CoA ligase [ADP-forming] subunit beta, mitochondrial (EC 6.2.1.5) (ATP-specific succinyl-CoA synthetase subunit beta) (A-SCS) (Succinyl-CoA synthetase beta-A chain) (SCS-betaA)	Metabolite interconversion enzyme
266	Q9NYU2	UDP-glucose:glycoprotein glucosyltransferase 1 (UGT1) (hUGT1) (EC 2.4.1.-) (UDP--Glc:glycoprotein glucosyltransferase) (UDP-glucose ceramide glucosyltransferase-like 1)	Metabolite interconversion enzyme
267	Q9NUJ1	Palmitoyl-protein thioesterase ABHD10, mitochondrial (EC 3.1.2.22) (Acyl-protein thioesterase ABHD10) (Alpha/beta hydrolase domain-containing protein 10) (Abhydrolase domain-containing protein 10) (Mycophenolic acid acyl-glucuronide esterase, mitochondrial) (EC 3.1.1.93)	Metabolite interconversion enzyme

268	Q9H857	5'-nucleotidase domain-containing protein 2 (EC 3.1.3.-)	Metabolite interconversion enzyme
269	Q9H773	dCTP pyrophosphatase 1 (EC 3.6.1.12) (Deoxycytidine-triphosphatase 1) (dCTPase 1) (RS21C6) (XTP3-transactivated gene A protein)	Metabolite interconversion enzyme
270	Q9BWD1	Acetyl-CoA acetyltransferase, cytosolic (EC 2.3.1.9) (Acetyl-CoA transferase-like protein) (Cytosolic acetoacetyl-CoA thiolase)	Metabolite interconversion enzyme
271	Q99798	Aconitate hydratase, mitochondrial (Aconitase) (EC 4.2.1.3) (Citrate hydro-lyase)	Metabolite interconversion enzyme
272	Q99714	3-hydroxyacyl-CoA dehydrogenase type-2 (EC 1.1.1.35) (17-beta-estradiol 17-dehydrogenase) (EC 1.1.1.62) (2-methyl-3-hydroxybutyryl-CoA dehydrogenase) (MHBD) (3-alpha-(17-beta)-hydroxysteroid dehydrogenase (NAD(+))) (EC 1.1.1.239) (3-hydroxy-2-methylbutyryl-CoA dehydrogenase) (EC 1.1.1.178) (3-hydroxyacyl-CoA dehydrogenase type II) (3alpha(or 20beta)-hydroxysteroid dehydrogenase) (EC 1.1.1.53) (7-alpha-hydroxysteroid dehydrogenase) (EC 1.1.1.159) (Endoplasmic reticulum-associated amyloid beta-peptide-binding protein) (Mitochondrial ribonuclease P protein 2) (Mitochondrial RNase P protein 2) (Short chain dehydrogenase/reductase family 5C member 1) (Short-chain type dehydrogenase/reductase XH98G2) (Type II HADH)	Metabolite interconversion enzyme
273	Q8TCS8	Polyribonucleotide nucleotidyltransferase 1, mitochondrial (EC 2.7.7.8) (3'-5' RNA exonuclease OLD35) (PNPase old-35) (Polynucleotide phosphorylase 1) (PNPase 1) (Polynucleotide phosphorylase-like protein)	Metabolite interconversion enzyme
274	Q16881	Thioredoxin reductase 1, cytoplasmic (TR) (EC 1.8.1.9) (Gene associated with retinoic and interferon-induced mortality 12 protein) (GRIM-12) (Gene associated with retinoic and IFN-induced mortality 12 protein) (KM-102-derived reductase-like factor) (Thioredoxin reductase TR1)	Metabolite interconversion enzyme
275	Q16822	Phosphoenolpyruvate carboxykinase [GTP], mitochondrial (PEPCK-M) (EC 4.1.1.32)	Metabolite interconversion enzyme
276	Q16795	NADH dehydrogenase [ubiquinone] 1 alpha subcomplex subunit 9, mitochondrial (Complex I-39kD) (CI-39kD) (NADH-ubiquinone oxidoreductase 39 kDa subunit)	Metabolite interconversion enzyme
277	Q16555	Dihydropyrimidinase-related protein 2 (DRP-2) (Collapsin response mediator protein 2) (CRMP-2) (N2A3) (Unc-33-like phosphoprotein 2) (ULIP-2)	Metabolite interconversion enzyme
278	Q15181	Inorganic pyrophosphatase (EC 3.6.1.1) (Pyrophosphate phospho-hydrolase) (PPase)	Metabolite interconversion enzyme
279	Q14739	Delta(14)-sterol reductase LBR (Delta-14-SR) (EC 1.3.1.70) (3-beta-hydroxysterol Delta (14)-reductase) (C-14 sterol reductase) (C14SR) (Integral nuclear envelope inner membrane protein) (LMN2R) (Lamin-B receptor) (Sterol C14-reductase)	Metabolite interconversion enzyme
280	Q13423	NAD(P) transhydrogenase, mitochondrial (EC 7.1.1.1) (Nicotinamide nucleotide transhydrogenase) (Pyridine nucleotide transhydrogenase)	Metabolite interconversion enzyme
281	Q13162	Peroxiredoxin-4 (EC 1.11.1.24) (Antioxidant enzyme AOE372) (AOE37-2) (Peroxiredoxin IV) (Prx-IV) (Thioredoxin peroxidase AO372) (Thioredoxin-dependent peroxide reductase A0372) (Thioredoxin-dependent peroxiredoxin 4)	Metabolite interconversion enzyme
282	Q08257	Quinone oxidoreductase (EC 1.6.5.5) (NADPH:quinone reductase) (Zeta-crystallin)	Metabolite interconversion enzyme
283	Q06830	Peroxiredoxin-1 (EC 1.11.1.24) (Natural killer cell-enhancing factor A) (NKEF-A) (Proliferation-associated gene protein) (PAG) (Thioredoxin peroxidase 2) (Thioredoxin-dependent peroxide reductase 2) (Thioredoxin-dependent peroxiredoxin 1)	Metabolite interconversion enzyme
284	Q04760	Lactoylglutathione lyase (EC 4.4.1.5) (Aldoketomutase) (Glyoxalase I) (Glx I) (Ketone-aldehyde mutase) (Methylglyoxalase) (S-D-lactoylglutathione methylglyoxal lyase)	Metabolite interconversion enzyme
285	P60891	Ribose-phosphate pyrophosphokinase 1 (EC 2.7.6.1) (PPRibP) (Phosphoribosyl pyrophosphate synthase I) (PRS-I)	Metabolite interconversion enzyme
286	P60174	Triosephosphate isomerase (TIM) (EC 5.3.1.1) (Methylglyoxal synthase) (EC 4.2.3.3) (Triose-phosphate isomerase)	Metabolite interconversion enzyme
287	P55809	Succinyl-CoA:3-ketoacid coenzyme A transferase 1, mitochondrial (EC 2.8.3.5) (3-oxoacid CoA-transferase 1) (Somatic-type succinyl-CoA:3-oxoacid CoA-transferase) (SCOT-s)	Metabolite interconversion enzyme
288	P54886	Delta-1-pyrroline-5-carboxylate synthase (P5CS) (Aldehyde dehydrogenase family 18 member A1) [Includes: Glutamate 5-kinase (GK) (EC 2.7.2.11) (Gamma-glutamyl kinase); Gamma-glutamyl phosphate reductase (GPR) (EC 1.2.1.41) (Glutamate-5-semialdehyde dehydrogenase) (Glutamyl-gamma-semialdehyde dehydrogenase)]	Metabolite interconversion enzyme
289	P53597	Succinate--CoA ligase [ADP/GDP-forming] subunit alpha, mitochondrial (EC 6.2.1.4) (EC 6.2.1.5) (Succinyl-CoA synthetase subunit alpha) (SCS-alpha)	Metabolite interconversion enzyme
290	P53004	Biliverdin reductase A (BVR A) (EC 1.3.1.24) (Biliverdin-IX alpha-reductase)	Metabolite interconversion enzyme
291	P50213	Isocitrate dehydrogenase [NAD] subunit alpha, mitochondrial (EC 1.1.1.41) (Isocitric dehydrogenase subunit alpha) (NAD(+)-specific ICDH subunit alpha)	Metabolite interconversion enzyme
292	P49821	NADH dehydrogenase [ubiquinone] flavoprotein 1, mitochondrial (EC 7.1.1.2) (Complex I-51kD) (CI-51kD) (NADH dehydrogenase flavoprotein 1) (NADH-ubiquinone oxidoreductase 51 kDa subunit)	Metabolite interconversion enzyme
293	P49189	4-trimethylaminobutyraldehyde dehydrogenase (TMABA-DH) (TMABALDH) (EC 1.2.1.47) (Aldehyde dehydrogenase E3 isozyme) (Aldehyde dehydrogenase family 9 member A1) (EC 1.2.1.3) (Gamma-aminobutyraldehyde dehydrogenase) (EC 1.2.1.19) (R-aminobutyraldehyde dehydrogenase) [Cleaved into: 4-trimethylaminobutyraldehyde dehydrogenase, N-terminally processed]	Metabolite interconversion enzyme
294	P48735	Isocitrate dehydrogenase [NADP], mitochondrial (IDH) (EC 1.1.1.42) (ICD-M) (IDP) (NADP(+)-specific ICDH) (Oxalosuccinate decarboxylase)	Metabolite interconversion enzyme
295	P43490	Nicotinamide phosphoribosyltransferase (NAmPRTase) (Nampt) (EC 2.4.2.12) (Pre-B-cell colony-enhancing factor 1) (Pre-B cell-enhancing factor) (Visfatin)	Metabolite interconversion enzyme
296	P43304	Glycerol-3-phosphate dehydrogenase, mitochondrial (GPD-M) (GPDH-M) (EC 1.1.5.3) (mitohondrial glycerophosphate dehydrogenase gene) (mGDH) (mtGPD)	Metabolite interconversion enzyme
297	P42126	Enoyl-CoA delta isomerase 1, mitochondrial (EC 5.3.3.8) (3,2-trans-enoyl-CoA isomerase) (Delta(3),Delta(2)-enoyl-CoA isomerase) (D3,D2-enoyl-CoA isomerase) (Dodecenoyl-CoA isomerase)	Metabolite interconversion enzyme
298	P40926	Malate dehydrogenase, mitochondrial (EC 1.1.1.37)	Metabolite interconversion enzyme
299	P39656	Dolichyl-diphosphooligosaccharide--protein glycosyltransferase 48 kDa subunit (DDOST 48 kDa subunit) (Oligosaccharyl transferase 48 kDa subunit)	Metabolite interconversion enzyme
300	P38117	Electron transfer flavoprotein subunit beta (Beta-ETF)	Metabolite interconversion enzyme
301	P37837	Transaldolase (EC 2.2.1.2)	Metabolite interconversion enzyme
302	P36957	Dihydrolipoyllysine-residue succinyltransferase component of 2-oxoglutarate dehydrogenase complex, mitochondrial (EC 2.3.1.61) (2-oxoglutarate dehydrogenase complex component E2) (OGDC-E2) (Dihydrolipoamide succinyltransferase component of 2-oxoglutarate dehydrogenase complex) (E2K)	Metabolite interconversion enzyme
303	P36551	Oxygen-dependent coproporphyrinogen-III oxidase, mitochondrial (COX) (Coprogen oxidase) (Coproporphyrinogenase) (EC 1.3.3.3)	Metabolite interconversion enzyme
304	P34897	Serine hydroxymethyltransferase, mitochondrial (SHMT) (EC 2.1.2.1) (Glycine hydroxymethyltransferase) (Serine methylase)	Metabolite interconversion enzyme
305	P33316	Deoxyuridine 5'-triphosphate nucleotidohydrolase, mitochondrial (dUTPase) (EC 3.6.1.23) (dUTP pyrophosphatase)	Metabolite interconversion enzyme

306	P32322	Pyrroline-5-carboxylate reductase 1, mitochondrial (P5C reductase 1) (P5CR 1) (EC 1.5.1.2)	Metabolite interconversion enzyme
307	P32119	Peroxiredoxin-2 (EC 1.11.1.24) (Natural killer cell-enhancing factor B) (NKEF-B) (PRP) (Thiol-specific antioxidant protein) (TSA) (Thioredoxin peroxidase 1) (Thioredoxin-dependent peroxide reductase 1) (Thioredoxin-dependent peroxiredoxin 2)	Metabolite interconversion enzyme
308	P31040	Succinate dehydrogenase [ubiquinone] flavoprotein subunit, mitochondrial (EC 1.3.5.1) (Flavoprotein subunit of complex II) (Fp)	Metabolite interconversion enzyme
309	P30837	Aldehyde dehydrogenase X, mitochondrial (EC 1.2.1.3) (Aldehyde dehydrogenase 5) (Aldehyde dehydrogenase family 1 member B1)	Metabolite interconversion enzyme
310	P30419	Glycylpeptide N-tetradecanoyltransferase 1 (EC 2.3.1.97) (Myristoyl-CoA:protein N-myristoyltransferase 1) (NMT 1) (Type I N-myristoyltransferase) (Peptide N-myristoyltransferase 1)	Metabolite interconversion enzyme
311	P30084	Enoyl-CoA hydratase, mitochondrial (EC 4.2.1.17) (Enoyl-CoA hydratase 1) (Short-chain enoyl-CoA hydratase) (SCEH)	Metabolite interconversion enzyme
312	P30048	Thioredoxin-dependent peroxide reductase, mitochondrial (EC 1.11.1.24) (Antioxidant protein 1) (AOP-1) (HBC189) (Peroxiredoxin III) (Prx-III) (Peroxiredoxin-3) (Protein MER5 homolog) (Thioredoxin-dependent peroxiredoxin 3)	Metabolite interconversion enzyme
313	P30046	D-dopachrome decarboxylase (EC 4.1.1.84) (D-dopachrome tautomerase) (Phenylpyruvate tautomerase II)	Metabolite interconversion enzyme
314	P30044	Peroxiredoxin-5, mitochondrial (EC 1.11.1.24) (Alu corepressor 1) (Antioxidant enzyme B166) (AOEB166) (Liver tissue 2D-page spot 71B) (PLP) (Peroxiredoxin V) (Prx-V) (Peroxisomal antioxidant enzyme) (TPx type VI) (Thioredoxin peroxidase PMP20) (Thioredoxin-dependent peroxiredoxin 5)	Metabolite interconversion enzyme
315	P30041	Peroxiredoxin-6 (EC 1.11.1.27) (1-Cys peroxiredoxin) (1-Cys PRX) (24 kDa protein) (Acidic calcium-independent phospholipase A2) (aiPLA2) (EC 3.1.1.4) (Antioxidant protein 2) (Glutathione-dependent peroxiredoxin) (Liver 2D page spot 40) (Lysophosphatidylcholine acyltransferase 5) (LPC acyltransferase 5) (LPCAT-5) (Lyso-PC acyltransferase 5) (EC 2.3.1.23) (Non-selenium glutathione peroxidase) (NSGPx) (Red blood cells page spot 12)	Metabolite interconversion enzyme
316	P26440	Isovaleryl-CoA dehydrogenase, mitochondrial (IVD) (EC 1.3.8.4) (Butyryl-CoA dehydrogenase) (EC 1.3.8.1)	Metabolite interconversion enzyme
317	P25325	3-mercaptopyruvate sulfurtransferase (MST) (EC 2.8.1.2)	Metabolite interconversion enzyme
318	P24752	Acetyl-CoA acetyltransferase, mitochondrial (EC 2.3.1.9) (Acetoacetyl-CoA thiolase) (T2)	Metabolite interconversion enzyme
319	P23786	Carnitine O-palmitoyltransferase 2, mitochondrial (EC 2.3.1.21) (Carnitine palmitoyltransferase II) (CPT II)	Metabolite interconversion enzyme
320	P23368	NAD-dependent malic enzyme, mitochondrial (NAD-ME) (EC 1.1.1.38) (Malic enzyme 2)	Metabolite interconversion enzyme
321	P21912	Succinate dehydrogenase [ubiquinone] iron-sulfur subunit, mitochondrial (EC 1.3.5.1) (Iron-sulfur subunit of complex II) (Ip)	Metabolite interconversion enzyme
322	P20674	Cytochrome c oxidase subunit 5A, mitochondrial (Cytochrome c oxidase polypeptide Va)	Metabolite interconversion enzyme
323	P19404	NADH dehydrogenase [ubiquinone] flavoprotein 2, mitochondrial (EC 7.1.1.2) (NADH-ubiquinone oxidoreductase 24 kDa subunit)	Metabolite interconversion enzyme
324	P18669	Phosphoglycerate mutase 1 (EC 5.4.2.11) (EC 5.4.2.4) (BPG-dependent PGAM 1) (Phosphoglycerate mutase isozyme B) (PGAM-B)	Metabolite interconversion enzyme
325	P17812	CTP synthase 1 (EC 6.3.4.2) (CTP synthetase 1) (UTP--ammonia ligase 1)	Metabolite interconversion enzyme
326	P16435	NADPH--cytochrome P450 reductase (CPR) (P450R) (EC 1.6.2.4)	Metabolite interconversion enzyme
327	P15954	Cytochrome c oxidase subunit 7C, mitochondrial (Cytochrome c oxidase polypeptide VIIc)	Metabolite interconversion enzyme
328	P14618	Pyruvate kinase PKM (EC 2.7.1.40) (Cytosolic thyroid hormone-binding protein) (CTHBP) (Opa-interacting protein 3) (OIP-3) (Pyruvate kinase 2/3) (Pyruvate kinase muscle isozyme) (Thyroid hormone-binding protein 1) (THBP1) (Tumor M2-PK) (p58)	Metabolite interconversion enzyme
329	P14406	Cytochrome c oxidase subunit 7A2, mitochondrial (Cytochrome c oxidase subunit VIIa-liver/heart) (Cytochrome c oxidase subunit VIIa-L) (Cytochrome c oxidase subunit VIIaL)	Metabolite interconversion enzyme
330	P14174	Macrophage migration inhibitory factor (MIF) (EC 5.3.2.1) (Glycosylation-inhibiting factor) (GIF) (L-dopachrome isomerase) (L-dopachrome tautomerase) (EC 5.3.3.12) (Phenylpyruvate tautomerase)	Metabolite interconversion enzyme
331	P13804	Electron transfer flavoprotein subunit alpha, mitochondrial (Alpha-ETF)	Metabolite interconversion enzyme
332	P13073	Cytochrome c oxidase subunit 4 isoform 1, mitochondrial (Cytochrome c oxidase polypeptide IV) (Cytochrome c oxidase subunit IV isoform 1) (COX IV-1)	Metabolite interconversion enzyme
333	P12277	Creatine kinase B-type (EC 2.7.3.2) (Brain creatine kinase) (B-CK) (Creatine kinase B chain) (Creatine phosphokinase B-type) (CPK-B)	Metabolite interconversion enzyme
334	P12268	Inosine-5'-monophosphate dehydrogenase 2 (IMP dehydrogenase 2) (IMPD 2) (IMPDH 2) (EC 1.1.1.205) (Inosine-5'-monophosphate dehydrogenase type II) (IMP dehydrogenase II) (IMPDH-II)	Metabolite interconversion enzyme
335	P11216	Glycogen phosphorylase, brain form (EC 2.4.1.1)	Metabolite interconversion enzyme
336	P11177	Pyruvate dehydrogenase E1 component subunit beta, mitochondrial (PDHE1-B) (EC 1.2.4.1)	Metabolite interconversion enzyme
337	P10606	Cytochrome c oxidase subunit 5B, mitochondrial (Cytochrome c oxidase polypeptide Vb)	Metabolite interconversion enzyme
338	P10599	Thioredoxin (Trx) (ATL-derived factor) (ADF) (Surface-associated sulphydryl protein) (SASP) (allergen Hom s Trx)	Metabolite interconversion enzyme
339	P10515	Dihydrolipoyllysine-residue acetyltransferase component of pyruvate dehydrogenase complex, mitochondrial (EC 2.3.1.12) (70 kDa mitochondrial autoantigen of primary biliary cirrhosis) (PBC) (Dihydrolipoamide acetyltransferase component of pyruvate dehydrogenase complex) (M2 antigen complex 70 kDa subunit) (Pyruvate dehydrogenase complex component E2) (PDC-E2) (PDCE2)	Metabolite interconversion enzyme
340	P09972	Fructose-bisphosphate aldolase C (EC 4.1.2.13) (Brain-type aldolase)	Metabolite interconversion enzyme
341	P09622	Dihydrolipoyl dehydrogenase, mitochondrial (EC 1.8.1.4) (Dihydrolipoamide dehydrogenase) (Glycine cleavage system L protein)	Metabolite interconversion enzyme
342	P09211	Glutathione S-transferase P (EC 2.5.1.18) (GST class-pi) (GSTP1-1)	Metabolite interconversion enzyme
343	P09110	3-ketoacyl-CoA thiolase, peroxisomal (EC 2.3.1.16) (Acetyl-CoA C-myristoyltransferase) (EC 2.3.1.155) (Acetyl-CoA acyltransferase) (EC 2.3.1.9) (Beta-ketothiolase) (Peroxisomal 3-oxoacyl-CoA thiolase)	Metabolite interconversion enzyme
344	P07686	Beta-hexosaminidase subunit beta (EC 3.2.1.52) (Beta-N-acetylhexosaminidase subunit beta) (Hexosaminidase subunit B) (Cervical cancer proto-oncogene 7 protein) (HCC-7) (N-acetyl-beta-glucosaminidase subunit beta) [Cleaved into: Beta-hexosaminidase subunit beta chain B; Beta-hexosaminidase subunit beta chain A]	Metabolite interconversion enzyme
345	P07195	L-lactate dehydrogenase B chain (LDH-B) (EC 1.1.1.27) (LDH heart subunit) (LDH-H) (Renal carcinoma antigen NY-REN-46)	Metabolite interconversion enzyme

346	P06733	Alpha-enolase (EC 4.2.1.11) (2-phospho-D-glycerate hydro-lyase) (C-myc promoter-binding protein) (Enolase 1) (MBP-1) (MPB-1) (Non-neural enolase) (NNE) (Phosphopyruvate hydratase) (Plasminogen-binding protein)	Metabolite interconversion enzyme
347	P05091	Aldehyde dehydrogenase, mitochondrial (EC 1.2.1.3) (ALDH class 2) (ALDH-E2) (ALDHI)	Metabolite interconversion enzyme
348	P04844	Dolichyl-diphosphooligosaccharide--protein glycosyltransferase subunit 2 (Dolichyl-diphosphooligosaccharide--protein glycosyltransferase 63 kDa subunit) (RIBIIR) (Ribophorin II) (RPN-II) (Ribophorin-2)	Metabolite interconversion enzyme
349	P04406	Glyceraldehyde-3-phosphate dehydrogenase (GAPDH) (EC 1.2.1.12) (Peptidyl-cysteine S-nitrosylase GAPDH) (EC 2.6.99.-)	Metabolite interconversion enzyme
350	P04181	Ornithine aminotransferase, mitochondrial (EC 2.6.1.13) (Ornithine delta-aminotransferase) (Ornithine--oxo-acid aminotransferase) [Cleaved into: Ornithine aminotransferase, hepatic form; Ornithine aminotransferase, renal form]	Metabolite interconversion enzyme
351	P04179	Superoxide dismutase [Mn], mitochondrial (EC 1.15.1.1)	Metabolite interconversion enzyme
352	P03905	NADH-ubiquinone oxidoreductase chain 4 (EC 7.1.1.2) (NADH dehydrogenase subunit 4)	Metabolite interconversion enzyme
353	P00558	Phosphoglycerate kinase 1 (EC 2.7.2.3) (Cell migration-inducing gene 10 protein) (Primer recognition protein 2) (PRP 2)	Metabolite interconversion enzyme
354	P00505	Aspartate aminotransferase, mitochondrial (mAspAT) (EC 2.6.1.1) (EC 2.6.1.7) (Fatty acid-binding protein) (FABP-1) (Glutamate oxaloacetate transaminase 2) (Kynurenine aminotransferase 4) (Kynurenine aminotransferase IV) (Kynurenine--oxoglutarate transaminase 4) (Kynurenine--oxoglutarate transaminase IV) (Plasma membrane-associated fatty acid-binding protein) (FABPpm) (Transaminase A)	Metabolite interconversion enzyme
355	P00492	Hypoxanthine-guanine phosphoribosyltransferase (HGPRT) (HGPRTase) (EC 2.4.2.8)	Metabolite interconversion enzyme
356	P00403	Cytochrome c oxidase subunit 2 (EC 7.1.1.9) (Cytochrome c oxidase polypeptide II)	Metabolite interconversion enzyme
357	P00390	Glutathione reductase, mitochondrial (GR) (GRase) (EC 1.8.1.7)	Metabolite interconversion enzyme
358	P00367	Glutamate dehydrogenase 1, mitochondrial (GDH 1) (EC 1.4.1.3)	Metabolite interconversion enzyme
359	O95831	Apoptosis-inducing factor 1, mitochondrial (EC 1.6.99.-) (Programmed cell death protein 8)	Metabolite interconversion enzyme
360	O94925	Glutaminase kidney isoform, mitochondrial (GLS) (EC 3.5.1.2) (K-glutaminase) (L-glutamine amidohydrolase) [Cleaved into: Glutaminase kidney isoform, mitochondrial 68 kDa chain; Glutaminase kidney isoform, mitochondrial 65 kDa chain]	Metabolite interconversion enzyme
361	O76003	Glutaredoxin-3 (PKC-interacting cousin of thioredoxin) (PICOT) (PKC-theta-interacting protein) (PKCq-interacting protein) (Thioredoxin-like protein 2)	Metabolite interconversion enzyme
362	O75489	NADH dehydrogenase [ubiquinone] iron-sulfur protein 3, mitochondrial (EC 7.1.1.2) (Complex I-30kD) (CI-30kD) (NADH-ubiquinone oxidoreductase 30 kDa subunit)	Metabolite interconversion enzyme
363	O75390	Citrate synthase, mitochondrial (EC 2.3.3.1) (Citrate (Si)-synthase)	Metabolite interconversion enzyme
364	O75306	NADH dehydrogenase [ubiquinone] iron-sulfur protein 2, mitochondrial (EC 7.1.1.2) (Complex I-49kD) (CI-49kD) (NADH-ubiquinone oxidoreductase 49 kDa subunit)	Metabolite interconversion enzyme
365	O43837	Isocitrate dehydrogenase [NAD] subunit beta, mitochondrial (Isocitric dehydrogenase subunit beta) (NAD(+)-specific ICDH subunit beta)	Metabolite interconversion enzyme
366	O00483	Cytochrome c oxidase subunit NDUFA4 (Complex I-MLRQ) (CI-MLRQ) (NADH-ubiquinone oxidoreductase MLRQ subunit)	Metabolite interconversion enzyme
367	Q9UQ80	Proliferation-associated protein 2G4 (Cell cycle protein p38-2G4 homolog) (hG4-1) (ErbB3-binding protein 1)	Protein modifying enzyme
368	Q9UNE7	E3 ubiquitin-protein ligase CHIP (EC 2.3.2.27) (Antigen NY-CO-7) (CLL-associated antigen KW-8) (Carboxy terminus of Hsp70-interacting protein) (RING-type E3 ubiquitin transferase CHIP) (STIP1 homology and U box-containing protein 1)	Protein modifying enzyme
369	Q9UBE0	SUMO-activating enzyme subunit 1 (Ubiquitin-like 1-activating enzyme E1A) [Cleaved into: SUMO-activating enzyme subunit 1, N-terminally processed]	Protein modifying enzyme
370	Q9H3G5	Probable serine carboxypeptidase CPVL (EC 3.4.16.-) (Carboxypeptidase, vitellogenic-like) (Vitellogenic carboxypeptidase-like protein) (VCP-like protein) (hVLP)	Protein modifying enzyme
371	Q9BYT8	Neurolysin, mitochondrial (EC 3.4.24.16) (Angiotensin-binding protein) (Microsomal endopeptidase) (MEP) (Mitochondrial oligopeptidase M) (Neurotensin endopeptidase)	Protein modifying enzyme
372	Q99873	Protein arginine N-methyltransferase 1 (EC 2.1.1.319) (Histone-arginine N-methyltransferase PRMT1) (Interferon receptor 1-bound protein 4)	Protein modifying enzyme
373	Q99797	Mitochondrial intermediate peptidase (MIP) (EC 3.4.24.59)	Protein modifying enzyme
374	Q93009	Ubiquitin carboxyl-terminal hydrolase 7 (EC 3.4.19.12) (Deubiquitinating enzyme 7) (Herpesvirus-associated ubiquitin-specific protease) (Ubiquitin thioesterase 7) (Ubiquitin-specific-processing protease 7)	Protein modifying enzyme
375	Q8TAA3	Proteasome subunit alpha-type 8 (Proteasome alpha 4 subunit) (Alpha4s) (Proteasome subunit alpha-type 7-like)	Protein modifying enzyme
376	Q53GS9	U4/U6.U5 tri-snRNP-associated protein 2 (Inactive ubiquitin-specific peptidase 39) (SAD1 homolog) (U4/U6.U5 tri-snRNP-associated 65 kDa protein) (65K)	Protein modifying enzyme
377	Q12797	Aspartyl/asparaginyl beta-hydroxylase (EC 1.14.11.16) (Aspartate beta-hydroxylase) (ASP beta-hydroxylase) (Peptide-aspartate beta-dioxygenase)	Protein modifying enzyme
378	Q10713	Mitochondrial-processing peptidase subunit alpha (Alpha-MPP) (Inactive zinc metalloprotease alpha) (P-55)	Protein modifying enzyme
379	Q00526	Cyclin-dependent kinase 3 (EC 2.7.11.22) (Cell division protein kinase 3)	Protein modifying enzyme
380	P62195	26S proteasome regulatory subunit 8 (26S proteasome AAA-ATPase subunit RPT6) (Proteasome 26S subunit ATPase 5) (Proteasome subunit p45) (Thyroid hormone receptor-interacting protein 1) (TRIP1) (p45/SUG)	Protein modifying enzyme
381	P61081	NEDD8-conjugating enzyme Ubc12 (EC 2.3.2.34) (NEDD8 carrier protein) (Ubiquitin-conjugating enzyme E2 M)	Protein modifying enzyme
382	P60900	Proteasome subunit alpha type-6 (27 kDa prosomal protein) (PROS-27) (p27K) (Macropain iota chain) (Multicatalytic endopeptidase complex iota chain) (Proteasome iota chain)	Protein modifying enzyme
383	P55786	Puromycin-sensitive aminopeptidase (PSA) (EC 3.4.11.14) (Cytosol alanyl aminopeptidase) (AAP-S)	Protein modifying enzyme
384	P52888	Thimet oligopeptidase (EC 3.4.24.15) (Endopeptidase 24.15) (MP78)	Protein modifying enzyme
385	P50579	Methionine aminopeptidase 2 (MAP 2) (MetAP 2) (EC 3.4.11.18) (Initiation factor 2-associated 67 kDa glycoprotein) (p67) (p67eIF2) (Peptidase M)	Protein modifying enzyme
386	P49721	Proteasome subunit beta type-2 (Macropain subunit C7-I) (Multicatalytic endopeptidase complex subunit C7-I) (Proteasome component C7-I)	Protein modifying enzyme
387	P49720	Proteasome subunit beta type-3 (Proteasome chain 13) (Proteasome component C10-II) (Proteasome theta chain)	Protein modifying enzyme
388	P48556	26S proteasome non-ATPase regulatory subunit 8 (26S proteasome regulatory subunit RPN12) (26S proteasome regulatory subunit S14) (p31)	Protein modifying enzyme

389	P45974	Ubiquitin carboxyl-terminal hydrolase 5 (EC 3.4.19.12) (Deubiquitinating enzyme 5) (Isopeptidase T) (Ubiquitin thioesterase 5) (Ubiquitin-specific-processing protease 5)	Protein modifying enzyme
390	P36776	Lon protease homolog, mitochondrial (EC 3.4.21.53) (LONHs) (Lon protease-like protein) (LONP) (Mitochondrial ATP-dependent protease Lon) (Serine protease 15)	Protein modifying enzyme
391	P31930	Cytochrome b-c1 complex subunit 1, mitochondrial (Complex III subunit 1) (Core protein I) (Ubiquinol-cytochrome-c reductase complex core protein 1)	Protein modifying enzyme
392	P28838	Cytosol aminopeptidase (EC 3.4.11.1) (Cysteinylglycine-S-conjugate dipeptidase) (EC 3.4.13.23) (Leucine aminopeptidase 3) (LAP-3) (Leucyl aminopeptidase) (Peptidase S) (Proline aminopeptidase) (EC 3.4.11.5) (Prolyl aminopeptidase)	Protein modifying enzyme
393	P28066	Proteasome subunit alpha type-5 (Macropain zeta chain) (Multicatalytic endopeptidase complex zeta chain) (Proteasome zeta chain)	Protein modifying enzyme
394	P25789	Proteasome subunit alpha type-4 (Macropain subunit C9) (Multicatalytic endopeptidase complex subunit C9) (Proteasome component C9) (Proteasome subunit L)	Protein modifying enzyme
395	P25788	Proteasome subunit alpha type-3 (Macropain subunit C8) (Multicatalytic endopeptidase complex subunit C8) (Proteasome component C8)	Protein modifying enzyme
396	P25787	Proteasome subunit alpha type-2 (Macropain subunit C3) (Multicatalytic endopeptidase complex subunit C3) (Proteasome component C3)	Protein modifying enzyme
397	P24666	Low molecular weight phosphotyrosine protein phosphatase (LMW-PTP) (LMW-PTPase) (EC 3.1.3.48) (Adipocyte acid phosphatase) (Low molecular weight cytosolic acid phosphatase) (EC 3.1.3.2) (Red cell acid phosphatase 1)	Protein modifying enzyme
398	P22695	Cytochrome b-c1 complex subunit 2, mitochondrial (Complex III subunit 2) (Core protein II) (Ubiquinol-cytochrome-c reductase complex core protein 2)	Protein modifying enzyme
399	P02786	Transferrin receptor protein 1 (TR) (TfR) (TfR1) (Trfr) (T9) (p90) (CD antigen CD71) [Cleaved into: Transferrin receptor protein 1, serum form (sTfR)]	Protein modifying enzyme
400	O75439	Mitochondrial-processing peptidase subunit beta (EC 3.4.24.64) (Beta-MPP) (P-52)	Protein modifying enzyme
401	O43242	26S proteasome non-ATPase regulatory subunit 3 (26S proteasome regulatory subunit RPN3) (26S proteasome regulatory subunit S3) (Proteasome subunit p58)	Protein modifying enzyme
402	O15355	Protein phosphatase 1G (EC 3.1.3.16) (Protein phosphatase 1C) (Protein phosphatase 2C isoform gamma) (PP2C-gamma) (Protein phosphatase magnesium-dependent 1 gamma)	Protein modifying enzyme
403	O14773	Tripeptidyl-peptidase 1 (TPP-1) (EC 3.4.14.9) (Cell growth-inhibiting gene 1 protein) (Lysosomal pepstatin-insensitive protease) (LPIC) (Tripeptidyl aminopeptidase) (Tripeptidyl-peptidase I) (TPP-I)	Protein modifying enzyme
404	P49755	Transmembrane emp24 domain-containing protein 10 (Protein TMED10) (21 kDa transmembrane-trafficking protein) (S31I125) (S31III125) (Tmp-21-I) (Transmembrane protein Tmp21) (p23) (p24 family protein delta-1) (p24delta1) (p24delta)	Membrane traffic protein
405	P43307	Translocon-associated protein subunit alpha (TRAP-alpha) (Signal sequence receptor subunit alpha) (SSR-alpha)	Membrane traffic protein
406	P30040	Endoplasmic reticulum resident protein 29 (ERp29) (Endoplasmic reticulum resident protein 28) (ERp28) (Endoplasmic reticulum resident protein 31) (ERp31)	Membrane traffic protein
407	Q5JWF2	Guanine nucleotide-binding protein G(s) subunit alpha isoforms XLas (Adenylate cyclase-stimulating G alpha protein) (Extra large alphas protein) (XLalphas)	Protein-binding activity modulator
408	P40616	ADP-ribosylation factor-like protein 1	Protein-binding activity modulator
409	P50395	Rab GDP dissociation inhibitor beta (Rab GDI beta) (Guanosine diphosphate dissociation inhibitor 2) (GDI-2)	Protein-binding activity modulator
410	P50454	Serpin H1 (47 kDa heat shock protein) (Arsenic-transactivated protein 3) (AsTP3) (Cell proliferation-inducing gene 14 protein) (Collagen-binding protein) (Colligin) (Rheumatoid arthritis-related antigen RA-A47)	Protein-binding activity modulator
411	P62826	GTP-binding nuclear protein Ran (Androgen receptor-associated protein 24) (GTPase Ran) (Ras-like protein TC4) (Ras-related nuclear protein)	Protein-binding activity modulator
412	P62834	Ras-related protein Rap-1A (EC 3.6.5.2) (C21KG) (G-22K) (GTP-binding protein smg p21A) (Ras-related protein Krev-1)	Protein-binding activity modulator
413	P14314	Glucosidase 2 subunit beta (80K-H protein) (Glucosidase II subunit beta) (Protein kinase C substrate 60.1 kDa protein heavy chain) (PKCSH)	Protein-binding activity modulator
414	P08240	Signal recognition particle receptor subunit alpha (SR-alpha) (Docking protein alpha) (DP-alpha)	Protein-binding activity modulator
415	P52565	Rho GDP-dissociation inhibitor 1 (Rho GDI 1) (Rho-GDI alpha)	Protein-binding activity modulator
416	P30086	Phosphatidylethanolamine-binding protein 1 (PEBP-1) (HCNPpp) (Neuropolypeptide h3) (Prostatic-binding protein) (Raf kinase inhibitor protein) (RKIP) [Cleaved into: Hippocampal cholinergic neurostimulating peptide (HCNP)]	Protein-binding activity modulator
417	P61204	ADP-ribosylation factor 3	Protein-binding activity modulator
418	Q9NTK5	Obg-like ATPase 1 (DNA damage-regulated overexpressed in cancer 45) (DOC45) (GTP-binding protein 9)	Protein-binding activity modulator
419	Q15293	Reticulocalbin-1	Calcium-binding protein
420	P31949	Protein S100-A11 (Calgizzarin) (Metastatic lymph node gene 70 protein) (MLN 70) (Protein S100-C) (S100 calcium-binding protein A11) [Cleaved into: Protein S100-A11, N-terminally processed]	Calcium-binding protein
421	P04083	Annexin A1 (Annexin I) (Annexin-1) (Calpactin II) (Calpactin-2) (Chromobindin-9) (Lipocortin I) (Phospholipase A2 inhibitory protein) (p35)	Calcium-binding protein
422	P08758	Annexin A5 (Anchorin CII) (Annexin V) (Annexin-5) (Calphobindin I) (CBP-I) (Endonexin II) (Lipocortin V) (Placental anticoagulant protein 4) (PP4) (Placental anticoagulant protein I) (PAP-I) (Thromboplastin inhibitor) (Vascular anticoagulant-alpha) (VAC-alpha)	Calcium-binding protein
423	P20073	Annexin A7 (Annexin VII) (Annexin-7) (Synexin)	Calcium-binding protein
424	P08133	Annexin A6 (67 kDa calelectrin) (Annexin VI) (Annexin-6) (Calphobindin-II) (CPB-II) (Chromobindin-20) (Lipocortin VI) (Protein III) (p68) (p70)	Calcium-binding protein
425	P60903	Protein S100-A10 (Calpactin I light chain) (Calpactin-1 light chain) (Cellular ligand of annexin II) (S100 calcium-binding protein A10) (p10 protein) (p11)	Calcium-binding protein
426	Q8IYU8	Calcium uptake protein 2, mitochondrial (EF-hand domain-containing family member A1)	Calcium-binding protein
427	Q14257	Reticulocalbin-2 (Calcium-binding protein ERC-55) (E6-binding protein) (E6BP)	Calcium-binding protein
428	Q13123	Protein Red (Cytokine IK) (IK factor) (Protein RER)	intercellular signal molecule
429	P42166	Lamina-associated polypeptide 2, isoform alpha (Thymopoietin isoform alpha) (TP alpha) (Thymopoietin-related peptide isoform alpha) (TPRP isoform alpha) [Cleaved into: Thymopoietin (TP) (Splenin); Thymopentin (TP5)]	intercellular signal molecule
430	Q7Z4V5	Hepatoma-derived growth factor-related protein 2 (HDGF-related protein 2) (HRP-2) (Hepatoma-derived growth factor 2) (HDGF-2)	gene-specific transcriptional regulator
431	O94776	Metastasis-associated protein MTA2 (Metastasis-associated 1-like 1) (MTA1-L1 protein) (p53 target protein in deacetylase complex)	gene-specific transcriptional regulator

432	O75475	PC4 and SFRS1-interacting protein (CLL-associated antigen KW-7) (Dense fine speckles 70 kDa protein) (DFS 70) (Lens epithelium-derived growth factor) (Transcriptional coactivator p75/p52)	gene-specific transcriptional regulator
433	Q12905	Interleukin enhancer-binding factor 2 (Nuclear factor of activated T-cells 45 kDa)	gene-specific transcriptional regulator
434	P20671	Histone H2A type 1-D (Histone H2A.3) (Histone H2A/g)	chromatin/chromatin-binding, or -regulatory protein
435	Q8TAQ2	SWI/SNF complex subunit SMARCC2 (BRG1-associated factor 170) (BAF170) (SWI/SNF complex 170 kDa subunit) (SWI/SNF-related matrix-associated actin-dependent regulator of chromatin subfamily C member 2)	chromatin/chromatin-binding, or -regulatory protein
436	Q71UI9	Histone H2A.V (H2A.F/Z) (H2A.Z variant histone 2)	chromatin/chromatin-binding, or -regulatory protein
437	Q01105	Protein SET (HLA-DR-associated protein II) (Inhibitor of granzyme A-activated DNase) (IGAAD) (PHAPII) (Phosphatase 2A inhibitor I2PP2A) (I-2PP2A) (Template-activating factor I) (TAF-I)	chromatin/chromatin-binding, or -regulatory protein
438	Q6DN03	Putative histone H2B type 2-C (H2B-clustered histone 20 pseudogene) (Histone H2B.t) (H2B/t)	chromatin/chromatin-binding, or -regulatory protein
439	P55209	Nucleosome assembly protein 1-like 1 (NAP-1-related protein) (hNRP)	chromatin/chromatin-binding, or -regulatory protein
440	P39687	Acidic leucine-rich nuclear phosphoprotein 32 family member A (Acidic nuclear phosphoprotein pp32) (pp32) (Leucine-rich acidic nuclear protein) (LANP) (Mapmodulin) (Potent heat-stable protein phosphatase 2A inhibitor I1PP2A) (Putative HLA-DR-associated protein I) (PHAPI)	chromatin/chromatin-binding, or -regulatory protein
441	Q92688	Acidic leucine-rich nuclear phosphoprotein 32 family member B (Acidic protein rich in leucines) (Putative HLA-DR-associated protein I-2) (PHAPI2) (Silver-stainable protein SSP29)	chromatin/chromatin-binding, or -regulatory protein
442	Q99733	Nucleosome assembly protein 1-like 4 (Nucleosome assembly protein 2) (NAP-2)	chromatin/chromatin-binding, or -regulatory protein
443	P16402	Histone H1.3 (Histone H1c) (Histone H1s-2)	chromatin/chromatin-binding, or -regulatory protein
444	O75367	Core histone macro-H2A.1 (Histone macroH2A1) (mH2A1) (Histone H2A.y) (H2A/y) (Medulloblastoma antigen MU-MB-50.205)	chromatin/chromatin-binding, or -regulatory protein
445	P68431	Histone H3.1 (Histone H3/a) (Histone H3/b) (Histone H3/c) (Histone H3/d) (Histone H3/f) (Histone H3/h) (Histone H3/i) (Histone H3/j) (Histone H3/k) (Histone H3/l)	chromatin/chromatin-binding, or -regulatory protein
446	Q9Y5B9	FACT complex subunit SPT16 (Chromatin-specific transcription elongation factor 140 kDa subunit) (FACT 140 kDa subunit) (FACTp140) (Facilitates chromatin transcription complex subunit SPT16) (hSPT16)	chromatin/chromatin-binding, or -regulatory protein
447	P62805	Histone H4	chromatin/chromatin-binding, or -regulatory protein
448	P35659	Protein DEK	chromatin/chromatin-binding, or -regulatory protein
449	Q9BTT0	Acidic leucine-rich nuclear phosphoprotein 32 family member E (LANP-like protein) (LANP-L)	chromatin/chromatin-binding, or -regulatory protein

Table A6. A protein-wide list of the enzymes among the high-confidence protein hits categorized according to their catalytic mechanisms as per the UniProt database. This table was used to generate Figure 4.10b.

S. No.	UniProt ID	Protein name	Enzyme Class on UniProt database
1	P12268	Inosine-5'-monophosphate dehydrogenase 2	Oxidoreductase
2	P31040	Succinate dehydrogenase [ubiquinone] flavoprotein subunit	Oxidoreductase
3	P30044	Peroxiredoxin-5	Oxidoreductase
4	P00390	Glutathione reductase	Oxidoreductase
5	P36551	Oxygen-dependent coproporphyrinogen-III oxidase	Oxidoreductase
6	P21912	Succinate dehydrogenase [ubiquinone] iron-sulfur subunit	Oxidoreductase
7	P04179	Superoxide dismutase [Mn]	Oxidoreductase
8	P13995	Bifunctional methylenetetrahydrofolate dehydrogenase/cyclohydrolase	Oxidoreductase
9	Q99714	3-hydroxyacyl-CoA dehydrogenase type-2	Oxidoreductase
10	P08559	Pyruvate dehydrogenase E1 component subunit alpha	Oxidoreductase
11	P32322	Pyrroline-5-carboxylate reductase 1	Oxidoreductase
12	Q13162	Peroxiredoxin-4 (EC 1.11.1.24)	Oxidoreductase
13	Q08257	Quinone oxidoreductase (EC 1.6.5.5) (NADPH:quinone reductase) (Zeta-crystallin)	Oxidoreductase
14	P30041	Peroxiredoxin-6 (EC 1.11.1.27)	Oxidoreductase
15	Q06830	Peroxiredoxin-1 (EC 1.11.1.24)	Oxidoreductase
16	P32119	Peroxiredoxin-2 (EC 1.11.1.24)	Oxidoreductase
17	P51649	Succinate-semialdehyde dehydrogenase	Oxidoreductase
18	P09622	Dihydrolipoyl dehydrogenase	Oxidoreductase
19	P05091	Aldehyde dehydrogenase	Oxidoreductase
20	Q12797	Aspartyl/asparaginyl beta-hydroxylase	Oxidoreductase
21	P11310	Medium-chain specific acyl-CoA dehydrogenase	Oxidoreductase
22	Q9UDR5	Alpha-aminoadipic semialdehyde synthase	Oxidoreductase
23	P40925	Malate dehydrogenase	Oxidoreductase
24	P40926	Malate dehydrogenase	Oxidoreductase
25	P30837	Aldehyde dehydrogenase X	Oxidoreductase
26	P04406	Glyceraldehyde-3-phosphate dehydrogenase (GAPDH)	Oxidoreductase
27	P40939	Trifunctional enzyme subunit alpha	Oxidoreductase
28	P49189	4-trimethylaminobutyraldehyde dehydrogenase (TMABA-DH)	Oxidoreductase
29	P53004	Biliverdin reductase A (BVR A)	Oxidoreductase
30	P00367	Glutamate dehydrogenase 1	Oxidoreductase
31	P50213	Isocitrate dehydrogenase [NAD] subunit alpha	Oxidoreductase
32	P48735	Isocitrate dehydrogenase [NADP]	Oxidoreductase
33	P00338	L-lactate dehydrogenase A chain (LDH-A)	Oxidoreductase
34	Q9UBM7	7-dehydrocholesterol reductase (7-DHC reductase)	Oxidoreductase
35	Q53GQ0	Very-long-chain 3-oxoacyl-CoA reductase	Oxidoreductase
36	O95831	Apoptosis-inducing factor 1	Oxidoreductase
37	P26440	Isovaleryl-CoA dehydrogenase	Oxidoreductase
38	P23368	NAD-dependent malic enzyme	Oxidoreductase
39	Q14739	Delta(14)-sterol reductase LBR (Delta-14-SR)	Oxidoreductase
40	P43304	Glycerol-3-phosphate dehydrogenase	Oxidoreductase
41	P07195	L-lactate dehydrogenase B chain (LDH-B)	Oxidoreductase
42	Q16836	Hydroxyacyl-coenzyme A dehydrogenase	Oxidoreductase
43	P11177	Pyruvate dehydrogenase E1 component subunit beta	Oxidoreductase
44	Q16881	Thioredoxin reductase 1	Oxidoreductase
45	P16435	NADPH--cytochrome P450 reductase (CPR) (P450R) (EC 1.6.2.4)	Oxidoreductase
46	Q9UHG3	Prenylcysteine oxidase 1 (EC 1.8.3.5) (Prenylcysteine lyase)	Oxidoreductase

47	P30048	Thioredoxin-dependent peroxide reductase	Oxidoreductase
48	P54886	Delta-1-pyrroline-5-carboxylate synthase (P5CS)	Oxidoreductase
49	P55809	Succinyl-CoA:3-ketoacid coenzyme A transferase 1	Transferase
50	P25325	3-mercaptopyruvate sulfurtransferase (MST)	Transferase
51	Q9Y6E0	Serine/threonine-protein kinase 24	Transferase
52	P24928	DNA-directed RNA polymerase II subunit RPB1	Transferase
53	Q8TCS8	Polyribonucleotide nucleotidyltransferase 1	Transferase
54	P11216	Glycogen phosphorylase	Transferase
55	P09110	3-ketoacyl-CoA thiolase	Transferase
56	Q8IY81	pre-rRNA 2'-O-ribose RNA methyltransferase FTSJ3	Transferase
57	P43490	Nicotinamide phosphoribosyltransferase (NAmPRTase) (Nampt)	Transferase
58	P00558	Phosphoglycerate kinase 1	Transferase
59	P36957	Dihydrolipoyllysine-residue succinyltransferase component of 2-oxoglutarate dehydrogenase complex	Transferase
60	P10515	Dihydrolipoyllysine-residue acetyltransferase component of pyruvate dehydrogenase complex	Transferase
61	Q4G0N4	NAD kinase 2	Transferase
62	P09211	Glutathione S-transferase P (GST class-pi) (GSTP1-1)	Transferase
63	Q7L0Y3	tRNA methyltransferase 10 homolog C	Transferase
64	P37837	Transaldolase (EC 2.2.1.2)	Transferase
65	P22102	Trifunctional purine biosynthetic protein adenosine-3 (GART)]	Transferase
66	Q08J23	RNA cytosine C(5)-methyltransferase NSUN2	Transferase
67	P30041	Peroxiredoxin-6 (EC 1.11.1.27)	Transferase
68	Q9UMS4	Pre-mRNA-processing factor 19	Transferase
69	Q96T88	E3 ubiquitin-protein ligase UHRF1	Transferase
70	P09874	Poly [ADP-ribose] polymerase 1 (PARP-1)	Transferase
71	Q96SB4	SRSF protein kinase 1	Transferase
72	Q9H993	Damage-control phosphatase ARMT1	Transferase
73	Q9UIG0	Tyrosine-protein kinase BAZ1B	Transferase
74	Q9UNE7	E3 ubiquitin-protein ligase CHIP	Transferase
75	Q99873	Protein arginine N-methyltransferase 1	Transferase
76	Q00526	Cyclin-dependent kinase 3	Transferase
77	P41250	Glycine--tRNA ligase	Transferase
78	P04406	Glyceraldehyde-3-phosphate dehydrogenase	Transferase
79	P40939	Trifunctional enzyme subunit alpha	Transferase
80	Q8NI60	Atypical kinase COQ8A	Transferase
81	P00505	Aspartate aminotransferase	Transferase
82	P12277	Creatine kinase B-type	Transferase
83	O75390	Citrate synthase	Transferase
84	P23786	Carnitine O-palmitoyltransferase 2	Transferase
85	P34897	Serine hydroxymethyltransferase	Transferase
86	P14618	Pyruvate kinase PKM	Transferase
87	P46087	Probable 28S rRNA (cytosine(4447)-C(5))-methyltransferase	Transferase
88	P22087	rRNA 2'-O-methyltransferase fibrillarin	Transferase
89	Q9NVV4	Poly(A) RNA polymerase	Transferase
90	P30419	Glycylpeptide N-tetradecanoyltransferase 1	Transferase
91	P00492	Hypoxanthine-guanine phosphoribosyltransferase (HGPRT) (HGPRTase) (EC 2.4.2.8)	Transferase
92	P24752	Acetyl-CoA acetyltransferase	Transferase
93	Q9NYU2	UDP-glucose:glycoprotein glucosyltransferase 1 (UGT1) (hUGT1)	Transferase
94	P61081	NEDD8-conjugating enzyme Ubc12	Transferase
95	Q13263	Transcription intermediary factor 1-beta (TIF1-beta) (E3 SUMO-protein ligase TRIM28)	Transferase
96	Q9BWD1	Acetyl-CoA acetyltransferase	Transferase
97	P68036	Ubiquitin-conjugating enzyme	Transferase
98	Q9C0C9	(E3-independent) E2 ubiquitin-conjugating enzyme	Transferase
99	P60891	Ribose-phosphate pyrophosphokinase 1	Transferase
100	P04181	Ornithine aminotransferase	Transferase

101	P22392	Nucleoside diphosphate kinase B (NDK B) (NDP kinase B)	Transferase
102	P22061	Protein-L-isoaspartate(D-aspartate) O-methyltransferase (PIMT)	Transferase
103	P54886	Delta-1-pyrroline-5-carboxylate synthase (P5CS)	Transferase
104	P51532	Transcription activator BRG1	Hydrolase
105	Q9Y265	RuvB-like 1	Hydrolase
106	Q9Y230	RuvB-like 2	Hydrolase
107	P62820	Ras-related protein Rab-1A	Hydrolase
108	Q5JRX3	Presequence protease	Hydrolase
109	O60264	SWI/SNF-related matrix-associated actin-dependent regulator of chromatin subfamily A member 5	Hydrolase
110	Q9H9J2	39S ribosomal protein L44	Hydrolase
111	P62834	Ras-related protein Rap-1A	Hydrolase
112	P13995	Bifunctional methylenetetrahydrofolate dehydrogenase/cyclohydrolase	Hydrolase
113	P36776	Lon protease homolog	Hydrolase
114	Q9BYT8	Neurolysin	Hydrolase
115	P62136	Serine/threonine-protein phosphatase PP1-alpha catalytic subunit (PP-1A)	Hydrolase
116	P55786	Puromycin-sensitive aminopeptidase (PSA)	Hydrolase
117	P55072	Transitional endoplasmic reticulum ATPase (TER ATPase)	Hydrolase
118	P45974	Ubiquitin carboxyl-terminal hydrolase 5	Hydrolase
119	Q9ULX3	RNA-binding protein NOB1	Hydrolase
120	O43847	Nardilysin	Hydrolase
121	Q9H0D6	5'-3' exoribonuclease 2	Hydrolase
122	O75439	Mitochondrial-processing peptidase subunit beta	Hydrolase
123	P52948	Nuclear pore complex protein Nup98-Nup96	Hydrolase
124	P50579	Methionine aminopeptidase 2 (MAP 2) (MetAP 2)	Hydrolase
125	P30041	Peroxiredoxin-6	Hydrolase
126	Q93009	Ubiquitin carboxyl-terminal hydrolase 7	Hydrolase
127	O00487	26S proteasome non-ATPase regulatory subunit 14	Hydrolase
128	P51148	Ras-related protein Rab-5C	Hydrolase
129	Q92900	Regulator of nonsense transcripts 1	Hydrolase
130	O15355	Protein phosphatase 1G	Hydrolase
131	O94925	Glutaminase kidney isoform	Hydrolase
132	Q9NUJ1	Palmitoyl-protein thioesterase ABHD10	Hydrolase
133	Q9NVP1	ATP-dependent RNA helicase DDX18	Hydrolase
134	Q7L2E3	ATP-dependent RNA helicase DHX30	Hydrolase
135	Q96GQ7	Probable ATP-dependent RNA helicase DDX27	Hydrolase
136	Q14566	DNA replication licensing factor MCM6	Hydrolase
137	P33993	DNA replication licensing factor MCM7	Hydrolase
138	P17844	Probable ATP-dependent RNA helicase DDX5	Hydrolase
139	Q9H993	Damage-control phosphatase ARMT1	Hydrolase
140	Q9H4A4	Aminopeptidase B (AP-B)	Hydrolase
141	P60953	Cell division control protein 42 homolog	Hydrolase
142	Q13838	Spliceosome RNA helicase DDX39B	Hydrolase
143	Q13283	Ras GTPase-activating protein-binding protein 1 (G3BP-1)	Hydrolase
144	P28838	Cytosol aminopeptidase	Hydrolase
145	Q9H3G5	Probable serine carboxypeptidase CPVL	Hydrolase
146	Q8TDD1	ATP-dependent RNA helicase DDX54	Hydrolase
147	Q9NR30	Nucleolar RNA helicase 2	Hydrolase
148	P11021	Endoplasmic reticulum chaperone BiP	Hydrolase
149	Q92841	Probable ATP-dependent RNA helicase DDX17	Hydrolase
150	P27695	DNA-(apurinic or apyrimidinic site) endonuclease	Hydrolase
151	Q15181	Inorganic pyrophosphatase	Hydrolase
152	Q92769	Histone deacetylase 2 (HD2)	Hydrolase
153	Q9H2U2	Inorganic pyrophosphatase 2	Hydrolase
154	P11142	Heat shock cognate 71 kDa protein	Hydrolase

155	P38919	Eukaryotic initiation factor 4A-III (eIF-4A-III) (eIF4A-III)	Hydrolase
156	P07686	Beta-hexosaminidase subunit beta	Hydrolase
157	Q86XP3	ATP-dependent RNA helicase DDX42	Hydrolase
158	P33316	Deoxyuridine 5'-triphosphate nucleotidohydrolase	Hydrolase
159	Q9Y305	Acyl-coenzyme A thioesterase 9	Hydrolase
160	Q9H773	dCTP pyrophosphatase 1	Hydrolase
161	P60842	Eukaryotic initiation factor 4A-I (eIF-4A-I) (eIF4A-I)	Hydrolase
162	P41091	Eukaryotic translation initiation factor 2 subunit 3	Hydrolase
163	P07900	Heat shock protein HSP 90-alpha	Hydrolase
164	Q99797	Mitochondrial intermediate peptidase (MIP)	Hydrolase
165	P33991	DNA replication licensing factor MCM4	Hydrolase
166	P24666	Low molecular weight phosphotyrosine protein phosphatase (LMW-PTP) (LMW-PTPase)	Hydrolase
167	Q9H857	5'-nucleotidase domain-containing protein 2	Hydrolase
168	O14773	Tripeptidyl-peptidase 1 (TPP-1)	Hydrolase
169	P52888	Thimet oligopeptidase	Hydrolase
170	P12956	X-ray repair cross-complementing protein 6	Hydrolase
171	P51149	Ras-related protein Rab-7a	Hydrolase
172	Q9Y3E5	Peptidyl-tRNA hydrolase 2	Hydrolase
173	Q99497	Parkinson disease protein 7	Hydrolase
174	P25205	DNA replication licensing factor MCM3	Hydrolase
175	P33992	DNA replication licensing factor MCM5	Hydrolase
176	P13010	X-ray repair cross-complementing protein 5	Hydrolase
177	P55265	Double-stranded RNA-specific adenosine deaminase (DRADA)	Hydrolase
178	P22234	Multifunctional protein ADE2	Lyase
179	P23396	40S ribosomal protein S3	Lyase
180	Q16822	Phosphoenolpyruvate carboxykinase [GTP]	Lyase
181	P30046	D-dopachrome decarboxylase	Lyase
182	P40939	Trifunctional enzyme subunit alpha	Lyase
183	P04075	Fructose-bisphosphate aldolase A	Lyase
184	P06733	Alpha-enolase	Lyase
185	P09972	Fructose-bisphosphate aldolase C	Lyase
186	Q04760	Lactoylglutathione lyase	Lyase
187	Q99798	Aconitate hydratase	Lyase
188	P30084	Enoyl-CoA hydratase	Lyase
189	P60174	Triosephosphate isomerase (TIM)	Lyase
190	P12956	X-ray repair cross-complementing protein 6	Lyase
191	P18669	Phosphoglycerate mutase 1	Isomerase
192	P62937	Peptidyl-prolyl cis-trans isomerase A (PPIase A)	Isomerase
193	Q02880	DNA topoisomerase 2-beta	Isomerase
194	P13667	Protein disulfide-isomerase A4	Isomerase
195	P30405	Peptidyl-prolyl cis-trans isomerase F	Isomerase
196	P11387	DNA topoisomerase 1	Isomerase
197	P30101	Protein disulfide-isomerase A3	Isomerase
198	P11388	DNA topoisomerase 2-alpha	Isomerase
199	P23284	Peptidyl-prolyl cis-trans isomerase B	Isomerase
200	O95394	Phosphoacetylglucosamine mutase (PAGM)	Isomerase
201	P42126	Enoyl-CoA delta isomerase 1	Isomerase
202	Q02790	Peptidyl-prolyl cis-trans isomerase FKBP4 (PPIase FKBP4)	Isomerase
203	P10809	60 kDa heat shock protein	Isomerase
204	P14174	Macrophage migration inhibitory factor (MIF)	Isomerase
205	Q15084	Protein disulfide-isomerase A6	Isomerase
206	Q15185	Prostaglandin E synthase 3	Isomerase
207	P60174	Triosephosphate isomerase (TIM)	Isomerase
208	P07237	Protein disulfide-isomerase (PDI)	Isomerase

209	P53597	Succinate--CoA ligase [ADP/GDP-forming] subunit alpha	Ligase
210	Q6PI48	Aspartate--tRNA ligase	Ligase
211	Q5JTZ9	Alanine--tRNA ligase	Ligase
212	P22234	Multifunctional protein ADE2	Ligase
213	Q9P2R7	Succinate--CoA ligase [ADP-forming] subunit beta	Ligase
214	P22102	Trifunctional purine biosynthetic protein adenosine-3 [Includes: Phosphoribosylamine--glycine ligase	Ligase
215	P17812	CTP synthase 1	Ligase
216	Q5JPH6	Probable glutamate--tRNA ligase	Ligase
217	Q9NSE4	Isoleucine--tRNA ligase	Ligase
218	P49589	Cysteine--tRNA ligase	Ligase
219	Q6UB35	Monofunctional C1-tetrahydrofolate synthase	Ligase
220	P41250	Glycine--tRNA ligase	Ligase
221	P54577	Tyrosine--tRNA ligase	Ligase

Table A7. List of the gene IDs of our high-confidence protein hits that are genetically linked to various disease classes as per the DAVID bioinformatics resource. This table was used to generate Figure 4.11a.

	Disease Classes on DAVID Bioinformatics Resource												
S. No.	**Aging**	**Cancer**	**Cardiovascular**	**Developmental**	**Hematological**	**Immune**	**Infection**	**Metabolic**	**Neurological**	**Pharmacogenomic**	**Psychiatric**	**Renal**	**Reproduction**
1	ATP5O	ATP5O	OXCT1	DHCR7	DEK	ABCF1	OXCT1	DHCR7	ATP5C1	DHCR7	DHCR7	CD81	DHCR7
2	ATP5C1	ATP5A1	ATP5B	ATP5A1	RAB7A	DEK	ATP5O	ATP5O	DDX21	ARF3	DDX27	DDX18	FUS
3	DNAJA3	ATP5C1	DEK	ATP5G2	RNPS1	DDX39B	ATP5A1	DDX27	DDX39B	ABCB7	GNL3	DDX5	RBMX
4	NDUFS1	ATP5G2	DDX39B	GRPEL1	SERBP1	FKBP4	ATP5C1	DNAJC11	FUS	ABCF1	GNAS	NDUFS2	ACP1
5	NDUFS2	BCLAF1	DNAJC11	RAD23B	SMARCA4	GNAS	ATP5G2	FKBP4	GDI2	CD81	H2AFY	NSUN2	ALDH2
6	NDUFS3	CD81	GNAS	S100A11	XRCC5	IK	ATP5H	FXR2	GNAS	CRKL	NDUFV2	PDLIM5	ANXA5
7	NDUFV1	DDX18	GRPEL1	SET	AARS2	NDUFS2	ATAD3A	FUS	GTPBP4	DDT	NDUFAB1	RAD23B	APEX1
8	NDUFV2	DDX39B	RAD23B	ACP1	ALDH2	NDUFAB1	ATPIF1	GFM1	IK	DDX39B	PDLIM5	TAF15	CS
9	NDUFA9	SMU1	RAP1A	ANXA1	ALDOA	PARK7	CD81	GNL3	NDUFS1	ELAVL1	PARK7	TRAP1	DLAT
10	NDUFAB1	GNAS	RBBP4	APEX1	ANXA1	RAB7A	DDX5	GNAS	NDUFS2	GNAS	RAN	WDR1	FMR1
11	PDLIM5	NDUFS1	RUVBL2	CALM1	ANXA5	RAD23B	DDX39B	GRPEL1	NDUFS3	NDUFS1	S100A10	XRCC6	GSTP1
12	SDAD1	NDUFS2	SERBP1	CDC5L	ASPH	S100A10	DNAJA3	MYBBP1A	NDUFV1	NDUFS2	TARDBP	ACAA1	HSP90AA1
13	SERBP1	NDUFV2	SMARCA4	CCT2	BLVRA	SAE1	DNAJC11	NSUN2	NDUFV2	NDUFS3	ACAT1	ALDH2	HSPA1A
14	ACIN1	NDUFA9	TSR1	CS	CPVL	XRCC5	FASTKD2	PDLIM5	NDUFA9	NDUFV1	ACAT2	ANXA1	HSPA4
15	CARS	PDLIM5	U2AF1	CPSF6	COX5A	XRCC6	GFM1	RAB2A	NDUFAB1	NDUFV2	ACP1	ANXA5	HADHA
16	DLAT	RAD23B	WDR1	CFL1	COX7C	ACP1	GRSF1	RAD23B	PARK7	NDUFA9	ALDH2	APEX1	KPNA3
17	FMR1	RANBP1	XRCC5	EIF6	DPYSL2	ANP32B	GNAS	RAN	RAB7A	NDUFAB1	ALDOA	CARS	LMNA
18	GOT2	RAN	ACAT2	FUBP3	GSTP1	ARPC1A	GRPEL1	RAP1A	TARDBP	NSUN2	CALM1	POR	MIF
19	GLRX3	RAP1A	ACP1	FSCN1	GSR	ARPC2	NMT1	POLR2A	ACAT1	RBBP4	CCT5	GLRX3	MDC1
20	GSTP1	POLR2A	AARS2	FMR1	GPD2	ADAR	NDUFAF4	SERBP1	ACP1	RCOR3	POR	GSTP1	GART
21	GSR	RUVBL1	ALDH1B1	GSTP1	LDHA	ALDH2	NDUFS1	SMARCA4	ALDH18A1	POLR2A	DPYSL2	GSR	PRPF40A
22	GAPDH	S100A10	ALDH2	HSP90AA1	MIF	ANXA5	NDUFS2	TAF15	ALDH2	S100A10	EIF3D	GARS	PGRMC1
23	HSPA1A	SH3GLB1	ALDH9A1	HIST1H1D	MYL12B	APEX1	NDUFS3	WDR1	ALDH5A1	SMARCA4	FMR1	GLO1	PCMT1
24	HSPA4	SMARCA4	ANXA1	IGF2BP1	NPM1	CPVL	NDUFV1	ACAT1	ANXA7	THOC6	GLUD1	HSP90AB1	SERPINH1
25	HSPA5	XRCC5	ANXA5	MTHFD1L	PITRM1	CDC42	NDUFV2	ACAT2	API5	TRAP1	GLS	HSP90B1	SDHA
26	HSPA8	XRCC6	APEX1	MTHFD2	PSMD3	CDC5L	NDUFA9	ACP1	APEX1	XRCC6	GLRX3	HSPA1A	SDHB
27	HSPA9	ACAA1	BLVRA	PPIF	RPL11	CLIC1	NDUFAB1	ANP32A	ATXN10	ACAT2	GSTP1	HSPA5	SOD2
28	HP1BP3	ACP1	BAZ1B	GART	RPL35A	C21orf33	NDUFA4	ARPC1A	CPVL	ACAA1	GLO1	HSPA8	TFAM
29	HEXB	ARPC1A	CALM1	PNPT1	RPL5	CUTA	NME2	ACADM	CDC42	ANP32A	HSPA1A	IMPDH2	TFRC
30	IPO9	ADAR	CAPZA1	PCMT1	RPS14	CARS	PARK7	AARS2	CDC5L	ACADM	HSPA4	LMNA	USP7
31	LMNA	ALDH18A1	CAPZB	PTMA	RPS16	COX7C	RAB2A	ALDH1B1	CCT5	ADAR	HSPA5	MIF	
32	MCM4	ALDH2	CPVL	RPL12	STK24	DLAT	RANBP1	ALDH2	CRYZ	ALDH1B1	IMPDH2	MCM5	
33	MRPS30	ANXA1	CPT2	RPS20	SSBP1	DLD	SSB	ALDH9A1	DLST	ALDH2	KPNA3	MSH2	
34	NUCKS1	ANXA2	CCT2	RPLP1	SOD2	DDOST	TRAP1	AASS	DLD	ALDH5A1	LDHA	NAMPT	
35	PRDX1	AIFM1	COX5B	SRRM1	TFAM	ETFA	TSFM	ANXA1	FMR1	ALDH9A1	LDHB	PPIA	
36	PRDX2	APEX1	COX7C	SHMT2	TFRC	EIF2S3	TUFM	ANXA2	GLUD1	ANXA1	MCM7	PITRM1	
37	PRDX3	RNPEP	DUT	SERPINH1	TPM4	EIF2B2	ABHD10	ANXA5	GLRX3	ANXA2	NEFM	PARP1	
38	PRDX4	CPT2	DLD	SLC25A13	UBE2L3	EIF3L	ACAT1	APEX1	GSTP1	AIFM1	PAICS	PCNA	
39	PRDX5	C1QBP	DPYSL2	SMC1A	ZNF326	EZR	ACAT2	ASPH	GSR	APEX1	PITRM1	PSMA4	
40	PGM3	COX7A2	ENO1	SDHB		GSTP1	ACAA1	DARS2	GAPDH	BAZ1B	PHB	PSMA5	
41	PYGB	CYC1	EIF3D	TMED10		GLO1	ACP1	BAZ1B	GARS	CALM1	PSMB2	PSMA6	

42	PARP1	POR	GOT2	TCOF1		HSP90AA1	ACO2	CALM1	HSPA1A	CANX	RCN1	PSMB2	
43	PDIA4	EZR	GLRX3	VCL		HSP90AB1	ARPC1A	CAPZB	HSPA4	CALR	RPL10	SOD2	
44	PCMT1	LGALS3BP	GSTP1	ZNF326		HSPA1A	ACADM	CPVL	HSPA5	CPT2	RPL5	TXN	
45	RPN2	GTF2F1	GSR			HSPA8	ADAR	CPT2	HSPA8	C1QBP	SHMT2	TOMM40	
46	RPL12	GLS	GPD2			HSPD1	AARS2	CCT2	HSPA9	CPOX	STK24	TPP1	
47	STK24	GSTP1	GLO1			HMGB1	ALDH1B1	POR	HSPD1	POR	SLC1A5		
48	SOD2	GSR	HSPA1A			HIST1H1D	ALDH18A1	DUT	HNRNPF	DDOST	SLC25A13		
49	TXNDC5	GLO1	HSPA4			HDAC2	ALDH2	DPYSL2	HNRNPH3	ECHS1	SOD2		
50	TXNRD1	HSP90AA1	HSPA8			HPRT1	ALDH5A1	DDOST	HNRNPU	EIF2B2	TXNDC5		
51	TXN	HSPA1A	HSPD1			IMPDH2	ALDH9A1	ETFA	HSD17B12	EZR	TRA2B		
52	TOP2A	HSPA5	HNRNPUL1			LMNB1	AASS	ETFB	LDHA	FBL	TUBA1A		
53	TOP2B	HSPA8	HSD17B12			MIF	ANXA1	EIF2B2	LMNA	GSTP1	YWHAE		
54	TCOF1	HSPE1	IPO7			MDC1	DARS2	EIF6	MIF	GSR	YWHAZ		
55	VIM	HNRNPDL	IVD			MTPAP	CPT2	EZR	ME2	HSP90AA1	VCP		
56		HDAC2	LMNA			MRPS9	CDC42	FMR1	MTHFD1L	HSP90AB1	VIM		
57		HADHA	LMNB1			NUP98	CCT7	GLUD1	MTHFD2	HSP90B1			
58		HSD17B12	MIF			PRDX5	CLNS1A	GLS	MTPAP	HSPA1A			
59		HPRT1	MTHFD1L			PARP1	C21orf33	GSTP1	MRPL39	HSPA8			
60		IGF2BP1	MTHFD2			PNPT1	CS	GPD2	MRPS16	HNRNPUL1			
61		IDH2	MTCH2			PRPF40A	C1QBP	GLO1	MSH2	HEXB			
62		KPNA2	MTPAP			PCNA	CPOX	HSPA1A	NEFM	HDAC2			
63		KPNB1	MRPL15			PTGES3	COX4I1	HSPA8	NUCKS1	HCFC1			
64		MIF	MTPN			PSMD3	COX5A	HSPH1	NOLC1	HSD17B10			
65		MATR3	NNT			PSMG1	COX5B	HNRNPD	OAT	HYOU1			
66		MDC1	NAMPT			PSMA4	COX7A2	HNRNPUL1	PPIF	IMPDH2			
67		METAP2	PPIA			PSMA6	CYC1	HEXB	PRDX1	ILF3			
68		MTHFD2	PRDX5			PRKCSH	DUT	HADH	PRDX2	LMNA			
69		MAPRE1	PRDX6			RPL5	DLAT	HADHA	PRDX3	LBR			
70		MCM3	PYGB			RPLP1	DLST	HPRT1	PRDX4	LMNB1			
71		MCM4	PITRM1			SRSF3	DLD	HYOU1	PRDX5	LMNB2			
72		MCM5	PNPT1			STK24	DDOST	IGF2BP1	GART	MIF			
73		MCM6	PRPF40A			SLC25A1	ETFA	IARS2	PYGB	MDH1			
74		MCM7	PHB			SOD2	ETFB	IVD	PITRM1	MTHFD1L			
75		MRPS30	PSMD14			TXNDC5	ECHS1	LDHA	PARP1	MCM4			
76		MRPS9	PSMD3			TXN	EIF2S1	LMNA	PTBP1	MRPL4			
77		MSH2	PSMA4			TMPO	ETF1	LRPPRC	PNPT1	NAMPT			
78		NPM1	PSMA6			TOP2B	GLUD1	LCP1	PSMD6	PTCD3			
79		PRDX4	PDIA6			TCERG1	GOT2	MIF	PRMT1	PRDX2			
80		PGK1	PPA1			TFRC	GLS	MDH1	PCMT1	PEBP1			
81		GART	RCN1			TOMM40	EARS2	MPST	RPN2	PARP1			
82		PARP1	RPS11			TUBB	GLRX3	MTHFD1L	RPLP1	PCNA			
83		PHB	RPLP1			YWHAG	GSTP1	MCM6	SRSF1	P4HB			
84		PCNA	SRSF3			UBE2L3	GSR	MICU2	STK24	PSMA6			
85		PSMA4	SRRT			VDAC1	GPD2	MRPL15	SDHB	PCMT1			
86		PSMA6	SFXN1				GARS	MRPL3	SOD2	PKM			
87		PRMT1	SOD2				GLO1	MRPS27	TXNRD1	RPL10			
88		PDIA3	TXN				HSPA1A	MRPS9	TXN	RPL18			
89		RCC2	TOP2B				HSPA4	MYL12B	TFAM	RPL7A			

90		RNH1	TFAM				HSPA9	NAMPT	TOMM40	SRSF6			
91		RPLP1	TOMM40				HSPD1	NUCKS1	TUBB	SHMT2			
92		SHMT2	TUBB				HSPE1	OAT	TPT1	SDHB			
93		SRP14	YWHAQ				HNRNPF	PPIF	YWHAZ	SOD2			
94		SNRPB	YWHAZ				HMGB1	PRDX6	UQCRC2	TXNRD1			
95		SDHA	UHRF1				HADH	PCK2	VCP	TXN			
96		SDHB	USP7				HADHA	PITRM1	VIM	TMPO			
97		SOD2	VIM				IMMT	PLS3	VCL	TOP1			
98		TXNRD1	VCL				IDH2	PARP1	VDAC1	TOP2A			
99		TXN	ZNF326				IDH3A	PNPT1	VDAC2	TOP2B			
100		TOP2A					IDH3B	PSMD6		TFRC			
101		TALDO1					IARS2	PSMA2		TOMM40			
102		TFRC					IVD	PSMA6		VCP			
103		TOMM40					LDHA	PSMA8		VCL			
104		TUBB					LDHB	PSMB2		ZNF326			
105		YWHAE					LAP3	PDIA6					
106		YWHAG					LRPPRC	PKM					
107		YWHAQ					LETM1	RCN2					
108		USP7					LONP1	RPS11					
109		VCP					MIF	RPLP2					
110							MDH1	SHMT2					
111							MDH2	SFXN1					
112							ME2	SRP14					
113							MPST	SLC25A13					
114							MTHFD1L	SPAG9					
115							MTHFD2	SUCLA2					
116							MICU2	SOD2					
117							MTCH2	TXNRD1					
118							MTPAP	TOP1					
119							MRPL14	TFAM					
120							MRPL15	TFRC					
121							MRPL20	TRA2A					
122							MRPL21	TRA2B					
123							MRPL3	TOMM40					
124							MRPL37	TUBA1A					
125							MRPL39	YWHAQ					
126							MRPL4	YWHAZ					
127							MRPL44	UBE2L3					
128							MRPS14	UHRF1					
129							MRPS16						
130							MRPS27						
131							MRPS30						
132							MRPS9						
133							NLN						
134							NNT						
135							OAT						
136							PTCD3						
137							PMPCA						
138							PMPCB						
139							PTRH2						
140							PPIA						
141							PPIB						
142							PPIF						
143							PRDX1						

144							PRDX3						
145							PRDX5						
146							PRDX6						
147							PCK2						
148							PITRM1						
149							PARP1						
150							PNPT1						
151							PGRMC1						
152							PHB2						
153							PHB						
154							PDIA6						
155							PPA2						
156							PDHB						
157							RCC2						
158							RCN1						
159							RSL1D1						
160							RPL10A						
161							RPL34						
162							RPL35A						
163							RPS14						
164							SHMT2						
165							SERPINH1						
166							SFXN1						
167							SSBP1						
168							SLC25A1						
169							SLC25A13						
170							SLC25A3						
171							STOML2						
172							SDHA						
173							SDHB						
174							SUCLA2						
175							SUCLG1						
176							SOD2						
177							TRMT10C						
178							TXNRD1						
179							TXN						
180							TFAM						
181							TFRC						
182							TIMM44						
183							TOMM20						
184							TOMM40						
185							TPI1						
186							UQCRC1						
187							UQCRC2						
188							VDAC1						
189							VDAC2						
190							VDAC3						

Table A8. The gene IDs for the high-confidence protein hits categorized with respect to the number of the types of cancer they are overexpressed in as per the Oncomine database.

S. No.	Gene ID	UniProt ID	No. of types of cancers the gene is overexpressed in	Protein description
1	TOP2A	P11388-4	18	Isoform 4 of DNA topoisomerase 2-alpha
2	KPNA2	P52292	17	Importin subunit alpha-1
3	TUBB	P07437	17	Tubulin beta chain
4	CCT5	P48643	17	T-complex protein 1 subunit epsilon
5	H2AFV	Q71UI9	16	Histone H2A.V
6	CBX3	Q13185	16	Chromobox protein homolog 3
7	MCM3	P25205	16	DNA replication licensing factor MCM3
8	PCNA	P12004	16	Proliferating cell nuclear antigen
9	MCM7	P33993	16	DNA replication licensing factor MCM7
10	MCM4	P33991	16	DNA replication licensing factor MCM4
11	MCM5	P33992	16	DNA replication licensing factor MCM5
12	SYNCRIP	O60506	16	Heterogeneous nuclear ribonucleoprotein Q
13	MARCKSL1	P49006	15	MARCKS-related protein
14	UHRF1	Q96T88-2	15	Isoform 2 of E3 ubiquitin-protein ligase UHRF1
15	MCM6	Q14566	15	DNA replication licensing factor MCM6
16	PAICS	P22234-2	15	Isoform 2 of Multifunctional protein ADE2
17	SHMT2	P34897	14	Serine hydroxymethyltransferase, mitochondrial
18	MTHFD2	P13995	14	Bifunctional methylenetetrahydrofolate dehydrogenase/cyclohydrolase, mitochondrial
19	RCN2	Q14257	14	Reticulocalbin-2
20	PTMA	P06454	14	Prothymosin alpha
21	RANBP1	P43487	14	Ran-specific GTPase-activating protein
22	RCC1	P18754-2	14	Isoform 2 of Regulator of chromosome condensation
23	LMNB1	P20700	14	Lamin-B1
24	RAN	P62826	14	GTP-binding nuclear protein Ran
25	LGALS3BP	Q08380	14	Galectin-3-binding protein
26	MIF	P14174	14	Macrophage migration inhibitory factor
27	ILF3	Q12906-7	14	Isoform 7 of Interleukin enhancer-binding factor 3
28	ANP32E	Q9BTT0	13	Acidic leucine-rich nuclear phosphoprotein 32 family member E
29	SNRPE	P62304	13	Small nuclear ribonucleoprotein E
30	TMEM97	Q5BJF2	13	Transmembrane protein 97
31	PKM	P14618	13	Pyruvate kinase PKM
32	ILF2	Q12905	13	Interleukin enhancer-binding factor 2
33	GART	P22102	13	Trifunctional purine biosynthetic protein adenosine-3
34	PGK1	P00558	13	Phosphoglycerate kinase 1
35	HSPD1	P10809	12	60 kDa heat shock protein, mitochondrial
36	CALR	P27797	12	Calreticulin
37	ACP1	P24666	12	Low molecular weight phosphotyrosine protein phosphatase
38	NASP	P49321-3	12	Isoform 3 of Nuclear autoantigenic sperm protein
39	RBBP4	Q09028	12	Histone-binding protein RBBP4
40	PSMA4	P25789	12	Proteasome subunit alpha type-4
41	S100A11	P31949	12	Protein S100-A11
42	LMNB2	Q03252	12	Lamin-B2

43	GARS	P41250	12	Glycine--tRNA ligase
44	TFRC	P02786	12	Transferrin receptor protein 1
45	ENO1	P06733	12	Alpha-enolase
46	MSH2	P43246	12	DNA mismatch repair protein Msh2
47	CCT2	P78371	12	T-complex protein 1 subunit beta
48	GAPDH	P04406	12	Glyceraldehyde-3-phosphate dehydrogenase
49	PDIA4	P13667	12	Protein disulfide-isomerase A4
50	NT5DC2	Q9H857	12	5'-nucleotidase domain-containing protein 2
51	LDHA	P00338-3	12	Isoform 3 of L-lactate dehydrogenase A chain
52	SET	Q01105	11	Protein SET
53	TPM4	P67936	11	Tropomyosin alpha-4 chain
54	MARCKS	P29966	11	Myristoylated alanine-rich C-kinase substrate
55	RCN1	Q15293	11	Reticulocalbin-1
56	SERBP1	Q8NC51	11	Plasminogen activator inhibitor 1 RNA-binding protein
57	SSRP1	Q08945	11	FACT complex subunit SSRP1
58	NAP1L1	P55209	11	Nucleosome assembly protein 1-like 1
59	NUCKS1	Q9H1E3	11	Nuclear ubiquitous casein and cyclin-dependent kinase substrate 1
60	MRPL15	Q9P015	11	39S ribosomal protein L15, mitochondrial
61	PHB	P35232	11	Prohibitin
62	CKAP4	Q07065	11	Cytoskeleton-associated protein 4
63	PRMT1	Q99873	11	Protein arginine N-methyltransferase 1
64	DPYSL2	Q16555	11	Dihydropyrimidinase-related protein 2
65	PFN1	P07737	11	Profilin-1
66	SNRPD2	P62316	11	Small nuclear ribonucleoprotein Sm D2
67	RUVBL1	Q9Y265	11	RuvB-like 1
68	HSPA4	P34932	11	Heat shock 70 kDa protein 4
69	HSPH1	Q92598	11	Heat shock protein 105 kDa
70	HPRT1	P00492	11	Hypoxanthine-guanine phosphoribosyltransferase
71	PRDX4	Q13162	11	Peroxiredoxin-4
72	FSCN1	Q16658	11	Fascin
73	PSMB3	P49720	11	Proteasome subunit beta type-3
74	IMPDH2	P12268	11	Inosine-5'-monophosphate dehydrogenase 2
75	IPO9	Q96P70	11	Importin-9
76	TSR1	Q2NL82	11	Pre-rRNA-processing protein TSR1 homolog
77	NPM1	P06748	10	Nucleophosmin
78	RPN2	P04844	10	Dolichyl-diphosphooligosaccharide--protein glycosyltransferase subunit 2
79	TSPAN3	O60637	10	Tetraspanin-3
80	SOD2	P04179	10	Superoxide dismutase [Mn], mitochondrial
81	HNRNPU	Q00839	10	Heterogeneous nuclear ribonucleoprotein U
82	PPIB	P23284	10	Peptidyl-prolyl cis-trans isomerase B
83	YWHAZ	P63104	10	14-3-3 protein zeta/delta
84	NOP56	O00567	10	Nucleolar protein 56
85	RCC2	Q9P258	10	Protein RCC2
86	DCTPP1	Q9H773	10	dCTP pyrophosphatase 1
87	PRPF40A	O75400	10	Pre-mRNA-processing factor 40 homolog A
88	ALDH18A1	P54886	10	Delta-1-pyrroline-5-carboxylate synthase
89	ADAR	P55265-4	10	Isoform 4 of Double-stranded RNA-specific adenosine deaminase
90	TPI1	P60174	10	Triosephosphate isomerase
91	NME2	P22392-2	10	Isoform 3 of Nucleoside diphosphate kinase B
92	PARP1	P09874	10	Poly [ADP-ribose] polymerase 1
93	SMARCA4	P51532	10	Transcription activator BRG1
94	SSR1	P43307	9	Translocon-associated protein subunit alpha
95	DEK	P35659	9	Protein DEK
96	VIM	P08670	9	Vimentin

97	MRPL3	P09001	9	39S ribosomal protein L3, mitochondrial
98	RRP15	Q9Y3B9	9	RRP15-like protein
99	G3BP1	Q13283	9	Ras GTPase-activating protein-binding protein 1
100	GLS	O94925	9	Glutaminase kidney isoform, mitochondrial
101	HMGB1	P09429	9	High mobility group protein B1
102	HSPA9	P38646	9	Stress-70 protein, mitochondrial
103	PNPT1	Q8TCS8	9	Polyribonucleotide nucleotidyltransferase 1, mitochondrial
104	HSP90B1	P14625	9	Endoplasmin
105	H2AFY	O75367	9	Core histone macro-H2A.1
106	EZR	P15311	9	Ezrin
107	SSBP1	Q04837	9	Single-stranded DNA-binding protein, mitochondrial
108	MSN	P26038	9	Moesin
109	MAPRE1	Q15691	9	Microtubule-associated protein RP/EB family member 1
110	ANXA2	P07355-2	9	Isoform 2 of Annexin A2
111	SSB	P05455	9	Lupus La protein
112	ASPH	Q12797	9	Aspartyl/asparaginyl beta-hydroxylase
113	HNRNPAB	Q99729-2	9	Isoform 2 of Heterogeneous nuclear ribonucleoprotein A/B
114	OLA1	Q9NTK5	9	Obg-like ATPase 1
115	FKBP4	Q02790	9	Peptidyl-prolyl cis-trans isomerase FKBP4
116	CNN3	Q15417	9	Calponin-3
117	LBR	Q14739	9	Lamin-B receptor
118	SNRPB	P14678-3	9	Isoform SM-B1 of Small nuclear ribonucleoprotein-associated proteins B and B'
119	HNRNPR	O43390	9	Heterogeneous nuclear ribonucleoprotein R
120	TAGLN2	P37802	9	Transgelin-2
121	TUBA1B	P68363	9	Tubulin alpha-1B chain
122	KPNB1	Q14974	9	Importin subunit beta-1
123	GSTP1	P09211	9	Glutathione S-transferase P
124	PSMD8	P48556	9	26S proteasome non-ATPase regulatory subunit 8
125	TUBB3	Q13509	9	Tubulin beta-3 chain
126	EIF4A1	P60842	9	Eukaryotic initiation factor 4A-I
127	GTPBP4	Q9BZE4	9	Nucleolar GTP-binding protein 1
128	CLIC1	O00299	9	Chloride intracellular channel protein 1
129	SERPINH1	P50454	9	Serpin H1
130	SMC1A	Q14683	8	Structural maintenance of chromosomes protein 1A
131	C1QBP	Q07021	8	Complement component 1 Q subcomponent-binding protein (or p32), mitochondrial
132	NOLC1	Q14978-2	8	Isoform Beta of Nucleolar and coiled-body phosphoprotein 1
133	HSPE1	P61604	8	10 kDa heat shock protein, mitochondrial
134	CLNS1A	P54105	8	Methylosome subunit pICln
135	CANX	P27824	8	Calnexin
136	CAPRIN1	Q14444	8	Caprin-1
137	HNRNPA1	P09651	8	Heterogeneous nuclear ribonucleoprotein A1
138	HNRNPA2B1	P22626	8	Heterogeneous nuclear ribonucleoproteins A2/B1
139	YWHAQ	P27348	8	14-3-3 protein theta
140	MTHFD1L	Q6UB35	8	Monofunctional C1-tetrahydrofolate synthase, mitochondrial
141	ACOT9	Q9Y305-4	8	Isoform 4 of Acyl-coenzyme A thioesterase 9, mitochondrial
142	PYCR1	P32322	8	Pyrroline-5-carboxylate reductase 1, mitochondrial
143	ANXA5	P08758	8	Annexin A5
144	P4HB	P07237	8	Protein disulfide-isomerase
145	S100A10	P60903	8	Protein S100-A10
146	EIF3B	P55884-2	8	Isoform 2 of Eukaryotic translation initiation factor 3 subunit B
147	YWHAE	P62258	8	14-3-3 protein epsilon
148	PPA1	Q15181	8	Inorganic pyrophosphatase
149	CPSF6	Q16630-2	8	Isoform 2 of Cleavage and polyadenylation specificity factor subunit 6

150	PDIA3	P30101	8	Protein disulfide-isomerase A3
151	GTF2I	P78347	8	General transcription factor II-I
152	DHCR7	Q9UBM7	8	7-dehydrocholesterol reductase
153	TRIM28	Q13263	8	Transcription intermediary factor 1-beta
154	GINS4	Q9BRT9	8	DNA replication complex GINS protein SLD5
155	HEXB	P07686	8	Beta-hexosaminidase subunit beta
156	HSP90AB1	P08238	8	Heat shock protein HSP 90-beta
157	DDOST	P39656	8	Dolichyl-diphosphooligosaccharide--protein glycosyltransferase 48 kDa subunit
158	PTBP1	P26599-3	8	Isoform 3 of Polypyrimidine tract-binding protein 1
159	APEX1	P27695	8	DNA-(apurinic or apyrimidinic site) lyase
160	LDHB	P07195	8	L-lactate dehydrogenase B chain
161	PSMA5	P28066	8	Proteasome subunit alpha type-5
162	MATR3	P43243	8	Matrin-3
163	HDAC2	Q92769	8	Histone deacetylase 2
164	TXN	P10599	8	Thioredoxin
165	PRPS1	P60891	8	Ribose-phosphate pyrophosphokinase 1
166	ALDOA	P04075-2	8	Isoform 2 of Fructose-bisphosphate aldolase A
167	XRCC5	P13010	8	X-ray repair cross-complementing protein 5
168	PSMA2	P25787	8	Proteasome subunit alpha type-2
169	CCT8	P50990	8	T-complex protein 1 subunit theta
170	BRIX1	Q8TDN6	8	Ribosome biogenesis protein BRX1 homolog
171	IPO7	O95373	8	Importin-7
172	CPOX	P36551	8	Coproporphyrinogen-III oxidase, mitochondrial
173	GLO1	Q04760	8	Lactoylglutathione lyase
174	DDX18	Q9NVP1	8	ATP-dependent RNA helicase DDX18
175	YARS	P54577	7	Tyrosine--tRNA ligase, cytoplasmic
176	HIST1H2AD	P20671	7	Histone H2A type 1-D
177	PRKCSH	P14314	7	Glucosidase 2 subunit beta
178	HIST2H2BF	Q5QNW6-2	7	Isoform 2 of Histone H2B type 2-F
179	ANP32A	P39687	7	Acidic leucine-rich nuclear phosphoprotein 32 family member A
180	HNRNPC	P07910	7	Heterogeneous nuclear ribonucleoproteins C1/C2
181	MRPS30	Q9NP92	7	28S ribosomal protein S30, mitochondrial
182	COX5A	P20674	7	Cytochrome c oxidase subunit 5A, mitochondrial
183	TFAM	Q00059	7	Transcription factor A, mitochondrial
184	TIMM50	Q3ZCQ8-2	7	Isoform 2 of Mitochondrial import inner membrane translocase subunit TIM50
185	PPIF	P30405	7	Peptidyl-prolyl cis-trans isomerase F, mitochondrial
186	RPSA	P08865	7	40S ribosomal protein SA
187	IDH2	P48735	7	Isocitrate dehydrogenase [NADP], mitochondrial
188	NMT1	P30419	7	Glycylpeptide N-tetradecanoyltransferase 1
189	SUMO2	P61956	7	Small ubiquitin-related modifier 2
190	HSD17B10	Q99714	7	3-hydroxyacyl-CoA dehydrogenase type-2
191	PTGES3	Q15185	7	Prostaglandin E synthase 3
192	PGRMC1	O00264	7	Membrane-associated progesterone receptor component 1
193	LMNA	P02545	7	Prelamin-A/C
194	BCLAF1	Q9NYF8	7	Bcl-2-associated transcription factor 1
195	UBE2M	P61081	7	NEDD8-conjugating enzyme Ubc12
196	TRAP1	Q12931	7	Heat shock protein 75 kDa, mitochondrial
197	HNRNPA3	P51991	7	Heterogeneous nuclear ribonucleoprotein A3
198	HNRNPUL1	Q9BUJ2	7	Heterogeneous nuclear ribonucleoprotein U-like protein 1
199	RPL14	P50914	7	60S ribosomal protein L14
200	DUT	P33316	7	Deoxyuridine 5'-triphosphate nucleotidohydrolase, mitochondrial
201	TXNRD1	Q16881	7	Thioredoxin reductase 1, cytoplasmic
202	SNRPD3	P62318	7	Small nuclear ribonucleoprotein Sm D3
203	LRRC59	Q96AG4	7	Leucine-rich repeat-containing protein 59

204	EIF6	P56537	7	Eukaryotic translation initiation factor 6
205	RUVBL2	Q9Y230	7	RuvB-like 2
206	PSMB2	P49721	7	Proteasome subunit beta type-2
207	RPS16	P62249	7	40S ribosomal protein S16
208	CRKL	P46109	7	Crk-like protein
209	RAB7A	P51149	7	Ras-related protein Rab-7a
210	PSMG1	O95456	7	Proteasome assembly chaperone 1
211	DDX21	Q9NR30	7	Nucleolar RNA helicase 2
212	SRPK1	Q96SB4-3	7	Isoform 1 of SRSF protein kinase 1
213	ARHGDIA	P52565	7	Rho GDP-dissociation inhibitor 1
214	PDIA6	Q15084-2	7	Isoform 2 of Protein disulfide-isomerase A6
215	HSPA8	P11142	7	Heat shock cognate 71 kDa protein
216	MIPEP	Q99797	7	Mitochondrial intermediate peptidase
217	VBP1	P61758	7	Prefoldin subunit 3
218	ALDH1B1	P30837	7	Aldehyde dehydrogenase X, mitochondrial
219	PDLIM5	Q96HC4	7	PDZ and LIM domain protein 5
220	PLS3	P13797	7	Plastin-3
221	AHSA1	O95433	7	Activator of 90 kDa heat shock protein ATPase homolog 1
222	SMARCA5	O60264	7	SWI/SNF-related matrix-associated actin-dependent regulator of chromatin subfamily A member 5
223	RAB2A	P61019	7	Ras-related protein Rab-2A
224	ANXA1	P04083	7	Annexin A1
225	GNB2L1	P63244	7	Guanine nucleotide-binding protein subunit beta-2-like 1
226	UTP14A	Q9BVJ6	7	U3 small nucleolar RNA-associated protein 14 homolog A
227	PYGB	P11216	7	Glycogen phosphorylase, brain form
228	EEF2	P13639	7	Elongation factor 2
229	CCT4	P50991	7	T-complex protein 1 subunit delta
230	UGGT1	Q9NYU2	7	UDP-glucose:glycoprotein glucosyltransferase 1
231	CCT7	Q99832	7	T-complex protein 1 subunit eta
232	MLLT4	P55196-5	6	Isoform 5 of Afadin
233	YBX1	P67809	6	Nuclease-sensitive element-binding protein 1
234	CALM1	P62158	6	Calmodulin
235	GRSF1	Q12849	6	G-rich sequence factor 1
236	RBMX	P38159	6	RNA-binding motif protein, X chromosome
237	ATP5H	O75947	6	ATP synthase subunit d, mitochondrial
238	PHB2	Q99623	6	Prohibitin-2
239	TRA2A	Q13595	6	Transformer-2 protein homolog alpha
240	NOP2	P46087-4	6	Isoform 4 of Putative ribosomal RNA methyltransferase NOP2
241	SH3GLB1	Q9Y371-2	6	Isoform 2 of Endophilin-B1
242	MDH2	P40926	6	Malate dehydrogenase, mitochondrial
243	TMPO	P42166	6	Lamina-associated polypeptide 2, isoform alpha
244	MRPL4	Q9BYD3	6	39S ribosomal protein L4, mitochondrial
245	KHDRBS1	Q07666	6	KH domain-containing, RNA-binding, signal transduction-associated protein 1
246	RPL29	P47914	6	60S ribosomal protein L29
247	RAD23B	P54727	6	UV excision repair protein RAD23 homolog B
248	CYC1	P08574	6	Cytochrome c1, heme protein, mitochondrial
249	TOMM20	Q15388	6	Mitochondrial import receptor subunit TOM20 homolog
250	EIF5A	P63241-2	6	Isoform 2 of Eukaryotic translation initiation factor 5A-1
251	ATP5O	P48047	6	ATP synthase subunit O, mitochondrial
252	TOP1	P11387	6	DNA topoisomerase 1
253	EEF1D	P29692-2	6	Isoform 2 of Elongation factor 1-delta
254	METAP2	P50579	6	Methionine aminopeptidase 2
255	SLC25A5	P05141	6	ADP/ATP translocase 2
256	MDC1	Q14676	6	Mediator of DNA damage checkpoint protein 1

257	LAP3	P28838	6	Cytosol aminopeptidase
258	HNRNPH1	P31943	6	Heterogeneous nuclear ribonucleoprotein H
259	RPS2	P15880	6	40S ribosomal protein S2
260	SLC25A6	P12236	6	ADP/ATP translocase 3
261	SRRT	Q9BXP5	6	Serrate RNA effector molecule homolog
262	RPS15A	P62244	6	40S ribosomal protein S15a
263	CAPZA1	P52907	6	F-actin-capping protein subunit alpha-1
264	GNL3	Q9BVP2	6	Guanine nucleotide-binding protein-like 3
265	RPL30	P62888	6	60S ribosomal protein L30
266	DDT	P30046	6	D-dopachrome decarboxylase
267	TUBA1A	Q71U36	6	Tubulin alpha-1A chain
268	EIF4G1	Q04637-9	6	Isoform 9 of Eukaryotic translation initiation factor 4 gamma 1
269	GNAS	Q5JWF2	6	Guanine nucleotide-binding protein G(s) subunit alpha isoforms XLas
270	TXNDC5	Q8NBS9	6	Thioredoxin domain-containing protein 5
271	PRDX1	Q06830	6	Peroxiredoxin-1
272	ELAVL1	Q15717	6	ELAV-like protein 1
273	HSP90AA1	P07900-2	6	Isoform 2 of Heat shock protein HSP 90-alpha
274	RRS1	Q15050	6	Ribosome biogenesis regulatory protein homolog
275	RPL8	P62917	6	60S ribosomal protein L8
276	PSMD3	O43242	6	26S proteasome non-ATPase regulatory subunit 3
277	VCP	P55072	6	Transitional endoplasmic reticulum ATPase
278	RPL10A	P62906	6	60S ribosomal protein L10a
279	RPS8	P62241	6	40S ribosomal protein S8
280	NLN	Q9BYT8	6	Neurolysin, mitochondrial
281	RPL13	P26373	6	60S ribosomal protein L13
282	PPIA	P62937	6	Peptidyl-prolyl cis-trans isomerase A
283	CDC5L	Q99459	6	Cell division cycle 5-like protein
284	PSMD11	O00231-2	6	Isoform 2 of 26S proteasome non-ATPase regulatory subunit 11
285	ESYT1	Q9BSJ8-2	6	Isoform 2 of Extended synaptotagmin-1
286	GPD2	P43304	6	Glycerol-3-phosphate dehydrogenase, mitochondrial
287	PCK2	Q16822	6	Phosphoenolpyruvate carboxykinase [GTP], mitochondrial
288	THOC6	Q86W42	6	THO complex subunit 6 homolog
289	CARS	P49589-3	5	Isoform 3 of Cysteine--tRNA ligase, cytoplasmic
290	RNPEP	Q9H4A4	5	Aminopeptidase B
291	NACA	Q13765-2	5	Isoform 2 of Nascent polypeptide-associated complex subunit alpha
292	NCL	P19338	5	Nucleolin
293	RPLP2	P05387	5	60S acidic ribosomal protein P2
294	FUS	P35637	5	RNA-binding protein FUS
295	CUTA	O60888-2	5	Isoform A of Protein CutA
296	RPS3	P23396	5	40S ribosomal protein S3
297	UQCRC2	P22695	5	Cytochrome b-c1 complex subunit 2, mitochondrial
298	SARNP	P82979	5	SAP domain-containing ribonucleoprotein
299	PSIP1	O75475	5	PC4 and SFRS1-interacting protein
300	ATP5B	P06576	5	ATP synthase subunit beta, mitochondrial
301	ETFA	P13804	5	Electron transfer flavoprotein subunit alpha, mitochondrial
302	ATP5C1	P36542	5	ATP synthase subunit gamma, mitochondrial
303	SRRM1	Q8IYB3	5	Serine/arginine repetitive matrix protein 1
304	DLAT	P10515	5	Dihydrolipoyllysine-residue acetyltransferase component of pyruvate dehydrogenase complex, mitochondrial
305	NUDC	Q9Y266	5	Nuclear migration protein nudC
306	TUFM	P49411	5	Elongation factor Tu, mitochondrial
307	CBX5	P45973	5	Chromobox protein homolog 5
308	CFL1	P23528	5	Cofilin-1
309	UQCRC1	P31930	5	Cytochrome b-c1 complex subunit 1, mitochondrial

310	HNRNPK	P61978-3	5	Isoform 3 of Heterogeneous nuclear ribonucleoprotein K
311	HNRNPH3	P31942	5	Heterogeneous nuclear ribonucleoprotein H3
312	SUPT16H	Q9Y5B9	5	FACT complex subunit SPT16
313	SDHA	P31040	5	Succinate dehydrogenase [ubiquinone] flavoprotein subunit, mitochondrial
314	LRPPRC	P42704	5	Leucine-rich PPR motif-containing protein, mitochondrial
315	PTCD3	Q96EY7	5	Pentatricopeptide repeat domain-containing protein 3, mitochondrial
316	HSPA5	P11021	5	78 kDa glucose-regulated protein
317	RSL1D1	O76021	5	Ribosomal L1 domain-containing protein 1
318	WDR43	Q15061	5	WD repeat-containing protein 43
319	PA2G4	Q9UQ80	5	Proliferation-associated protein 2G4
320	RPL31	P62899-2	5	Isoform 2 of 60S ribosomal protein L31
321	U2AF1	Q01081	5	Splicing factor U2AF 35 kDa subunit
322	YWHAG	P61981	5	14-3-3 protein gamma
323	VDAC2	P45880-1	5	Isoform 1 of Voltage-dependent anion-selective channel protein 2
324	PCBP2	Q15366-2	5	Isoform 2 of Poly(rC)-binding protein 2
325	HYOU1	Q9Y4L1	5	Hypoxia up-regulated protein 1
326	RAB5C	P51148-2	5	Isoform 2 of Ras-related protein Rab-5C
327	MYL12B	O14950	5	Myosin regulatory light chain 12B
328	DDX39B	Q13838-2	5	Isoform 2 of Spliceosome RNA helicase DDX39B
329	HNRNPF	P52597	5	Heterogeneous nuclear ribonucleoprotein F
330	EIF5	P55010	5	Eukaryotic translation initiation factor 5
331	SRP9	P49458	5	Signal recognition particle 9 kDa protein
332	NUDT21	O43809	5	Cleavage and polyadenylation specificity factor subunit 5
333	RPS3A	P61247	5	40S ribosomal protein S3a
334	ARPC1A	Q92747	5	Actin-related protein 2/3 complex subunit 1A
335	CD81	P60033	5	CD81 antigen
336	EIF3D	O15371	5	Eukaryotic translation initiation factor 3 subunit D
337	PARK7	Q99497	5	Protein DJ-1
338	NNT	Q13423	5	NAD(P) transhydrogenase, mitochondrial
339	CDC42	P60953-1	5	Isoform 1 of Cell division control protein 42 homolog
340	KHSRP	Q92945	5	Far upstream element-binding protein 2
341	ARF3	P61204	5	ADP-ribosylation factor 3
342	UBE2L3	P68036-3	5	Isoform 3 of Ubiquitin-conjugating enzyme E2 L3
343	HADHA	P40939	5	Trifunctional enzyme subunit alpha, mitochondrial
344	RPL35A	P18077	5	60S ribosomal protein L35a
345	RPL38	P63173	5	60S ribosomal protein L38
346	PSMA6	P60900	5	Proteasome subunit alpha type-6
347	TUBB2B	Q9BVA1	5	Tubulin beta-2B chain
348	SFXN1	Q9H9B4	5	Sideroflexin-1
349	RPL18A	Q02543	5	60S ribosomal protein L18a
350	XRN2	Q9H0D6	5	5'-3' exoribonuclease 2
351	EIF3CL	B5ME19	5	Eukaryotic translation initiation factor 3 subunit C-like protein
352	RPL12	P30050	5	60S ribosomal protein L12
353	GDI2	P50395	5	Rab GDP dissociation inhibitor beta
354	RPL10	P27635	5	60S ribosomal protein L10
355	RBM4	Q9BWF3	5	RNA-binding protein 4
356	CAPZB	P47756-2	5	Isoform 2 of F-actin-capping protein subunit beta
357	RPL18	Q07020	5	60S ribosomal protein L18
358	RPL23	P62829	5	60S ribosomal protein L23
359	EIF2S1	P05198	5	Eukaryotic translation initiation factor 2 subunit 1
360	FUBP1	Q96AE4-2	5	Isoform 2 of Far upstream element-binding protein 1
361	WDR1	O75083	5	WD repeat-containing protein 1
362	PEBP1	P30086	5	Phosphatidylethanolamine-binding protein 1
363	RPL36A	P83881	5	60S ribosomal protein L36a

364	SLC1A5	Q15758	5	Neutral amino acid transporter B(0)
365	BLVRA	P53004	5	Biliverdin reductase A
366	TCERG1	O14776	5	Transcription elongation regulator 1
367	ARPC2	O15144	5	Actin-related protein 2/3 complex subunit 2
368	FUBP3	Q96I24	5	Far upstream element-binding protein 3
369	BAZ1B	Q9UIG0	5	Tyrosine-protein kinase BAZ1B
370	PPP1CA	P62136-2	5	Isoform 2 of Serine/threonine-protein phosphatase PP1-alpha catalytic subunit
371	RPL17	P18621-3	4	Isoform 3 of 60S ribosomal protein L17
372	PTRH2	Q9Y3E5	4	Peptidyl-tRNA hydrolase 2, mitochondrial
373	PSMD13	Q9UNM6-2	4	Isoform 2 of 26S proteasome non-ATPase regulatory subunit 13
374	ANXA6	P08133	4	Annexin A6
375	C6orf211	Q9H993	4	UPF0364 protein C6orf211
376	C7orf55	Q96HJ9-2	4	Isoform 2 of UPF0562 protein C7orf55
377	CPVL	Q9H3G5	4	Probable serine carboxypeptidase CPVL
378	TRA2B	P62995	4	Transformer-2 protein homolog beta
379	TPM3	J3KN67	4	Tropomyosin alpha-3 chain
380	TPP1	O14773	4	Tripeptidyl-peptidase 1
381	C21orf33	P30042	4	ES1 protein homolog, mitochondrial
382	ABHD10	Q9NUJ1	4	Mycophenolic acid acyl-glucuronide esterase, mitochondrial
383	AIFM1	O95831	4	Apoptosis-inducing factor 1, mitochondrial
384	COX5B	P10606	4	Cytochrome c oxidase subunit 5B, mitochondrial
385	UBE2O	Q9C0C9	4	Ubiquitin-conjugating enzyme E2 O
386	PSMA3	P25788	4	Proteasome subunit alpha type-3
387	SNRNP70	P08621	4	U1 small nuclear ribonucleoprotein 70 kDa
388	NPEPPS	P55786	4	Puromycin-sensitive aminopeptidase
389	LETM1	O95202	4	LETM1 and EF-hand domain-containing protein 1, mitochondrial
390	ZNF259	O75312	4	Zinc finger protein ZPR1
391	MRPL14	Q6P1L8	4	39S ribosomal protein L14, mitochondrial
392	GLUD1	P00367	4	Glutamate dehydrogenase 1, mitochondrial
393	OCLN	Q16625	4	Occludin
394	NDUFAF4	Q9P032	4	NADH dehydrogenase [ubiquinone] 1 alpha subcomplex assembly factor 4
395	PPM1G	O15355	4	Protein phosphatase 1G
396	GOT2	P00505	4	Aspartate aminotransferase, mitochondrial
397	ATAD3A	Q9NVI7-2	4	Isoform 2 of ATPase family AAA domain-containing protein 3A
398	RPLP1	P05386	4	60S acidic ribosomal protein P1
399	RPL11	P62913	4	60S ribosomal protein L11
400	RPLP0	P05388	4	60S acidic ribosomal protein P0
401	RPS17L	P0CW22	4	40S ribosomal protein S17-like
402	SDHB	P21912	4	Succinate dehydrogenase [ubiquinone] iron-sulfur subunit, mitochondrial
403	ST13	P50502	4	Hsc70-interacting protein
404	NOP14	P78316	4	Nucleolar protein 14
405	SON	P18583-9	4	Isoform I of Protein SON
406	LONP1	P36776	4	Lon protease homolog, mitochondrial
407	RAB1A	P62820	4	Ras-related protein Rab-1A
408	DAZAP1	Q96EP5	4	DAZ-associated protein 1
409	XRCC6	P12956	4	X-ray repair cross-complementing protein 6
410	HNRNPA0	Q13151	4	Heterogeneous nuclear ribonucleoprotein A0
411	ABCF1	Q8NE71	4	ATP-binding cassette sub-family F member 1
412	HNRNPD	Q14103	4	Heterogeneous nuclear ribonucleoprotein D0
413	NSUN2	Q08J23	4	tRNA (cytosine(34)-C(5))-methyltransferase
414	DARS2	Q6PI48	4	Aspartate--tRNA ligase, mitochondrial
415	NDUFS2	O75306	4	NADH dehydrogenase [ubiquinone] iron-sulfur protein 2, mitochondrial
416	NDUFA4	O00483	4	NADH dehydrogenase [ubiquinone] 1 alpha subcomplex subunit 4
417	PRPF19	Q9UMS4	4	Pre-mRNA-processing factor 19

418	SEC31A	O94979-8	4	Isoform 8 of Protein transport protein Sec31A
419	SEC63	Q9UGP8	4	Translocation protein SEC63 homolog
420	SLC25A1	P53007	4	Tricarboxylate transport protein, mitochondrial
421	PRDX2	P32119	4	Peroxiredoxin-2
422	TOMM40	O96008	4	Mitochondrial import receptor subunit TOM40 homolog
423	NDUFV2	P19404	4	NADH dehydrogenase [ubiquinone] flavoprotein 2, mitochondrial
424	LCP1	P13796	4	Plastin-2
425	SLC25A13	Q9UJS0-2	4	Isoform 2 of Calcium-binding mitochondrial carrier protein Aralar2
426	SLC25A3	Q00325	4	Phosphate carrier protein, mitochondrial
427	SDAD1	Q9NVU7	4	Protein SDA1 homolog
428	PES1	O00541	4	Pescadillo homolog
429	ATXN10	Q9UBB4	4	Ataxin-10
430	EIF3K	Q9UBQ5	4	Eukaryotic translation initiation factor 3 subunit K
431	RPL7	P18124	4	60S ribosomal protein L7
432	DDX17	Q92841	4	Probable ATP-dependent RNA helicase DDX17
433	SNRNP40	Q96DI7	4	U5 small nuclear ribonucleoprotein 40 kDa protein
434	NUP98	P52948	4	Nuclear pore complex protein Nup98-Nup96
435	SFPQ	P23246	4	Splicing factor, proline- and glutamine-rich
436	NOP58	Q9Y2X3	4	Nucleolar protein 58
437	PGM3	O95394-4	4	Isoform 3 of Phosphoacetylglucosamine mutase
438	ANXA7	P20073	4	Annexin A7
439	EIF4A3	P38919	4	Eukaryotic initiation factor 4A-III
440	NOL11	Q9H8H0	4	Nucleolar protein 11
441	IPO4	Q8TEX9-2	4	Isoform 2 of Importin-4
442	ACAA1	P09110	4	3-ketoacyl-CoA thiolase, peroxisomal
443	RPL24	P83731	4	60S ribosomal protein L24
444	VCL	P18206	4	Vinculin
445	DDX5	P17844	4	Probable ATP-dependent RNA helicase DDX5
446	GLRX3	O76003	4	Glutaredoxin-3
447	EIF2S3	P41091	4	Eukaryotic translation initiation factor 2 subunit 3
448	PCYOX1	Q9UHG3	4	Prenylcysteine oxidase 1
449	NAMPT	P43490	4	Nicotinamide phosphoribosyltransferase
450	RPL7A	P62424	4	60S ribosomal protein L7a
451	DDX27	Q96GQ7	4	Probable ATP-dependent RNA helicase DDX27
452	DHX30	Q7L2E3-2	4	Isoform 2 of Putative ATP-dependent RNA helicase DHX30
453	ESYT2	A0FGR8-6	4	Isoform 6 of Extended synaptotagmin-2
454	COX4I1	P13073	3	Cytochrome c oxidase subunit 4 isoform 1, mitochondrial
455	HADH	Q16836-2	3	Isoform 2 of Hydroxyacyl-coenzyme A dehydrogenase, mitochondrial
456	NEFM	P07197	3	Neurofilament medium polypeptide
457	MRPS27	Q92552	3	28S ribosomal protein S27, mitochondrial
458	MRPL21	Q7Z2W9	3	39S ribosomal protein L21, mitochondrial
459	NDUFAB1	O14561	3	Acyl carrier protein, mitochondrial
460	RPS27A	P62979	3	Ubiquitin-40S ribosomal protein S27a
461	RALY	Q9UKM9	3	RNA-binding protein Raly
462	GTF2F1	P35269	3	General transcription factor IIF subunit 1
463	CS	O75390	3	Citrate synthase, mitochondrial
464	TCOF1	Q13428-4	3	Isoform 4 of Treacle protein
465	MRPL37	Q9BZE1	3	39S ribosomal protein L37, mitochondrial
466	TIMM44	O43615	3	Mitochondrial import inner membrane translocase subunit TIM44
467	NAP1L4	Q99733	3	Nucleosome assembly protein 1-like 4
468	MRPS9	P82933	3	28S ribosomal protein S9, mitochondrial
469	OXCT1	P55809	3	Succinyl-CoA:3-ketoacid coenzyme A transferase 1, mitochondrial
470	IDH3A	P50213	3	Isocitrate dehydrogenase [NAD] subunit alpha, mitochondrial
471	NDUFS1	P28331-2	3	Isoform 2 of NADH-ubiquinone oxidoreductase 75 kDa subunit, mitochondrial

472	MRPS14	O60783	3	28S ribosomal protein S14, mitochondrial
473	RPL22	P35268	3	60S ribosomal protein L22
474	MTPAP	Q9NVV4-2	3	Isoform 2 of Poly(A) RNA polymerase, mitochondrial
475	NDUFS3	O75489	3	NADH dehydrogenase [ubiquinone] iron-sulfur protein 3, mitochondrial
476	RPS11	P62280	3	40S ribosomal protein S11
477	HNRNPDL	O14979	3	Heterogeneous nuclear ribonucleoprotein D-like
478	RPL9	P32969	3	60S ribosomal protein L9
479	FMR1	Q06787	3	Fragile X mental retardation protein 1
480	RPS25	P62851	3	40S ribosomal protein S25
481	PRDX6	P30041	3	Peroxiredoxin-6
482	RBM39	Q14498	3	RNA-binding protein 39
483	CPT2	P23786	3	Carnitine O-palmitoyltransferase 2, mitochondrial
484	VDAC1	P21796	3	Voltage-dependent anion-selective channel protein 1
485	ME2	P23368	3	NAD-dependent malic enzyme, mitochondrial
486	TSFM	P43897	3	Elongation factor Ts, mitochondrial
487	STK24	Q9Y6E0	3	Serine/threonine-protein kinase 24
488	ERP29	P30040	3	Endoplasmic reticulum resident protein 29
489	EEF1B2	P24534	3	Elongation factor 1-beta
490	NDUFA9	Q16795	3	NADH dehydrogenase [ubiquinone] 1 alpha subcomplex subunit 9, mitochondrial
491	PPAN	Q9NQ55-3	3	Isoform 3 of Suppressor of SWI4 1 homolog
492	ALDH5A1	P51649-2	3	Isoform 2 of Succinate-semialdehyde dehydrogenase, mitochondrial
493	AASS	Q9UDR5	3	Alpha-aminoadipic semialdehyde synthase, mitochondrial
494	EXOSC9	Q06265-2	3	Isoform 2 of Exosome complex component RRP45
495	POR	P16435	3	NADPH--cytochrome P450 reductase
496	FBL	P22087	3	rRNA 2'-O-methyltransferase fibrillarin
497	RPS6	P62753	3	40S ribosomal protein S6
498	RAP1A	P62834	3	Ras-related protein Rap-1A
499	PSMA1	P25786-2	3	Isoform Long of Proteasome subunit alpha type-1
500	MTCH2	Q9Y6C9	3	Mitochondrial carrier homolog 2
501	MYL6	P60660-2	3	Isoform Smooth muscle of Myosin light polypeptide 6
502	ATP5G2	Q06055-2	3	Isoform 2 of ATP synthase F(0) complex subunit C2, mitochondrial
503	RPS23	P62266	3	40S ribosomal protein S23
504	STUB1	Q9UNE7	3	E3 ubiquitin-protein ligase CHIP
505	CAPZA2	P47755	3	F-actin-capping protein subunit alpha-2
506	TOP2B	Q02880	3	DNA topoisomerase 2-beta
507	SPAG9	O60271	3	C-Jun-amino-terminal kinase-interacting protein 4
508	RPS20	P60866-2	3	Isoform 2 of 40S ribosomal protein S20
509	SAR1B	Q9Y6B6	3	GTP-binding protein SAR1b
510	PGAM1	P18669	3	Phosphoglycerate mutase 1
511	CRYZ	Q08257	3	Quinone oxidoreductase
512	SAE1	Q9UBE0	3	SUMO-activating enzyme subunit 1
513	SAFB	Q15424-3	3	Isoform 3 of Scaffold attachment factor B1
514	COX7C	P15954	3	Cytochrome c oxidase subunit 7C, mitochondrial
515	HSPA1A	P08107	3	Heat shock 70 kDa protein 1A/1B
516	USP7	Q93009	3	Ubiquitin carboxyl-terminal hydrolase 7
517	UTP15	Q8TED0	3	U3 small nucleolar RNA-associated protein 15 homolog
518	PMPCA	Q10713	3	Mitochondrial-processing peptidase subunit alpha
519	EEF1G	P26641	3	Elongation factor 1-gamma
520	MDH1	P40925-3	3	Isoform 3 of Malate dehydrogenase, cytoplasmic
521	HSD17B12	Q53GQ0	3	Estradiol 17-beta-dehydrogenase 12
522	RPS26	P62854	3	40S ribosomal protein S26
523	USP5	P45974	3	Ubiquitin carboxyl-terminal hydrolase 5
524	RPS4X	P62701	3	40S ribosomal protein S4, X isoform
525	UPF1	Q92900	3	Regulator of nonsense transcripts 1

526	ACAT2	Q9BWD1	3	Acetyl-CoA acetyltransferase, cytosolic
527	CSRP2	Q16527	3	Cysteine and glycine-rich protein 2
528	USP39	Q53GS9	3	U4/U6.U5 tri-snRNP-associated protein 2
529	COX7A2	P14406	2	Cytochrome c oxidase subunit 7A2, mitochondrial
530	PDHB	P11177	2	Pyruvate dehydrogenase E1 component subunit beta, mitochondrial
531	TAF15	Q92804	2	TATA-binding protein-associated factor 2N
532	SRSF6	Q13247	2	Serine/arginine-rich splicing factor 6
533	RNPS1	Q15287	2	RNA-binding protein with serine-rich domain 1
534	PRDX3	P30048	2	Thioredoxin-dependent peroxide reductase, mitochondrial
535	OAT	P04181	2	Ornithine aminotransferase, mitochondrial
536	DLD	P09622	2	Dihydrolipoyl dehydrogenase, mitochondrial
537	PPA2	Q9H2U2-2	2	Isoform 2 of Inorganic pyrophosphatase 2, mitochondrial
538	ANP32B	Q92688	2	Acidic leucine-rich nuclear phosphoprotein 32 family member B
539	ATPIF1	Q9UII2	2	ATPase inhibitor, mitochondrial
540	GFM1	Q96RP9-2	2	Isoform 2 of Elongation factor G, mitochondrial
541	IARS2	Q9NSE4	2	Isoleucine--tRNA ligase, mitochondrial
542	ACIN1	Q9UKV3	2	Apoptotic chromatin condensation inducer in the nucleus
543	EWSR1	Q01844-5	2	Isoform 5 of RNA-binding protein EWS
544	MRPL44	Q9H9J2	2	39S ribosomal protein L44, mitochondrial
545	IMMT	Q16891	2	Mitochondrial inner membrane protein
546	SUCLG1	P53597	2	Succinyl-CoA ligase [ADP/GDP-forming] subunit alpha, mitochondrial
547	DNAJA3	Q96EY1	2	DnaJ homolog subfamily A member 3, mitochondrial
548	GRPEL1	Q9HAV7	2	GrpE protein homolog 1, mitochondrial
549	RPL23A	P62750	2	60S ribosomal protein L23a
550	HIST1H1D	P16402	2	Histone H1.3
551	PDHA1	P08559-4	2	Isoform 4 of Pyruvate dehydrogenase E1 component subunit alpha, somatic form, mitochondrial
552	TMED10	P49755	2	Transmembrane emp24 domain-containing protein 10
553	LTV1	Q96GA3	2	Protein LTV1 homolog
554	NDUFV1	P49821	2	NADH dehydrogenase [ubiquinone] flavoprotein 1, mitochondrial
555	ACTR1A	P61163	2	Alpha-centractin
556	PCBP1	Q15365	2	Poly(rC)-binding protein 1
557	SF3A3	Q12874	2	Splicing factor 3A subunit 3
558	FASTKD2	Q9NYY8	2	FAST kinase domain-containing protein 2
559	EIF3G	O75821	2	Eukaryotic translation initiation factor 3 subunit G
560	PSMC5	P62195	2	26S protease regulatory subunit 8
561	NRD1	O43847-2	2	Isoform 2 of Nardilysin
562	ACADM	P11310-2	2	Isoform 2 of Medium-chain specific acyl-CoA dehydrogenase, mitochondrial
563	NOC2L	Q9Y3T9	2	Nucleolar complex protein 2 homolog
564	RCOR3	Q9P2K3-3	2	Isoform 3 of REST corepressor 3
565	GTPBP10	A4D1E9	2	GTP-binding protein 10
566	CDC37	Q16543	2	Hsp90 co-chaperone Cdc37
567	RPL5	P46777	2	60S ribosomal protein L5
568	RPS14	P62263	2	40S ribosomal protein S14
569	PCMT1	P22061-2	2	Isoform 2 of Protein-L-isoaspartate(D-aspartate) O-methyltransferase
570	SMU1	Q2TAY7	2	WD40 repeat-containing protein SMU1
571	SF3B2	Q13435	2	Splicing factor 3B subunit 2
572	MPST	P25325	2	3-mercaptopyruvate sulfurtransferase
573	EIF2B2	P49770	2	Translation initiation factor eIF-2B subunit beta
574	U2AF2	P26368	2	Splicing factor U2AF 65 kDa subunit
575	IGF2BP1	Q9NZI8	2	Insulin-like growth factor 2 mRNA-binding protein 1
576	EIF3L	Q9Y262	2	Eukaryotic translation initiation factor 3 subunit L
577	ALDOC	P09972	2	Fructose-bisphosphate aldolase C
578	ETF1	P62495	2	Eukaryotic peptide chain release factor subunit 1

579	HAUS4	Q9H6D7	2	HAUS augmin-like complex subunit 4
580	ALDH9A1	P49189	2	4-trimethylaminobutyraldehyde dehydrogenase
581	RPS13	P62277	2	40S ribosomal protein S13
582	ARL1	P40616	2	ADP-ribosylation factor-like protein 1
583	MYBBP1A	Q9BQG0-2	2	Isoform 2 of Myb-binding protein 1A
584	GSR	P00390	2	Glutathione reductase, mitochondrial
585	RPL34	P49207	2	60S ribosomal protein L34
586	RPL19	P84098	2	60S ribosomal protein L19
587	PSMD6	Q15008	2	26S proteasome non-ATPase regulatory subunit 6
588	CDK3	Q00526	2	Cyclin-dependent kinase 3
589	SMARCC2	Q8TAQ2	2	SWI/SNF complex subunit SMARCC2
590	NOB1	Q9ULX3	2	RNA-binding protein NOB1
591	ETFB	P38117	1	Electron transfer flavoprotein subunit beta
592	MRPL39	Q9NYK5-2	1	Isoform 2 of 39S ribosomal protein L39, mitochondrial
593	AAMP	Q13685	1	Angio-associated migratory cell protein
594	PMPCB	O75439	1	Mitochondrial-processing peptidase subunit beta
595	ADCK3	Q8NI60	1	Chaperone activity of bc1 complex-like, mitochondrial
596	ATP5A1	P25705	1	ATP synthase subunit alpha, mitochondrial
597	EARS2	Q5JPH6	1	Probable glutamate--tRNA ligase, mitochondrial
598	ECHS1	P30084	1	Enoyl-CoA hydratase, mitochondrial
599	ACAT1	P24752	1	Acetyl-CoA acetyltransferase, mitochondrial
600	HIST1H3A	P68431	1	Histone H3.1
601	PRDX5	P30044	1	Peroxiredoxin-5, mitochondrial
602	SRP14	P37108	1	Signal recognition particle 14 kDa protein
603	IVD	P26440	1	Isovaleryl-CoA dehydrogenase, mitochondrial
604	IK	Q13123	1	Protein Red
605	VDAC3	Q9Y277-2	1	Isoform 2 of Voltage-dependent anion-selective channel protein 3
606	MRPL20	Q9BYC9	1	39S ribosomal protein L20, mitochondrial
607	FXR2	P51116	1	Fragile X mental retardation syndrome-related protein 2
608	TPT1	P13693	1	Translationally-controlled tumor protein
609	AARS2	Q5JTZ9	1	Alanine--tRNA ligase, mitochondrial
610	HNRNPUL2	Q1KMD3	1	Heterogeneous nuclear ribonucleoprotein U-like protein 2
611	EXOSC6	Q5RKV6	1	Exosome complex component MTR3
612	DNAJC11	Q9NVH1	1	DnaJ homolog subfamily C member 11
613	ALDH2	P05091	1	Aldehyde dehydrogenase, mitochondrial
614	POLR2A	P24928	1	DNA-directed RNA polymerase II subunit RPB1
615	SUCLA2	Q9P2R7	1	Succinyl-CoA ligase [ADP-forming] subunit beta, mitochondrial
616	UFM1	P61960-2	1	Isoform 2 of Ubiquitin-fold modifier 1
617	API5	Q9BZZ5	1	Apoptosis inhibitor 5
618	MRPS16	Q9Y3D3	1	28S ribosomal protein S16, mitochondrial
619	DDX54	Q8TDD1-2	1	Isoform 2 of ATP-dependent RNA helicase DDX54
620	TARDBP	Q13148	1	TAR DNA-binding protein 43
621	FTSJ3	Q8IY81	1	pre-rRNA processing protein FTSJ3
622	DDB1	Q16531	1	DNA damage-binding protein 1
623	KPNA3	O00505	1	Importin subunit alpha-4
624	TALDO1	P37837	1	Transaldolase
625	DDX42	Q86XP3	1	ATP-dependent RNA helicase DDX42
626	THOP1	P52888	1	Thimet oligopeptidase
627	LRRC47	Q8N1G4	1	Leucine-rich repeat-containing protein 47
628	HNRNPCL1	O60812	0	Heterogeneous nuclear ribonucleoprotein C-like 1
629	STOML2	Q9UJZ1	0	Stomatin-like protein 2, mitochondrial
630	HP1BP3	Q5SSJ5	0	Heterochromatin protein 1-binding protein 3
631	SF3A1	Q15459	0	Splicing factor 3A subunit 1
632	HIST1H4A	P62805	0	Histone H4

633	PITRM1	Q5JRX3-2	0	Isoform 2 of Presequence protease, mitochondrial
634	MTPN	P58546	0	Myotrophin
635	IDH3B	O43837	0	Isocitrate dehydrogenase [NAD] subunit beta, mitochondrial
636	DLST	P36957	0	Dihydrolipoyllysine-residue succinyltransferase component of 2-oxoglutarate dehydrogenase complex, mitochondrial
637	MRPS5	P82675	0	28S ribosomal protein S5, mitochondrial
638	RPS12	P25398	0	40S ribosomal protein S12
639	ACO2	Q99798	0	Aconitate hydratase, mitochondrial
640	PSMA8	Q8TAA3	0	Proteasome subunit alpha type-7-like
641	CKB	P12277	0	Creatine kinase B-type
642	SRPR	P08240	0	Signal recognition particle receptor subunit alpha
643	MTA2	O94776	0	Metastasis-associated protein MTA2
644	PHF5A	Q7RTV0	0	PHD finger-like domain-containing protein 5A
645	HCFC1	P51610-4	0	Isoform 4 of Host cell factor 1
646	POLDIP3	Q9BY77	0	Polymerase delta-interacting protein 3
647	RNH1	P13489	0	Ribonuclease inhibitor
648	MT-ND4	P03905	No data	NADH-ubiquinone oxidoreductase chain 4
649	U2SURP	O15042	No matches	U2 snRNP-associated SURP motif-containing protein
650	TUBB4B	P68371	No matches	Tubulin beta-4B chain
651	PSMD14	O00487	No matches	26S proteasome non-ATPase regulatory subunit 14
652	CCAR2	Q8N163-2	No macthes	Isoform 2 of Cell cycle and apoptosis regulator protein 2
653	SRSF8	Q9BRL6	No data	Serine/arginine-rich splicing factor 8
654	SRSF7	Q16629	No data	Serine/arginine-rich splicing factor 7
655	SRSF5	Q13243	No data	Serine/arginine-rich splicing factor 5
656	HIST2H2BC	Q6DN03	No data	Putative histone H2B type 2-C
657	NADK2	Q4G0N4	No data	NAD kinase 2, mitochondrial
658	SRSF3	P84103	No data	Serine/arginine-rich splicing factor 3
659	HDGFRP2	Q7Z4V5	No data	Hepatoma-derived growth factor-related protein 2
660	FLJ35645	Q8NAB5	No data	Putative uncharacterized protein FLJ35645 PE
661	SRSF1	Q07955-2	No data	Isoform ASF-2 of Serine/arginine-rich splicing factor 1
662	SRSF4	Q08170	No data	Serine/arginine-rich splicing factor 4
663	TRMT10C	Q7L0Y3	No data	Mitochondrial ribonuclease P protein 1
664	SRSF9	Q13242	No data	Serine/arginine-rich splicing factor 9
665	SRSF11	Q05519	No data	Serine/arginine-rich splicing factor 11
666	ABCB7	O75027-2	No data	Isoform 2 of ATP-binding cassette sub-family B member 7, mitochondrial
667	UQCRFS1P1	P0C7P4	No data	Putative cytochrome b-c1 complex subunit Rieske-like protein 1
668	TMA16	Q96EY4	No data	Translation machinery-associated protein 16
669	ECI1	P42126	No data	Enoyl-CoA delta isomerase 1, mitochondrial
670	ZNF326	Q5BKZ1	No data	DBIRD complex subunit ZNF326
671	MT-CO2	P00403	No data	Cytochrome c oxidase subunit 2
672	MICU2	Q8IYU8	No data	Calcium uptake protein 2, mitochondrial
673	CTPS1	P17812	No data	CTP synthase 1
674	EEF1A1P5	Q5VTE0	No data	Putative elongation factor 1-alpha-like 3

Table A9. The list of 250 proteins among our 674 high-confidence protein hits that were identified as DrugBank targets on the UniProt database. This list was used to generate the pie chart on Figure 4.11b.

S. No.	UniProt ID	Protein description	Accesion number of the associated drug(s) on DrugBank database
1	Q07021	Complement component 1 Q subcomponent-binding protein, mitochondrial or p32	DB09130 DB08818
2	Q14978	Nucleolar and coiled-body phosphoprotein 1	DB00997
3	P0DP23	Calmodulin-1	DB08039 DB01429 DB01244 DB01373 DB11093 DB13800 DB11348 DB14481 DB00477 DB00527 DB02868 DB01023 DB04841 DB00623 DB00753 DB00836 DB01065 DB08231 DB04513 DB00622 DB01115 DB00850 DB00925 DB01100 DB04825 DB01069 DB03900 DB00831 DB03977
4	P0DP24	Calmodulin-2	DB11093 DB11348 DB14481
5	P0DP25	Calmodulin-3	DB11093 DB11348 DB14481
6	P61604	10 kDa heat shock protein, mitochondrial	DB12695
7	P11177	Pyruvate dehydrogenase E1 component subunit beta, mitochondrial	DB00157 DB00119
8	P13073	Cytochrome c oxidase subunit 4 isoform 1, mitochondrial	DB02659 DB04464
9	Q16836	Hydroxyacyl-coenzyme A dehydrogenase, mitochondrial	DB03612 DB03059 DB00157 DB09568
10	P13995	Bifunctional methylenetetrahydrofolate dehydrogenase/cyclohydrolase, mitochondrial [Includes: NAD-dependent methylenetetrahydrofolate dehydrogenase]	DB00157 DB00116
11	P10809	60 kDa heat shock protein, mitochondrial	DB09130
12	P06748	Nucleophosmin	DB11638
13	P27797	Calreticulin	DB00025 DB11093 DB11348 DB14481 DB09130 DB13949 DB06245 DB13998 DB01065 DB13999 DB00031 DB14520
14	P22695	Cytochrome b-c1 complex subunit 2, mitochondrial	DB07763 DB07778 DB04141 DB08453 DB04799 DB07401 DB08330 DB08690
15	Q9NYK5	39S ribosomal protein L39, mitochondrial	
16	P04181	Ornithine aminotransferase, mitochondrial	DB02821 DB02054 DB00129 DB00114
17	P08670	Vimentin	DB11638 DB12695
18	P09622	Dihydrolipoyl dehydrogenase, mitochondrial	DB03147 DB00145 DB00157
19	P67936	Tropomyosin alpha-4 chain	DB12695
20	P20674	Cytochrome c oxidase subunit 5A, mitochondrial	DB02659 DB04464
21	P06576	ATP synthase subunit beta, mitochondrial	DB07384 DB07394 DB08949 DB08629 DB12695 DB08399 DB04216
22	Q99623	Prohibitin-2	DB06774 DB15496 DB15495
23	O14561	Acyl carrier protein, mitochondrial	DB00157
24	Q7Z4V5	Hepatoma-derived growth factor-related protein 2	
25	P24666	Low molecular weight phosphotyrosine protein phosphatase	DB04214 DB00173
26	Q07955	Serine/arginine-rich splicing factor 1	DB09130
27	Q5SSJ5	Heterochromatin protein 1-binding protein 3	DB11638

28	Q8NI60	Atypical kinase COQ8A, mitochondrial	DB12010
29	P36542	ATP synthase subunit gamma, mitochondrial	DB07384 DB07394 DB08629 DB08399 DB04216
30	O95831	Apoptosis-inducing factor 1, mitochondrial	DB03147 DB05282
31	O75390	Citrate synthase, mitochondrial	DB03182 DB04272 DB01992 DB03499 DB04230 DB02637 DB01969
32	P27824	Calnexin	DB00025 DB11093 DB11348 DB14481 DB06245 DB13998 DB13999 DB00031
33	Q08170	Serine/arginine-rich splicing factor 4	DB11638
34	P10515	Dihydrolipoyllysine-residue acetyltransferase component of pyruvate dehydrogenase complex, mitochondrial	DB03760 DB00157 DB03758
35	P10606	Cytochrome c oxidase subunit 5B, mitochondrial	DB02659 DB04464
36	Q9Y266	Nuclear migration protein nudC	DB12695
37	P62805	Histone H4	
38	O94925	Glutaminase kidney isoform, mitochondrial	DB13155 DB00142 DB09374 DB00130
39	P25705	ATP synthase subunit alpha, mitochondrial	DB07384 DB11638 DB07394 DB08629 DB08399 DB04216
40	P25788	Proteasome subunit alpha type-3	DB08515 DB12695
41	P09429	High mobility group protein B1	DB00608 DB05869
42	Q5JPH6	Probable glutamate--tRNA ligase, mitochondrial	DB00142
43	P49411	Elongation factor Tu, mitochondrial	DB04315 DB01593 DB14487 DB14533 DB14548
44	P45973	Chromobox protein homolog 5	DB09130
45	P30084	Enoyl-CoA hydratase, mitochondrial	DB04117 DB03059 DB02563 DB02910 DB09568
46	P55809	Succinyl-CoA:3-ketoacid coenzyme A transferase 1, mitochondrial	DB02731 DB00139
47	P50213	Isocitrate dehydrogenase [NAD] subunit alpha, mitochondrial	DB09130 DB06757 DB00157 DB09092
48	Q9NSE4	Isoleucine--tRNA ligase, mitochondrial	DB00167
49	P28331	NADH-ubiquinone oxidoreductase 75 kDa subunit, mitochondrial	DB00157
50	P24752	Acetyl-CoA acetyltransferase, mitochondrial	DB09061 DB14009 DB14011 DB00795
51	P68431	Histone H3.1	
52	P30044	Peroxiredoxin-5, mitochondrial	DB00995 DB03608 DB09221
53	P53597	Succinate--CoA ligase [ADP/GDP-forming] subunit alpha, mitochondrial	DB00787
54	P14625	Endoplasmin	DB08465 DB02103 DB09130 DB02935 DB02424 DB08464 DB03719 DB03758 DB00615
55	P55786	Puromycin-sensitive aminopeptidase	DB11638 DB11781
56	P30405	Peptidyl-prolyl cis-trans isomerase F, mitochondrial	DB08168 DB00091 DB00172 DB02078
57	P08865	40S ribosomal protein SA	DB09130 DB04985
58	P40926	Malate dehydrogenase, mitochondrial	DB04272 DB00157 DB09092
59	P43487	Ran-specific GTPase-activating protein	DB09130 DB12695
60	P42126	Enoyl-CoA delta isomerase 1, mitochondrial	DB03127 DB02910
61	P35232	Prohibitin	DB15496 DB15495

62	P23528	Cofilin-1	DB11638 DB09130 DB04147
63	P31930	Cytochrome b-c1 complex subunit 1, mitochondrial	DB07763 DB07778 DB04141 DB08453 DB04799 DB07401 DB08330 DB04741 DB08690
64	P62750	60S ribosomal protein L23a	DB02494 DB07374 DB11638 DB08437
65	P61978	Heterogeneous nuclear ribonucleoprotein K	DB11638 DB12695
66	P48735	Isocitrate dehydrogenase [NADP], mitochondrial	DB13874 DB01727
67	P31942	Heterogeneous nuclear ribonucleoprotein H3	DB09130
68	P22626	Heterogeneous nuclear ribonucleoproteins A2/B1	DB11638 DB09130
69	P08559	Pyruvate dehydrogenase E1 component subunit alpha, somatic form, mitochondrial	DB00157
70	P00367	Glutamate dehydrogenase 1, mitochondrial	DB11081 DB00142 DB04137 DB00756 DB00157
71	P30419	Glycylpeptide N-tetradecanoyltransferase 1	DB03062
72	P37108	Signal recognition particle 14 kDa protein	DB11638
73	P31040	Succinate dehydrogenase [ubiquinone] flavoprotein subunit, mitochondrial	DB04141 DB04657 DB00139 DB04795 DB09270 DB08689
74	Q99714	3-hydroxyacyl-CoA dehydrogenase type-2	DB02820 DB00157 DB09568
75	Q9P032	NADH dehydrogenase [ubiquinone] 1 alpha subcomplex assembly factor 4	
76	P00403	Cytochrome c oxidase subunit 2	DB02659 DB04464 DB05412
77	O75489	NADH dehydrogenase [ubiquinone] iron-sulfur protein 3, mitochondrial	DB00997 DB00157
78	P49821	NADH dehydrogenase [ubiquinone] flavoprotein 1, mitochondrial	DB00157
79	Q15185	Prostaglandin E synthase 3	DB00316 DB09130 DB05036
80	P11021	Endoplasmic reticulum chaperone BiP	DB00945 DB00025 DB09130 DB13998 DB13999
81	P26440	Isovaleryl-CoA dehydrogenase, mitochondrial	DB04036 DB03147
82	P32969	60S ribosomal protein L9	
83	P04179	Superoxide dismutase [Mn], mitochondrial	DB04436 DB03297 DB06796 DB09221 DB11590
84	O00264	Membrane-associated progesterone receptor component 1	DB00514 DB00540 DB01104
85	O43837	Isocitrate dehydrogenase [NAD] subunit beta, mitochondrial	DB00157
86	P08574	Cytochrome c1, heme protein, mitochondrial	DB07763 DB07778 DB04141 DB08453 DB07636 DB04799 DB07401 DB08330 DB08690
87	P00505	Aspartate aminotransferase, mitochondrial	DB02783 DB00128 DB00151 DB00142 DB00114
88	P30041	Peroxiredoxin-6	DB03814 DB09130
89	P62913	60S ribosomal protein L11	DB02494 DB07374 DB08437
90	Q99873	Protein arginine N-methyltransferase 1	DB01752
91	P08708	40S ribosomal protein S17	DB11638
92	P48047	ATP synthase subunit O, mitochondrial	DB11638
93	P21912	Succinate dehydrogenase [ubiquinone] iron-sulfur subunit, mitochondrial	DB04141 DB08689
94	P23786	Carnitine O-palmitoyltransferase 2, mitochondrial	DB00583 DB01074
95	P11387	DNA topoisomerase 1	DB07354 DB08159 DB05482 DB04690 DB05806 DB04882 DB05129 DB11254 DB00762 DB04967 DB06159 DB12893 DB05630 DB01030 DB14962 DB06069

96	P27348	14-3-3 protein theta	DB12695
97	Q9Y277	Voltage-dependent anion-selective channel protein 3	DB01375 DB06098
98	Q12874	Splicing factor 3A subunit 3	DB12695
99	P45880	Voltage-dependent anion-selective channel protein 2	DB01375 DB06098
100	P50579	Methionine aminopeptidase 2	DB03396 DB04108 DB07322 DB07323 DB02310 DB07746 DB07309 DB07313 DB02893 DB02640 DB00134 DB07377 DB03086 DB01422 DB04324 DB05864 DB03900 DB08633
101	P21796	Voltage-dependent anion-selective channel protein 1	DB01375 DB09061 DB14009 DB14011
102	P32322	Pyrroline-5-carboxylate reductase 1, mitochondrial	DB00157 DB00172
103	P18583	Protein SON	
104	P23368	NAD-dependent malic enzyme, mitochondrial	DB03499 DB01677 DB03589 DB00157 DB03680
105	P05141	ADP/ATP translocase 2	DB00720 DB01077
106	P23284	Peptidyl-prolyl cis-trans isomerase B	DB04447 DB00172
107	P11310	Medium-chain specific acyl-CoA dehydrogenase, mitochondrial	DB03415 DB03147 DB02910
108	P07355	Annexin A2	DB11638 DB00591 DB06245 DB00031
109	P08758	Annexin A5	DB03981 DB03935 DB09130 DB00591 DB02929 DB02497 DB02846 DB03959 DB03484
110	P13693	Translationally-controlled tumor protein	DB11093 DB11348 DB14481
111	Q13838	Spliceosome RNA helicase DDX39B	DB11638
112	P07237	Protein disulfide-isomerase	DB11638 DB09130 DB03615 DB01593 DB14487 DB14533 DB14548
113	P60903	Protein S100-A10	DB12695
114	P62826	GTP-binding nuclear protein Ran	DB04315
115	Q5JTZ9	Alanine--tRNA ligase, mitochondrial	DB00160
116	Q9Y6E0	Serine/threonine-protein kinase 24	DB12010
117	Q16555	Dihydropyrimidinase-related protein 2	DB11638
118	P52597	Heterogeneous nuclear ribonucleoprotein F	DB12695
119	Q12797	Aspartyl/asparaginyl beta-hydroxylase	DB00128 DB00139
120	P63104	14-3-3 protein zeta/delta	DB12695
121	Q16795	NADH dehydrogenase [ubiquinone] 1 alpha subcomplex subunit 9, mitochondrial	DB03147 DB00157
122	P07737	Profilin-1	DB07908 DB11638
123	P62258	14-3-3 protein epsilon	DB01780 DB12695
124	P51649	Succinate-semialdehyde dehydrogenase, mitochondrial	DB00534 DB00157 DB09072 DB00139 DB00313
125	P28838	Cytosol aminopeptidase	DB07448 DB02386 DB08766
126	Q9UDR5	Alpha-aminoadipic semialdehyde synthase, mitochondrial	DB00142 DB04207 DB00157 DB02338
127	P16435	NADPH--cytochrome P450 reductase	DB06263 DB00865 DB00694 DB00997 DB01466 DB03147 DB03247 DB09332 DB00166 DB00305 DB03461 DB00665 DB00698
128	P50914	60S ribosomal protein L14	DB11638

129	P25789	Proteasome subunit alpha type-4	DB08515
130	P31943	Heterogeneous nuclear ribonucleoprotein H	DB09130
131	Q14103	Heterogeneous nuclear ribonucleoprotein D0	DB11638
132	P33316	Deoxyuridine 5'-triphosphate nucleotidohydrolase, mitochondrial	DB04685 DB03413
133	Q16881	Thioredoxin reductase 1, cytoplasmic	DB01169 DB00126 DB03147 DB04106 DB05428 DB02338 DB05448 DB11127 DB11135 DB03566
134	P15880	40S ribosomal protein S2	DB09130
135	P12236	ADP/ATP translocase 3	DB00720 DB01077
136	Q99798	Aconitate hydratase, mitochondrial	DB03964 DB04351 DB04072 DB01727 DB04562
137	P30101	Protein disulfide-isomerase A3	DB09130 DB01593 DB14487 DB14533 DB14548
138	Q6PI48	Aspartate--tRNA ligase, mitochondrial	DB00128
139	P11388	DNA topoisomerase 2-alpha	DB05706 DB06013 DB05022 DB06263 DB00276 DB06420 DB04975 DB06362 DB00537 DB00970 DB00694 DB06421 DB00380 DB00997 DB05129 DB00467 DB00445 DB00773 DB09047 DB04576 DB01645 DB01177 DB00978 DB04967 DB01204 DB00218 DB01059 DB01165 DB00487 DB01179 DB05920 DB04978 DB01208 DB00444 DB00685 DB00385 DB06042
140	O75306	NADH dehydrogenase [ubiquinone] iron-sulfur protein 2, mitochondrial	DB00997 DB00157
141	O00483	Cytochrome c oxidase subunit NDUFA4	DB00157
142	P31949	Protein S100-A11	DB02482
143	P62753	40S ribosomal protein S6	DB11638
144	P56537	Eukaryotic translation initiation factor 6	DB09130
145	Q99497	Parkinson disease protein 7	DB09130
146	P25786	Proteasome subunit alpha type-1	DB08515
147	P62316	Small nuclear ribonucleoprotein Sm D2	DB11638
148	Q9UBM7	7-dehydrocholesterol reductase	DB00157
149	P22061	Protein-L-isoaspartate	DB01752
150	Q13423	NAD	DB01763 DB00157 DB03461 DB09092
151	P60953	Cell division control protein 42 homolog	DB02623 DB04315
152	Q92945	Far upstream element-binding protein 2	DB11638 DB02709
153	P41250	Glycine--tRNA ligase	DB00145
154	Q9Y230	RuvB-like 2	DB04216
155	P49721	Proteasome subunit beta type-2	DB08515 DB08889
156	P53007	Tricarboxylate transport protein, mitochondrial	DB09154
157	P05091	Aldehyde dehydrogenase, mitochondrial	DB01612 DB06770 DB04381 DB02115 DB00822 DB00536 DB00157 DB00435 DB00727 DB09117 DB06154
158	P32119	Peroxiredoxin-2	DB02153 DB09130 DB04048
159	P12004	Proliferating cell nuclear antigen	DB00945 DB00279
160	P40939	Trifunctional enzyme subunit alpha, mitochondrial	DB00157

161	P19404	NADH dehydrogenase [ubiquinone] flavoprotein 2, mitochondrial	DB00157
162	P07686	Beta-hexosaminidase subunit beta	DB03861 DB02813 DB09301 DB03747 DB00205
163	Q71U36	Tubulin alpha-1A chain	DB07574 DB00518 DB11638 DB15534 DB05147 DB01873 DB00643 DB03010 DB12695 DB00570
164	P51149	Ras-related protein Rab-7a	DB04315
165	Q9UJS0	Calcium-binding mitochondrial carrier protein Aralar2	DB00128
166	P60900	Proteasome subunit alpha type-6	DB08515
167	P14174	Macrophage migration inhibitory factor	DB01880 DB07888 DB08334 DB08335 DB08333 DB07718 DB08765 DB02728
168	P37802	Transgelin-2	DB11638
169	P08238	Heat shock protein HSP 90-beta	DB08293 DB08153 DB08292 DB08346 DB08465 DB08045 DB07877 DB02754 DB07594 DB02424 DB08464 DB09221 DB03758 DB06070 DB05134
170	Q9P2R7	Succinate--CoA ligase [ADP-forming] subunit beta, mitochondrial	DB00787
171	Q9BVA1	Tubulin beta-2B chain	DB07574 DB05147
172	P34932	Heat shock 70 kDa protein 4	DB12695
173	P14618	Pyruvate kinase PKM	DB07697 DB07692 DB02726 DB07628 DB00787 DB11638 DB09130 DB01733 DB00119
174	Q06830	Peroxiredoxin-1	DB11638 DB09130 DB09221 DB01593 DB14487 DB14533 DB14548
175	P11142	Heat shock cognate 71 kDa protein	DB07045 DB11638 DB09130 DB01254
176	P54886	Delta-1-pyrroline-5-carboxylate synthase	DB00142
177	Q02880	DNA topoisomerase 2-beta	DB08651 DB05022 DB06362 DB00970 DB00694 DB06421 DB00380 DB00773 DB04395 DB05488 DB06042
178	P17812	CTP synthase 1	DB00130
179	P07900	Heat shock protein HSP 90-alpha	DB07317 DB08197 DB08443 DB08557 DB08789 DB06969 DB08788 DB07324 DB02840 DB03749 DB08787 DB08786 DB07502 DB07100 DB06957 DB07601 DB08194 DB08442 DB07495 DB06964 DB06961 DB06958 DB07319 DB03137 DB03093 DB02550 DB04505 DB07877 DB04254 DB08436 DB04054 DB02359 DB03504 DB02754 DB03809 DB03899 DB12442 DB07594 DB09130 DB02424 DB06956 DB07325 DB04588 DB00716 DB09221 DB04216 DB00615 DB06070 DB05134
180	P27695	DNA-	DB04967
181	P07195	L-lactate dehydrogenase B chain	DB02401 DB11638 DB00157 DB03940 DB09118
182	P30837	Aldehyde dehydrogenase X, mitochondrial	DB00157
183	P68363	Tubulin alpha-1B chain	DB07574 DB05147 DB01873 DB03010
184	P12277	Creatine kinase B-type	DB00787 DB00148 DB13749 DB13191 DB00300
185	Q92598	Heat shock protein 105 kDa	DB12695
186	P28066	Proteasome subunit alpha type-5	DB08515
187	P00492	Hypoxanthine-guanine phosphoribosyltransferase	DB03153 DB02309 DB01632 DB04356 DB00993 DB01033 DB00352
188	Q9Y6B6	GTP-binding protein SAR1b	DB04315
189	P18669	Phosphoglycerate mutase 1	DB11638 DB09130
190	P27635	60S ribosomal protein L10	DB11638
191	Q08257	Quinone oxidoreductase	DB09061 DB00266 DB14009 DB14011 DB03461

192	P62917	60S ribosomal protein L8	DB02494 DB07374 DB08437
193	P07437	Tubulin beta chain	DB11638 DB05284 DB15534 DB01394 DB09130 DB05147 DB11731 DB01873 DB12334 DB03010 DB01179 DB06137 DB00570 DB00541 DB11641 DB00361 DB06042
194	P02786	Transferrin receptor protein 1	DB13949 DB15617 DB14490 DB14491 DB14488 DB14501 DB14489 DB13257 DB06784 DB05260 DB01592 DB14520
195	O60264	SWI/SNF-related matrix-associated actin-dependent regulator of chromatin subfamily A member 5	DB02670 DB02379
196	Q07020	60S ribosomal protein L18	DB11638
197	Q92769	Histone deacetylase 2	DB01223 DB01076 DB05015 DB01095 DB00227 DB11830 DB01303 DB06603 DB05223 DB00175 DB06176 DB00641 DB00277 DB09091 DB00313 DB02546
198	P15954	Cytochrome c oxidase subunit 7C, mitochondrial	DB02659 DB04464
199	P23246	Splicing factor, proline- and glutamine-rich	DB11638 DB09130
200	P10599	Thioredoxin	DB12695
201	P62829	60S ribosomal protein L23	DB02494 DB07374 DB08437
202	P49720	Proteasome subunit beta type-3	DB08515
203	P55072	Transitional endoplasmic reticulum ATPase	DB12695 DB04395
204	P06733	Alpha-enolase	DB11638 DB09130 DB01593 DB14487 DB14533 DB14548
205	P62241	40S ribosomal protein S8	DB11638
206	P12268	Inosine-5'-monophosphate dehydrogenase 2	DB03948 DB00993 DB04566 DB01033 DB00688 DB01024 DB00157 DB00811 DB03070 DB06103
207	Q96AE4	Far upstream element-binding protein 1	DB05786 DB12893
208	P09211	Glutathione S-transferase P	DB01834 DB03814 DB00316 DB14001 DB01008 DB04972 DB04339 DB00958 DB00291 DB02633 DB00515 DB01242 DB00363 DB11672 DB14635 DB14002 DB03619 DB11831 DB00903 DB00773 DB06246 DB05460 DB00143 DB03310 DB03003 DB13014 DB00526 DB08370 DB03686 DB04132 DB01915 DB07849 DB00197 DB00163
209	P04083	Annexin A1	DB00288 DB14669 DB01222 DB01013 DB01234 DB14649 DB00591 DB00741 DB14538 DB14539 DB14540 DB14541 DB14542 DB14543 DB14544 DB00959 DB14631
210	P63244	Receptor of activated protein C kinase 1	DB09130
211	P30086	Phosphatidylethanolamine-binding protein 1	DB09130 DB09568
212	P60174	Triosephosphate isomerase	DB04447 DB03379 DB02726 DB03132 DB07387 DB04510 DB03314 DB03135 DB11638 DB04326 DB01695 DB03026 DB03900 DB01593 DB14487 DB14533 DB14548
213	P22392	Nucleoside diphosphate kinase B	DB00787 DB00718 DB01262 DB04315 DB00709 DB14126 DB09299 DB00300
214	P04075	Fructose-bisphosphate aldolase A	DB04733 DB02512 DB11638 DB04326 DB08240 DB01593 DB14487 DB14533 DB14548
215	P49189	4-trimethylaminobutyraldehyde dehydrogenase	DB00157
216	P62277	40S ribosomal protein S13	DB11638
217	Q15758	Neutral amino acid transporter B	DB00174 DB13146 DB00130
218	P62937	Peptidyl-prolyl cis-trans isomerase A	DB01742 DB11638 DB09130 DB00091 DB02419 DB00172 DB03393
219	P40616	ADP-ribosylation factor-like protein 1	DB04315
220	Q13509	Tubulin beta-3 chain	DB05147 DB01873 DB04845 DB03010 DB12695 DB06042

221	P25787	Proteasome subunit alpha type-2	DB08515
222	P11216	Glycogen phosphorylase, brain form	DB03496 DB00114
223	P68371	Tubulin beta-4B chain	DB00518 DB05147 DB01873 DB00643 DB04910 DB03010 DB12695
224	P09110	3-ketoacyl-CoA thiolase, peroxisomal	DB09069
225	P09874	Poly [ADP-ribose] polymerase 1	DB04010 DB03509 DB03072 DB03722 DB03073 DB07787 DB07096 DB07330 DB02498 DB13877 DB02701 DB11793 DB02690 DB09074 DB12332 DB11760 DB00277 DB07232 DB01593 DB14487 DB14533 DB14548
226	P53004	Biliverdin reductase A	DB00157
227	P00390	Glutathione reductase, mitochondrial	DB07393 DB01644 DB02895 DB03867 DB02153 DB07714 DB09061 DB00262 DB09110 DB09130 DB03147 DB00143 DB03310 DB02553 DB14009 DB14011 DB00157 DB11135 DB11590
228	P40925	Malate dehydrogenase, cytoplasmic	DB11638 DB00157 DB03461
229	P22102	Trifunctional purine biosynthetic protein adenosine-3 (GART)	DB02236 DB03546 DB00642
230	P17844	Probable ATP-dependent RNA helicase DDX5	DB11638
231	P84098	60S ribosomal protein L19	DB02494 DB07374 DB08437
232	P60842	Eukaryotic initiation factor 4A-I	DB09130
233	P13639	Elongation factor 2	DB02059 DB03223 DB11823 DB04315 DB12688 DB08348
234	P41091	Eukaryotic translation initiation factor 2 subunit 3	DB04315
235	P04406	Glyceraldehyde-3-phosphate dehydrogenase	DB07347 DB02059 DB11638 DB09130 DB00157 DB03893 DB09092
236	P43490	Nicotinamide phosphoribosyltransferase	DB12731 DB05217
237	P00338	L-lactate dehydrogenase A chain	DB11638 DB09130 DB02483 DB00157 DB02701 DB03940 DB09118
238	Q9BWD1	Acetyl-CoA acetyltransferase, cytosolic	DB01992 DB01915
239	O00299	Chloride intracellular channel protein 1	DB11638 DB09130
240	P00558	Phosphoglycerate kinase 1	DB04510 DB00787 DB03909 DB11638 DB09130 DB00709
241	O15144	Actin-related protein 2/3 complex subunit 2	DB08236 DB08235
242	P22234	Multifunctional protein ADE2	DB00128
243	Q04760	Lactoylglutathione lyase	DB00143 DB00328 DB03345 DB08179 DB03330 DB03602 DB04132 DB03130
244	Q16822	Phosphoenolpyruvate carboxykinase [GTP], mitochondrial	DB00787
245	P62136	Serine/threonine-protein phosphatase PP1-alpha catalytic subunit	DB02506
246	P49589	Cysteine--tRNA ligase, cytoplasmic	DB00151
247	P54577	Tyrosine--tRNA ligase, cytoplasmic	DB08617 DB01766 DB07205 DB08371 DB02709 DB03978 DB00135
248	P34897	Serine hydroxymethyltransferase, mitochondrial	DB11638 DB00145 DB00114 DB00116
249	P03905	NADH-ubiquinone oxidoreductase chain 4	DB00157
250	P55196	Afadin	DB08574

Rights and Permissions

Rightslink® by Copyright Clearance Center https://s100.copyright.com/AppDispatchServlet

CCC RightsLink®

Home | Help | Email Support | Aditi Dixit

ACS Publications
Most Trusted. Most Cited. Most Read.

New Paradigm for Allosteric Regulation of Escherichia coli Aspartate Transcarbamoylase

Author: Gregory M. Cockrell, Yunan Zheng, Wenyue Guo, et al
Publication: Biochemistry
Publisher: American Chemical Society
Date: Nov 1, 2013

Copyright © 2013, American Chemical Society

PERMISSION/LICENSE IS GRANTED FOR YOUR ORDER AT NO CHARGE

This type of permission/license, instead of the standard Terms and Conditions, is sent to you because no fee is being charged for your order. Please note the following:

- Permission is granted for your request in both print and electronic formats, and translations.
- If figures and/or tables were requested, they may be adapted or used in part.
- Please print this page for your records and send a copy of it to your publisher/graduate school.
- Appropriate credit for the requested material should be given as follows: "Reprinted (adapted) with permission from {COMPLETE REFERENCE CITATION}. Copyright {YEAR} American Chemical Society." Insert appropriate information in place of the capitalized words.
- One-time permission is granted only for the use specified in your RightsLink request. No additional uses are granted (such as derivative works or other editions). For any uses, please submit a new request.

If credit is given to another source for the material you requested from RightsLink, permission must be obtained from that source.

BACK CLOSE WINDOW

© 2022 Copyright - All Rights Reserved | Copyright Clearance Center, Inc. | Privacy statement | Terms and Conditions
Comments? We would like to hear from you. E-mail us at customercare@copyright.com

1 of 1 3/29/2022, 12:02 PM

RightsLink Printable License https://s100.copyright.com/App/PrintableLicenseFrame.jsp?publisher...

ELSEVIER LICENSE
TERMS AND CONDITIONS

Mar 29, 2022

This Agreement between Ms. Aditi Dixit ("You") and Elsevier ("Elsevier") consists of your license details and the terms and conditions provided by Elsevier and Copyright Clearance Center.

License Number	5278051417255
License date	Mar 29, 2022
Licensed Content Publisher	Elsevier
Licensed Content Publication	Cell
Licensed Content Title	Extensive In Vivo Metabolite-Protein Interactions Revealed by Large-Scale Systematic Analyses
Licensed Content Author	Xiyan Li,Tara A. Gianoulis,Kevin Y. Yip,Mark Gerstein,Michael Snyder
Licensed Content Date	Nov 12, 2010
Licensed Content Volume	143
Licensed Content Issue	4
Licensed Content Pages	12
Start Page	639
End Page	650
Type of Use	reuse in a thesis/dissertation

1 of 7 3/29/2022, 12:00 PM

RightsLink Printable License https://s100.copyright.com/App/PrintableLicenseFrame.jsp?publisher...

Portion	figures/tables/illustrations
Number of figures/tables /illustrations	1
Format	both print and electronic
Are you the author of this Elsevier article?	No
Will you be translating?	No
Title	The Choline Metabolite-Interacting Proteome of Mammalian Cells: Discovery and Significance
Institution name	Indian Institute of Science Education and Research (IISER), Pune
Expected presentation date	May 2022
Portions	Figure 1
Requestor Location	Ms. Aditi Dixit Lab 304, AB-3, IISER Bhopal Bhopal Bypass Road, Bhauri Bhopal, Madhya Pradesh Bhopal, Madhya Pradesh 462066 India Attn: Ms. Aditi Dixit
Publisher Tax ID	GB 494 6272 12
Total	0.00 USD

Terms and Conditions

INTRODUCTION

1. The publisher for this copyrighted material is Elsevier. By clicking "accept" in connection with completing this licensing transaction, you agree that the following terms and conditions apply to this transaction (along with the Billing and Payment terms and conditions established by Copyright Clearance Center, Inc. ("CCC"), at the time that you

2 of 7 3/29/2022, 12:00 PM

RightsLink Printable License https://s100.copyright.com/App/PrintableLicenseFrame.jsp?publisher...

OXFORD UNIVERSITY PRESS LICENSE
TERMS AND CONDITIONS

Mar 29, 2022

This Agreement between Ms. Aditi Dixit ("You") and Oxford University Press ("Oxford University Press") consists of your license details and the terms and conditions provided by Oxford University Press and Copyright Clearance Center.

License Number	5278060320294
License date	Mar 29, 2022
Licensed content publisher	Oxford University Press
Licensed content publication	Journal of Experimental Botany
Licensed content title	Emerging strategies for the identification of protein–metabolite interactions
Licensed content author	Luzarowski, Marcin; Skirycz, Aleksandra
Licensed content date	May 14, 2019
Type of Use	Thesis/Dissertation
Institution name	
Title of your work	The Choline Metabolite-Interacting Proteome of Mammalian Cells: Discovery and Significance
Publisher of your work	Indian Institute of Science Education and Research (IISER), Pune
Expected publication date	May 2022

1 of 4 3/29/2022, 12:07 PM

RightsLink Printable License https://s100.copyright.com/App/PrintableLicenseFrame.jsp?publisher...

Permissions cost	0.00 USD
Value added tax	0.00 USD
Total	0.00 USD
Title	The Choline Metabolite-Interacting Proteome of Mammalian Cells: Discovery and Significance
Institution name	Indian Institute of Science Education and Research (IISER), Pune
Expected presentation date	May 2022
Portions	Figure 5
Requestor Location	Ms. Aditi Dixit Lab 304, AB-3, IISER Bhopal Bhopal Bypass Road, Bhauri Bhopal, Madhya Pradesh Bhopal, Madhya Pradesh 462066 India Attn: Ms. Aditi Dixit
Publisher Tax ID	GB125506730
Total	0.00 USD

Terms and Conditions

STANDARD TERMS AND CONDITIONS FOR REPRODUCTION OF MATERIAL FROM AN OXFORD UNIVERSITY PRESS JOURNAL

1. Use of the material is restricted to the type of use specified in your order details.

2. This permission covers the use of the material in the English language in the following territory: world. If you have requested additional permission to translate this material, the terms and conditions of this reuse will be set out in clause 12.

3. This permission is limited to the particular use authorized in (1) above and does not allow you to sanction its use elsewhere in any other format other than specified above, nor does it apply to quotations, images, artistic works etc that have been reproduced from other sources

2 of 4 3/29/2022, 12:07 PM

RightsLink Printable License https://s100.copyright.com/App/PrintableLicenseFrame.jsp?publisher...

ELSEVIER LICENSE
TERMS AND CONDITIONS

Mar 29, 2022

This Agreement between Ms. Aditi Dixit ("You") and Elsevier ("Elsevier") consists of your license details and the terms and conditions provided by Elsevier and Copyright Clearance Center.

License Number	5278060878309
License date	Mar 29, 2022
Licensed Content Publisher	Elsevier
Licensed Content Publication	Current Opinion in Microbiology
Licensed Content Title	Towards detecting regulatory protein–metabolite interactions
Licensed Content Author	Maren Diether,Uwe Sauer
Licensed Content Date	Oct 1, 2017
Licensed Content Volume	39
Licensed Content Issue	n/a
Licensed Content Pages	8
Start Page	16
End Page	23
Type of Use	reuse in a thesis/dissertation

1 of 7 3/29/2022, 12:16 PM

RightsLink Printable License https://s100.copyright.com/App/PrintableLicenseFrame.jsp?publisher...

Portion	figures/tables/illustrations
Number of figures/tables /illustrations	1
Format	both print and electronic
Are you the author of this Elsevier article?	No
Will you be translating?	No
Title	The Choline Metabolite-Interacting Proteome of Mammalian Cells: Discovery and Significance
Institution name	Indian Institute of Science Education and Research (IISER), Pune
Expected presentation date	May 2022
Portions	Figure 1
Requestor Location	Ms. Aditi Dixit Lab 304, AB-3, IISER Bhopal Bhopal Bypass Road, Bhauri Bhopal, Madhya Pradesh Bhopal, Madhya Pradesh 462066 India Attn: Ms. Aditi Dixit
Publisher Tax ID	GB 494 6272 12
Total	0.00 USD

Terms and Conditions

INTRODUCTION

1. The publisher for this copyrighted material is Elsevier. By clicking "accept" in connection with completing this licensing transaction, you agree that the following terms and conditions apply to this transaction (along with the Billing and Payment terms and conditions established by Copyright Clearance Center, Inc. ("CCC"), at the time that you

2 of 7 3/29/2022, 12:16 PM

CCC Marketplace™

This is a License Agreement between Aditi Dixit ("User") and Copyright Clearance Center, Inc. ("CCC") on behalf of the Rightsholder identified in the order details below. The license consists of the order details, the CCC Terms and Conditions below, and any Rightsholder Terms and Conditions which are included below.

All payments must be made in full to CCC in accordance with the CCC Terms and Conditions below.

Order Date	29-Mar-2022	**Type of Use**	Republish in a thesis/dissertation
Order License ID	1204739-1	**Publisher**	ROYAL SOCIETY OF CHEMISTRY
ISSN	1742-2051	**Portion**	Chart/graph/table/figure

LICENSED CONTENT

Publication Title	Molecular bioSystems	**Publication Type**	e-Journal
Article Title	Photocrosslinkers illuminate interactions in living cells.	**Start Page**	473
		End Page	480
Author/Editor	Royal Society of Chemistry (Great Britain)	**Issue**	6
		Volume	4
Date	06/01/2005	**URL**	http://www.rsc.org/Publishing/Journals/mb/index.asp
Language	English		
Country	United Kingdom of Great Britain and Northern Ireland		
Rightsholder	Royal Society of Chemistry		

REQUEST DETAILS

Portion Type	Chart/graph/table/figure	**Distribution**	Worldwide
Number of charts / graphs / tables / figures requested	1	**Translation**	Original language of publication
		Copies for the disabled?	No
Format (select all that apply)	Print, Electronic	**Minor editing privileges?**	No
		Incidental promotional use?	No
Who will republish the content?	Academic institution		
Duration of Use	Life of current edition	**Currency**	USD
Lifetime Unit Quantity	Up to 499		
Rights Requested	Main product		

NEW WORK DETAILS

Title	The Choline Metabolite-Interacting Proteome of Mammalian Cells: Discovery and Significance	**Institution name**	Indian Institute of Science Education and Research (IISER), Pune
		Expected presentation date	2022-05-30
Instructor name	Dr. Jeet Kalia		

ADDITIONAL DETAILS

Order reference number	N/A	**The requesting person / organization to appear on the license**	Aditi Dixit

REUSE CONTENT DETAILS

Title, description or numeric reference of the portion(s)	Figure 1	**Title of the article/chapter the portion is from**	Photocrosslinkers illuminate interactions in living cells.
Editor of portion(s)	Tanaka, Yoshihito; Bond, Michelle R.; Kohler, Jennifer J.	**Author of portion(s)**	Tanaka, Yoshihito; Bond, Michelle R.; Kohler, Jennifer J.
Volume of serial or monograph	4	**Issue, if republishing an article from a serial**	6
Page or page range of portion	473-480	**Publication date of portion**	2008-06-01

CCC Terms and Conditions

1. Description of Service; Defined Terms. This Republication License enables the User to obtain licenses for republication of one or more copyrighted works as described in detail on the relevant Order Confirmation (the "Work(s)"). Copyright Clearance Center, Inc. ("CCC") grants licenses through the Service on behalf of the rightsholder identified on the Order Confirmation (the "Rightsholder"). "Republication", as used herein, generally means the inclusion of a Work, in whole or in part, in a new work or works, also as described on the Order Confirmation. "User", as used herein, means the person or entity making such republication.

2. The terms set forth in the relevant Order Confirmation, and any terms set by the Rightsholder with respect to a particular Work, govern the terms of use of Works in connection with the Service. By using the Service, the person transacting for a republication license on behalf of the User represents and warrants that he/she/it (a) has been duly authorized by the User to accept, and hereby does accept, all such terms and conditions on behalf of User, and (b) shall inform User of all such terms and conditions. In the event such person is a "freelancer" or other third party independent of User and CCC, such party shall be deemed jointly a "User" for purposes of these terms and conditions. In any event, User shall be deemed to have accepted and agreed to all such terms and conditions if User republishes the Work in any fashion.

3. Scope of License; Limitations and Obligations.

   3.1. All Works and all rights therein, including copyright rights, remain the sole and exclusive property of the Rightsholder. The license created by the exchange of an Order Confirmation (and/or any invoice) and payment by User of the full amount set forth on that document includes only those rights expressly set forth in the Order Confirmation and in these terms and conditions, and conveys no other rights in the Work(s) to User. All rights not expressly granted are hereby reserved.

   3.2. General Payment Terms: You may pay by credit card or through an account with us payable at the end of the month. If you and we agree that you may establish a standing account with CCC, then the following terms apply: Remit Payment to: Copyright Clearance Center, 29118 Network Place, Chicago, IL 60673-1291. Payments Due: Invoices are payable upon their delivery to you (or upon our notice to you that they are available to you for downloading). After 30 days, outstanding amounts will be subject to a service charge of 1-1/2% per month or, if less, the maximum rate allowed by applicable law. Unless otherwise specifically set forth in the Order Confirmation or in a separate written agreement signed by CCC, invoices are due and payable on "net 30" terms. While User may exercise the rights licensed immediately upon issuance of the Order Confirmation, the license is automatically revoked and is null and void, as if it had never been issued, if complete payment for the license is not received on a timely basis either from User directly or through a payment agent, such as a credit card company.

   3.3. Unless otherwise provided in the Order Confirmation, any grant of rights to User (i) is "one-time" (including the editions and product family specified in the license), (ii) is non-exclusive and non-transferable and (iii) is subject to any and all limitations and restrictions (such as, but not limited to, limitations on duration of use or circulation) included in the Order Confirmation or invoice and/or in these terms and conditions. Upon completion of the licensed use, User shall either secure a new permission for further use of the Work(s) or immediately cease any new use of the Work(s) and shall render inaccessible (such as by deleting or by removing or severing links or other locators) any further copies of the Work (except for copies printed on paper in accordance with this license and still in User's stock at the end of such period).

   3.4. In the event that the material for which a republication license is sought includes third party materials (such as photographs, illustrations, graphs, inserts and similar materials) which are identified in such